Exploring New Methods for Polymer and Monomer Editing

A Dissertation Presented for the

Doctor of Philosophy

Degree

The University of Tennessee, Knoxville

Nicholas Jose Galan

August 2023

DEDICATION

I would like to dedicate this dissertation to my late mother and father, Jose, and Catherine Galan. My parents, both of whom were manual laborers, encouraged me from a young age to work hard in school so that I could live a better life and not destroy my body. Little did they know that I've likely done a different kind of harm to my body being around chemicals for nearly 6 years, but at least my joints are still functioning. My parents, mostly my mom, always fostered an inquisitive mindset that I have taken with me and applied to almost everything I've endeavored in. While my father instilled a fastidious resolve and work ethic, even if it means making some sacrifices along the way. While they won't be here in the physical sense to see the culmination of all my hard work the last five and a half years, I know they would be beyond proud.

I would also like to dedicate a part of this dissertation to my dear late friend and lab-mate Alan Fried. I met Alan when he was only a prospective student touring the university in March of 2018. We got along from the very beginning before he even formally joined the group. While he was here, Alan expanded my musical tastes to bands I'd never heard before and introduced me to the worlds of specialty coffee and collecting music on vinyl. While Alan tragically passed before he could see the completion of his work, I was honored to be able to complete them, one of which is included in this dissertation. I know he would be glad, albeit surprised that I stuck around and finished them.

ACKNOWLEDGEMENTS

First and foremost, I want to thank my late parents, Catherine, and Jose Galan, they pushed me to achieve things they never had the chance to. They supported me and made sure I had good support system during my time in undergrad and throughout most of my graduate career.

Secondly, I want to thank my PI, Professor Johnathan Brantley. When I was considering UTK as a serious graduate school choice in fall 2016, it never crossed my mind that it would be in the lab of someone who wasn't even employed there at the time. Who could've predicted how the last 6 years would have transpired after our first meeting in K brew in July 2017. Thank you for your mentorship, guidance, and always pushing us as scientists, despite the number of times you had to say, "we're back to where we were!" those first two years. I am extremely proud of the work we've been able to accomplish together over these years. It has been a challenging, but formative experience and I hope you're as proud of what we accomplished as I am.

Next, I want to thank Dr. Breana Wilson, Dr. Brian Jacobs, Chase Cromer, Boris Cobbold, and Hima Davit. While some of you didn't overlap in your time in the lab, I have enjoyed my time around all of you the last six years. From drawing the giraffes on the fume hoods and going to conferences together, to all the group outings and all the little mundane everyday things. One of the secrets to making it through grad school is having lab mates you enjoy being around, and I certainly lucked out in that regard.

I also want to thank the members of my dissertation committee, Professor Brian Long, Professor Michael Best, and Professor Gila Stein. Dr. Best, I have had the

opportunity to take two, very important classes with you during my time here at UTK. Furthermore, I had the privilege to conduct undergrad research in your lab for a year and a half including a paid summer of research. Thank you for that experience, and for all the times we've gotten to chit-chat about video games. It's always a treat walking into your office and seeing the new memorabilia you've acquired. Dr. Long, I'm so thankful for the collaboration between the groups when Dr. Brantley's group was first being established, and all of the discussions we've had throughout the years. At times, the Long group members feel like an extended family and we're always helping each other. I will certainly miss the walks up the 4th floor. Dr. Stein, thank you for helpful discussions regarding Gordon-Taylor analysis of one of my copolymers showcased in one of my publications. I also appreciate the thoughtful questions regarding my projects throughout my graduate career.

Lastly, I want to give a special tank you to all of my friends, family, and many others who have supported me throughout one of the most stressful periods in my life. It's so easy to get lost in grad school, so having those outside influences to maintain a somewhat normal life have helped keep me grounded. I wouldn't be where I am today without everyone mentioned here. Thank you all so much.

ABSTRACT

Soft polymers have become intricately woven into many facets of human society. One key motivation for their continued development is the link between polymer structure and material properties. Structure modification can be accomplished through the developing diverse monomers, or through direct polymer editing. As such, developing new methods to access materials with bespoke architectures and properties is of great importance. As such, there is a burgeoning interest in reaction manifolds that furnish highly reactive functional groups/intermediates, which open paths for degradation and functionalization previously inaccessible.

Polymers composed of rigid carbocycles possess desirable properties and exhibit predictable structure property trends, such as glass transition temperature (T_g), as a function of carbocycle content. However, longstanding synthetic limitations prevent investigation of cyclic monomers other than norbornene. Furthermore, terpenoids are bio-derived substrates which often possess carbocyclic cores. Terpenoids are not only ideal candidates to probe fundamental properties but could serve as supplements to petroleum-based materials. Herein, I present my contributions to the community's understanding of how reactive intermediates/functionalities expand the chemical space of polymer and monomer editing and expound upon our efforts to probe resulting structure property relationships.

My first project (Chapter II) centered on utilizing the Skattebøl rearrangement to embed allenes within polynorbornene. We found that these polyallenamers exhibited unique photophysical properties and retained intrinsic reactivity of the allene moiety (e.g. [2+2] cycloadditions and Au-I mediated couplings). In a subsequent study (Chapter III),

we devised a route to access polyallenamers from polymerizing a “masked” (i.e., *gem*-dibromocyclopropane) monomer. These polyallenamers exhibited similar photo-physical properties, were amenable to synthesis of block-like copolymers, and their mechanical properties could be tuned as a function of irradiation time. Chapter IV focused on investigating underutilized methods (i.e., photoredox catalysis) to generate high energy species (radical cations) along polyalkenamers backbones. These intermediates led to chain scission and functionalization. Mechanistic experiments were conducted to investigate this unique reactivity. The final project discussed (Chapter V and VI) explore the utility of cyclic allenes and terpenoid derived allene monomers as congeners for cyclic olefin copolymers and investigations into their innate structure property relationships as a function of carbocycle content.

TABLE OF CONTENTS

LIST OF TABLES

LIST OF FIGURES

LIST OF SCHEMES

CHAPTER I: INTRODUCTION

1.1 Polymer Structure Dictates Bulk Properties

Synthetic polymers have revolutionized nearly every aspect of human society since their discovery by Staudinger.[1] One of the key motivations behind their widespread adoption, and continued development, is the inextricable link between polymer structure and bulk material properties.[2] For example, small changes to polymer architecture (e.g., branching, unsaturation, and regiochemical connectivity) can have a substantial impact on overall physical properties. For instance, 3% alkyl branching in polyethylene (PE) significantly alters the thermomechanical properties of the polymer (i.e. modulus, viscosity), and, by extension, the applications for which the material can be used. [3,4] Altering bond type (e.g., $Csp^3 – Csp^3$ to $Csp^2 – Csp^2$) can influence both thermomechanical properties and chemical reactivity (i.e., oxidations, reductions, and crosslinking) which is demonstrated when comparing materials that possess similar structures such as polyethylene and polybutadiene (Figure 1.1). Furthermore, substitution (e.g., *meta* vs *para*) can also affect physical properties. For example, Kevlar is a polyaramide where the *para* arene regiochemistry facilitate additive interactions such as H-bonding (between N-H and C=O units) and π-stacking that affords a material with increased tensile strength.[5] However, modifying the arene regiochemistry from *para* to *meta* yields Nomex, a polyaramide that exhibits flame resistant properties commonly used for lab coats and firefighter jackets. (Figure 1.1). It is evident that altering polymer structure has significant implications regarding the bulk material properties. As such, developing strategies that permit access to structurally diverse macromolecules is of urgent need.

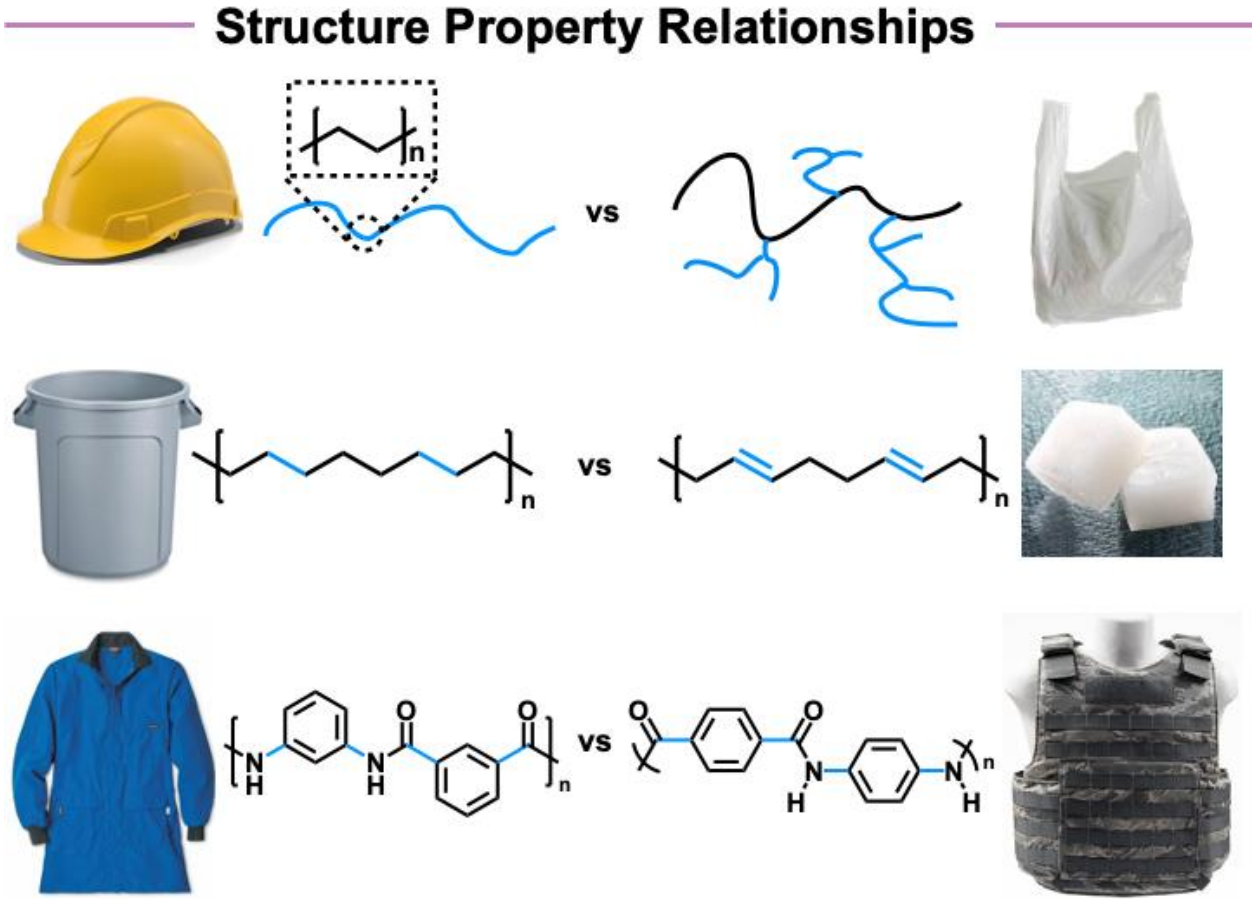

Figure 1.1: Cartoon examples of selected structure property relationships.

Polymer structure, and the resulting properties, can be tailored via two general strategies: (i) monomer editing (i.e., prior to polymer synthesis) or (ii) direct polymer editing, done post-polymerization. Monomer editing enables access to a diverse library of functionalized monomers. For example, chemistries such as cycloadditions, halogenation, and esterification permit the preparation of various monomers. Furthermore, judicious choice of monomer can afford access to soft materials with structures that were previously synthetic challenging. Alternatively, editing of extant macromolecules allows for introduction of functionalities that would normally be incompatible in the monomer. Furthermore, efforts to repurpose commodity materials at the end of their life (i.e., polymer upcycling), has ushered in a renaissance regarding the development of polymer editing methodologies. As such, investigating underexplored chemistries for both monomer and polymer editing is paramount for preparing materials with tailored architectures.

1.2 Altering Macromolecular Structure via Polymer Editing

Polymer editing can occur along the backbone or the side-chain. This feat is more readily accomplished on the polymer side-chain,[6,7] salient examples include facile "click" type reactions (e.g., thiol-ene coupling of 1,2 polybutadiene,[8] dipolar cycloadditions of azides with alkyne side-chains[9]), and even transition metal mediated cross-coupling reactions (e.g. Sonogashira[10] or Suzuki[11]) of various polymers. Despite the breadth of chemistries that have been developed for side-chain modification, direct editing of the backbone, is less common. Zhukovitsky and colleagues recently proposed using graph theory to distinguish main-chain and side-chain atoms in linear polymers (Figure 1.2). This

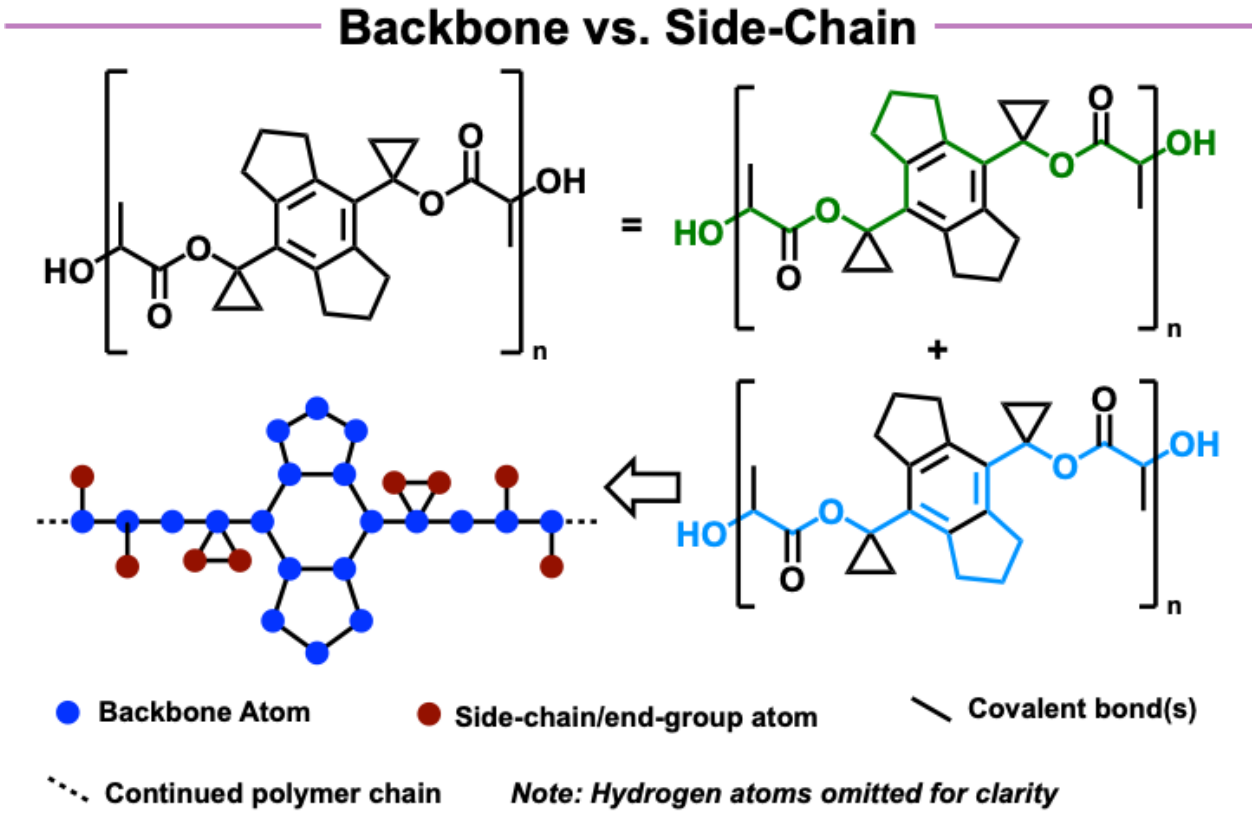

Figure 1.2: Distinguishing main-chain from side-chain.

convention reduces atoms to vertices and covalent bonds to single edges (regardless of bond order or atom identity). The end groups are defined to be the natural boundaries of the polymer, and the backbone is simply the set of all non-self-intersecting paths that connect the two boundaries. Any atoms not fulfilling these conditions is considered to be a side-chain element. As such, this model will be adopted in this dissertation when examining polymer main-chains.

Since 55% of the world's plastic production consists of polyolefins (e.g., polyethylene, polypropylene, polystyrene, etc.),[12] editing methodologies have largely focused on manipulating C–H and C−C bonds for upcycling efforts. These relatively inert bonds possess high bond-dissociation energies (BDEs) such as 83-90 kcal/mol (for C−C) and 96-105 kcal/mol (for C–H) that necessitate high energy intermediates for activation.[13] Notwithstanding this inherent synthetic challenge, there have been considerable achievements toward the direct chemical tailoring of polymer backbones. In a seminal report, Hartwig and Hillmyer detailed a Rh-catalyzed borylation/oxidation of substituted polyolefins.[14] Similar pioneering work by Coates and Goldman demonstrated that Iridium pincer complexes could install reactive olefins throughout various polyolefins via catalytic dehydrogenation (Scheme 1.1).[15] More recently, the Leibfarth group has reported the perfluoroalkylation of polystyrene[16] and the functionalization of linear and branched polyolefins through radical chain-transfer methodologies (Scheme 1.1).[17,18]

In an effort to expand the scope of available editing strategies, other transformations, aside from C-H activations, have been investigated. For example, methods for incorporating new atoms into the backbone (i.e., atom insertion) have been well studied,

Scheme 1.1: Selected examples of polymer editing.

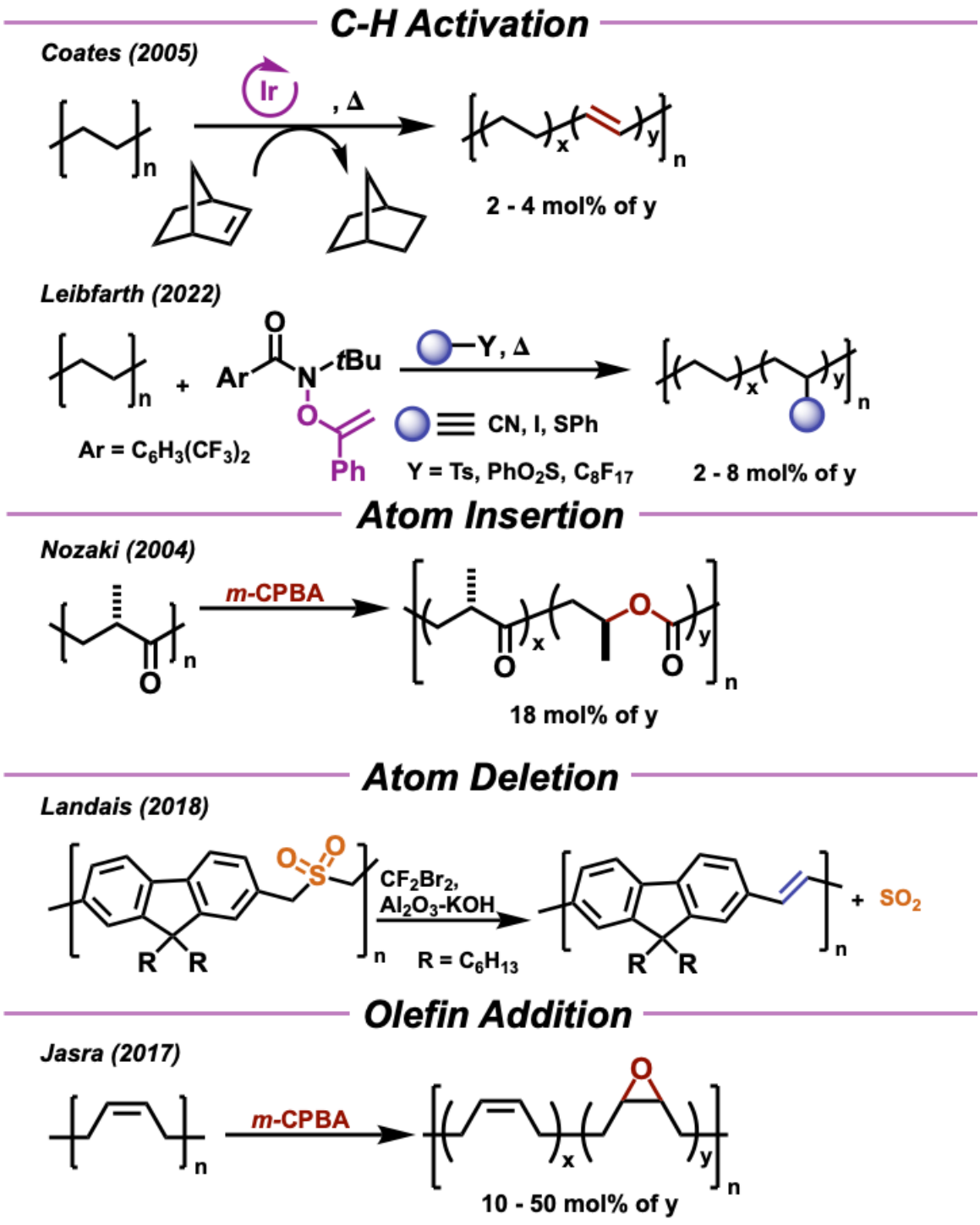

such as Nozaki's work detailing the insertion of O-atoms into a polyketone via Baeyer-Villiger oxidation. (Scheme 1.1). Conversely, atom deletions are significantly more challenging as these processes can promote unwanted chain-scission, however, Landais has accomplished the only example of atom deletion, without concomitant chain-scission, via Ramberg-Bäcklund extrusion of SO_2 from an aromatic macromolecule.[19] Further examples include simple olefin additions, which are often classified as cyclization, such as epoxidation,[20] and *gem*- dihalocyclopropanation[21–23] of polyalkenamer scaffolds (e.g., polybutadiene, polyisoprene, polynorbornene etc.) (Scheme 1.1). Despite these elegant examples, expanding the chemical space of polymer editing strategies would enable access to materials with tailored reactivities and bulk material properties. A major thrust of the work detailed in this dissertation describes how the scope of polymer editing methodologies were expanded through the investigation of underutilized reactive groups/intermediates.

1.2.1 Allenes in Macromolecular Materials

Functionalities incorporated via polymer editing strategies commonly result in modifying bulk physical properties However, the embedded groups rarely allow for further chemical elaborations to access 2nd and 3rd generation materials. There are, however, examples which detail the synthesis of 2nd generation daughter polymers after the initial functionalization. For example, epoxidized polyalkenamers can undergo nucleophilic ring-opening and subsequent cross-linking to form dynamic covalent networks.[24] Similarly, *gem*-dihalocyclopropanes are susceptible to force-induced ring-opening which is amenable

to mechanochemical strengthening through S_N2 chemistries.[25] Furthermore, aldehydes can be reversibly crosslinked with di-amines to form covalent networks or engage in 1,2-additions.[11] Moreover, introduction of azides allow for various successive transformations such as the copper-assisted azide-alkyne cycloaddition (CuAAC),[26] which has seen numerous biological applications. As such, embedding reactive functionalities within polymer matrices that facilitate further editing is highly enticing. These groups can even facilitate uncommon modifications, such as Zhukovitsky's report detailing Ireland-Claisen rearrangements of allylic ester-containing materials. Specific moieties can also serve as handles for polymer degradation. Mecking and coworkers have disclosed PE-like materials decorated with degradable ester linkages.[27] Thus, exploring underutilized reactive handles that are amenable to chemical elaboration and degradation is of increasing interest.

One moiety that remains largely underexplored in the polymer science community, is the allene. Indeed, allenes have emerged as linchpins within modern synthetic methodologies. For example, there have been myriad reports detailing metal mediated transformations such as hydroaminations,[28] hydroboration,[29] hydroacylation,[30] and hydroazidation.[31] Moreover, allenes can participate in an array of cycloadditions[32–34] toward the synthesis of complex heterocyclic molecules. Additionally, allenes can impart axial chirality, if prepared from enantioenriched precursors.[35] Despite these enticing benefits, the preparation of polyallenamers remain largely overlooked by the polymer science community. This oversight is presumably due to the intrinsic reactivity of the allene moiety. Indeed, there is extensive precedent detailing myriad methods of allene polymerization[36] such as uncontrolled[37] and controlled[38] radical, cationic,[39] anionic,[40]

coordination-insertion,[41,42] and living vinyl-addition.[43–47] Nonetheless, the allene moiety is consumed in these methods (Scheme 1.2). Thus, the preparation of materials with main-chain allenes, has remained a considerable synthetic challenge.

Regardless of longstanding synthetic difficulties, there has been some success regarding the preparation of polyallenamers. Seminal reports by Kijima and coworkers reported the synthesis of tetraphenylallene oligomers which exhibited tunable fluorescence (Scheme 1.3).[48–50] Shortly thereafter, Diedrich and colleagues detailed the preparation of allenyne oligomers that displayed enhanced chiroptical properties, as oligomer length increased (Scheme 1.3).[51,52] Similarly, Hasegawa disclosed the first redox-switchable oligomeric allene chromophore.[53] While these early reports demonstrated that polyallenamers could be prepared through elegant iterative coupling strategies, expanding to more modular methods of synthesis could enable access to various scaffolds, allow for control of the molecular weight of the material, and access advanced architectures (e.g., block copolymers).

Recently, the Bielawski and Moore groups have independently reported the synthesis of well-defined polyallenamers via ring-opening metathesis (ROMP) of cyclic allene monomers (Scheme 1.3). These materials were amenable to further chemical elaboration (e.g. hydrosilylation). However, these systems were limited to low (<20 kDa) number average molecular weight (M_n) materials and were not compatible for block copolymer architectures. Despite these promising examples, there remains significant

Scheme 1.2: Selected examples of polymerizing allene monomers.

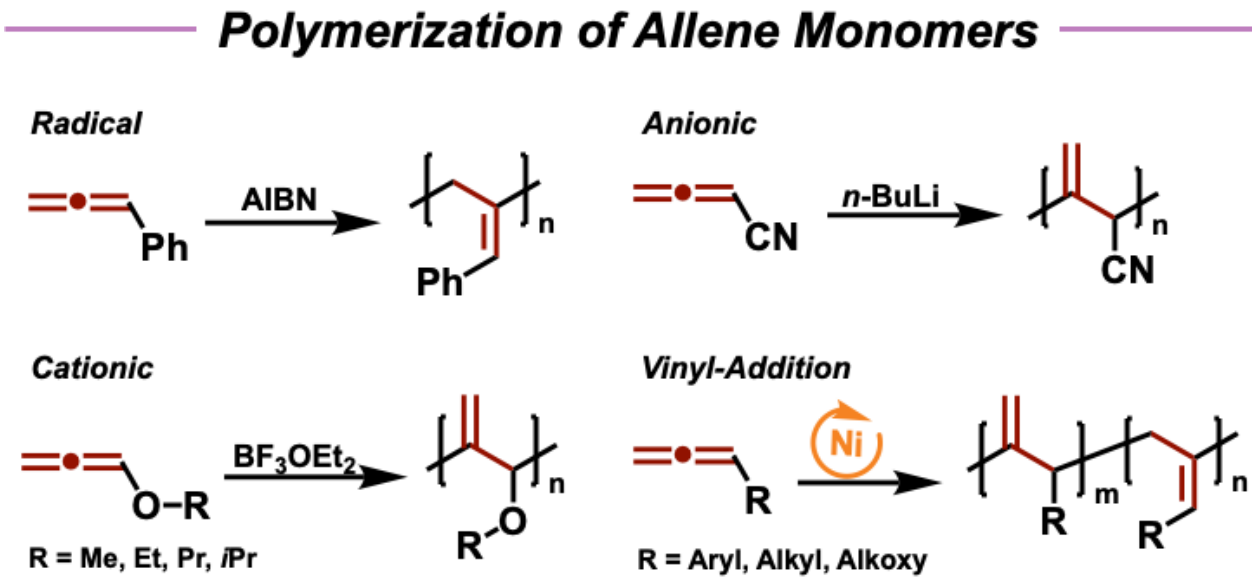

Scheme 1.3: Selected examples of methods to prepare polyallenamers.

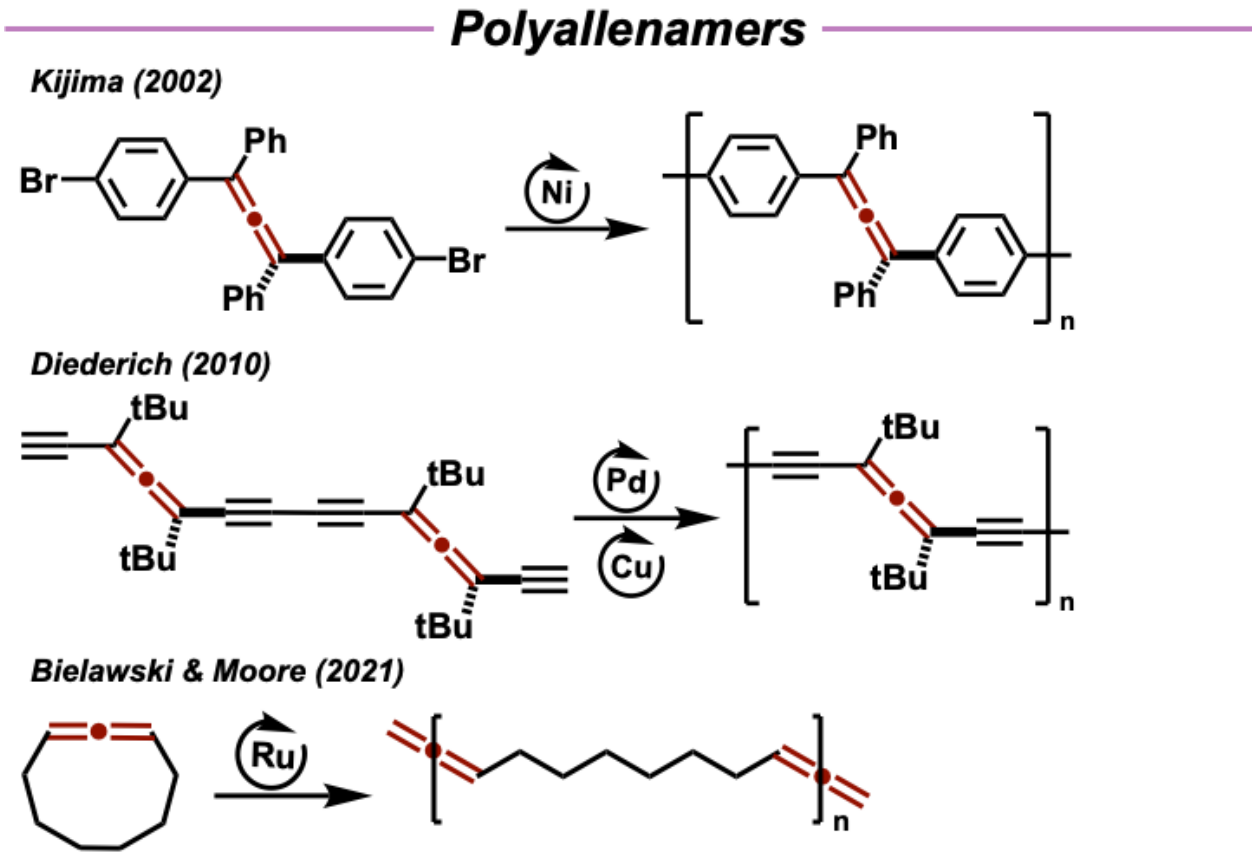

limitations that must be addressed, such as poor control of M_n, accessibility of various polymer scaffolds, and the construction of block copolymer systems. Part of the work demonstrated in this dissertation details the transformation of polyalkenamers to well-defined polyallenamers via a simple polymer editing protocol.

1.2.2 Polymer Editing via High Energy Species

Portions of this section were reproduced from a book chapter in submission by Hima Davit, Chase E. Cromer and Nicholas J. Galan.

Davit, H.; Galan, N. J.; Cromer, C. E.; Brantley, J. N. Exploring Sustainable Methods for Polymer Synthesis and Editing. In *Sustainable Green Chemistry in Polymer Science and Technology*. ACS Books. Ed. H. N. Cheng. **2023**. *Submitted.*

The majority of commodity plastics produced are comprised of C−H and C−C bonds that are relatively difficult to leverage for synthetic transformations. Indeed, the editing of synthetic macromolecules is no trivial task. Both kinetic and thermodynamic barriers impede our ability to insert or delete functional groups from polymer backbones. Frustratingly, transformations developed using small molecule substrates often demonstrate little success when applied to macromolecules. As such, reaction manifolds that can circumvent these limitations are critically needed. One such way to engender enhanced reactivity, of normally inert bonds, is through the generation of high energy species such as radical ions. However, accessing these species require the use of reaction manifolds that promote sing-electron oxidations/reductions. Within the last decade, methods that facilitate single-electron redox manipulations (i.e., photoredox catalysis and

synthetic electrochemistry) have undergone significant growth and development. However, this has been almost exclusively centered on small molecule substrates. Despite the wealth of transformations that are facilitated by photoredox and electrochemical methods, these methods remain underexplored in the polymer science community. For example, the Inagi group reported that conjugated polymers (e.g., polyhexylthiophene) were amenable to electrochemical chlorination via anodic oxidation, in an effort to tune the optoelectronic properties (Scheme 1.4).[54] Similarly, Sarlah and coworkers have reported the dearomatization of polystyrene via electroreduction (which implicated a radical anion intermediate[55]). These reduced materials were further elaborated using olefin chemistries (Scheme 1.4).[56] More recently, McNeil and colleagues reported that polyvinylchloride could function as a chloride source to access chlorinated arenes (Scheme 1.4). [57] Moreover, the Shida group detailed an electrochemical protocol for benzylic substitution of an aryl ether polymer (Scheme 1.4),[58] and our lab disclosed electrochemical single-electron editing, scission and azidation, of various polyalkenamers (Scheme 1.4). There are fewer reports regarding photoredox mediated polymer transformations. Early examples have focused on decarboxylation of various acrylate copolymers (Scheme 1.5) which required activated ester moieties. More recent work by the Sumerlin group have shown that an acridinium photoredox catalyst promotes single electron oxidation of polyacrylic acid/acrylate copolymers (Scheme 1.5). There have even been reports detailing direct depolymerization of thio-capped polyacrylates.[59] Despite these promising precedents of polymer editing through the generation of high energy species, expanding

Scheme 1.4: Examples of electrochemical polymer editing strategies. Adapted from a scheme originally published in *Sustainable Green Chemistry in Polymer Science and Technology*. ACS Books, **2023** Submitted.

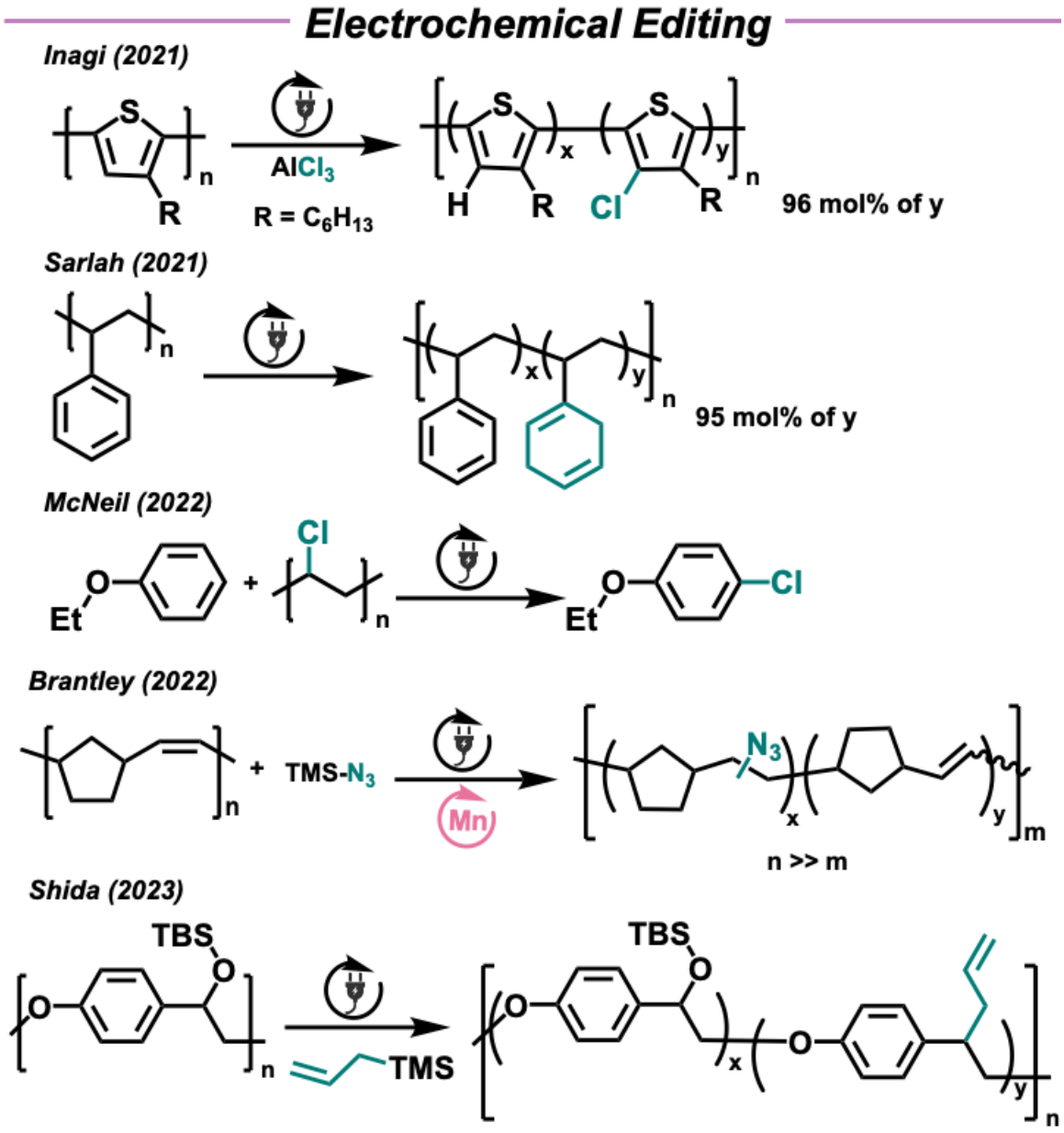

Scheme 1.5: Examples of polymer editing via photoredox catalysis.

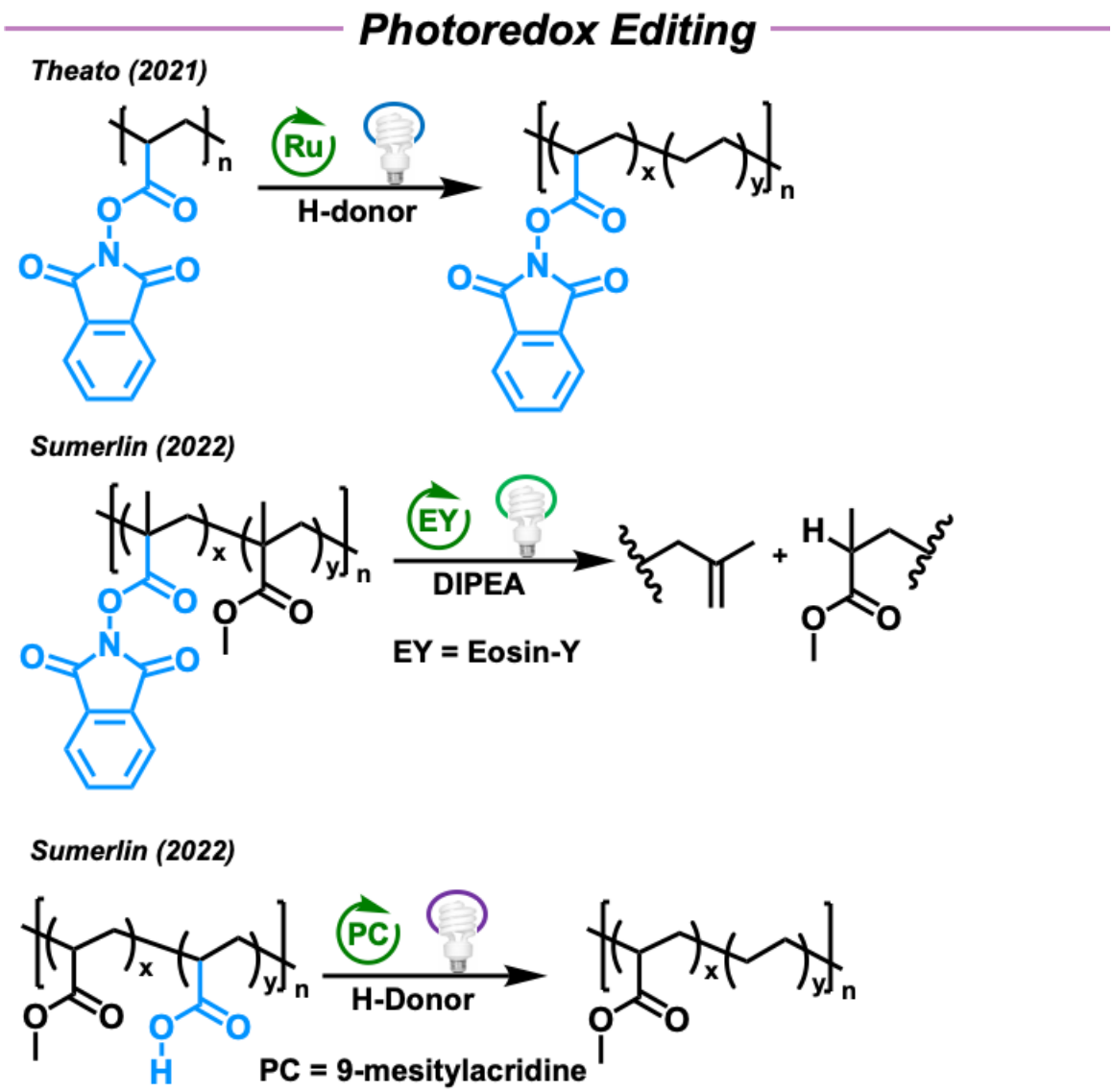

the available toolbox of editing methods is critical for the functionalization and degradation of extant macromolecules.

1.3 Structure Property Relationships in Cyclic-Olefin Copolymer Congeners

Portions of this section were reproduced from articles originally published by Nicholas J. Galan, Justin M. Burroughs, Chris Maroon, Alan D. Fried, and Chase Cromer:

Galan, N. J. [†]; Burroughs, J. M. [†]; Maroon, C. R.; Long, B. K.; Brantley, J. N.[*] Vinyl-Addition Polymerizations of Cycloallenes: Synthetic Access to Congeners of Cyclic-Olefin Polymers. *Polym. Chem.* **2020**, *11* (35), 5578–5581; .

[†] Indicates equal contribution, [*] Corresponding author

Galan, N. J. [†]; Fried, A. D. [†]; Cromer, C. E. [†]; Fish, A.; Coughlin, D. R.; Brantley, J. N.[*] Exploring the Influence of Rigid Carbocycles on Terpenoid Copolymer Properties. *J. Polym. Sci.* **2023**, 1-7.

[†] Indicates equal contribution, [*] Corresponding author

Given the intricate relationship between structure and bulk material properties (*vide supra*), designing materials with bespoke properties and architectures is a persistent challenge in the polymer community. Indeed, efforts to predict bulk material properties from polymer composition are often hindered by the nuance of these structure property relationships. However, macromolecules composed of rigid carbocyclic and acyclic units appear to be an exception to this issue. These cyclic olefin copolymers (COCs) have emerged as enticing synthetic targets due to their desirable physical properties (e.g. high

glass transition temperature [T_g],[60] optical transparency,[61,62] good processability,[63] enhanced modulus,[64] etc.). More importantly, bulk physical properties (i.e. Young's Modulus and T_g) seemingly correlate with cyclic monomer content in a linear/additive manner consistent with theoretical models such as the Fox relation.[65–67] Nonetheless, a more comprehensive understanding of how carbocyclic units influence copolymer properties remain elusive. This is attributed to enduring synthetic challenges that severely limit the scope of cyclic motifs that can be reliably embedded within soft polymers. For example, radical and cationic polymerizations suffer from deleterious rearrangements and chain termination events (affording low yields and oligomeric species).[68,69] Furthermore, ROMP intrinsically requires highly strained monomers (e.g. norbornene) which inherently limits monomer scope.[70] However, one method that successfully facilitates the polymerization of cyclic olefins is vinyl-addition polymerization.

While this method exhibits improved performance, it is not without synthetic obstacles. For example, off-cycle reactions (such as β-hydride elimination) often preclude the use of monomers aside from norbornene and its substituted derivatives.[71] Although many cyclic olefin substrates undergo copolymerization in the presence of ethylene, this strategy necessitates the use of highly reactive metal catalysts (which can exhibit poor functional group tolerance) along with harsh activators and cocatalysts (Scheme 1.6). For example, Group 3 complexes will polymerize norbornene in the presence of acyclic olefins, aside from ethylene, such as 1-hexene.[72] Moreover, Waymouth and colleagues reported that half-sandwich constrained geometry complexes could polymerize other cyclic olefins such as cyclooctene, cycloheptene, and cyclopentene (Scheme 1.6).[73] However, only

Scheme 1.6: Selected examples of cyclic olefin copolymers. Adapted from schemes originally published in *Polym. Chem.* **2020** *11*, 5578-5581 and *J. Poly. Sci.* **2023** 1-7.

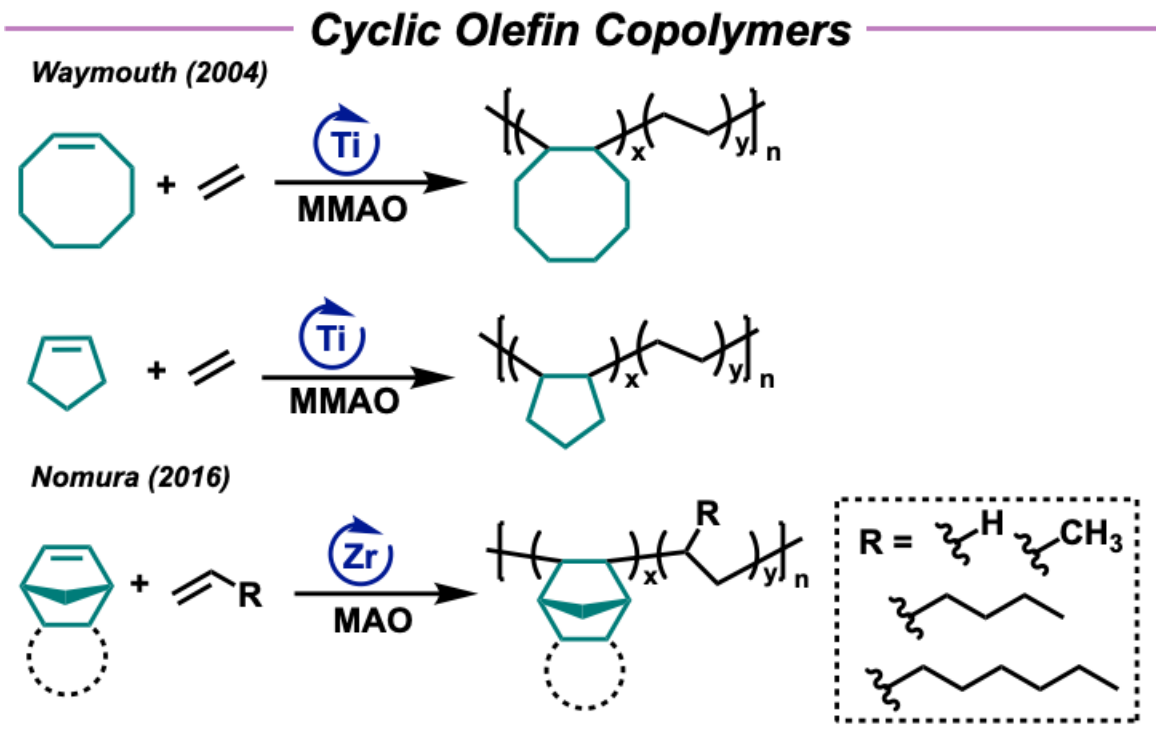

modest amounts (<50 mol%) of the cyclic motif was incorporated. Post-metallocene vinyl-addition catalysts are reported to polymerize sterically demanding (*t*-butyl) and functionally rich substituted norbornene monomers (e.g. alcohols, various esters) which were incompatible with traditional vinyl-addition catalysts (Scheme 1.5). Despite this promising precedent, exploring new pathways to access materials composed of rigid carbocyclic units is crucial for further elucidating how these architectural elements impact bulk material properties.

Similar to their olefin congeners, allenes can polymerize via vinyl-addition catalysts, [36,74] but exhibit superior functional group tolerance (Scheme 1.2) More specifically, Endo and colleagues have shown that [(π-allyl)NiOCOCF$_3$]$_2$ facilitates the living polymerization of structurally diverse (e.g. sterically bulky and cyclic) allene monomers bearing an array of functional groups (e.g. alcohols, esters, amides). Furthermore, 1,1-disubstitued allenes are reported to polymerize solely through the 2,3 carbons, which simplifies characterization of the resulting polymer. Since it has been demonstrated that cyclic allenes are amenable to homopolymerization,[75] these species may serve as adequate olefin analogues toward the investigation of how carbocyclic frameworks influence bulk material properties.

1.3.1 Terpenoids as a Source of Structurally and Functionally Diverse Monomers

Portions of this section were reproduced from a book chapter in submission by Hima Davit, Chase E. Cromer and Nicholas J. Galan.

Davit, H.; Galan, N. J.; Cromer, C. E.; Brantley, J. N. Exploring Sustainable Methods for Polymer Synthesis and Editing. In *Sustainable Green Chemistry in Polymer Science and Technology*. ACS Books. Ed. H. N. Cheng. **2023**. *Submitted.*

Accessing exotic architectures (e.g., fused rings, bicycles, spirocycles, etc.) to elucidate their impact on bulk material properties is challenging. There are few petroleum derived examples that are amenable to polymerization (i.e., norbornene). Conversely, biology affords unparalleled complexity and diversity in the context of chemical space. Leveraging these natural products as polymer feedstocks would enable fundamental investigations on how complex structural motifs influence polymer properties. There have been considerable achievements regarding the preparation of bio-based commodity materials such as polylactide and polyglycolide which see applications in packaging[76] and medical sutures,[77] respectively. However, broader adoption of these and other bio-based plastics has been hampered by their hydrolytic instability, inadequate physical properties (compared to polyolefins), or higher manufacturing costs.[78,79] However, one class of bio-derived materials that are not only architecturally diverse, but also replete with various functionalities are terpenoids. Terpenes have been investigated as potential monomer candidates since the early 20th century,[80] and have found various uses (e.g., as adhesives,[81] food packaging,[82] tackifiers,[83] and even latex substitutes[84]). Terpenes bearing rigid carbocycles are particularly attractive candidates, given their striking similarities to COCs comprised of norbornene.

There have been numerous recent reports detailing the preparation of terpenoid congeners of COCs. For instance, Nomura and coworkers have disclosed the Ti-catalyzed vinyl-addition copolymerization of ethylene, limonene, and β-pinene (Scheme 1.6).[85] Similarly, Kennemur and colleagues have shown that δ-pinene will undergo ROMP in the presence of trace α-pinene (Scheme 1.6).[86] The Howdle group have reported a series of triblock copolymers via reversible addition-fragmentation chain transfer (RAFT) polymerization of acrylate functionalized pinene and tetrahydrogeraniol derivatives (Scheme 1.6).[87,88] Aside from these clever reports, the controlled syntheses of bicyclic terpenoids without concomitant ring-opening, as observed in the cationic polymerization of β-pinene,[89,90] is challenging. There are several terpenoid candidates that possess a structural homology to common COCs (e.g., pinene, camphene, sabinene, etc.), thus overcoming this synthetic hurdle could allow a deeper understanding of how rigid carbocyclic motif influence bulk material properties.

Our lab has reported the synthesis of the allene congener of β-pinene (β-pinadiene) and subsequent vinyl-addition homopolymerization using the [(π-allyl)NiOCOCF$_3$] catalyst (Scheme 1.6).[44] This monomer polymerized in a living manner, exhibited enhanced thermal properties compared to ring-opened precedent, and retention of the bicyclic core was confirmed by 2-D NMR spectroscopic experiments. Encouraged by these results, a more in-depth investigation into the structure property relationship of copolymer architectures is needed. For example, how carbocycle content affects bulk material properties in block copolymers compared to statistical copolymers. We are also curious if trends observed in COCs with acyclic units are applicable to systems with units that are

Scheme 1.7: Selected examples of terpene-based polymers. Adapted from schemes originally published in *J. Poly. Sci.* **2023** 1-7. And *Sustainable Green Chemistry in Polymer Science and Technology*. ACS Books, **2023** Submitted.

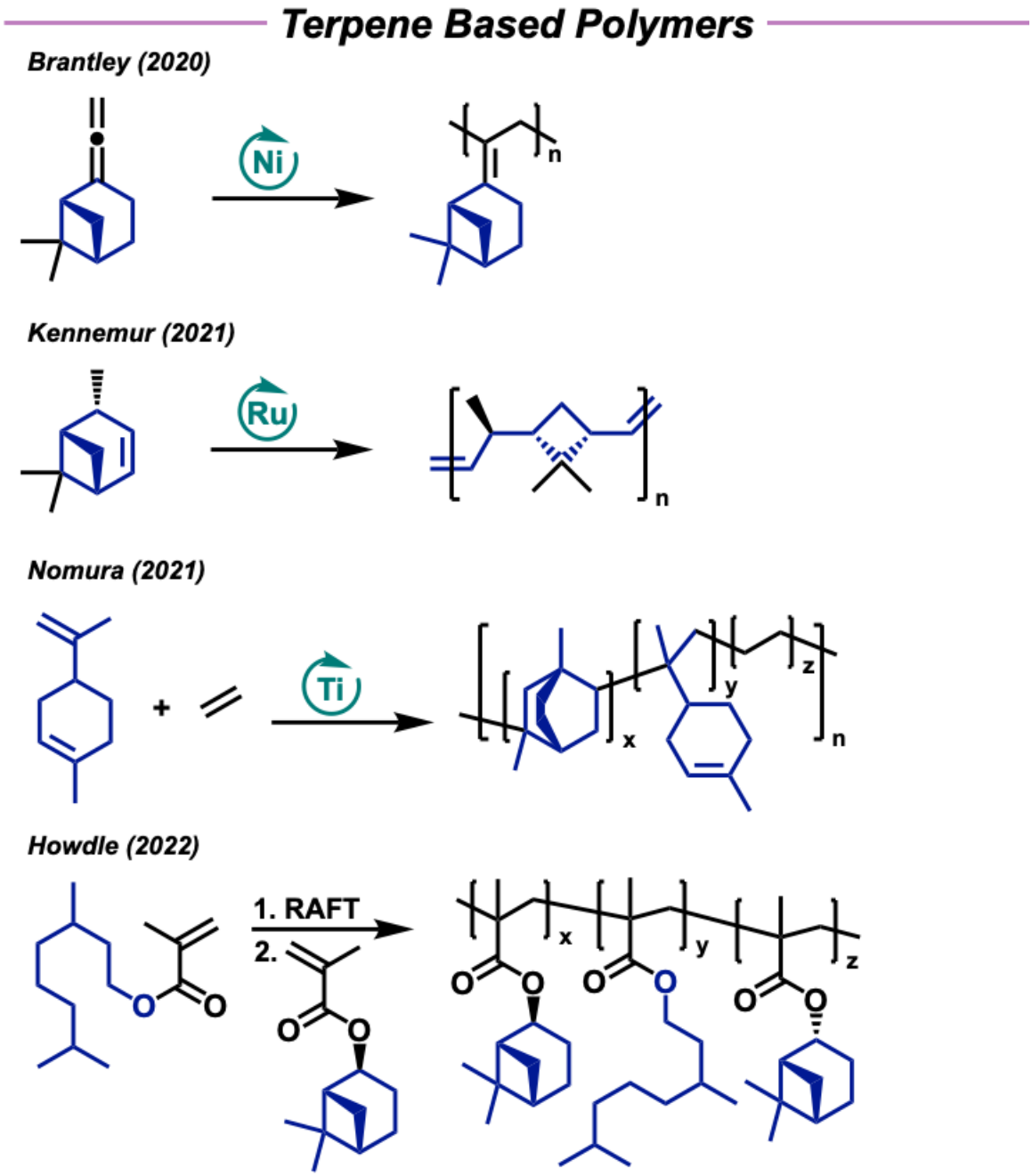

synthetically challenging to embed using traditional procedures, such as aromatic and polar co-monomers.

1.4 Conclusions and Outlook

Finding new methods to modify polymer architectures is critical for developing materials with enhanced chemical reactivity (for further elaborations) and understanding fundamental structure property relationships. As polymer editing strategies are commonly employed in upcycling efforts, expanding the chemical space of available editing methods is of urgent need. Similarly, the discovery of new monomer types and feedstocks can facilitate in-depth investigations into structure property relationships that are normally limited in terms of monomer scope.

The work in this dissertation outlines how we leveraged our synthetic expertise to expand the knowledge and understanding of developing new polymer editing and synthesis strategies by leveraging the chemistry of olefins. Herein, we detail how extant polyalkenamers scaffolds can be edited (functionalization, scission, or both) through the reactive olefin moiety. This was accomplished by embedding functional groups with enhanced reactivity (allenes) or through the generation of high energy species (e.g., radical cations via single-electron oxidation). Furthermore, COC congeners, comprised of alkyl and terpenoid units, were synthesized by extending cumulation of olefins to the allenes followed by vinyl-addition polymerization. The resulting materials were further investigated to elucidate how rigid carbocycles impact bulk material properties.

CHAPTER II: GENERAL ACCESS TO ALLENE-CONTAINING POLYMERS USING THE SKATTEBØL REARRANGEMENT

A version of this chapter was originally published by Nicholas J. Galan and Johnathan N. Brantley:

Galan, N. J., Brantley, J. N. *, General Access to Allene-Containing Polymers using the Skattebøl Rearrangement. *ACS Macro Lett.* **2020**, 1662-1666.

In this article, I was responsible for designing and synthesizing all polymers studied. I also performed all polymer characterization, reaction optimization, fluorescence studies, aggregation experiments. Dr. Johnathan Brantley organized this project and facilitated the writing of the manuscript.

2.1 Abstract

Post-synthetic modification is a powerful strategy for tuning soft materials. While methods for side-chain functionalization abound, modifications of backbone structural elements can be difficult to achieve. This challenge arises, in part, from a lack of intrinsically reactive motifs that can be installed in the main chain of a polymer. Incorporating established synthetic handles into polymer architectures is paramount for overcoming this limitation. Allenes are salient examples of moieties that could be leveraged in a wide range of post-synthetic modifications; however, the synthesis of a polyallene has proven elusive. Using the metathesis polymer of norbornene as a model architecture, we have established the Skattebøl rearrangement as a facile route to polyallenes. Polymers with varying allene content (20–95%) were readily prepared in excellent yields (89–94%). These materials possess unique optical properties and can be engaged through further post-synthetic

modifications. As such, polyallenes could serve as valuable platforms for developing functional soft materials.

2.2 Introduction

As polymer upcycling[91,92] continues to advance the forefront of materials science, post-synthetic modification chemistry (which can facilitate upcycling efforts) has undergone a veritable renaissance.[6,7] The prospect of transforming a single material into myriad daughter polymers with precisely tailored properties is enticing, but this requires the implementation of C–H/C–C activations or the pre-installation of synthetic handles.[16,17,93] The latter scenario is often more readily accomplished, and an array of functional groups have been leveraged in post-synthetic transformations. Salient examples include side-chain modifications via thiol-ene,[8,94] dipolar cycloaddition,[9] and even metal-mediated reactions (e.g. Sonogashira[10] or Suzuki couplings[95]). In contrast, backbone functionalization is typically limited to simple olefin manipulations[20,96,97] or modestly efficient C–H activations.[98] Expanding the scope of functional groups that can be incorporated into polymer main chains could potentially overcome these obstacles. Specifically, the installation of unique synthetic linchpins within polymers could dramatically enhance the efficacy of post-polymerization modifications.

One motif that holds great synthetic promise (but is largely absent in soft materials) is the allene (Scheme 2.1). Indeed, allenes have emerged as cornerstones of modern synthetic methodology. For example, Bertrand, Fürstner, and Toste have reported a variety of asymmetric Au(I)- catalyzed transformations involving allene derivatives, such as

Scheme 2.1: Selected Syntheses of Polymeric Allenes

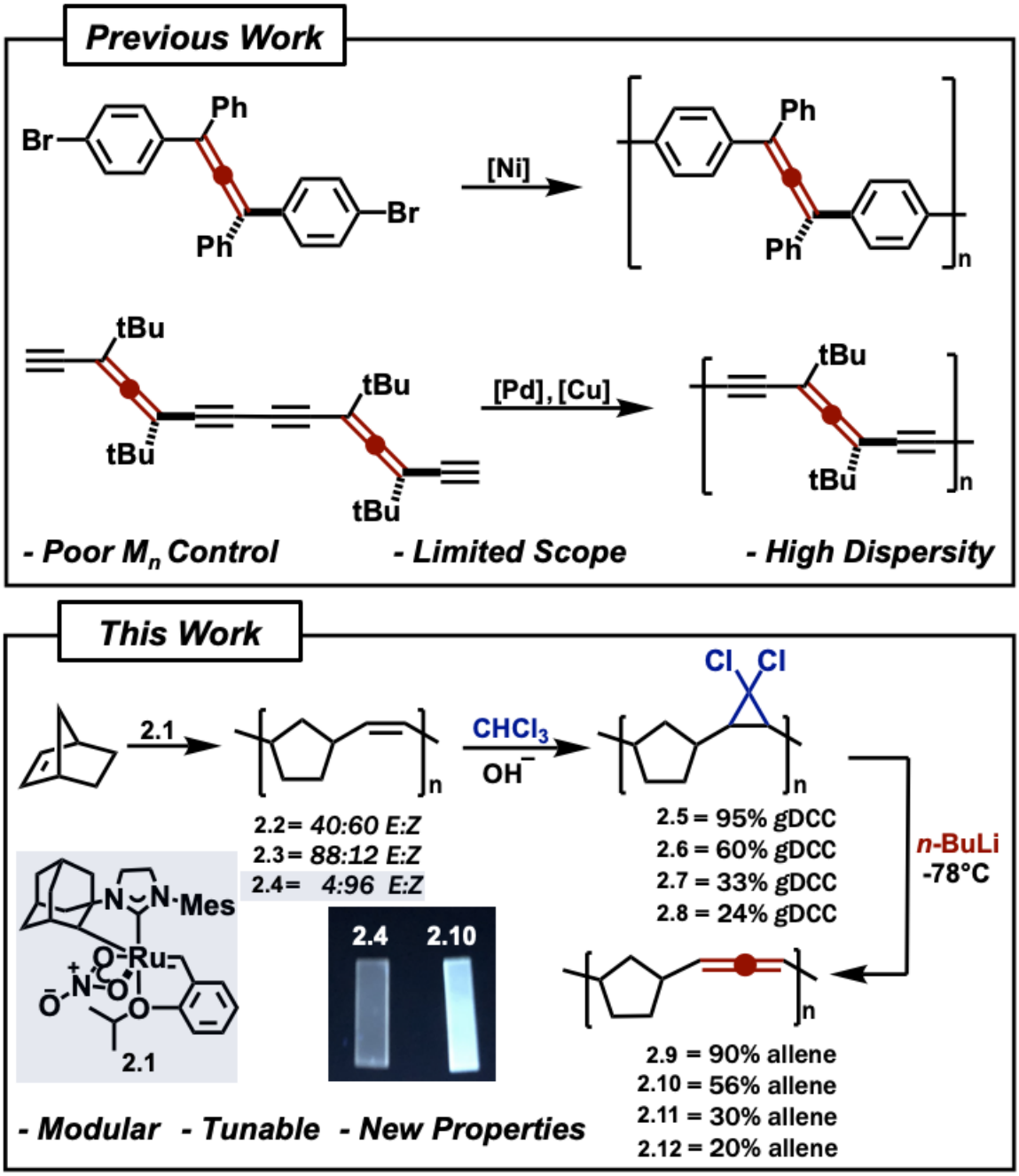

hydroaminations,[31,28] propargyl-Claisen rearrangements,[99] and fused-ring formations.[100] Fu and Garg have disclosed methods for synthesizing complex heteroatom ring systems via allene cycloadditions.[32–34] Trost and others have also reported myriad Pd-catalyzed transformations that can rapidly diversify allenes.[101–103] The application of this rich chemistry to polymer modifications is enticing, and the preparation of allene-containing polymers could dramatically expand the chemical space available for post-synthetic modifications of soft materials.

A potential impediment toward this synthetic goal, however, is the propensity of allenes to polymerize under a variety of conditions.[36] Indeed, Endo and others have demonstrated radical,[37] cationic,[39] vinyl-addition,[104,44] and coordination-insertion[42] polymerizations of allene-containing monomers. As such, the pre-installation of allenes within monomers could be impractical for incorporating cumulated bonds into a variety of materials. Incompatibilities notwithstanding, there have been some advancements toward accessing macromolecules comprised of allene functionalities.[105] Kijima demonstrated the synthesis of conjugated allene-containing oligomers that exhibited tunable fluorescent properties (Scheme 2.1).[48–50,106] Similarly, Diederich has disclosed the syntheses of macrocycles and allene-yne oligomers that exhibit unique chiroptical properties (Scheme 2.1).[51,52] Furthermore, Hasegawa reported the synthesis and chiroptical properties allene-containing tetrathiafulvalene materials.[53] Despite these promising precedents, we are unaware of any reports that detail a modular, broadly applicable approach to accessing polyallenes.

Given the intrinsic reactivity of allenes toward polymerization, we envisioned that a more reliable approach would involve post-polymerization installation of the cumulated bonds. Although there are several classical methods for accessing allenes (e.g. Claisen rearrangement,[107] the Myers allene synthesis,[108] etc.), the Doering-LaFlamme-Skattebøl rearrangement[109,110] immediately attracted our attention. The incorporation of *gem*-dichlorocyclopropanes (*g*DCCs) into polymer matrices is well established,[25,23] and we hypothesized that we could engage *g*DCC-containing materials through Skattebøl chemistry to access allenes (Scheme 2.1; Figure 2.1).

2.3 Results and Discussion

2.3.1 Synthetic Optimization and Characterization of Allene-Containing Polymers

We selected norbornene as our model scaffold, given the ease with which ring-opening metathesis polymerization (ROMP) can afford polynorbornene in a stereocontrolled manner. Our initial efforts employed the Hoveyda-Grubbs second generation catalyst to prepare a polynorbornene, **2.2**, that exhibited a modest number average molecular weight (M_n = 95 kDa; 1.99 Đ) and an olefin *E*:*Z* ratio of 40:60 (determined by ^{1}H NMR spectroscopy; Scheme 2.1; Table 2.1). Subsequent cyclopropanation with dichlorocarbene afforded **2.2.1** (83% cyclopropanation by ^{1}H NMR spectroscopy). Upon closer inspection of the ^{1}H NMR spectrum, however, we noted minor resonances in **2.2.1** that were not consistent with cyclopropanation (~17%).[23] Treatment of **2.2.1** with 0.9 equivalents of *n*-butyllithium (BuLi; -78 °C for 45 min) and subsequent quenching with MeOH afforded a precipitate, **2.2.2**, that proved difficult to dissolve in common solvents (e.g. THF, DCM, PhH, PhMe, DMSO, DMF). We were able to dissolve small portions in d-chloroform

Table 2.1: Initial Synthetic Optimization

Entry	Catalyst	E:Z[b]	*g*DCC (%)[b]	n-BuLi (eq.)	Time (h)	Allene (%)[b,c]	Yield (%)
1	Hoveyda-Grubbs II	40:60	83	0.9	0.75	15	-
2[d]	Grubbs I	88:12	-	1	1	-	-
3	1[a]	4:96	95	1	1	19	-
4	1[a]	4:96	94	5	1	47	-
5[e]	1[a]	4:96	95	5	5	95	90
6[e]	1[a]	4:96	95	2.5	3	85	87

[a]See Scheme 2.1. [b]Determined via ^{1}H NMR spectroscopy. [c]Based on residual 2.2 in ^{1}H NMR spectra. [d]Intractable material isolated. [e]Stored in solution (THF) at 5 °C.

($CDCl_3$), and we observed new resonances in the ^1H and ^{13}C NMR spectra that were consistent with allene formation (*c.f.* 5.21 and 201 ppm, respectively: Figures 2.46– 2.47). Although these data were encouraging, the alkyl region of the ^1H NMR spectrum exhibited considerable complexity. This, combined with (*i*) the poor solubility of **2.2.2** and (*ii*) the presence of unidentified byproducts in **2.2.1**, suggested to us that *E*-olefins might have poor compatibility with our reaction sequence. To probe this possibility, we synthesized a predominantly *E*-polynorbornene, **2.3**, using the Grubbs first-generation catalyst (M_n = 23 kDa, 2.17 Đ; *E:Z* = 88:12). Subjecting **2.3** to our cyclopropanation conditions afforded **2.3.1**; however, we found that NMR spectral data for this material were not consistent with *g*DCC formation. Instead, we observed a mixture of products that resembled the minor components of **2.2.1** (Figures 2.4-2.5). Although we were unable to confidently identify the structure of **2.3.1**, we noted that treatment of this material with BuLi did not afford allene moieites (as determined by ^1H NMR spectroscopy; Figure 2.6).

Having demonstrated the deleterious reactivity of polymers containing *E*-olefins, we sought to avoid this issue by employing a *Z*-selective[111] metathesis catalyst (**2.1**) for ROMP of norbornene (Scheme 2.1). The isolated polymer, **2.4** (M_n = 127 kDa; 1.76 Đ; *E:Z* = 4:96), smoothly reacted with dichlorocarbene to afford **2.5** (95% cyclopropanation). Treatment of **2.5** with BuLi (5.0 equivalents) at -78 °C for 1 h (followed by quenching with MeOH) resulted in incomplete conversion to the target allene (47%). Extending the reaction time to 5 h, however, afforded near quantitative allene incorporation (95% based on residual *g*DCC) into the final polymer (**2.9**, Figure 2.1).

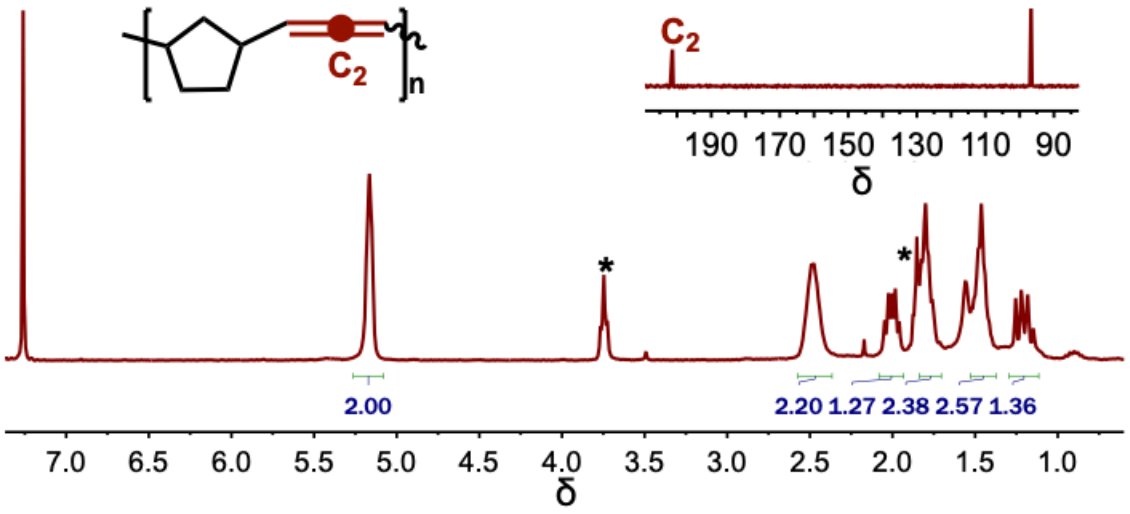

Figure 2.1: ^{1}H NMR spectrum of **2.9**. Inset shows partial ^{13}C NMR spectrum (allene resonances at 201 and 95 ppm are shown). * denotes residual THF.

Table 2.2: Selected Molecular Weight Data for **2.9**-**2.12**

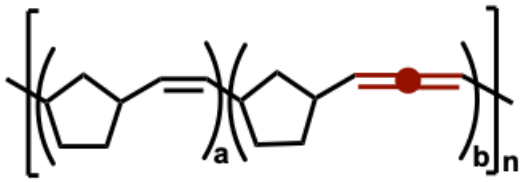

Polymer	a[a]	b[a]	Đ[b]	M_n (Da)[c]	Yield (%)
2.12	80	20	1.89	88,400	94
2.11	70	30	1.88	100,600	88
2.10	44	56	2.72	32,400	90
2.9	5	95	1.80	270,300	89

[a]Determined by ^{1}H NMR spectroscopy. [b]Calculated using M_w/M_n. [c]Measured by GPC (rounded values shown).

Controlling the extent of cyclopropanation allowed us to synthesize materials exhibiting varied allene composition (i.e. **2.10**, **2.11**, and **2.12**; Scheme 2.1; Table 2.2). We found that materials with < 35% allene incorporation could be isolated, dried, and dissolved in a variety of solvents. In contrast, > 50% cumulation required immediate dissolution of the freshly precipitated material. We found that freshly prepared polymers containing > 50% allene content could be indefinitely stored as dilute solutions in THF at 5 °C (under N_2).[112]

2.3.2 Thermal, Photophysical, and Aggregation Studies

Thermogravimetric analyses of **2.9–2.12** revealed major decomposition onset temperatures near 400 °C (similar to the T_d of polynorbornene; Figures 2.26–2.30). Given that allenes can undergo thermal [2+2] cycloadditions,[113,114] however, we also monitored thermal stability via ^{1}H NMR spectroscopy (Figure 2.7). Gelation was observed upon heating **2.11** to 140 °C, and new alkyl resonances were observed in the ^{1}H NMR spectrum of the soluble fraction. Taken together, we interpreted these data as evidence of thermal cross-linking. Unfortunately, this deleterious reactivity precluded the measurement of T_g by differential scanning calorimetry.

Closer inspection of the gel-permeation chromatography (GPC) data for **2.9–2.12** revealed a significant increase in Đ as overall allene content increased (*c.f.* Đ = 1.7 for **2.9** versus Đ = 2.7 for **2.10**).[115] This, combined with the reduced solubility of **2.9** and **2.10**, suggested to us that aggregation could be occurring. Consistent with this hypothesis, dynamic light scattering (DLS) measurements revealed larger average particle sizes in THF solutions of **2.11** (relative to **2.4** and **2.7**; Figure 2.9). To our surprise, irradiating **2.9–2.12**

with a 366 nm lamp resulted in visible fluorescence (both in the solid state and in solution; Scheme 2.1). Subsequent fluorimetry experiments revealed broad emissions (λ_{EM} = 360–660 nm) for $CHCl_3$ solutions of **2.9–2.12** excited at wavelengths near 350 nm (Figure 2.2A; see experimental).

These data (along with apparent solvatochromic effects upon changing solvent polarity; see experimental) suggested to us that exciplex formation could account for the photophysical properties of our **2.9**-**2.12** materials. Electron deficient arenes (e.g. nitrobenzene) are known to quench exciplex fluorescence,[116–118] and we surmised that similar fluorescence quenching should be observed with our **2.9**-**2.12** materials. Gratifyingly, treatment of **2.10** with nitrobenzene (2 equivalents) resulted in complete quenching of fluorescence (Figures 2.2B and 2.12). We are currently investigating the photophysical properties of these materials (and their potential applications as fluorescent sensors) in greater detail.

2.3.3 Investigating Chemical Reactivity of Allene-Containing Polymers

Finally, we sought to leverage intrinsic allene reactivity to modify our **2.9**-**2.12** materials. We hypothesized that these polymers could potentially participate in photochemical [2+2] reactions[119] to create networks. To test this, **2.11** was dissolved in d_8-THF and irradiated with 245 nm light under an N_2 atmosphere (T < 40 °C; Figure 2.2). As expected, the sample underwent complete gelation within 40 h.[120] We also explored Au-catalyzed multicomponent couplings with our allene-containing materials.[121] In a preliminary experiment, **2.9** was reacted with TMS-azide and trifluoroacetic acid under the

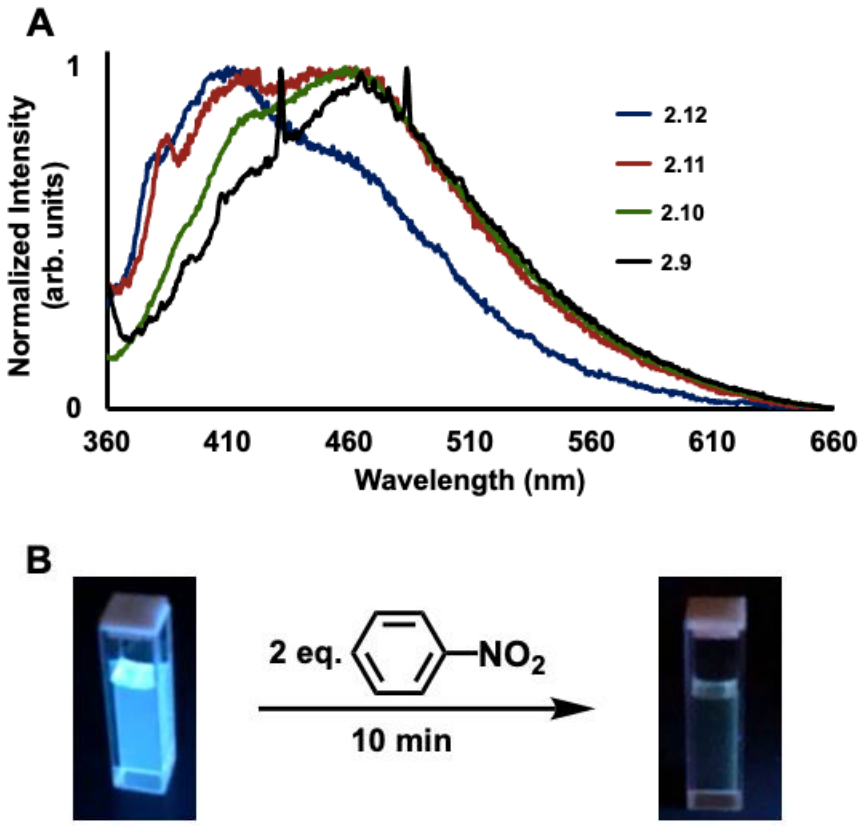

Figure 2.2: A) Normalized emission spectra of 2.9-2.12 in $CHCl_3$. B) 2.10 $CHCl_3$ solution irradiated with 360 nm light before (left) and after (right) addition of nitrobenzene.

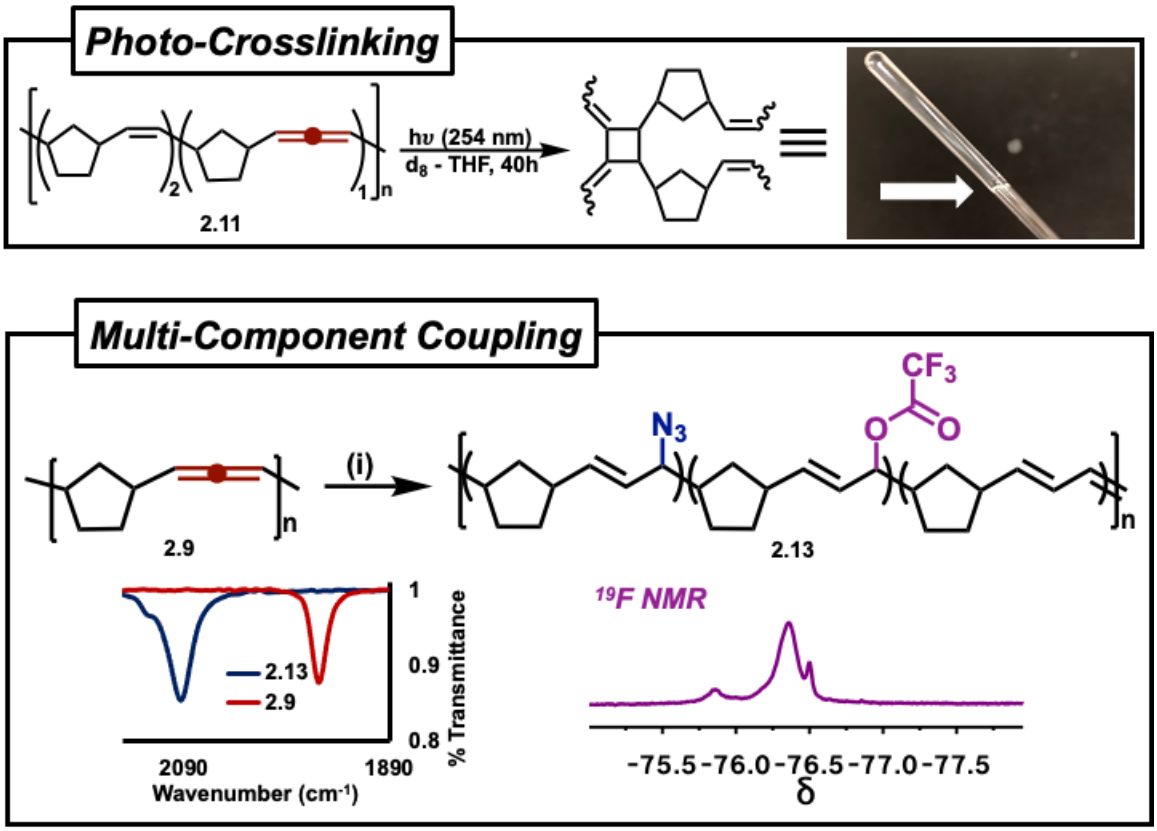

Figure 2.3: (Top) Photochemical crosslinking of **2.11**. Inset shows inverted NMR tube with gelation highlighted. (Bottom) Multi-component of **2.9**. Conditions (i): PPh_3AuCl (20 mol%); AgOTf (20 mol%); $TMSN_3$ (0.3 equiv.); TFA (0.3 equiv.); DCM (3 mL); 30 °C; 5 h. IR spectroscopy revealed consumption of allene (1959 cm^{-1}) and azide incorporation (2092 cm^{-1}) in **2.13**. ^{19}F NMR spectroscopy revealed a broad resonance (δ = -76.35) consistent with trifluoroacetate incorporation in **2.13**.

action of a Au(I) catalyst at 30 °C (experimental). Analysis of the resultant material, **2.13**, by IR spectroscopy revealed complete consumption of the allene motifs and concomitant growth of a new azide stretch (Figure 2.3, Figure 2.60). Additionally, ^{19}F NMR spectroscopic analysis of **2.13** revealed a broad resonance (δ = -76.35) that we attributed to incorporation of trifluoroacetates within the polymer backbone (Figure 2.3, Figure 2.55).[122] A control experiment in the absence of the Au(I) catalyst and AgOTf did not yield any functionalization of the allene moieties in **2.9** (Figures 2.56 and 2.59). Although preliminary, these data suggest that allene chemistry can be harnessed to rapidly diversify polymer structures (which could be of general benefit to post-synthetic modification studies).

2.4 Conclusions

We have developed a modular approach toward reliably incorporating allenes into polymeric matrices. Our methodology consists of *gem*-dichlorocyclopropanation of olefin-containing polymers and subsequent treatment with BuLi to afford the desired polyallene. The resulting materials exhibited unexpected photophysical properties (e.g. fluorescence), and the allenes could be engaged through a variety of post-synthetic manipulations (e.g. [2+2] cycloadditions and Au-catalyzed multicomponent couplings). Although our synthetic approach is expected to be quite general, there are some limitations that need to be addressed. For example, we are currently investigating methods to improve the solubility of materials with > 35 % allene content. Moreover, as the cyclopropanation step of the Skattebøl sequence is entirely stochastic, our current strategy could have limited applicability to the synthesis of allene-containing block copolymers. These limitations

notwithstanding, our results suggest that installing allenes within soft materials could open underexplored chemical space for polymer design and modification. As such, we expect that our work will serve as a general platform for developing new types of tunable or stimulus-responsive materials.

2.5 Acknowledgements

This study was supported in part by the Donors of the American Chemical Society Petroleum Research Fund.

2.6 Experimental

2.6.1 General Materials and Methods

Unless otherwise noted, solvents were dried on an MBraun solvent purification system with 3 Å molecular sieves and degassed with three freeze-pump-thaw cycles. All other reagents were obtained from commercial sources and used without further purification. Oxygen and water sensitive manipulations were performed in a nitrogen filled MBraun glovebox or using standard Schlenk techniques. ^{1}H and ^{13}C NMR spectroscopic data were collected on a Varian 300 MHz NMR, a Varian 500 MHz NMR, or a Varian 600 MHz NMR spectrometer. Chemical shifts (δ) are reported in ppm using the residual solvent as reference. IR spectra were collected on a Bruker Alpha II FT-IR spectrometer with an ATR attachment (diamond crystal) for solid samples and a Transmission iD1 attachment with flow cell for liquid samples. UV-visible absorbance spectra were recorded using an Agilent Cary 100 series UV-Vis spectrophotometer and quartz cuvettes. Fluorescence emission

spectra were recorded using an Agilent Cary Eclipse Fluorescence Spectrophotometer. Dynamic light scattering studies were performed using a Malvern Zetasizer Nano ZS instrument equipped with a He-Ne 633 nm laser and a temperature controller at a scattering angle at 173°. Thermogravimetric analysis (TGA) was performed on a TA Instruments TGA Q500. Gel Permeation Chromatography (GPC) data were collected on an Omnisec Resolve and Omnisec Reveal Sytem using triple detection with detectors in series: UV, light scattering, viscometer, and refractive index and three Viscotek styrene divinylbenzene copolymer columns (in series T3000, T4000, and T5000) at a flow rate of 1 mL/min and thermostatted to 30 °C using either tetrahydrofuran (THF) or chloroform ($CHCl_3$) as the eluent. Molecular weight and dispersity data from triple detection are reported.

2.6.2 Representative 2.2 Synthesis

A flame dried 100 mL round bottom flask was charged with norbornene (500 mg; 5.31 mmol), THF (20 mL), and a Teflon stir bar. A solution of Hoveyda-Grubbs II (11.7 mg; 0.0187 mmol) in THF (0.5 mL) was added via syringe, and the reaction was stirred for 40 min at 23 ºC. The polymerization was quenched with ethyl vinyl ether (1 mL; 10.52 mmol) and diluted with THF (25 mL). Polymeric material was precipitated from MeOH, collected on a medium porosity fritted funnel, and dried for 16 h *in vacuo*. Spectral data were consistent with literature reports,[111] and a representative ^{1}H NMR spectrum is shown in Figure 2.36. Olefin *E:Z* ratios were determined based on the relative integrations of the *Z* ($\delta = 5.22$) and *E* ($\delta = 5.35$) olefin resonances. Representative GPC data is shown in Figure 2.13.

Scheme 2.2: Synthesis of **2.2**

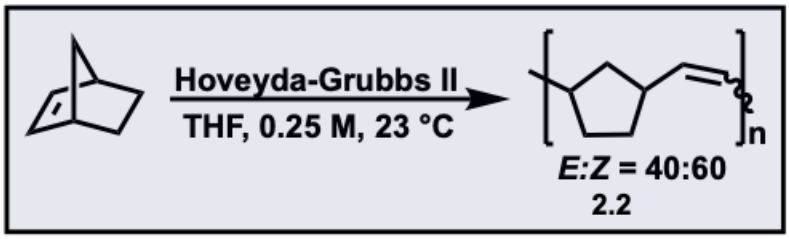

2.6.3 Representative 2.3 Synthesis

A flame dried 50 mL Schlenk flask was charged with norbornene (600 mg; 6.37 mmol), THF (25 mL), and a Teflon stir bar. A solution of Grubbs I (19.9 mg; 0.0242 mmol; in 0.7 mL THF) was prepared in an N_2 filled glovebox and added via syringe. The reaction was stirred for 15 min at 23 ºC, after which the polymerization was quenched with ethyl vinyl ether (1 mL; 10.52 mmol). Polymeric material was precipitated from MeOH, collected on a medium porosity fritted funnel, and dried *in vacuo*. The polymer was dissolved in minimal THF and precipitated from MeOH a second time, collected via filtration, and dried for 16 h *in vacuo*. Spectral data were consistent with literature reports,[23] and a representative ^{1}H NMR spectrum is shown in Figure 2.37. Olefin *E:Z* ratios were determined based on the relative integrations of the *Z* (δ = 5.22) and *E* (δ = 5.35) olefin resonances. Representative GPC data is shown in Figure 2.14.

2.6.4 Representative 2.4 Synthesis

A flame dried 50 mL Schlenk flask was charged with norbornene (300 mg; 3.186 mmol), THF (12 mL), and a Teflon stir bar. The monomer solution was degassed via three cycles of freeze-pump-thaw and cooled to -30 °C. A solution of **2.1** (Scheme 2.1; 15 mg; 0.024 mmol in 0.5 mL THF) was prepared in an N_2 fill glovebox and added via syringe. The reaction temperature was maintained between -40 °C and -20 °C for 4 h, after which the polymerization was quenched with ethyl vinyl ether (2 mL; 21.04 mmol) in THF (18 mL). Polymeric material was precipitated from MeOH, collected on a medium porosity fritted funnel, and dried *in vacuo*. The polymer was dissolved in minimal THF, precipitated from

Scheme 2.3: Synthesis of **2.3**

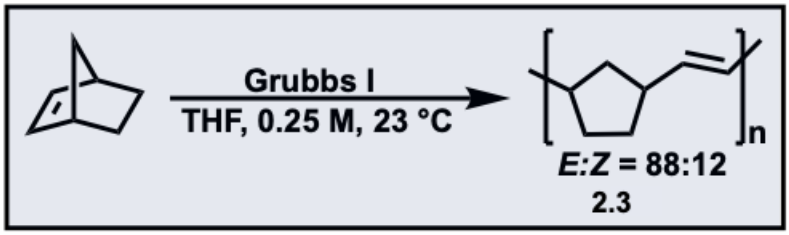

Scheme 2.4: Synthesis of **2.4**

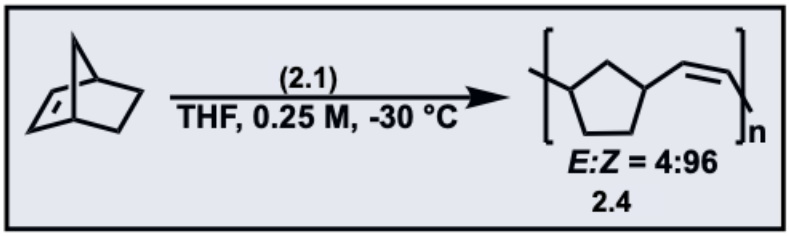

MeOH a second time, collected via filtration, and dried for 16 h *in vacuo*. Spectral data were consistent with literature reports,[111] and a representative ^{1}H NMR spectrum is shown in Figure 2.38. Olefin *E:Z* ratios were determined based on the relative integrations of the *Z* ($\delta = 5.22$) and *E* ($\delta = 5.35$) olefin resonances. Representative GPC data is shown in Figure 2.15.

2.6.5 Representative Synthesis of 2.2.1, 2.3.1, and 2.5-2.8

Following a modified procedure reported by Craig,[23,22] a 250 mL round bottom flask was charged with **2.4** (400 mg; 4.25 mmol) and a Teflon stir bar. $CHCl_3$ ([**2.4**] = 0.09 M), and cetyltrimethylammonium bromide (CTMA Br; 465 mg; 1.28 mmol) were added to the flask, and the mixture was sparged with N_2 for 30 min. In a separate vessel, a NaOH solution (8.49 g; 212.50 mmol; 33% w/w in water) was sparged with N_2 for 30 min. This NaOH solution was then added dropwise to the mixture containing **2.4** over the course of 5 min. The resulting mixture was stirred for 2 days at 23 °C. Aliquots were periodically removed, concentrated to dryness, and dissolved in $CDCl_3$ to monitor conversion by ^{1}H NMR spectroscopy. The extent of cyclopropanation was determined via ^{1}H NMR spectroscopy as follows:

$$\% \text{ Functionalization} = I_{al} - 4(I_{vin})/[I_{al} + I_{vin}]$$

Where: I_{vin} = integration from $\delta = 5.5\text{-}5.0$, and I_{al} = integration from $\delta = 3.0 - 0.8$. When necessary, residual solvent peaks were excluded from the integration ranges. There is a reported ± 5% uncertainty in the percent functionalization determined by this procedure.[23]

Upon reaching the desired degree of functionalization (95% in the case of **2.5**), the reaction was quenched with 2M HCl (50 mL) and added to a separatory funnel containing brine (5.0 mL) and $CHCl_3$ (5.0 mL). The organic layer was separated, washed with brine (2 x 40 mL), and reduced to a minimal volume under vacuum. The polymer product was precipitated from MeOH, collected on a medium porosity fritted funnel, and dried *in vacuo*. The material was dissolved in minimal $CHCl_3$, precipitated from MeOH a second time, collected via filtration, and dried for 16 h *in vacuo*. Spectral data were consistent with literature reports of similar materials,[23] and a representative ^{1}H NMR spectrum is shown in Figure 2.41. Representative GPC data are shown in Figures 2.16 – 2.21. The remaining **2.5 – 2.8** materials were synthesized using the procedure outlined above, with the following exceptions: NaOH (10 eq.) and CTMA Br (10 mol%) were used, and shorter reactions times (6 h – 1.5 days) were required (depending on desired *g*DCC content). The one noted exception for reaction time involved predominantly *E* olefin-containing materials, which required a reaction time of 3 days to reach the desired extent of functionalization.

2.6.6 Representative Synthesis of 2.9

In a representative Skattebøl procedure, a flame dried 25 mL Schlenk flask was charged with **2.5** (100 mg; 0.565 mmol), THF (11.3 mL), and a Teflon stir bar. The solution was then cooled to -78 °C. *n*-Butyllithium (1.13 mL of a 2.5 M solution in hexanes; 2.82 mmol; 5 equiv. relative to *g*DCC content), was slowly added to the flask via gas-tight syringe at -78 °C. The light pink solution (pale yellow if < 90% *g*DCC) was left to stir for 5 h at -78 °C. The reaction was quenched with MeOH (0.3 mL; 7.42 mmol) and two 1 mL aliquots

Scheme 2.5: Representative Synthesis of **2.5**

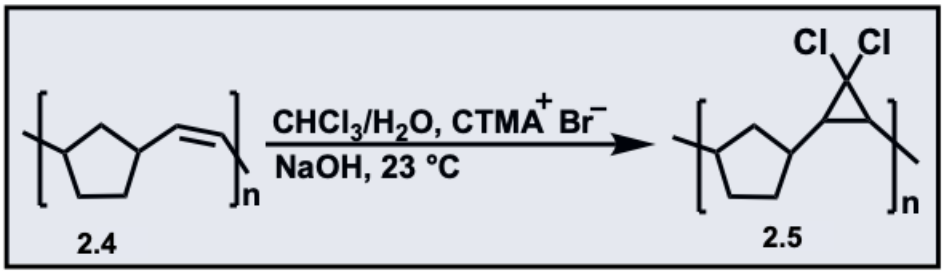

Scheme 2.6: Representative Synthesis of **2.9**

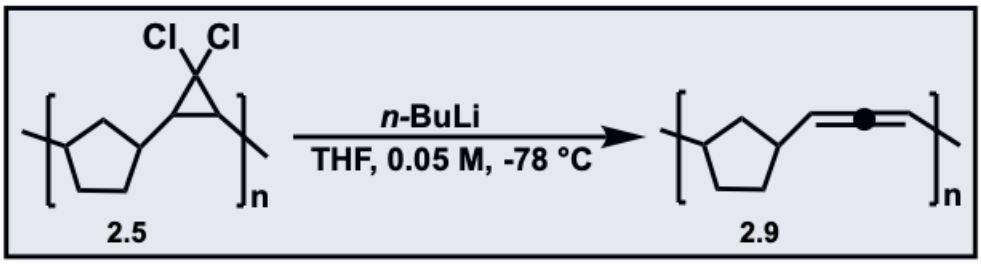

were removed, precipitated from MeOH, quickly dried *in vacuo* and used for ^{1}H NMR and GPC analyses. The bulk material was stored as a solution in THF at 5 °C for further use. **^{1}H NMR (500 MHz, $CDCl_3$):** δ = 5.26-5.09 (2H), δ 2.59-2.34 (2H), δ 2.08-1.92 (1H), δ 1.83-1.73 (2H), δ 1.52-1.38 (2H), δ 1.28-1.12 (1H). **^{13}C NMR (126 MHz, $CDCl_3$):** δ = 201.50, 96.83, 40.43, 39.56, 32.24. Representative ^{1}H and ^{13}C NMR spectra shown in Figures 2.48 – 2.50. Representative GPC data shown in Figure 2.22.

Partially functionalized materials (**2.10** – **2.12**) were synthesized according to this procedure using fewer equivalents of *n*-BuLi (2.5 equiv. relative to *g*DCC content) and shorter reaction times (2.5 h). Representative spectral data are shown in Figures 2.51 – 2.53. Representative GPC data are shown in Figures 2.23 – 2.25. Extent of allene formation (for **2.10** – **2.12**) was determined via integration of the residual **2.9** methine (δ = 2.8) relative to the methine of the allene-containing material (δ = 2.5).

To arrive at the optimized conditions outlined above, modifications to reaction time and equivalents of *n*-BuLi were explored. Using 1 equiv. *n*-BuLi (relative to *g*DCC content) for 1 h resulted in poor conversion to allene (Table 2.3, Entry 3). Increasing the equivalents of *n*-BuLi facilitated higher conversions (Table 2.3, Entry 4). Extending reaction times to 5 h yielded the greatest amount of allene formation (Table 2.3, Entry 5). Attempts using the **2.2.1** and **2.3.1** materials resulted in poor conversion (Table 2.3, Entry 1) and intractable materials (Table 2.3, Entry 2) which was attributed to deleterious reactivity of *E* olefins during cyclopropanation (see experimental sections ***2.5.7*** & ***2.5.8***).

The proposed structure of **2.9** was further supported using $^{1}H–^{13}C$ Heteronuclear Multiple Bond Correlation NMR spectroscopy (HMBC; Figure 2.50). The vinyl protons (δ = 5.16; 2H) correlated with all carbon signals, suggesting they are within three bonds of every carbon atom. Furthermore, only the resonances at δ = 5.16 ppm (2H) and δ = 2.5 ppm (2H) correlated to the *sp*-hybridized allene carbon (δ = 201 ppm). As only two sets of protons are within 3 bonds of the *sp*-hybridized allene carbon in our proposed structure (i.e. the vinyl and methine protons), this data further supports our structural assignment.

2.6.7 Comparison of 2.2.1, 2.3.1, and 2.5

^{1}H and ^{13}C NMR spectroscopic analyses of the materials isolated following cyclopropanation revealed distinct differences. Both **2.2.1** and **2.3.1** exhibited resonances from byproducts that were inconsistent with the targeted *g*DCC motifs (Figures 2.4 and 2.5)**.**

2.6.8 Titration of 2.3.1 with n-BuLi

A flame dried 50 mL Schlenk flask was charged with **2.3.1** (204 mg; 2.17 mmol; due to the inability to identify the exact repeating unit, the molar mass of **2.3** was used to determine amounts), a Teflon stir bar, THF (23 mL), and mesitylene (25 μL; 0.179 mmol; added as an internal standard). A 0.9 mL aliquot was removed for ^{1}H NMR spectral analysis, and the reaction vessel was cooled to -78 °C. *n*-BuLi (0.1 mL of a 0.87 M solution in Et_2O; 0.05 equiv.) was added via syringe, and the reaction mixture was stirred for 30

Table 2.3: Initial Skattebøl optimization

Entry	Polymer	E:Z	*g*DCC (%)	n-BuLi (eq.)	Time (h)	% Allene
1	**2.2.1**	40:60	83	0.9	0.75	15
2	**2.3.1**	88:12	-	1	1	-
3	**2.5**	4:96	95	1	1	19
4	**2.5**	4:96	94	5	1	47
5	**2.5**	4:96	95	5	5	95
6	**2.5**	4:96	95	2.5	3	85

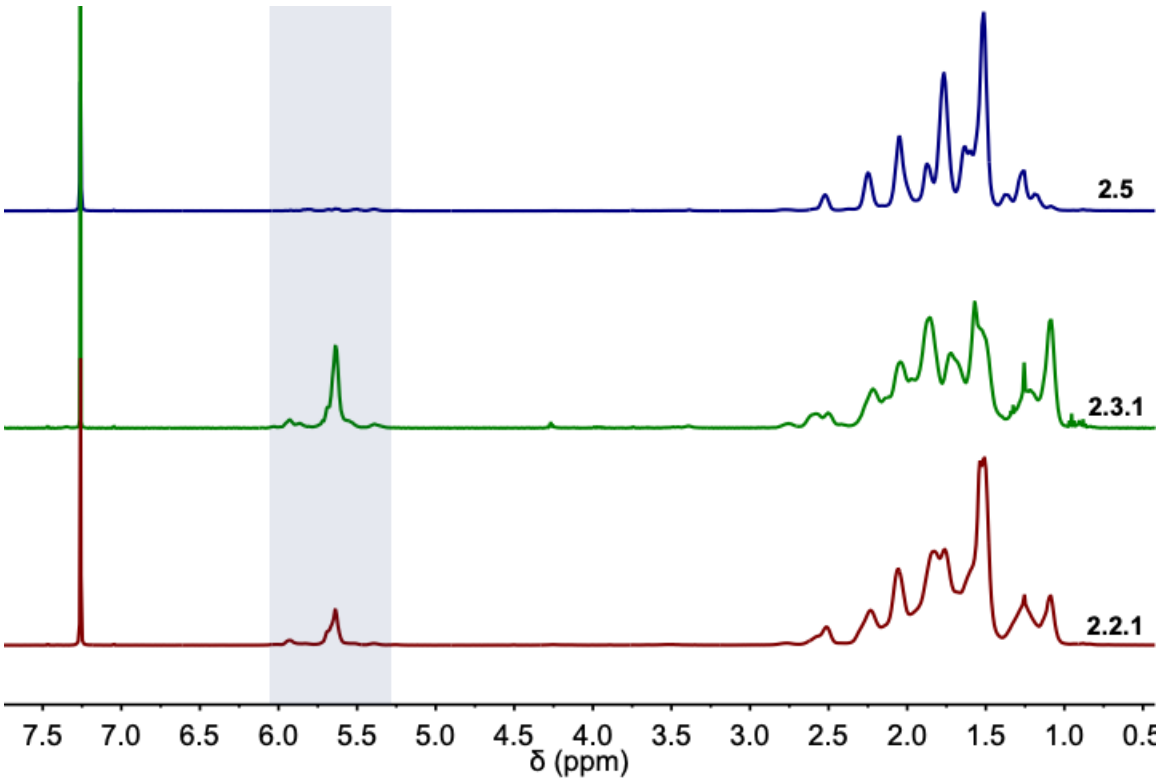

Figure 2.4: ^{1}H NMR spectra of **2.2.1**, **2.3.1**, and **2.5**. Distinct byproduct resonances highlighted by blue box.

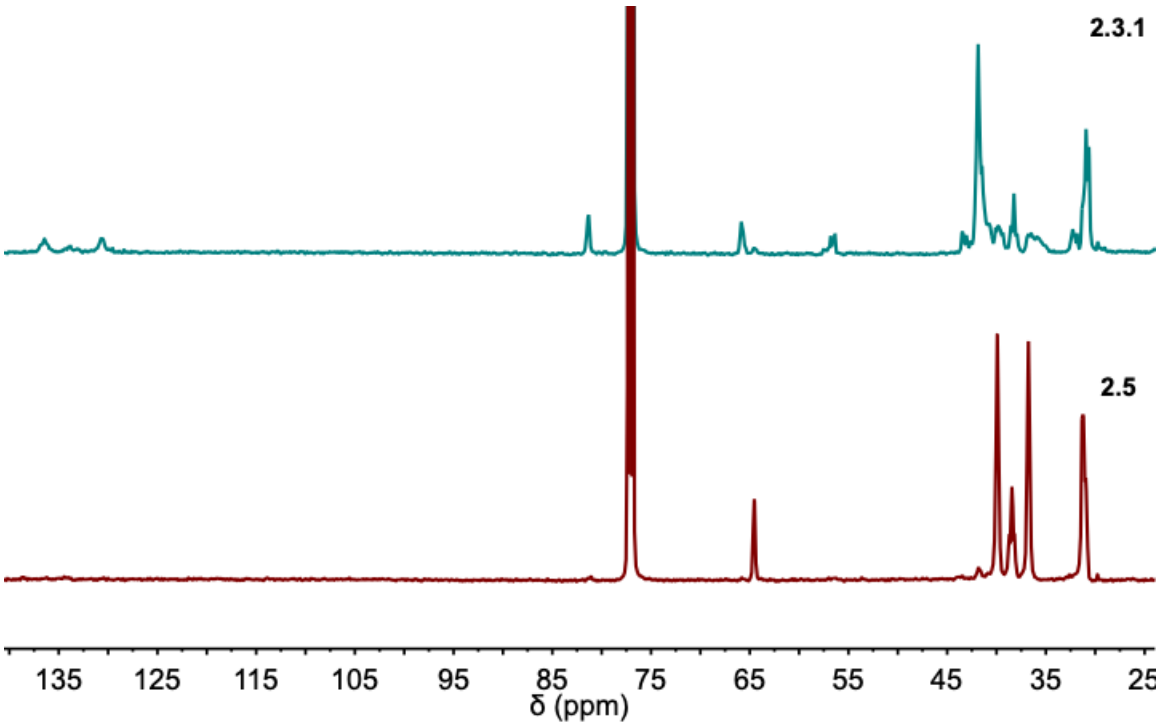

Figure 2.5: ^{13}C NMR spectra of **2.3.1** and **2.5**.

min at -78 °C. Another aliquot (0.9 mL) was removed for ^{1}H NMR spectral analysis, and another portion of *n*-BuLi (0.12 mL, 0.05 equiv. relative to remaining material) was added to the reaction mixture. This protocol was repeated until a total of 0.2 equiv. of *n*-BuLi were added. Each aliquot was concentrated under reduced pressure and dissolved in $CDCl_3$; however, aliquots after addition of 0.1–0.2 equiv. *n*-BuLi exhibited poor solubility. These aliquots were heated at 50 °C for 48 h to achieve solvation. All aliquots were then characterized by ^{1}H NMR spectroscopy (Figure 2.6, A). The downfield byproduct resonances were consumed without concomitant growth of allene (Figure 2.6, A). A final portion of *n*-BuLi was added (0.44 mL; 0.25 – 0.5 equiv. relative to material) which afforded a polymer with poor solubility. Subsequent IR spectroscopy (Figure 2.6, B) confirmed no allene formation.

2.6.9 Thermal Crosslinking Experiment

A 1 mL vial was charged with **2.11** (4.7 mg), a Teflon stir bar, and C_6D_6 (0.7 mL). The polymer solution was transferred to a J-young NMR tube and degassed via three cycles of freeze-pump-thaw. The solution was heated at 140 °C for 36 h in the absence of light. Visible gelation within the J-Young tube (Figure 2.7, inset) suggested network formation via thermal crosslinking. The soluble portion was precipitated from MeOH, mother liquor decanted, dried *in vacuo*, and dissolved in $CDCl_3$. ^{1}H NMR spectroscopic analysis revealed broadening of the alkyl region and traces of new vinyl resonances (Figure 2.7).

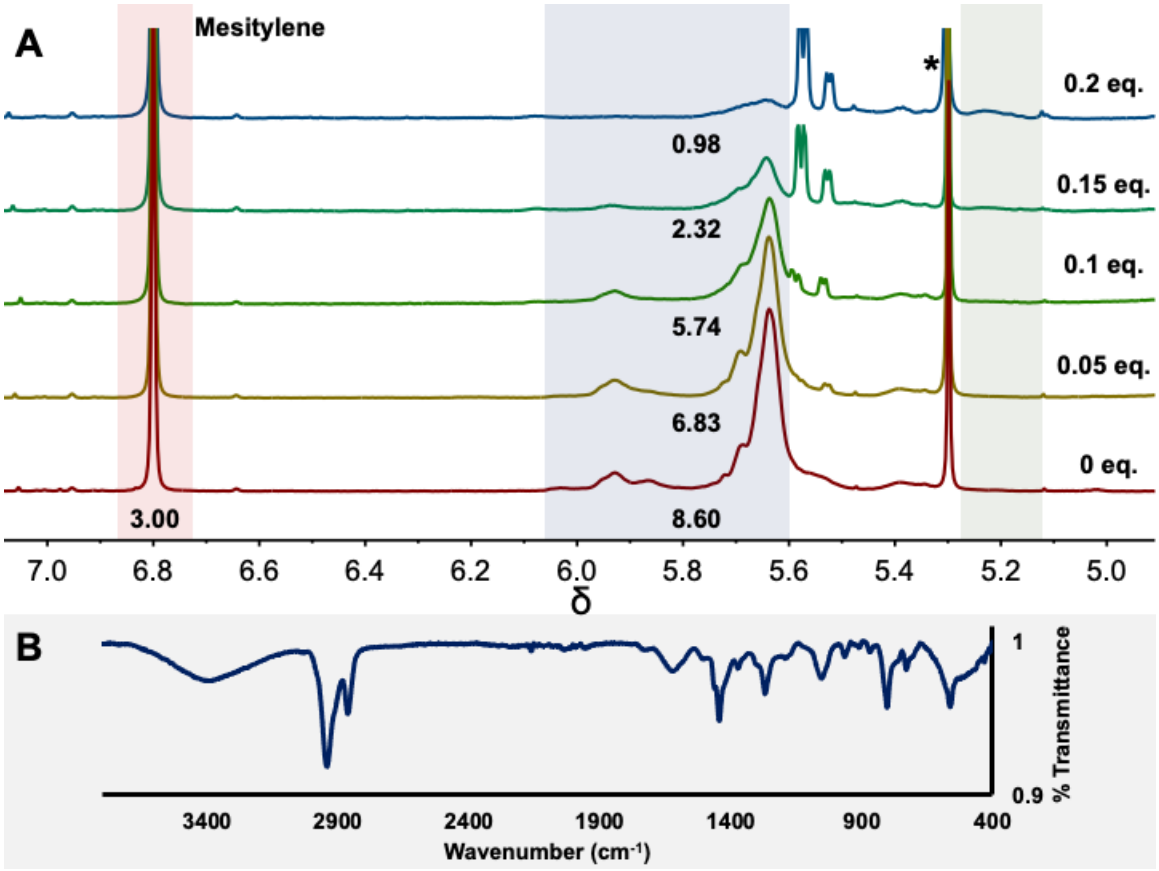

Figure 2.6: ^{1}H NMR spectra for n-BuLi titration of **2.3.1**. Mesitylene (red), byproduct (blue), and range for allene (green) resonances are highlighted. * denotes DCM (δ = 5.3 ppm). B) IR spectrum of precipitated material after addition of 0.5 equiv. of n-BuLi, the characteristic allene stretch at 1959 cm^{-1} (see Figure 2.58) was not observed.

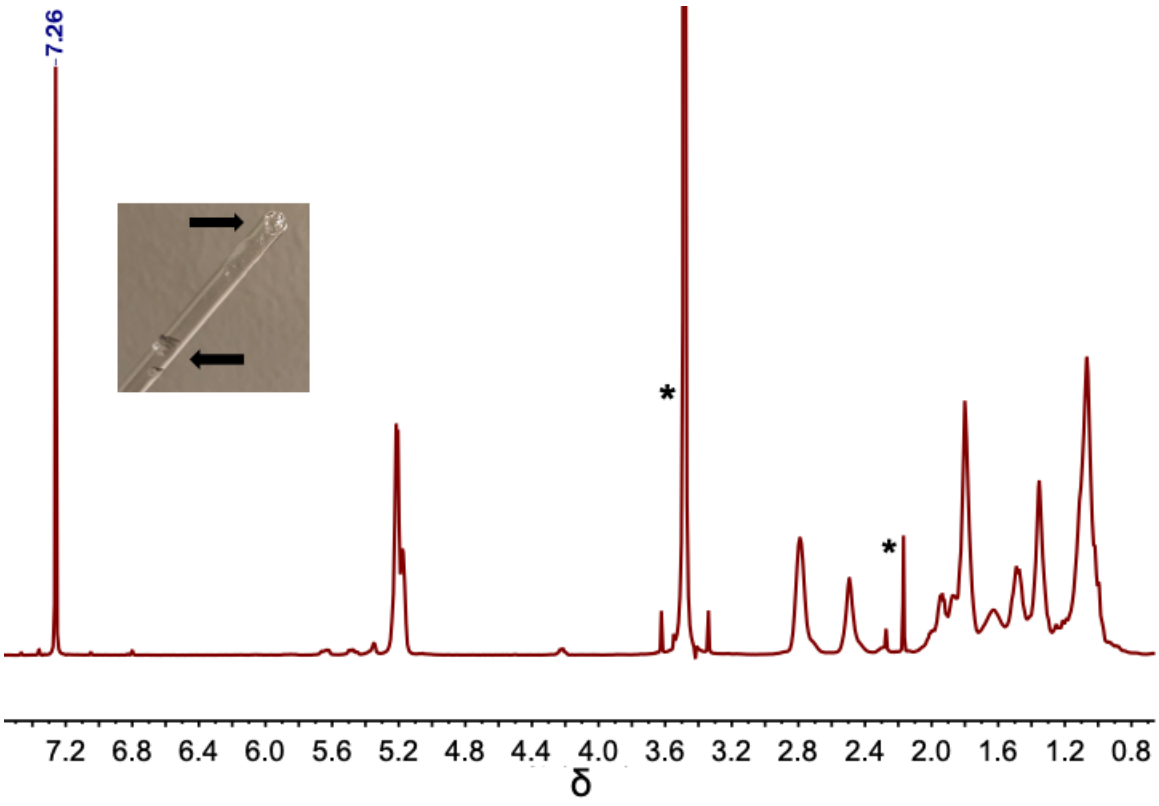

Figure 2.7: ^{1}H NMR spectrum ($CDCl_3$) of precipitated sample that was heated at 140 °C. Inset shows gelation within the J-young tube. * denotes residual solvent (MeOH: δ = 3.5; acetone: δ = 2.16).

2.6.10 O_2 Sensitivity (solution)

A 1 mL vial was charged with **2.9** (4.7 mg), $CDCl_3$ (0.8 mL), a Teflon stir bar, and mesitylene (1.50 μL; 0.0108 mmol; added as an internal standard). The polymer solution was transferred to a J-young NMR tube, degassed via three cycles of freeze-pump-thaw, and analyzed by ^{1}H NMR spectroscopy (red spectra, Figure 2.8). The NMR tube was placed under an O_2 atmosphere, and the sample was heated at 40 °C for 24 hours. ^{1}H NMR spectroscopy revealed a slight decrease in allene content (green spectra, Figure 2.8). The sample was then heated at 80 °C for 48 hours. ^{1}H NMR spectroscopy revealed significant consumption of the allene (blue spectra, Figure 2.8).

2.5.11 Representative UV-Vis and Fluorescence Experimental Setup

2.9 – 2.12 polymer samples were dissolved in HPLC-grade $CHCl_3$ or DCM (0.5 – 1 mg/mL) and filtered through 0.45 μm syringe filters into a quartz cuvette. UV-vis absorbance (Figures 2.31 – 2.35) and fluorescence (Figure 2.2) spectra were collected for each sample.

2.6.12 DLS Measurements

Polymer samples of **2.4**, **2.7**, and **2.11** (note: the **2.7** and **2.11** samples were synthesized from the **2.4** material analyzed here) were dissolved in HPLC-grade THF (0.25 mg/mL). The samples were transferred to a quartz cuvette and analyzed without prior filtration. **2.11** was found to have an average particle radius of 162.5 nm, which contrasted to both **2.7** (55.45 nm) and **2.4** (70.44 nm; Figure 2.9).

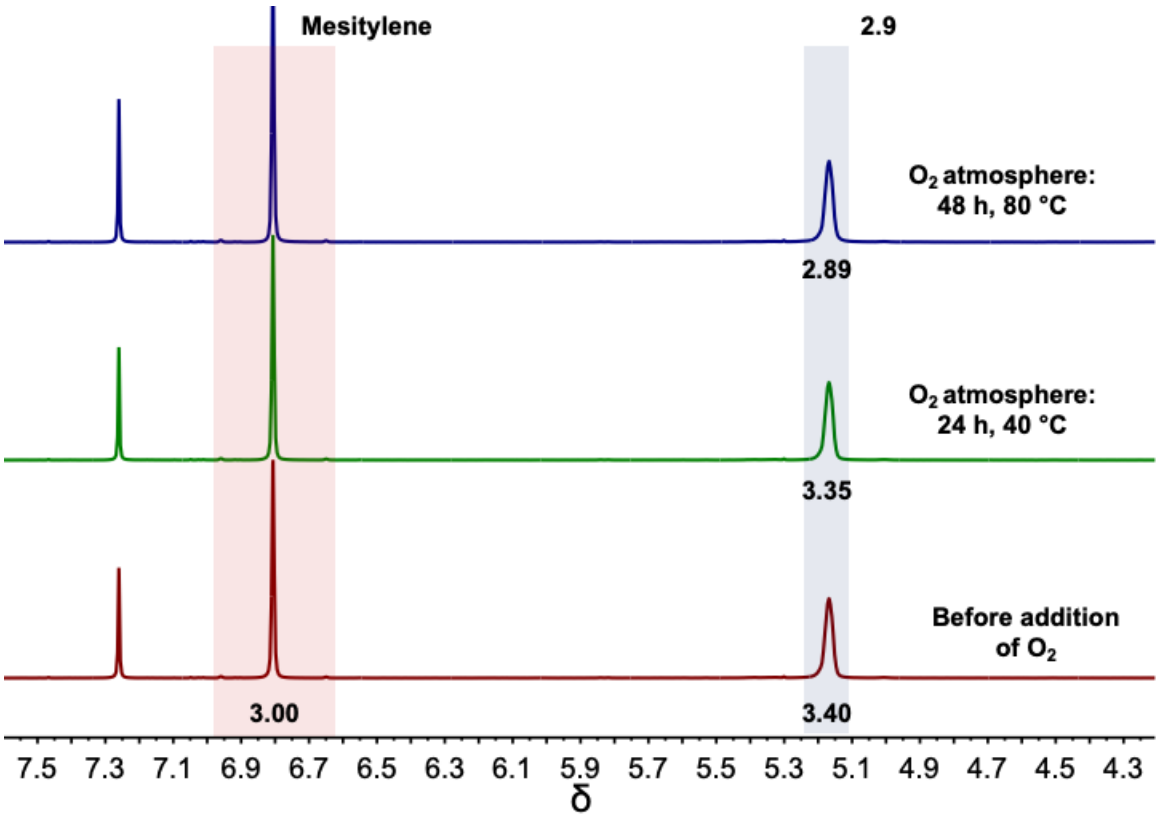

Figure 2.8: ^{1}H NMR spectra ($CDCl_3$) for O_2 sensitivity of **2.9** after heating under an O_2 atmosphere at 40 ºC (green) and 80 ºC (blue). Mesitylene (red box) and allene (blue box) resonances are highlighted.

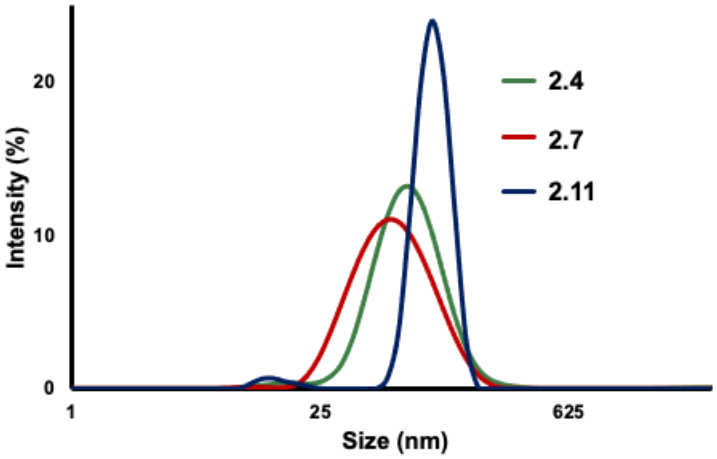

Figure 2.9: DLS plot showing the average particle size of **2.4**, **2.7**, and **2.11** in HPLC THF.

2.6.13 Sonication Experiment

2.10 (5.6 mg) was added to a 7 mL vial charged with a Teflon stir bar, followed by HPLC-grade THF (5 mL). The solution was stirred with mild heating for 24 h. Two portions of this solution (1 mL) were removed and filtered through 0.2μ syringe filters into separate 1 mL vials. One sample was immediately analyzed via GPC (Đ = 1.86; Figure 2.10). The other sample was sonicated for 45 minutes prior to GPC analysis, which revealed a narrower dispersity (Đ =1.49; Figure 2.10).

2.6.14 DLS Measurements: Solvent Effects

Samples of **2.9** (M_n = 178 kDa) were dissolved in HPLC-grade $CHCl_3$ or DCM (1.2 mg/mL in both cases) and filtered through 0.45 μm syringe filters into quartz cuvettes. DLS measurements revealed distinct aggregation populations in each solvent (c.f. average radius of 40.48 nm in $CHCl_3$ *versus* 34.70 nm in DCM; Figure 2.11). The fluorescence spectrum of **2.9** in $CHCl_3$ (Figure 2.2 in the main text) was also found to be distinct from the spectrum of **2.9** in DCM (Figure 2.11, inset). Note: fluorescence data are from unfiltered samples.

2.6.15 Fluorescence Quenching Experiment

A $CHCl_3$ solution of **2.10** (1 mg/ml; 0.040 mmol polymer) was analyzed by fluorescence spectroscopy (λ_{EX} = 350 nm; Figure 2.12, blue). The **2.10** solution was transferred to a 7 mL vial, and nitrobenzene (10 μL; 0.097 mmol) was added. After stirring at 23 ºC for 10 min, the solution was transferred to quartz cuvette and analyzed by fluorescence spectroscopy, which revealed complete quenching of fluorescence (Figure 2.12, red). Photographs of the samples (irradiated with a 350 nm lamp) are shown in Figure 2.2.

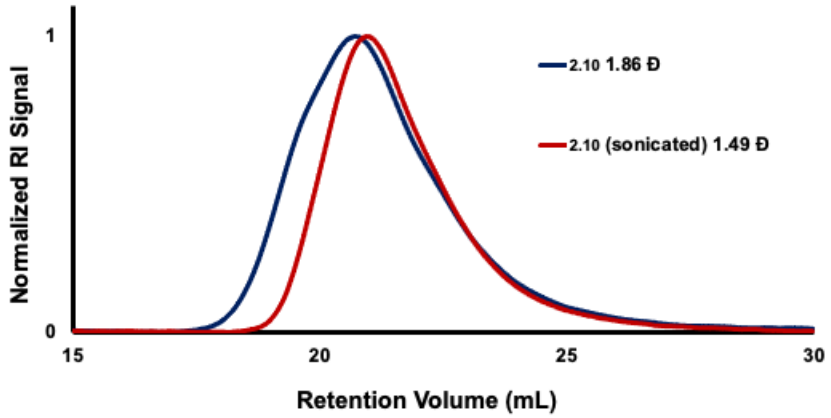

Figure 2.10: GPC traces of **2.10** samples that were not sonicated (blue) or sonicated for 45 min (red).

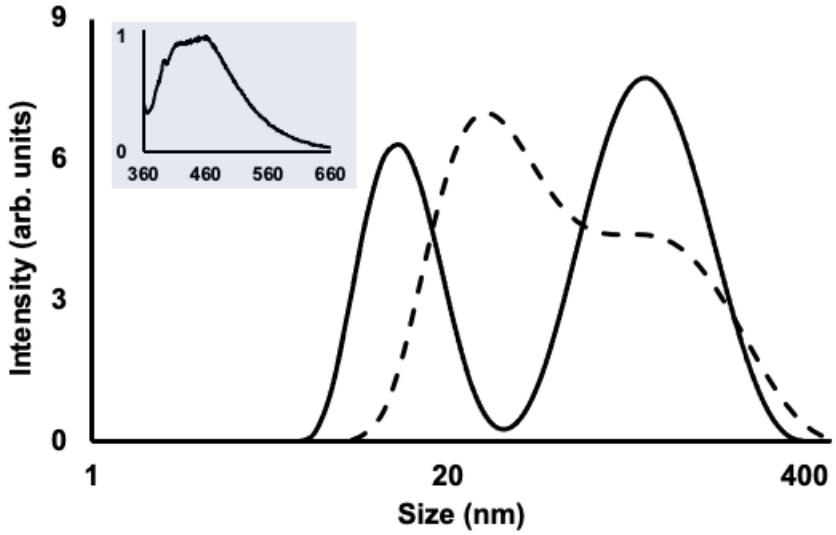

Figure 2.11: DLS plot showing the average particle size of **2.9** in $CHCl_3$ (dashed), and DCM (solid). Inset shows normalized fluorescence spectra of **2.9** in DCM.

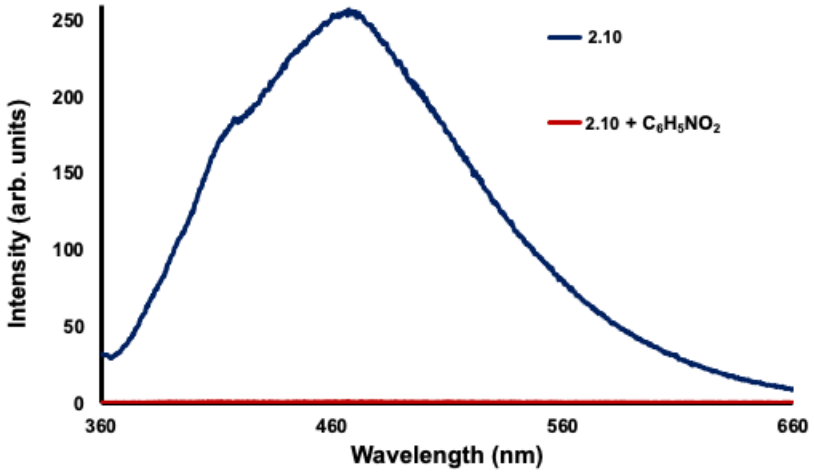

Figure 2.12: Fluorescence spectra of **2.10** before and after addition of nitrobenzene ($CHCl_3$, 1 mg/mL).

2.6.16 Photochemical Crosslinking of 2.11

A J-young tube was charged with a d_8 – THF (0.7 mL) solution of **2.11** (7.7 mg) and mesitylene (0.5 μL; 0.0036 mmol; added as an internal standard). The solution was degassed via three cycles of freeze-pump-thaw and placed under an N_2 atmosphere. The sample was analyzed by ^{1}H NMR spectroscopy and then placed in an enclosed photoreactor (consisting of 4 bulbs orthogonally arranged) and irradiated with 254 nm light for 40 h (note: the temperature inside the reactor did not exceed 40 °C). Complete gelation of the sample was observed, which precluded further analysis by ^{1}H NMR spectroscopy (Scheme 2.7, inset).

2.6.17 Photochemical Crosslinking Control of 2.4

In a N_2 filled glovebox, a J-young tube was charged with a d_8 – THF (0.7 mL) solution of **2.4** (5.7 mg; 0.0605 mmol) and mesitylene (2.5 μL; 0.0179 mmol; added as an internal standard). The sample was analyzed by ^{1}H NMR spectroscopy (Scheme 2.8, red) and then placed in an enclosed photoreactor (consisting of 4 bulbs orthogonally arranged) and irradiated (254 nm) for 67 h (note: the temperature inside the reactor did not exceed 40 °C). The resultant solution was free flowing (Scheme 2.8, inset), and subsequent ^{1}H NMR spectroscopic analysis revealed partial isomerization of the olefins had occurred (Scheme 2.8, blue). Additional spectral data shown in Figure 2.57.

Scheme 2.7: Photochemical Crosslinking of **2.11**

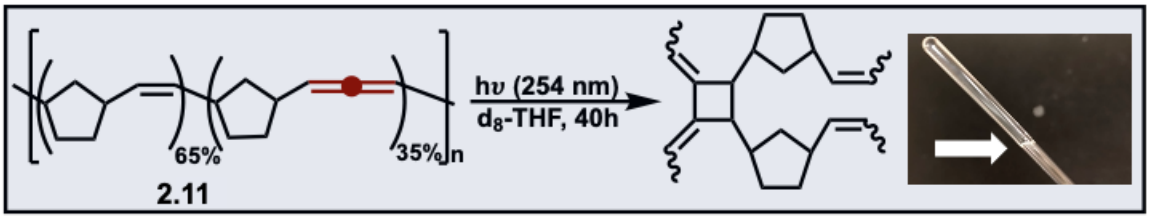

Scheme 2.8: ^{1}H NMR spectrum (d_8 - THF) of **2.4** before (red) and after (blue) irradiation with 254 nm light. Inset shows free-flowing polymer solution within following irradiation. * denotes internal standard (Mesitylene: δ = 6.90, 2.38)

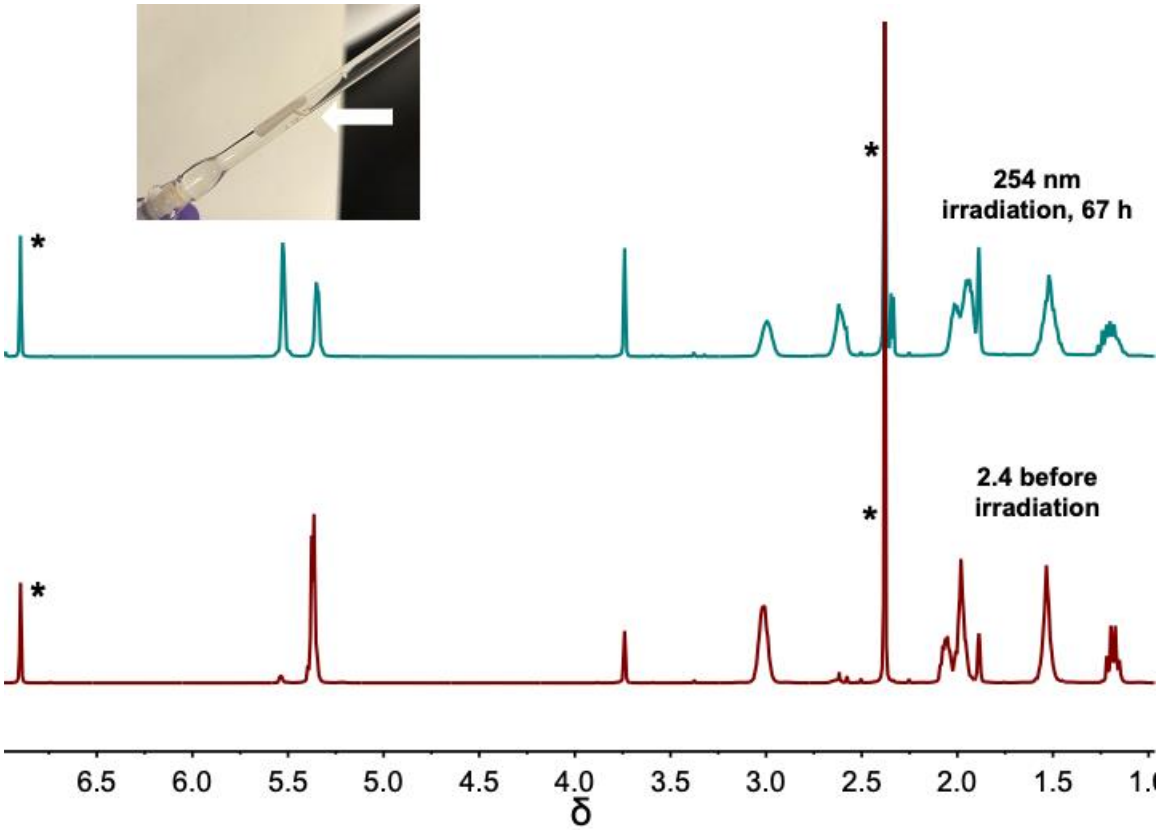

2.6.18 Au(I) Catalyzed Multicomponent Coupling of 2.9

A 7 mL vial was charged with chloro(triphenylphosphine)gold(I) (PPh_3AuCl; 29.6 mg; 0.0599 mmol), silver triflate (AgOTf; 16 mg; 0.0625 mmol), a Teflon stir bar, and DCM (1 mL). The suspension was stirred for 5 minutes at 0 °C, after which a DCM solution of **2.9** (31.6 mg; 0.298 mmol; in 2 mL DCM) was slowly added. Trimethylsilylazide (TMS-azide; 12 μL, 0.0894 mmol) and trifluoroacetic acid (TFA; 6.8 μL, 0.0894 mmol) were added at 0 °C to the resultant ochre solution, and the reaction was then heated at 30 °C for 5 hours in the absence of light. The resulting orange suspension was filtered through a pad of celite, washed with DCM (3 mL), and concentrated to a minimal volume. Polymeric material was precipitated from pentane, immediately dissolved in minimal DMSO, and precipitated a second time from pentane:*i*PrOH (90:10). IR spectroscopic analysis of **2.13** revealed complete consumption of the allene stretch and appearance of an azide stretch (Figure 2.3, Figure 2.60). ^{19}F NMR spectroscopy (2:1 d_6-DMSO:d_6-acetone) revealed broad resonances consistent with installation of trifluoroacetate groups (Figure 2.3, Figure 2.55). Additional spectral data shown in Figure 2.54.

A control experiment was conducted following the conditions outlined above, except with no chloro(triphenylphosphine)gold(I) and silver triflate. ^1H NMR (Figure 2.56), and IR spectroscopy (Figure 2.59) of the precipitated material revealed no functionalization of the allene moieties.

Scheme 2.9: Au(I) catalyzed Multicomponent Coupling of **2.9**

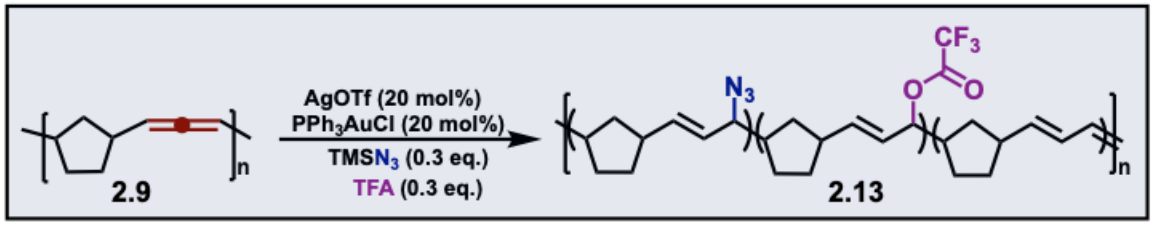

APPENDIX

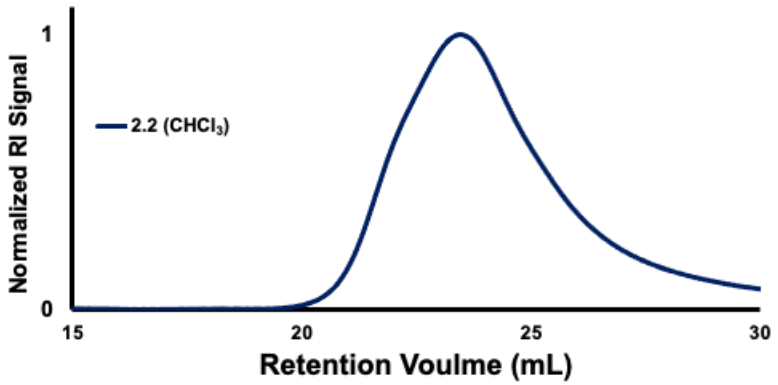

Figure 2.13: Representative **2.2** GPC trace. M_n = 94,790 Da, Đ = 1.99

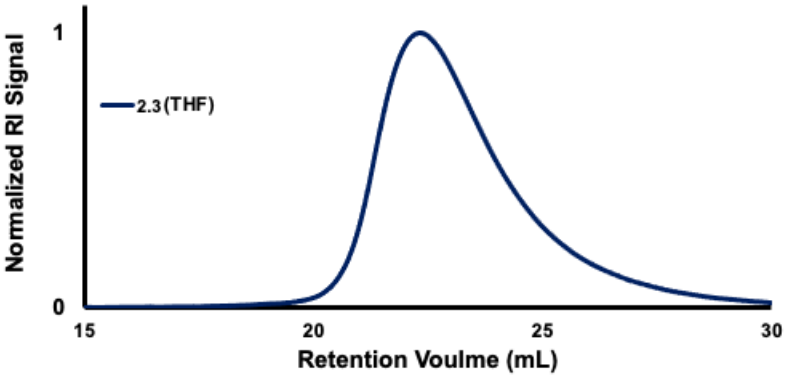

Figure 2.14: Representative **2.3** GPC trace. M_n = 23,110 Da, Đ = 2.17

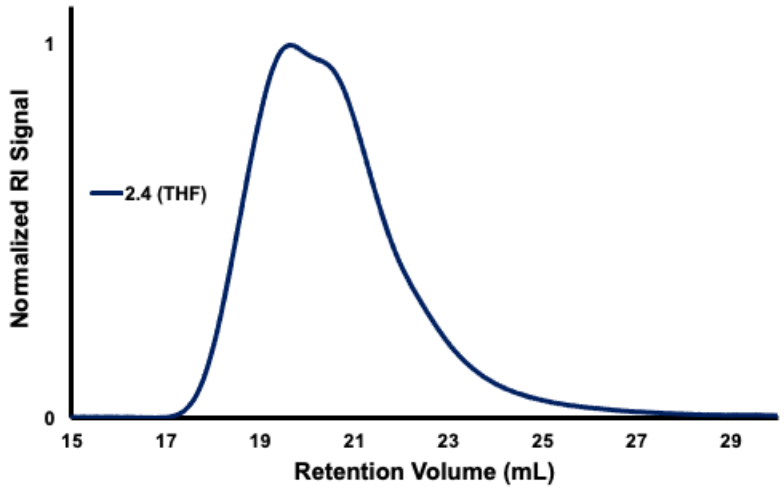

Figure 2.15: Representative **2.4** GPC trace. M_n = 259,700 Da, Đ = 1.79

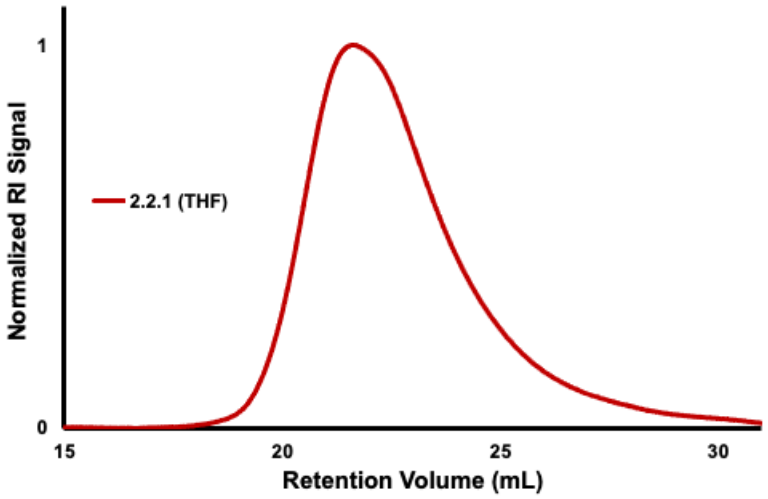

Figure 2.16: Representative **2.2.1** GPC trace. M_n = 83,700 Da, Đ = 1.71

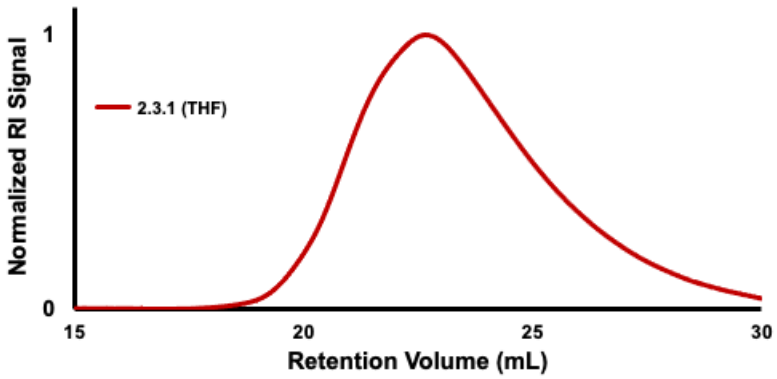

Figure 2.17: Representative **2.3.1** GPC trace. M_n = 46,020 Da, Đ = 2.21

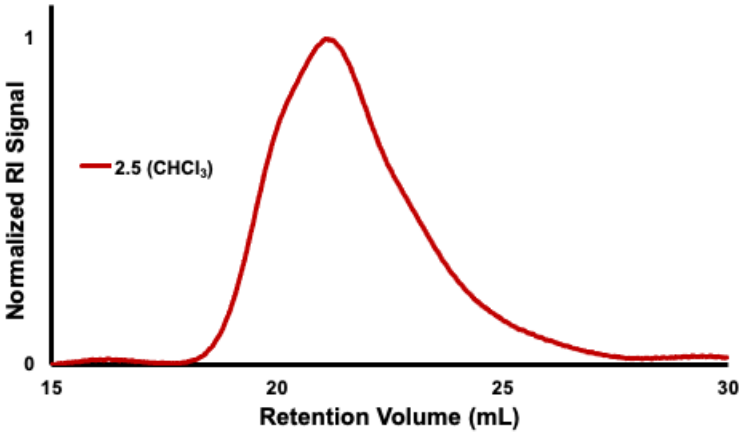

Figure 2.18: Representative **2.5** GPC trace. M_n = 257,300 Da, Đ = 1.63

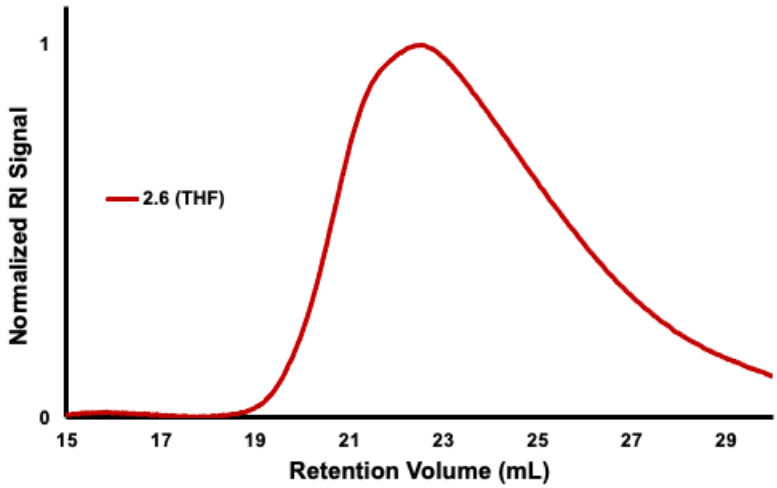

Figure 2.19: Representative **2.6** GPC trace. M_n = 45,580 Da Đ = 2.46

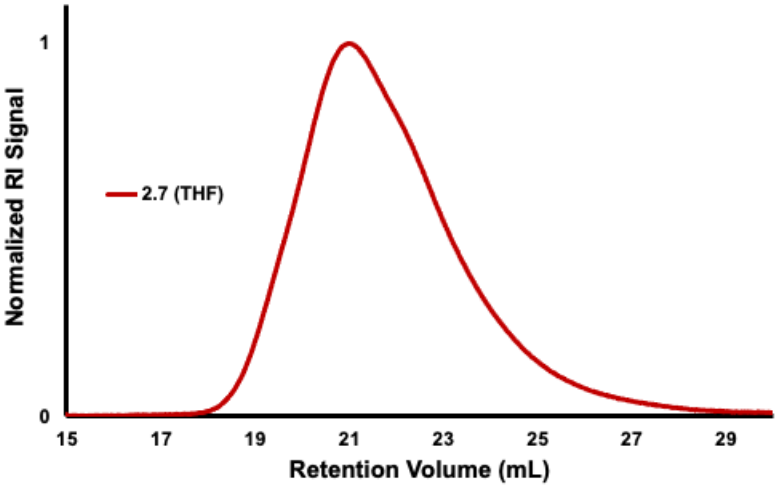

Figure 2.20: Representative **2.7** GPC trace. M_n = 114,100 Da, Đ = 1.82

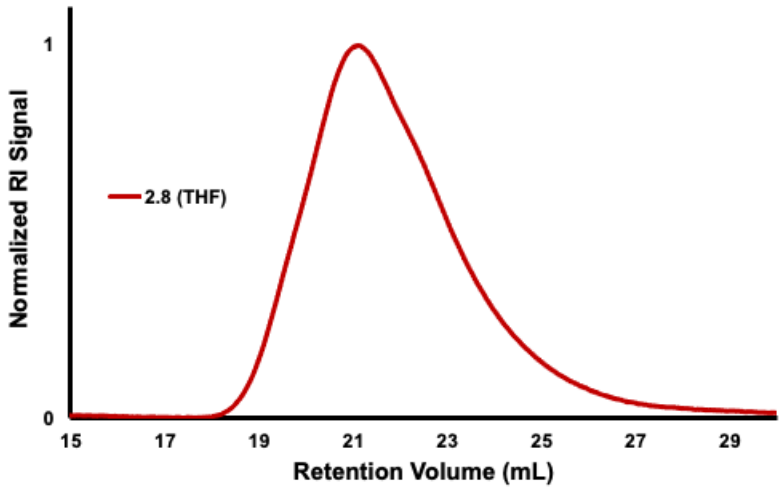

Figure 2.21: Representative **2.8** GPC trace. M_n = 120,500 Da, Đ = 1.79

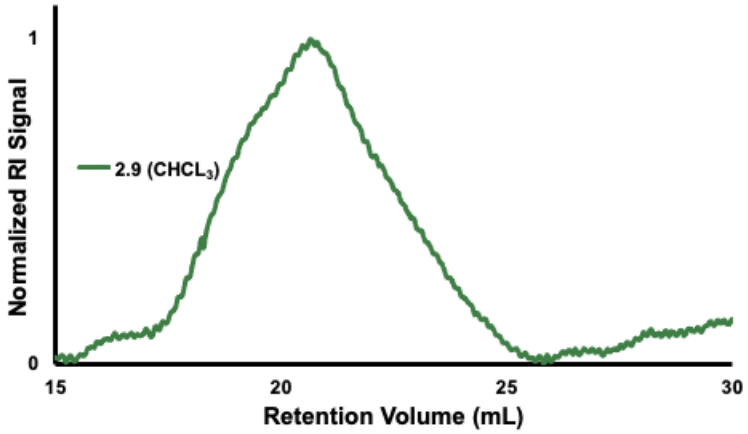

Figure 2.22: Representative **2.9** GPC trace. Low concentrations (~0.25 mg/mL) were required for **2.9 – 2.12** materials due to poor solubility. M_n = 270,300 Da, Đ = 1.76

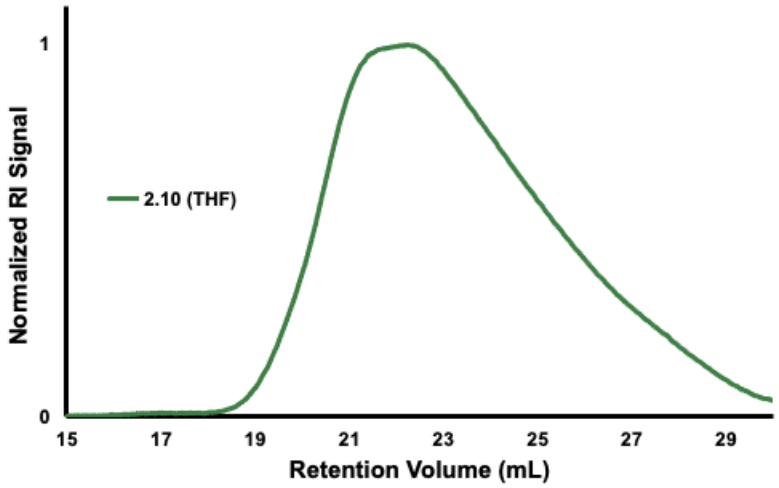

Figure 2.23: Representative **2.10** GPC trace. M_n = 32,430 Da, Đ = 2.72

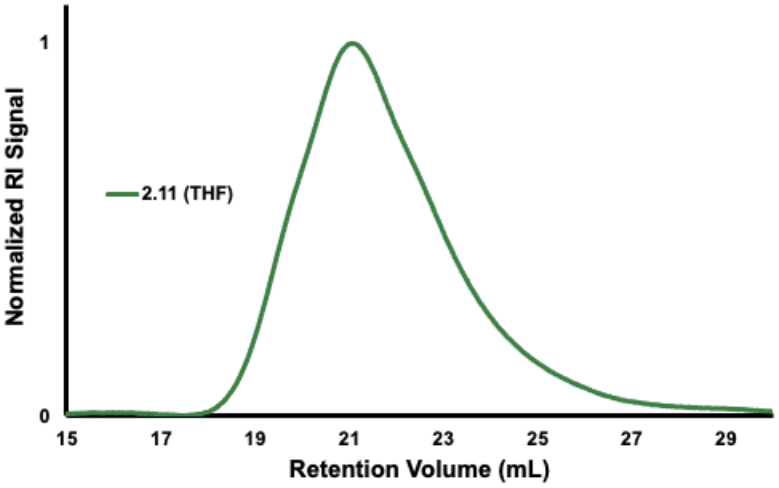

Figure 2.24: Representative **2.11** GPC trace. M_n = 100,600 Da, Đ = 1.88

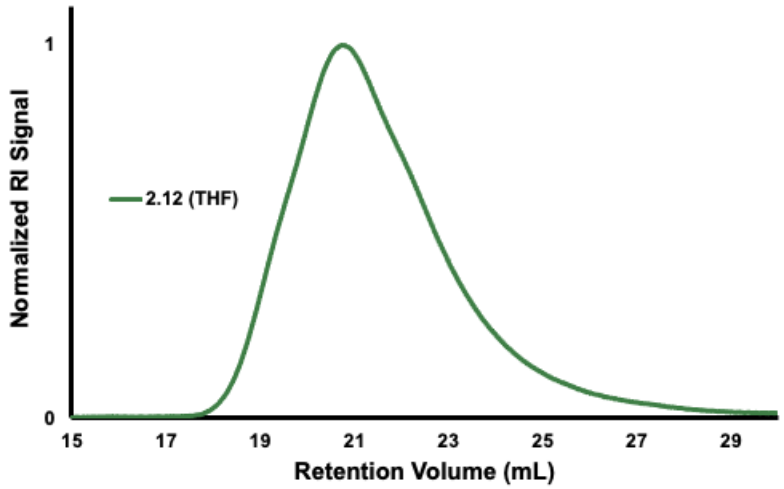

Figure 2.25: Representative **2.12** GPC trace. M_n = 88,380 Da, Đ = 1.90

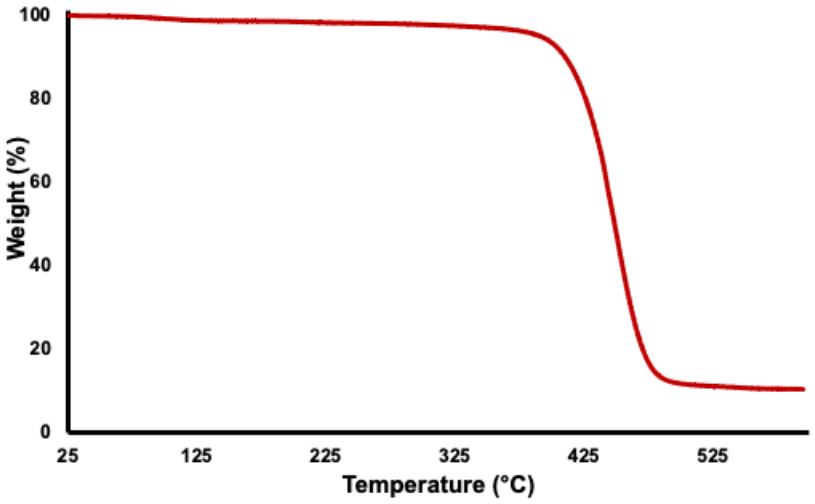

Figure 2.26: Representative **2.9** TGA thermogram (Heating Rate: 10 °C/min in N_2)

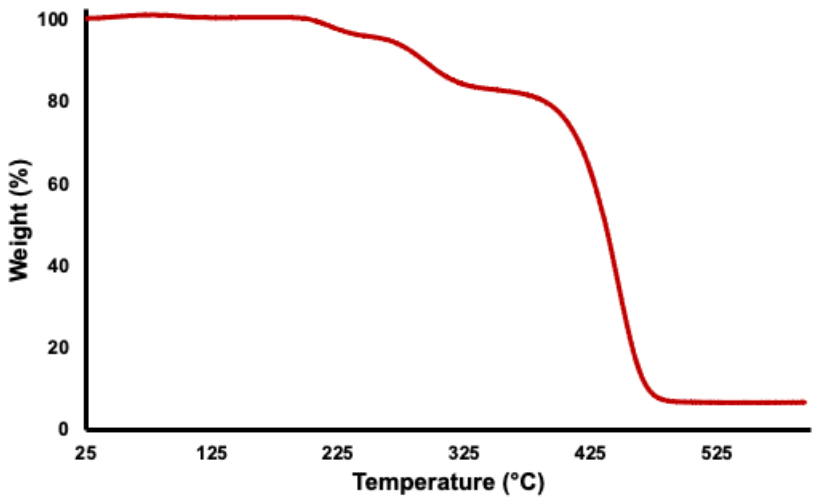

Figure 2.27: Representative **2.10** TGA thermogram (Heating Rate: 10 °C/min in N_2)

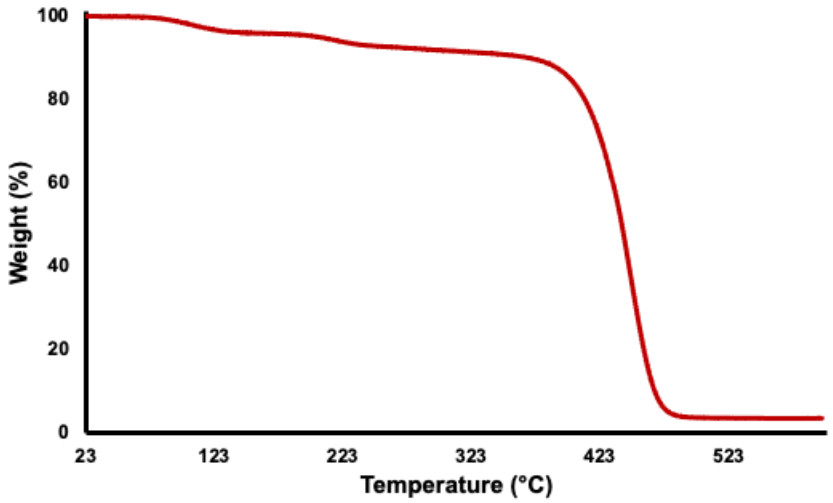

Figure 2.28: Representative **2.11** TGA thermogram (Heating Rate: 10 °C/min in N_2)

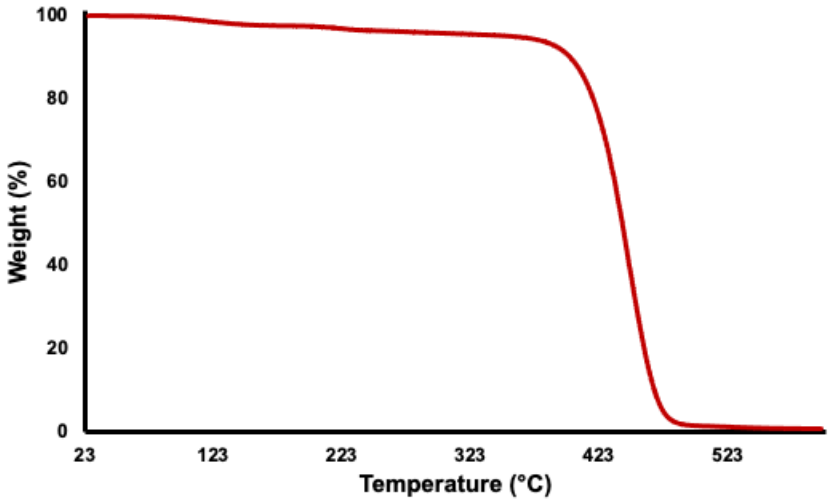

Figure 2.29: Representative **2.12** TGA thermogram (Heating Rate: 10 °C/min in N_2)

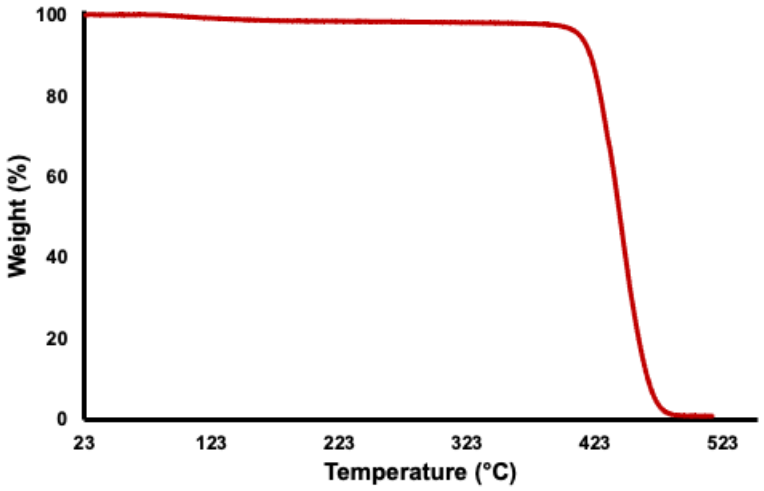

Figure 2.30: Representative **2.4** TGA thermogram (Heating Rate: 10 °C/min in N_2)

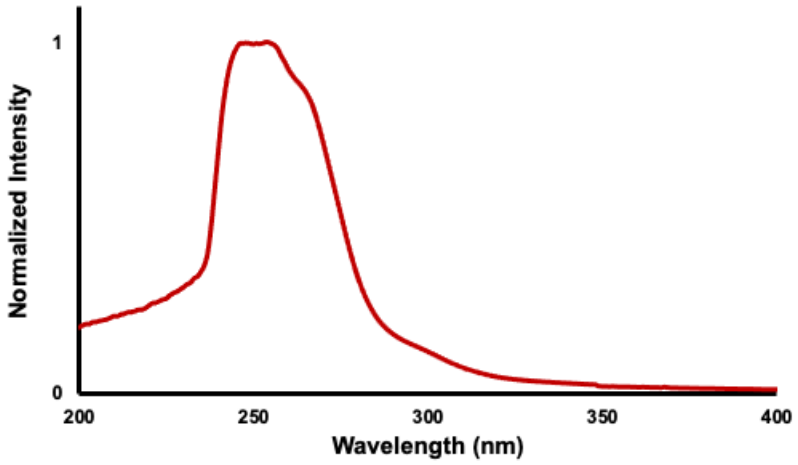

Figure 2.31: Representative UV-Vis spectrum of **2.9** ($CHCl_3$, 1.2 mg/mL)

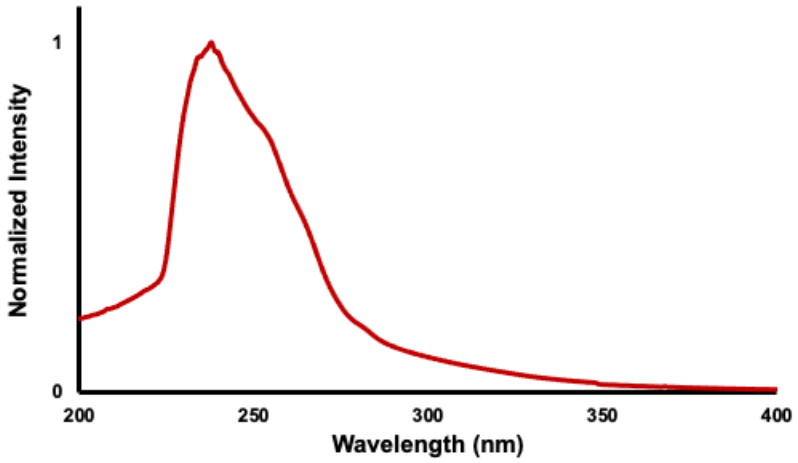

Figure 2.32: Representative UV-Vis spectrum of **2.9** (DCM, 1.2 mg/mL)

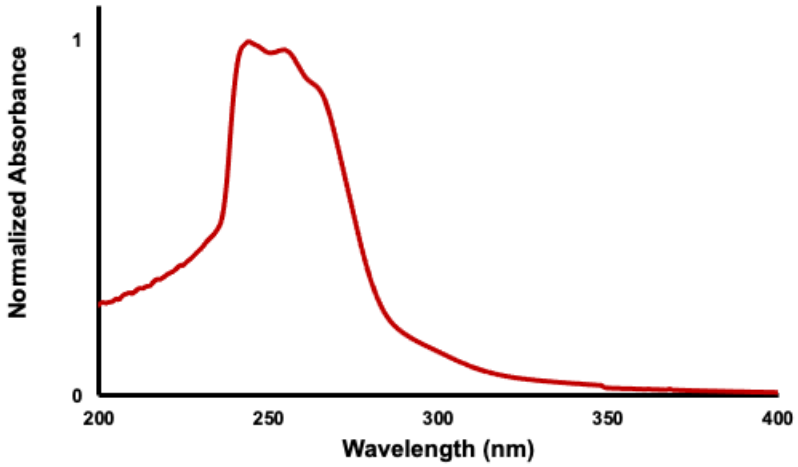

Figure 2.33: Representative UV-Vis spectrum of **2.10** ($CHCl_3$, 1.0 mg/mL)

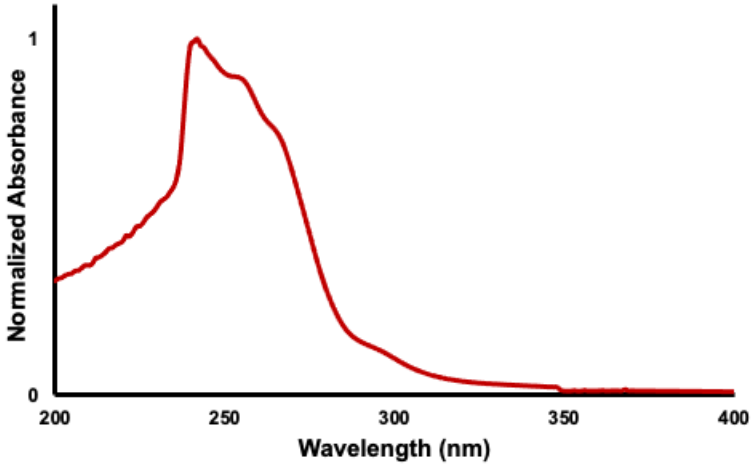

Figure 2.34: Representative UV-Vis spectrum of **2.11** ($CHCl_3$, 0.9 mg/mL)

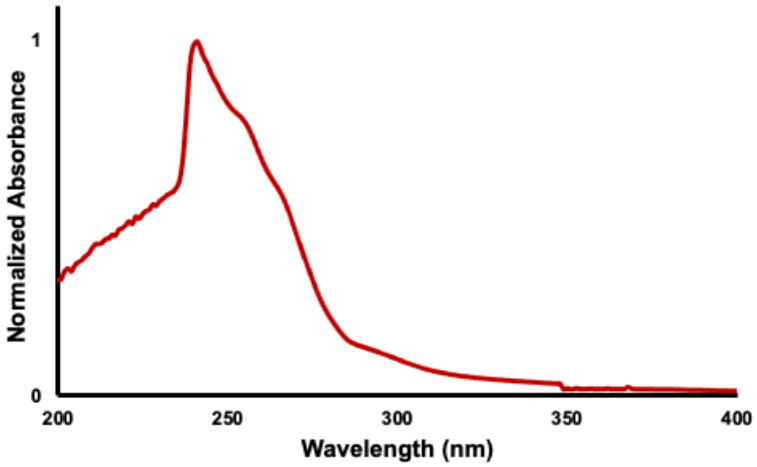

Figure 2.35: Representative UV-Vis spectrum of **2.12** ($CHCl_3$, 1.0 mg/mL)

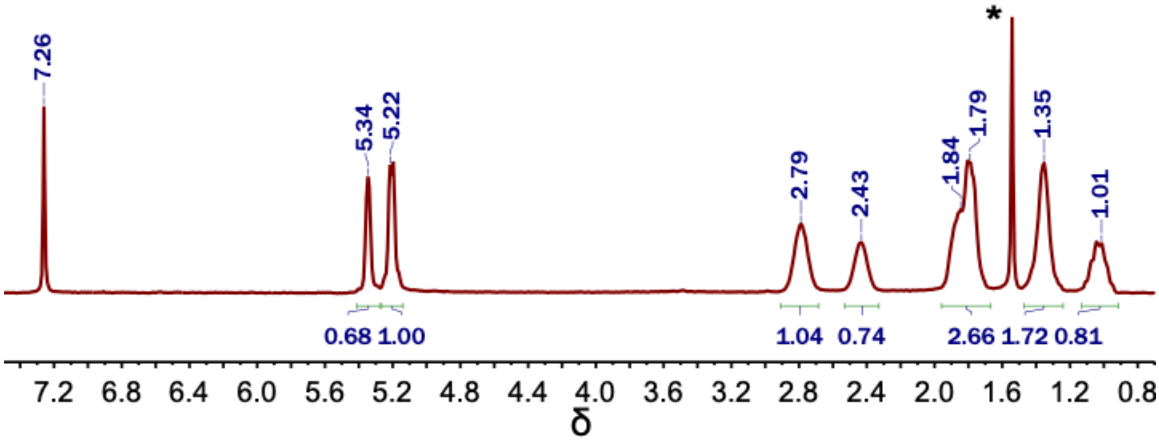

Figure 2.36: Representative ^1H NMR of **2.2** in $CDCl_3$. *Z*:*E* ratio determined by integration of peaks at δ = 5.22 and 5.34. Residual solvent (H_2O: δ = 1.56) denoted with *.

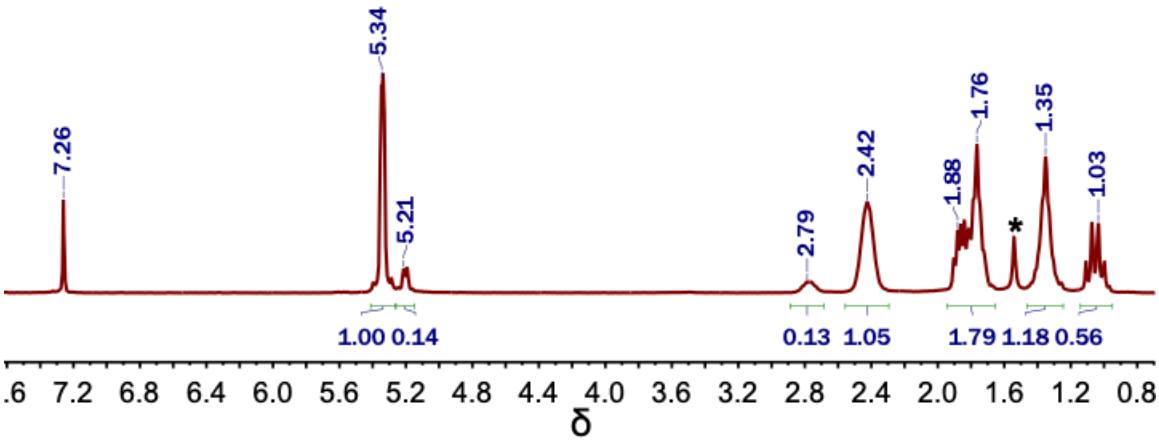

Figure 2.37: Representative ^{1}H NMR of **2.3** in $CDCl_3$. *Z*:*E* ratio determined by integration of peaks at δ = 5.21 and 5.34. Residual solvent (H_2O: δ = 1.56) denoted with *.

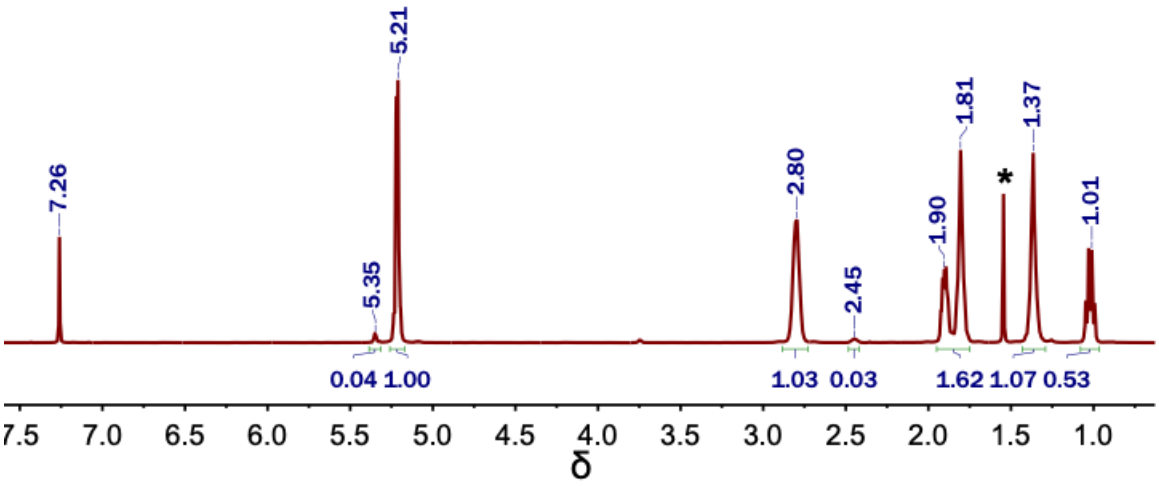

Figure 2.38: Representative ^{1}H NMR of **2.4** in $CDCl_3$. *Z*:*E* ratio determined by integration of peaks at δ = 5.21 and 5.35. Residual solvent (H_2O: δ = 1.56) denoted with *.

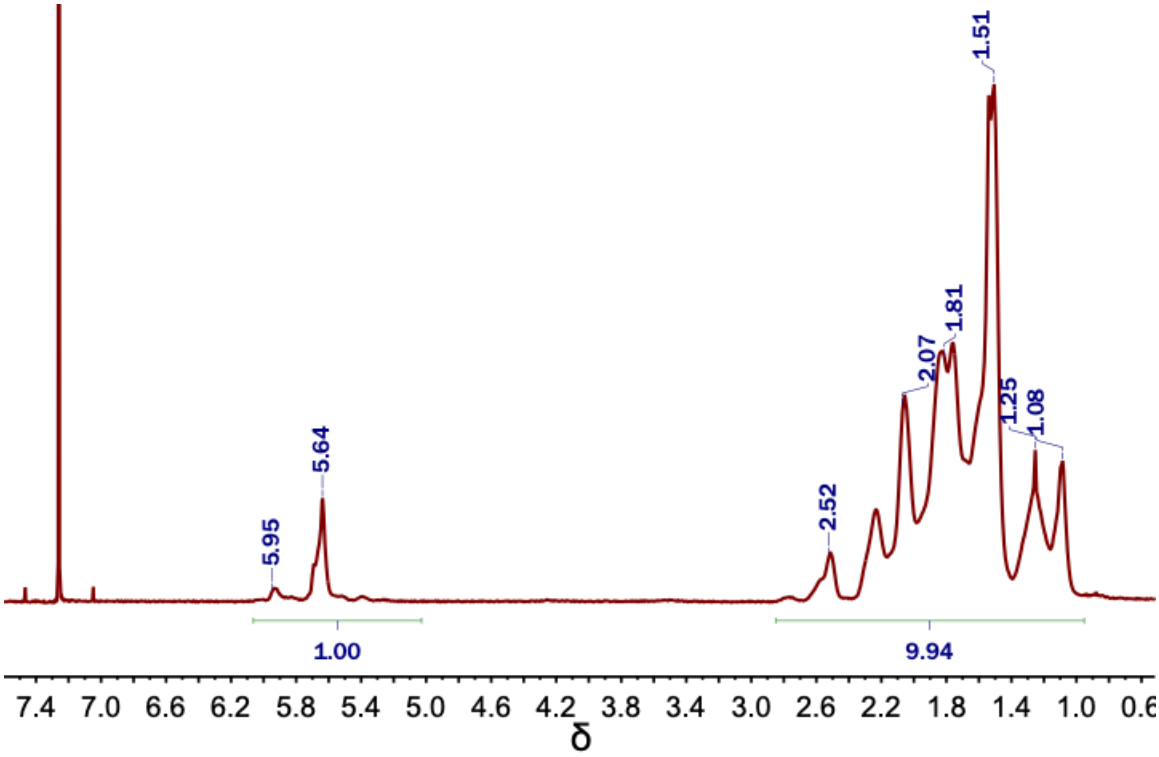

Figure 2.39: Representative ^{1}H NMR of **2.2.1** in $CDCl_3$.

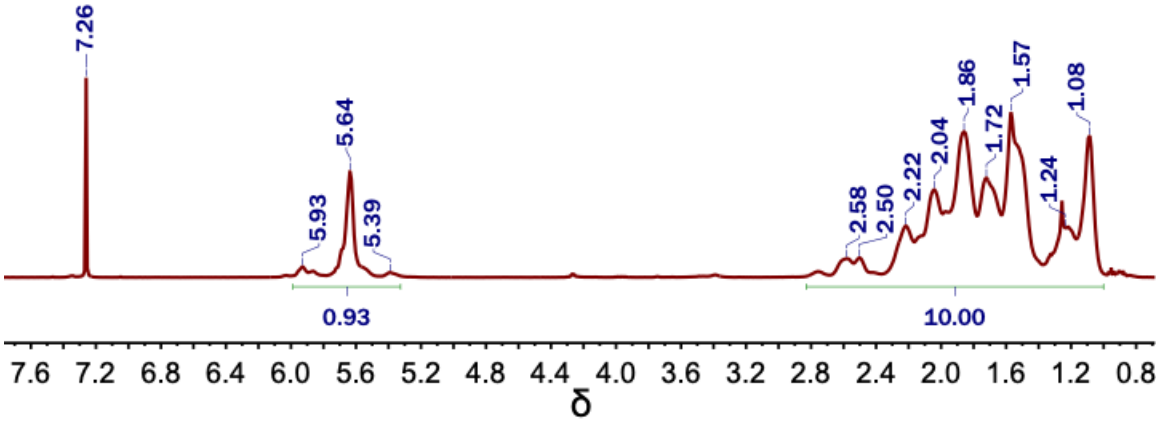

Figure 2.40: Representative ^{1}H NMR of **2.3.1** in $CDCl_3$.

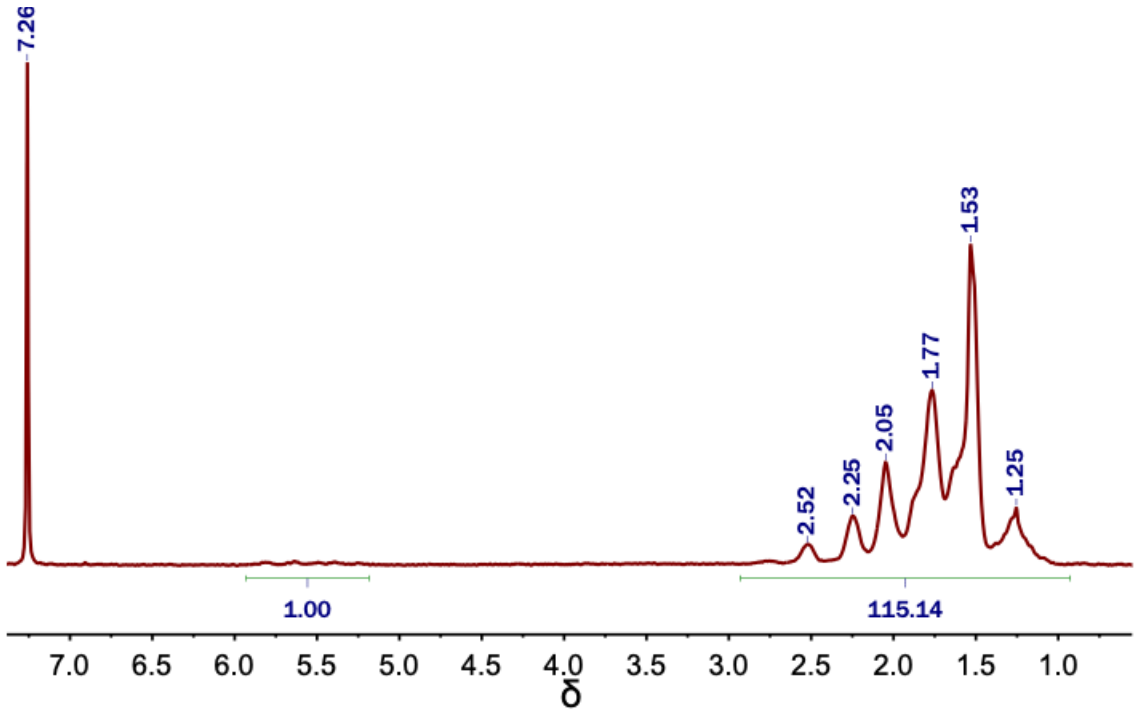

Figure 2.41: Representative ^{1}H NMR of **2.5** in $CDCl_3$.

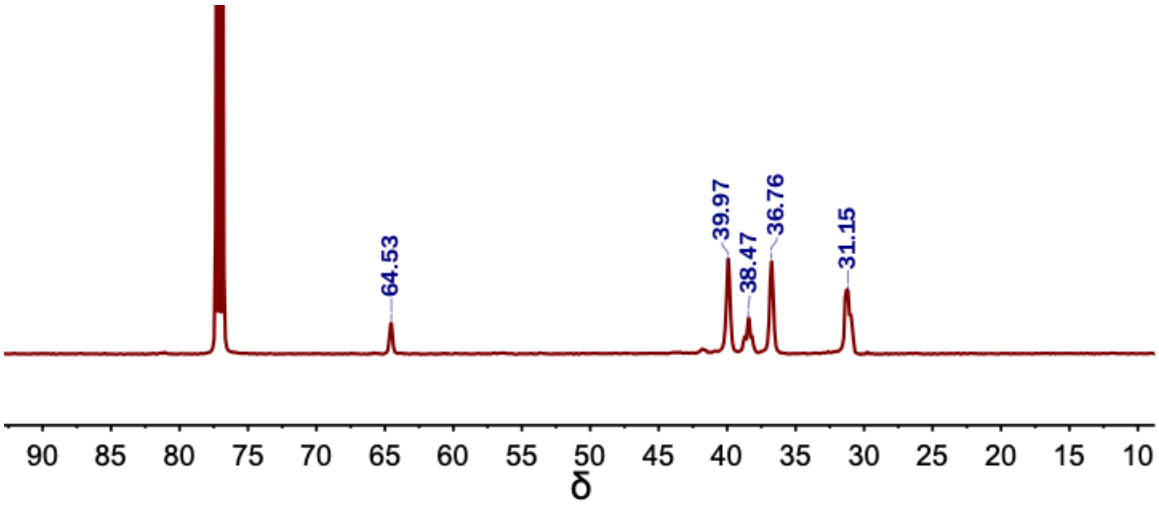

Figure 2.42: Representative ^{13}C NMR of **2.5** in $CDCl_3$.

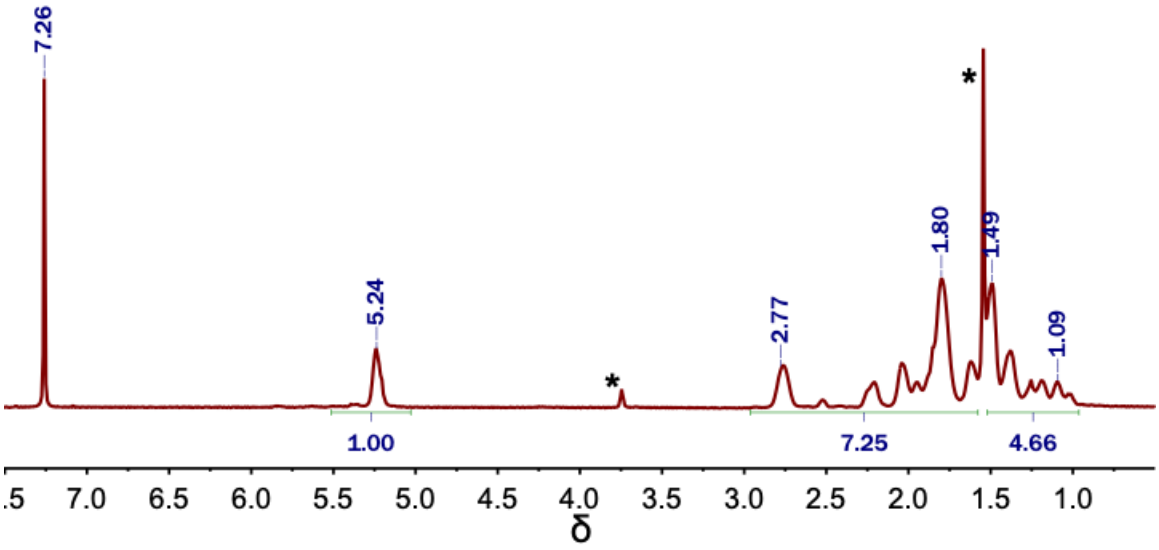

Figure 2.43: Representative ^{1}H NMR of **2.6** in $CDCl_3$. Residual solvent (THF: δ = 3.74, H_2O: δ = 1.56) denoted with *.

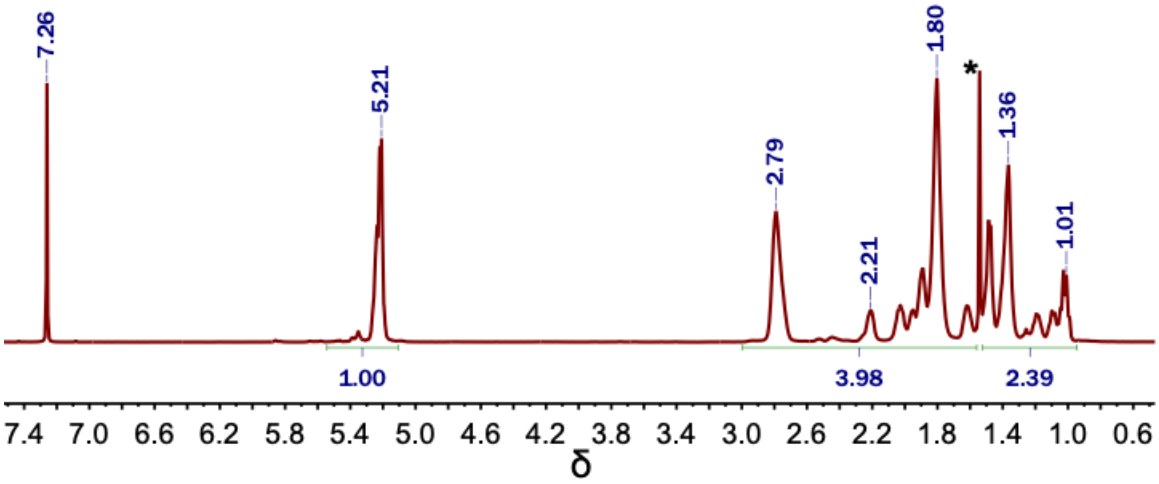

Figure 2.44: Representative ^{1}H NMR of **2.7** in $CDCl_3$. Residual solvent (H_2O: δ = 1.56) denoted with *.

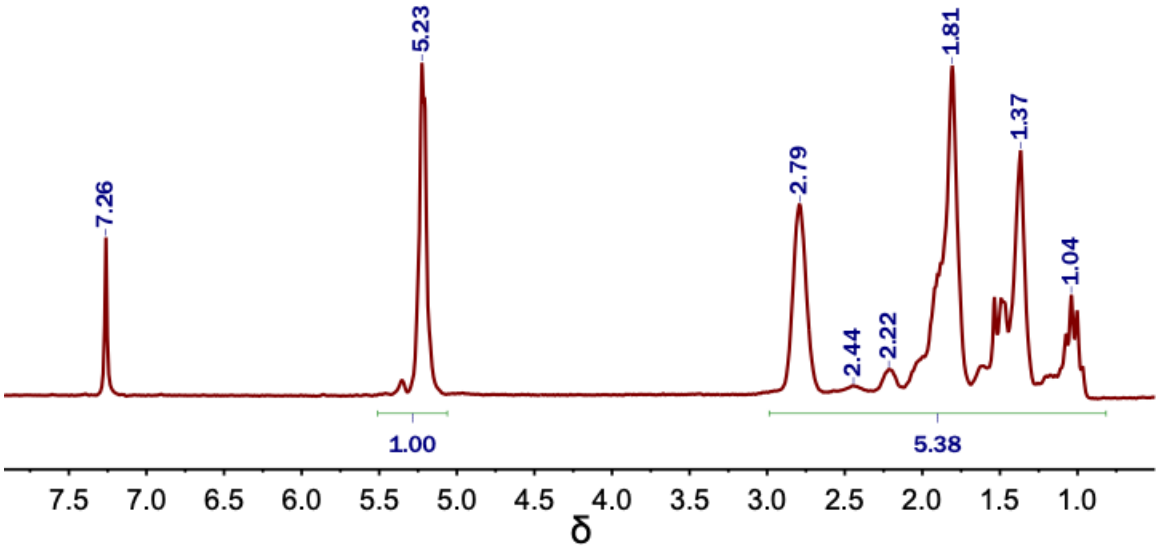

Figure 2.45: Representative ^{1}H NMR of **2.8** in $CDCl_3$.

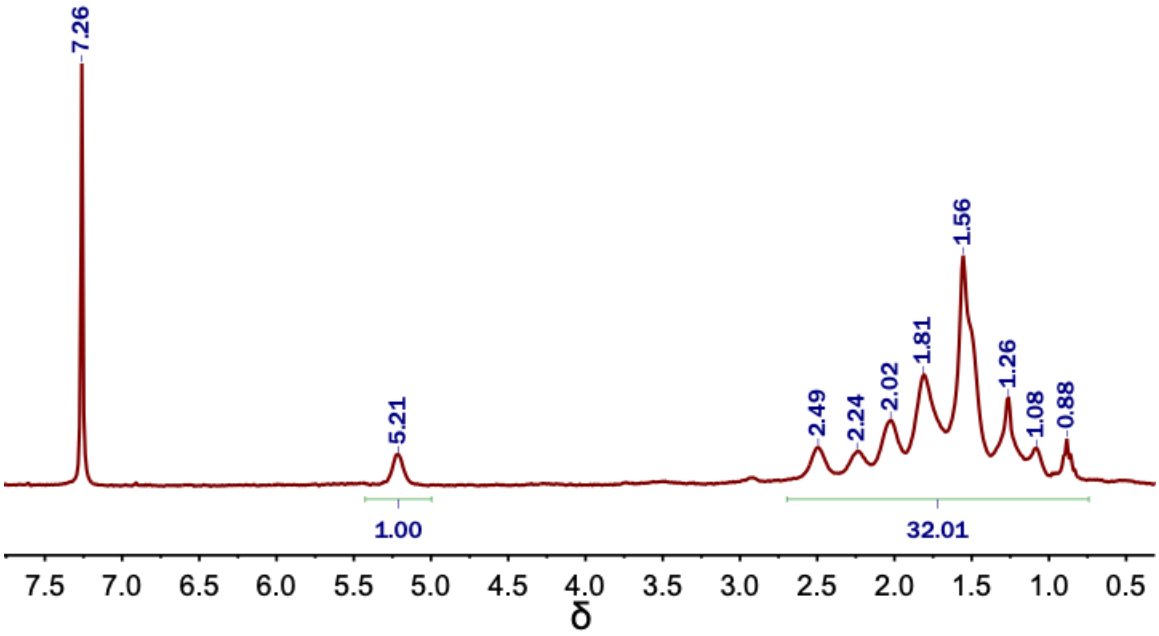

Figure 2.46: Representative ^{1}H NMR of **2.2.2** in $CDCl_3$.

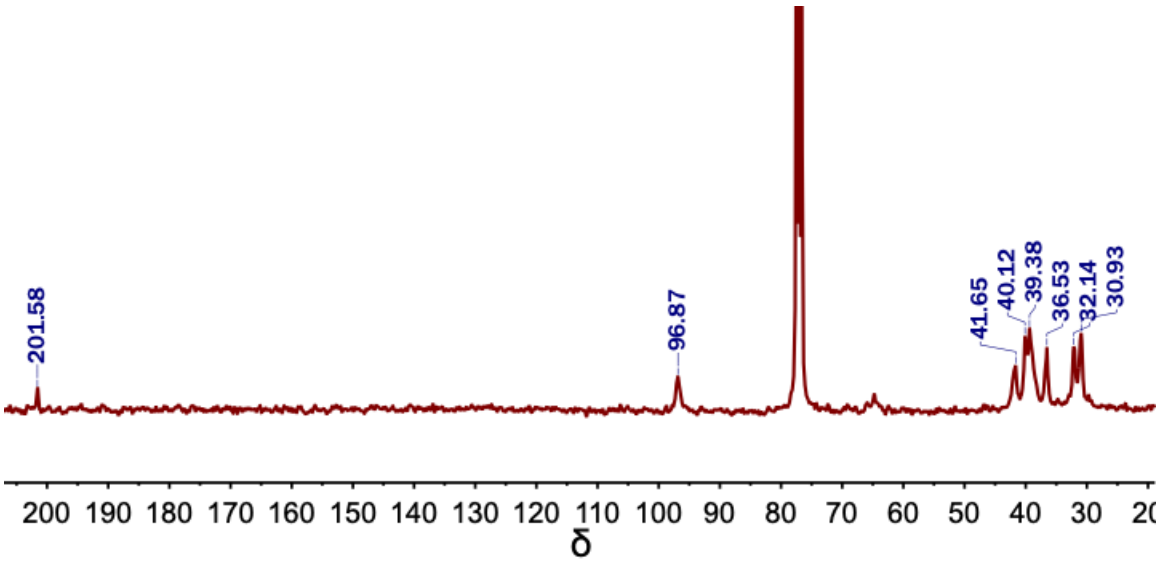

Figure 2.47: Representative ^{13}C NMR of **2.2.2** in $CDCl_3$.

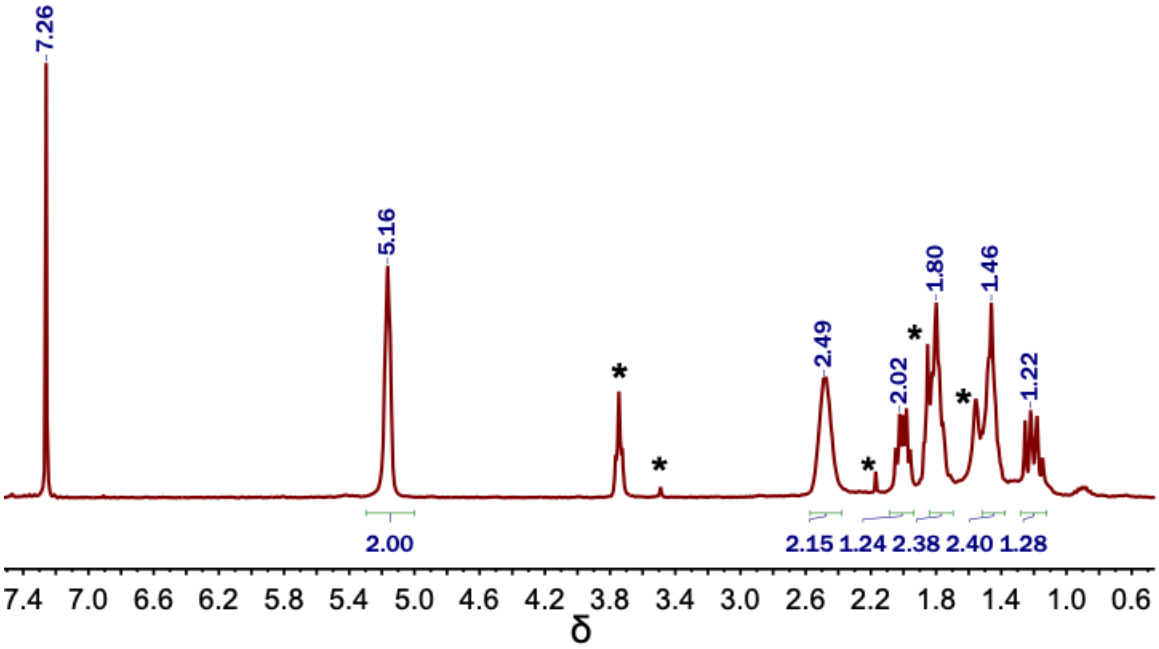

Figure 2.48: Representative ^{1}H NMR of **2.9** in $CDCl_3$. Residual solvent (THF: δ = 3.74,1.85. MeOH: δ = 3.50, Acetone: δ = 2.17, H_2O: δ = 1.56) denoted with *.

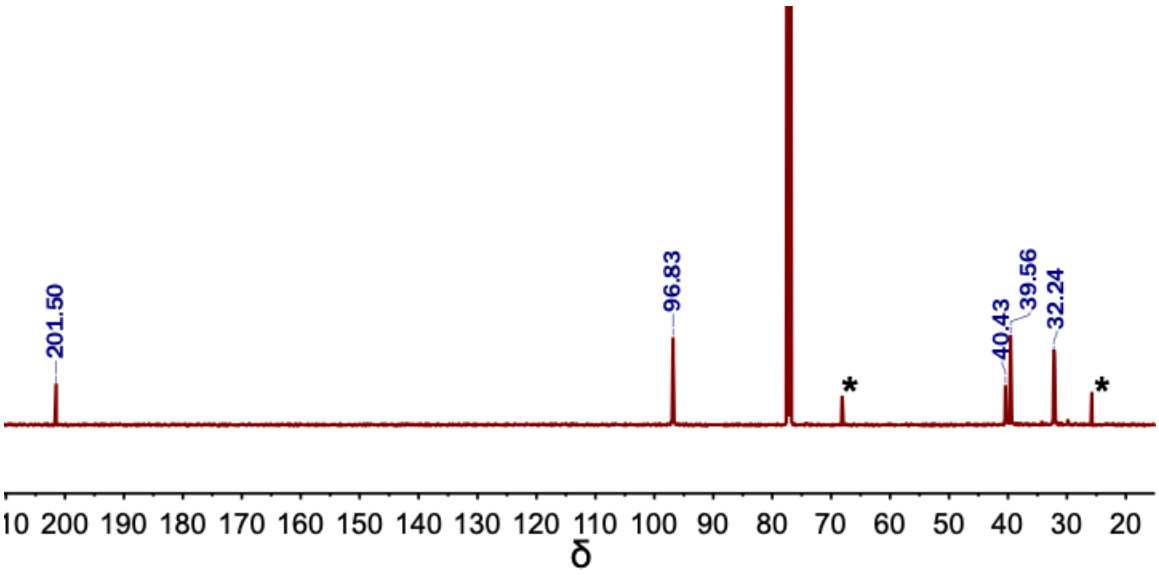

Figure 2.49: Representative ^{13}C NMR of **2.9** in $CDCl_3$. Residual solvent (THF: δ = 67.97, 25.62) denoted with *.

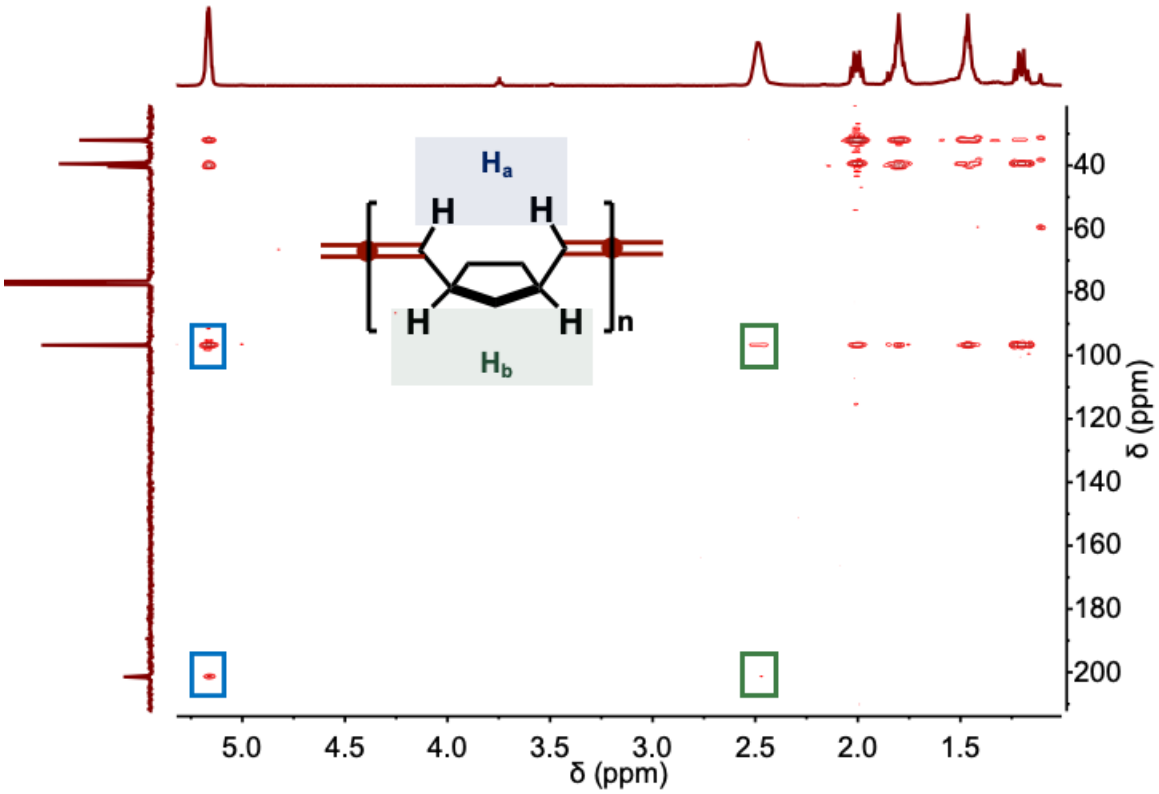

Figure 2.50: HMBC spectra of **2.9**. Correlations of H_a to allene carbons highlighted in blue. Correlations of H_b to allene carbons highlighted in green.

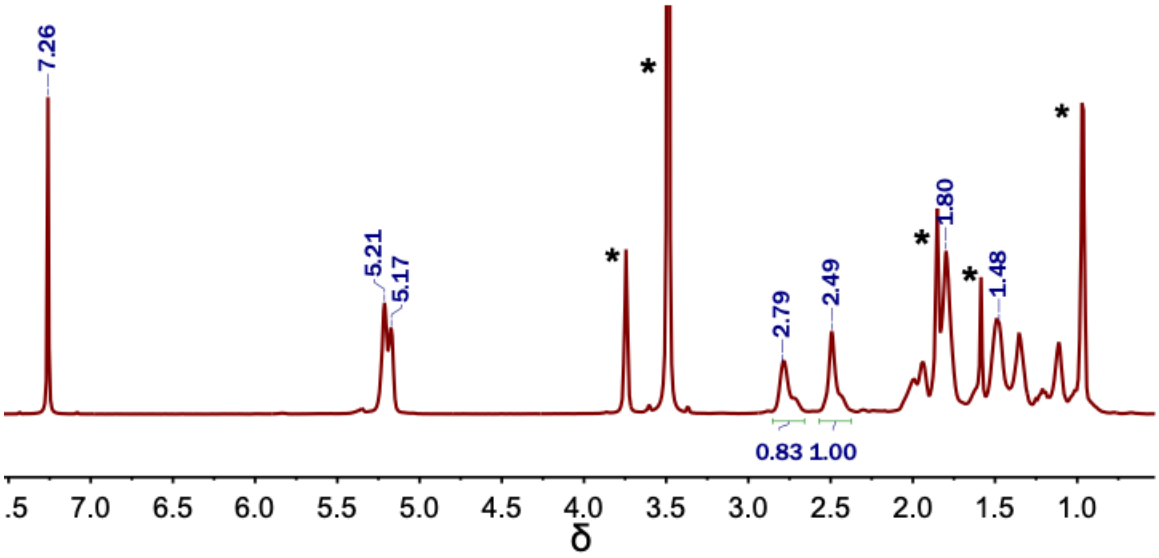

Figure 2.51: Representative ^{1}H NMR of **2.10** in $CDCl_3$. Residual solvent (THF: δ = 3.74,1.85. MeOH: δ = 3.50,0.9 H_2O: δ = 1.56) denoted with *.

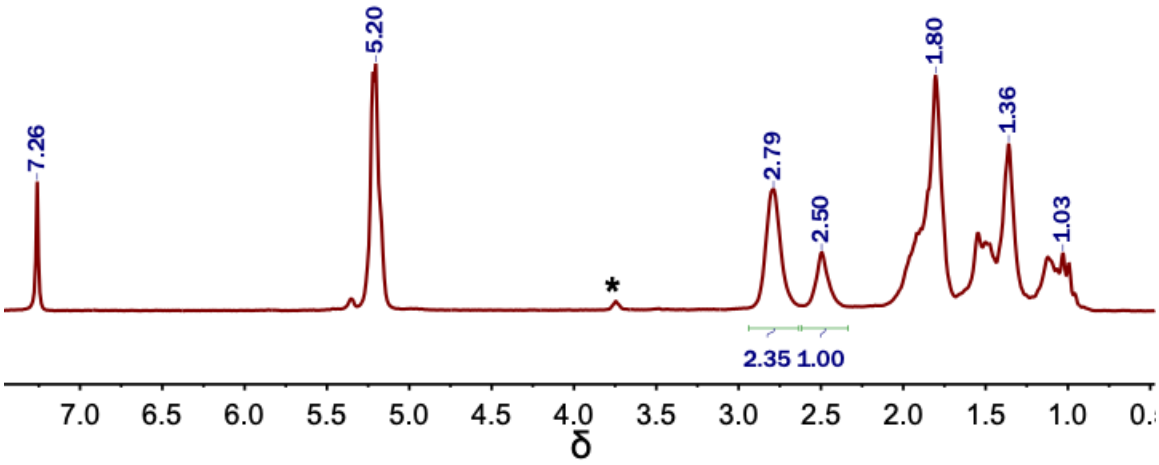

Figure 2.52: Representative ^{1}H NMR of **2.11** in $CDCl_3$. Residual solvent (THF: δ = 3.74) denoted with *.

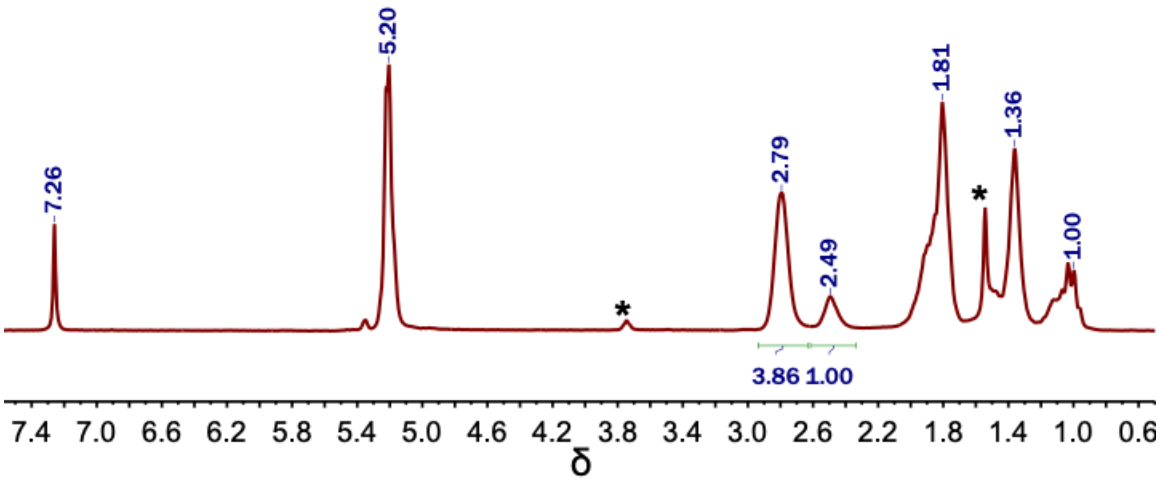

Figure 2.53: Representative ^{1}H NMR of **2.12** in $CDCl_3$. Residual solvent (THF: δ = 3.74, H_2O: δ = 1.56) denoted with *.

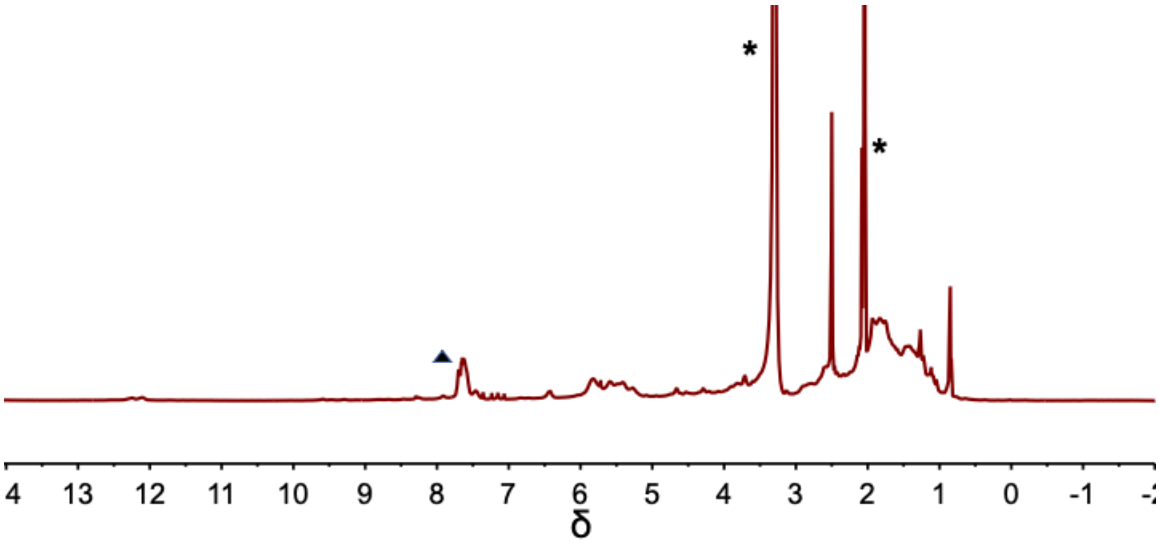

Figure 2.54: ^{1}H NMR of **2.13** in d_6-DMSO:d_6-acetone (2:1). Residual solvent (H_2O: δ = 3.33, acetone: δ = 2.09) denoted with *. Triphenylphosphine denoted by ▲.

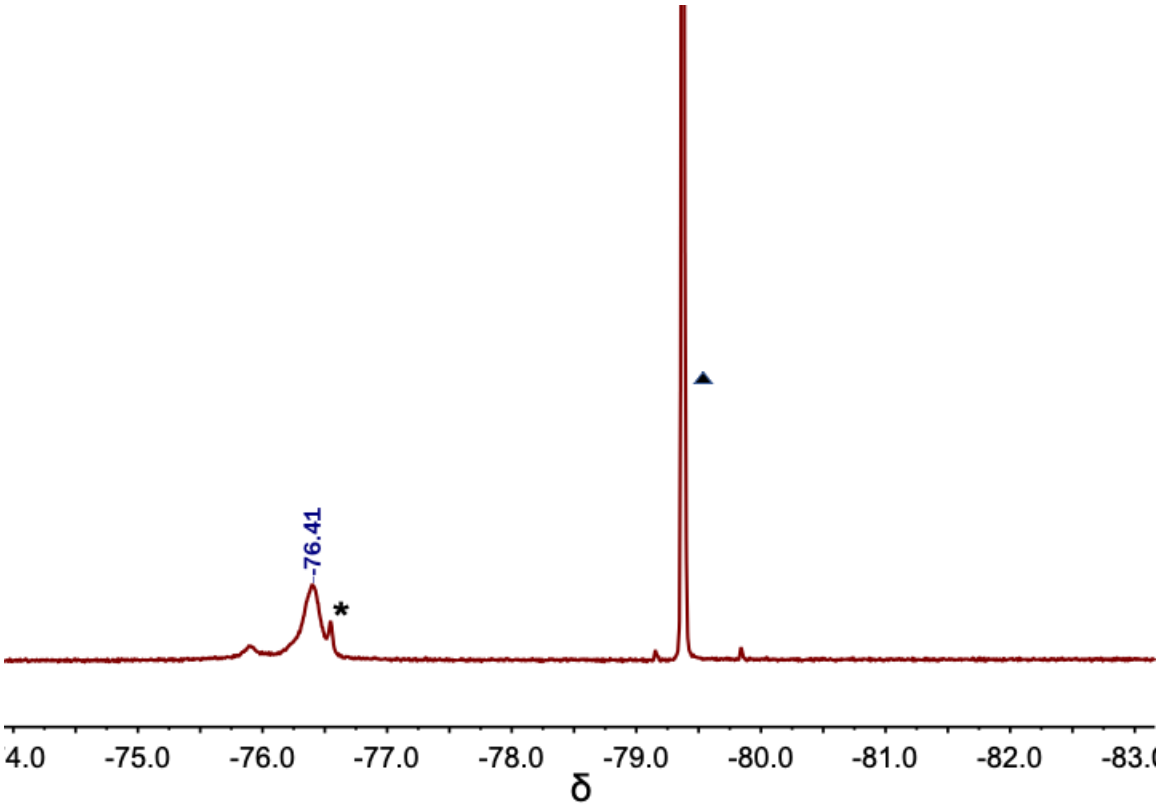

Figure 2.55: ^{19}F NMR of **2.13** in d_6-DMSO:d_6-acetone (2:1). Trace trifluoroacetic acid (TFA: δ = -76.55) denoted with *. Residual triflate denoted by ▲.

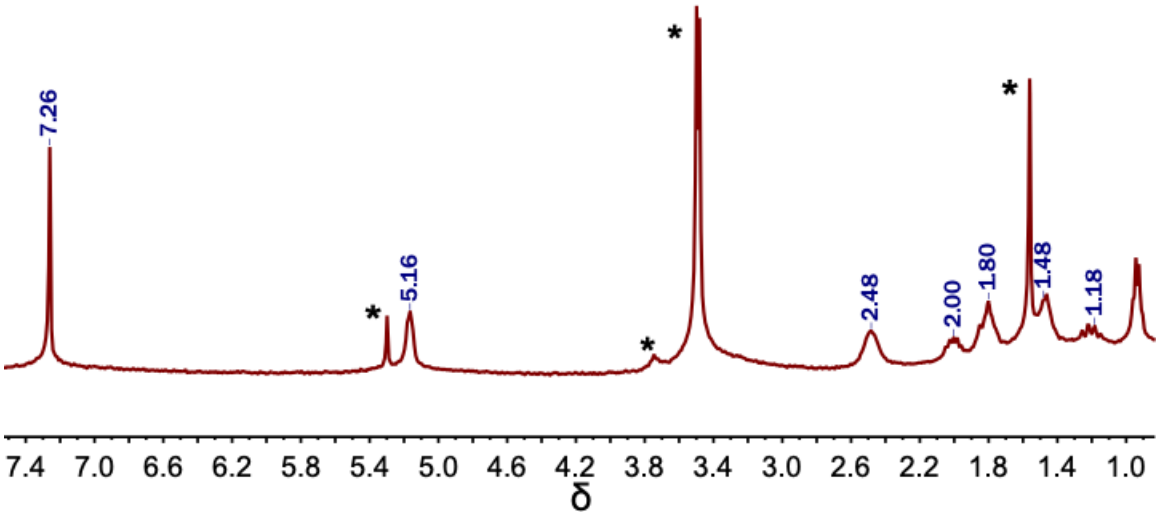

Figure 2.56: ^{1}H NMR of multicomponent coupling control reaction of 2.9 in $CDCl_3$. Residual solvent (DCM: δ = 5.33, THF: δ = 3.74, MeOH: δ = 3.50, H_2O: δ = 1.56) denoted with *.

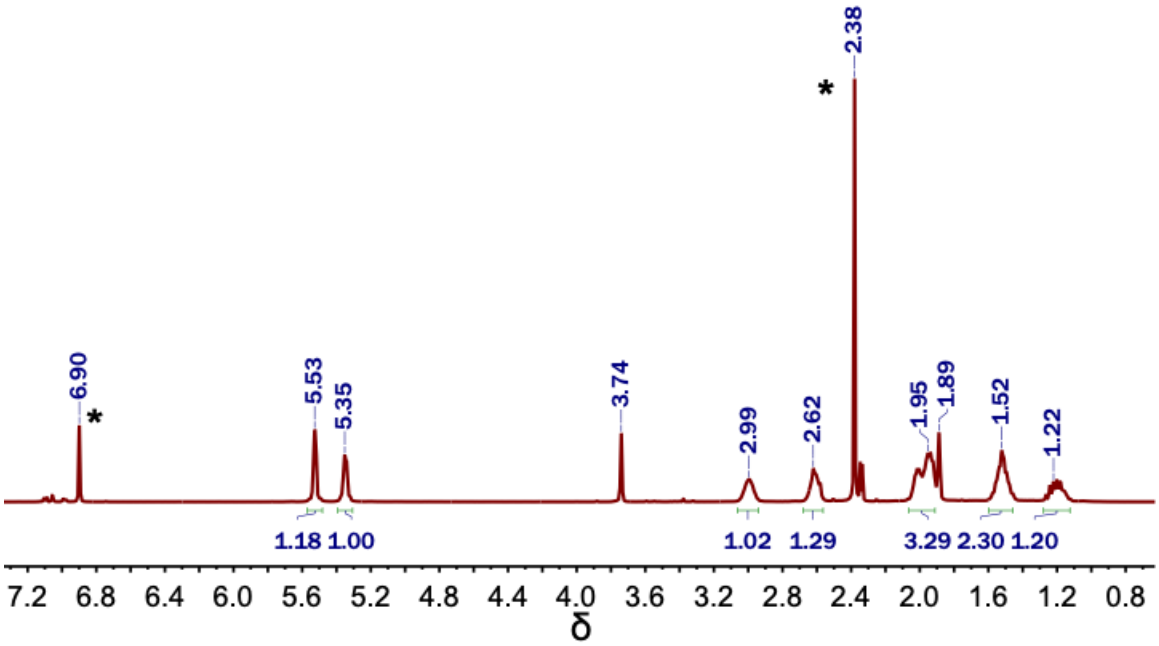

Figure 2.57: ^{1}H NMR of 2.4 in d_8 - THF after irradiation at 254 nm for 67 h. in $CDCl_3$. *Z*:*E* ratio determined by integration of peaks at δ = 5.35 and 5.53. Internal standard (Mesitylene: δ = 6.90, 2.38) denoted with *.

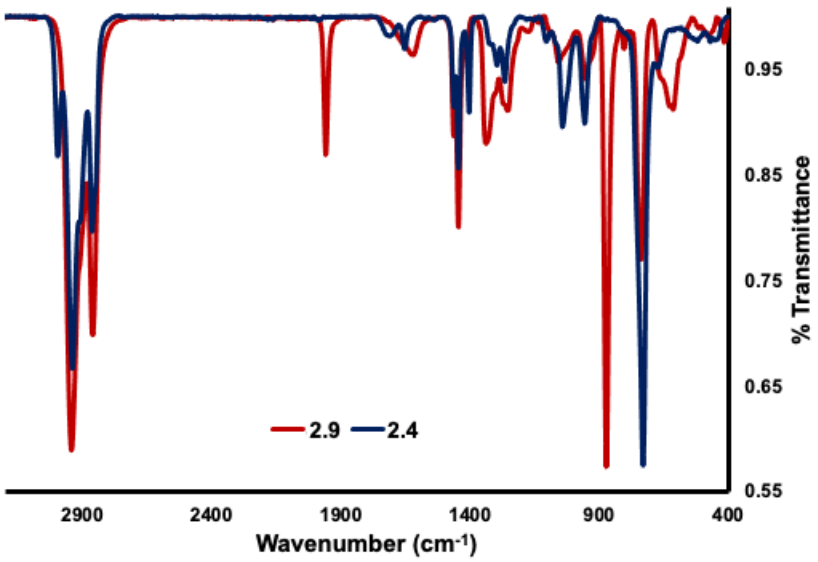

Figure 2.58: Overlaid representative IR spectra of **2.4** and **2.9** depicting the characteristic allene stretch (1959 cm^{-1}) in **2.9**, consistent with literature reports of allenic carbons.[123]

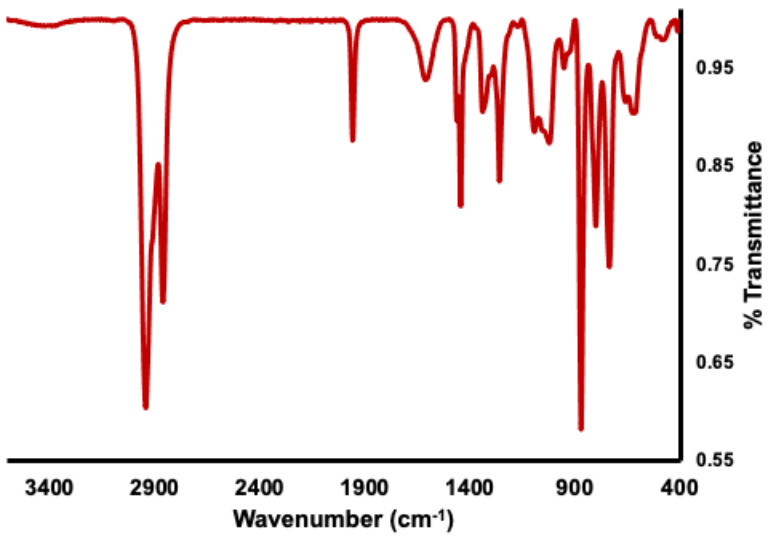

Figure 2.59: IR spectra of precipitated material from the multicomponent coupling control reaction depicting retention of the characteristic allene stretch (1959 cm^{-1}) in **2.9**.

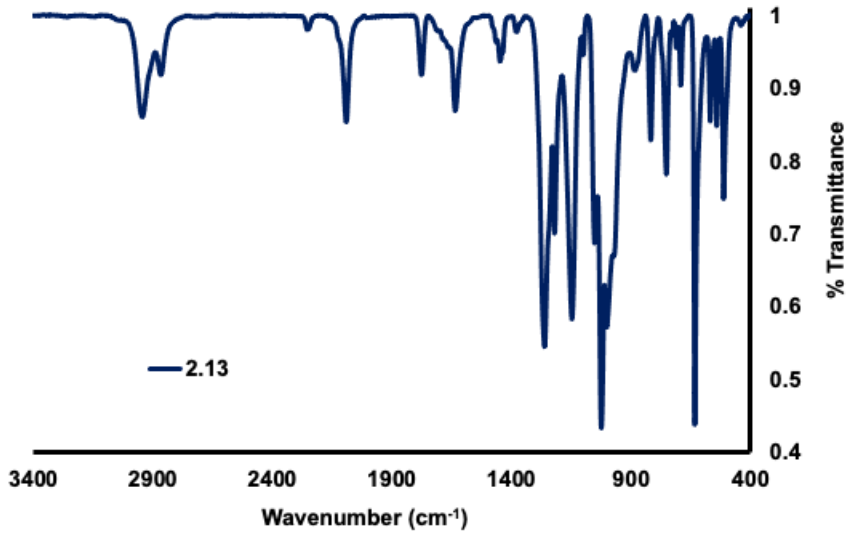

Figure 2.60: IR spectra of precipitated **2.13** material.

CHAPTER III: PRECISION SYNTHESIS OF TUNABLE POLYALLENAMERS FROM "MASKED" PRECURSORS

A version of this chapter was originally published by Nicholas J. Galan and Johnathan N. Brantley:

Galan, N. J., Brantley, J. N. *, Precision Synthesis of Tunable Polyallenamers from "Masked" Precursors. *Macromolecules.* **2023**, 305-310.

*corresponding author

In this article, I was responsible for designing and synthesizing all polymers studied. I also performed all polymer characterization, reaction optimization, fluorescence studies, and tensile testing experiments. Dr. Johnathan Brantley organized this project and facilitated the writing of the manuscript.

3.1 Abstract

Incorporating reactive functional groups within polymer matrices is a promising avenue toward achieving intrinsically tunable materials. Motifs that respond to external stimuli and/or participate in a diverse array of chemical transformations are particularly enabling in the context of designing multipurpose materials. For example, polyallenamers are an emerging class of materials that exhibit stimulus responsive behavior and are readily tailored through post-synthetic manipulations. Unfortunately, current synthetic methods for accessing these scaffolds suffer from poor control (either with respect to molecular weight or the preparation of more complex microstructures). Here, we report a new synthetic strategy that addresses these limitations by polymerizing "masked" allene precursors. Ring-opening metathesis polymerization (ROMP) of a *gem*-

dibromobicyclo[6.1.0]non-4-ene monomer, and a subsequent Skattebøl rearrangement, afforded the target polymers in good yields (85–88%; M_n = 7,900–55,000 Da). Saturated congeners of these materials, which exhibit structural homology to polyolefins, could also be prepared using a simple hydrogenation protocol. Solid films of this reduced material were susceptible to photochemical tuning of bulk mechanical properties (via network formation). Moreover, our saturated polymers were readily transformed into 1,8-octandioic acid (a valuable feedstock for polyesters) using a simple ozonolysis protocol. Finally, we could leverage our synthetic strategy to prepare discrete block-like copolymer architectures with controlled allene content.

3.2 Introduction

Post-synthetic modifications of soft materials are emerging as valuable strategies for accessing bespoke polymers. The prospect of building a library of precisely tailored materials from a single polymer is enticing, but this approach necessitates either bond activation (either C–H or C–C) or the preinstallation of reactive handles within the parent material. Indeed, both general strategies have been implemented in various polymer valorization efforts, such as upcycling and depolymerization. For example, C–H bond activations have been applied toward the direct chemical tailoring of various polyolefins (e.g., via installation of xanthyl groups,[17] olefins,[15] and alcohols[14,124]). Additionally, Mecking recently reported the syntheses of recyclable polyethylene-like materials containing hydrolytically unstable linking groups (e.g., esters).[27,125] Importantly, these reports have demonstrated that modest degrees of functional group incorporation can

change bulk material properties, which serves as a potent impetus to explore how other unique motifs can be installed (and chemically manipulated) within soft materials.

Inspired by these seminal efforts, we became keenly interested in leveraging allene-based motifs to access functional (and tunable) soft materials (Scheme 3.1). Allenes are emerging as powerful synthetic handles, and they participate in a diverse array of chemical transformations (e.g., hydroborations,[29] metal-catalyzed cycloadditions,[126] hydroacylations,[30] and others[127]). The application of these reactive motifs in soft material tailoring is enticing, given the significant expansion of post-polymerization modification space this could represent. Unfortunately, strategies for incorporating allenes within polymers are largely underdeveloped. This is due, in part, to the fact that allenes are prone to polymerization under a variety of conditions[36] (e.g., radical,[37] cationic,[39] anionic,[40] vinyl-addition[43,44,74]). However, there have been advancements in synthesizing macromolecules that retain cumulated bonds.[105] Indeed, Diederich,[51] Hasegawa,[53] and Kijima[50] have established that oligomeric allenes can be prepared through various cross-coupling strategies (Scheme 3.1). Our lab later showed that polyallenamers could be synthesized through backbone editing via the Skattebøl rearrangement (Scheme 3.1).[128] More recently, Bielawski[129] and Moore[130] disclosed that cyclic allenes could undergo ring-opening metathesis polymerization (ROMP) to afford polyallenamers. While these studies represent important synthetic advancements, they are not without their limitations (especially regarding molecular weight control and access to well-defined block copolymers). As such, new methods that can overcome these challenges are urgently needed.

Scheme 3.1: Syntheses of Polyallenamers

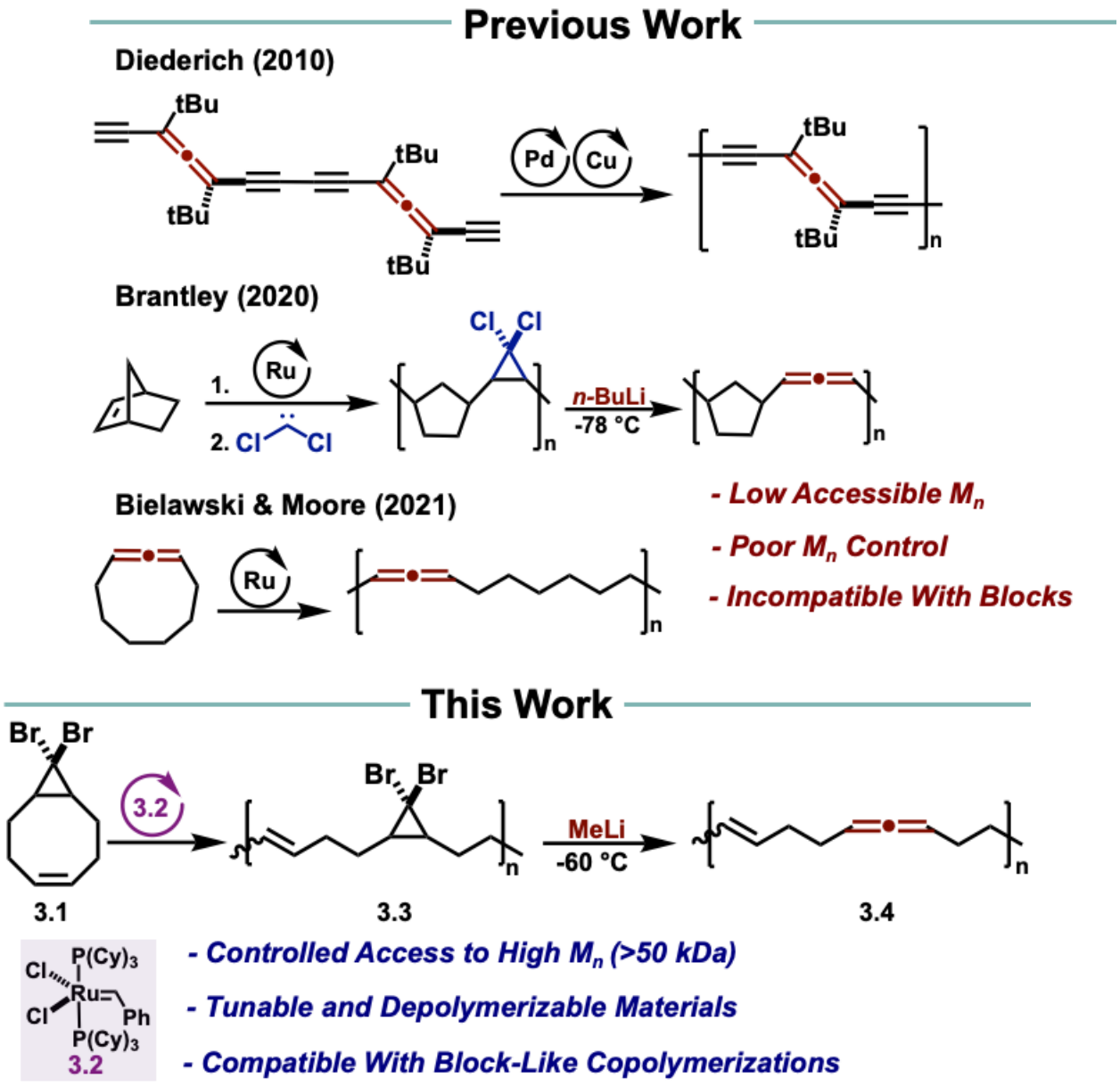

3.3 Results and Discussion

3.3.1 Initial Synthetic Optimization and Characterization of Polyallenamers

We envisioned that polymerizing a "masked" allene precursor could potentially circumvent many of the challenges associated with polyallenamer synthesis. Specifically, we hypothesized that pre-installation of a *gem*-dihalocyclopropane synthon within a judiciously chosen monomer (e.g., *gem*-dibromobicyclo[6.1.0]non-4-ene; **3.1**; Scheme 3.1)[131,132] would enable us to precisely control allene incorporation within a variety of (co)polymers. To explore this concept, **3.1** was synthesized according to previously reported[133] conditions (see experimental). With our target monomer in hand, we focused on ring-opening metathesis polymerization (ROMP) as a strategy for preparing both homopolymers and copolymers. A recent report by Wang and coworkers revealed that fused ring systems can promote reverse metathesis under the action of Grubbs' 2nd generation catalyst.[134] To avoid this deleterious reactivity (which could lead to oligomerization of **3.1**), our initial studies employed Grubbs' 1st generation catalyst (**3.2**). Gratifyingly, **3.1** readily polymerized under the action of **3.2** to afford the desired polymer, **3.3$_{DP}$** (where the subscript here and throughout denotes the degree of polymerization of the parent polymer in the synthetic sequence) as a tacky solid in good yield (87%; Table 3.1). Analysis by size-exclusion chromatography (SEC) revealed that the polymer, **3.3$_{55}$**, exhibited a number average molecular weight (M_n = 15,620 Da) in good agreement with the targeted value. Encouraged by this result, we prepared materials exhibiting a range of molecular weights (**3.3$_{41}$** – **3.3$_{453}$**; Table 3.1). Consistent with Wang's report, polymerization of **3.1** with the 2nd generation Grubbs

Table 3.1: Molecular Weight Data for **3.3$_{DP}$**

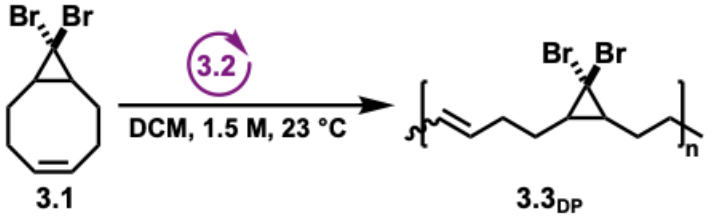

Entry	**3.3$_{DP}$**	[**1**]$_0$	Time (h)	M_n^{theo} (Da)[a]	M_n^{expt} (Da)[b]	Đ[c]	Yield (%)
1	**3.3$_{41}$**	1.5	0.75	10,000	11,600	1.75	90
2	**3.3$_{55}$**	1.5	0.75	15,000	15,600	1.88	87
3	**3.3$_{110}$**	1.5	0.75	30,000	30,800	1.76	79
4	**3.3$_{201}$**	1.5	0.75	46,000	56,500	1.86	88
5	**3.3$_{392}$**	1.5	1	115,000	110,000	1.76	89
6	**3.3$_{429}$**	1.5	1	120,000	120,300	1.71	85
7	**3.3$_{453}$**	1.5	1	150,000	126,900	1.89	73

[a]Calculated using [**3.1**]$_0$:[**3.2**]$_0$×280. [b]Measured by SEC (triple detection) and rounded. [c]Calculated using M_w/M_n.

catalyst resulted in lower yields (<70%) and significant oligomerization (as determined by SEC; Figure 3.4).

Having prepared our precursor polymers, we next evaluated Skattebøl conditions to access the desired polyallenamers. As alkyllithiums have recently been shown to react with allylic protons in polymer matrices,[135] we initially hypothesized that the olefins throughout **3.3$_{DP}$** could hinder the Skattebøl rearrangement. To explore this, **3.3$_{55}$** was treated with MeLi (5 equiv.) at -78 °C for 5 h, which yielded a tacky material (80% yield). ^{1}H NMR spectroscopic analysis of the isolated polymer revealed incomplete conversion to the allene (~82%), and new broad signals in the alkyl region (δ = 1.21 – 1.54 ppm; Figure 3.5) were observed (which we attributed to network formation). Reducing the amount of MeLi used during the Skattebøl rearrangement, however, appeared to mitigate this issue. Indeed, treatment of **3.3$_{55}$** with 1.5 equivalents of MeLi for 5 h resulted in ~90% conversion to the desired polyallenamer, **3.4$_{DP}$** (Scheme 3.1). ^{1}H and ^{13}C NMR spectroscopic analysis revealed new vinyl and allenic carbon resonances (δ = 5.09 ppm, and 204.05 ppm, respectively; Figures 3.34, and 3.35) that were consistent with our target material. With optimized conditions in hand, our **3.3$_{DP}$** materials were smoothly converted to the corresponding polyallenamers (**3.4$_{DP}$**) in good yields and conversions (Table 3.2). These materials also exhibited photoluminescent properties consistent with previous reports (Figure 3.23 – 3.24),[128,130] could be thermally crosslinked above 100 °C (Figure 3.6), displayed good thermal stability (Figure 3.6), and demonstrated good oxidative stability in solution (Figure 3.7).

Table 3.2: Molecular Weight Data for **3.4$_{DP}$**

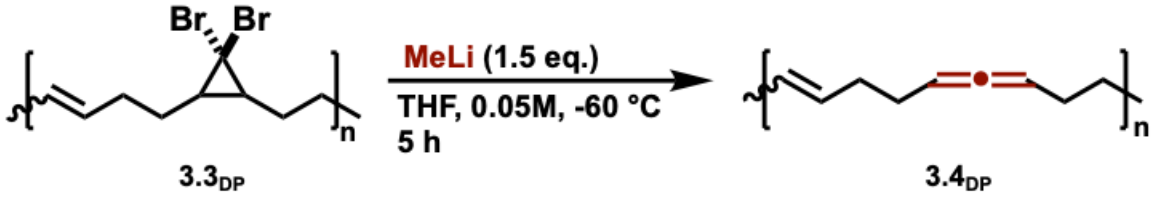

3.3$_{DP}$ **3.4$_{DP}$**

Entry	**3.3$_{DP}$**	**3.4$_{DP}$**	M_n (Da)[a]	Đ[b]	Allene (%)[c]	Yield (%)
1	**3.3$_{55}$**	**3.4$_{55}$**	7,900	1.85	94[c]	85
2	**3.3$_{110}$**	**3.4$_{110}$**	12,800	1.97	95[c]	87
3	**3.3$_{429}$**	**3.4$_{429}$**	55,400	2.24	96[c]	87

[a]Measured by SEC (triple detection). [b]Calculated using M_w/M_n. [c]Determined via ^{1}H NMR spectroscopy.

3.3.2 Synthesis of Block-Like Copolymers

Encouraged by this success, we turned our attention toward the challenge of accessing polyallenamer block copolymers. Block copolymer architectures often exhibit distinct (and desirable) physical properties when compared to their constituent homopolymers (e.g., due to microphase-separation[136]). Unfortunately, the established protocols for preparing polyallenamers are not compatible with block copolymer syntheses (either due to stochastic reactivity during the cyclopropanation step of our original Skattebøl route,[128] or poor stability of the Ru vinylidene generated during ROMP of cyclic allenes[129,130]). However, we surmised that our current strategy could overcome these obstacles. To demonstrate this concept, we attempted to prepare a block copolymer through sequential addition of **3.1** and *cis*-cyclooctene (COE). We first polymerized **3.1** (150 mg, 1M DCM) under the optimized conditions described above (Figure 3.1). An aliquot (~45 μL) was removed after 45 min and quenched with excess ethyl vinyl ether (10 μL). Subsequent ^{1}H NMR spectral analysis confirmed the complete consumption of **3.1**, and SEC analysis of the sample (M_n^{expt} = 19 kDa) closely matched the target value (M_n^{theo} = 15 kDa). COE (494 mg, 1.5 M in DCM) was subsequently added to the polymerization reaction and allowed to react for 1 h. The viscous mixture was then quenched with a 0.66 M solution of ethyl vinyl ether in DCM (3.2 mL). The new copolymer, **3.5**, was isolated by filtration following precipitation from MeOH. Successful COE incorporation was supported by SEC analysis (Figure 3.1), which revealed the copolymer exhibited an M_n that that closely matched the expected value (c.f., M_n^{expt} = 66 kDa versus M_n^{theo} = 65 kDa). Furthermore, ^{1}H NMR spectroscopy revealed the relative composition of the copolymer

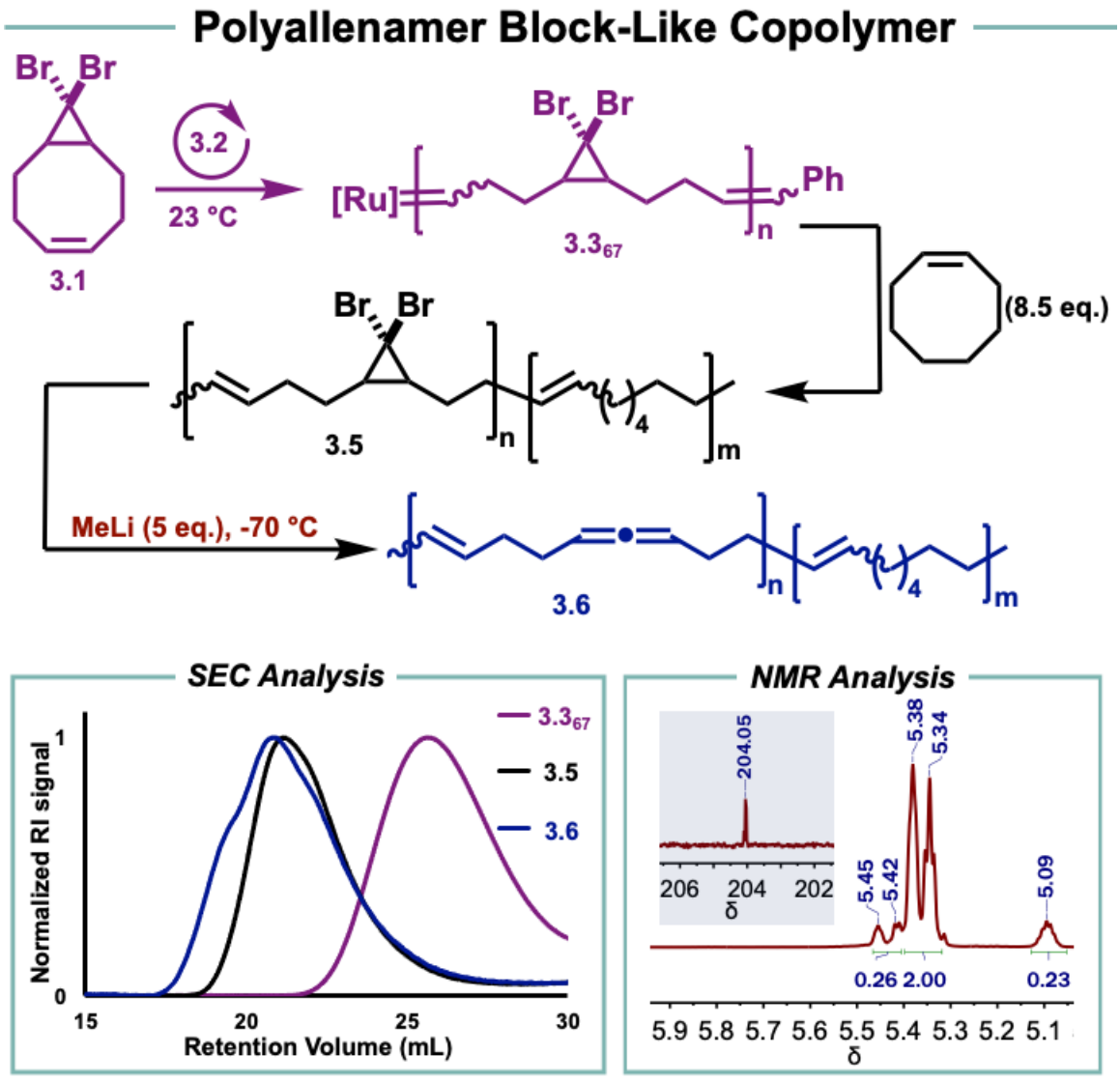

Figure 3.1: Polyalleneamer copolymer synthesis. SEC analysis was consistent with chain extension following addition of COE. Characteristic allene resonances were observed in the ^{1}H (δ = 5.09 ppm) and ^{13}C (δ = 203.96 ppm; blue inset) NMR spectra of the final copolymer (**3.6**).

was ~12:88 (**3.1**:**COE**), which was in excellent agreement with the targeted composition (**3.1**:**COE** = 10:90). With **3.5** in hand, we subjected the material to Skattebøl conditions (5 equiv.[137] MeLi; THF; -70 °C; 5 h) and quenched with excess MeOH to afford **3.6** (M_n = 56 kDa, Đ = 2.55; Figure 3.1). To our delight, characteristic allene resonances were observed in the ^{1}H (δ = 5.09 ppm) and ^{13}C (δ = 204.05 ppm) NMR spectra of **3.6** (Figure 3.1), and integration of the new proton resonances was consistent with ~90% conversion from **3.5**. Taken together, these data suggest that our methodology could provide unprecedented access to polyallenamer block-like copolymers.

3.3.3 Synthesis of Polyallenamers from Reduced 3.3$_{DP}$

We also explored saturated congeners of **3.3$_{DP}$**, given that these polyolefin homologues could simplify characterization for subsequent reactivity studies. We initially pursued catalytic hydrogenation strategies, since alternative methods (such as hydrazide reductions[138]) typically require harsh conditions that could promote ring-opening of the *gem*-dibromocyclopropanes in **3.3$_{DP}$**.[139] Crabtree's catalyst (**3.7**) immediately attracted our attention, as it exhibits excellent functional group tolerance, high activity at low loadings (2-0.5 mol%),[140] and has been used to reduce polymeric substrates.[141] Unfortunately, hydrogenation of **3.3$_{535}$** (14.7 psi H_2; 0.5 mol% **3.7**) only reached ~8% conversion after 18 h (Figure 3.9). Following a brief optimization study, we found that hydrogenations conducted at higher H_2 pressures (i.e., 600 psi; 0.5 mol% **3.7**)[142] afforded the best conversions while avoiding putative chain scission.[143–145] Gratifyingly, treatment of our **3.3$_{DP}$** materials under these conditions afforded near quantitative olefin hydrogenation (> 95% by ^{1}H NMR spectroscopy). The resulting polymers, **3.8$_{DP}$**, were isolated in good yield

(83 – 93%; Table 3.3). With these **3.8$_{DP}$** materials in hand, we found that our original[128] Skattebøl reaction conditions (5 equiv. MeLi; -78 °C; 5 h) furnished the desired polyallenamers, **3.9$_{DP}$** in excellent yields (89 – 99%; Table 3.4). ^{1}H and ^{13}C NMR spectral analyses of **3.9$_{DP}$** were consistent with the expected allene proton and carbon resonances (δ = 5.06 ppm and 203 ppm, respectively; Figures 3.42 and 3.43).[146] We also found that backbone saturation significantly impacted the intrinsic viscosity ([η]) of our polyallenamers. For example, while **3.9$_{392}$** exhibited [η] = 0.74 dL/g (as determined by SEC), **3.4$_{392}$** exhibited [η] = 1.39 dL/g. The lower [η] of **3.9$_{DP}$** could reflect this material's propensity to adopt a more tightly coiled conformation than **3.4$_{DP}$** (a consequence of chain rigidification from the olefin in the latter). This conclusion was also supported by Mark-Houwink analyses, which revealed that **3.9$_{DP}$** was indeed higher density than **3.4$_{DP}$**. It is also worth noting that the [η] of **3.4$_{DP}$** closely resembles that of polyoctenamer ([η] ~ 1.21 dL/g) (Figure 3.47), which suggests that olefins may have a more substantial impact on chain entanglement than allenes.

3.3.4 Solid-State Photochemical Crosslinking

As we previously demonstrated that polyallenamers are susceptible to photochemical crosslinking in solution,[128,147] we became intrigued by the prospect of exploiting analogous reaction manifolds in solid films. We hypothesized that photochemical crosslinking in the solid state would allow us to reinforce the film through putative [2+2] cycloadditions (thereby modulating bulk thermomechanical properties). Importantly, we surmised that we could potentially tailor bulk properties by controlling the duration of photoexposure. To explore this concept, solid films of **3.9$_{453}$** were cast from

Table 3.3: Molecular Weight Data for **3.8$_{DP}$**

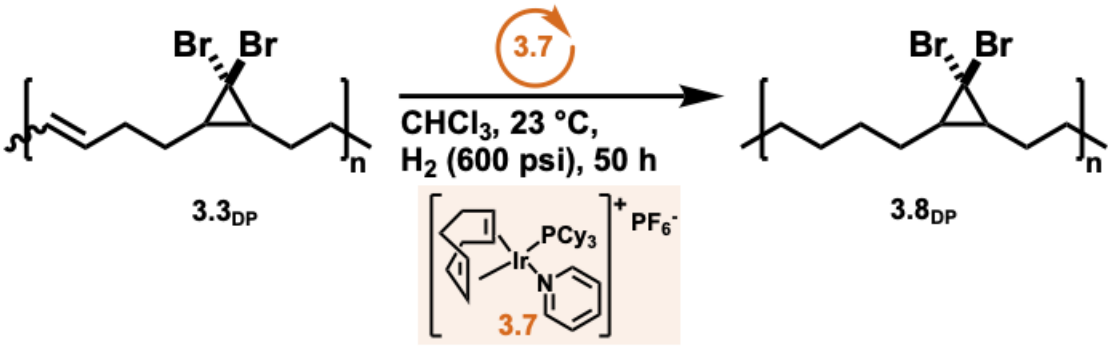

Entry	**3.3$_{DP}$**	**3.8$_{DP}$**	M_n (Da)[a]	Đ[b]	[H] (%)[c,d]	Yield (%)
1	**3.3$_{41}$**	**3.8$_{41}$**[e]	11,900	1.80	>99[d]	86
2	**3.3$_{55}$**	**3.8$_{55}$**[e]	15,500	1.73	>99[d]	96
3	**3.3$_{201}$**	**3.8$_{201}$**	57,700	1.88	95[d]	83
4	**3.3$_{392}$**	**3.8$_{392}$**	105,700	1.84	97[d]	92
5	**3.3$_{453}$**	**3.8$_{453}$**	132,100	1.77	99[c]	93

[a]Measured by SEC (triple detection). [b]Calculated using M_w/M_n. [c]Determined using ^{1}H NMR spectroscopy (mesitylene as an external standard). [d]Back calculated by comparing residual olefin and allene proton resonances in **3.9$_{DP}$**. [e]Reduced using Adam's catalyst (PtO_2).

Table 3.4: Molecular Weight Data for **3.9_{DP}**

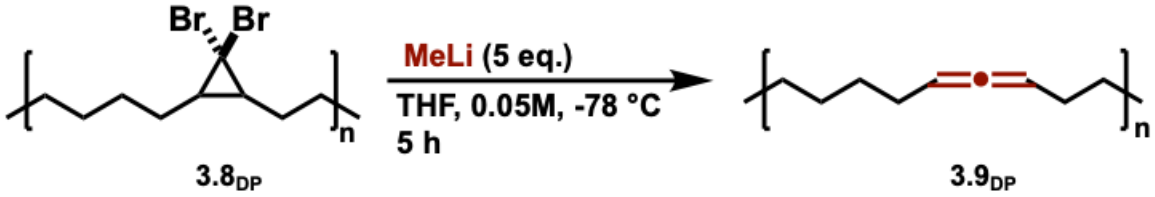

3.8_{DP} 3.9_{DP}

Entry	3.8_{DP}	3.9_{DP}	M_n (Da)[a]	Đ[b]	Allene (%)[c]	Yield (%)
1	3.8_{41}	3.9_{41}	5,500	1.91	99	95
2	3.8_{55}	3.9_{55}	8,000	1.71	99	98
3	3.8_{201}	3.9_{201}	23,800	2.01	>95	89
4	3.8_{392}	3.9_{392}	50,300	1.87	>95	99
5	3.8_{453}	3.9_{453}	78,900	2.07	>95	98

[a]Measured by SEC (triple detection). [b]Calculated using M_w/M_n. [c]Determined via integration of the allene vinyl resonances relative to the *gem*-dihalocyclopropane proton resonances.

$CHCl_3$ and irradiated (λ = 254 nm) for either 24 h or 48 h (under an N_2 atmosphere). The samples were then subjected to a uniaxial tension test using a dynamic mechanical analyzer (See experimental). Gratifyingly, we found that doubling the irradiation time resulted in a nearly three-fold increase in the measured Young's moduli (c.f. 1.84 ± 0.20 MPa versus 5.09 ± 0.38 MPa for 24 and 48 h irradiation time, respectively; Figure 3.2). Similar trends were observed using lower M_n samples. For example, solid films of **3.9$_{336}$** were cast from $CHCl_3$ and irradiated as described above. Tensile testing revealed that increasing the irradiation time from 24 h to 48 h increased the measured Young's modulus from 1.32 ± 0.34 MPa to 4.60 ± 1.1 MPa. These proof-of-concept data suggest that judiciously selected photocuring conditions can be used to tailor the bulk properties of polyallenamers.

3.3.5 Oxidative Degradation of 3.9$_{DP}$

We also envisioned that our **3.9$_{453}$** materials could be susceptible to depolymerization by virtue of their main chain allene motifs. Intrinsic degradability is a highly desirable property for polyolefin surrogates, especially with regard to end-of-life fate and material recycling.[148,149] In an ideal scenario, polyolefin-like materials could be shunted into a closed-loop lifecycle (consider, for example, Mecking's recent reports detailing degradable polyethylene-like materials[27,125]). We hypothesized that oxidative allene cleavage (e.g., via ozonolysis) could facilitate depolymerization with concomitant formation of α,ω-dicarboxylic acids (e.g., **3.10**; Figure 3.3). As these byproducts are benign precursors to intrinsically biodegradable polyesters, we could effectively transform

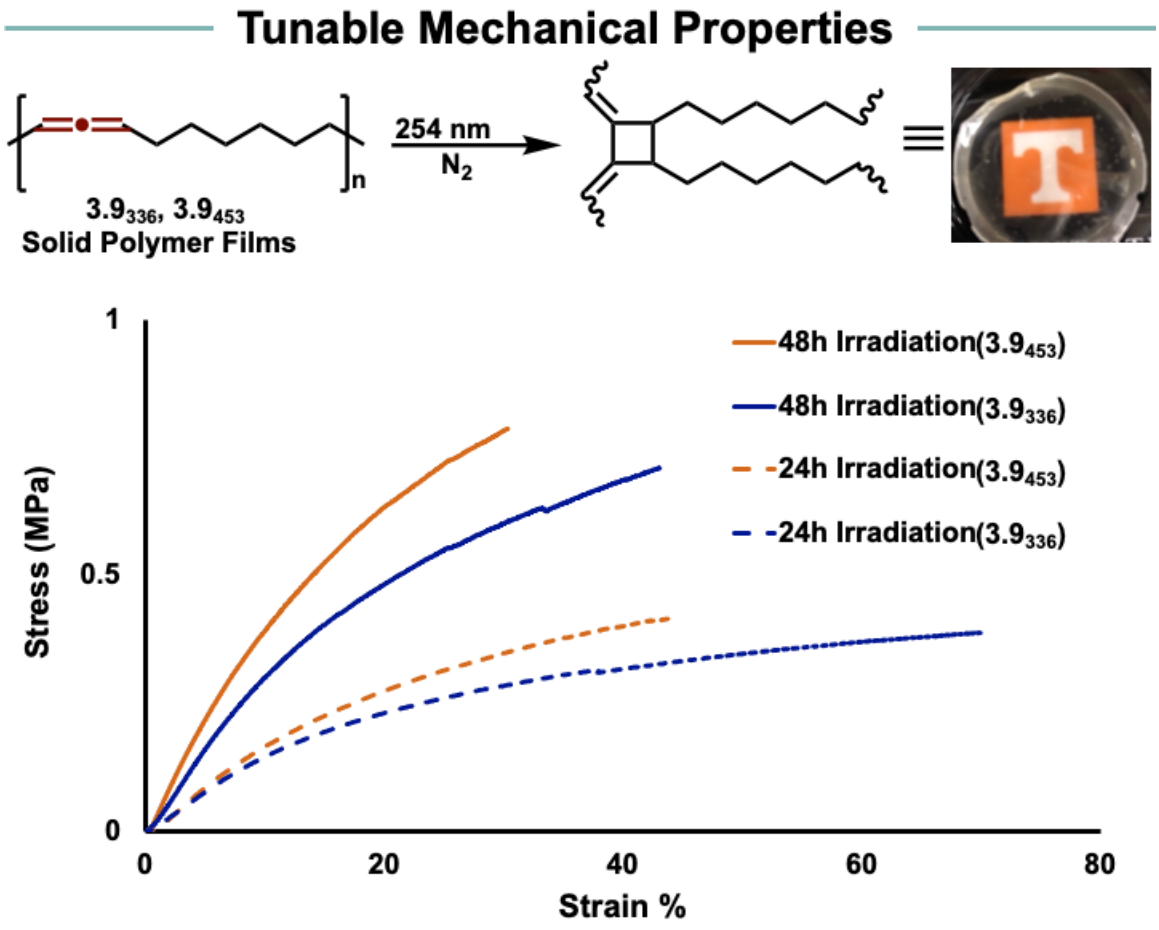

Figure 3.2: Idealized solid-state photochemical crosslinking scheme for **3.9**$_{336}$ and **3.9**$_{453}$ films. Inset shows free-standing film after 24 h irradiation. Representative Stress vs. Strain plots shown for films irradiated for 24 and 48 h.

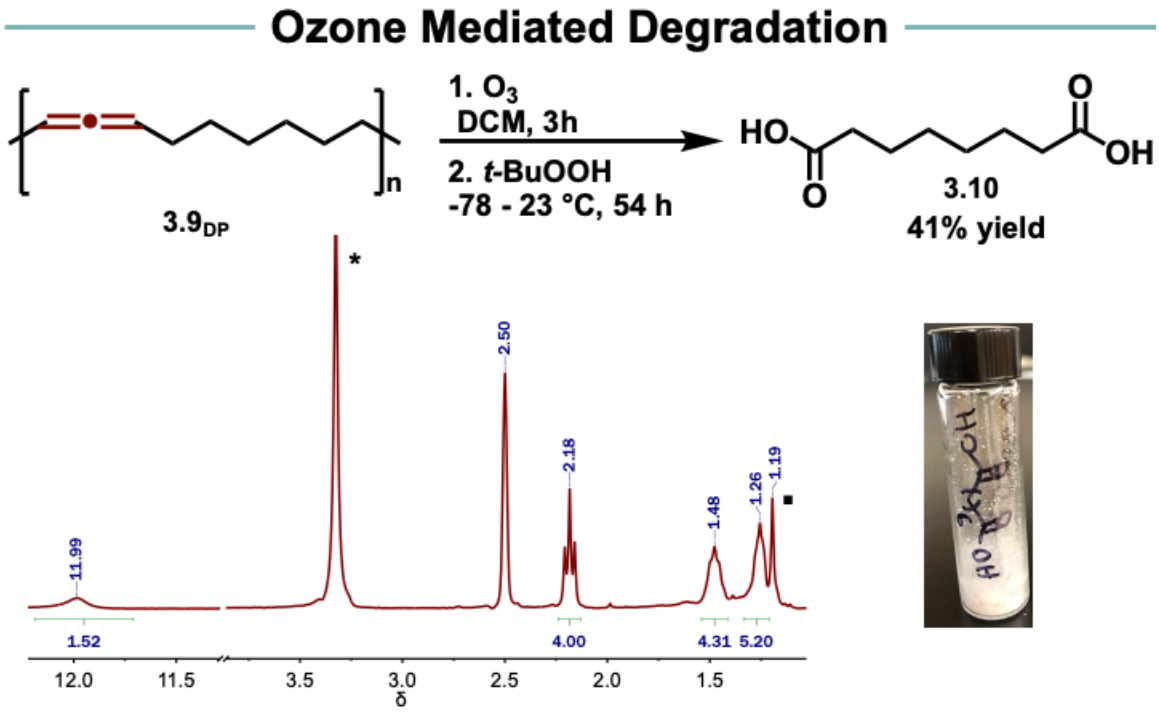

Figure 3.3: Ozone mediated degradation of **3.9**$_{55}$. Inset shows isolated recrystallized **3.10**. ^{1}H NMR of **3.10** in d_6-DMSO. * denotes residual H_2O; ▪ denotes residual impurity (attributed to formation of trace *tert*-butyl diester).

polyolefin congeners into a recyclable polyester feedstock using mild oxidants.[150] Furthermore, we surmised that the allene motifs in our materials would serve as critical handles for cleavage[151] (as ozonolysis of olefins in polymers results in a complex mixture of only partially degraded products[152–154]). In a proof-of-concept experiment, a solution of **3.9$_{55}$** (3.9 mg/mL in DCM) was treated with a stream of ozone at -78 °C for 3 h. *t*-Butyl hydroperoxide (2 equiv. relative to allene) was then added, and the reaction was slowly warmed from -78 to 23 °C (see experimental). Evaporation of the solvent followed by recrystallization from EtOAc:Hex (80:20 v/v) afforded **3.10** in modest yield (41%; Figure 3.3). The supernatant was analyzed by ^{1}H NMR spectroscopy and SEC, which suggested the remaining mass balance consisted of oligomeric species, residual **3.10**, and the *t*-butyl diester of **3.10** (Figure 3.16 – 3.17). While these conditions are unoptimized, these results indicate that mild conditions can be employed to transform allene-containing polyolefin congeners into valuable small molecule feedstocks.

3.4 Conclusion

The demand to access intrinsically tunable materials is rapidly growing. Here, we have disclosed an improved strategy to afford polyallenamers that can be tailored through various post-synthetic modifications. These materials can be accessed in good yield and conversion (>90%), and our synthetic method could be applied toward block-like copolymer preparation (which has defied synthetic logic). The mechanical properties of these materials could be tuned (e.g., through photomodulation of crosslink density), and they could undergo controlled depolymerization to afford diaicd monomers (thereby creating a pathway to transform our polyolefin congeners into recyclable polyesters). We

anticipate this work will serve as inspiration for future studies targeted toward intrinsically modifiable platforms.

3.5 Acknowledgements

This work was supported in part by the donors of the American Chemical Society Petroleum Research Fund and The University of Tennessee Science Alliance. I thank Natalie Parsons for synthetic assistance.

3.6 Experimental

3.6.1 General Materials and Methods

Unless otherwise noted, solvents were dried on an MBraun solvent purification system with 3 Å molecular sieves and degassed with three freeze-pump-thaw cycles. All other reagents were obtained from commercial sources and used without further purification. Oxygen and water sensitive manipulations were performed in a nitrogen filled MBraun glovebox or using standard Schlenk techniques. ^{1}H and ^{13}C NMR spectroscopic data were collected on a Varian 300 MHz NMR, a Varian 500 MHz NMR, or a Varian 600 MHz NMR spectrometer. Chemical shifts (δ) are reported in ppm using the residual solvent as reference. IR spectra were collected on a Bruker Alpha II FT-IR spectrometer with an ATR attachment (diamond crystal) for solid samples and a Transmission iD1 attachment with flow cell for liquid samples. UV-visible absorbance spectra were recorded using an Agilent Cary 100 series UV-Vis spectrophotometer and quartz cuvettes. Fluorescence emission spectra were recorded using an Agilent Cary Eclipse Fluorescence Spectrophotometer. Thermogravimetric analysis (TGA) was performed on a TA Instruments TGA Q500.

Dynamic Mechanical Analysis (DMA) data was collected on a TA instruments DMA Q800 with powder and film tension clamp attachments. Size Exclusion Chromatography (SEC) data were collected on an Omnisec Resolve and Omnisec Reveal Sytem using triple detection with detectors in series: UV, light scattering, viscometer, and refractive index and three Viscotek styrene divinylbenzene copolymer columns (in series T3000, T4000, and T5000) at a flow rate of 1 mL/min and thermostatted to 30 °C using tetrahydrofuran (THF) as the eluent. Molecular weight and dispersity data are from triple detection. dn/dc values were calculated assuming 100% mass elution.

3.6.2 Representative Synthesis of 3.1

A flame dried, 250 mL two-neck round bottom flask was charged with potassium *tert*-butoxide (KO*t*-Bu; 9.3 g; 83 mmol) and a Teflon stir bar under positive nitrogen flow. Hexanes (40 mL) and 1,5-cyclooctaidene (6.0 g; 55 mmol) were added via syringe, and the reaction vessel was cooled to 0 ºC. Bromoform ($CHBr_3$; 7.3 mL; 83 mmol) was then added dropwise via syringe over a period of 5 min. The resulting mixture was stirred for 24 h while slowly warming to room temperature. The reaction mixture was then diluted with DI H_2O (200 mL) and hexanes (20 mL). The organic phase was separated, and the aqueous phase was extracted with hexanes (2 x 20 mL). The combined organic layers were washed with DI H_2O (1 x 100 mL), brine (1 x 100 mL), dried over sodium sulfate, and filtered. The solvent was removed *in vacuo*, after which the crude product was dissolved in hexanes and passed through a plug of silica gel. Subsequent solvent removal and vacuum distillation (105 °C, at 1 mmHg) afforded **3.1** as a colorless oil (3.79 g, 25% yield). Spectral data were consistent with literature reports.[155] Representative spectral data are shown in Figure 3.31.

Scheme 3.2: Synthesis of **3.1**

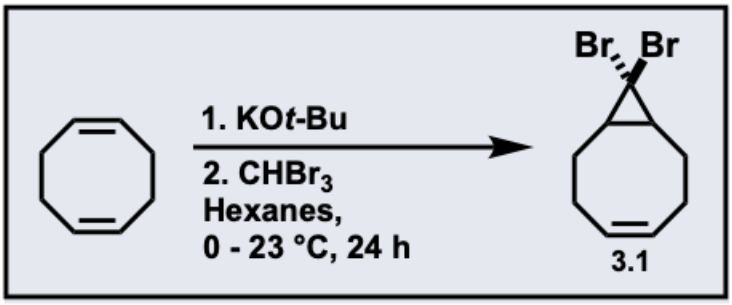

3.6.3 Polymerization of 3.1 with Grubbs 2nd Generation Catalyst

In an N_2 filled glovebox, **3.1** (280 mg; 1.00 mmol) was added to a 2-dram vial charged with a Teflon stir bar. DCM (3.5 mL) was added via syringe and the solution was stirred at 23 °C. In a separate 1-dram vial, Grubbs 2nd Generation catalyst (2.4 mg; 0.0028 mmol) was added and dissolved in DCM (0.5 mL). This freshly prepared catalyst solution was added to the DCM solution of **3.1** and stirred for 20 min at 23 °C. The polymerization was removed from the glovebox, quenched with excess ethyl vinyl ether (EVE) (1 mL; 10.5 mmol), and stirred for 45 min. The solution was concentrated to a minimal volume and added to stirring MeOH to precipitate any polymeric material. The supernatant was decanted, and the solid polymer was dried *in vacuo* (151 mg; 54% yield). Subsequent SEC analysis revealed significant formation of oligomeric species (Figure 3.4).

3.6.3 Polymerization of 3.1 with 3.2

Polymerization of **3.1** using Grubbs 1st Generation catalyst (**3.2**) was also explored. In an N_2 filled glovebox, **3.1** (290 mg; 1.036 mmol) was added to a 2-dram vial charged with a Teflon stir bar. DCM (0.3 mL) was added via syringe and the solution was stirred at 23 °C. In a separate 1-dram vial, **3.2** (5.3 mg; 0.0064 mmol) was added and dissolved in DCM (0.39 mL). This freshly prepared catalyst solution was added to the DCM solution of **3.1** and stirred for 45 min at 23 °C. The polymerization was removed from the glovebox, quenched with excess ethyl vinyl ether (EVE) (0.2 mL; 2.105 mmol), and stirred for 20 min. The solution was then diluted with DCM and passed through a short plug of basic alumina. The resulting solution was concentrated *in vacuo* and added to excess MeOH to precipitate any polymeric material. The supernatant was decanted, and the solid polymer

Scheme 3.3: Polymerization of **3.1** using Grubbs 2nd Generation Catalyst

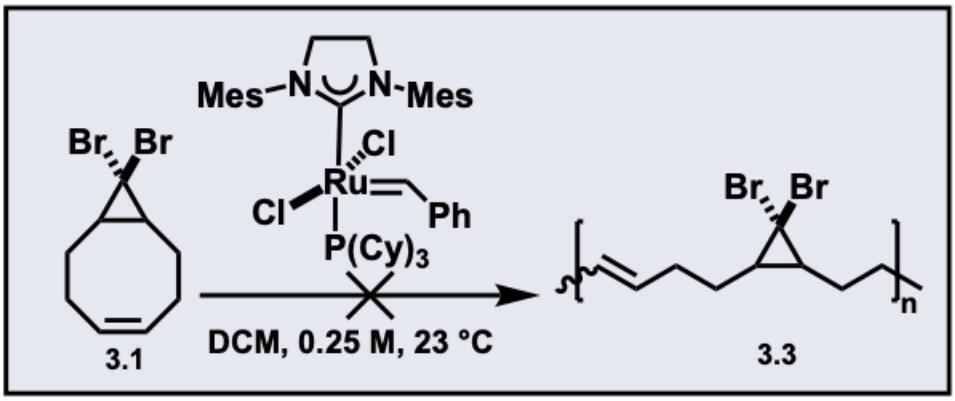

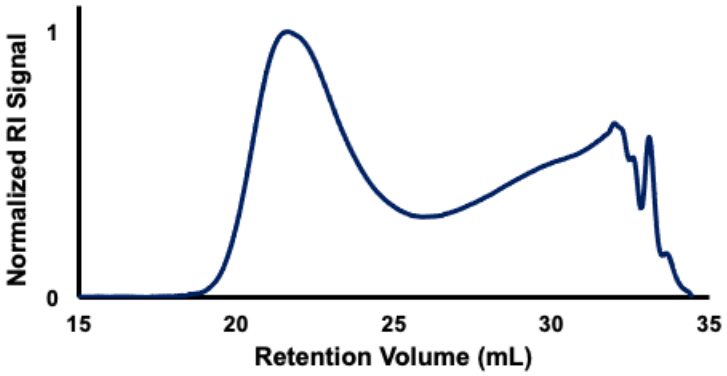

Figure 3.4: Representative SEC data for the polymerization of **3.1** with Grubbs 2nd generation catalyst (0.25 M).

was dried *in vacuo* for 2h (246 mg; 85% yield). Portions of the dried solid were analyzed using ^{1}H NMR spectroscopy and SEC; however, the bulk polymer was stored in DCM (10 mg/mL) to prevent physical crosslinking.[156] Spectral data for **3.3** were consistent with literature reports.[157] Varying molecular weights of **3.3** were prepared using this procedure (but changing the [**3.1**]$_0$:[**3.2**]$_0$ ratios; see Table 3.1 in the main text. To ensure reproducibility, two separate sets of **3.3$_{DP}$** materials (with varying M_n values; see Figure 3.18 & 3.19 for representative SEC data) were synthesized using the above protocol. Representative spectral data are shown in Figures 3.32 – 3.33 dn/dc = 0.109 mL/g

3.6.4 Representative Synthesis of 3.4$_{DP}$ Materials

In an N_2 filled glovebox, a 10 mL Schlenk flask was charged with **3.3$_{DP}$** (49.7 mg; 0.178 mmol), THF (3 mL), and a Teflon stir bar. The flask was sealed with a rubber septum, removed from the glovebox, and connected to a Schlenk line. The solution was cooled to -60 °C under N_2, and methyllithium (0.24 mL of a 1.1 M solution in Et_2O; 0.267 mmol; 1.5 equiv. per *g*DBC) was slowly added via gas-tight syringe over the course of 1 min. The resulting pale-yellow solution was then warmed with stirring to -50 °C over the course of 5 h. The reaction was then quenched with MeOH (0.3 mL; 7.42 mmol), concentrated *in vacuo,* and added to vigorously stirring MeOH to precipitate the polymeric product. The supernatant was decanted, and the solid polymer was dried *in vacuo* for 1 h (~18 mg; 87% yield). The bulk polymer was stored in DCM (9 mg/mL) for further use. Aliquots (0.2 mL) were removed and concentrated to dryness for NMR spectral and SEC analysis. Conversion was determined using the relative integrations of the allene (δ = 5.06 – 5.14 ppm) and olefin

Scheme 3.4: Representative Synthesis of **3.3$_{DP}$**

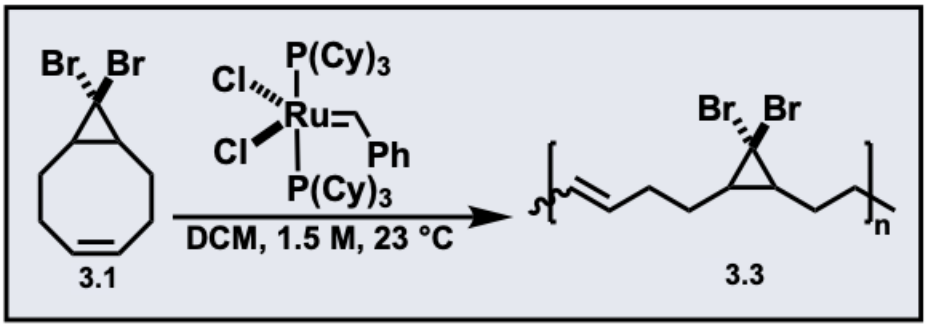

Scheme 3.5: Representative Synthesis of **3.4$_{DP}$**

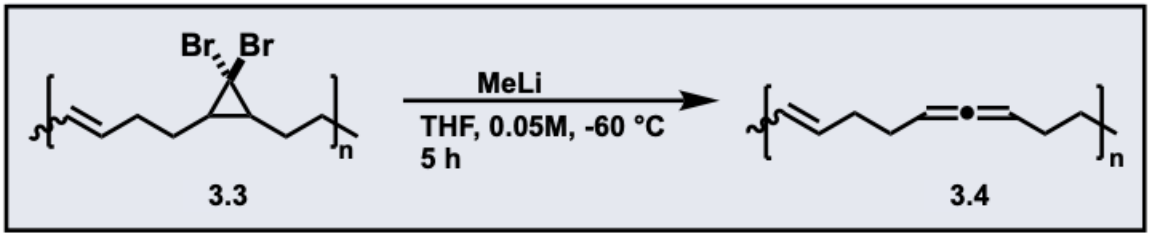

(δ = 5.39 – 5.48 ppm) ^{1}H NMR resonances (compared to the theoretical total). **^{1}H NMR (500 MHz, $CDCl_3$):** δ = 5.39-5.48(2H), δ 5.06-5.14(2H), δ 1.99-2.18(8H). **^{13}C NMR (126 MHz, $CDCl_3$):** δ = 204.05, 130.26, 129.69, 90.87, 32.39, 29.25, 27.17. Molecular weight data is given in Table 3.2. Representative SEC data for the isolated polymers are shown in Figure 3.20. Representative spectral data shown in Figures 3.34 – 3.35. dn/dc = 0.168 mL/g

We also explored the impact of additional equivalents of methyllithium (MeLi) on the Skattebøl step. In an N_2 filled glovebox, a 10 mL Schlenk flask was charged with **3.3_{DP}** (337 mg; 1.20 mmol), THF (23 mL), and a Teflon stir bar. The flask was sealed with a rubber septum, removed from the glovebox, and connected to a Schlenk line. The solution was cooled to -60 °C under N_2, and MeLi (3.38 mL; 1.6 M in Et_2O; 5 equiv. per *g*DBC) was slowly added via gas-tight syringe over the course of 1 min. The solution was kept at -50 °C for 5 h. The reaction was quenched with MeOH (0.3 mL; 7.42 mmol), followed by removal of solvent, and addition to stirring MeOH to precipitate polymeric material. The solid polymer was collected via filtration (80% yield), dried *in vacuo* for 1 h, and then analyzed by ^{1}H NMR spectroscopy. Incomplete conversion to the allene (~82%; Figure 3.5) was noted, and new broad signals in the alkyl region (Figure 3.5) were observed.

3.6.5 Thermal Crosslinking of 3.4_{DP}

A 1-dram vial was charged with **3.4_{DP}** (8.1 mg; 0.067 mmol), a Teflon stir bar, C_6D_6 (0.7 mL), and mesitylene (1.5 μL; 0.0107 mmol; added as an internal standard). The polymer solution was transferred to a J-young NMR tube and degassed via three cycles of freeze-pump-thaw. The solution was heated under the conditions specified in Figure 3.6 in the

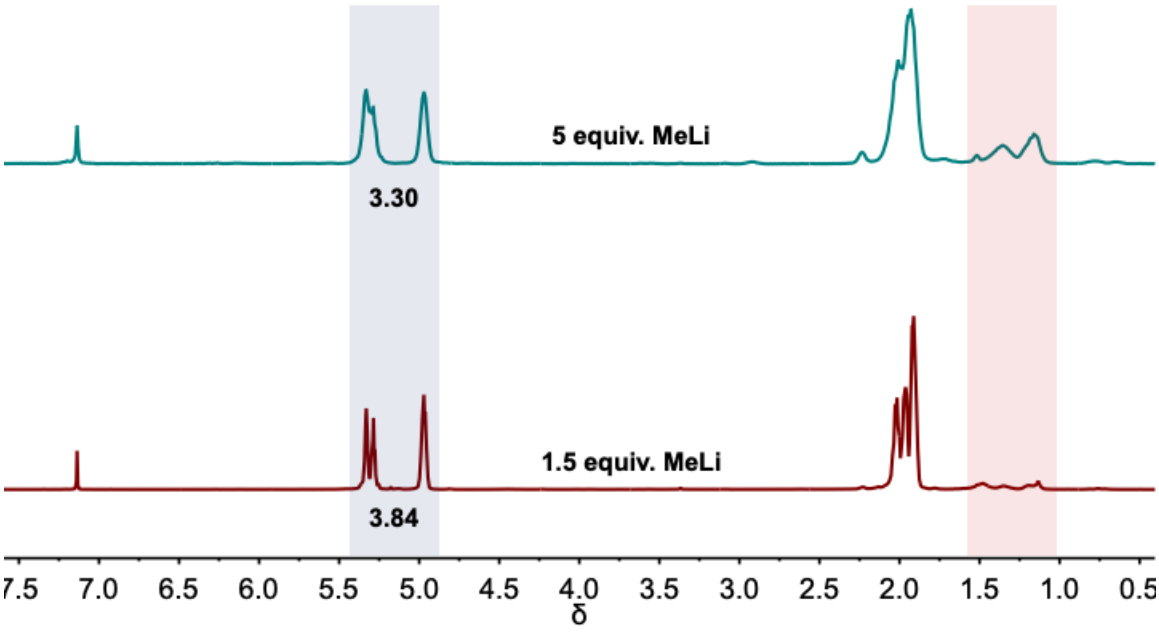

Figure 3.5: ^{1}H NMR spectra for **3.4$_{DP}$** prepared using 1.5 equiv. (bottom) and 5.0 equiv. (top) of MeLi. Combined allene and olefin integrations are shown (blue box; Note: the alkene proton resonances were set to 2, and the combined theoretical integration for allene/olefin should be 4 protons). New alkyl resonances are highlighted (red box).

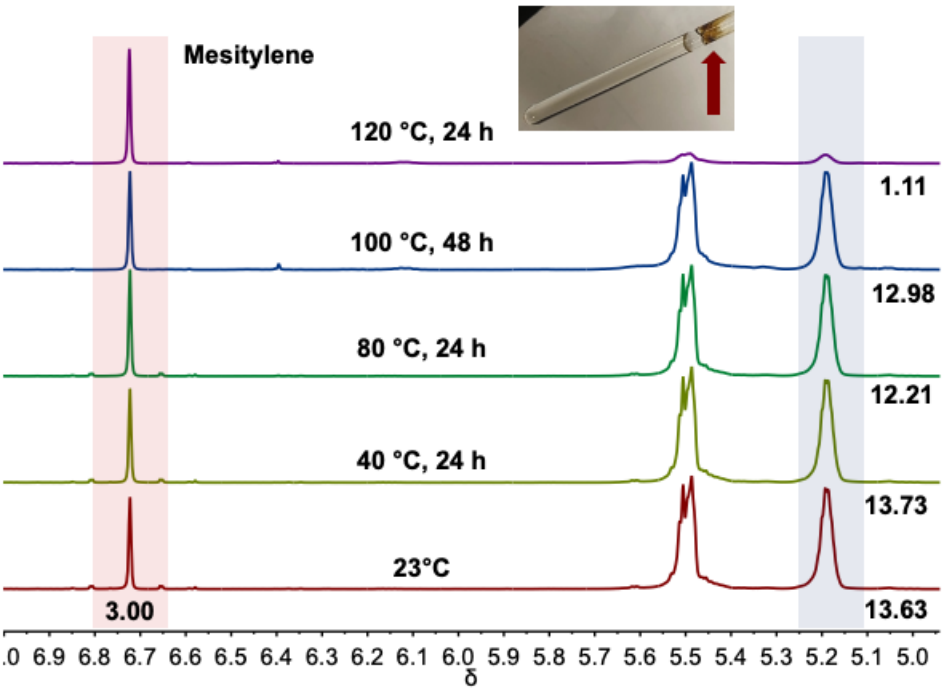

Figure 3.6: ^{1}H NMR spectrum ($CDCl_3$) of **3.4$_{DP}$** sample that was heated at varying temperatures. Mesitylene (red box) and allene resonances (blue box) are highlighted. Inset shows gelation within the J-young tube.

absence of light. Visible gelation occurred within the J-Young tube (Figure 3.6, inset) after heating at 120 °C for 24 h, which suggested significant network formation had occurred via thermal [2+2] cycloadditions.

3.6.6 O_2 Sensitivity (solution) of 3.4$_{DP}$

A 1-dram vial was charged with **3.4$_{DP}$** (14.4 mg; 0.12 mmol), $CDCl_3$ (0.7 mL), a Teflon stir bar, and mesitylene (1.5 μL; 0.0107 mmol; added as an internal standard). The polymer solution was transferred to a J-young NMR tube, degassed via three cycles of freeze-pump-thaw, and then placed under an O_2 atmosphere. The solution was allowed to equilibrate at 23 °C for 24 h prior to analysis by ^{1}H NMR spectroscopy (red spectra, Figure 3.7). The sample was then heated at 40 °C for 72 h. ^{1}H NMR spectroscopy revealed a slight decrease in allene and olefin content (green spectra, Figure 3.7). The sample was then heated at 80 °C for 48 hours. ^{1}H NMR spectroscopy revealed a further decrease in allene and olefin content (blue spectra, Figure 3.7).

3.6.7 Sample Preparation and Fluorescence Quenching Experiment of 3.4$_{DP}$

3.4$_{DP}$ polymer samples were dissolved in HPLC-grade $CHCl_3$ (~1 mg/mL) and transferred into a quartz cuvette. UV-vis absorbance (Figures 3.23) and fluorescence (Figure 3.24) spectra were collected.

A 3 mL (3 mg; 0.0246 mmol) aliquot was taken from a **3.4$_{DP}$** stock solution (1 mg/mL in HPLC $CHCl_3$) added to a quartz cuvette and analyzed by fluorescence spectroscopy (λ_{EX} = 350 nm; Figure 3.8, blue). Following irradiation, nitrobenzene (5 μL; 0.0492 mmol; 2 equiv. per allene unit) was added and the solution was thoroughly mixed for 1 minute. The

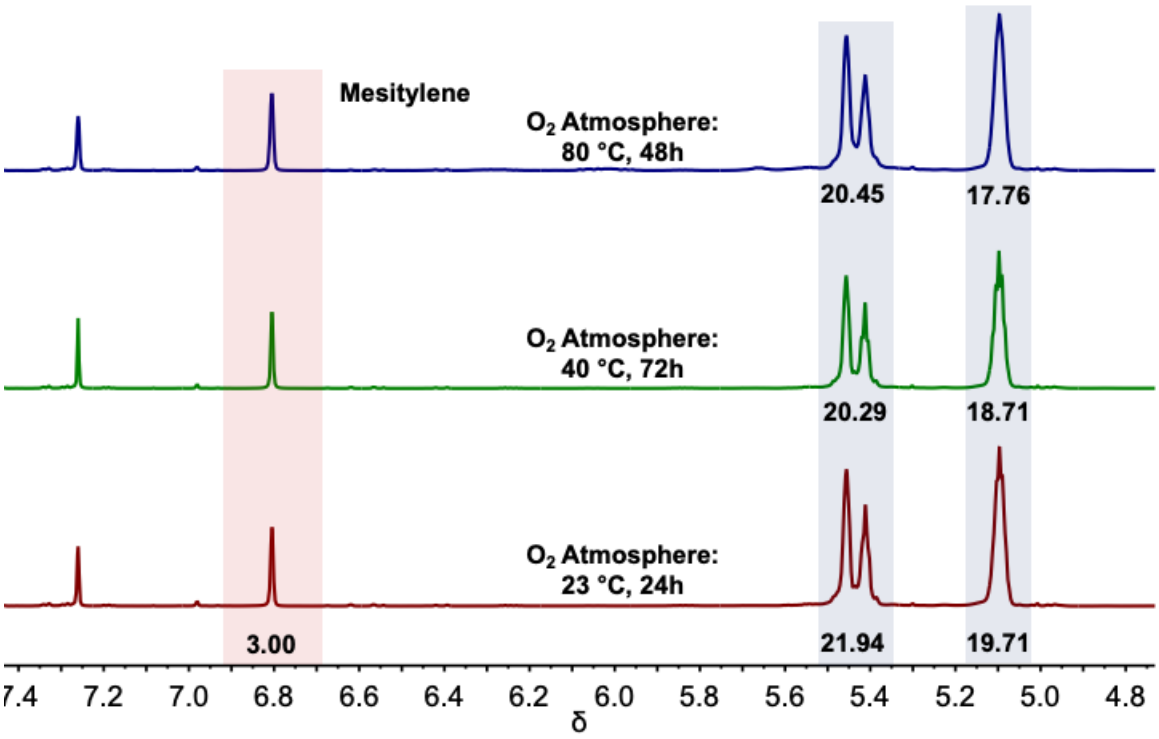

Figure 3.7: ^{1}H NMR spectra ($CDCl_3$) for O_2 sensitivity of **3.4$_{DP}$** after equilibration at 23 °C for 24 h under an O_2 atmosphere (bottom), heating at 40 ºC (middle), and heating at 80 ºC (top). Mesitylene (red box), and allene/olefin (blue boxes) resonances are highlighted.

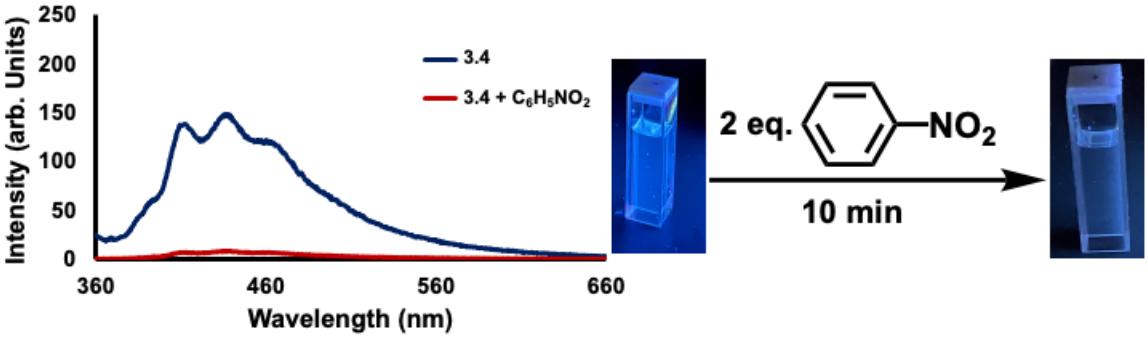

Figure 3.8: Fluorescence spectra of **3.4$_{DP}$** before and after addition of nitrobenzene ($CHCl_3$, 1 mg/mL). Photographs showing **3.4$_{DP}$** before (left) and after (right) addition of nitrobenzene.

mixture was subsequently analyzed by fluorescence spectroscopy, which revealed quenching of fluorescence (Figure 3.8, red). Photographs of the samples (irradiated with a 350 nm lamp) are shown in Figure 3.8.

3.6.8 Photochemical Crosslinking of 3.4$_{DP}$

A J-young tube was charged with a d_8 – THF (0.7 mL) solution of **3.4$_{DP}$** (15 mg; 0.125 mmol) and mesitylene (1.5 μL; 0.0107 mmol; as an internal standard). The solution was degassed via three cycles of freeze-pump-thaw and placed under an N_2 atmosphere. The sample was analyzed by ^{1}H NMR spectroscopy and then placed in an enclosed photoreactor (consisting of 4 bulbs orthogonally arranged) and irradiated with 254 nm light for 7 days (note: the temperature inside the reactor did not exceed 40 °C). Complete gelation of the sample was observed, which precluded further analysis by ^{1}H NMR spectroscopy (Scheme 3.6, inset).

3.6.9 Procedure for Polyallenamer Block-Like Copolymer Synthesis

In an N_2 filled glovebox, **3.1** (150 mg; 0.535 mmol) was added to a 2-dram vial charged with a Teflon stir bar and stirred at 23 °C. In a separate 1-dram vial, **3.2** (8.15 mg; 0.0099 mmol) was added and dissolved in DCM (0.53 mL). This freshly prepared catalyst solution was added to the solution of **3.1** and stirred for 45 min at 23 °C. After which an aliquot (~45 μL) was removed, quenched with excess EVE (10 μL; 0.105 mmol) and diluted with $CDCl_3$ (0.65 mL). Complete consumption of **3.1** was confirmed by ^{1}H NMR spectroscopy, and subsequent SEC analysis revealed the number average molecular weight (M_n) of the formed polymer was ~19 kDa (**3.3$_{67}$**; Table 3.5). A DCM solution (2.3 mL) of COE (494

Scheme 3.6: Photochemical Crosslinking of **3.4$_{DP}$**

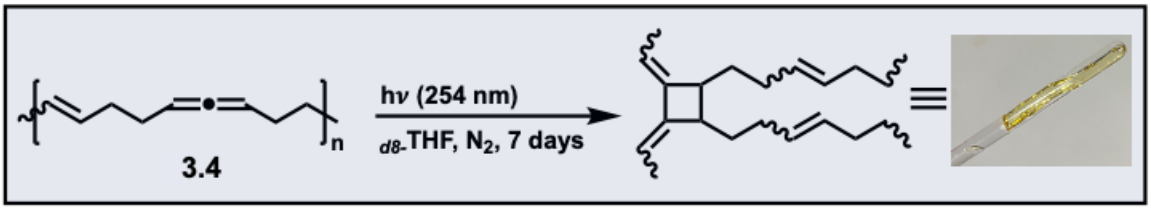

Scheme 3.7: Representative Synthesis of **3.5**

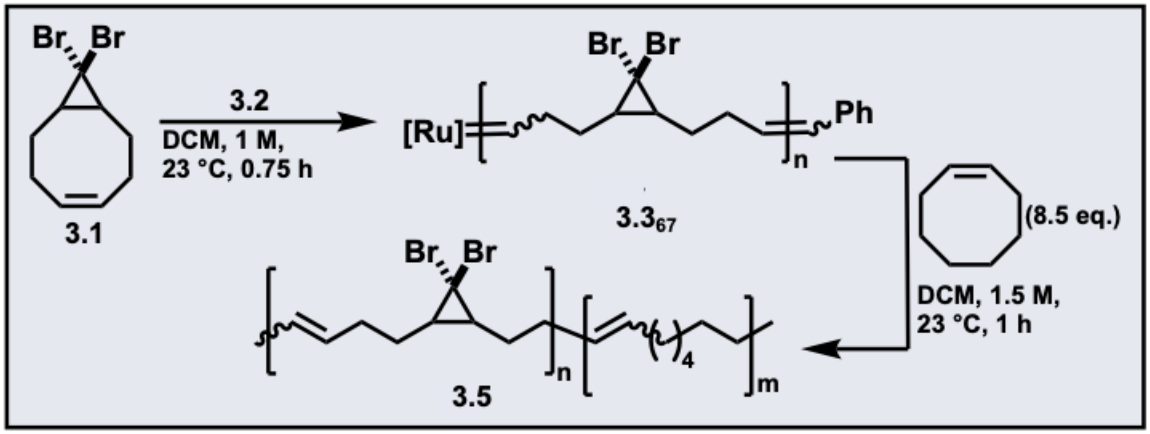

mg; 4.49 mmol) was added to the polymerization reaction and stirred for 1 h. The bulk polymerization was removed from the glovebox after 1h, diluted with DCM (3 mL), quenched with EVE (0.2 mL; 2.105 mmol) and stirred for 30 minutes. The solution was added to excess MeOH to precipitate polymeric material. The supernatant was decanted, and the solid polymer was dried *in vacuo* for 1 h. The solid polymer was redissolved in DCM (10 mL) and passed through a short plug of basic alumina. The polymer solution was then concentrated and added to excess MeOH to precipitate polymeric product. The solid polymer, **3.5**, was collected by filtration and dried *in vacuo* for 2h (543 mg; 84% yield). Portions of the dried solid were used for NMR spectral and SEC analysis; however, the bulk polymer was stored in the glovebox as a solution in THF (53 mg/mL) to use for subsequent Skattebøl reactions. Molecular weight data for **3.5** is given in Table 3.5. Representative SEC data for **3.5** is shown in Figure 3.1 in the main text. Representative spectral data are shown in Figures 3.36 – 3.37. dn/dc = 0.098 mL/g

3.6.10 Procedure for Conversion of 3.5 into 3.6

In an N_2 filled glovebox, a 25 mL Schlenk flask was charged with 1 mL of **3.5** (53 mg; 0.447 mmol total; 0.0227 mmol *g*DBC repeat) stock solution, THF (7.5 mL), and a Teflon stir bar. The flask was sealed with a rubber septum, removed from the glovebox, and connected to a Schlenk line. The solution was cooled to -70 °C under N_2, and MeLi (0.10 mL of a 1.1 M solution in Et_2O; 0.114 mmol; 5 equiv. per *g*DBC) was slowly added via gas-tight syringe over the course of 1 min. The resulting pale-yellow solution was warmed with stirring to -50 °C over the course of 5 h. The reaction was quenched with MeOH (0.2 mL; 4.94 mmol), concentrated *in vacuo*, and added to vigorously stirring MeOH to

Scheme 3.8: Representative Synthesis of **3.6**

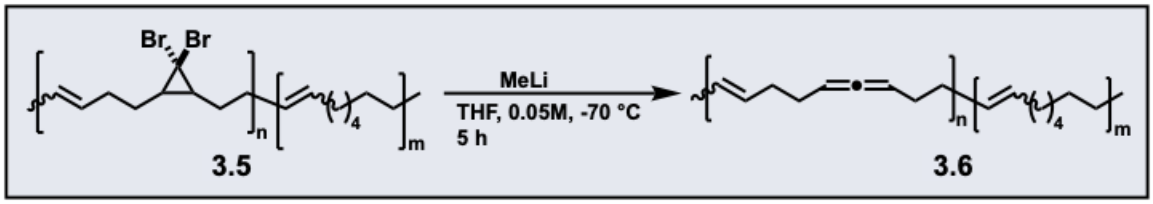

Table 3.5: Molecular Weight Data for **3.3$_{67}$**, **3.5**, and **3.6** materials (Triple Detection)

Entry	Polymer	M_n^{expt} (Da)	M_n^{theo} (Da)	Đ	Yield (%)
1	3.3$_{67}$	19,300	15,000	1.72	--
2	3.5	66,500	65,000	1.57	84
3	3.6	56,300	55,900	2.55	72

precipitate any polymeric product. The supernatant was decanted, and the solid polymer, **3.6**, was dried *in vacuo* for 1.5 h (35 mg; 72% yield) The bulk polymer was stored as a solution in DCM (9 mg/mL) for further use. Aliquots (0.2 mL) were removed and concentrated to dryness for NMR spectral and SEC analysis. Conversion was determined using the relative integrations of the allene (δ = 5.06 – 5.14 ppm) and olefin (δ = 5.39 – 5.48 ppm) ^{1}H NMR resonances (compared to the theoretical total). Molecular weight data for **3.6** is given in Table 3.5. Representative SEC data for **3.6** is shown in Figure 3.1. Representative spectral data are shown in Figures 3.38 – 3.39. dn/dc = 0.125 mL/g

3.6.11 Hydrogenation Optimization and Synthesis of 3.8$_{DP}$ Materials

A 2-dram vial was charged with **3.3$_{DP}$** (95.8 mg; 0.342 mmol), $CHCl_3$ (4 mL), and a Teflon stir bar. In a separate 1-dram vial, **3.7** (1.5 mg; 0.00188 mmol) was added and dissolved in $CHCl_3$ (0.5 mL). The freshly prepared catalyst solution was added to the solution of **3.3$_{DP}$**, the vial was sealed with a septa cap, punctured with two 18G needles. The vial was placed in a Parr reactor and secured in place with crumpled paper. The Parr reactor was sealed, placed behind a blast shield, purged with ultra-high purity H_2 for 30 seconds, and subsequently charged to 600 psi. The reaction was stirred for 50 h at 23 °C. The H_2 was vented, the solution was diluted with $CHCl_3$ (2 mL) and passed through a short plug of basic alumina. The solution was concentrated to dryness and the solid polymer was dried *in vacuo* for 4 h (89 mg; 92% yield). Portions were used for NMR spectral and SEC analysis; however, the bulk material was stored as a THF (~17 mg/mL) stock solution in an N_2 filled glovebox to use for subsequent Skattebøl chemistry. Conversion was determined by the integration of the olefinic region (δ = 5.40 - 5.60 ppm) against an

Scheme 3.9: Representative Synthesis of $\mathbf{3.8_{DP}}$

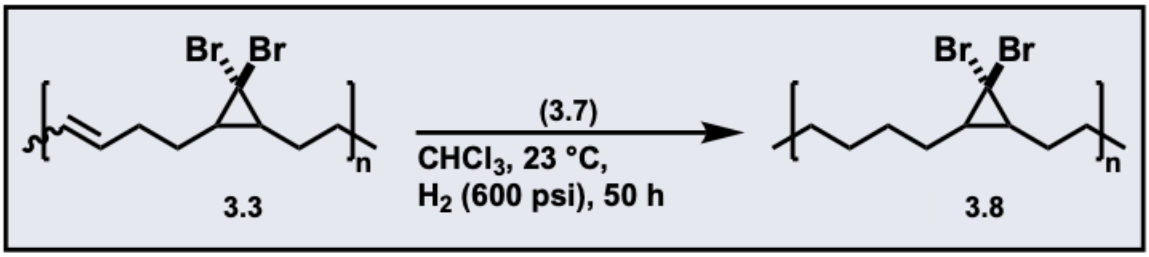

external standard, mesitylene. Conversion can also be determined post-Skattebøl rearrangement by integrating the allene resonance (δ = 5.06 ppm) against residual vinyl signals (δ = 5.40 - 5.60 ppm) of the **3.3$_{DP}$** polymer. Molecular weight data is given in Table 3.3 in the main text. Representative SEC data for the isolated polymers are shown in Figure 3.25. Representative spectral data shown in Figures 3.32 – 3.33. dn/dc = 0.095 mL/g

Lower molecular weight polymers (**3.3$_{41}$, 3.3$_{55}$**,) could be hydrogenated using Adam's catalyst (PtO_2, 20 mol%) under the same reaction conditions. These polymers are purified via dilution with $CHCl_3$, filtration through a 0.45 μm syringe filter, removal of solvent and precipitation from MeOH. Larger M_n polymers (> 25 kDa) reduced using Pd/C or PtO_2 required exceptionally long reaction times (>9 days) to achieve high conversions (~95%). Using 0.5 mol% of **3.7** with 14.7 psi of H_2 for 18 h resulted in poor reduction conversion (~8%; Figure 3.9). Increasing the H_2 pressure (150 psi; 0.25 mol% of **3.7**) for 33 h led to increased; however, incomplete conversion (~74%; Figure 3.10). Further increasing H_2 pressure (300 psi; 0.5 mol% of **3.7**) for 51 h led to higher conversion to the saturated product (~79%; Figure 3.11). We found that extended reaction times (72 hours) at higher H_2 pressure (700 psi; 0.5 mol% of **3.7**) led to an observed reduction in molecular weight (Figure 3.12) which was attributed to hydrogenolysis.

3.6.12 General Skattebøl Procedure for the Synthesis of 3.9$_{DP}$ Materials

In an N_2 filled glovebox, a 25 mL Schlenk flask was charged with 4.5 mL of the **3.8$_{DP}$** (77 mg; 0.27 mmol) stock solution, THF (0.1 mL), and a Teflon stir bar. THF (0.1 mL) The flask was sealed with a rubber septum and connected to a Schlenk line. The solution was

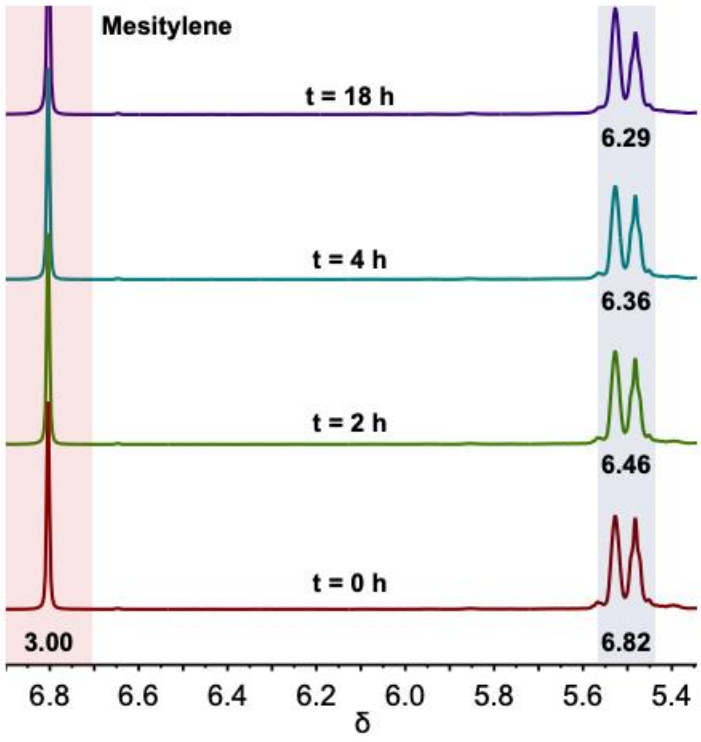

Figure 3.9: ^{1}H NMR ($CDCl_3$) spectra of 14.7 psi reduction of **3.3$_{DP}$**. Mesitylene (red box) and olefin resonances (blue box) highlighted. Time points and integrations listed.

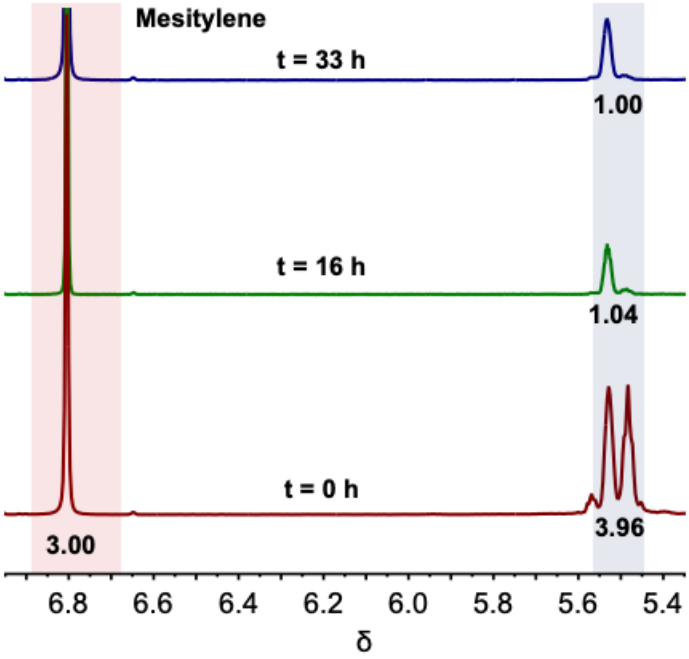

Figure 3.10: ^{1}H NMR ($CDCl_3$) spectra of 150 psi reduction of **3.3$_{DP}$**. Mesitylene (red box) and olefin resonances (blue box) highlighted. Time points and integrations listed.

cooled to -78 °C under N_2, and methyllithium (0.85 mL of a 1.6 M solution in Et_2O; 1.35 mmol; 5 equiv. per *g*DBC) was slowly added via gas-tight syringe over the course of 1 min. The resulting pale-yellow solution was then warmed with stirring to -70 °C over the course of 5 h. The reaction was quenched with MeOH (0.3 mL; 7.42 mmol), concentrated *in vacuo*, and added to stirring MeOH to precipitate polymeric product. The supernatant was decanted, and the solid polymer was dried *in vacuo* for 1 h (30 mg; 89% yield). The bulk polymer was stored in DCM (9 mg/mL) for further use. Aliquots (0.2 mL) were removed and concentrated to dryness for NMR spectral and SEC analysis. Spectral data were consistent with literature reports.[129,130] Molecular weight data is given in Table 3.4 in the main text. Representative SEC data for the isolated polymers are shown in Figure 3.26. Representative spectral data shown in Figures 3.38 – 3.39. dn/dc = 0.130 mL/g.

Higher molecular weight polymers (**3.3**$_{429}$**, 3.8**$_{392}$, **3.8**$_{453}$) required higher reaction temperatures (-40 °C) to prevent precipitation out of solution.

3.6.13 General Procedure for Stress Strain Experiments

Circular films of the respective polymers (**3.9**$_{336}$, **3.9**$_{453}$) were cast from $CHCl_3$ (5 wt% polymer) in a Teflon dish, and subsequently dried *in vacuo* for 48 h. The films were placed in a glass drying chamber, filled with an N_2 atmosphere, and irradiated for the specified time. The films were cut into rectangular strips and analyzed using DMA (Film tension clamp at 0.1% strain/min). Representative Stress v. Strain plots shown in Figure 3.2 of the main text.

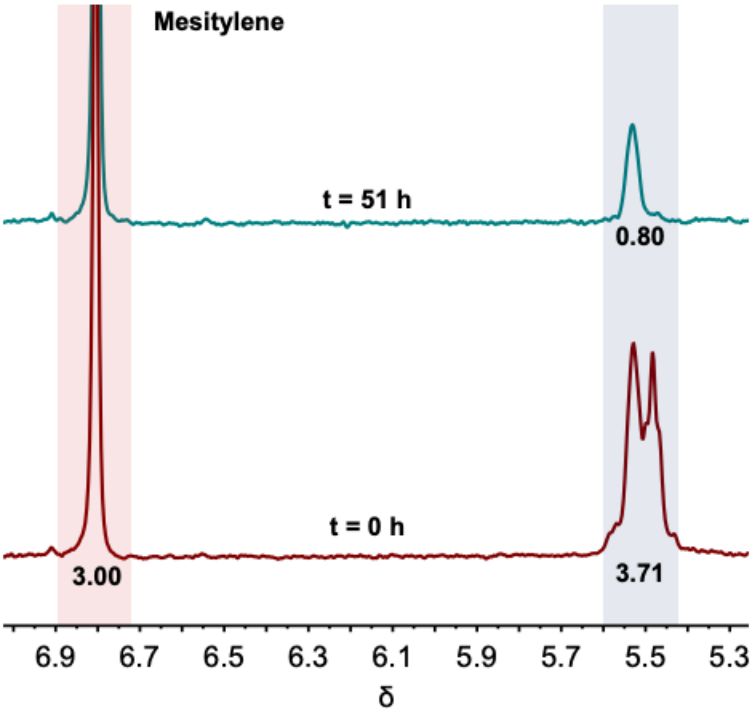

Figure 3.11: ^{1}H NMR ($CDCl_3$) spectra of 300 psi reduction of **3.3$_{DP}$**. Mesitylene (red box) and olefin resonances (blue box) highlighted. Time points and integrations listed.

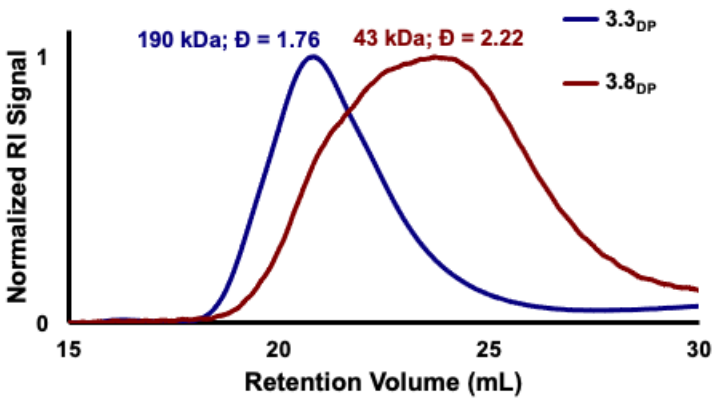

Figure 3.12: Overlaid SEC traces for **3.3$_{DP}$**, and **3.8$_{DP}$** following hydrogenation using **3.7** for 72 h, with 700 psi H_2. Decrease in M_n attributed to hydrogenolysis.

Scheme 3.10: Representative Synthesis of **3.9$_{DP}$**

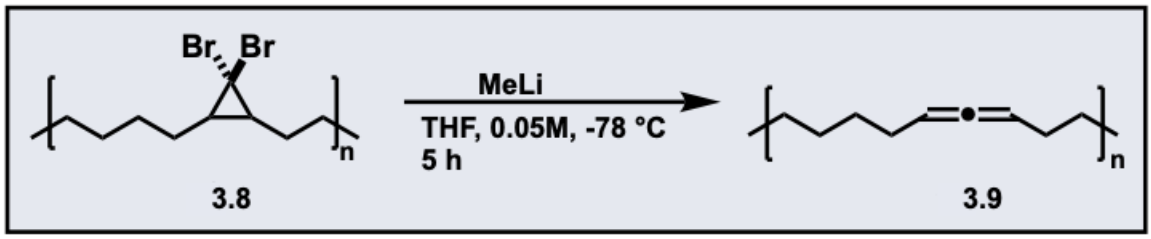

3.6.14 Thermal Crosslinking of 3.9$_{DP}$ Materials

1-dram vial was charged with **3.9$_{DP}$** (4.4 mg; 0.036 mmol), a Teflon stir bar, C_6D_6 (0.7 mL), and mesitylene (1.5 μL; 0.0107 mmol; added as internal standard). The polymer solution was transferred to a J-young NMR tube and degassed via three cycles of freeze-pump-thaw. The solution was heated at the specified temperature for the stated time (Figure 3.13) in the absence of light. Visible gelation occurred within the J-Young tube (Figure 3.13, inset) after heating at 120 °C for 23 h, which suggested network formation had occurred via thermal [2+2] cycloadditions ^{1}H NMR spectroscopic analysis revealed significant consumption of the starting allene resonance after heating at 120 °C for 23 h and appearance of new vinyl resonances (Figure 3.13).

3.6.15 O_2 Sensitivity (Solution) 3.9$_{DP}$ Materials

A 1 mL vial was charged with **3.9$_{DP}$** (5 mg; 0.041 mmol), $CDCl_3$ (0.7 mL), a Teflon stir bar, and mesitylene (1.5 μL; 0.0107 mmol; added as an internal standard). The polymer solution was transferred to a J-young NMR tube, degassed via three cycles of freeze-pump-thaw, and placed under an O_2 atmosphere and allowed to equilibrate at 23 °C for 24 h and analyzed by ^{1}H NMR spectroscopy (red spectra, Figure 3.14). The sample was then heated at 40 °C for 72 hours. ^{1}H NMR spectroscopy revealed a slight decrease in allene content (green spectra, Figure 3.14). The sample was then heated at 80 °C for 48 hours. ^{1}H NMR spectroscopy revealed a significant decrease in allene content accompanied by the appearance of new vinyl resonances (blue spectra, Figure 3.14).

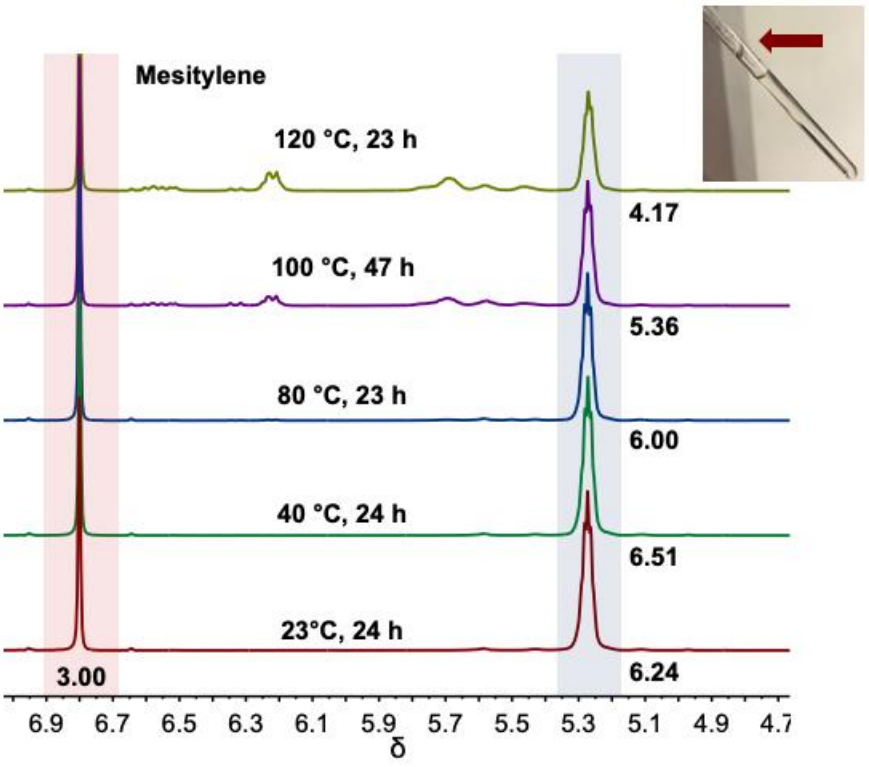

Figure 3.13: ^{1}H NMR spectrum ($CDCl_3$) of **3.9$_{DP}$** sample that was heated at varying temperatures for the specified times. Mesitylene (red box) and allene resonance (blue box) are highlighted. Inset shows gelation within the J-young tube.

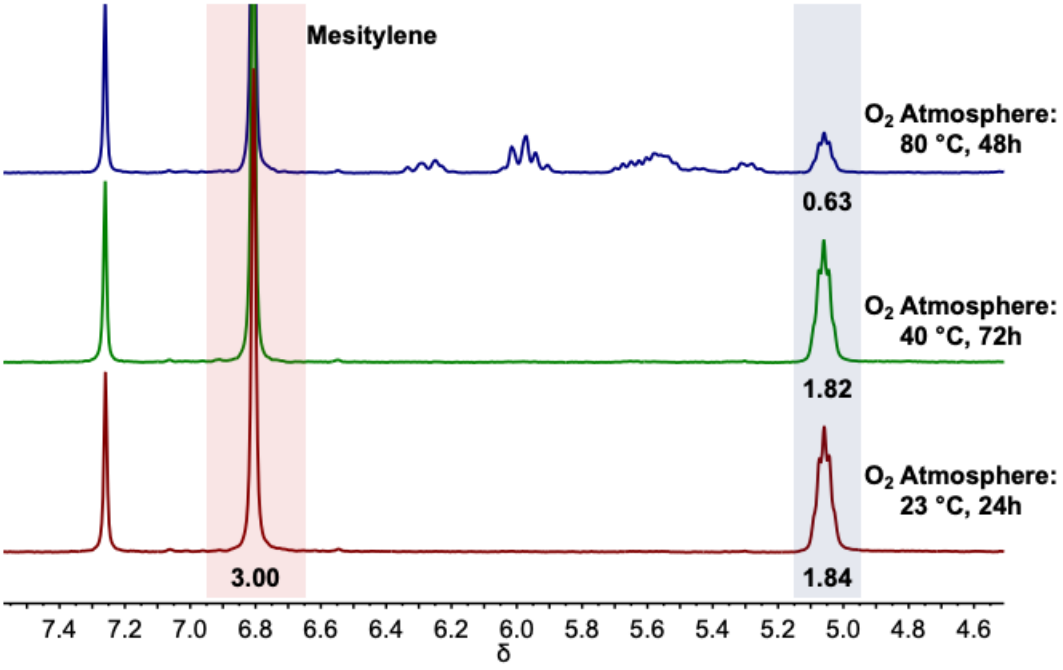

Figure 3.14: ^{1}H NMR spectra ($CDCl_3$) for O_2 sensitivity of **3.9$_{DP}$** after equilibration at 23 °C for 24 h under an O_2 atmosphere (bottom), followed by heating at 40 ºC (middle) and 80 ºC (top). Mesitylene (red box), and allene (blue box) resonances are highlighted.

3.6.16 Sample Preparation and Fluorescence Quenching Experiment of 3.9$_{DP}$

3.9$_{DP}$ polymer samples were dissolved in HPLC-grade $CHCl_3$ (~1 mg/mL) and transferred into a quartz cuvette. UV-vis absorbance (Figures 3.29) and fluorescence (Figure 3.30) spectra were collected.

A 3 mL (3 mg; 0.0246 mmol) aliquot was taken from a **3.9$_{DP}$** stock solution (1 mg/mL in HPLC $CHCl_3$) added to a quartz cuvette and analyzed by fluorescence spectroscopy (λ_{EX} = 350 nm; Figure 3.15, blue). Following irradiation, nitrobenzene (5 μL; 0.0492 mmol; 2 equiv. per allene unit) was added and the solution was thoroughly mixed for 1 minute. The mixture was subsequently analyzed by fluorescence spectroscopy, which revealed complete quenching of fluorescence (Figure 3.15, red). Photographs of the samples (irradiated with a 350 nm lamp) are shown in Figure 3.15.

3.6.17 Photochemical Crosslinking of 3.9$_{DP}$

A J-young tube was charged with a d_8 – THF (0.7 mL) solution of **3.9$_{DP}$** (4.4 mg; 0.036 mmol) and mesitylene (1.5 μL; 0.0107 mmol; as an internal standard). The solution was degassed via three cycles of freeze-pump-thaw and placed under an N_2 atmosphere. The sample was analyzed by ^{1}H NMR spectroscopy and then placed in an enclosed photoreactor (consisting of 4 bulbs orthogonally arranged) and irradiated with 254 nm light for 7 days (note: the temperature inside the reactor did not exceed 40 °C). Complete gelation of the sample was observed, which precluded further analysis by ^{1}H NMR spectroscopy (Scheme 3.11, inset).

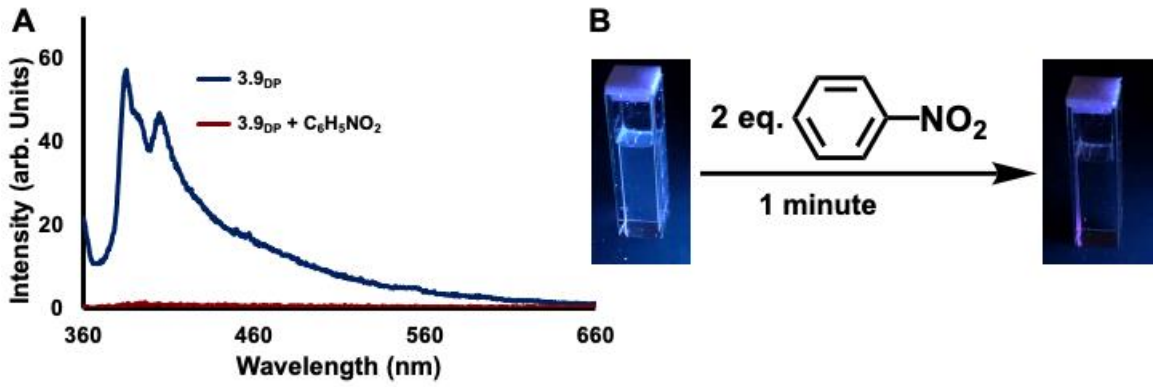

Figure 3.15: A) Fluorescence spectra of **3.9$_{DP}$** before and after addition of nitrobenzene ($CHCl_3$, 1 mg/mL). B) photographs showing the **3.9$_{DP}$** before (left) and after (right) addition of nitrobenzene.

Scheme 3.11: Photochemical Crosslinking of **3.9$_{DP}$**

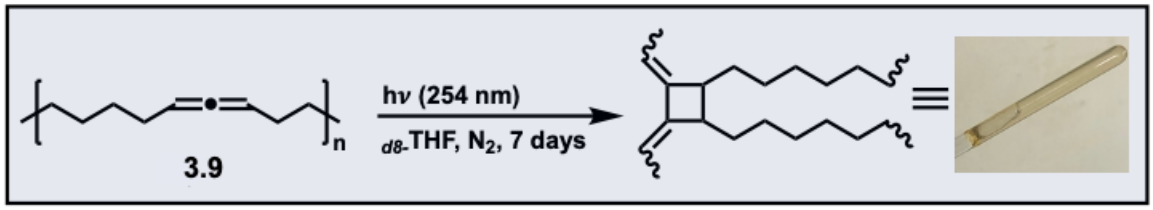

3.6.18 Procedure for Ozone Mediated Degradation of 3.9$_{DP}$

A 50 mL round bottom flask was charged a 10 mL DCM solution of **3.9$_{DP}$** (176 mg; 1.44 mmol) DCM (35 mL) and a Teflon stir bar. The reaction vessel was cooled to -78 °C with stirring. The solution was sparged with a constant stream of ozone for 3 hours once the solution turned blue. After which *tert*-hydroperoxide (*t*BuOOH; 0.52 mL, 2.86 mmol; ~5.5 M in decane) was added via syringe at -78 °C. The resulting colorless solution was then warmed with stirring to 23 °C over the course of 54 h. The solvent was subsequently removed *in vacuo* yielding a powdery/oily residue. **3.10** was recrystallized from dissolving in warm EtOAc (0.5 mL) followed dropwise addition of hexanes until cloudy. The solution was cooled to -5 °C for 1 h, the suspension was separated by centrifugation, the supernatant decanted, and the white powdery solid was dried *in vacuo* for 13 h. Following concentration of the supernatant, the purification protocol was repeated two more times to increase the recovery of **3.10** (103 mg; 41% yield). Representative SEC data for **3.9$_{DP}$** and the recrystallization supernatant (a mixture of oligomeric species, **3.10**, and the *t*-butyl diester of **3.10**) are shown in Figure 3.16. ^{1}H NMR spectra of the supernatant residues are compared to **3.9$_{DP}$** in Figure 3.17. Spectral data for **3.10** were consistent with literature results.[158] Spectral data shown in Figure 3.44.

Scheme 3.12: Ozone mediated degradation of **3.9$_{DP}$**

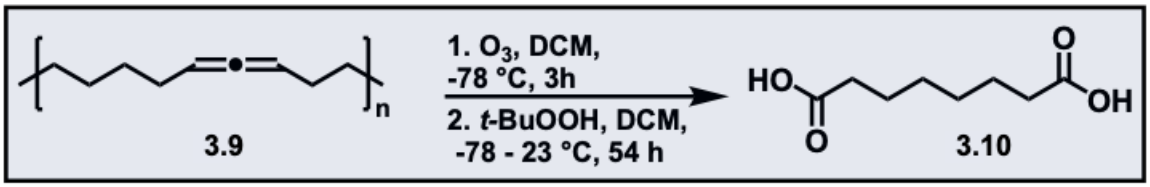

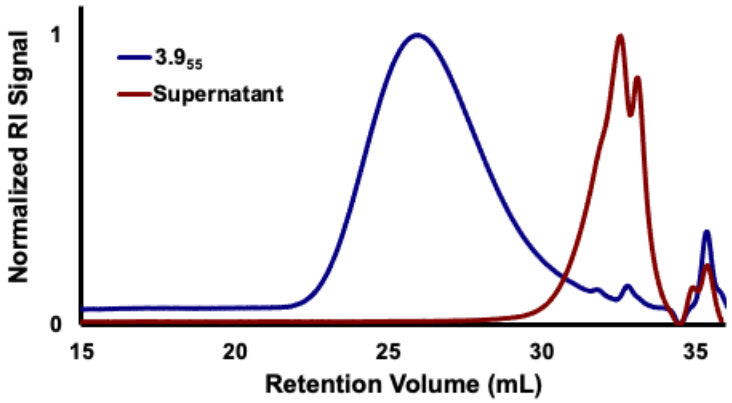

Figure 3.16: Overlaid SEC traces of **3.9$_{DP}$** (blue) and the isolated residue after ozonolysis (red).

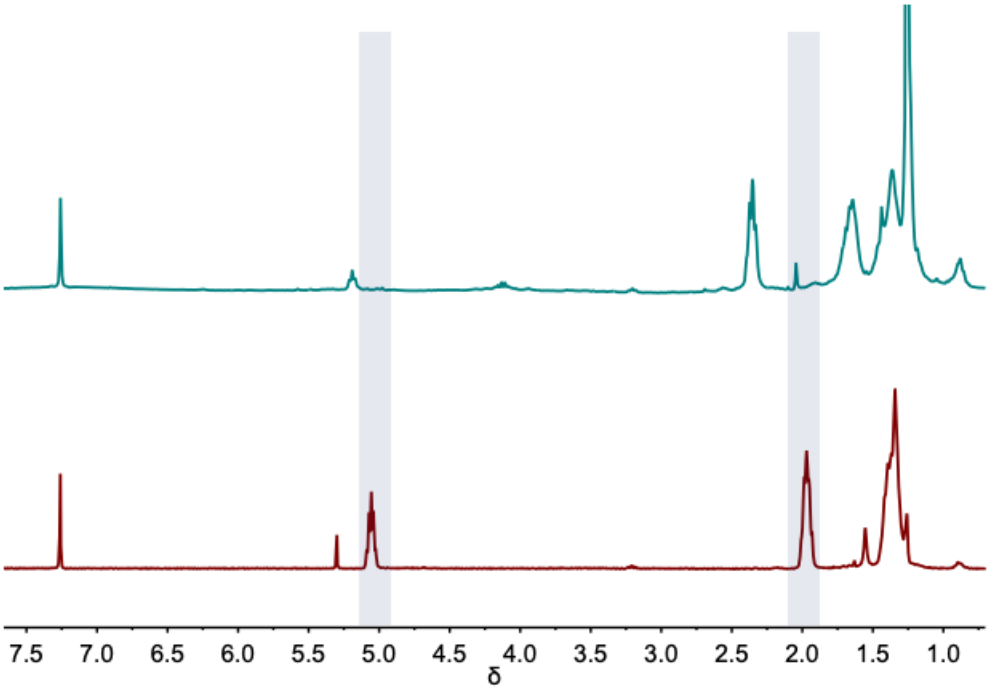

Figure 3.17: ^{1}H NMR ($CDCl_3$) spectra of **3.9$_{55}$** (bottom) and the supernatant following recrystallization of **3.10** (top). The allene and allenylic methylene signals are highlighted (blue boxes).

APPENDIX

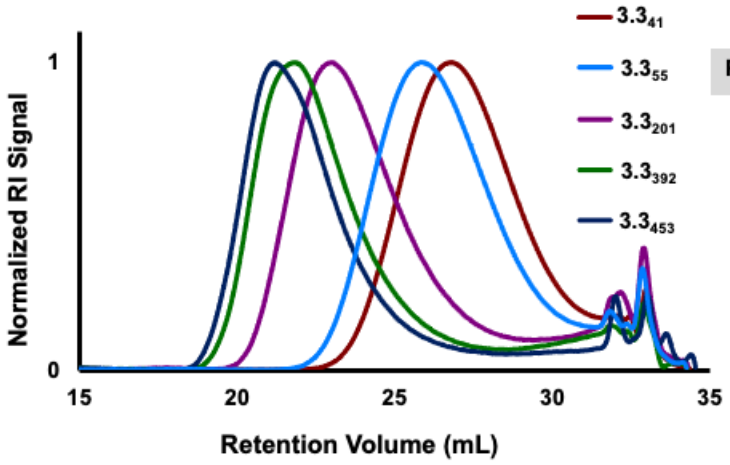

Polymer	M_n (Da)	Đ
3.3$_{41}$	11,600	1.75
3.3$_{55}$	15,600	1.88
3.3$_{201}$	56,500	1.86
3.3$_{392}$	110,000	1.76
3.3$_{453}$	126,900	1.89

Figure 3.18: Representative SEC data for **3.3$_{41}$**, **3.3$_{55}$**, **3.3$_{201}$**, **3.3$_{392}$**, and **3.3$_{453}$** materials. Note: this set of **3.3$_{DP}$** materials was used to prepare the **3.8$_{DP}$** materials.

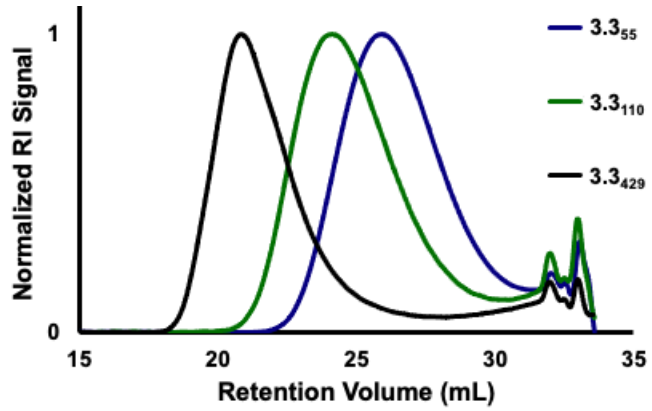

Polymer	M_n (Da)	Đ
3.3$_{55}$	15,800	1.69
3.3$_{110}$	30,800	1.76
3.3$_{429}$	120,300	1.71

Figure 3.19: Selected SEC data for **3.3$_{55}$**, **3.3$_{110}$**, and **3.3$_{429}$** materials. Note: this set of **3.3$_{DP}$** materials was used to prepare the **3.4$_{DP}$** materials.

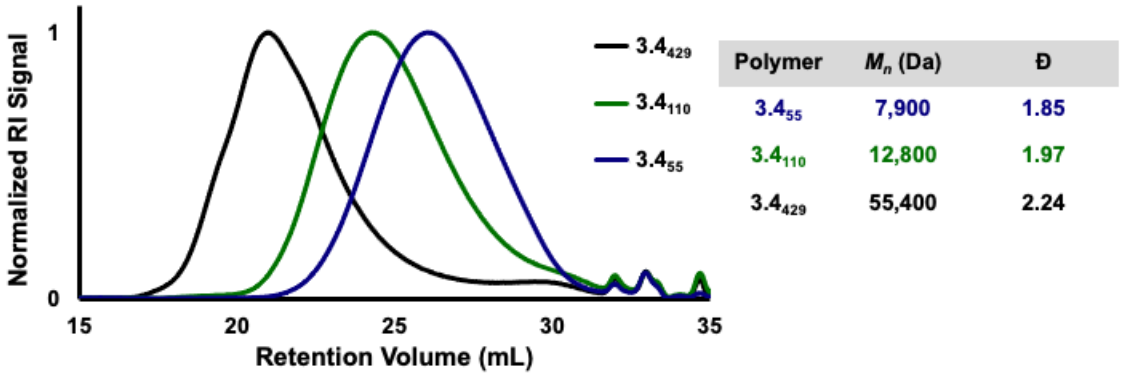

Polymer	M_n (Da)	Đ
3.4_{55}	7,900	1.85
3.4_{110}	12,800	1.97
3.4_{429}	55,400	2.24

Figure 3.20: Representative SEC data for **3.4_{55}** – **3.4_{429}** materials.

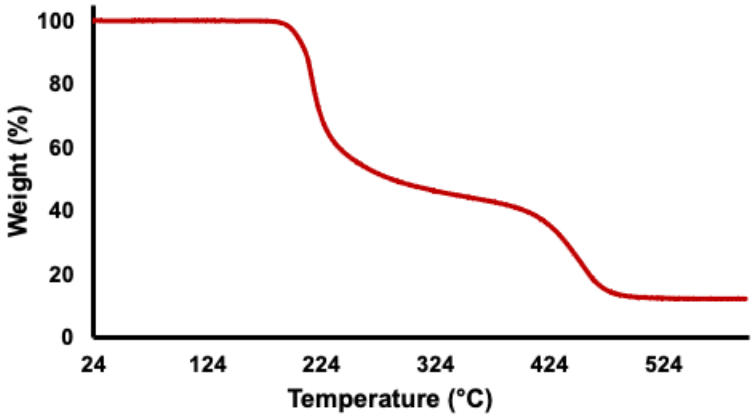

Figure 3.21: Representative **3.3_{DP}** TGA thermogram (Heating Rate: 10 °C/min in N_2)

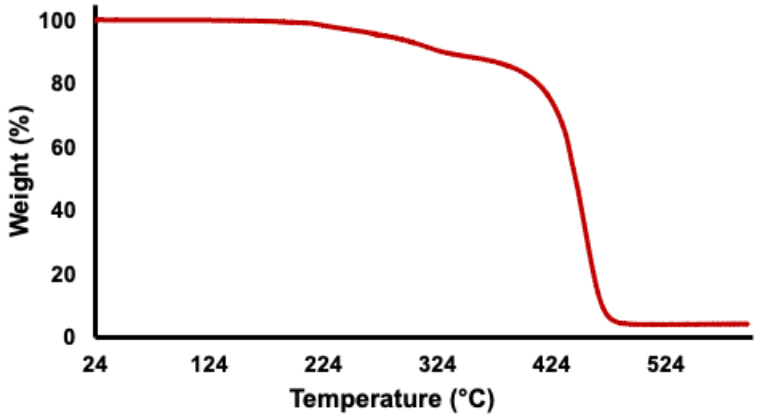

Figure 3.22: Representative **3.4$_{DP}$** TGA thermogram (Heating Rate: 10 °C/min in N_2)

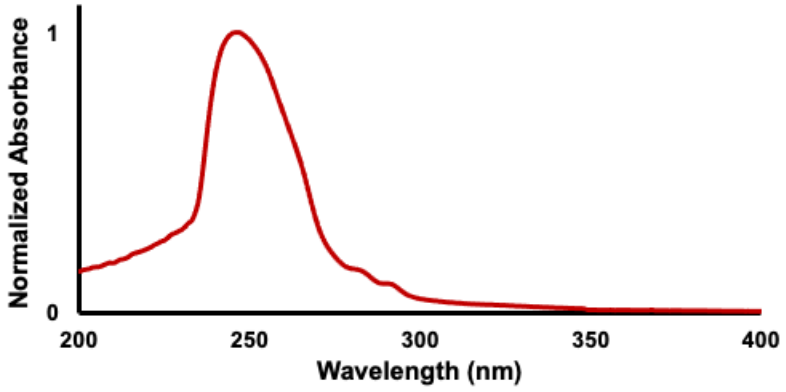

Figure 3.23: Representative UV-Vis spectrum of **3.4$_{DP}$** ($CHCl_3$, ~1.0 mg/mL)

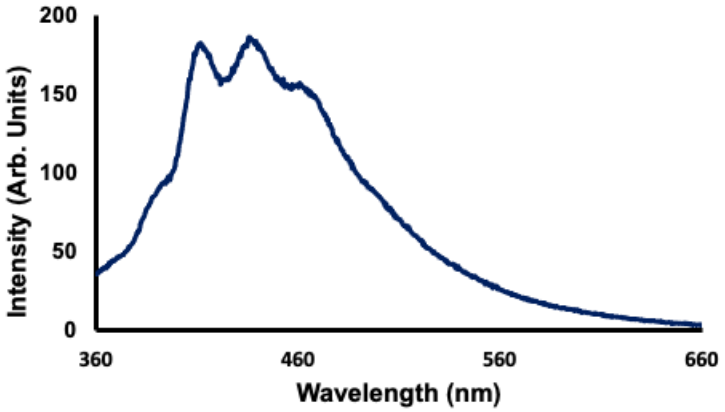

Figure 3.24: Representative Fluorescence spectrum of **3.4$_{DP}$** ($CHCl_3$, ~1.0 mg/mL; λ_{EX} = 350 nm).

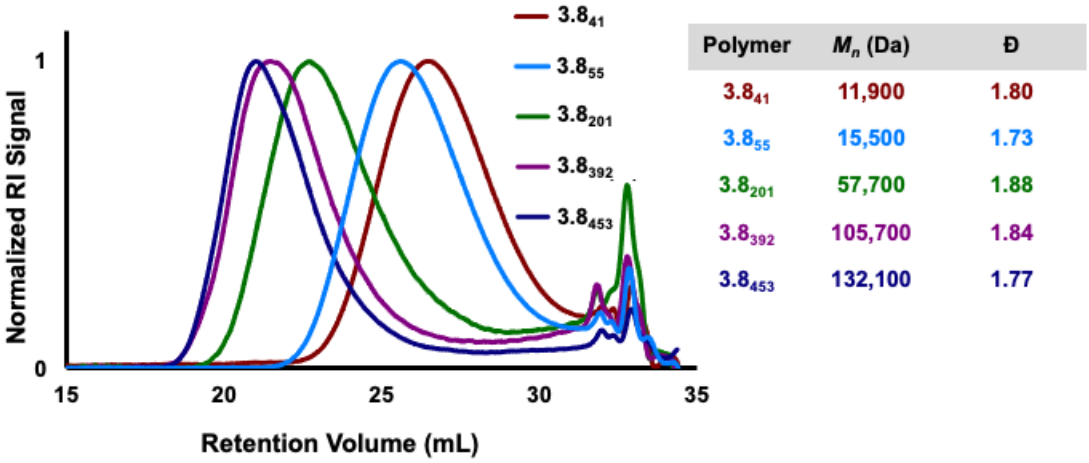

Polymer	M_n (Da)	Đ
3.8$_{41}$	11,900	1.80
3.8$_{55}$	15,500	1.73
3.8$_{201}$	57,700	1.88
3.8$_{392}$	105,700	1.84
3.8$_{453}$	132,100	1.77

Figure 3.25: Representative SEC data for **3.8$_{41}$** – **3.8$_{453}$** materials.

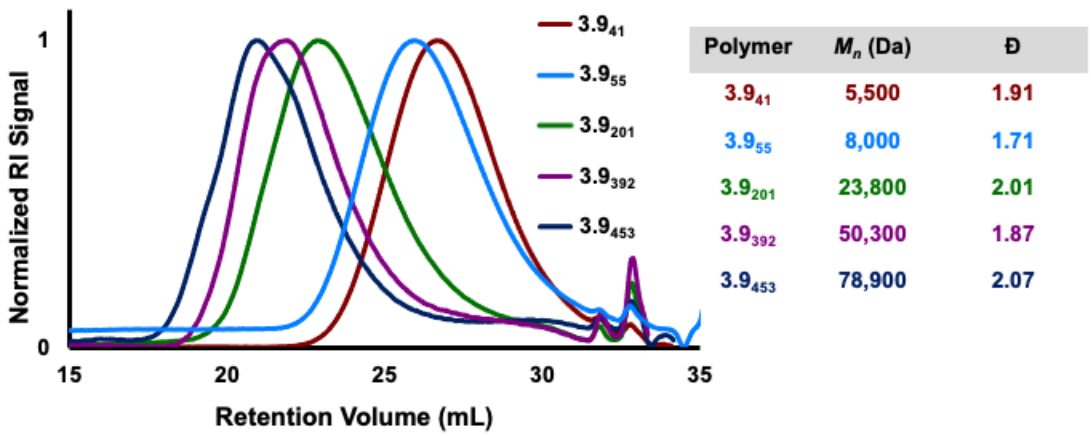

Polymer	M_n (Da)	Đ
3.9$_{41}$	5,500	1.91
3.9$_{55}$	8,000	1.71
3.9$_{201}$	23,800	2.01
3.9$_{392}$	50,300	1.87
3.9$_{453}$	78,900	2.07

Figure 3.26: Representative SEC data for **3.9$_{41}$** – **3.9$_{453}$** materials.

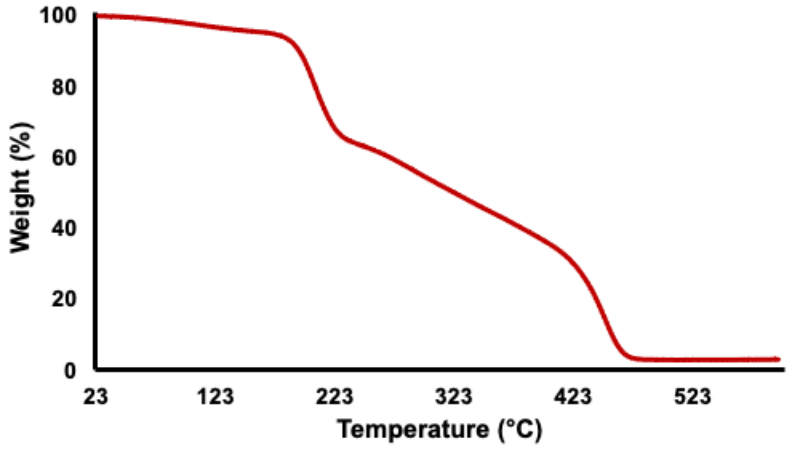

Figure 3.27: Representative **3.8$_{DP}$** TGA thermogram (Heating Rate: 10 °C/min in N_2)

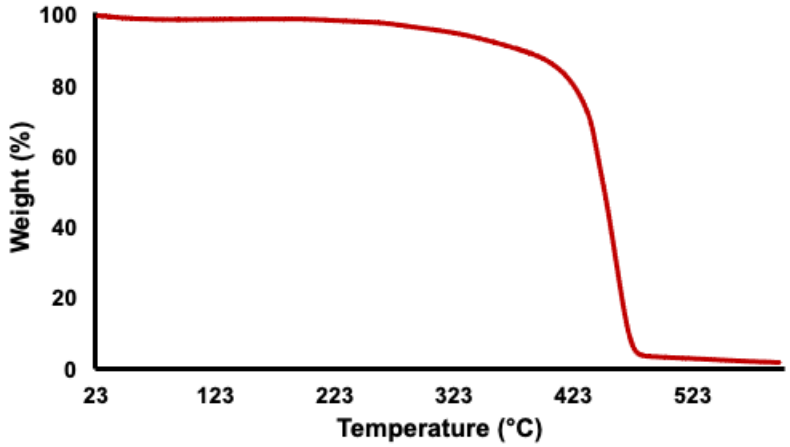

Figure 3.28: Representative **3.9$_{DP}$** TGA thermogram (Heating Rate: 10 °C/min in N_2).

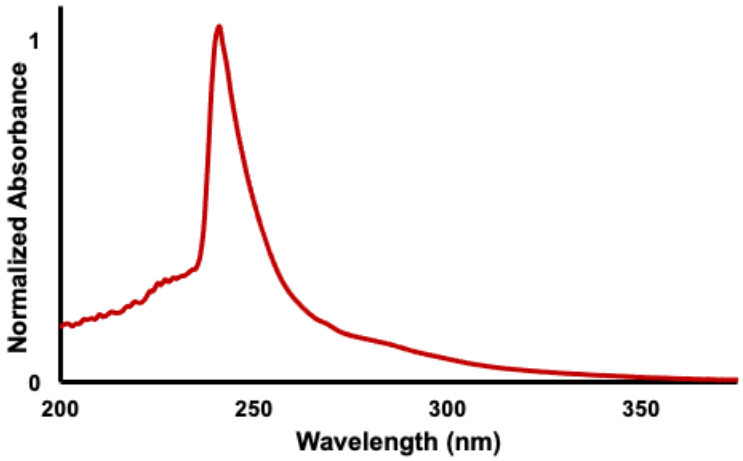

Figure 3.29: Representative UV-Vis spectrum of **3.9$_{DP}$** ($CHCl_3$, ~1.0 mg/mL).

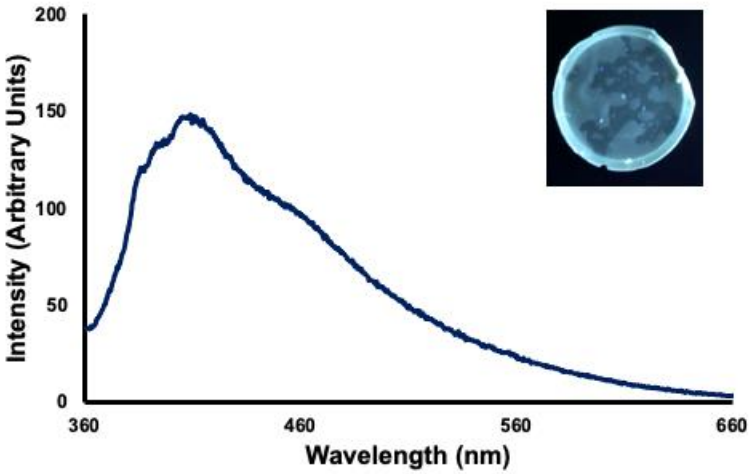

Figure 3.30: Representative Fluorescence spectrum of **3.9$_{DP}$** ($CHCl_3$, ~1.0 mg/mL; λ_{EX} = 350 nm). Inset shows a circular film of **3.9$_{DP}$** irradiated with a 350 nm lamp.

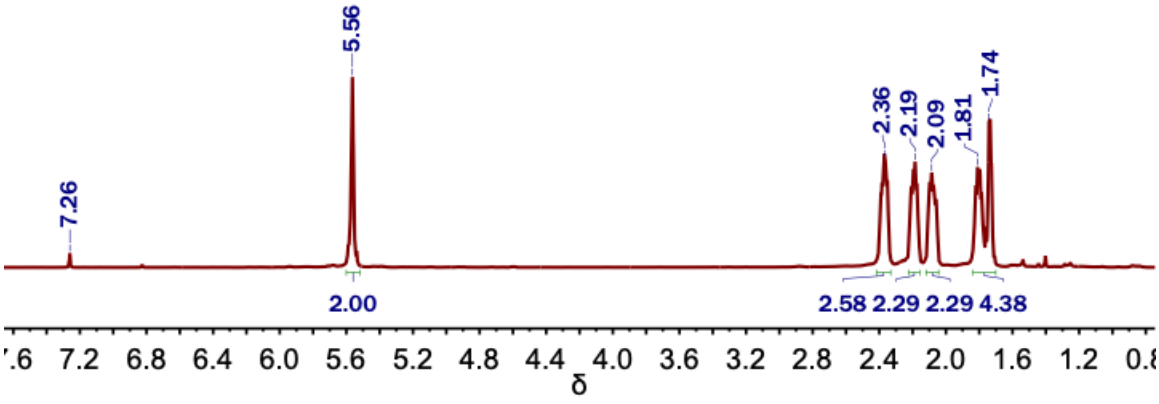

Figure 3.31: Representative ^{1}H NMR of **3.1** in $CDCl_3$.

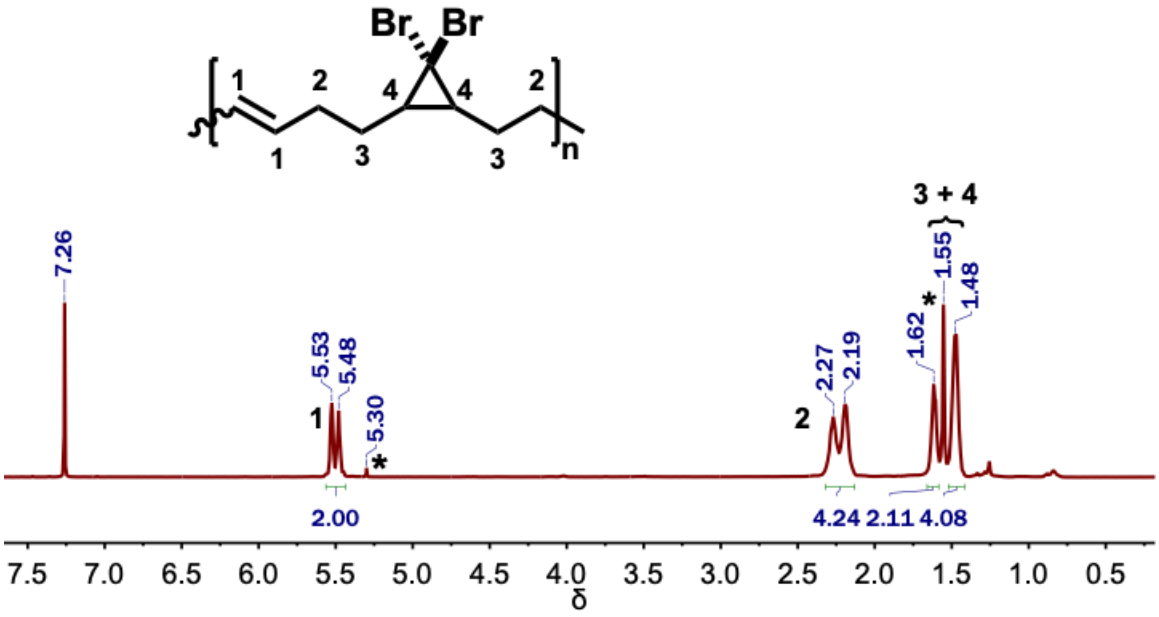

Figure 3.32: Representative ^{1}H NMR of **3.3$_{DP}$** in $CDCl_3$. Residual solvent (H_2O: δ = 1.55, and DCM: δ = 5.30) denoted with *.

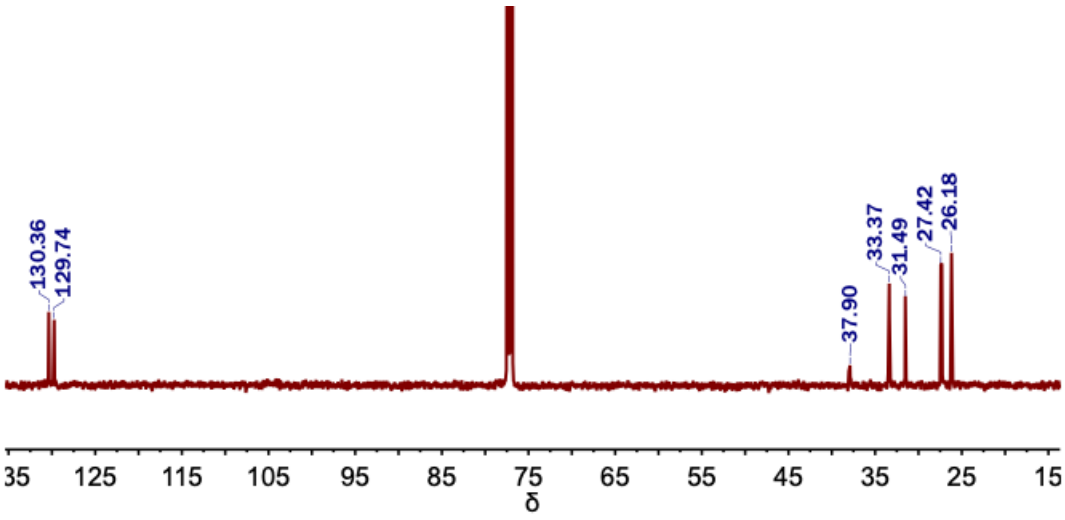

Figure 3.33: Representative ^{13}C NMR of **3.3$_{DP}$** in $CDCl_3$.

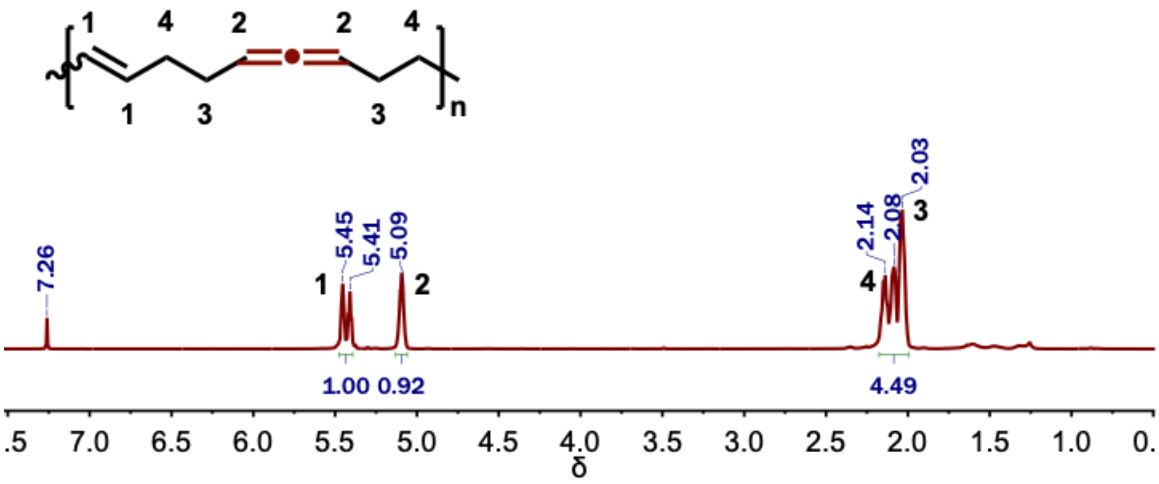

Figure 3.34: Representative ^{1}H NMR of **3.4$_{DP}$** in $CDCl_3$.

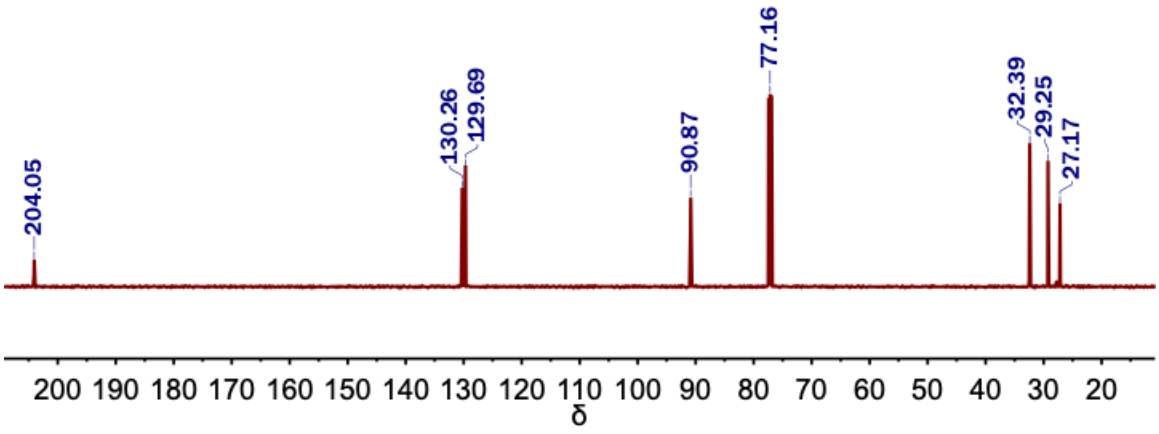

Figure 3.35: Representative ^{13}C NMR of **3.4$_{DP}$** in $CDCl_3$.

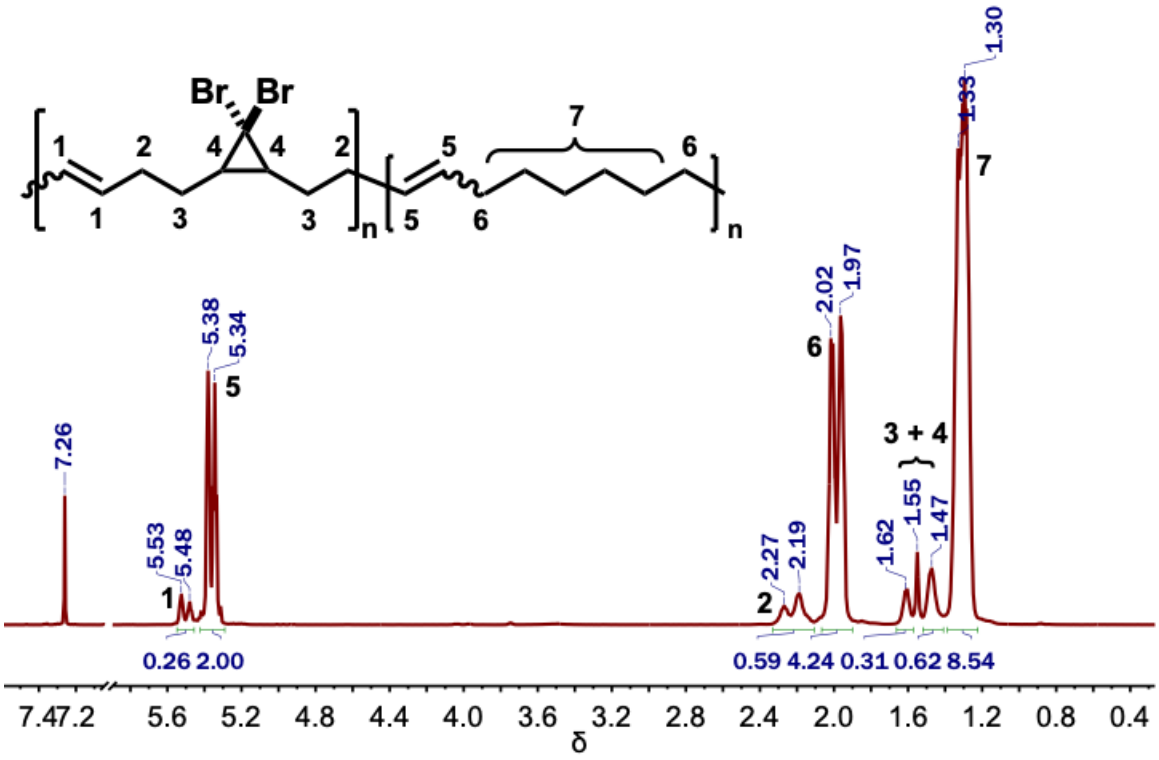

Figure 3.36: Representative ^{1}H NMR of **3.5** in $CDCl_3$.

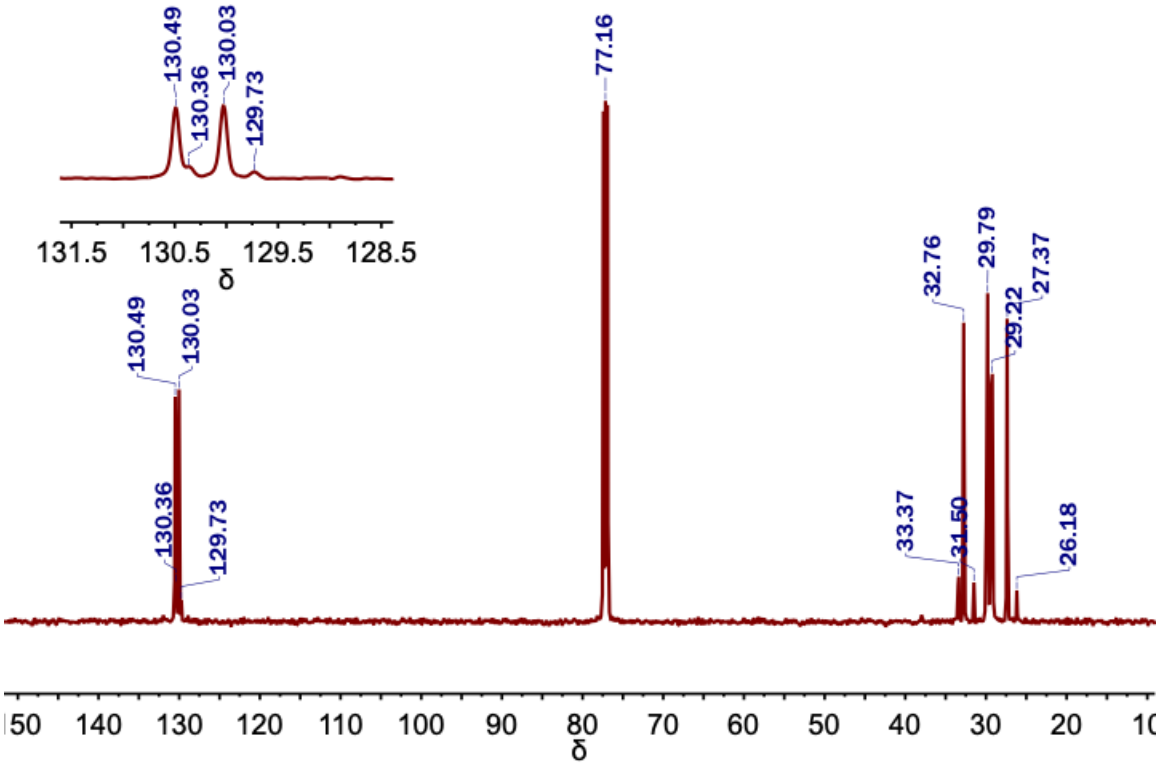

Figure 3.37: Representative ^{13}C NMR of **3.5** in $CDCl_3$. Inset shows magnified view of the vinyl region.

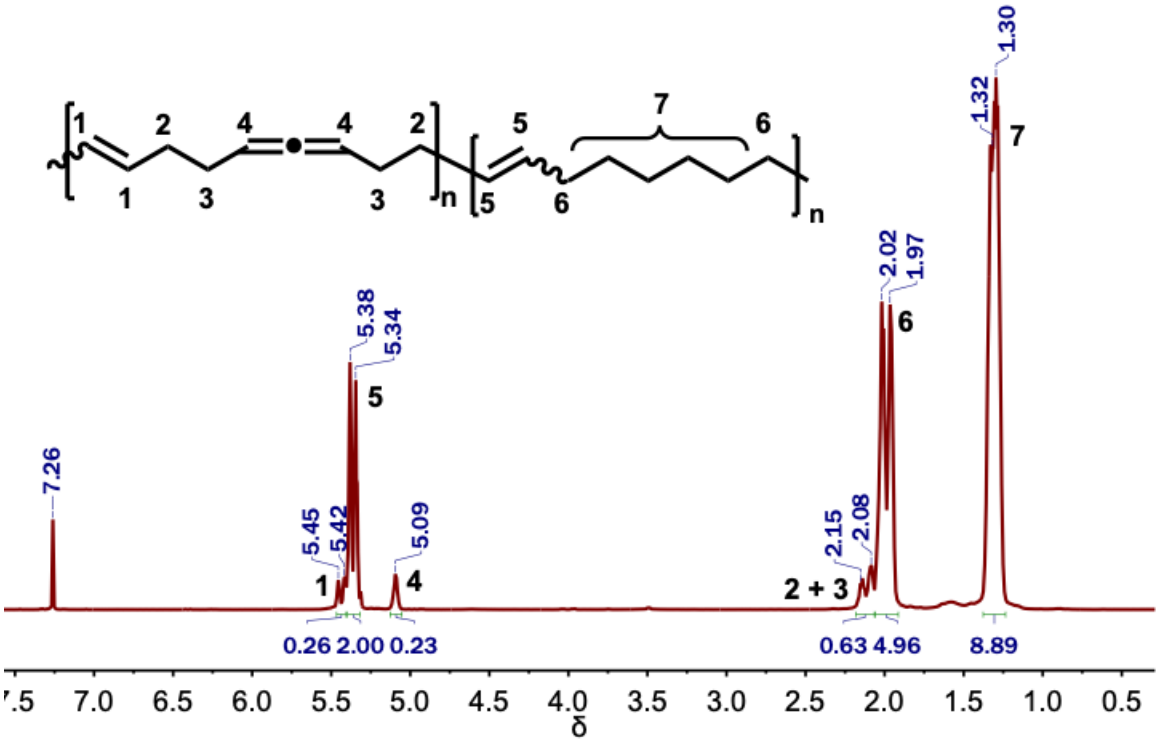

Figure 3.38: Representative ^{1}H NMR of **3.6** in $CDCl_3$.

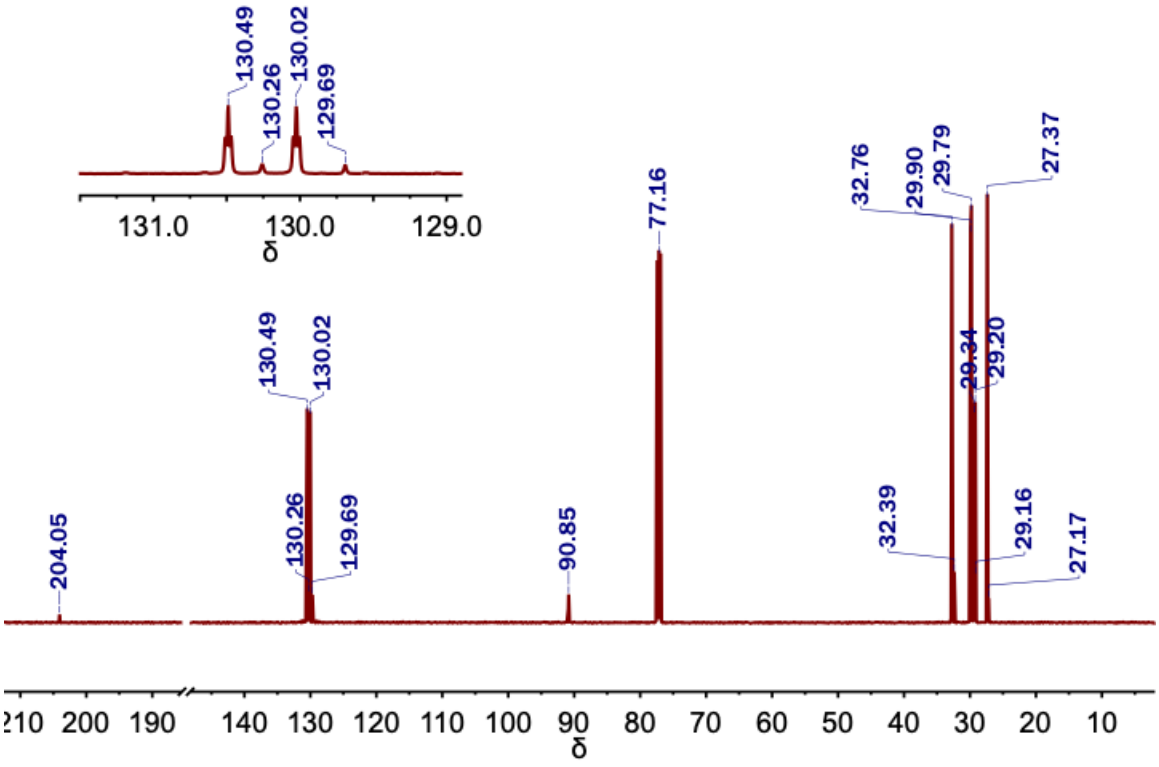

Figure 3.39: Representative ^{13}C NMR of **3.6** in $CDCl_3$. Inset shows magnified view of the vinyl region.

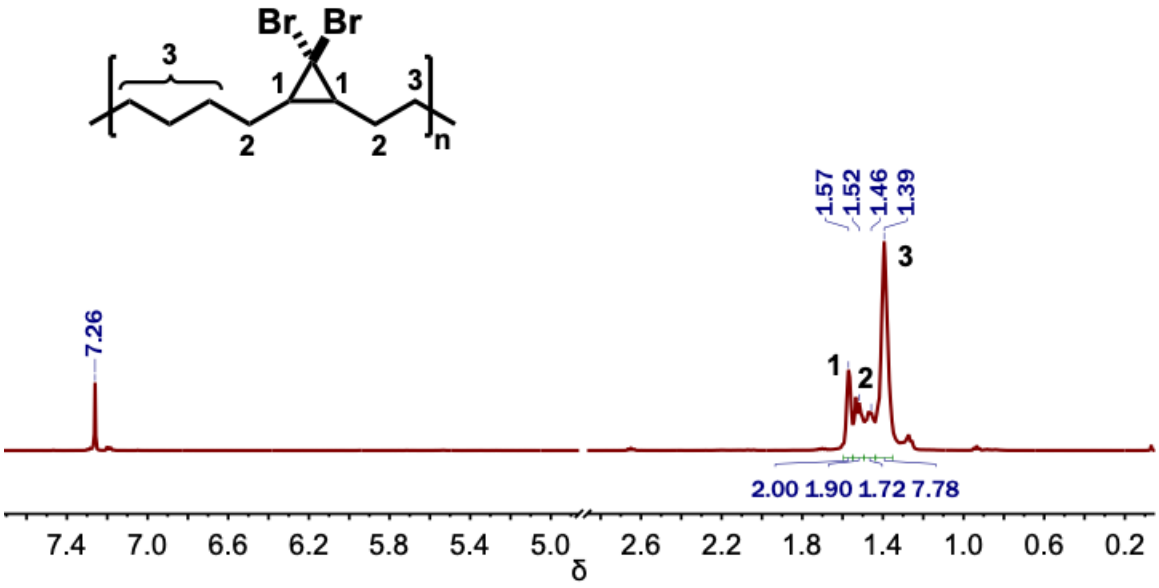

Figure 3.40: Representative ^{1}H NMR of **3.8$_{DP}$** in $CDCl_3$.

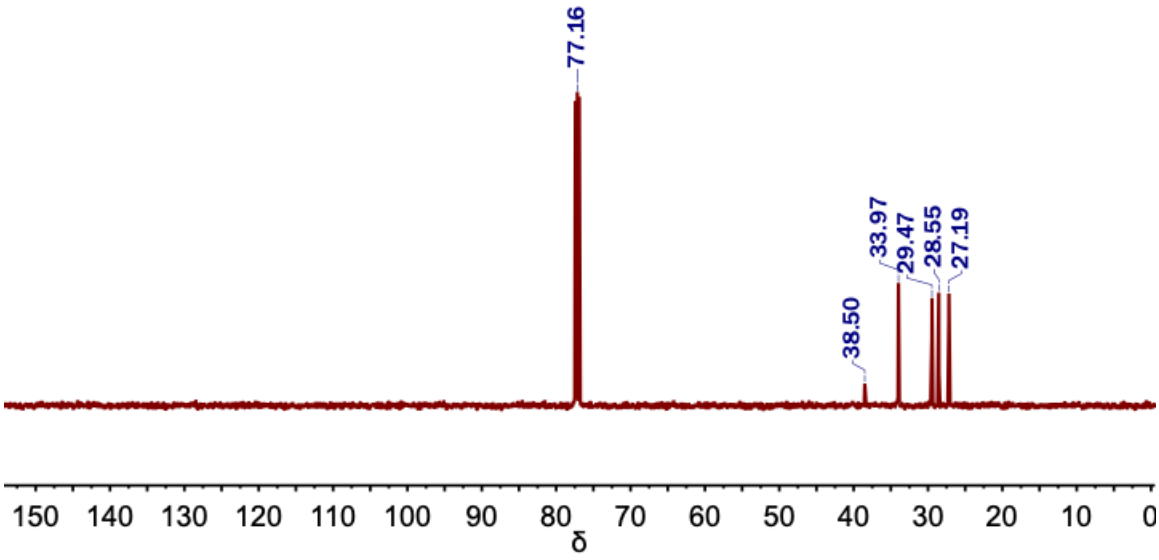

Figure 3.41: Representative ^{13}C NMR of **3.8$_{DP}$** in $CDCl_3$.

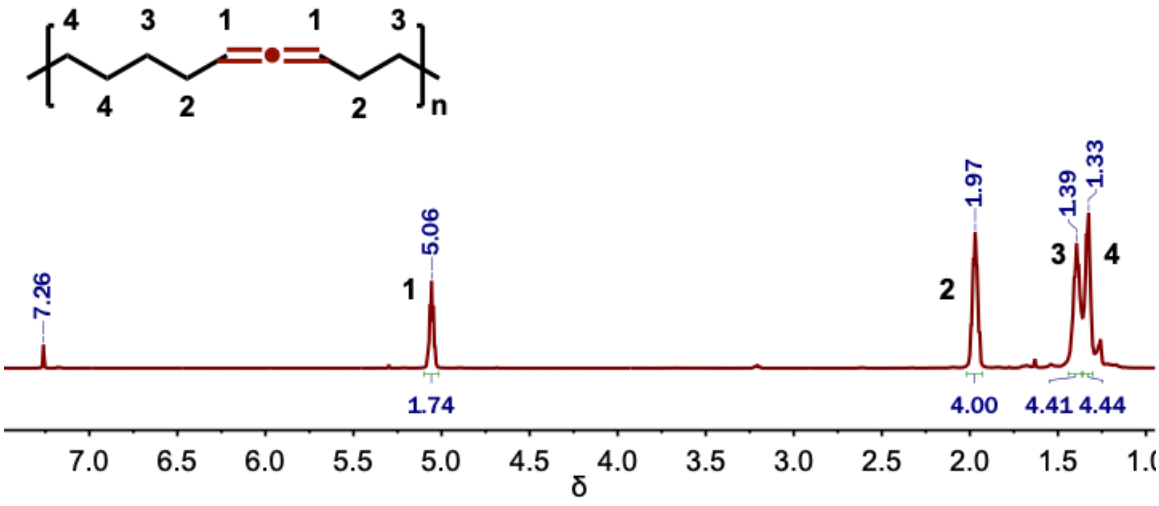

Figure 3.42: Representative ^{1}H NMR of **3.9$_{DP}$** in $CDCl_3$.

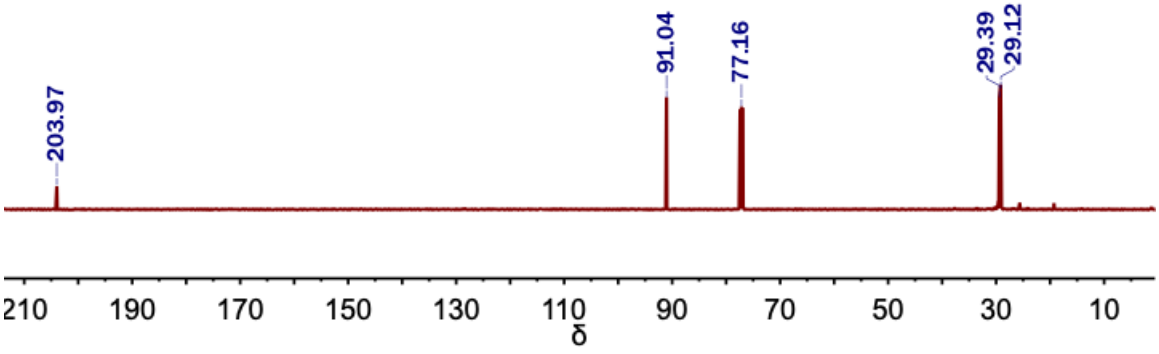

Figure 3.43: Representative ^{13}C NMR of **3.9$_{DP}$** in $CDCl_3$.

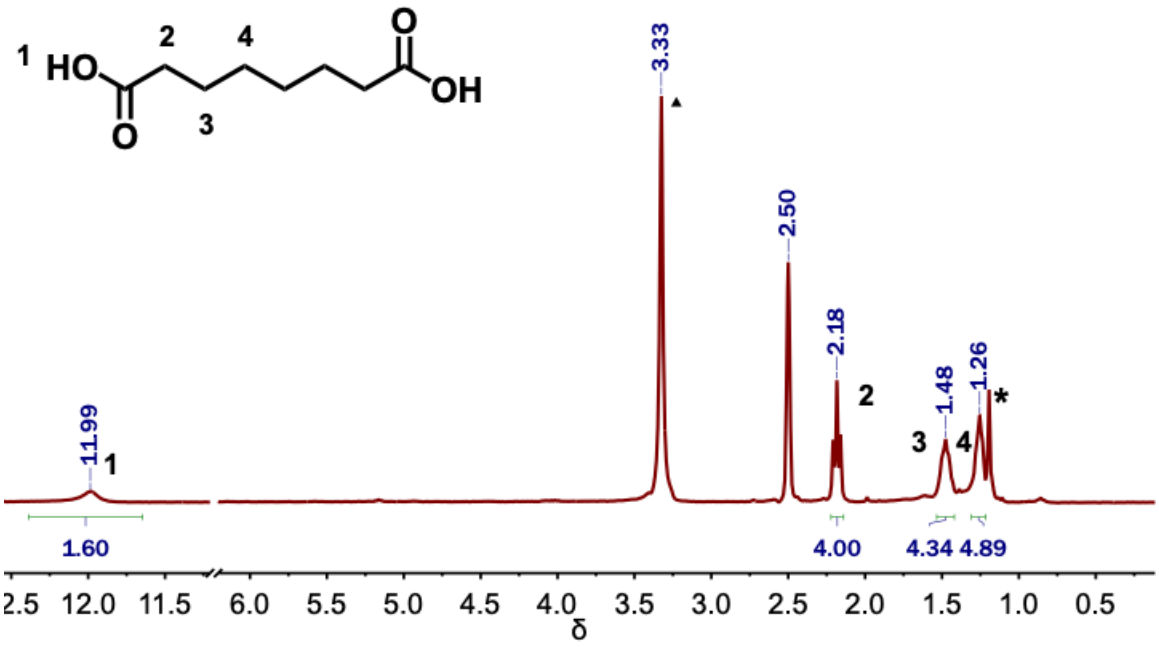

Figure 3.44: Representative ^{1}H NMR of **3.10** in d_6 – DMSO. Residual solvent (H_2O, δ = 3.33 ppm) denoted with ▲. Impurity attributed to trace t-butyl diester denoted with *.

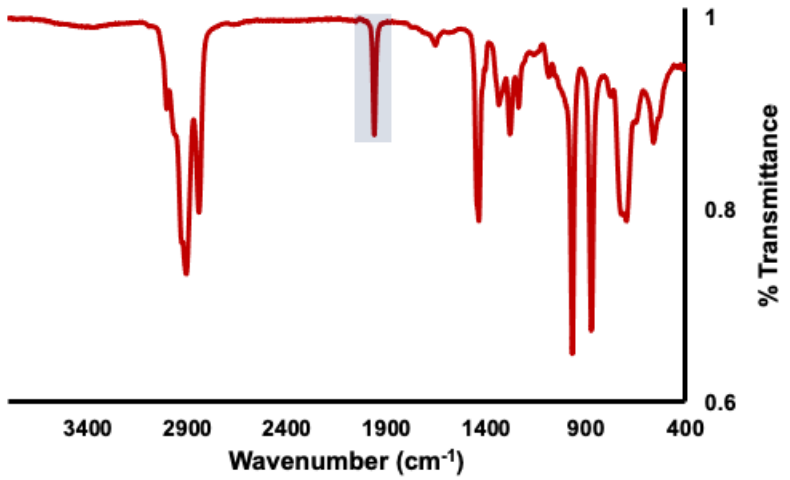

Figure 3.45: Representative IR spectra of a **3.4$_{DP}$** material, the characteristic allene stretch (1961 cm^{-1}, highlighted in blue) is consistent with literature reports of allenic carbons.[123]

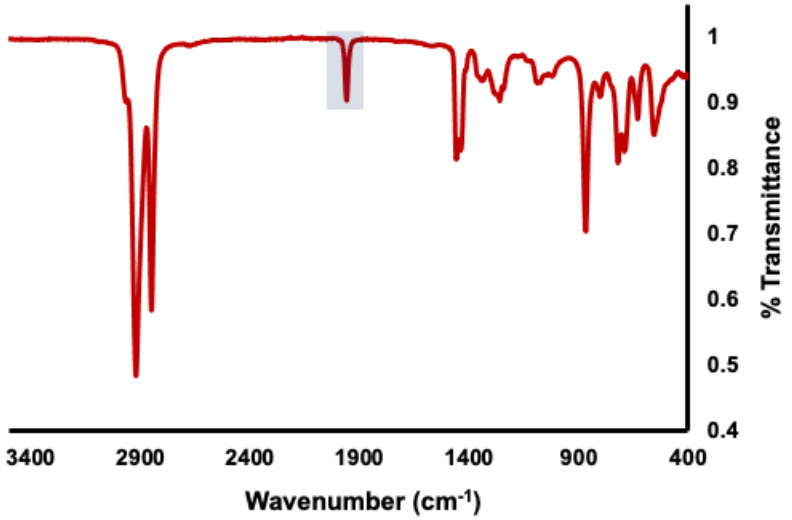

Figure 3.46: Representative IR spectra of a **3.9$_{DP}$** material, the characteristic allene stretch (1961 cm^{-1}, highlighted in blue) is consistent with literature reports of allenic carbons.[123]

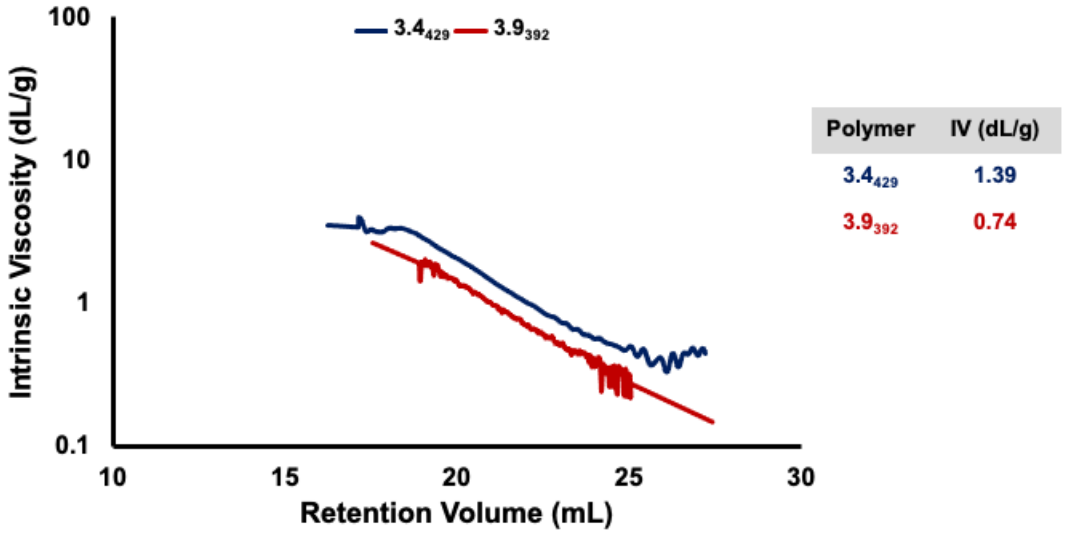

Figure 3.47: Mark-Houwink Plots of **3.4**$_{429}$ and **3.9**$_{392}$.

CHAPTER IV: PHOTOEDITING OF SOFT POLYMER BACKBONES VIA ORGANIC PHOTOREDOX CATALYSIS

4.1 Abstract

Accessing the chemistry of reactive intermediates under mild conditions has significantly expanded chemical space for small molecule transformations. Nowhere is this more apparent than in the context of photoredox catalysis. Despite abundant literature precedents for using this powerful methodology to build complex targets, there are comparatively few reports that leverage photoredox catalysis for polymer editing. Here, we report a mild photoredox approach that enables both the functionalization and degradation of polyalkenamers to valuable feedstocks. Irradiation with visible light (including natural sunlight) in the presence of a pyrillium photoredox catalyst promoted facile chain scission in a variety of substrates. This metal-free approach transformed high molar mass materials (> 300 kDa) to lower molar mass species (<30 kDa) within 10 min. Moreover, we could completely degrade macromolecules into a range of useful targets within 96 h. Mechanistic and kinetic experiments were carried out to understand this unique reactivity, which could be coupled with various hydrofunctionalizations.

4.2 Introduction

Light-driven[159–161] reaction manifolds have revolutionized retrosynthetic logic in the context of small molecule targets. Photoredox catalysis is particularly enabling in this regard, as various reactive intermediates[162] (e.g., radical anions/cations) can be accessed under mild conditions through single electron transfer (SET) processes. Indeed, precise redox matching between catalyst and substrate has enabled mild alkene

hydrofunctionalizations,[163] nucleophilic aromatic substitutions,[164] cycloadditions,[165,166] and direct C–H activations[167] with excellent functional group compatibility.[168]

Unfortunately, photoredox catalysis remains an underexplored platform for polymer editing (a fact that is partially attributable to the challenges of translating small molecule reactivity to macromolecular substrates). In a seminal report, Theato and coworkers detailed the $Ru(bpy)_3Cl_2$ catalyzed decarboxylation of polyacrylate copolymers containing redox-active esters to afford polyethylene/polyacrylate copolymers.[169] More recently, Sumerlin and colleagues have reported the direct decarboxylation of polyacrylate/polyacrylic acid copolymers via an acridine photoredox catalyst.[170] The resulting polymer compositions could even be tailored through the use of H-atom donors or a Co co-catalyst (Scheme 4.1).[171] These precedents demonstrate the possibility for chemoselective, spatiotemporally-controlled polymer editing through photoredox catalysis; yet, they also highlight the fact that a vast area of chemical space remains untapped for photoredox-mediated polymer editing.

We became intrigued by reports of using photoredox catalysis to synthesize poly(4-methoxystyrene),[172] polyvinylethers,[173] polynorbornene[174] and other polymers[175] through mechanisms involving radical cations (Scheme 4.1). We reasoned that polymer deconstruction through these same species should be viable (per microscopic reversibility). Recent reports from Sumerlin and Anatasaki, which have shown that reversible addition-fragmentation chain-transfer (RAFT) polymers can undergo photoredox-mediated radical depolymerizations,[59,176] were particularly encouraging in this regard (Scheme 4.1). Organic photoredox catalysts are well-known to promote single-electron oxidations of olefins to

Scheme 4.1: Selected examples of photoredox-enabled polymer synthesis and editing.

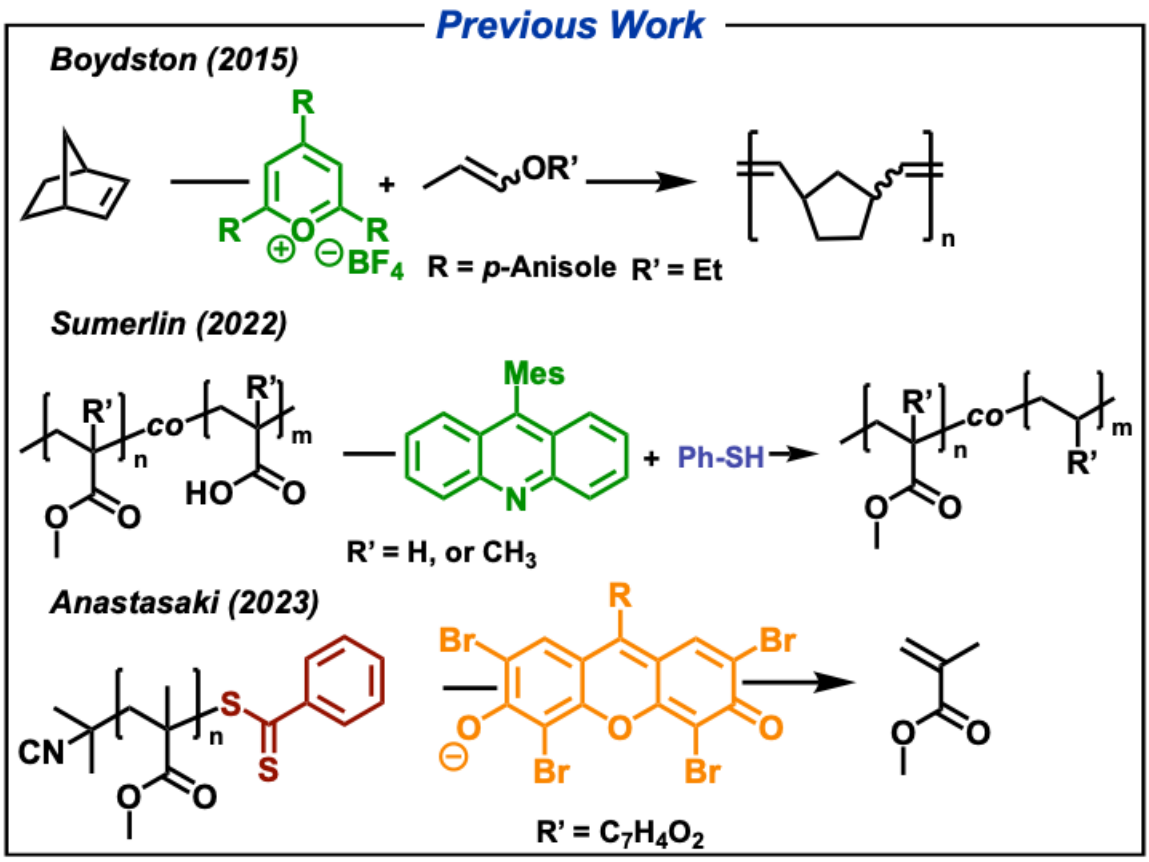

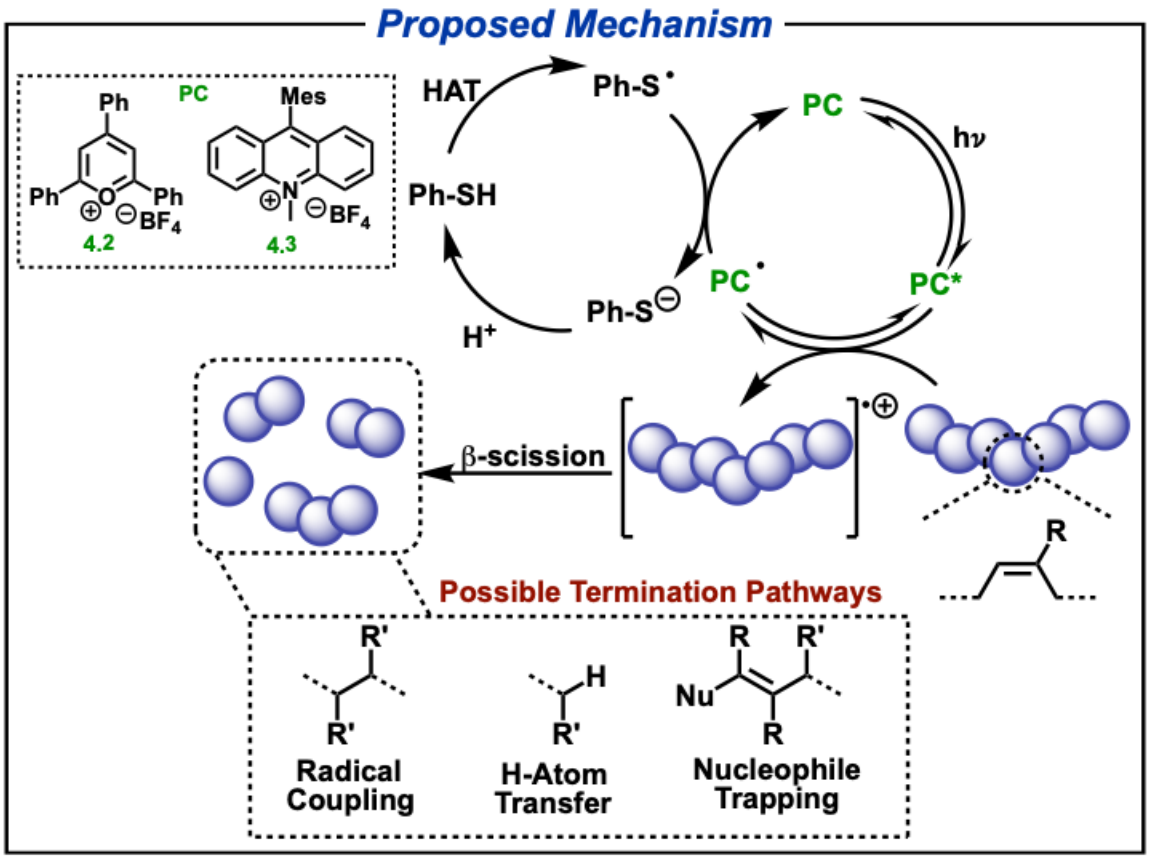

Figure 4.1: Proposed mechanism for polyalkenamer single-electron photoediting (SEPE).

afford radical cation intermediates.[177,178] We posited that generating these high-energy species on polyalkenamer substrates would promote chain cleavage through β-scission. Importantly, these radical cation intermediates might also be susceptible to trapping with exogenous species (such as nucleophiles or other radicals).

4.3 Results and Discussion

4.3.1 Initial Reaction Condition Optimization

To explore this concept, polynorbornene (**4.1**, E_{red} = +2.18 V)[26] was selected as our model substrate. A high number average molar mass (M_n) sample of **4.1** was prepared using a commercially available Z-selective Grubbs catalyst[111] (M_n = 330 kDa). Organic photoredox catalysts with excited state reduction potentials matching those of unactivated olefins,[168] such as 2,4,6-triphenylpyrylium tetrafluoroborate (**4.2**, E^*_{red} = +2.55 V vs SCE[161]) and 9-mesityl-10-methylacridinium tetrafluoroborate (**4.3**, E^*_{red} = +2.18 V vs SCE[161]), were selected for our preliminary photoediting studies. We also selected diphenyldisulfide $(PhS)_2$ as an H-atom transfer (HAT) catalyst, as this has been shown to turn over photoredox catalysts.[179,180] Initially, $(PhS)_2$ (6.1 mg; 0.28 mmol; 10 mol%) and **4.2** (5.6 mg; 0.014 mmol; 5 mol%) were dissolved in DCM (0.5 mL) and added to a solution of **4.1** (26 mg; 0.28 mmol; 0.075 M in anhydrous DCM) under an N_2 atmosphere in a glovebox. The reaction mixture was then irradiated with a 12W blue LED lamp (λ_{EM} = 450-460 nm) for 1 h.[181] Following irradiation, the mixture was diluted with DCM, filtered through a short plug of silica, and concentrated under a stream of N_2. Excess MeOH was added to precipitate any polymeric material, which was isolated with good mass recovery

(76%) following centrifugation. Consistent with our initial hypothesis, analysis of this material by size-exclusion chromatography (SEC) revealed a 59% reduction in M_n relative to **4.1** (ΔM_n = -192 kDa; Figure 4.11; Table 4.2).

We briefly explored other reaction conditions to ascertain their impact on polymer degradation. Surprisingly, chain scission was observed when **4.1** was irradiated in the absence of both **4.2** and $(PhS)_2$ (Table 4.11; entry 3). Analysis of the post-irradiated material by ^{1}H NMR spectroscopy revealed scrambling of the backbone olefin stereochemistry (Figure 4.49). Presumably, the diradical intermediate during olefin isomerization can also undergo a background β-scission reaction. However, a sufficiently oxidizing catalyst is necessary to observe enhanced degradation. For example, irradiating **4.1** in the presence of a weakly oxidizing catalyst, $Ru(bpy)_3Cl_2$ (E_{red}^* = +0.77 V vs SCE[159]), resulted in only background scission (Table 4.1). Conversely, **4.3** was also found to be a competent catalyst for degradation, albeit with poorer control (as determined by the increased dispersity of the degraded material; Figure 4.9). These data suggest that a slight overpotential is required to achieve larger reductions in M_n with good fidelity. Replacing $(PhS)_2$ with alkyl thiols (such as 1-adamantanethiol or 1-dodecanethiol) afforded intractable materials that could not be further characterized. Increasing the loading of $(PhS)_2$ to 25 mol% increased the observed extent of degradation (ΔM_n = -245 kDa);

Table 4.1: Control experiments for polyalkenamer photoediting

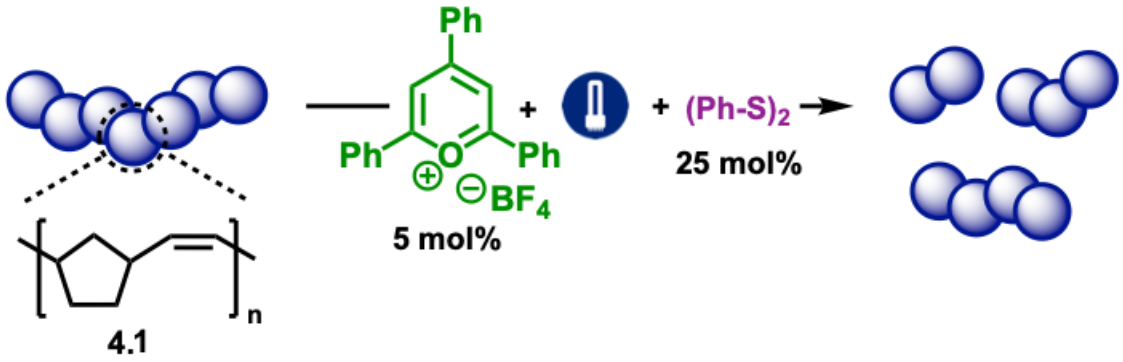

Entry	Deviation from Standard Conditions	Initial M_n (kDa)[a]	Final M_n (kDa)	Yield (%)[b]
1	None	328	103	96
2[c]	-$(PhS)_2$	328	--	90
3	-**4.2**; -$(PhS)_2$	328	138	88
4	+$Ru(bpy)_3Cl_2$; -**4.2**	328	137	82
5	+Ambient Atmosphere	328	12	66

[a]Calculated using triple detection. [b]Recovered mass. [c]Isolated material was intractable.

however, higher loadings (50 mol%) did not substantially improve beyond this (ΔM_n = -244 kDa). Interestingly, the loading of **4.2** appeared to have minimal impact on the extent of polymer degradation (Figure 4.10) . For example, addition of 1 mol% **4.2** resulted in degradation that was similar to what was observed with 10 mol% **4.2** (ΔM_n = -223 kDa versus -230 kDa, respectively; Table 4.2). As such, we elected to use an intermediate loading of **2.2** (5 mol%) and $(PhS)_2$ (25 mol%) for all subsequent studies.

We were also curious if this reactivity would be operative under less rigorous conditions (i.e., ambient atmosphere and technical-grade solvent), as **4.2** has been shown to facilitate transformations in the presence of oxygen.[161] To our delight, we could achieve nearly complete polymer degradation (~96%) under an ambient atmosphere (ΔM_n = -315 kDa; Figure 4.13; Table 4.1). Additionally, we found that natural sunlight[182] could also be used in this ambient photoediting methodology. As a proof of concept, a solution of **4.1** (0.075 in DCM) was placed in sunlight under otherwise identical conditions to those described above for 2 h.[183] We were delighted to observe that SEC characterization of the isolated polymeric residue revealed an 81% reduction in molecular weight (ΔM_n = -131 kDa; Figure 4.30). Finally, other polyalkenmers were competent substrates for our photoredox degradation. For example, both *cis*-1,4-polyisoprene (**4.4**) and *cis*-1,4-polybutadiene (**4.5**) showed 98% and 93% degradation under our optimized conditions (c.f. ΔM_n = -611 kDa and -160 kDa, respectively; Figures 4.27 and 4.28). Importantly, **4.4** and **4.5** could also be degraded (92% and 86%) using ambient sunlight as described above (ΔM_n = -205 kDa, and ΔM_n = -115 kDa, respectively; Figures 4.31 and 4.32).

4.3.2 Impact of H_2O and O_2 on Degradation Efficacy and Rate

Given the enhanced activity observed under ambient conditions, we surmised that either H_2O or O_2 must be playing some role. Initially, we suspected that increased H_2O could provide a secondary source of H-atoms, which would enable rapid turnover of the HAT catalyst and faster regeneration of the ground state photoredox catalyst. To test this, we prepared a solution of **4.1** (26 mg; 0.028 mmol) in technical-grade DCM (3 mL) in a Schlenk flask. Oxygen was removed via two degassing (freeze/pump/thaw) cycles, after which a DCM (0.7 mL) solution of **4.2** and $(PhS)_2$ (prepared as described above) was added to the vessel. The reaction was subjected to a final degassing cycle, placed under a balloon of argon, and irradiated for 1 h with blue light. The resulting polymeric material was isolated, and subsequent SEC analysis revealed a ~75% reduction in M_n relative to **4.1** had been achieved (Figure 4.25).[184] Considering these results, O_2 seemed the more likely origin of the enhanced degradation. Pyrillium catalysts, among others, are known to sensitize $^1O_2$, which can add to olefins to form reactive peroxide species (which, in turn, are known to promote polymer cracking).[180,185–188] To investigate this hypothesis, samples of **4.1** (25.1 mg; 0.27 mmol), **4.2** (5.5 mg; 0.014 mmol), and $(PhS)_2$ (15.2 mg; 0.07 mmol) were dried over P_2O_5 for 16 h. The dried reagents were dissolved in anhydrous DCM (0.075 M) in a glovebox and irradiated with blue light under a balloon of O_2. After irradiation for 1 h, SEC analysis revealed a 96% reduction in M_n relative to **4.1** (ΔM_n = -113 kDa), which mirrored the enhanced activity we originally observed under ambient conditions (Figure 4.25; Table 4.1). Conducting a similar experiment in the presence of a colorimetric peroxide indicator was consistent with the formation of organic peroxides under the reaction conditions

(Figure 4.4). We note that no peroxide formation was observed when an analogous experiment was conducted with O_2 being rigorously excluded (Figure 4.5). Furthermore, irradiating **4.1** under an argon atmosphere in the presence of an exogenous peroxide (i.e., *t*-butyl hydroperoxide) resulted in a 94% reduction compared to an analogous experiment conducted without added peroxide (i.e., 72% reduction) (Figure 4.26). These results are consistent with previous observations of peroxide-mediated polymer degradation,[186,187] and they suggest that photoredox catalysis can couple multiple single-electron editing coordinates to achieve nearly quantitative polymer consumption under mild conditions.

Not only does ambient atmosphere afford more degradation, but it also increased the rate at which polymer degradation occurred. Using standard air-free techniques, a DCM (3 mL) solution of **4.1** (25 mg; 0.27 mmol; 0.075 M) was added to a Schlenk flask under N_2, followed by a DCM (0.55 mL) solution of **4.2** (5.4 mg; 0.013 mmol) and $(PhS)_2$ (14.5 mg; 0.07 mmol). The vessel was irradiated with blue light under an N_2 atmosphere, and aliquots (0.1 mL) were removed every minute for a period of 10 min. The samples were diluted with THF, and the changes in polymer molar mass were determined using SEC (Figure 4.19), which indicated a ~60% reduction in molar mass.[189] A plot of M_n vs irradiation time revealed a monotonic decrease in molecular weight (Figure 4.20), which would be consistent with random chain-scission along the backbone. We posited that a model used to empirically elucidate the rate of stochastic degradation, such as the example (eq 1) developed by Malhotra and coworkers,[190] could be used fit our data.

$$\frac{1}{M_t} = \frac{1}{M_i} + K't \qquad (1)$$

Here, $K' = k_{obs}/M_0$, k_{obs} is the polymer cleavage rate constant, M_0 is the molar mass of the repeat unit, M_i is the initial M_z of the polymer, and M_t is the M_z following irradiation for time *t*. A representative plot of $1/M_t - 1/M_i$ versus irradiation time (Figure 4.2) reveals the expected linear correlation ($k_{obs} = 1.96 \times 10^{-2} \pm 2.37 \times 10^{-4}$). We then repeated these kinetic studies under an ambient atmosphere. A DCM (3 mL) solution of **4.1** (27 mg; 0.28 mmol) was added to a vessel, followed by a DCM (0.7 mL) solution of **4.2** (5.6 mg; 0.014 mmol) and $(PhS)_2$ (15.4 mg; 0.07 mmol). The reaction solution was irradiated with a blue LED lamp, and aliquots (0.1 mL) were removed as described above for SEC analysis, which revealed an 88% reduction in molar mass.[191] A representative plot of $1/M_t - 1/M_i$ versus irradiation time revealed the observed rate of degradation increased 6-fold relative to the inert conditions ($k_{obs} = 1.21 \times 10^{-1} \pm 6.66 \times 10^{-3}$; Figure 4.2). Furthermore, irradiating **4.1** under ambient conditions in the presence of a radical trap (i.e., (2,2,6,6-tetramethylpiperidin-1-yl)oxyl; TEMPO) resulted in a near complete shutdown of the degradation activity ($k_{obs} = 2.35 \times 10^{-3} \pm 5.65 \times 10^{-4}$; Figure 4.2), which further implicated the need for oxidatively generated radical species. Efforts are currently underway to further elucidate the exact mechanistic role of oxygen in this SEPE strategy.

4.3.3 Prolonged Degradation of cis-Polyisoprene

We were curious if prolonging the irradiation time (e.g., 96 h) would result in products with significantly reduced molar mass that would be analogous to waxes and fuels (i.e., C_{20} - C_{60}). Since these materials are typically derived from petroleum feedstocks, we posited that the degradation of linear polyalkenamers, such as **4.4,** would afford comparable species. To test this concept, a DCM (18 mL) solution of **4.4** (95.3 mg; 1.4

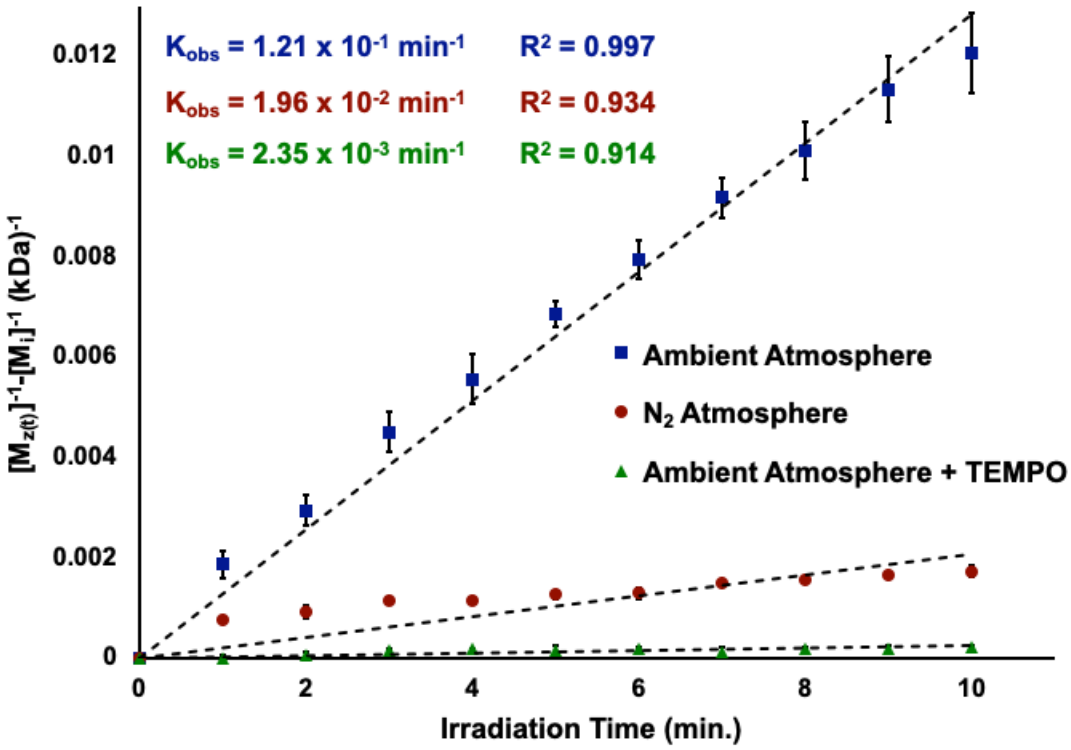

Figure 4.2: Representative kinetic plots for photoediting of **4.1** highlighting the differences in rates when conducted under ambient atmosphere (blue squares), under N_2 atmosphere (red circles), or under ambient atmosphere with an added radical trap (green triangles).

mmol) was added to a scintillation vial followed by a DCM (0.5 mL) solution of **4.2** (27.7 mg; 0.070 mmol) and $(PhS)_2$ (76 mg; 0.35 mmol). The vessel was irradiated with a blue LED lamp under ambient conditions for 96 h. The crude mixture was passed through a short plug of silica and solvent was removed under a gentle stream of N_2. Subsequent SEC analysis of the isolated residue (**4.6**) revealed a 99.5% reduction in molar mass (ΔM_n = -445 kDa) (Figure 4.28), however, this was accompanied by extensive (>30%) thiol-ene coupling supported by ^{1}H NMR spectroscopic analysis (Figure 4.55; note: >5% of thiol-ene coupling is only observed reactions that go for extended periods [> 6 h]). To remove the coupled thioethers, we conducted a simple desulfurization protocol with Raney Nickel in the presence of H_2. A THF (10 mL) solution of **4.6** (124 mg) was added to a THF (10 mL) suspension of Raney Nickel, placed under a balloon of H_2, and stirred for 20 hours. After which the mixture was filtered through short plugs of celite and basic alumina and stored as a THF solution for further characterization. SEC analysis revealed a further decrease in molar mass attributed to loss of the thioethers (Figure 4.29). However, in-depth characterization (i.e., GC-MS) of the products of degradation are currently ongoing.

4.3.4 Hydroaddition Substrate Scope

Finally, we were curious if we could trap the putative radical cation intermediate with nucleophiles to access functionalized species. We initially targeted hydroetherifications,[178] as this chemistry has been well-established with **4.3**. We prepared a solution of **4.3** (5 mg; 0.013 mmol; 5 mol%) and $(PhS)_2$ (6 mg; 0.028 mmol; 10 mol%) in 50:50 DCE:DCM (0.5 mL). The catalyst solution was added to a separate vessel containing **4.1** (25 mg; 0.26 mmol; 0.075 M in 50:50 DCE:DCM), followed by MeOH (30μL; 0.78 mmol; 300 mol%

relative to **4.1**). The reaction mixture was then irradiated under an N_2 atmosphere with blue light. After 48 h, the reaction mixture was filtered through a short plug of silica gel and concentrated to afford a viscous solution. Polymeric materials were precipitated by adding excess MeOH, isolated by filtration, and washed with excess pentane. The resultant solid, **4.7**, (50% yield) was subjected to ^{1}H NMR spectroscopic analysis, which revealed the presence of characteristic methoxy and methine protons (δ = 3.35 and 3.02 ppm, respectively; Figure 4.39) consistent with hydroetherification. Integration of the new methoxy protons relative to the residual olefin protons was consistent with ~50% hydroetherification (Figure 4.39). SEC analysis of the isolated material revealed an 86% reduction in molar mass, consistent with our prior observations (Figure 4.15.[192] We found that alcohols with bulkier substituents (i.e., benzyl alcohol) could also be coupled to the polymer fragments using an analogous protocol (Figure 4.41). We next sought to investigate the viability of other nucleophilic species such as thiols, carboxylic acids,[193] and azides,[194] as these functionalities can alter physical properties and facilitate further elaborations. These experiments were carried out using the same conditions described above (**4.3**, 5 mol%, $(Ph\text{-}S)_2$ 10 mol%, 50:50 DCM:DCE) with nucleophiles (300 mol%.) such as acetic acid, thiophenol, and trimethylsilylazide ($TMSN_3$). Extended reaction times (7 days) were required to achieve modest conversion (7-30%; Figure 4.3; Bottom). More specifically, hydroacetoxylation was achieved in low conversion (~7%), and respectable yield (97%) (see experimental; Figure 4.45 and 4.57). This SEPE protocol also facilitates the hydroaddition of simple thioethers (i.e., thiophenol) (Figure 4.3). ^{1}H NMR

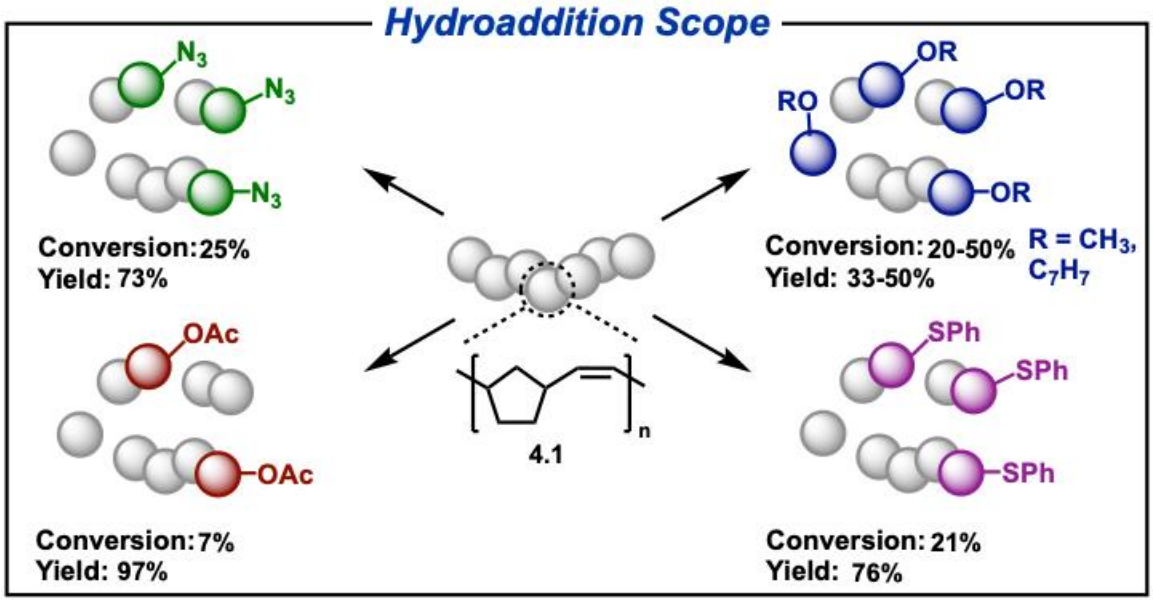

Figure 4.3: Cartoon depicting hydroaddition substrate scope of **4.1.**

spectroscopic analysis of the isolated residue (76% yield) revealed new aromatic and methine signals consistent with thioetherification (δ = 6.9 -7.3 ppm, and 2.9 ppm, respectively) which indicated 21% conversion (Figure 4.43). Moreover, we could leverage this methodology to access azide functionalized materials (Figure 4.3). Presence of the azide (determined to be a major product) was supported by IR spectroscopy (Figure 4.58), and ^{1}H NMR spectroscopic analysis suggested 25% conversion to the azidated product (73% yield) (Figure 4.47).[195] While preliminary, these results illustrate that this photoediting strategy will facilitate myriad hydroadditions of polyalkenamers to access functionalized species.

4.4 Conclusions

In conclusion, we have shown that photoredox manipulation of olefins can be leveraged toward the editing of various polyalkenamer scaffolds. This single-electron editing approach can reduce the molar mass by 96%. Oxygen also has a significant role in the degradation mechanism, as this allows access to even lower molecular weight species. This SEPE approach can leverage natural sunlight as a light source to promote degradation of various polyalkenamers. This methodology can be conducted for longer periods (96 h) to afford low molar mass carbon fragments. Furthermore, the reactive species generated upon single-electron oxidation can be trapped using exogenous reagents (e.g., alcohols, carboxylic acids, thiols, and nitrogen groups) to afford functionalized scaffolds. We envision this work will serve as inspiration to apply further photoredox chemistries toward polymeric architectures and further expand the chemical space for polymer editing strategies.

4.5 Acknowledgements

I thank Dominic Coughlin for assistance with synthetic work.

4.6 Experimental

4.6.1 General Materials and Methods

Unless otherwise noted, solvents were dried on an MBraun solvent purification system with 3Å molecular sieves and degassed via three freeze-pump-thaw cycles. *Cis*-1,4-polybutadiene and *cis*-1,4-polyisoprene (purified by precipitation from methanol) were purchased from Sigma. All other reagents and materials were obtained from commercial sources and used without further purification unless otherwise noted. Oxygen and water sensitive manipulations were performed in a N_2 filled MBraun glovebox or using standard Schlenk techniques with oven- and flame- dried glassware. ^{1}H and ^{13}C NMR spectral data were collected on a Bruker 500 MHz NMR, Varian 600 MHz NMR, Varian 500 MHz NMR, or Varian 300 MHz NMR spectrometer. Chemical shifts (δ) are reported in ppm using the residual solvent as reference. IR spectra were collected on a Bruker Alpha II FT-IR with Platinum ATR accessory or a Thermo Scientific Nicolet IS5 spectrometer with an ATR iD7 attachment (germanium crystal). Centrifugation was conducted using a OHAUS Frontier 5306 mini centrifuge spun at 6,000 rpm for 20-minute cycles. Size Exclusion Chromatography (SEC) data were collected on an Omnisec Resolve and Omnisec Reveal System using triple detection with detectors in series: UV, light scattering, viscometer, and refractive index and three Viscotek styrene divinylbenzene copolymer columns (in series T3000, T4000, and T5000) at a flow rate of 1 mL/min and thermostatted to 30°C using tetrahydrofuran (THF) as the eluent (SEC 1) or an Agilent 1260 infinity II SEC equipped

with a Wyatt Dawn Helios 8 multiangle light scattering detector, ViscoStar III, and an Optilab T-rEX at a flow of 1 mL/min with THF as the eluent (SEC 2). Unless otherwise noted, Molecular weight data were acquired with SEC 1. Molecular weight and dispersity data calculated from triple detection or conventional calibration relative to polystyrene standards are reported. All photochemical transformations were performed using an ABI 12w Blue LED lamp (λ_{EX} = 450 – 460 nm), where the reaction vessels were placed 10 cm away from the light source and the temperature did not exceed 35 °C.

4.6.2 Representative Procedure for the Preparation of cis-Polynorbornene (4.1)

A flame dried 250 mL Schlenk flask was charged with norbornene (3.0179 g; 31.9 mmol), THF (126 mL), and a Teflon stir bar. The monomer solution was degassed via three cycles of freeze-pump-thaw and cooled to -30 °C. A solution of Z-selective Grubbs catalyst (40 mg; 0.05 mmol in 1 mL THF) was prepared in an N_2 filled glovebox and then added to the monomer solution via syringe. The reaction temperature was maintained between -40 °C and -20 °C for 4 h, after which the polymerization was quenched with ethyl vinyl ether (2 mL; 25.05 mmol) in THF (1 mL). Polymeric material was precipitated from methanol, collected on a medium porosity fritted funnel, and dried in vacuo. The polymer was dissolved in minimal DCM, precipitated from MeOH a second time, collected via filtration, and dried in vacuo. The polymer was dissolved in THF and precipitated from methanol two additional times. The title material (**4.1**) was recovered as a white solid (1.4323 g, 47.5% yield) representative SEC data for this isolated polymer shown in Figure 4.6 (red Trace, 328 kDa). Spectral data were consistent with literature reports, and representative ^{1}H

Scheme 4.2: Z-selective Polymerization to afford **4.1**

and ^{13}C NMR spectra are shown in Figure 4.33 and Figure 4.34, respectively. Olefin E:Z ratio of 1:24 was determined based on the relative integrations of the Z (δ = 5.20) and E (δ = 5.35) olefin resonances. SEC data for all polymer used in this study are shown in Figure 4.6.

4.6.3 Representative Procedure for the Preparation of Low M_n Polynorbornene (4.1)

A flame dried 25 mL Schlenk flask was charged with norbornene (500 mg; 5.31 mmol), DCM (20 mL), and a Teflon stir bar. A solution of Grubbs 3rd generation catalyst (85 mg; 0.10 mmol in 1.5 mL DCM) was added via syringe. The reaction was stirred at 0 °C for 30 min, after which the polymerization was quenched with excess ethyl vinyl ether (0.5 mL; 0.91 mmol) and concentrated to minimal volume. The solution was passed over a plug of basic alumina twice and concentrated to minimal volume for precipitation from MeOH before drying in vacuo. The title material was recovered as an off-white powder (423 mg, 85% yield). SEC data for all polymers utilized for SEPE degradation and hydroaddition studies is provided in Figure 4.7. Spectral data were consistent with literature reports.[26]

4.6.4 Procedure for Inert Atmosphere Photoediting of Polyalkenamers (Method A)

In a N_2 filled glovebox, a 2-dram vial was charged with **4.1** (25 mg; 0.266 mmol), a Teflon stir bar, and DCM (3.54 mL). The mixture was stirred until all polymer was dissolved. In a separate vessel, **4.2** (5.3 mg; 0.013 mmol), and $(PhS)_2$ (14.5 mg; 0.067 mmol) were added followed by DCM (0.5 mL). After which the combined catalyst solution was added to the mixture of **4.1**, sealed with a Teflon lined cap, removed from the glovebox, and irradiated with a 12W blue LED lamp (λ_{EM} = 450 – 460 nm) for 1 h with stirring. After which the

crude reaction mixture was filtered over a plug of silica and concentrated to a volume of ~1mL under a gentle stream of N_2. Polymeric material was precipitated from addition to MeOH, followed by centrifugation. The resulting supernatant was decanted, and the isolated solids were dried for 16 in vacuo.

4.6.5 Procedure for Ambient Atmosphere Photoediting of Polyalkenamers (Method B)

A 2-dram vial was charged with **4.1** (25 mg; 0.266 mmol), a Teflon stir bar, and technical-grade DCM (3.04 mL). The mixture was stirred until all polymer was dissolved. In a separate vessel, **4.2** (5.3 mg; 0.013 mmol), and $(PhS)_2$ (14.5 mg; 0.067 mmol) were added followed by DCM (0.5 mL). After which the combined catalyst solution was added to the mixture of **4.1** and irradiated with a 12 W blue LED lamp (λ_{EM} = 450 – 460 nm) for 1 h with stirring. After which the crude reaction mixture was filtered over a plug of silica and concentrated to a volume of ~1mL under a gentle stream of N_2. Polymeric material was precipitated from addition to MeOH, followed by centrifugation. The resulting supernatant was decanted, and the isolated solids were dried for 16 in vacuo.

4.6.6 Details for Photoediting Reaction Optimization

Reaction optimizations were conducted under N_2 and followed the general procedure outlined above (Method A). We varied conditions such as: HAT catalyst identity (note: alkyl thiols such as 1-adamantane thiol and 1-dodecanethiol afforded intractable materials which precluded characterization), Photoredox catalyst identity (2,4,6-Triphenylpyryllium

Scheme 4.3: Generalized Photoediting Scheme

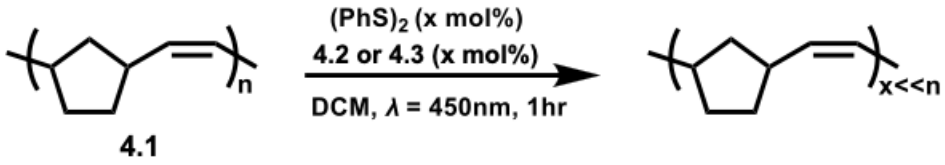

4.1

tetrafluoroborate; **4.2**, & 9-Mesityl-10-methylacridinium tetrafluoroborate; **4.3**) and their loadings (1-10 mol%), HAT catalyst loadings (10-50 mol%), Reaction concentrations (0.075M & 0.15M), and reaction atmosphere (N_2 and Ambient) (see Table 4.2). Representative SEC data shown in Figures 4.8 – 4.13.

4.6.7 Details for Photoediting Control Experiments

Control experiments were conducted under N_2 following the general procedure outlined above (Method A). Deviations and Molecular weight data are shown in Table 4.1. SEC data shown in Figure 4.14 Spectral data showing olefin isomerization shown in Figure 4.50.

4.6.8 Degradation of cis-1,4-polyisoprene (4.4)

A 20 mL scintillation vial was charged with **4.4** (50 mg, 0.734 mmol), DCM (8.88 mL), and a Teflon stir bar. A separate 1-dram vial was charged with $(PhS)_2$ (41 mg, 0.184 mmol), **4.2** (14.9 mg, 0.037 mmol), DCM (1 mL) and added to the solution of **4.4**. The reaction mixture was irradiated with 12W Blue LED for 1 hour with stirring. After which the crude solution was filtered through plug of silica, concentrated to a minimal volume, and precipitated from addition to MeOH. Polymeric material was isolated following centrifugation and decanting of the supernatant. The residue was washed with hexanes and dried for 16 in vacuo. SEC data of the isolated solids (40 mg; 80% mass recovery) shown in Figure 4.27. Representative spectral data shown in Figures 4.51 and 4.52.

This material was also utilized for prolonged degradation experiments (i.e., 96 h irradiation)

Table 4.2: Results from optimization experiments.

Entry	$(PhS)_2$ (Xmol%)	Atmosphere	PC (Xmol%)	[M]	Initial M_n (kDa)	Final M_n (kDa)	Reduction (%)	Yield (%)
1	25 mol%	Nitrogen	4.2 (5mol%)	0.075M	328	103	68.6	95.7
2	25 mol%	Nitrogen	4.3 (5 mol%)	0.075M	328	124	62.2	27.9
3	25 mol%	Nitrogen	4.2 (1 mol%)	0.075M	328	106	67.7	82.1
4	25 mol%	Nitrogen	4.2 (10 mol%)	0.075M	328	100	69.5	98.1
5	10 mol%	Nitrogen	4.2 (5 mol %)	0.075M	328	136	58.5	75.5
6	50 mol%	Nitrogen	4.2 (5 mol %)	0.075M	328	100	69.5	90.2
7	25 mol%	Nitrogen	4.2 (5 mol %)	0.150M	328	128	61.0	82.9
8	25 mol%	Ambient	4.2 (5 mol %)	0.075M	328	12	96.3	65.8

Note: the degradation of **4.4** could also be prolonged (96 h) to afford materials with a 99.5 reduction in molar mass. This was conducted on a larger scale to aid in subsequent characterization. **4.4** (95.3 mg, 1.399 mmol), **4.2** (27.7 mg, 0.070 mmol), $(PhS)_2$ (76.4 mg, 0.350 mmol), and DCM (18.7 mL). Reaction setup and purification was outlined above (Method B). SEC data of the isolated pale-yellow residue shown in Figure 4.29. Spectral data shown in Figures 4.55 – 4.56.

4.6.9 Degradation of cis-1,4-polybutadiene (4.5)

A 20 mL scintillation vial was charged with **4.5** (57.3 mg, 1.06 mmol), DCM (13 mL), and a Teflon stir bar. A separate 1-dram vial was charged with $(PhS)_2$ (57.8 mg, 0.233 mmol), **4.2** (21 mg, 0.053 mmol), DCM (1.1 mL) and added to the solution of **4.5**. The reaction mixture was irradiated with 12W Blue LED for 1 hour with stirring. After which the crude solution was filtered through plug of silica, concentrated to a minimal volume, and precipitated from addition to MeOH. Polymeric material was isolated following centrifugation and decanting of the supernatant. The residue was washed with hexanes and dried for 16 in vacuo. SEC data of the isolated solids (50 mg; 88% mass recovery) shown in Figure 4.28. Representative spectral data shown in Figures 4.53 and 4.54

4.6.9 Degradation of 4.1, 4.4, and 4.5 Using Natural Sunlight

Reaction setup was consistent with our general procedure (Method B). **4.1** (26.3 mg, 0.279 mmol), $(PhS)_2$ (15.1 mg, 0.069 mmol) **4.2** (6.1 mg, 0.015 mmol), and technical-grade DCM (3.72 mL). Reaction vessels were placed on a raised windowsill in direct sunlight for 2 h. A thermometer was placed next to vials and the temperature did not exceed 40 °C. Workup

Scheme 4.4: Photoediting of **4.4**

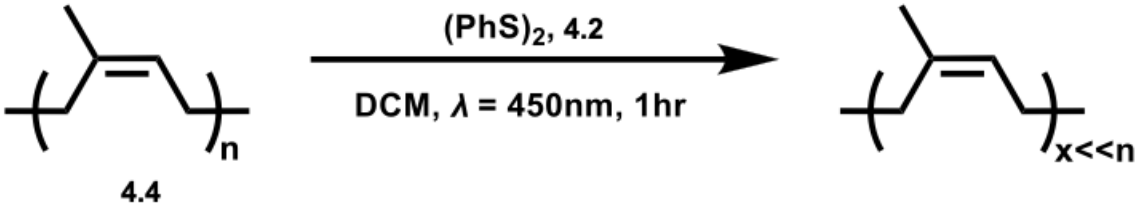

4.4

Scheme 4.5: Prolonged photoediting of **4.4**

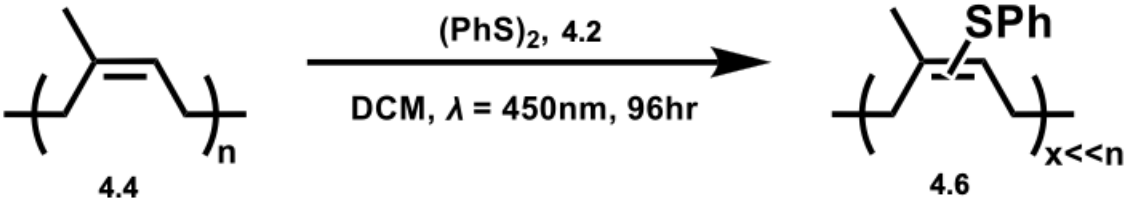

4.4 4.6

and isolation is outlined above (Method B). SEC data of the isolated solids (25.9 mg; 98% mass recovery) shown in Figure 4.30.

Reaction setup was consistent with our general procedure (Method B). **4.4** (20.4 mg, 0.299 mmol), $(PhS)_2$ (16.7 mg, 0.076 mmol) **4.2** (6 mg, 0.015 mmol), and technical-grade DCM (4 mL). Reaction vessels were placed on a raised windowsill in direct sunlight for 2 h. A thermometer was placed next to vials and the temperature did not exceed 40 °C. Workup and isolation is outlined above (Method B). SEC data of the isolated solids (20.2 mg; 99% mass recovery) shown in Figure 4.31.

Reaction setup was consistent with our general procedure (Method B). **4.5** (20.4 mg, 0.377 mmol), $(PhS)_2$ (21 mg, 0.096 mmol) **4.2** (7.5 mg, 0.019 mmol), and technical-grade DCM (5 mL). Reaction vessels were placed on a raised windowsill in direct sunlight for 2 h. A thermometer was placed next to vials and the temperature did not exceed 40 °C. Workup and isolation is outlined above (Method B). SEC data of the isolated solids (18.7 mg; 92% mass recovery) shown in Figure 4.32.

4.6.10 Investigation on the Impact of H_2O

A 10 mL Schlenk flask was charged with a technical grade DCM (2.71 mL) solution of **4.1** (26.2 mg, 0.278 mmol) and a Teflon stir bar. The vessel was sealed with a rubber septum followed by 2 cycles of degassing (freeze/pump/thaw). In a separate vessel, **4.2** (6.1 mg, 0.017 mmol), $(PhS)_2$ (15.2 mg, 0.070 mmol) were added followed by technical grade DCM (1.0mL). The catalyst solution was taken up in a syringe and added to the frozen solution

Scheme 4. 6: Photoediting of **4.5**

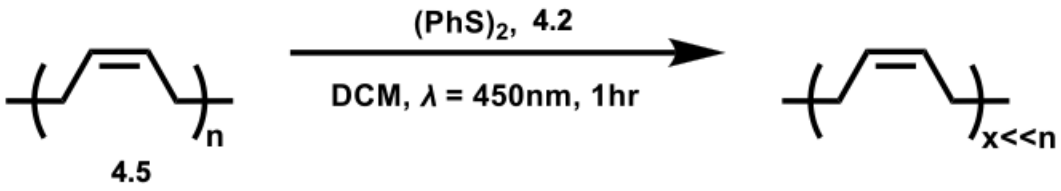

of **4.1**, after which a final degas cycle was performed and allowed to thaw under an argon balloon. The vessel was irradiated with 12W Blue LED for 1hr with stirring. The workup and isolation were performed as outlined above (Method B) Experiment was conducted in triplicate. Average SEC data shown in Figure 4.25.

4.6.11 Investigation on the Impact of Oxygen

In a N_2 filled glovebox, a 10 mL Schlenk flask was charged with an anhydrous/degassed DCM (2.57 mL) solution of **4.1** (25.2 mg, 0.268 mmol) and a Teflon stir bar. The vessel was sealed with a rubber septum, removed from the glovebox and the atmosphere removed via 2 cycles of degassing (freeze/pump/thaw). In a separate vessel, **4.2** (5.5 mg, 0.015 mmol), $(PhS)_2$ (15.0 mg, 0.069 mmol) followed by anhydrous/degassed DCM (1.0mL). The catalyst solution was taken up in a gas-tight syringe and the needle inserted into septa-capped 1-dram vial to protect from air exposure. This solution was injected into frozen solution of **4.1** under positive N_2 flow followed by a final degassing cycle. The solution was allowed to thaw under a balloon of ~98% oxygen, which was passed over 3 Å molecular sieves. The solution was irradiated with a 12W Blue LED for 1hr with stirring. The workup and isolation were performed as outlined above (Method B) Experiment was conducted in triplicate. Average SEC data shown in Figure 4.25.

4.6.12 Investigation on the Impact of Exogenous Peroxides

A 10 mL Schlenk flask was charged with a technical-grade DCM (2.57 mL) solution of **4.1** (25.2 mg, 0.268 mmol) and a Teflon stir bar. The vessel was sealed with a rubber septum, and the atmosphere was removed via 2 degassing cycles (freeze/pump/thaw). In a separate

vessel, **4.2** (5.5 mg, 0.015 mmol), $(PhS)_2$ (15.1 mg, 0.069 mmol) and *t*-Butyl hydroperoxide (51 µL, 0.535 mmol; ~5-6M in decane) were added, followed by technical-grade DCM (1.0mL). This catalyst/peroxide solution was taken up in a syringe and added to the frozen solution of **4.1** under positive N_2 pressure followed by a final degassing cycle. The solution was allowed to thaw under a balloon of argon. The solution was irradiated with a 12W Blue LED for 1hr with stirring. The workup and isolation were performed as outlined above (Method B). Experiment was conducted in triplicate. SEC data shown in Figure 4.26.

4.6.13 Qualitative Investigation for the Presence of Organic Peroxide Species

The experimental setup was outlined above (Method B) and used the optimized conditions on a 0.27 mmol scale with respect to **4.1**. Prior to irradiation a CTL Scientific Supply Corp QUANTOFIX Peroxide Test Strip was dipped into the solution and allowed to dry (Figure 4.4, top). The solution was irradiated with 12W Blue LED for 10 minutes with stirring. A second peroxide test strip was dipped into the solution and allowed to dry (Figure 4.4, bottom). The dry test strip turned a blue color, which indicated presence of organic peroxides. A control experiment (using Method A) was conducted as described above, and a peroxide strip was dipped in the solution under positive N_2 pressure before irradiation (Figure 4.5 top), and a second test strip was dipped into the solution after 10 minutes of irradiation under positive N_2 pressure (Figure 4.5, bottom). No change in color indicated a negative result for presence of peroxides. Photographs of each experiment shown below.

4.6.14 Degradation Kinetics of 4.1 Under N_2 Atmosphere

In a N_2 filled glovebox, a 10 mL Schlenk flask was charged with a DCM (3.18 mL) solution

Figure 4.4: Photograph showing peroxide test strips after being dipped into the solution prior to irradiation (top) and after 10 minutes (bottom) during the photoediting of **4.1** under ambient atmosphere.

Figure 4.5: Photograph showing peroxide test strips after being dipped into the solution prior to irradiation (top) and after 10 minutes (bottom) during the photoediting of **4.1** under N_2.

Table 4.3: Kinetic study for photoediting degradation of **4.1** under N_2

Entry	Irradiation Time (min)	M_n[a] (kDa)	M_z[a] (kDa)
1	0	292 ±9	960±59
2	1	188±2	549±14
3	2	171±5	509±25
4	3	156±7	459±7
5	4	152±4	457±6
6	5	144±7	432±12
7	6	139±6	428±15
8	7	134±3	393±6
9	8	130±3	383±4
10	9	123±2	368±6
11	10	116±2	362±12

[a]Average of three experiments

of **4.1** (26 mg, 0.276 mmol) and a Teflon stir bar. The vessel was sealed with a rubber septum and covered with aluminum foil. In a separate vessel, **4.2** (5.5 mg, 0.014 mmol) and $(PhS)_2$ (15.1 mg, 0.069 mmol) were dissolved in DCM (0.5 mL), taken up in a syringe and added to the solution of **4.1**. The vessel was removed from the glovebox, equipped to a Schlenk line and the solution placed under an atmosphere of N_2. After which an aliquot (0.1 mL) was removed and diluted to 1 mL with THF for SEC analysis (t_0). Aluminum foil was removed, and the bulk solution was irradiated with a 12w Blue LED. At 1-minute intervals, an aliquot (0.1 mL) was removed, the process for t_0 was repeated until 10 aliquots had been removed (t_1-t_{10}). Aliquot vials were covered from ambient light for the remainder of the experiment. Aliquot solutions were filtered through a 0.2µm syringe filter into autosampler vials for SEC characterization. Experiment was conducted in triplicate. The rate of chain cleavage was calculated according to equation 1 to be $1.96 \times 10^{-2} \pm 2.37 \times 10^{-4}$ min^{-1}. A plot of $1/M_t - 1/M_i$ versus irradiation time is shown in Figure 4.2. Evolution of M_n over time is shown in Figures 4.20 and Table 4.3

4.6.15 Degradation Kinetics of 4.1 Under Ambient Atmosphere

A 2-dram vial was charged with a technical-grade DCM (3 mL) solution of **4.1** (26.6 mg, 0.283 mmol) and a Teflon stir bar. The vial was sealed with a septa-cap with a needle inserted for venting. In a separate vessel, **4.2** (5.6 mg, 0.014 mmol) and $(PhS)_2$ (15.1 mg, 0.071 mmol) were dissolved in DCM (0.77 mL) and injected into polymer solution. An aliquot (0.1 mL) was quickly removed and diluted to 1 mL with THF for SEC analysis (t_0). After which the bulk solution was irradiated with a 12W Blue LED. At 1-minute intervals, an aliquot (0.1 mL) was removed, the process for t_0 was repeated until 10 aliquots had been

removed (t_1-t_{10}). Aliquot vials were covered from ambient light for the remainder of the experiment. Aliquot solutions were filtered through a 0.2μm syringe filter into autosampler vials for SEC characterization. Experiment was conducted in triplicate. The rate of chain cleavage was calculated according to equation 1 to be $1.21 \times 10^{-1} \pm 6.66 \times 10^{-3} min^{-1}$. A plot of $1/M_t - 1/M_i$ versus irradiation time is shown in Figure 4.2. SEC data shown in Figure 4.21 Evolution of M_n over time is shown in Figure 4.22 and Table 4.4

4.6.16 Degradation Kinetics of 4.1 Under Ambient Atmosphere with TEMPO

A 2-dram vial was charged with a DCM (3 mL) solution of **4.1** (26.2 mg, 0.278 mmol) and a Teflon stir bar. The vial was sealed with a septa-cap with a needle inserted for venting. In a separate vessel, **4.2** (5.6 mg, 0.014 mmol) and $(PhS)_2$ (15.1 mg, 0.069 mmol) and (2,2,6,6-Tetramethylpiperidin-1-yl)oxyl (TEMPO, 131mg, 0.838mmol) were dissolved in DCM (0.71 mL) and injected into the polymer solution. An aliquot (0.1 mL) was removed and diluted to 1 mL with THF for SEC analysis (t_0) (Table 4.5). After which the bulk solution was irradiated with 12W Blue LED. At 1-minute intervals, aliquots (0.1) were removed, via the same technique as described above, and diluted to 1 mL with THF (samples t_1-t_{10}). Aliquot vials were covered from ambient light for the remainder of the experiment. Solutions filtered through a 0.2μm syringe filter into SEC vials for characterization. Experiment was conducted in triplicate. The rate of chain cleavage was calculated according to equation 1 to be $2.35 \times 10^{-3} \pm 5.65 \times 10^{-4} min^{-1}$. A plot of $1/M_t - 1/M_i$ versus irradiation time is shown in Figure 4.2. SEC data shown in Figure 4.23. Evolution of M_n over time is shown in Figures 4.24 and Table 4.5

Table 4.4: Kinetic study for photoediting degradation of **4.1** under ambient atmosphere

Entry	Irradiation Time (min)	M_n[a] (kDa)	M_z[a] (kDa)
1	0	271±	865±71
2	1	138±	330±24
3	2	109±	243±15
4	3	87±	176±10
5	4	69±	149±9
6	5	62±	125±3
7	6	52±	110±4
8	7	45±	97±3
9	8	42±	89±4
10	9	36±	80±4
11	10	33±	76±4

[a]Average of three experiments

Table 4.5: Kinetic study for photoediting degradation of **4.1** under ambient atmosphere + TEMPO

Entry	Irradiation Time (min)	M_n[a] (kDa)	M_z[a] (kDa)
1	0	240 ±7	677±41
2	1	234±8	672±41
3	2	226±6	646±41
4	3	225±7	606±11
5	4	223±7	604 ±16
6	5	220±6	608±31
7	6	218±6	601±21
8	7	217±5	624±34
9	8	216±5	594±21
10	9	215±5	599±18
11	10	214±5	591±28

[a]Average of three experiments

4.6.17 Raney Nickel Catalyzed Desulfurization of Degraded 4.4

Raney Nickel (12 mL of 50% w/w in H_2O) vacuum filtered through a fritted filter sealed with a septum. The Raney Nickel solids were washed with 1,4-dioxane (2 x 5 mL) and dry/degassed Tetrahydrofuran (THF, 2 x 10 mL) and subsequently dried for 16 h in vacuo. The dry Raney Nickel solids were suspended in dry/degassed THF and transferred via syringe into 20mL scintillation vial to prepare a ~6g Raney nickel suspension in 20mL THF. This solution was sparged with a H_2 balloon, and (3g, 10mL) of this solution was transferred to a 50 mL Schlenk flask under an H_2 atmosphere. After which a THF (10 mL) solution of **4.6** (124mg, 0.052mmol) was added to the Raney Nickel suspension under positive H_2 pressure followed by methanol (2 mL, 49.4 mmol). The reaction mixture was stirred for 20 hours at room temperature. The crude suspension was filtered through a plug of celite and basic alumina to remove Raney Nickel solids. The product was stored as THF solution and aliquots were removed as needed for subsequent characterization. SEC data of the desulfurized material are shown in Figure 4.29.

4.6.18 Hydroetherification (Methanol) of 4.1

In a N_2 filled glovebox, a 10 mL Schlenk flask was charged with 50:50 DCM:DCE (3 mL) solution of **4.1** (24.6 mg; 0.261 mmol) and a Teflon stir bar. The vessel was sealed with a rubber septum, removed from the glovebox, and MeOH (30 μL; 0.783 mmol) was added under a positive flow of N_2 followed by 2 cycles of degassing via freeze/pump/thaw. In a separate vessel, **4.3** (5.2 mg; 0.013 mmol) and $(PhS)_2$ (6 mg; 0.027 mmol) were dissolved in 50:50 DCM:DCE (0.5 mL), taken up in a gas-tight syringe and the needle inserted into a septa-capped 1-dram vial to protect from air exposure. This catalyst solution was added

Scheme 4.7: Raney Nickel Catalyzed Desulfurization of **4.6**

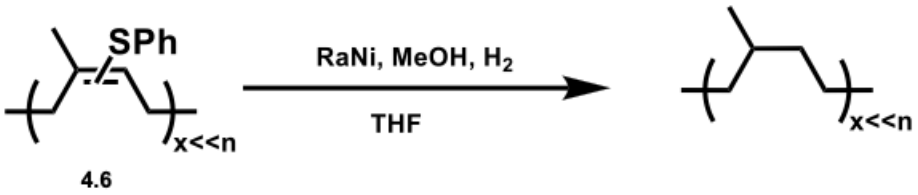

Scheme 4.8: MeOH hydroetherification of **4.1**

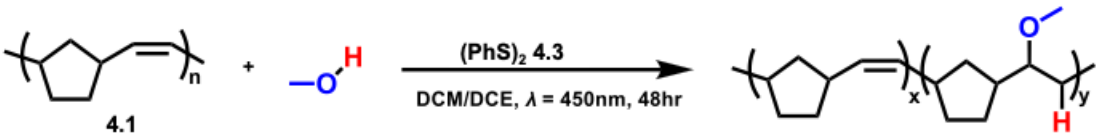

to the frozen solution of **4.1** under positive N_2 pressure, after which a final degas cycle was performed. The reaction mixture was warmed to ambient temperature (23 ° C) and irradiated with a 12W blue LED lamp (λ_{EM} = 450 – 460 nm) for 48 h under static N_2 with stirring. The crude reaction mixture was filtered through a silica plug and concentrated to a minimal volume (~ 1 mL). Polymeric material was precipitated from addition to pentane followed by centrifugation and decanting of the supernatant. The solids were dried for 16 h in vacuo (14.3 mg, 49.7% yield). Representative spectral data are shown in Figures 4.39 – 4.40. ^{1}H NMR of the residual olefin (δ = 5.2 – 5.4 ppm) against the new methoxy signal (δ = 3.35 ppm) suggest ~50% conversion to the hydroetherified product. Representative SEC data shown in Figure 4.15.

4.6.19 Hydroetherification (Benzyl Alcohol) of 4.1

In a N_2 filled glovebox, a 10 mL Schlenk flask was charged with 35:65 DCM:DCE (3 mL) solution of low M_n **4.1** (24 mg, 0.255 mmol) and a Teflon stir bar. The vessel was sealed with a rubber septum, removed from the glovebox, and benzyl alcohol (163 µL, 0.765 mmol) was added under a positive flow of N_2 followed by 2 cycles of degassing via freeze/pump/thaw. In a separate vessel, **4.3** (2.3 mg; 0.006 mmol) and $(PhS)_2$ (6.6 mg; 0.030 mmol) were dissolved in 50:50 DCM:DCE (0.4 mL), taken up in a gas-tight syringe and the needle inserted into septa-capped 1-dram vial to protect from air exposure. This catalyst solution was added to the frozen solution of **4.1** under positive N_2 pressure, after which a final degas cycle was performed. The reaction mixture was warmed to ambient temperature (23 ° C) and irradiated with a 12 W blue LED lamp (λ_{EM} = 450 – 460 nm) for 48 h under static N_2 with stirring. The crude reaction mixture was filtered through a silica

plug and concentrated to a minimal volume (~ 1 mL). Polymeric material was precipitated from addition to pentane followed by centrifugation and decanting of the supernatant. The solids were dried for 16 h in vacuo (10.2 mg, 33% yield). Representative spectral data are shown in Figures 4.41 – 4.42. ^{1}H NMR of the residual olefin (δ = 5.2 – 5.4 ppm) against the new benzyl methylene signal (δ = 4.53 ppm) suggest ~20% conversion to the hydroetherified product. Representative SEC data shown in Figure 4.16.

4.6.20 Hydrothioetherification (Thiophenol) of 4.1

In a N_2 filled glovebox, a 10 mL Schlenk flask was charged with 50:50 DCM:DCE (3.1 mL) solution of **4.1** (25.5 mg, 0.271 mmol) and a Teflon stir bar. The vessel was sealed with a rubber septum, removed from the glovebox, and thiophenol (110 µL, 1.08 mmol) was added under a positive flow of N_2 followed by 2 cycles of degassing via freeze/pump/thaw. In a separate vessel, **4.3** (5.5 mg, 0.014 mmol) was dissolved in 50:50 DCM:DCE (0.5 mL), taken up in a gas-tight syringe and the needle inserted into septa-capped 1-dram vial to protect from air exposure. This catalyst solution was added to the frozen solution of **4.1** under positive N_2 pressure, after which a final degas cycle was performed. The reaction mixture was warmed to ambient temperature (23 ° C) and irradiated with a 12 W blue LED lamp (λ_{EM} = 450 – 460 nm) for 168 h under static N_2 with stirring. The crude reaction mixture was filtered through a silica plug and concentrated to dryness under N_2 pressure. The solids were washed with pentane (2 x 3 mL) and dried for 16 h in vacuo (24 mg, 75.5% yield). Representative spectral data are shown in Figures 4.43 – 4.44. ^{1}H NMR of the residual olefin (δ = 5.2 – 5.4 ppm) against the new methine signal (δ = 2.90 ppm) suggest ~21% conversion to the hydrothioetherified product.

Scheme 4.9: Benzyl alcohol hydroetherification of low M_n **4.1**

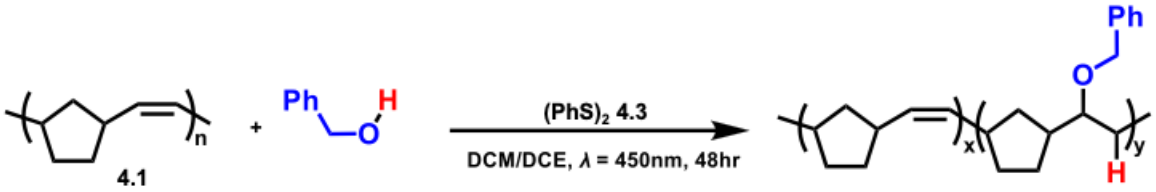

Scheme 4.10: Hydrothioetherification of **4.1**

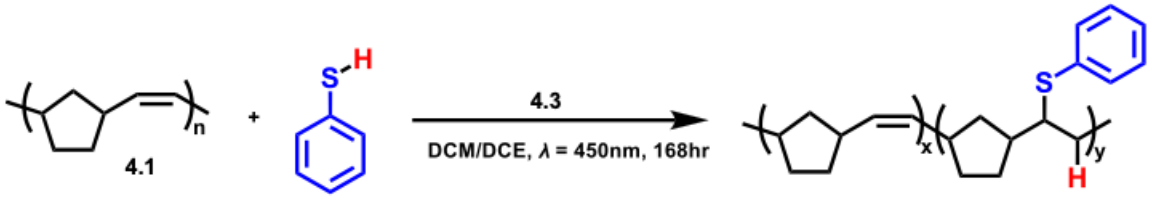

Representative SEC data shown in Figure 4.17.

4.6.21 Hydrocarboxylation (Acetic Acid) of 4.1

In a N_2 filled glovebox, a 10 mL Schlenk flask was charged with 50:50 DCM:DCE (3.06 mL) solution of **4.1** (25.1 mg, 0.267 mmol) and a Teflon stir bar. The vessel was sealed with a rubber septum, removed from the glovebox. Glacial acetic acid (46 µL, 0.8 mmol) and 2,6-Lutidine (8 µL, 0.067 mmol) were added under a positive flow of N_2 followed by 2 cycles of degassing via freeze/pump/thaw. In a separate vessel, **4.3** (5.4 mg, 0.014 mmol) and $(PhS)_2$ (5.8 mg, 0.0266 mmol) were dissolved in 50:50 DCM:DCE (0.5 mL), taken up in a gas-tight syringe and the needle inserted into septa-capped 1-dram vial to protect from air exposure. This catalyst solution was added to the frozen solution of **4.1** under positive N_2 pressure, after which a final degas cycle was performed. The reaction mixture was warmed to ambient temperature (23 ° C) and irradiated with a 12 W blue LED lamp (λ_{EM} = 450 – 460 nm) for 168 h under static N_2 with stirring. The crude reaction mixture was filtered through a silica plug and concentrated to dryness under N_2 pressure. The solids were washed with pentane (2 x 3 mL) and dried for 16 h in vacuo (26 mg, 97% yield). Representative spectral data are shown in Figures 4.45 – 4.46. ^{1}H NMR of the residual olefin (δ = 5.2 – 5.4 ppm) against the new methine signal (δ = 4.87 ppm) suggest ~5% conversion to the hydrocarboxylated product. IR spectra shown in Figure 4.56 Representative SEC data shown in Figure 4.18.

4.6.21 Hydroazidation (Trimethylsilyl Azide) of 4.1

In a N_2 filled glovebox, a 10 mL Schlenk flask was charged with 50:50 DCM:DCE (3 mL) solution of **4.1** (24.7 mg, 0.262 mmol) and a Teflon stir bar. The vessel was sealed with a rubber septum, removed from the glovebox. Trimethylsilyl azide (100 µL, 0.760 mmol) and 2,2,2-trifluoroethanol (100 µL, 1.389 mmol) were added under a positive flow of N_2 followed by 2 cycles of degassing via freeze/pump/thaw. In a separate vessel, **4.3** (5.2 mg, 0.013 mmol) and $(PhS)_2$ (5.7 mg, 0.0261 mmol) were dissolved in 50:50 DCM:DCE (0.5 mL), taken up in a gas-tight syringe and the needle inserted into septa-capped 1-dram vial to protect from air exposure. This catalyst solution was added to the frozen solution of **4.1** under positive N_2 pressure, after which a final degas cycle was performed. The reaction mixture was warmed to ambient temperature (23 ° C) and irradiated with a 12 W blue LED lamp (λ_{EM} = 450 – 460 nm) for 168 h under static N_2 with stirring. The crude reaction mixture was filtered through a silica plug and concentrated to dryness under N_2 pressure. The solids were washed with pentane (2 x 3 mL) and dried for 16 h in vacuo (26 mg, 97% yield). Representative spectral data are shown in Figures 4.47 – 4.48. ^{1}H NMR of the residual olefin (δ = 5.2 – 5.4 ppm) against the new methines signal (δ = 3.87 ppm for azido methine) δ = 3.00 ppm for thioether methine, and δ = 3.6 ppm for thrifluoroethyl ether methine) suggest ~25% conversion to the hydroazidated product, ~37% conversion to the thioetherified product, and ~10% to the trifluoroethyl etherified product. ^{19}F NMR spectra shown in Figure 4.49. IR spectra shown in Figure 4.58.

Scheme 4.11: Hydrocarboxylation of **4.1**

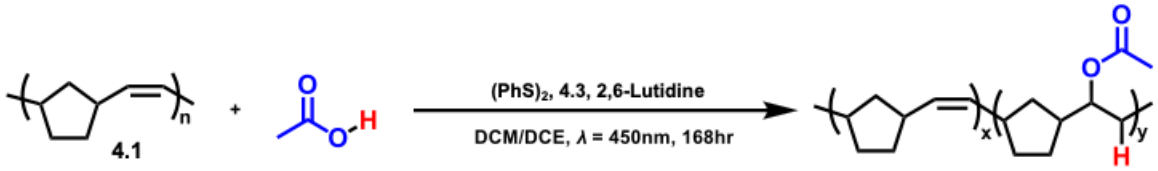

Scheme 4.12: Hydroazidation of **4.1**

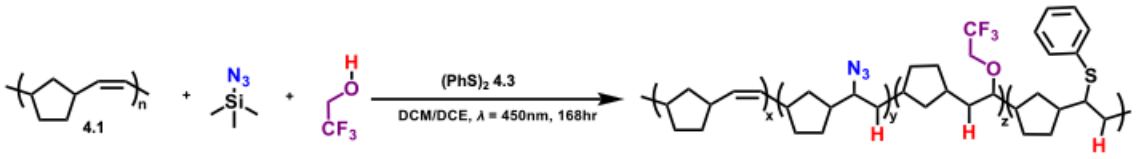

APPENDIX

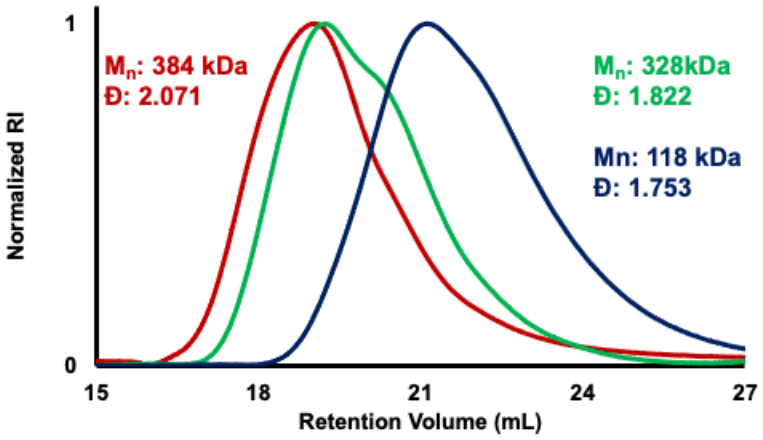

Figure 4.6: SEC data from triple detection for high M_n **4.1** samples used in this study.

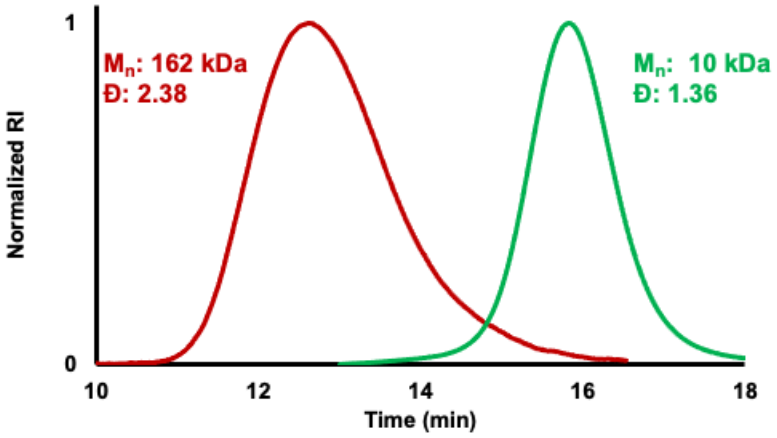

Figure 4.7: SEC data from conventional calibration (acquired on SEC 2) for high and low M_n **4.1** samples used in this study.

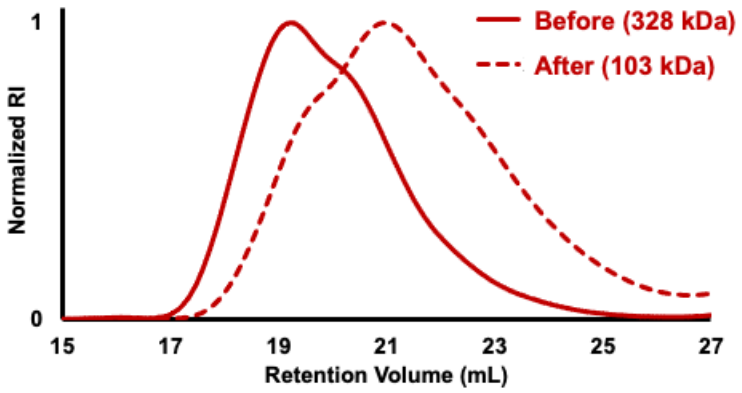

Figure 4.8: SEC data from triple detection for the degradation of **4.1**with **4.2** under N_2 (Table 4.2, entry 1). Solid trace represents starting polymer, and the dotted trace represents the isolated material following irradiation.

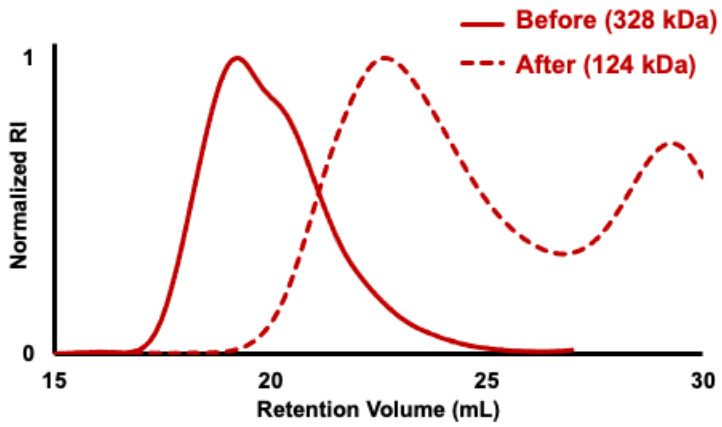

Figure 4.9: SEC data from triple detection for the degradation of **4.1**with **4.3** under N_2 (Table 4.2, entry 2). Solid trace represents starting polymer, and the dotted trace represents the isolated material following irradiation.

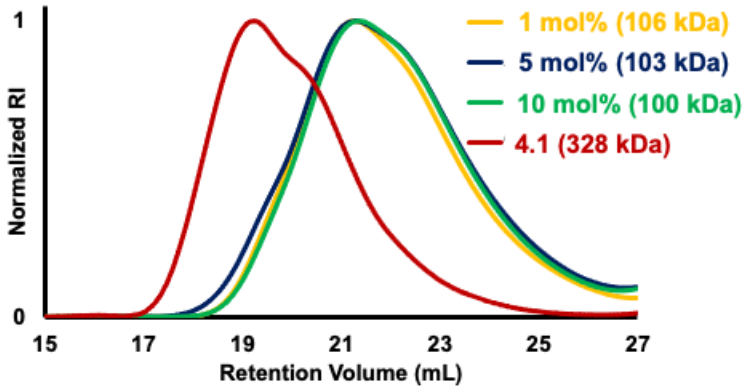

Figure 4.10: SEC data from triple detection for varied catalyst loadings of **4.2** (Table 4.2)

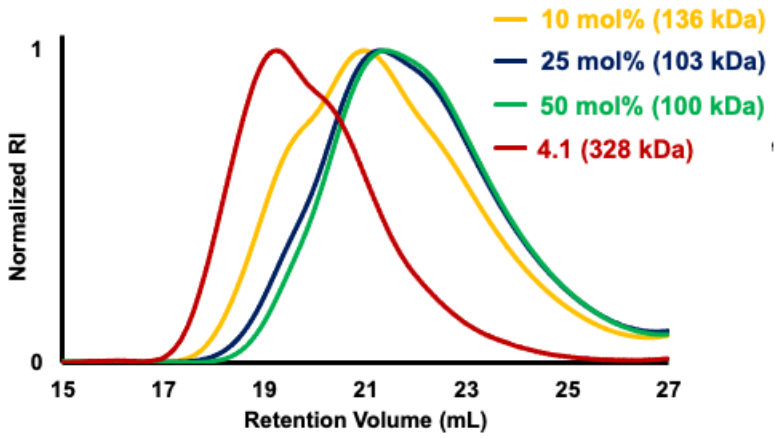

Figure 4.11: SEC data from triple detection for varied catalyst loadings of $(PhS)_2$ (Table 4.2)

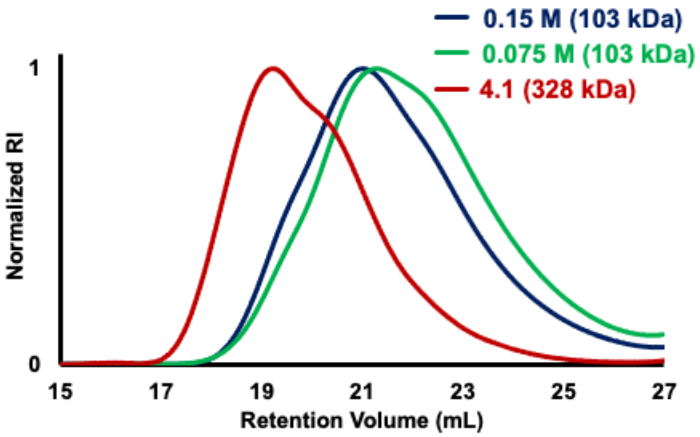

Figure 4.12: SEC data from triple detection for varied concentrations (Table 4.2)

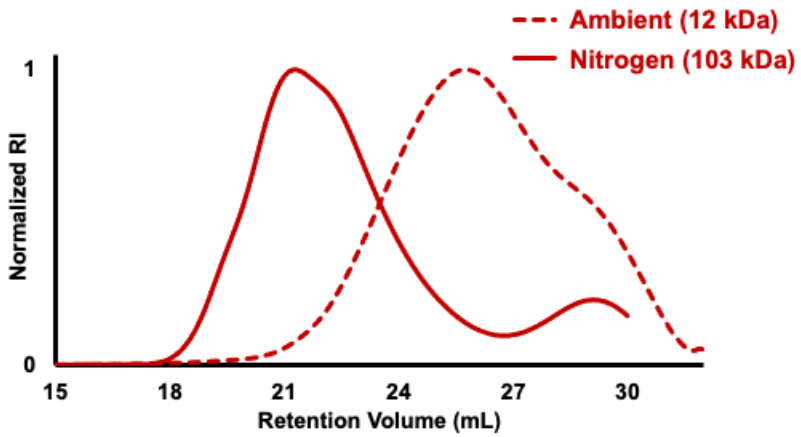

Figure 4.13: SEC data from triple detection for degradation of **4.1** under inert and ambient conditions (Table 4.2)

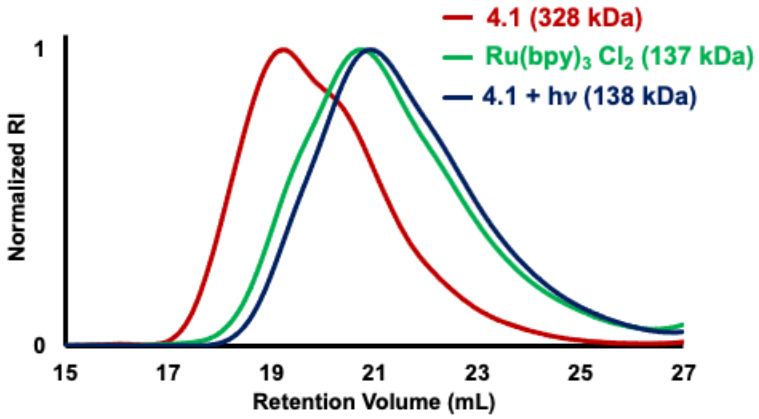

Figure 4.14: SEC data from triple detection for control experiments (Table 4.1)

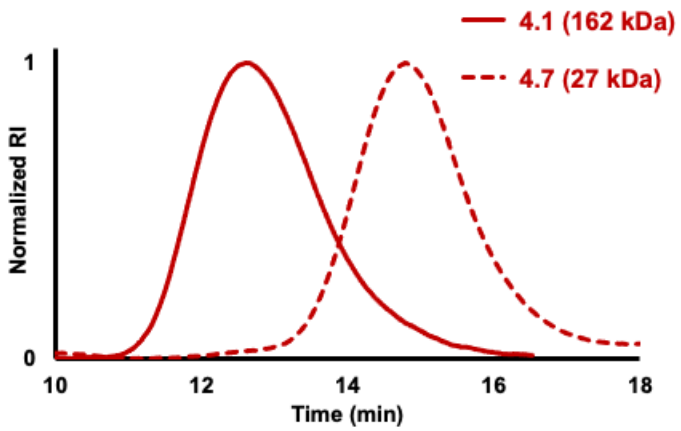

Figure 4.15: SEC data from conventional calibration (SEC 2) for the hydroetherification (MeOH) of **4.1**

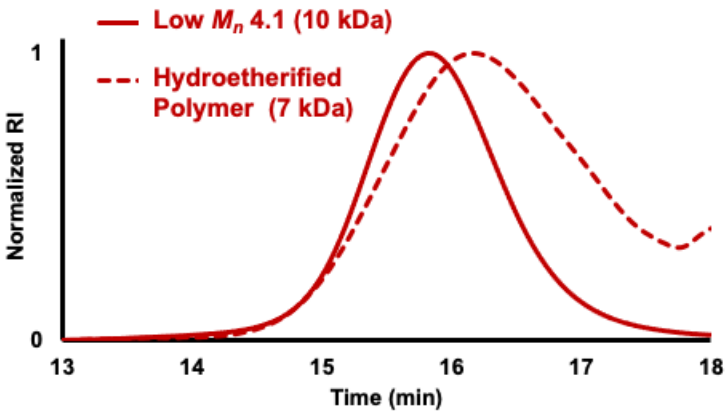

Figure 4.16: SEC data from conventional calibration (SEC 2) for the hydroetherification (BnOH) of low M_n **4.1**

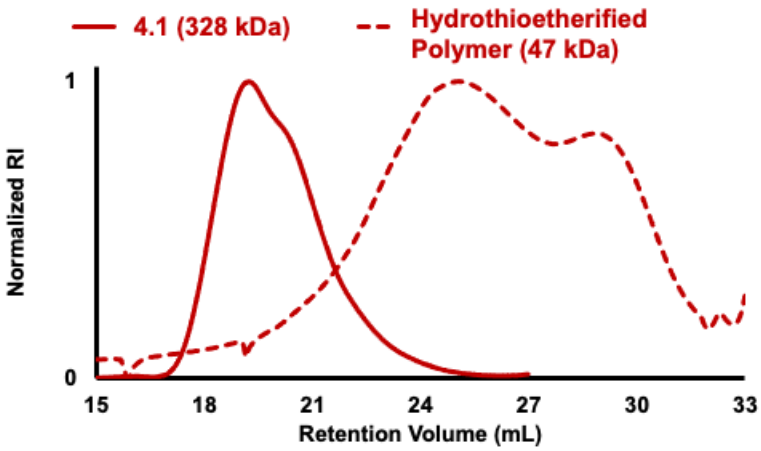

Figure 4.17: SEC data from conventional calibration for the hydrothioetherification (PhSH) of **4.1**

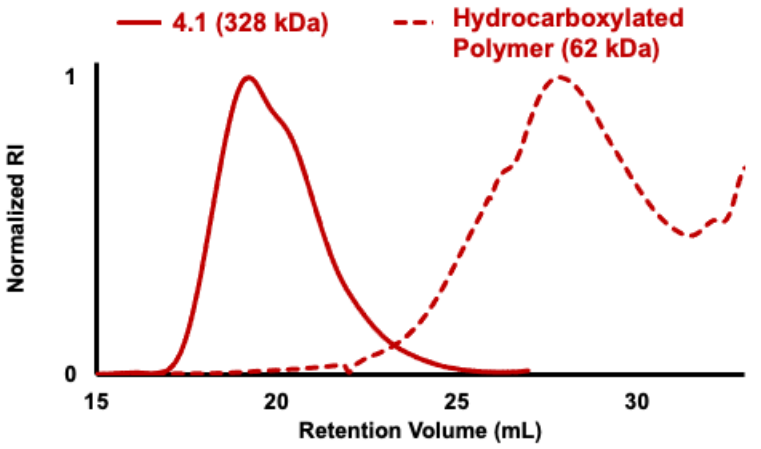

Figure 4.18: SEC data from triple detection for the hydrocarboxylation (AcOH) of **4.1**

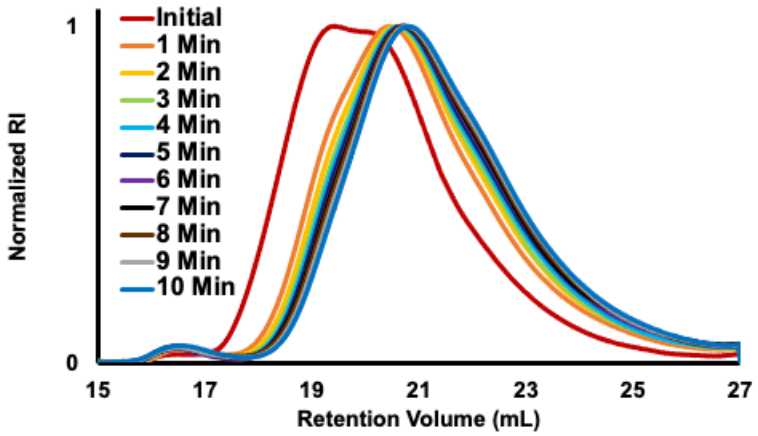

Figure 4.19: SEC data from triple detection for the degradation kinetics of **4.1** under N_2

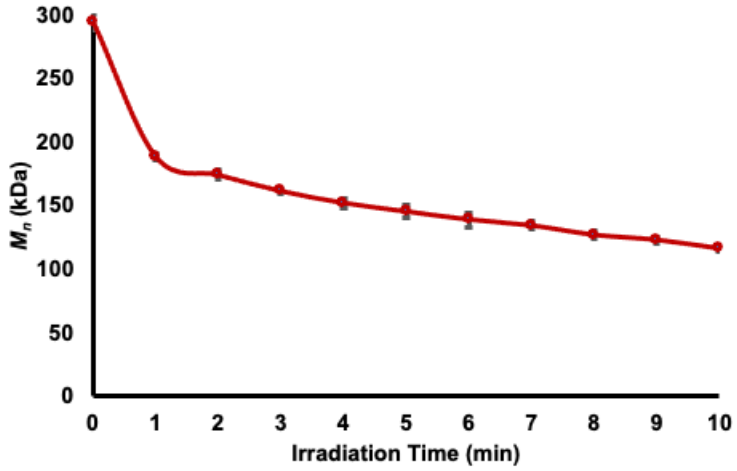

Figure 4.20: M_n (determined by triple detection SEC) as a function of irradiation time during photoediting of **4.1** under N_2

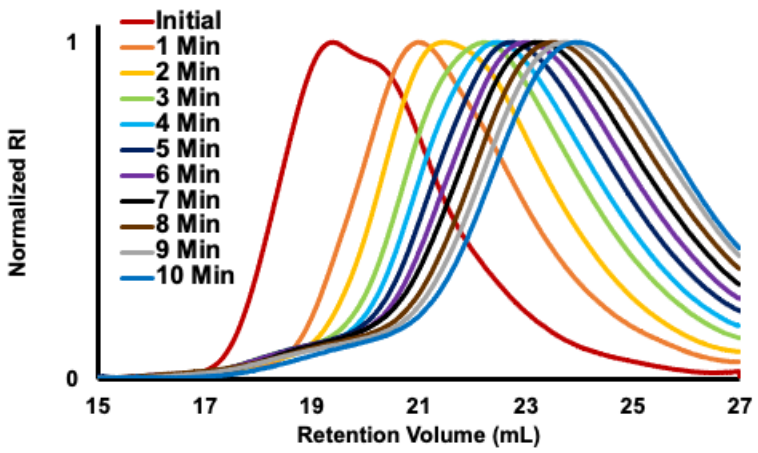

Figure 4.21: SEC data from triple detection for the degradation kinetics of **4.1** under ambient atmosphere.

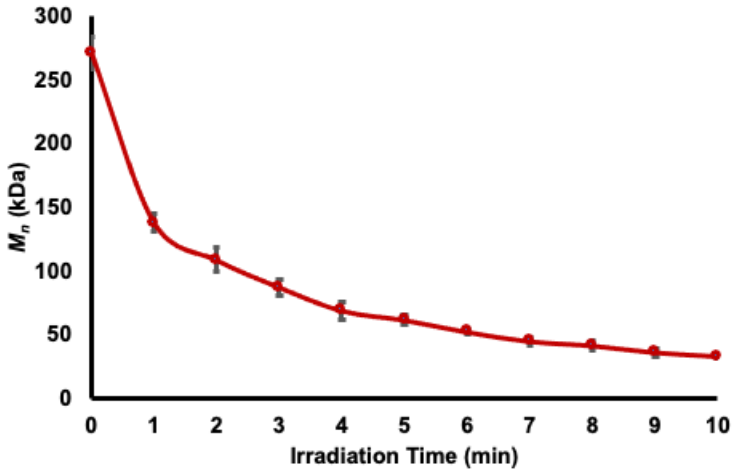

Figure 4.22: M_n (determined by triple detection SEC) as a function of irradiation time during photoediting of **4.1** under ambient atmosphere.

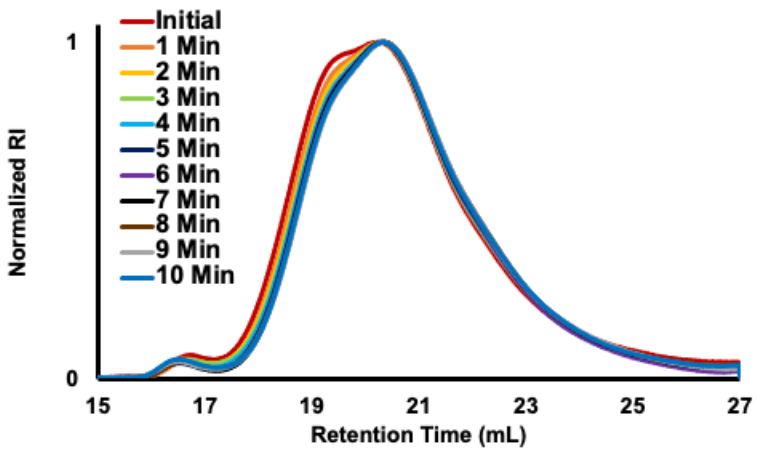

Figure 4.23: SEC data from triple detection for the degradation kinetics of **4.1** under ambient atmosphere with TEMPO additive.

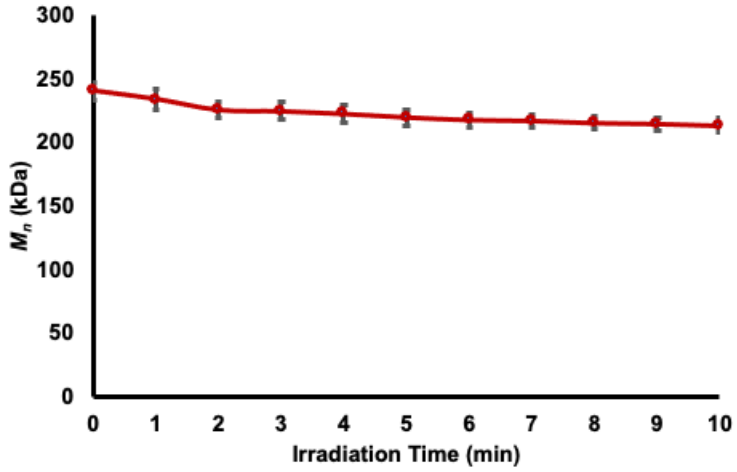

Figure 4.24: M_n (determined by triple detection SEC) as a function of irradiation time during photoediting of **4.1** under ambient atmosphere with TEMPO additive.

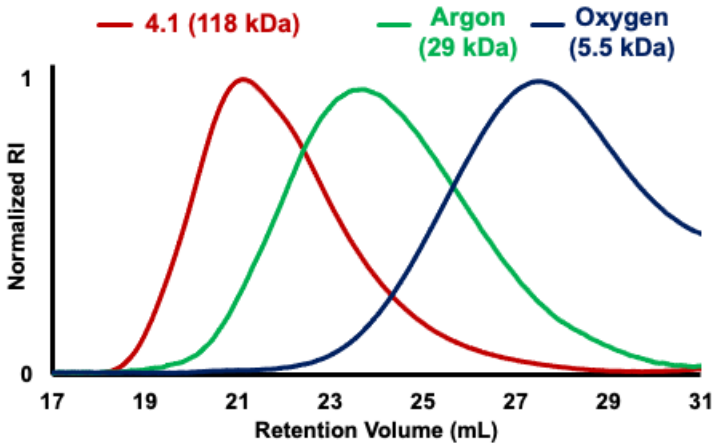

Figure 4.25: Overlaid SEC data from triple detection for the impact of H_2O and oxygen on the degradation of **4.1**

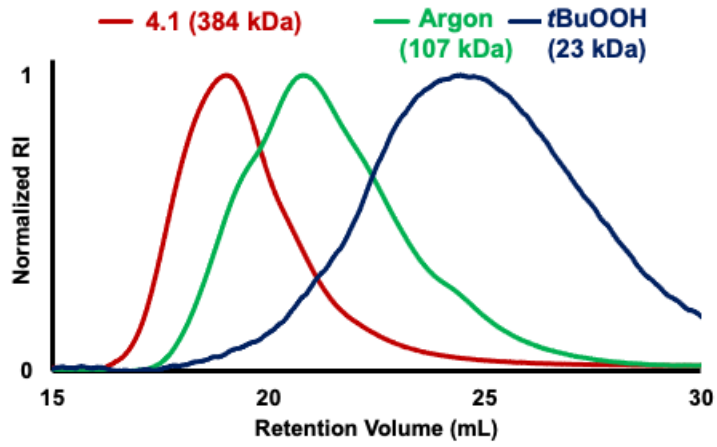

Figure 4.26: Overlaid SEC data from triple detection for the impact of exogenous tBuOOH on the degradation of **4.1**

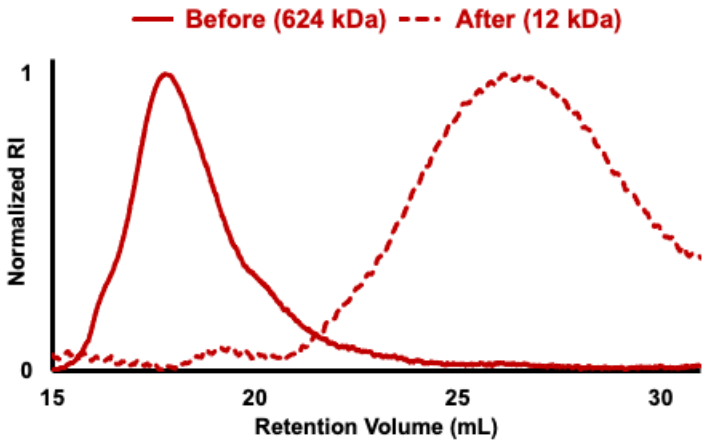

Figure 4.27: SEC data from conventional calibration for the photoediting of **4.4**

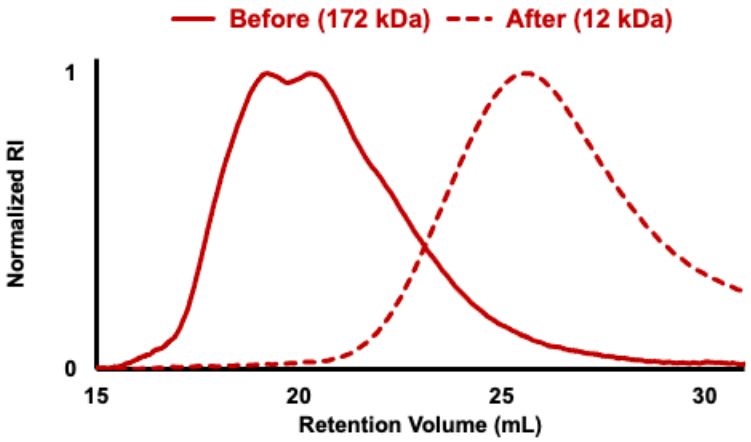

Figure 4.28: SEC data from conventional calibration for the photoediting of **4.5**

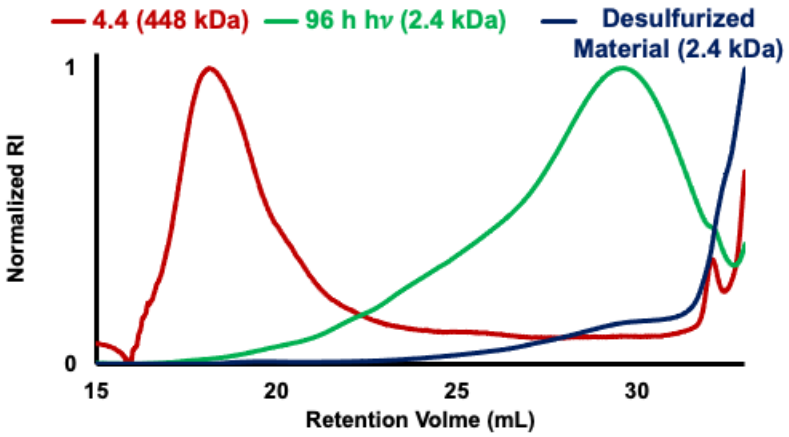

Figure 4.29: SEC data from triple detection for the prolonged (96 h) photoediting of **4.4** and the products after desulfurization.

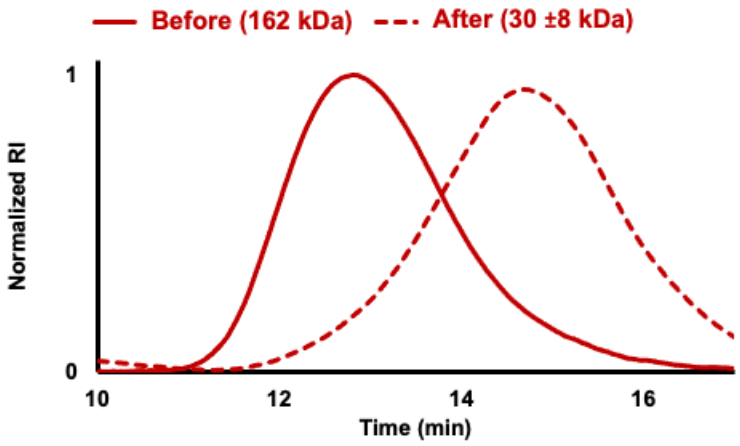

Figure 4.30: SEC data from conventional calibration (SEC 2) for the sunlight mediated photoediting of **4.1.**

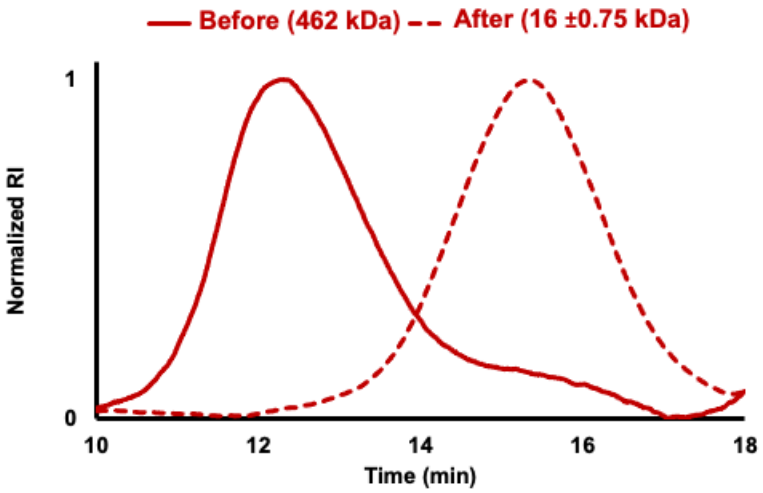

Figure 4.31: SEC data from conventional calibration (SEC 2) for the sunlight mediated photoediting of **4.4**.

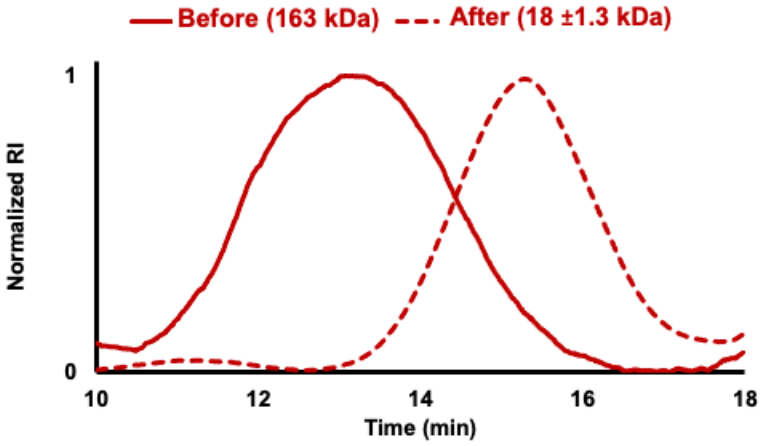

Figure 4.32: SEC data from conventional calibration (SEC 2) for the sunlight mediated photoediting of **4.5**.

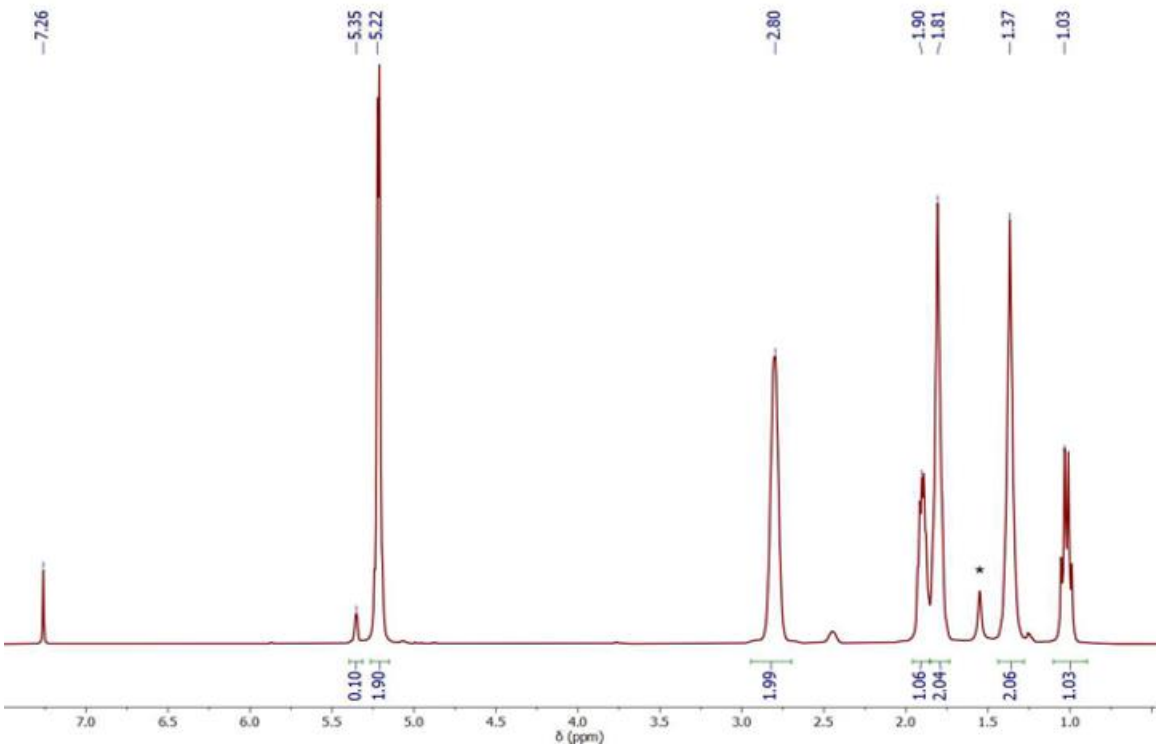

Figure 4.33: Representative ^{1}H NMR spectrum of **4.1** in $CDCl_3$. (* denotes water)

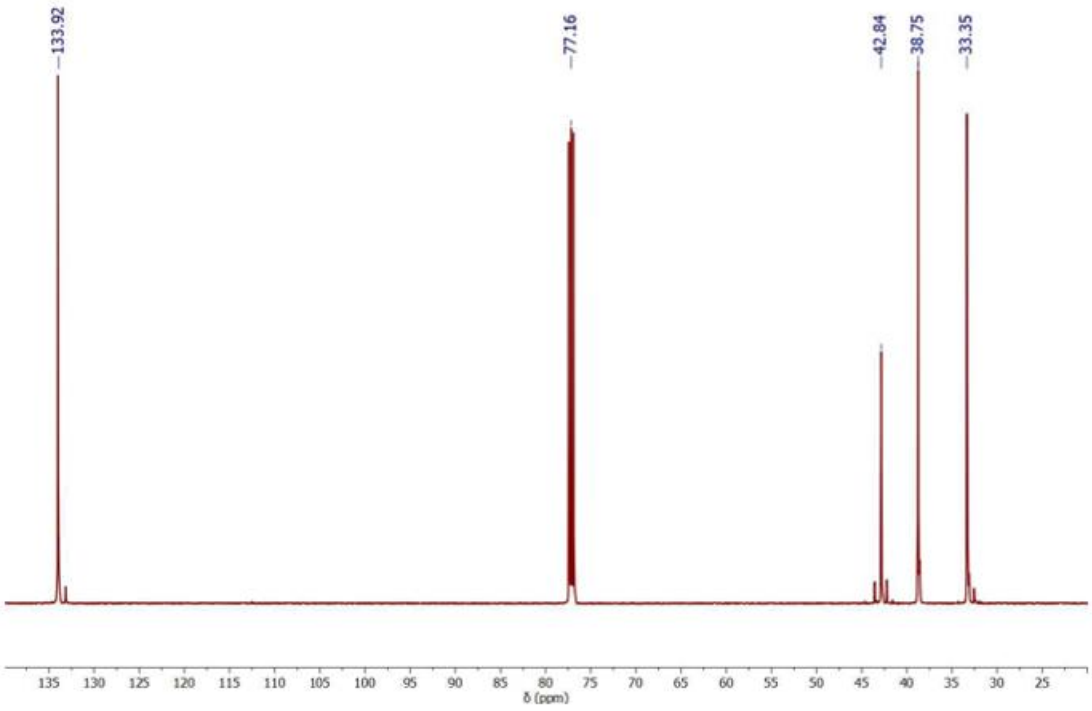

Figure 4.34: Representative ^{13}C NMR spectrum of **4.1** in $CDCl_3$.

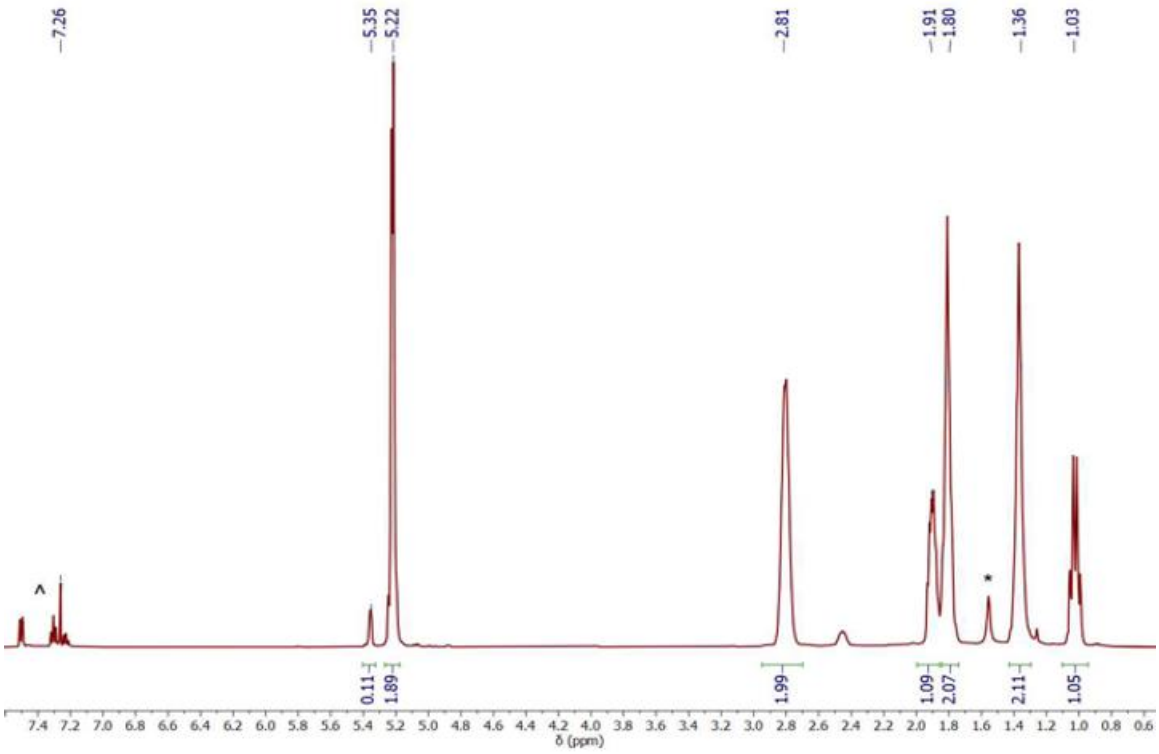

Figure 4.35: Representative ^{1}H NMR of the reduced molar mass product from the photoediting of **4.1** under N_2 (* denotes water δ=1.56 ppm; ^ denotes diphenyl disulfide δ= 7.3, 7.5 ppm)

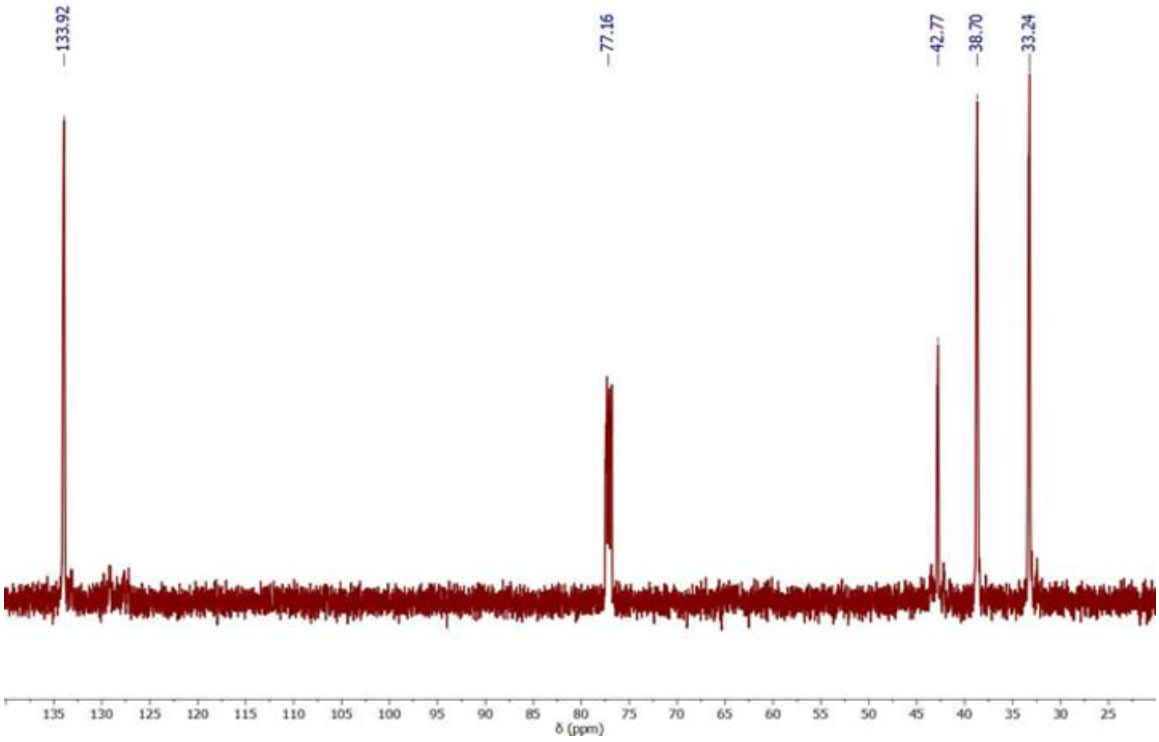

Figure 4.36: Representative ^{13}C NMR of the reduced molar mass product from the photoediting of **4.1** under N_2

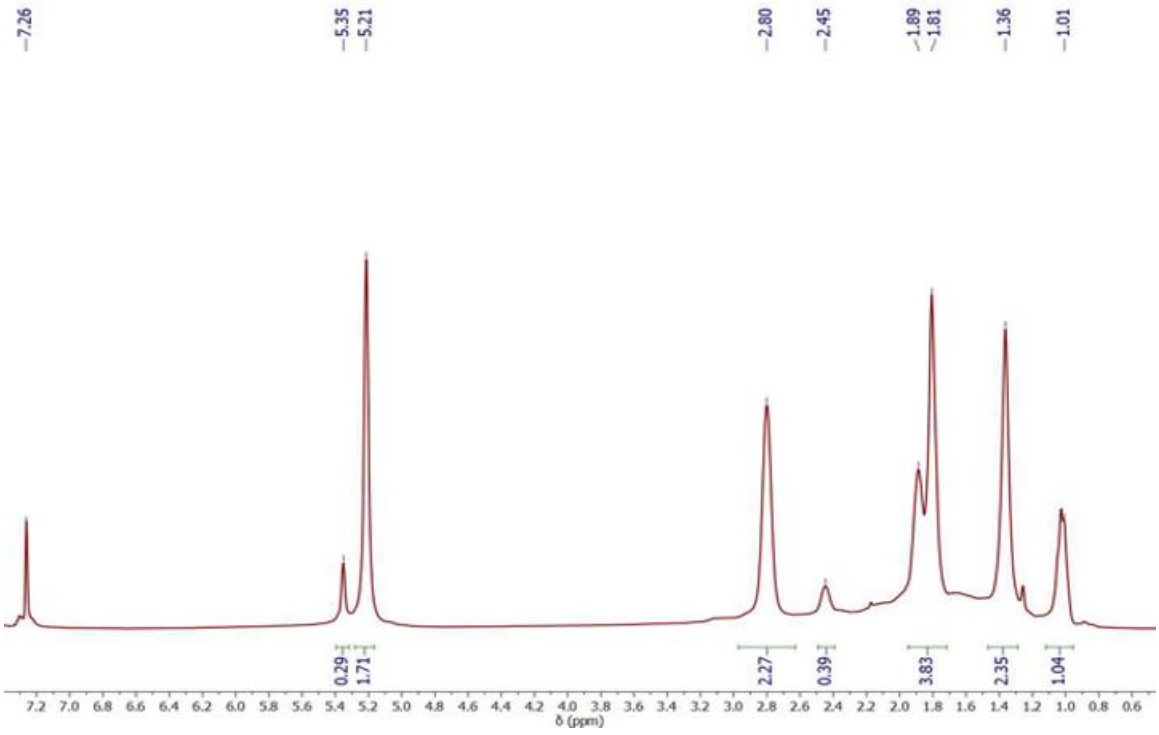

Figure 4.37: Representative ^{1}H NMR of the reduced molar mass product from the photoediting of **4.1** under ambient atmosphere

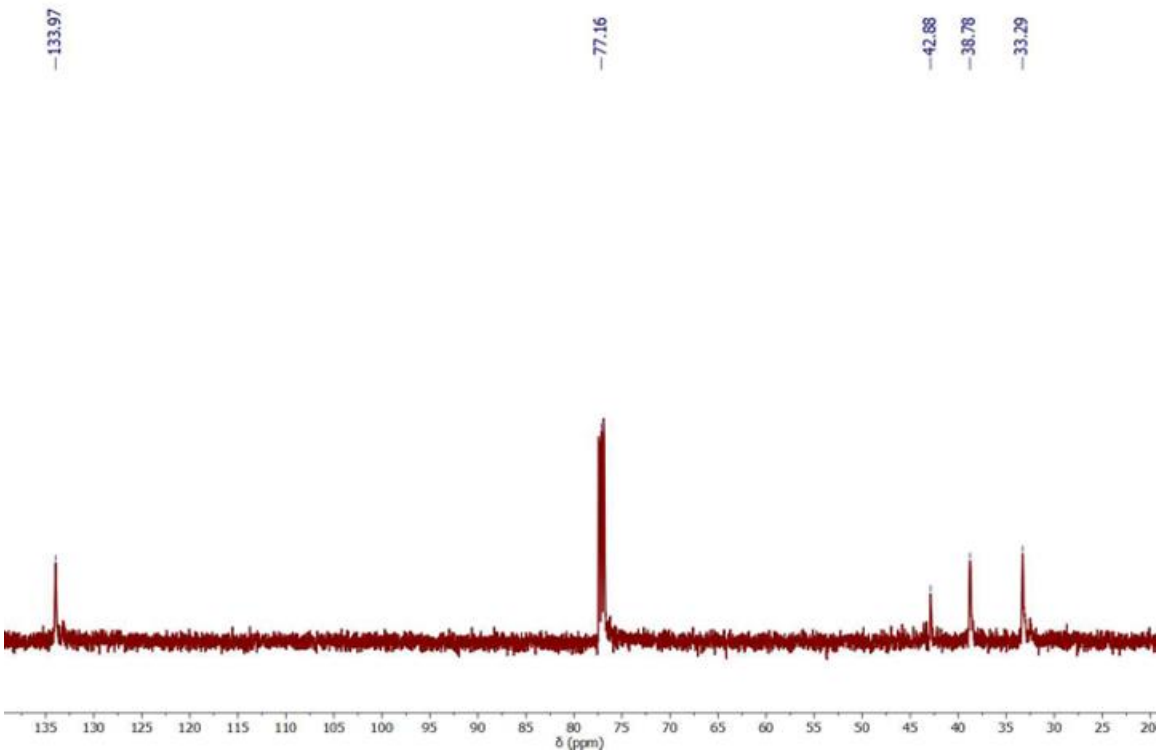

Figure 4.38: Representative ^{13}C NMR of the reduced molar mass product from the photoediting of **4.1** under ambient atmosphere

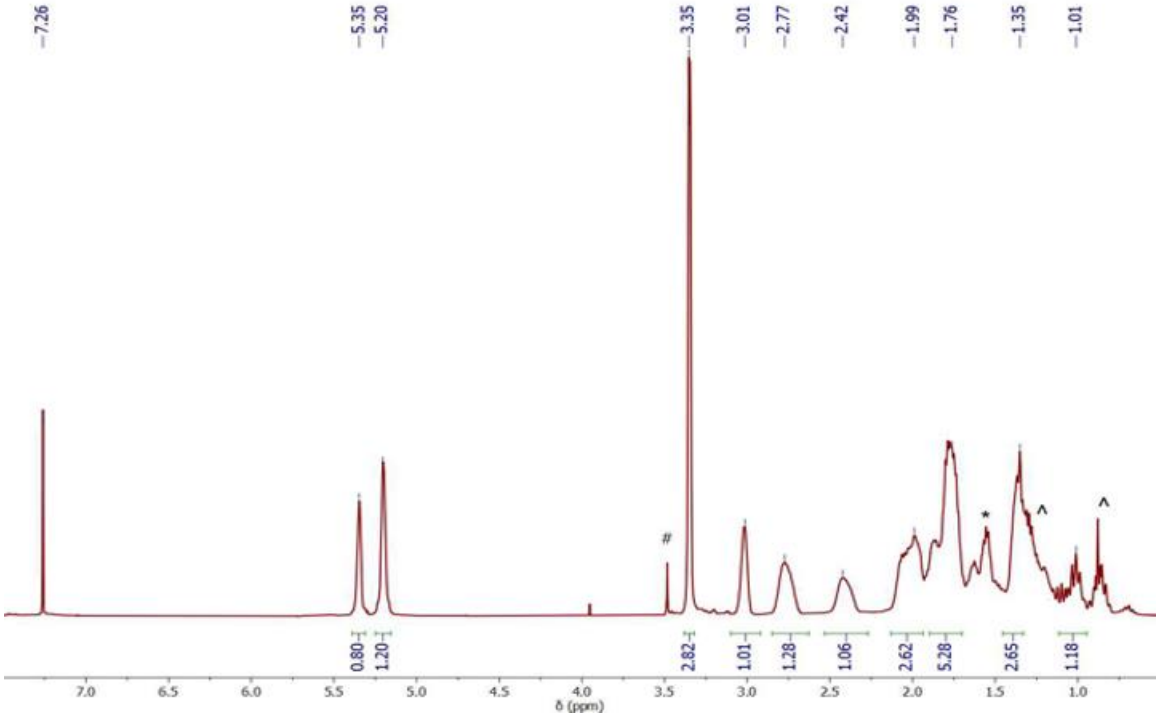

Figure 4.39: Representative ^{1}H NMR of **4.7** in $CDCl_3$ (* denotes water δ=1.56; ^ denotes pentane δ=0.88, and 1.29 ppm; # denotes methanol δ=3.49 ppm)

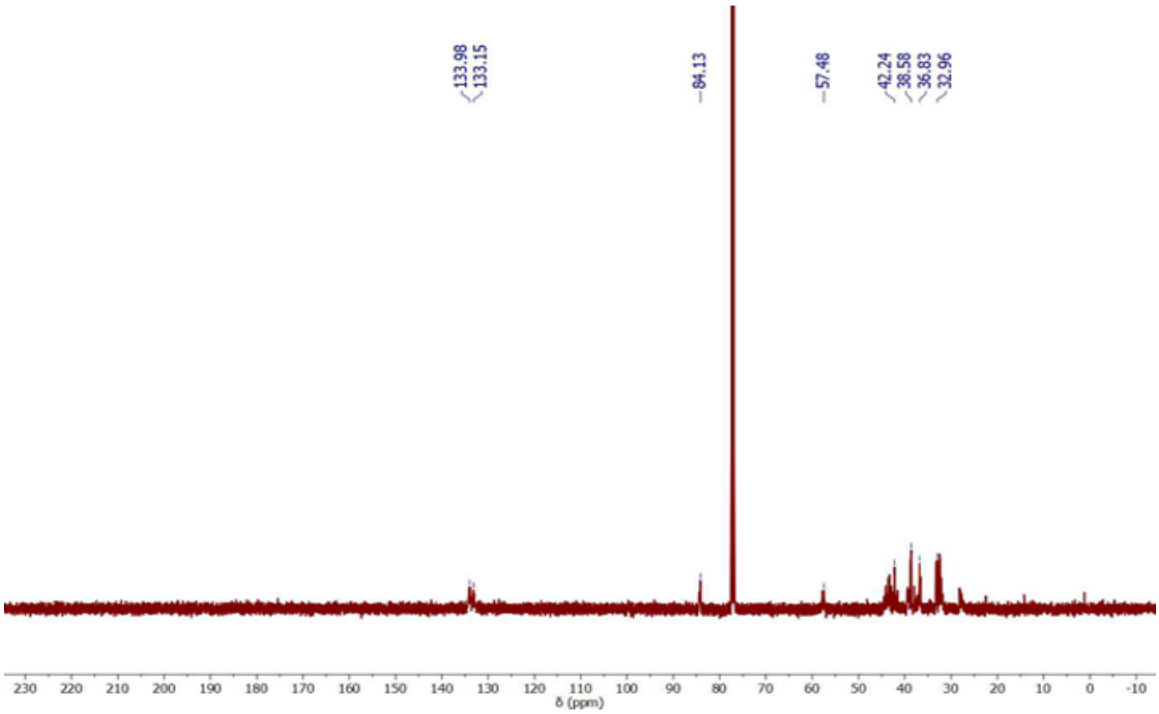

Figure 4.40: Representative ^{13}C NMR of **4.7** in $CDCl_3$

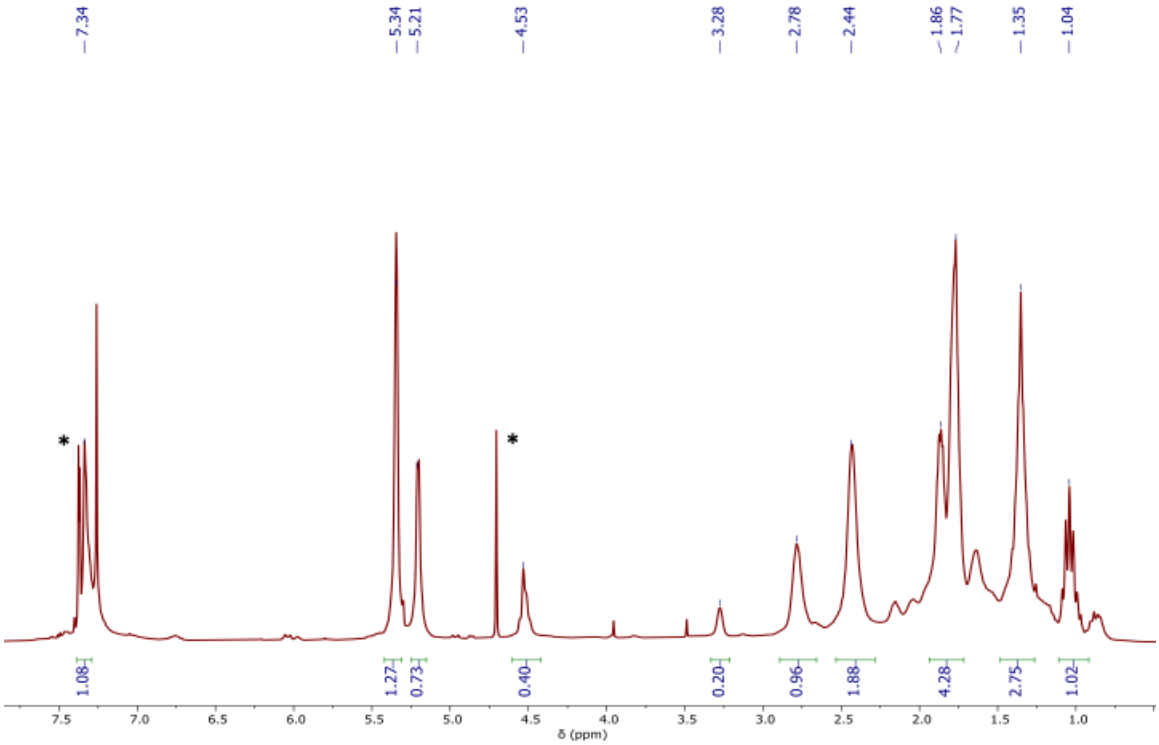

Figure 4.41: Representative ^{1}H NMR of hydroetherification (BnOH) of **4.1** in $CDCl_3$ (* denotes residual BnOH δ=4.6 and 7.2-7.4 ppm)

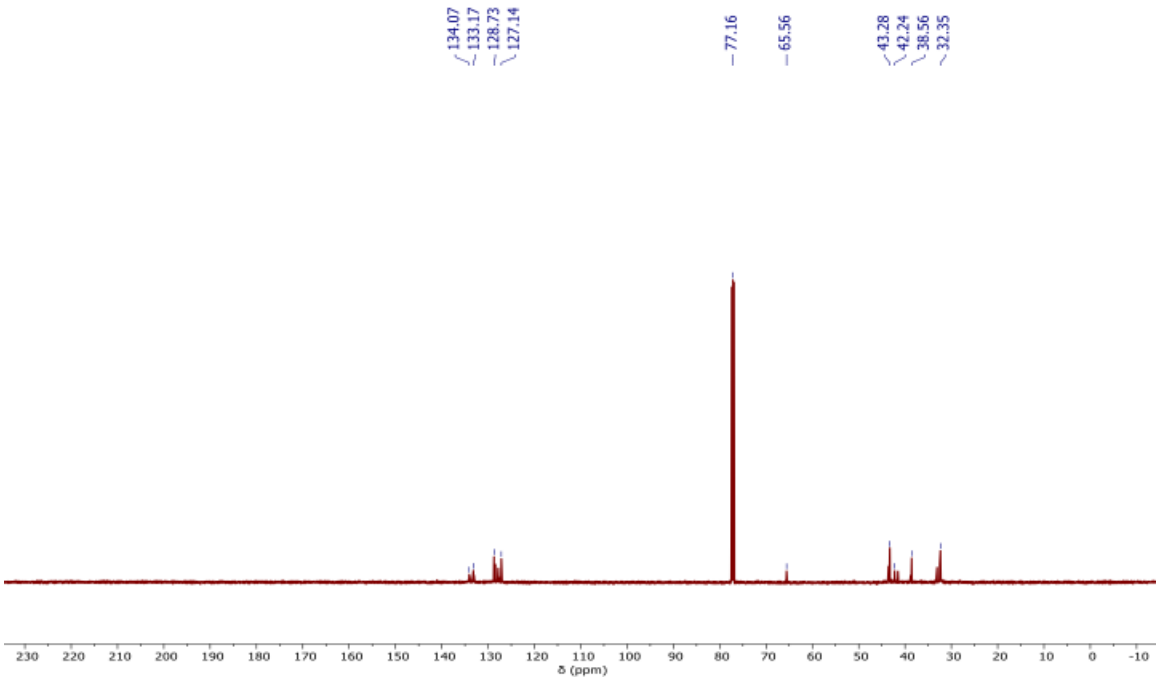

Figure 4.42: Representative ^{13}C NMR of hydroetherification (BnOH) of **4.1** in $CDCl_3$

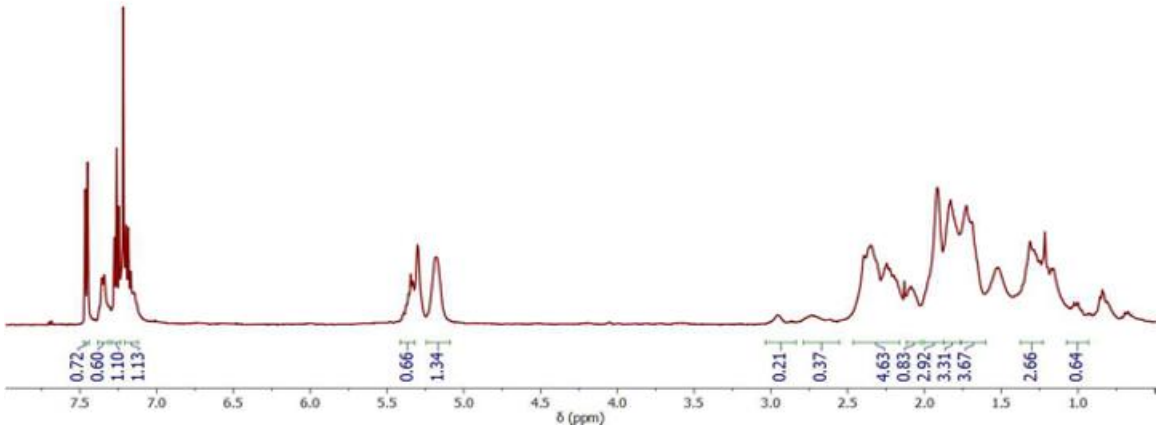

Figure 4.43: Representative ^{1}H NMR of hydrothioetherification (PhSH) of **4.1** in $CDCl_3$

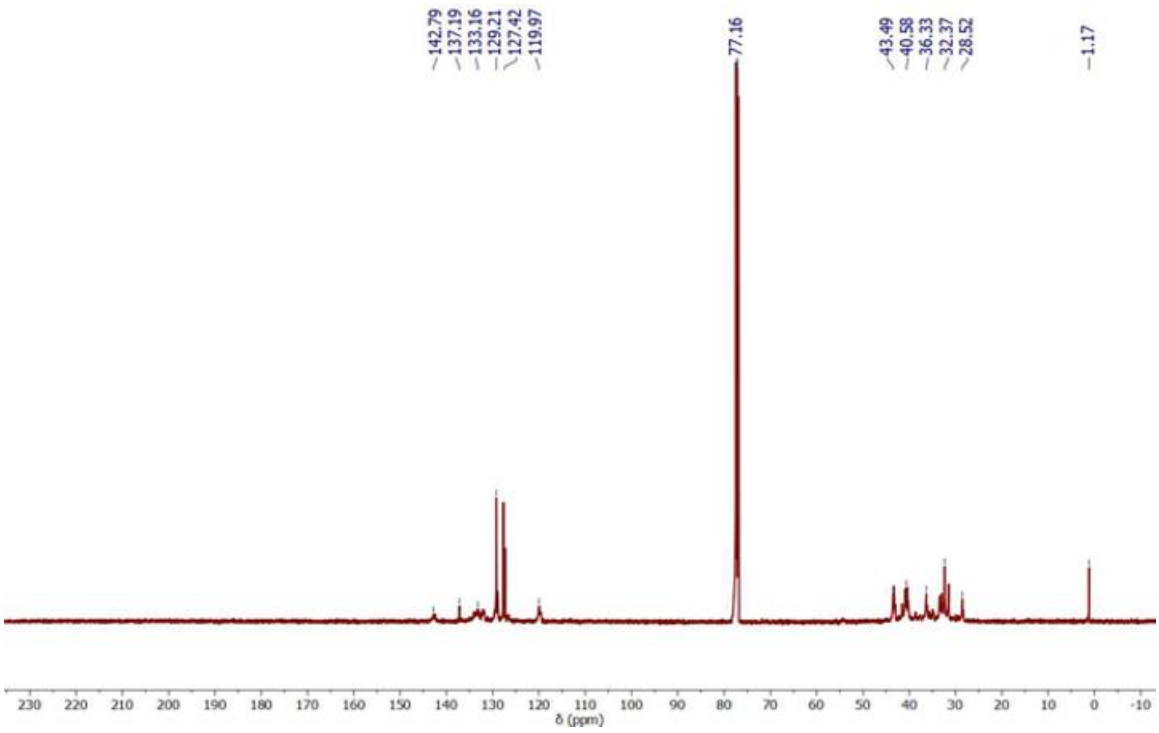

Figure 4.44: Representative ^{13}C NMR of hydrothioetherification (PhSH) of **4.1** in $CDCl_3$

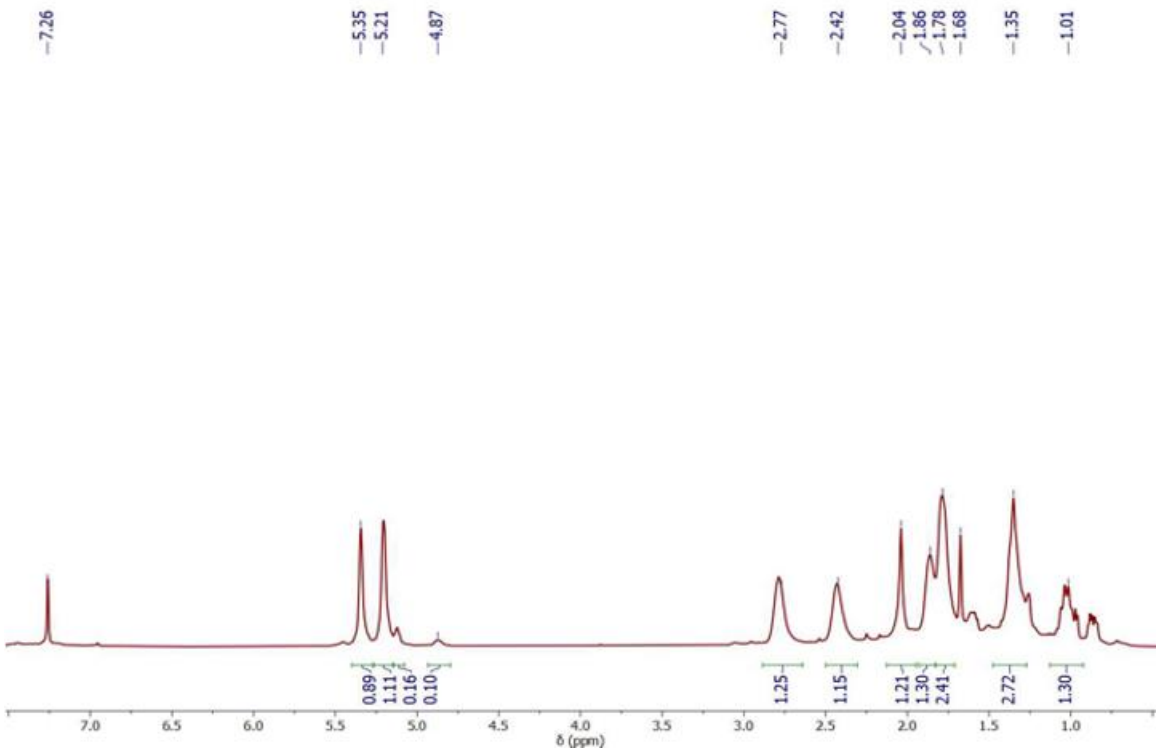

Figure 4.45: Representative ^{1}H NMR of hydrocarboxylation (AcOH) of **4.1** in $CDCl_3$

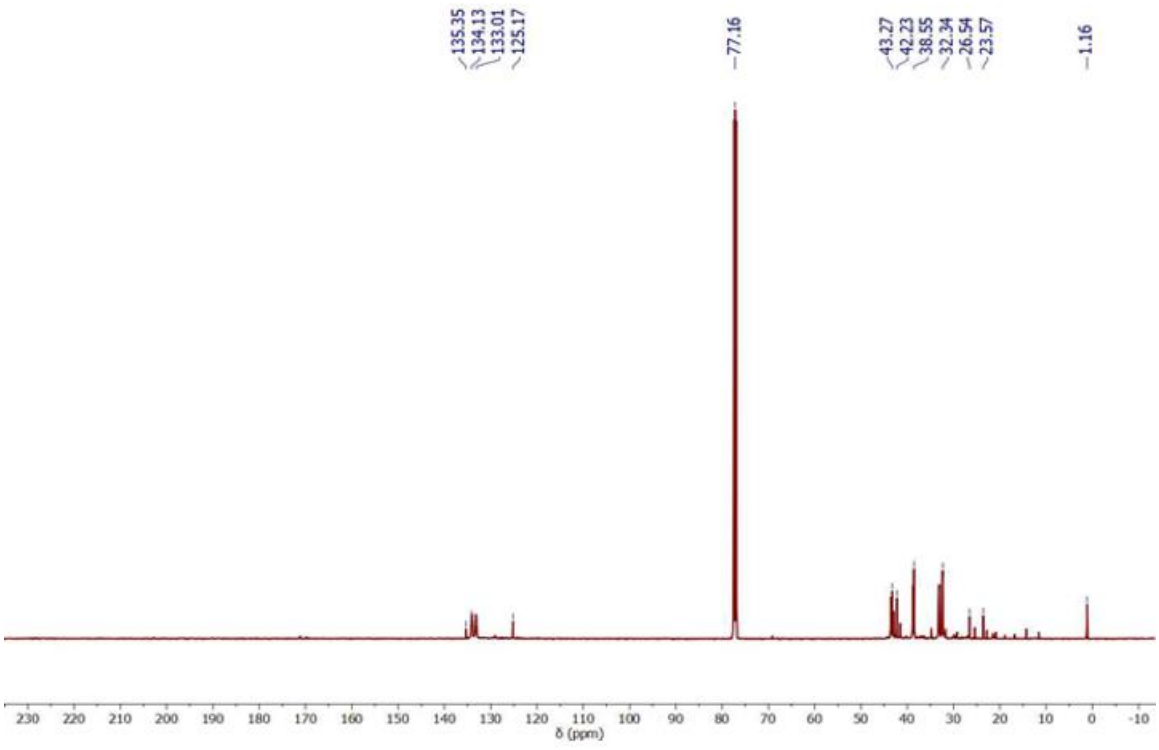

Figure 4.46: Representative ^{13}C NMR of hydrocarboxylation (AcOH) of **4.1** in $CDCl_3$

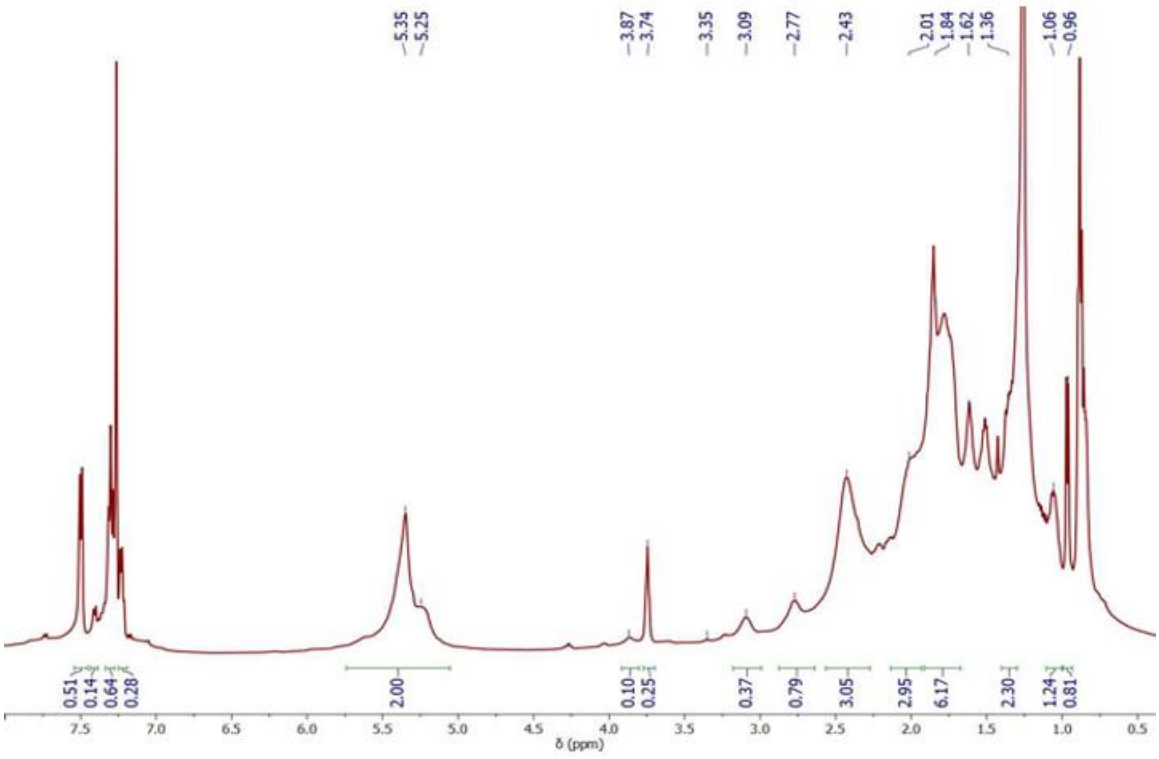

Figure 4.47: Representative ^{1}H NMR of hydroazidation ($TMSN_3$) of **4.1** in $CDCl_3$

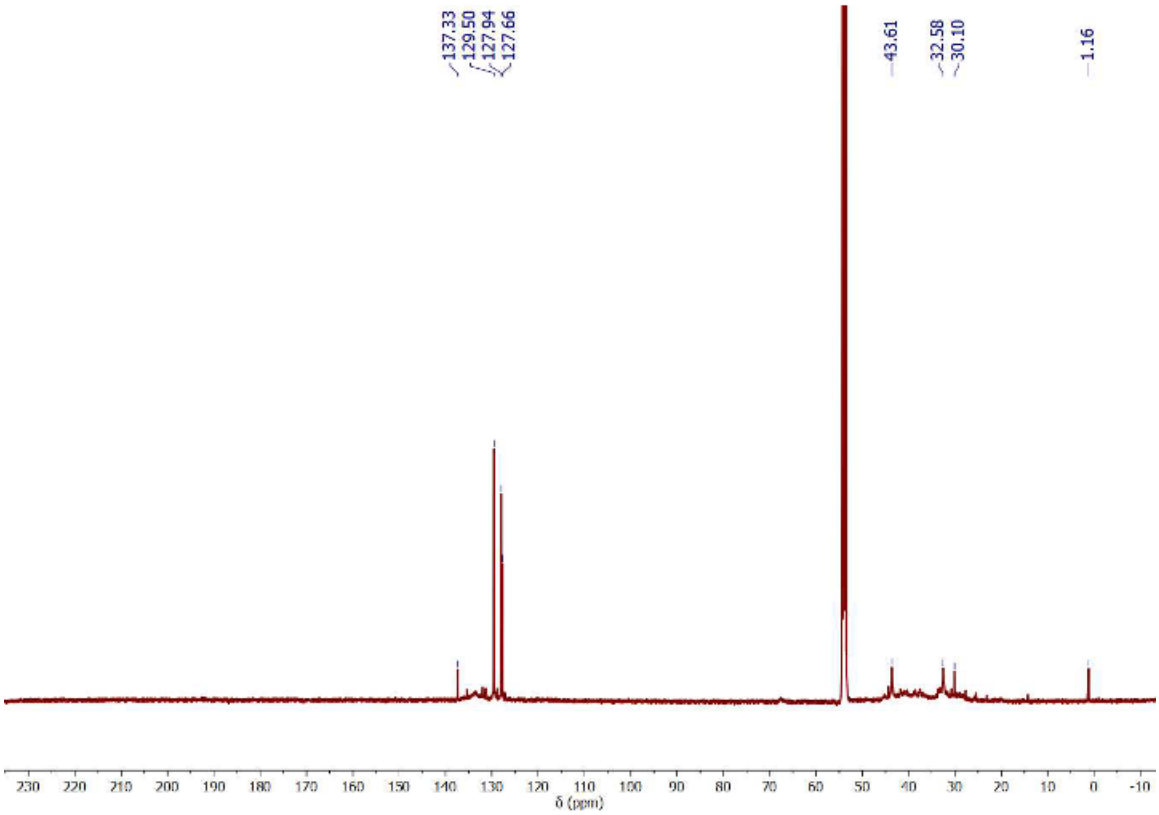

Figure 4.48: Representative ^{13}C NMR of hydroazidation ($TMSN_3$) of **4.1** in $CDCl_3$

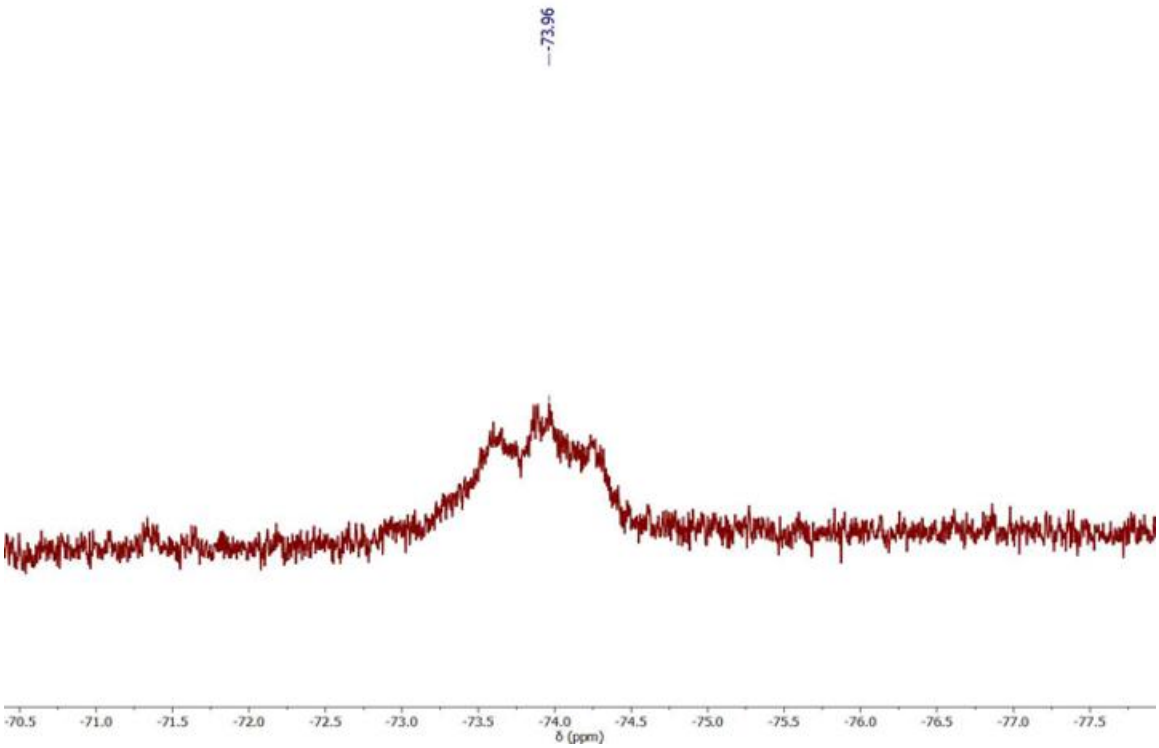

Figure 4.49: ^{19}F NMR of the product from the hydroazidation of **4.1**

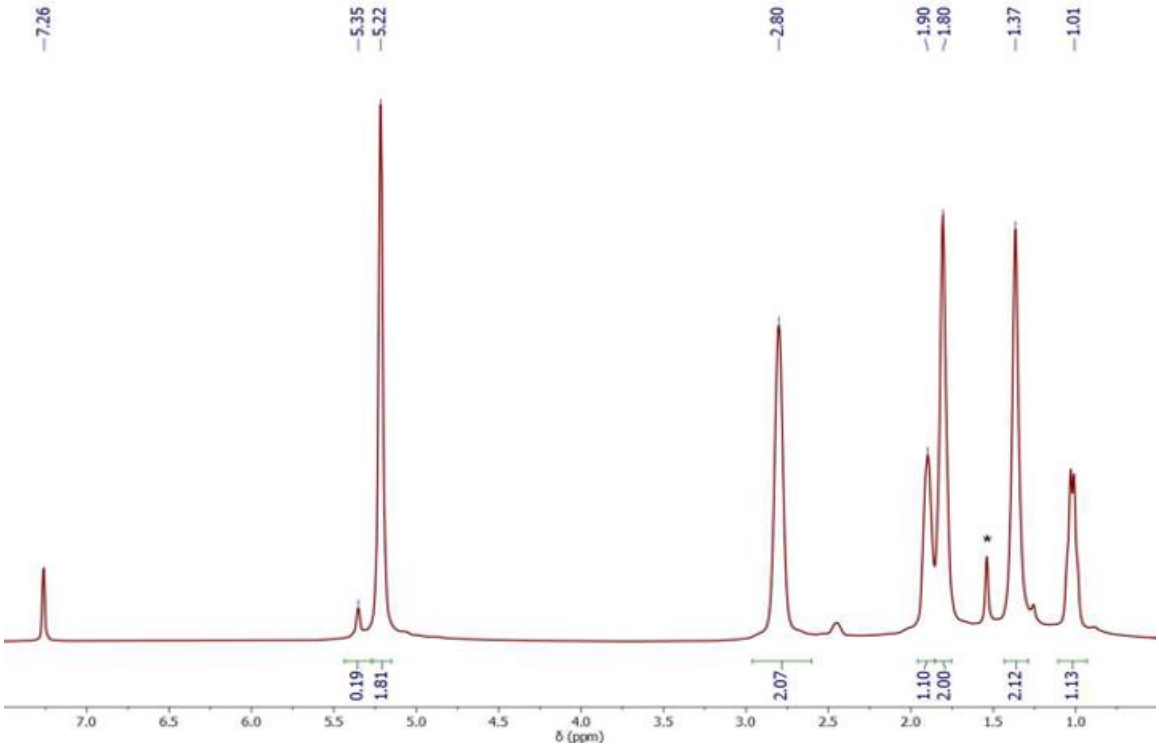

Figure 4.50: ^{1}H NMR of product from the control experiment - **4.2**, - $(PhS)_2$ (Table 4.1)

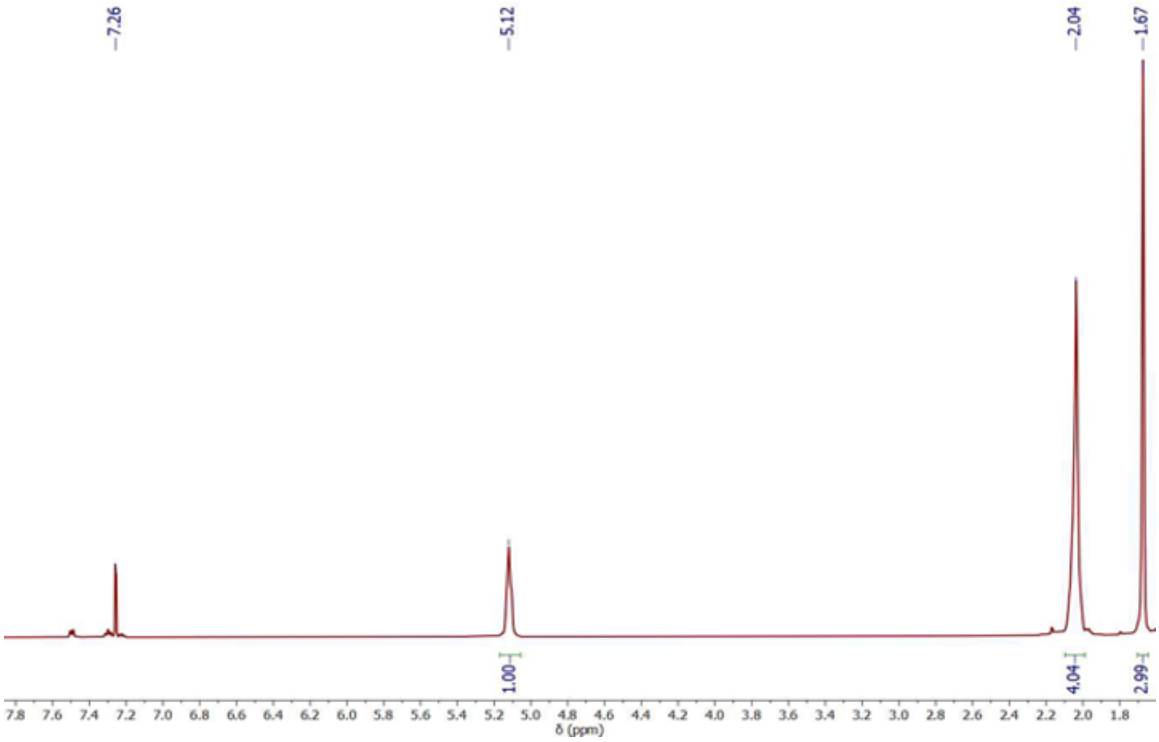

Figure 4.51: Representative ^{1}H NMR of the product from photoediting (1 h) of **4.4** in $CDCl_3$

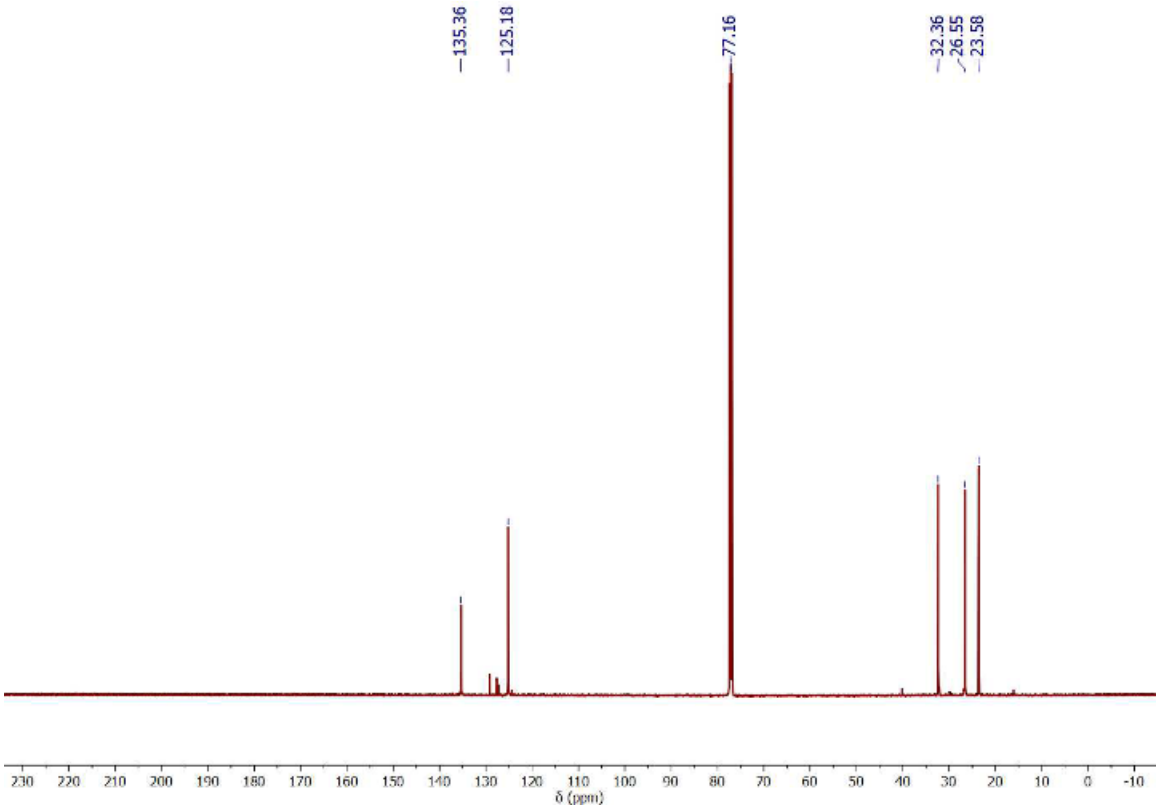

Figure 4.52: Representative ^{13}C NMR of the product from photoediting (1 h) of **4.4** in $CDCl_3$

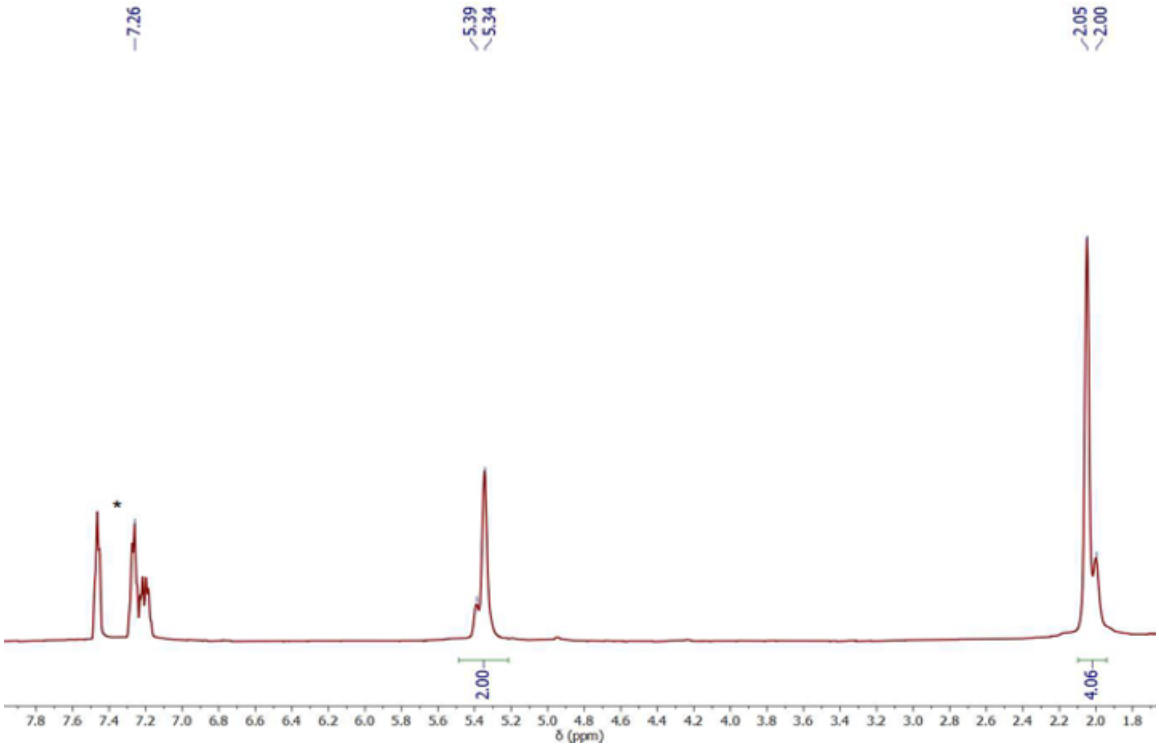

Figure 4.53: Representative ^{1}H NMR of the product from photoediting (1 h) of **4.5** in $CDCl_3$ (*denotes diphenyl disulfide δ= 7.3, 7.5 ppm)

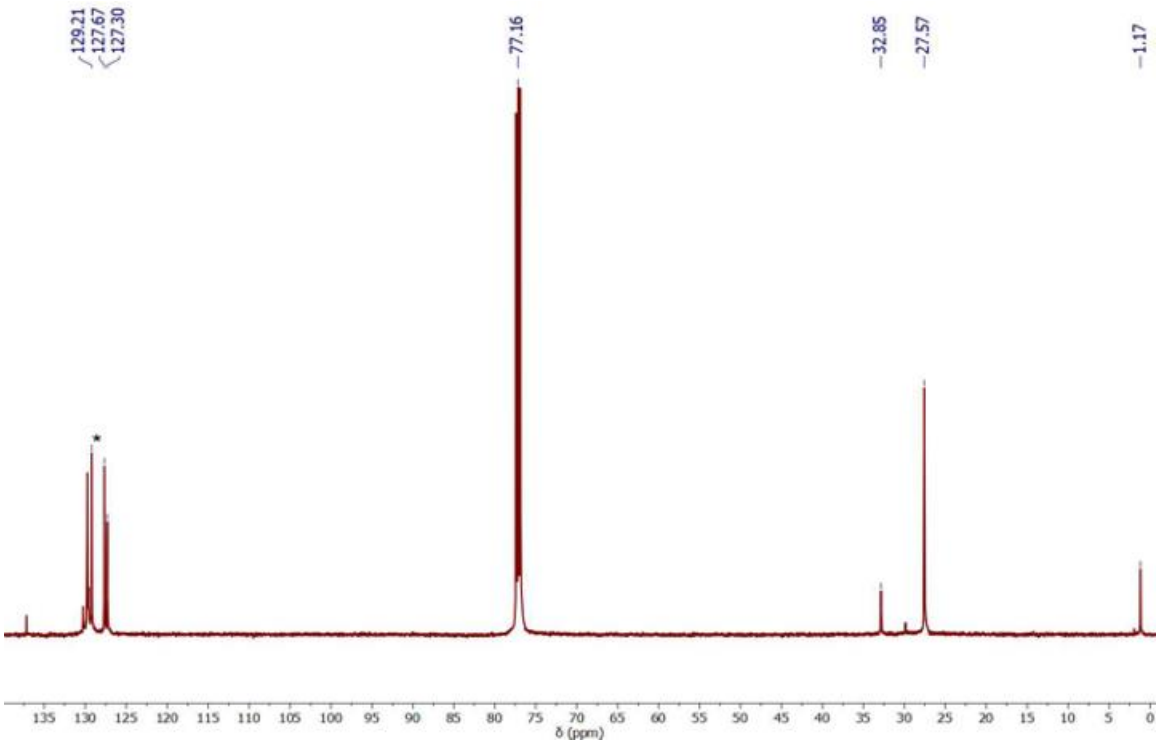

Figure 4.54: Representative ^{13}C NMR of the product from photoediting (1 h) of **4.5** in $CDCl_3$

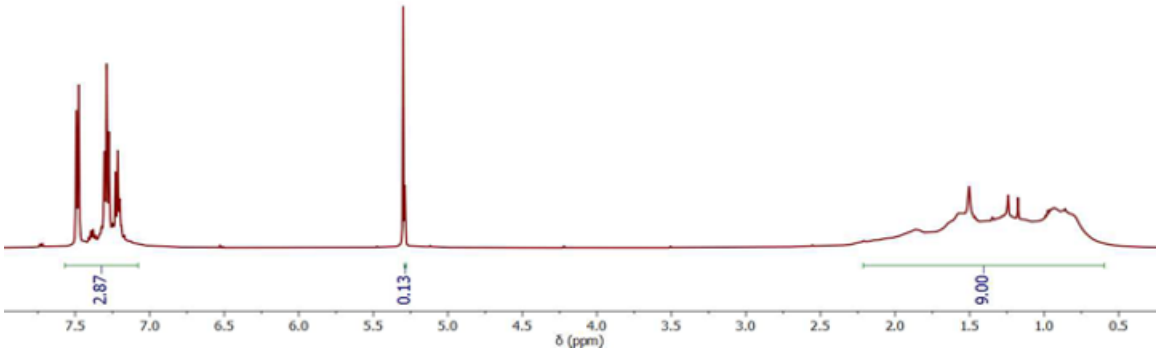

Figure 4.55: Representative ^{1}H NMR of the product from prolonged photoediting (96 h) of **4.4** in CD_2Cl_2

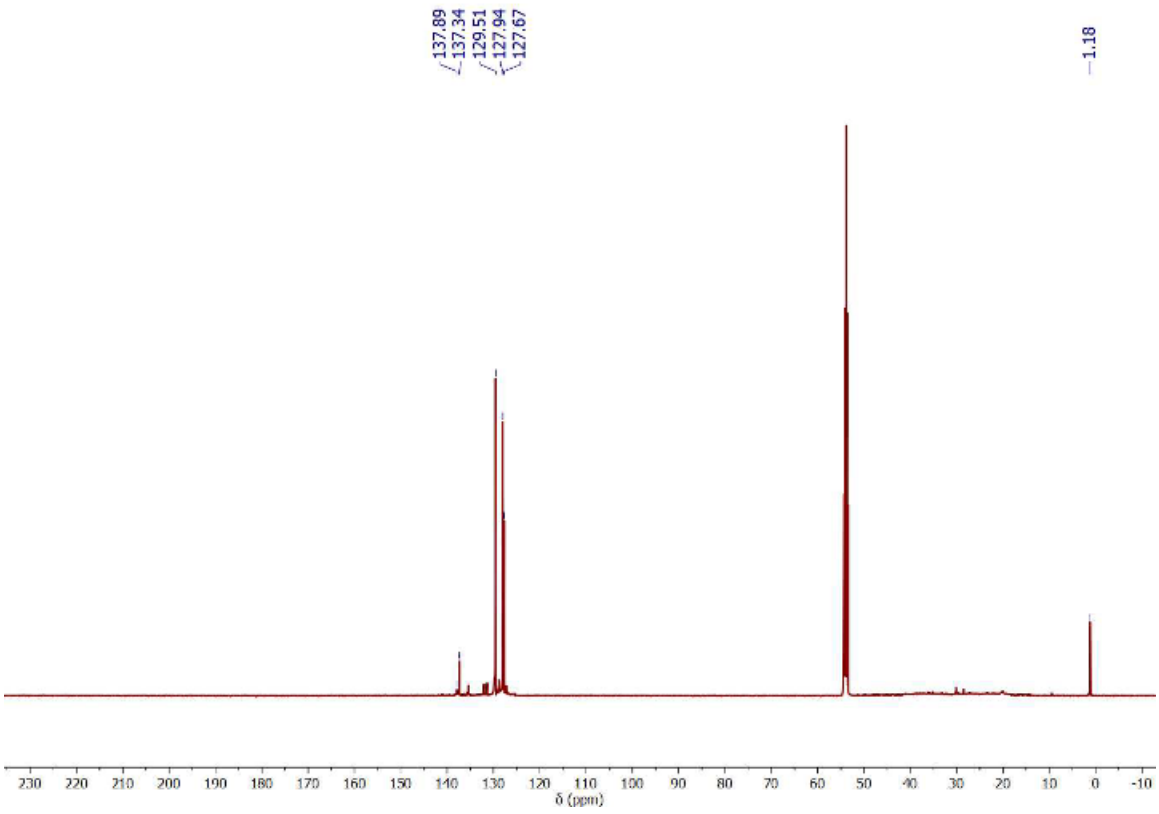

Figure 4.56: Representative ^{13}C NMR of the product from prolonged photoediting (96 h) of **4.4** in CD_2Cl_2

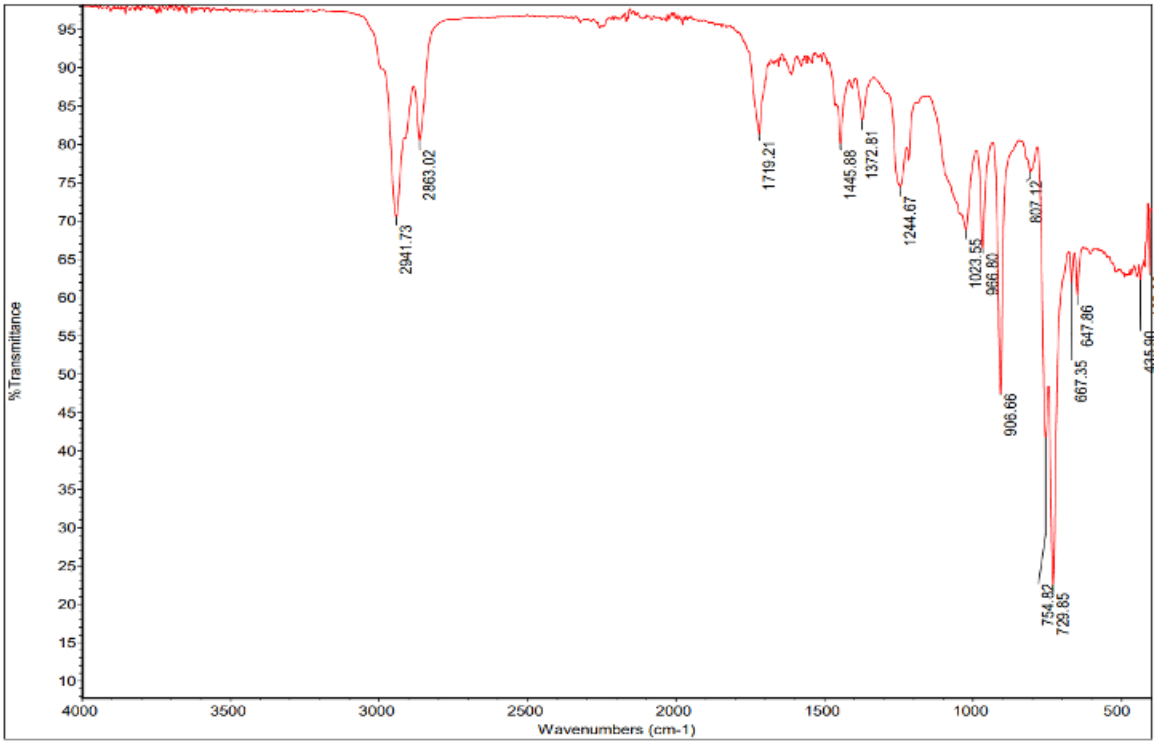

Figure 4.57: IR Spectra of the product of hydrocarboxylation of **4.1.** Ester stretch at 1791 cm^{-1}

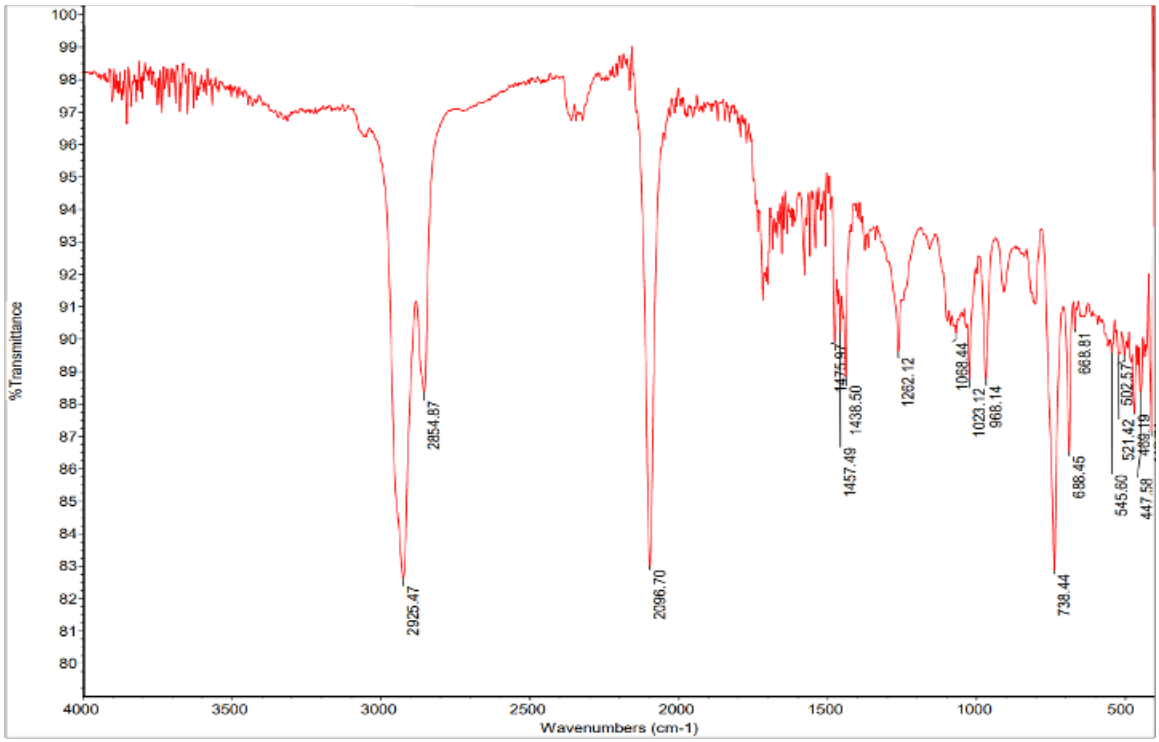

Figure 4.58: IR Spectra of the product of hydroazidation of **4.1**. Azide stretch at 2096 cm^{-1}

CHAPTER V: VINYL-ADDITION POLYMERIZATIONS OF CYCLOALLENES: SYNTHETIC ACCESS TO CONGENERS OF CYCLIC-OLEFIN COPOLYMERS

A version of this chapter was originally published by Nicholas J. Galan, Justin M. Burroughs, Christopher R. Maroon, Brain K. Long, and Johnathan N. Brantley:

Galan, N. J., Burroughs, J.M., Maroon, C. R., Long, B.K., Brantley, J. N. *, Vinyl-Addition Polymerizations of Cycloallenes: Synthetic Access to Congeners of Cyclic-Olefin Copolymers. *Polymer Chemistry*. **2020**, 5578-5581.

In this article, I aided in designing and synthesizing all monomers and polymers studied. I also performed most of the polymer characterization, and tensile testing. Dr. Justin Burroughs also synthesized monomers and polymers used in this study. Dr. Christopher Maroon conducted the initial catalyst screen and optimization. Dr. Johnathan Brantley and Dr. Brian Long organized this project and facilitated the writing of the manuscript.

5.1 Abstract

Expanding the scope of cycloolefin monomers that polymerize via coordination-insertion mechanisms is an enduring synthetic challenge. Vinyl-addition polymerizations of cyclic olefins are almost exclusively limited to norbornene scaffolds and/or copolymerizations with ethylene. To circumvent these synthetic limitations, we report the vinyl-addition polymerization of cycloallenes using a [{(π-allyl)NiOCOCF$_3$}$_2$] catalyst. The polycyclic materials could be accessed in excellent yields (up to 97%), and the polymerization exhibited living character (which was leveraged for copolymerizations with acyclic monomers). Importantly, we found that multiple ring sizes could be incorporated into

polymer architectures, and material properties could be tailored by controlling the cycloallene feed ratios.

5.2 Introduction

Relative to their acyclic congeners, cycloolefin polymers are enticing synthetic targets that frequently exhibit unique physical properties. Indeed, the incorporation of small carbocyclic motifs into soft materials can impact optical transparency,[61,62] modify viscosity,[196] increase T_g,[60] and enhance modulus.[64] In principle, cyclic motifs can be introduced into polymer matrices through a variety of polymerization manifolds; however, practical considerations often narrow the scope of applicable methods. For example, radical and ionic polymerizations can undergo deleterious chain termination events or undesired rearrangements (resulting in low yields and oligomeric products).[68,69] Furthermore, ring-opening polymerizations typically require highly strained monomers (e.g. norbornene), which intrinsically limits monomer scope.

In contrast, vinyl-addition polymerizations of cyclic olefins typically exhibit improved performance, but such polymerizations are not without synthetic obstacles. For example, vinyl-addition homopolymerizations of cyclic olefins other than norbornene and cyclopentene are virtually unknown.[197] Although many cyclic olefins can be copolymerized with ethylene, this strategy usually requires highly reactive catalysts (which can exhibit poor functional group tolerance) and harsh co-catalysts or activators (Scheme 5.1). Given these limitations, exploring new monomer and catalyst space is imperative for overcoming these obstacles.

Scheme 5.1: Routes to Cycloolefin Copolymers

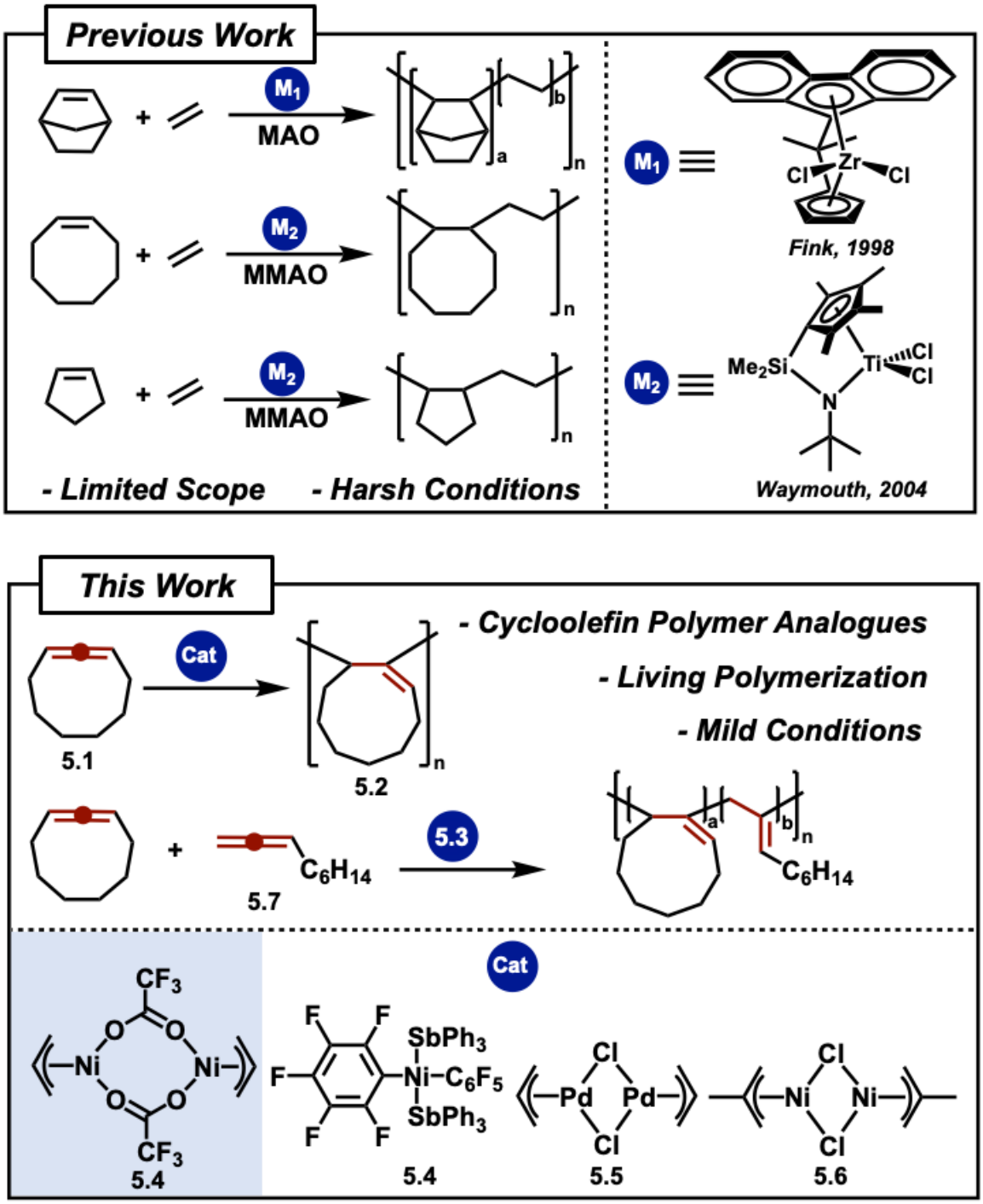

Much like their olefin congeners, allenes polymerize under a variety of conditions[36] (e.g. radical,[37] cationic,[39] anionic,[40] and coordination-insertion[42,198–200]). We were particularly inspired by the work of Endo and colleagues, who have shown that[(π-allyl)NiOCOCF$_3$]$_2$ (**5.3**; Scheme 5.1) catalyses the living polymerization of allenes bearing an array of functional groups (e.g. alcohols,[45] esters,[46] or amides,[201]). One brief report by Endo and colleagues revealed that catalyst **5.3** can facilitate the polymerization of cycloallenes; however, this succinct note lacked detailed analyses of polymerization kinetics, living character at higher conversions, copolymerizations, or bulk material properties.[75] As these materials can be considered analogues of cycloolefin polymers, we envisioned that a more detailed study of their syntheses and properties could reveal important design elements for creating a spate of advanced architectures. Indeed, cycloolefins can be efficiently transformed into cycloallenes using the two-step Skattebøl rearrangement.[109] This operationally simple strategy, combined with a deeper understanding of cycloallene polymerization tendencies and the functional group tolerance of **5.3**, could significantly expand the scope of potential monomers[202] for vinyl-addition polymerizations. Given these considerations, we envisioned that vinyl-addition polymerizations of cyclic allenes would afford access to novel derivatives of cycloolefin (co)polymers.

5.3 Results and Discussion

5.3.1 Initial Monomer Syntheses and Kinetic Study

We selected 1,2-cyclononadiene (**5.1**) as our model substrate, given that (i) it is

easily synthesized from cyclooctene on a multi-gram scale, and (ii) the resultant polymer would contain rings that are difficult to incorporate using traditional monomers.[203] Our initial studies commenced with the homopolymerization of **5.1** using catalyst **5.3** (Scheme 5.1)**.** Gratifyingly, the polymerization proceeded rapidly (*vide infra*) to afford the desired polymer, **5.2**, as a white powder in excellent yield (94%, Table 5.1). Analysis by gel-permeation chromatography (GPC) revealed that polymer **5.2** exhibited low dispersity ($Đ$ = 1.11) and a number-average molecular weight (M_n = 36 kDa) similar to the targeted value. We note that we consistently observed a high molecular weight impurity that we were unable to avoid.[204] Thermogravimetric analysis of **5.2** revealed a relatively high decomposition temperature (T_d = 350 °C), which is comparable to cycloolefin polymers.[205] Unfortunately, we were unable to observe any thermal transitions using differential scanning calorimetry.

The predicted[206] ring strain of **5.1** is typical for other 9-membered rings (~12 kcal/mol); thus, the rapid polymerization we observed suggested that unusually high strain may not be required to access our target materials. To benchmark this, we monitored homopolymerizations of **5.1** and an acyclic analogue [1,2-nonadiene (**5.7**)] via ^{1}H NMR spectroscopy (see experimental). We observed >95% conversion of **5.1** within 20 min, compared to approximately 60 min for >95% consumption of **5.7** (Figure 5.1). Furthermore, **5.1** exhibited a 6-fold increase in polymerization rate relative to **5.7** (c.f. k_{obs} = 0.296 for **5.1** versus k_{obs} = 0.052 for **5.7**; Figure 5.1). These studies demonstrate that modestly strained cycloallenes possess enhanced reactivity relative to acyclic allenes. This behaviour starkly contrasts cyclic olefin polymerization tendencies, and these promising

Table 5. 1: Initial Catalyst Screen and Polymerization Optimization

Entry	Catalyst*	$[\mathbf{5.1}]_0$	Time (h)	Temp. (°C)	M_n^{theo} (Da)	M_n^{expt} (Da)[c]	$Đ$[d]	Yield (%)
1	**3**	0.1	1	23	24,400[a]	35,600	1.11	94
2	**3**	0.1	1	35	24,400[a]	50,500	1.11	93
3	**3**	0.1	1	50	24,400[a]	48,900	1.13	97
4	**3**	0.1	1	65	24,400[a]	73,300	1.12	53
5	**4**	1.5	1	23	24,400[b]	133,00	1.62	57
6	**5**[f]	1.5	24	23	24,400[a]	32,000	1.37	63
7[e]	**6**[f]	1.5	1	23	24,400[a]	--	--	59
8	**3**[f]	1.5	24	23	24,400[a]	8,100	2.73	99

[a]Calculated using $[\mathbf{5.1}]_0$:$[\mathbf{Metal}]_0$ X 122.12. [b]Calculated using $[\mathbf{5.1}]_0$:$[\mathbf{Catalyst}]_0$ X 122.12. [c] Measured by GPC (triple detection). [d] Calculated using M_w/M_n. [e] Insoluble material. [f] activated with $AgSbF_6$. * See Scheme 5.1.

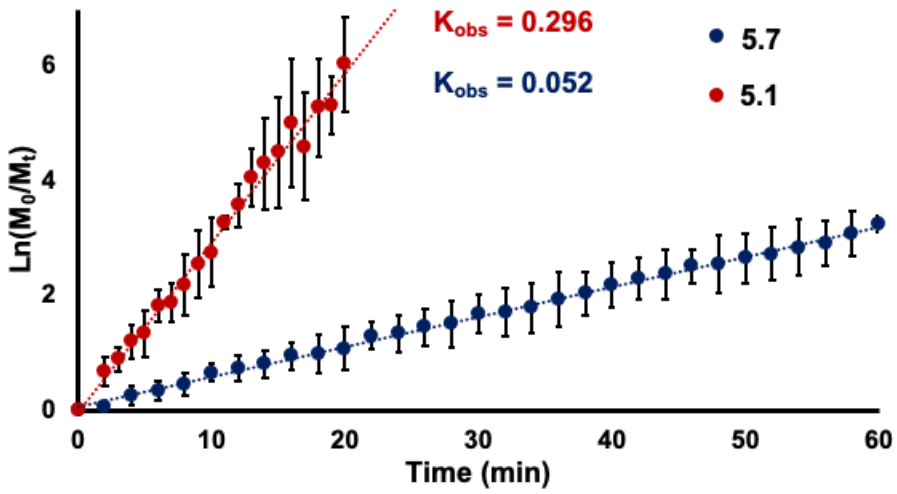

Figure 5.1: Kinetic plots for the polymerization of **5.1** (red) and **5.7** (blue)

results suggest that our strategy could accommodate monomers bearing larger ring sizes (*vide infra*).

5.3.2 Catalyst Scope and Investigation of Living Character

Having identified **5.3** as a highly active catalyst, we sought to further optimize the polymerization. We began our studies by examining other vinyl-addition polymerization catalysts[207] (**5.4** – **5.6**; Scheme 5.1). Although **5.1** polymerized in the presence of catalyst **5.4**, GPC analysis revealed that the M_n of the isolated material was significantly higher than the theoretical value (Table 5.1)**.** Polymerizations in the presence of catalyst **5.5** (activated with $AgSbF_6$) required lengthy reaction times (24 h), whereas catalyst **5.6** (also activated with $AgSbF_6$) afforded low yields of highly insoluble materials (Table 5.1). The addition of $AgSbF_6$ to **5.3** (which is known to enhance the activity of Ni based catalysts[207]) resulted in materials with low M_n and broad Đ. Finally, polymerizations at elevated temperatures (35, 50, and 65 °C) afforded materials with (i) M_n values that exceeded the theoretical values (M_n = 50, 49, and 73 kDa, respectively); (ii) slightly higher dispersities ($Đ$ = 1.13, 1.12); and (iii) reduced yields, which we hypothesize may be due to catalyst decomposition (Table 5.1).

With our selected polymerization conditions in hand, we next evaluated the living character of these polymerizations. Briefly, aliquots were periodically removed during the polymerization of **5.1** and quenched by exposure to air. Monomer conversion was determined via ^{1}H NMR spectroscopy, and M_n and $Đ$ values were determined by GPC. As shown in Figure 5.2, a linear correlation between M_n and monomer conversion was observed while maintaining relatively narrow dispersities ($Đ \leq 1.2$). Moreover, chain

extension via sequential addition of **5.1** was successful (see experimental for more details), further supporting the living nature of this polymerization (Figure 5.2). Importantly, these data suggest that cycloallenes may be readily integrated into an array of soft materials through copolymerizations.

5.3.3 Investigating the Impact of Cyclic (Co)units on Mechanical Properties

Given that polymers containing cyclic motifs often exhibit unique thermomechanical properties, we sought to investigate the effect of cycloallene moieties on mechanical properties (i.e. Young's modulus). In a preliminary study, we synthesized a series of high M_n (> 100 kDa) statistical copolymers by varying the feed ratio of **5.1**:**5.7** (70:30, 50:50, and 30:70; Table 5.2). These materials were then cast into films from $CHCl_3$ and used for subsequent tensile testing. We surmised that increased cycloallene content would result in an increased Young's modulus (in direct analogy to reports of more traditional cycloolefin copolymers).[208] Conversely, we expected increased acyclic allene content would lower the modulus [in direct analogy to poly(α-olefins)]. Tension tests were conducted for materials containing 70 and 50 mol% **5.1**. The homopolymer of **5.1** proved too brittle for analysis, whereas both the homopolymer of **5.7** and the 30 mol% material proved too tacky for mechanical analysis. We measured a Young's modulus of 1367 ± 15 MPa [strain at break = 2.5% (± 0.6%)] for the 70 mol% polymer (Figure 5.3). Conversely, tensile testing of the 50 mol% material revealed a Young's modulus of 263 ± 30 MPa [strain at break = 5.2% (± 2.4%)]. These data are consistent with observations from cyclic

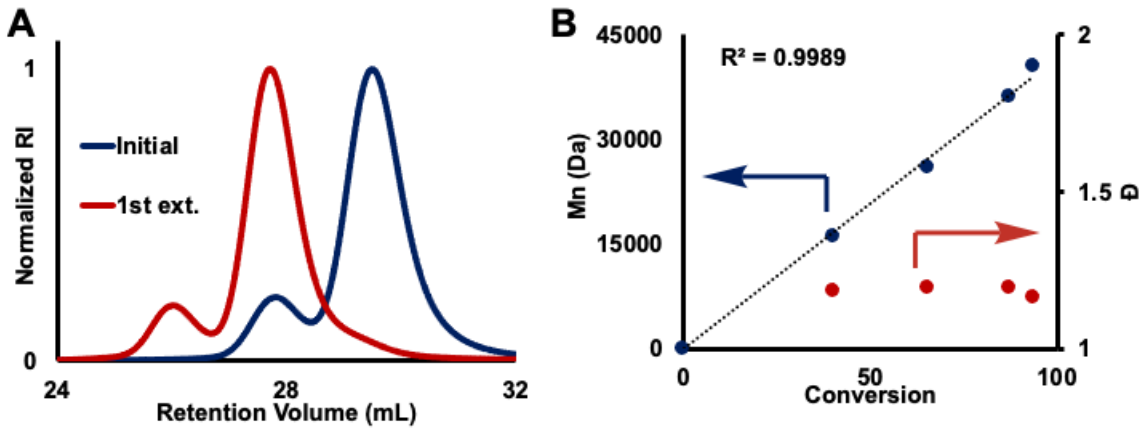

Figure 5.2: A) GPC plot showing chain extension of **5.1**. B) M_n vs. Conversion plot of **5.1**.

olefin polymers,[208] and they demonstrate that relatively modest changes in cycloallene feed ratios can dramatically impact the mechanical properties of the resultant materials. Slouf reported similar trends in copolymers with varied norbornene content (15 – 30% norbornene),[209] which further illustrates the apparent similarity between cycloolefin and cycloallene polymers. Although preliminary, these results suggest that our approach could be amenable to synthesizing a spate of soft materials with highly tunable physical properties.

5.3.4 Polymerizing Larger Ring Motifs

Finally, we sought to demonstrate the compatibility of our polymerization strategy with other cycloallene ring sizes. Synthesizing materials with large ring sizes is inherently difficult,[21] with cycloolefin scaffolds being limited primarily to fused polycycles (e.g. tetracyclododecene). However, increased ring sizes could further modify bulk material properties, such as T_d[210] or modulus.[208] We prepared 1,2-cyclotridecadiene (**5.8**) and subjected it to our optimized polymerization conditions (experimental). Interestingly, the polymerization of **5.8** required longer reaction times (72 h) to achieve modest conversions (67%), which is likely due to the steric hindrance of incorporating 13-membered rings into the growing polymer chain. The resultant material exhibited poor solubility in common solvents ($CHCl_3$, DCM, THF, PhMe, etc.); however, some portions could be dissolved in $CDCl_3$, and subsequent ^{1}H NMR spectroscopic analysis was consistent with the proposed polymer (Figure 5.27). Molecular weight data could only be determined using high-temperature GPC, which revealed that we could access relatively high M_n polymers despite the sluggish nature of the polymerization (M_n = 47,289; Đ = 1.99; Figure 5.44). Although

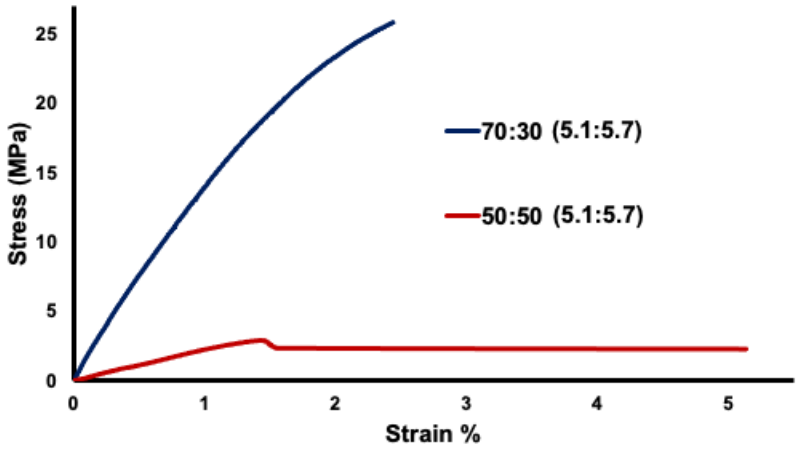

Figure 5.3: Stress vs. strain plots for copolymers of **5.1** and **5.7**. Results for 70:30 (5.1:5.7, blue) and 50:50 (red) copolymer films are shown.

Table 5.2: Polymerization results for (co)polymers of **5.1** and **5.7**

Entry	(**1**:7)	Yield (%)	M_n (Da)[a]	Đ[b]
1	100:0	76	61,356	1.32
2	0:100	74	67,570	1.15
3	70:30	97	129,100	1.38
4	50:50	92	98,360	1.85
5	30:70	78	99,270	1.75

[a]Measured by GPC (triple detection). [b] Calculated using M_w/M_n

further work is needed, these preliminary studies demonstrate that lower strain cyclic motifs can successfully be incorporated into polymer matrices.

5.4 Conclusions

In conclusion, we have demonstrated that vinyl-addition polymerization of cycloallenes is a potentially valuable strategy for preparing analogues of cycloolefin polymers that obviate current limitations. Importantly, cycloallenes can be polymerized in a well-controlled manner at room temperature using a simple Ni catalyst. Moreover, this route does not require high strain monomers (e.g., norbornene) to achieve cyclic motif incorporation. Lastly, copolymerization with acyclic monomers is possible, but not required to achieve good conversion. Taken together, these results suggest that vinyl-addition polymerizations of cyclic allenes could provide a reliable synthetic route toward previously inaccessible materials.

5.5 Acknowledgements

This work was partially supported by the donors of the American Chemical Society Petroleum Research Fund.

5.6 Experimental

5.6.1 General Materials and Methods

The following compounds were prepared according to literature procedures: 9,9-dibromobicyclo[6.1.0]nonane,[211] 1,2-cyclononadiene,[212] 1,1-dibromo-2-

hexylcyclopropane,[213] 1,2-nonadiene,[110] [(π-allyl)NiOCOCF$_3$]$_2$,[214] and *trans*-[Ni(C$_6$F$_5$)$_2$(SbPh$_3$)$_2$].[207] All other reagents and solvents were obtained from commercial sources and used without further purification. Unless otherwise noted, solvents were dried on an MBraun solvent purification system or Pure Solve solvent purification system with 3Å molecular sieves and degassed with three freeze-pump-thaw cycles. Oxygen and water sensitive manipulations were performed in a N_2-filled MBraun glovebox or using standard Schlenk techniques. All polymerizations were performed in a N_2-filled glovebox. ^{1}H and ^{13}C NMR spectroscopic data were collected on a Bruker 400 MHz NMR, Varian 300 MHz NMR, a Varian 500 MHz NMR, or a Varian 600 MHz spectrometer. Chemical shifts (δ) are reported in ppm using the residual solvent as reference. Thermogravimetric analysis (TGA) was performed on a TA Instruments TGA Q500. Dynamic mechanical analysis (DMA) was performed on a TA Instruments DMA Q800 with a film tension clamp. Gel permeation chromatography (GPC) data, unless otherwise stated, were collected on an Omnisec Resolve and Omnisec Reveal system using triple detection with detectors in series: UV, light scattering, viscometer, and refractive index and three Viscotek styrene divinylbenzene copolymer columns (in series T3000, T4000, and T5000) at a flow rate of 1 mL/min and thermostatted to 30 °C using either tetrahydrofuran (THF) or chloroform ($CHCl_3$) as the eluent. Molecular weight and dispersity data reported are from triple detection. Poly(1,2-cyclotridecadiene) was analyzed via GPC using 1,2,4-trichlorobenezene (TCB) as the eluent using a Malvern High Temperature OMNISEC system equipped with one TSK gel column thermostatted to 150 °C. Molecular weight and

polydispersity data are reported using triple detection: refractive index, viscometer, low angle light scattering and right-angle light scattering.

5.6.2 Synthesis of 9,9-Dibromobicyclo[6.1.0]nonane

9,9-Dibromobicyclo[6.1.0]nonane was synthesized following a modified procedure.[211] A 250 mL 2-neck flask was charged with a Teflon stir bar, cyclooctene (11 g; 99.81 mmol), bromoform ($CHBr_3$, 50.4 g; 199.62 mmol), DCM (30 mL), EtOH (2 mL), and cetyltrimethylammonium bromide ($CTMA^+ Br^-$, 250 mg; 0.686 mmol). The mixture was cooled to 0°C and NaOH (15.96 g; 399 mmol; 50% w/w in water) was added dropwise via cannula over the course of 10 minutes. The resulting mixture was left to stir for 48 hours while warming to room temperature (23 °C). The reaction mixture was neutralized with 2 M HCl and diluted with water (50 mL). The organic phase was separated, and the aqueous phase was extracted with DCM (2 x 30 mL). The combined organic layers were washed with water (1 x 100 mL), brine (1 x 100 mL), dried over anhydrous sodium sulfate, and filtered. The solvent was removed under vacuum, after which the crude product was dissolved in hexanes and filtered through a plug of silica gel. Residual bromoform and cyclooctene were removed under vacuum (5 torr) with gentle heating (55 °C) for 16 h to afford 9,9-Dibromobicyclo[6.1.0]nonane (17 g; 60% yield) as a colorless oil. Spectral data are consistent with known reports[211]. ^{1}H NMR ($CDCl_3$ 7.26), δ = 1.07 - 1.25 (m, 2 H), 1.30 - 1.70 (m, 10 H), 2.00 - 2.10 (m, 2 H); ^{13}C ($CDCl_3$) δ = 25.3, 26.3, 27.8, 33.2, 37. Spectral data are shown in Figures 5.9 and 5.10.

Scheme 5.2: Synthesis of 9,9-Dibromobicyclo[6.1.0]nonane

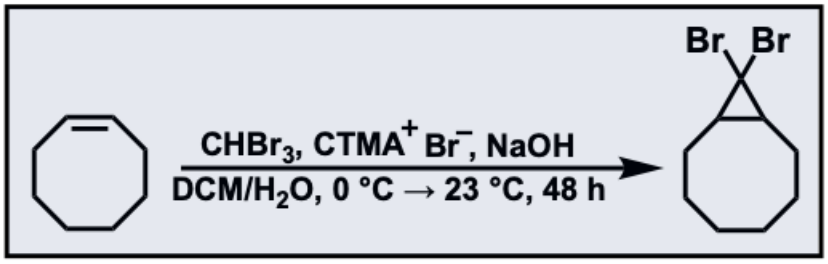

5.6.3 Synthesis of 5.1

1,2-Cyclononadiene (5.1) was synthesized following a modified procedure.[212] A flame dried 250 mL round bottom flask was charged with a Teflon stir bar, 9,9-Dibromobicyclo[6.1.0]nonane (14.3 g; 50.7 mmol), and diethyl ether (Et_2O, 25 mL) before cooling the solution to -50 °C (5 minute isotherm). Methyllithium (1.6 M in Et_2O; 36 mL; 57.6 mmol) was added slowly and the reaction was stirred at -50 °C for 30 minutes. The reaction mixture was warmed to 0 °C and quenched with water (6 mL). The mixture was then warmed to room temperature (23 °C) and further diluted with water (20 mL). The organic phase was separated, and the aqueous layer was extracted with Et_2O (2 x 20 mL). The combined organic layers were washed with water (1 x 40 mL), brine (1 x 40 mL) dried over anhydrous sodium sulfate and filtered. Solvent was removed under vacuum to yield a pale-yellow oil. Vacuum distillation (2 Torr) at 45 °C afforded **5.1** as a colorless oil (5.5 g; 89% yield). Spectral data are consistent with literature reports.[212] ^{1}H NMR ($CDCl_3$ 7.26), δ = 1.38-1.40 (m, 2H), 1.54-1.67 (m, 6H), 1.74-1.82 (m, 2H), 2.18-2.27 (m, 2H), 5.26 (m, 2H); ^{13}C ($CDCl_3$) δ = 25.5, 27.5, 28.2, 92.6, 205.8. Spectral data are shown in Figures 5.11 and 5.12.

5.6.4 Synthesis of 1,1-dibromo-2-hexylcyclopropane

1,1-dibromo-2-hexylcyclopropane was synthesized following a modified procedure.[213] A 250 mL 2-neck flask was charged with a Teflon stir bar, 1-octene (10 g; 89.1 mmol), bromoform ($CHBr_3$, 33.6 g; 133 mmol), DCM (100 mL), and cetyltrimethylammonium bromide ($CTMA^+$ Br^-, 3.27 g, 8.91 mmol). The mixture was cooled to 0 °C, and KOH (25.00 g; 445 mmol; 50% w/w in water) was added dropwise via cannula over the course

Scheme 5.3: Synthesis of **5.1**

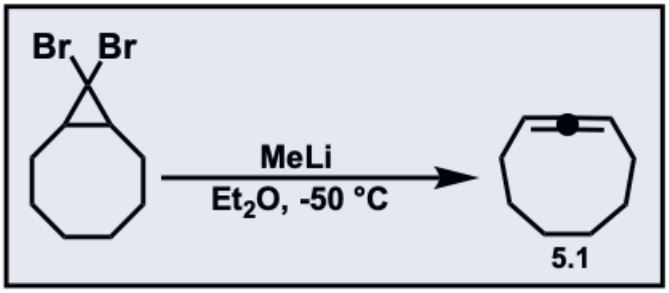

Scheme 5.4: Synthesis of 1,1-dibromo-2-hexylcyclopropane

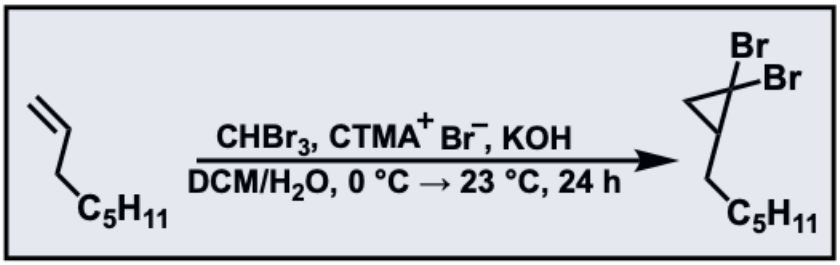

of 30 minutes. The resulting mixture was left to stir for 24 hours while warming to room temperature (23 °C), after which time the reaction mixture was neutralized using 6 M HCl. The organic phase was separated, and the aqueous layer was extracted with DCM (3 x 50 mL). The combined organic layers were washed with water (2 x 50 mL), brine (1 x 50 mL), dried over anhydrous magnesium sulfate, and filtered. Solvent was removed under vacuum, after which the crude product was dissolved in hexanes and filtered through a plug of silica gel. Vacuum distillation (2 Torr) at 85 °C afforded 1,1-dibromo-2-hexylcyclopropane as a colorless oil (20.0 g, 79% yield). Spectral data are consistent with literature reports.[213] ^{1}H NMR ($CDCl_3$ 7.26), δ = 0.92 (t, 3H),1.22 (t, 1H), 1.28–1.42 (m, 6H),1.43-1.65 (m, 5H), 1.76 (dd, 1H); ^{13}C ($CDCl_3$) δ = 14.1, 22.6, 28.3, 28.6, 29.0, 29.7, 31.5, 31.7, 32.6. Spectral data are shown in Figures 5.13 and 5.14.

5.6.5 Synthesis of 5.7

1,2-nonadiene (**5.7**) was synthesized following a modified procedure.[110] A 100 mL Schlenk flask was charged with a Teflon stir bar, 1,1-dibromo-2-hexylcyclopropane (10 g, 35.2 mmol), and diethyl ether (Et_2O, 25 mL) before cooling the solution to -78 °C (x minutes isotherm). Methyllithium (1.56 M in Et_2O; 27 mL; 42.2 mmol) was added dropwise over the course of 15 minutes and the reaction was stirred at -78 °C for 20 minutes. The reaction mixture was warmed to room temperature (23 °C) and allowed to stir for 1 hour. The mixture was quenched with water (25 mL) the organic phase separated, and the aqueous layer was extracted with Et_2O (2 x 50 mL). The combined organic layers were washed with water (2 x 50 mL), brine (1 x 50 mL), dried over magnesium sulfate, and filtered. Solvent was removed under vacuum, and vacuum distillation (60 torr) at 70 –

Scheme 5.5: Synthesis of **5.7**

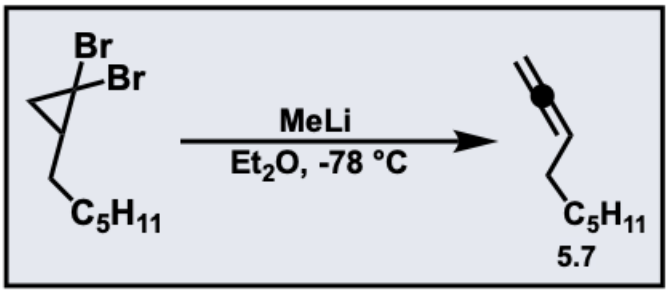

80 °C, afforded **5.7** as a colorless oil (4.0g, 93% yield). Spectral data are consistent with literature reports.[110] ^{1}H NMR ($CDCl_3$ 7.26), δ = 5.10 (quint, 1H), 4.66 (dt, 2H), 2.03-1.98 (m, 2H), 1.43-1.26 (m, 8H), 0.90 (t, 3H); ^{13}C NMR (CDCl3): δ = 208.7, 90.1, 74.5, 31.6, 29.1, 28.7, 28.2, 22.6, 14.0. Spectral data are shown in Figures 5.15 and 5.16.

5.6.6 Separation of cis-cyclododecene

***Cis*-cyclododecene** was isolated following a previously reported procedure.[215] Commercially available cyclododecene (7 g; 42.09 mmol; 65% *cis* via ^{1}H NMR spectroscopy) was added to a boiling (65 °C) MeOH solution of silver nitrate ($AgNO_3$, 4.28 g; 25.18 mmol, 0.92 equivalent relative to *trans* cyclododecene). The boiling solution was stirred for 5 minutes at 65 °C. The solution was cooled to room temperature and subsequently stored at -20 for 16 hours, after which time white needles crystallized within the flask. The white needles were collected on a medium porosity fritted funnel and transferred to a 150 mL beaker equipped with a stir bar. A mixture of water (30 mL) and Et_2O (30 mL) was added followed by vigorous stirring for 5 minutes at 23 °C. The organic layer was separated, and the aqueous layer was washed with Et_2O (2 x 30 mL). The combined organic layers were washed with water (1 x 100 mL), brine (1 x 100 mL), dried over anhydrous sodium sulfate, and filtered. Solvent was removed under vacuum to afford *cis*-cyclodocene (94% *cis* via ^{1}H NMR spectroscopy) as a colorless oil (3.16 g; 64% yield). Spectral data are consistent with literature reports.[216] ^{1}H NMR ($CDCl_3$ 7.26), δ = 5.32 (quint, 2H), 2.16-2.07 (m, 4H), 1.48-1.41 (quint, 4H), 1.37-1.31 (s, 10H), 1.30-1.22 (m, 6H); ^{13}C NMR ($CDCl_3$): δ = 130.43, 27.00, 24.68, 24.41, 23.99, 22.11. Spectral data are shown in Figures 5.17 and 5.18.

5.6.7 Synthesis of 13,13-dibromobicyclo[10.1.10]decane

13,13-dibromobicyclo[10.1.10]decane was synthesized following a modified procedure.[217] A 250 mL round bottom flask was charged with a Teflon stir bar, *cis*-cyclododecene (3.16 g; 19.06 mmol), bromoform ($CHBr_3$, 5 mL; 57.18 mmol), cetyltrimethylammonium bromide ($CTMA^+ Br^-$, 228 mg; 0.625 mmol) and EtOH (1 mL). The mixture was cooled to 0 °C and KOH (9.6 g; 171.5 mmol; 50% w/w in water) was added dropwise via syringe over the course of 6 minutes. The resulting mixture was left to stir for 48 hours while warming to room temperature (23 °C). The reaction mixture was diluted with water (50 mL) and hexanes (30 mL). The organic phase was separated, and the aqueous layer was extracted with hexanes (2 x 30 mL). The combined organic layers were washed with water (1 x 60 mL), brine (1 x 90 mL), dried over anhydrous sodium sulfate and filtered. Solvent was removed under vacuum. Unreacted cyclododecene was removed via vacuum distillation (5 torr) at 90 °C. The product was taken up in hexanes, filtered through a plug of silica gel, and removal of solvent under vacuum afforded 13,13-dibromobicyclo[10.1.10]decane as colorless crystals (4.3 g; 67% yield). ^{1}H NMR ($CDCl_3$ 7.26), δ = 1.73-1.65 (m, 2H), 1.65-1.49 (m, 4H), 1.49-1.31 (m, 10H), 1.29-1.15 (m, 4H); ^{13}C NMR (CDCl3): δ = 34.29, 26.88, 26.72, 26.06, 24.06, 22.64. Spectral data are shown in Figures 5.19 and 5.20.

5.6.8 Synthesis of 5.8

1,2-cyclotridecadiene (**5.8**) was synthesized following a modified procedure.[217] A flame dried 50 mL round bottom flask was charged with a Teflon stir bar, 13,13-

Scheme 5.6: Separation of cis-cyclododecene

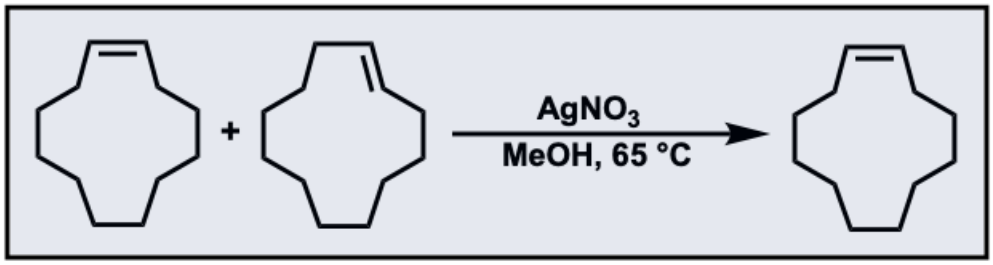

Scheme 5.7: Synthesis of 13,13-dibromobicyclo[10.1.10]decane

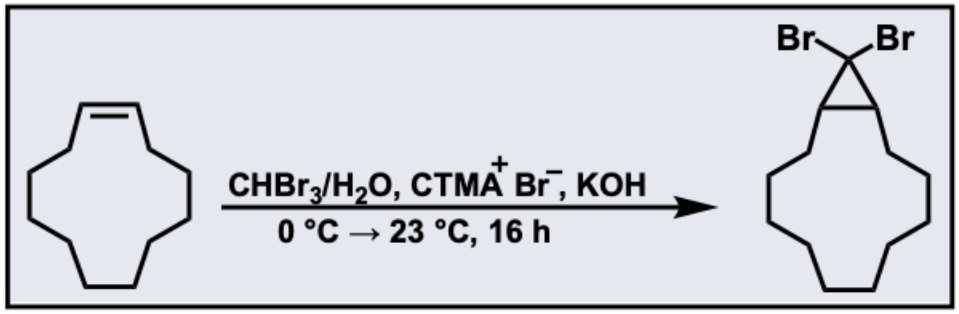

dibromobicyclo[10.1.10]decane (4 g; 11.83 mmol), and diethyl either (Et_2O, 15 mL) before cooling to solution to -40 °C (5 minute isotherm). Methyllithium (1.6 M in Et_2O; 8.13 mL; 13.01 mmol) was slowly added and the reaction was stirred at -40 °C for 1 hour. The reaction mixture was warmed to 0 °C and slowly quenched with water (5 mL). The mixture was then warmed to room temperature (23 °C) and further diluted with water (10 mL). The organic phase was separated, and the aqueous layer was extracted with Et_2O (3 x 15 mL). The combined organic layers were washed with water (1 x 60 mL), brine (1 x 60 mL brine), dried over anhydrous sodium sulfate. Solvent was removed under vacuum and the crude product was purified via vacuum distillation (15 torr) at 95 °C to afford **5.8** as a colorless oil (1.5 g; 71% yield). Spectral data are consistent with literature reports.[217] ^{1}H NMR ($CDCl_3$ 7.26), δ = 5.08 (quint, 2H), 2.15-1.95 (m, 4H), 1.62-1.50 (m, 4H), 1.50-1.37 (m, 8H), 1.37-1.23 (m, 8H); ^{13}C NMR ($CDCl_3$): δ = 204.31, 91.34, 27.47, 27.19, 27.12, 26.76, 26.52. Spectral data shown in Figures 5.21 and 5.22.

5.6.9 General Procedure for Vinyl-Addition Polymerization of 5.1 with 5.3

In an N_2 filled glovebox, bis(1,5-cyclooctadiene)nickel(0) (12.4 mg; 0.045 mmol) was dissolved in toluene (1.75 mL). Allyltrifluoroacetate (5.8 μL, 0.045mmol) was added with stirring at 23 °C for 20 minutes, which generated [{(π-allyl)NiOCOCF$_3$}$_2$] *in-situ* ([Ni] =0.026 M). An aliquot (0.15 mL, 0.004 mmol Ni) of this freshly prepared catalyst solution was added to a solution of **5.1** (100 mg; 0.818 mmol) in toluene (8.0 mL) and stirred for 1 hour at 23 °C. The polymerization was quenched via exposure to air and solvent was removed *in vacuo*. Polymeric material was then dissolved in minimal $CHCl_3$ and

Scheme 5.8: Synthesis of **5.8**

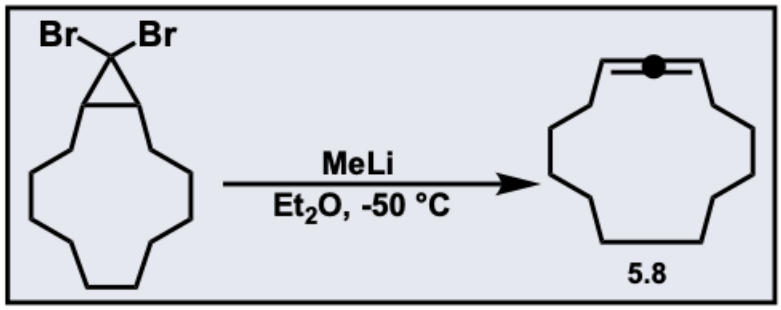

Scheme 5.9: Generation of **5.3** *in situ* and Synthesis of **5.2**

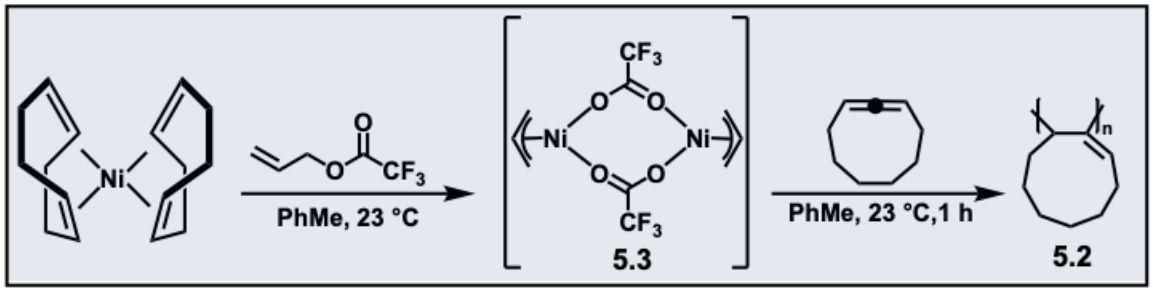

precipitated from MeOH. The white powder was collected on a medium porosity fritted funnel and dried for 16 hours *in vacuo*. Representative spectral data are shown in Figures 5.23 and 5.24. Representative GPC data shown in Figure 5.35.

5.7 was polymerized following the procedure outlined in section **5.6.9** with the following modifications: **5.3**, (0.26 mL; 0.0068 mmol Ni), **5.7** (3.3 mmol), and toluene (20 mL) were used. The polymerization was conducted for 16 hours, quenched via exposure to air, concentrated to a minimal volume, and precipitated from MeOH. Representative spectral data shown in Figures 5.25 and 5.26. GPC data shown in Figure 5.36.

5.6.10 General Procedure for Vinyl-Addition Polymerization of 5.1 with 5.3-5.6

In an N_2 filled glovebox, a 7 mL vial was charged with a Teflon stir bar and a solution of catalyst **5.3**, **5.5**, or **5.6** (0.004 mmol Ni/Pd in 0.5 mL toluene) activated with $AgSbF_6$ (1 equiv. with respect to Ni) or a solution of catalyst **5.4** (0.004 mmol Ni in 0.5 mL toluene). **5.1** (100 mg, 0.818 mmol) was added to the catalyst solution and stirred at 23 °C for 1 hour (catalysts **5.4** and **6.6**) or 24 hours (catalyst **5.5** and **5.3**). The polymerization was sparged with air and solvent was removed *in vacuo*. GPC data are shown in Figures 5.37 – 5.40. Results are tabulated in Table 5.1.

5.6.11 General Procedure for Quenching the Polymerization of 5.1 with 5.3

In an N_2 filled glovebox, bis(1,5-cyclooctadiene)nickel(0) (12.4 mg; 0.045 mmol) was dissolved in toluene (2.0 mL). Allyltrifluoroacetate (5.8 μL, 0.045mmol) was added with stirring at 23 °C for 20 minutes, which generated [{(π-allyl)NiOCOCF$_3$}$_2$] *in-situ* ([Ni] = 0.023 M). An aliquot (0.11 mL, 0.0025 mmol Ni) of this freshly prepared catalyst solution

was added to a solution of **5.1** (25 mg; 0.205 mmol) in toluene (2.0 mL) and stirred for 1 hour at 23 °C. Various quenching agents were used to terminate the active catalyst and stirred for 30 min. The inactive polymerization solution was then precipitated from MeOH. The white powder was collected on a medium porosity fritted funnel and dried for 16 hours *in vacuo*. The findings from this study are summarized in Table 5.3.

5.6.12 General Procedure for Additional Catalyst Studies to Alleviate High M_n Shoulder

In an N_2 filled glovebox, bis(1,5-cyclooctadiene)nickel(0) (12.4 mg; 0.045 mmol) was dissolved in toluene (1.75 mL). Allyltrifluoroacetate (5.8 μL, 0.045 mmol) was added with stirring at 23 °C for 10 minutes, which generated [{(π-allyl)NiOCOCF$_3$}$_2$] *in-situ* ([Ni] = 0.026 M). PPh_3 (11.8 mg; 0.045 mmol) or $SbPh_3$ (15.0 mg; 0.045 mmol) was added stirring at 23 °C for 10 minutes. An aliquot (0.38 mL, 0.010 mmol Ni) of this freshly prepared catalyst solution was added to a solution of **5.1** (100 mg; 0. 818 mmol) in toluene (8.0 mL) and stirred for 1 hour at 23 °C. The polymerization was quenched with 0.1 mL of dried and degassed MeOH and stirred for 30 min at 23 °C. The inactive polymerization solution was then precipitated from MeOH. The white powder was collected on a medium porosity fritted funnel and dried for 16 hours *in vacuo* (Table 5.4).

In an N_2 filled glovebox, **5.6** (3.0 mg; 0.010 mmol) and silver trifluoroacetate (4.4 mg; 0.021 mmol) were dissolved in toluene (1.0 mL) and stirred at 23 °C for 5 minutes. The resulting solution was filtered, using a 0.2 μm syringe filter, directly into a solution of **5.1** (100 mg; 0. 818 mmol) in toluene (8.0 mL) and stirred for 1 hour at 23 °C. The

Table 5.3: Quenching agent study for polymerization of **5.1** with **5.3**

Entry	[**5.1**]$_0$	Time (h)	Quenching Agent	High M_n Shoulder	M_n^{expt} (Da)	*Đ*	Yield (%)
1	0.1	1	Concentrated HCl (degassed)	present	20,600	1.18	90
2	0.1	1	Concentrated Trifluoroacetate (degassed)	present	21,000	1.23	98
3	0.1	1	MeOH (dried and degassed)	present	20,700	1.2	78
4	0.1	1	Air Sparge	present	23,000	1.21	89
5	0.1	1	MeOH (dried and aerated)	present	23,400	1.24	98
6	0.1	1	MeCN (dried and degassed)	present	23,900	1.16	99

Table 5.4: The polymerization of **5.1** with various catalytic species

Entry	Catalyst	[**5.1**]^0	Time (h)	Additive	High M_n Shoulder	M_n^{expt} *(Da)*	Đ	Yield (%)
1	5.3	0.1	1	PPh3	N/A	N/A	N/A	N/A
2	5.3	0.1	1	SbPh3	present	27,400	1.16	96
3	5.6	0.1	1	AgTFA	present	10,800	1.14	81

polymerization was quenched with 0.1 mL of dried and degassed MeOH and stirred for 30 min at 23 °C. The inactive polymerization solution was then precipitated from MeOH. The white powder was collected on a medium porosity fritted funnel and dried for 16 hours *in vacuo* (Table 5.4).

5.6.13 General Procedure for Statistical and Block Copolymerizations

Statistical copolymers were synthesized following the same procedure outlined in section **5.6.9** Note: both monomers were combined in a single vessel prior to addition of **5.3**. The solution was then stirred at 23 °C for 16 hours. The polymerization was quenched via exposure to air, concentrated to a minimal volume, precipitated from MeOH, collected on a medium porosity fritted funnel, and dried in a vacuum oven (65 °C) for 16 hours. Representative spectral data shown in Figures 5.29 – 5.34. Representative GPC data shown in Figures 5.41 – 5.43

5.6.14 General Procedure for Kinetics Experiments of 5.1 and 5.7

In an N_2 filled glovebox, a 3 mL vial was charged with **5.1** or **7** (30 mg; 0.25 mmol), d_8-toluene (0.5 mL) and trimethoxybenzene (4.8 mg; 0.026 mmol; used with **5.7**) or mesitylene (2.5 μL; 0.018 mmol; used with **5.1**) as an internal standard. The solution was transferred to a septa-capped NMR tube and an initial (T_0) ^{1}H NMR spectrum was collected. A separate 1 mL vial was charged with bis(1,5-cyclooctadiene)nickel(0) (12 mg; 0.044 mmol)**,** a Teflon stir bar, d_8-toluene (1 mL), and allyltrifluoroacetate (5.7 μL; 0.044 mmol). Stirring at 23 °C for 20 minutes generated **5.3** *in situ* ([Ni] = 0.044 M). An aliquot (0.14 mL; 0.0062 mmol Ni) was drawn up by an air-tight syringe and the needle tip inserted

into a rubber septum. The solution of **5.3** was quickly injected into the NMR tube (followed by mixing via inversion). ^{1}H NMR spectra were collected every two minutes over the course of 30 minutes (for **5.1**) or one hour (for **5.7**). Monomer consumption was determined via integration of the allene vinyl protons (δ = 5.1 – 5.3 for **5.1**; δ = 4.5 – 4.8 for **5.7**) versus the internal standard (δ = 6.1 – 6.3 for trimethoxybenzene; δ = 6.6 – 6.8 for mesitylene). The kinetics experiments were completed in triplicate for **5.1** and **5.7**, and error was determined by the standard deviation of the three trials. Kinetics plot comparing the rates of polymerization of **5.1** and **5.7** are shown in Figure 5.1.

5.6.15 General Procedure for Determination of Living Character of 5.1 and 5.7

In an N_2 filled glovebox, a 7 mL vial was charged with a Teflon stir bar, **5.1** (150 mg; 1.23 mmol), mesitylene (170 μL; 1.23 mmol; used as an internal standard) and an aliquot was removed via capillary action and diluted with $CDCl_3$ for ^{1}H NMR spectroscopic analysis (T_0). After which toluene (3 mL) was added. In a separate 7 mL vial, a stock solution of **5.3** ([Ni] = 0.026 M) was prepared as previously described in section **5.6.9**. An aliquot (0.2 mL; 0.0052 mmol Ni) of this freshly prepared stock solution was added to the vial containing **5.1** and stirred at 23 °C. Aliquots (0.2 mL) were removed every ~4 minutes, quenched via exposure to air, diluted with $CDCl_3$ (0.5 mL) and analyzed by ^{1}H NMR spectroscopy (Table 5.5). The NMR samples were transferred to 3 mL vials, concentrated to a residue, and dried *in vacuo* for 16 hours. The aliquots were dissolved in HPLC-THF (2 mL) and analyzed by GPC to determine the number average molecular weight (M_n) of any polymeric species (Table 5.5). The calculated M_n data were plotted as a function of monomer conversion, which revealed a linear correlation (Figure 5.2B).

Table 5.5: Living Plot Molecular Weight and Conversion Data for **5.1**

Entry	Monomer	Reaction Time (min)	Conversion (%)	M_n (Da)	Đ
0	5.1	0	0	-	-
1	5.1	4	40	16,000	1.18
2	5.1	8	65	26,000	1.19
3	5.1	13	87	36,000	1.19
4	5.1	18	94	40,470	1.16

This procedure was also conducted for **5.7** with the following amount/time modifications: **5.3** (0.13 mL; 0.0034 mmol Ni); aliquots removed every 5 to 10 minutes. The aliquots were analyzed as previously described in section **5.1** (Table 5.6). The calculated M_n data were plotted as a function of monomer conversion, which revealed a linear conversion Figure 5.4.

5.6.16 General Procedure for Chain Extension

In an N_2 filled glovebox, a stock solution of **5.3** ([Ni] = 0.0133 M) was prepared as described in section **5.6.9**. A separate 20 mL vial was charged with a Teflon stir bar, **5.1** (100 mg; 0.8188 mmol), and toluene (1 mL). An aliquot (0.6 mL; 0.00799 mmol Ni) of the stock solution of **5.3** was added to the solution of **5.1**, and stirred at 23 °C. After 20 minutes, an aliquot (0.15 mL) was removed, quenched via exposure to air, diluted with $CDCL_3$ (0.55 mL) and analyzed by ^{1}H NMR spectroscopy (which confirmed full conversion of **5.1**). At this point, another portion of **5.1** (100 mg; 0.8188 mmol) in toluene (1.6 mL) was added to the polymerization mixture and allowed to stir. After 20 minutes another aliquot (0.15 mL) was removed from the turbid solution, and ^{1}H NMR spectroscopic analysis confirmed quantitative conversion of **5.1**. The NMR aliquots were concentrated to a residue under vacuum and analyzed by GPC to determine the number average molecular weight (M_n) of any polymeric species (Table 5.7). The observed data were consistent with successful chain extension (Figure 5.2A).

5.6.17 General Procedure for Stress Strain Experiments

A rectangular film of the respective polymer was cast from $CHCl_3$ (5 w% polymer) and

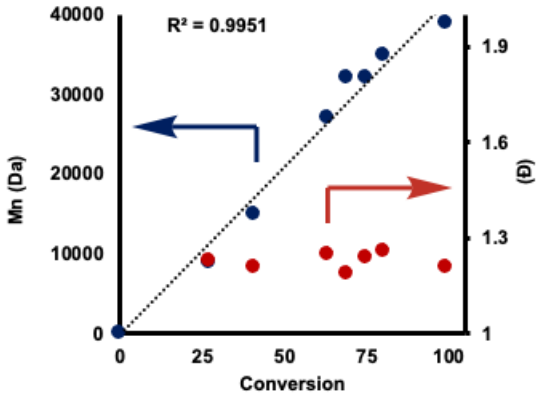

Figure 5.4: Number average molecular weight (M_n) as a function of monomer conversion (blue) and Dispersity (Đ; red) for polymerization of **5.7.**

Table 5.6: Living Plot Molecular Weight and Conversion Data for **5.7**

Entry	Monomer	Reaction Time (min)	Conversion (%)	M_n (Da)	Đ
0	5.7	0	0	-	-
1	5.7	9	27	9,000	1.23
2	5.7	15	41	15,000	1.21
3	5.7	35	63	27,000	1.25
4	5.7	45	69	32,000	1.19
5	5.7	65	75	32,000	1.24
6	5.7	85	80	35,000	1.26
7	5.7	115	99	39,000	1.21

Table 5.7: Molecular Weight Data for Chain Extension of **5.1**

Entry	Extensions	M_n (Da)	Target M_n (Da)	Đ
1	0	18,910	12,000	1.16
2	1	33,800	24,000	1.14

analyzed using DMA (film tension clamp at 0.1% strain/min). Representative Stress v. Strain plots are shown in Figure 5.3.

APPENDIX

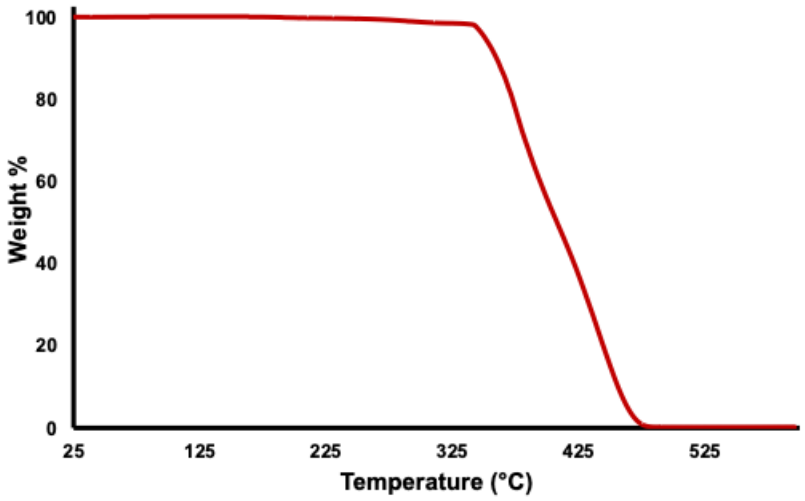

Figure 5.5: Representative **5.2** TGA thermogram (Heating Rate: 10 °C/min in N_2)

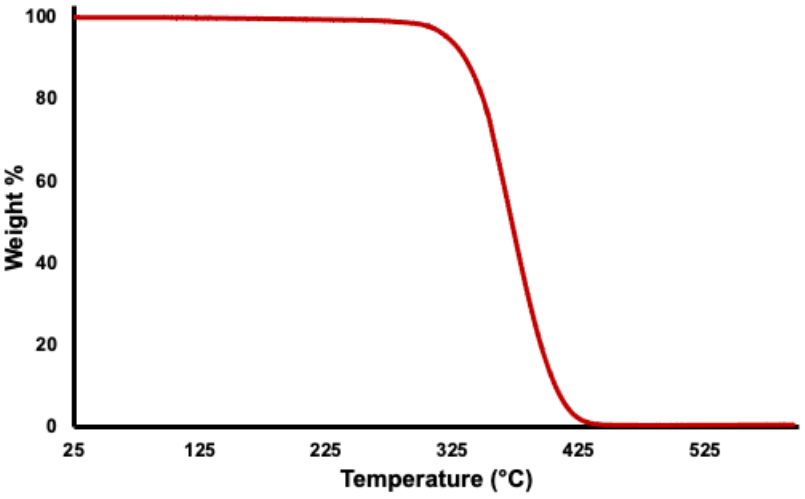

Figure 5.6: Representative poly(1,2-nonadiene) TGA thermogram (Heating Rate: 10 °C/min in N_2)

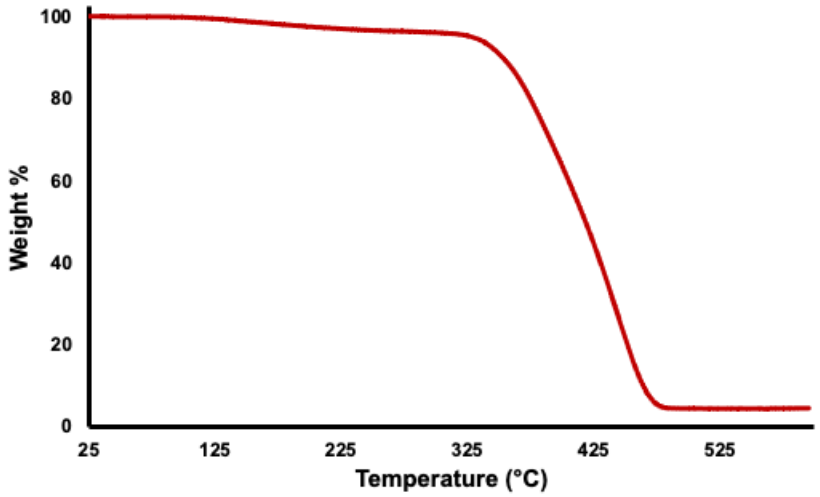

Figure 5.7: Representative poly(1,2-cyclotridecadiene) TGA thermogram (Heating Rate: 10 °C/min in N_2)

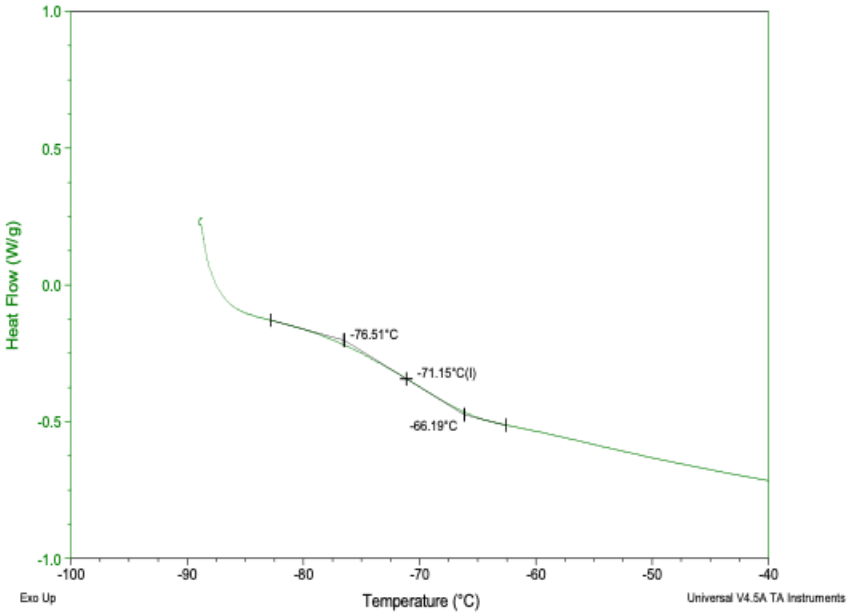

Figure 5.8: Representative DSC thermogram of poly(1,2-nonadiene). Second heating cycle (Heating Rate: 10 °C/min).

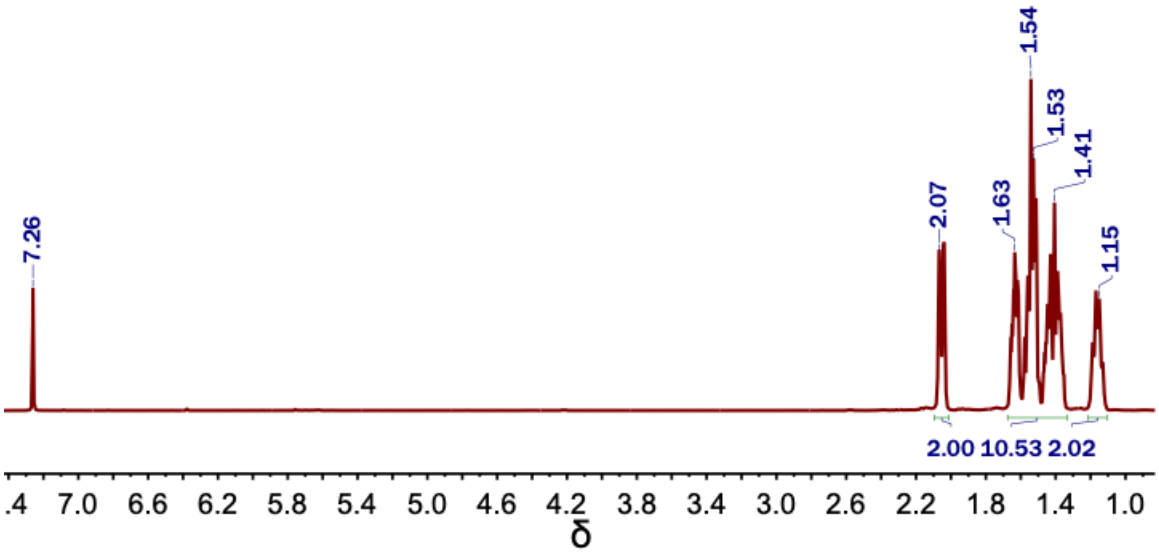

Figure 5.9: ^{1}H NMR spectrum of 9,9-Dibromobicyclo[6.1.0]nonane in $CDCl_3$.

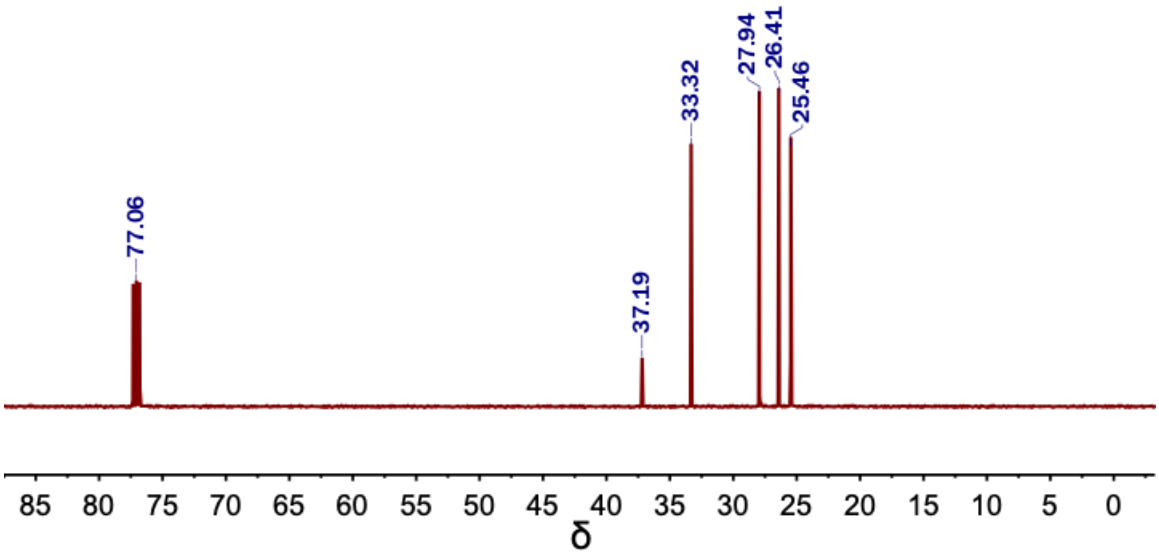

Figure 5.10: ^{13}C NMR spectrum of 9,9-Dibromobicyclo[6.1.0]nonane in $CDCl_3$.

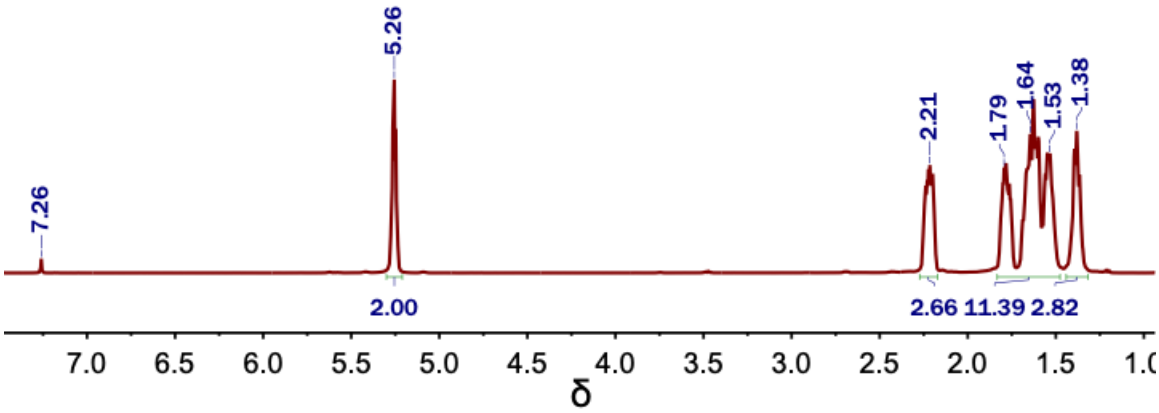

Figure 5.11: ^{1}H NMR spectrum of **5.1** in $CDCl_3$.

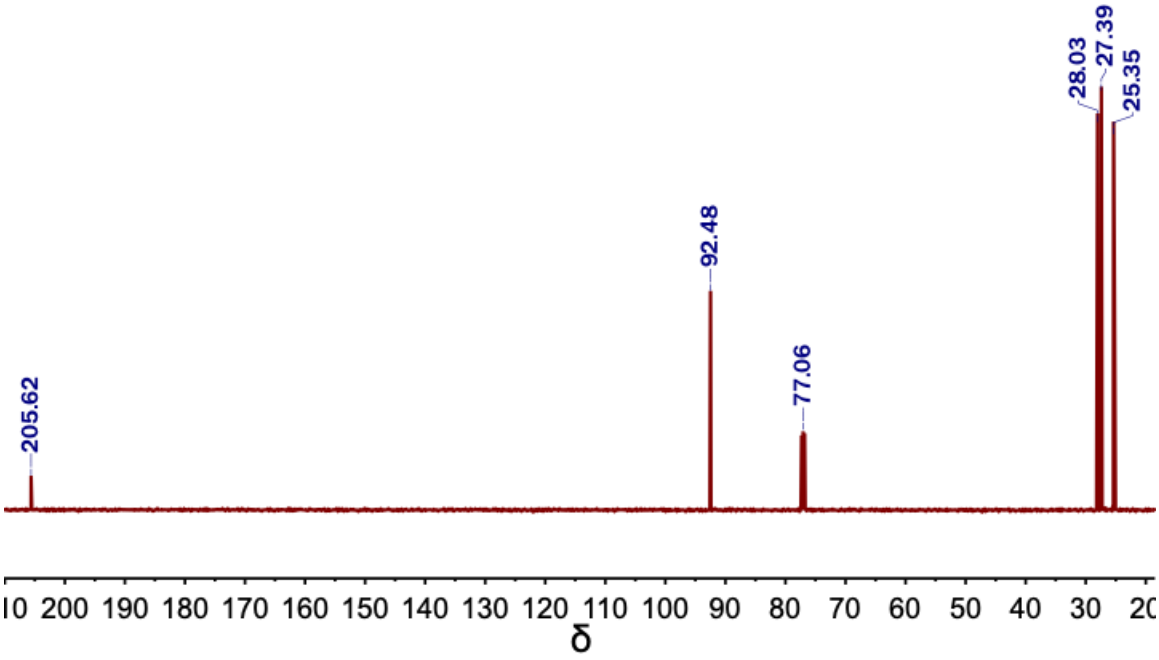

Figure 5.12: ^{13}C NMR spectrum of **5.1** in $CDCl_3$.

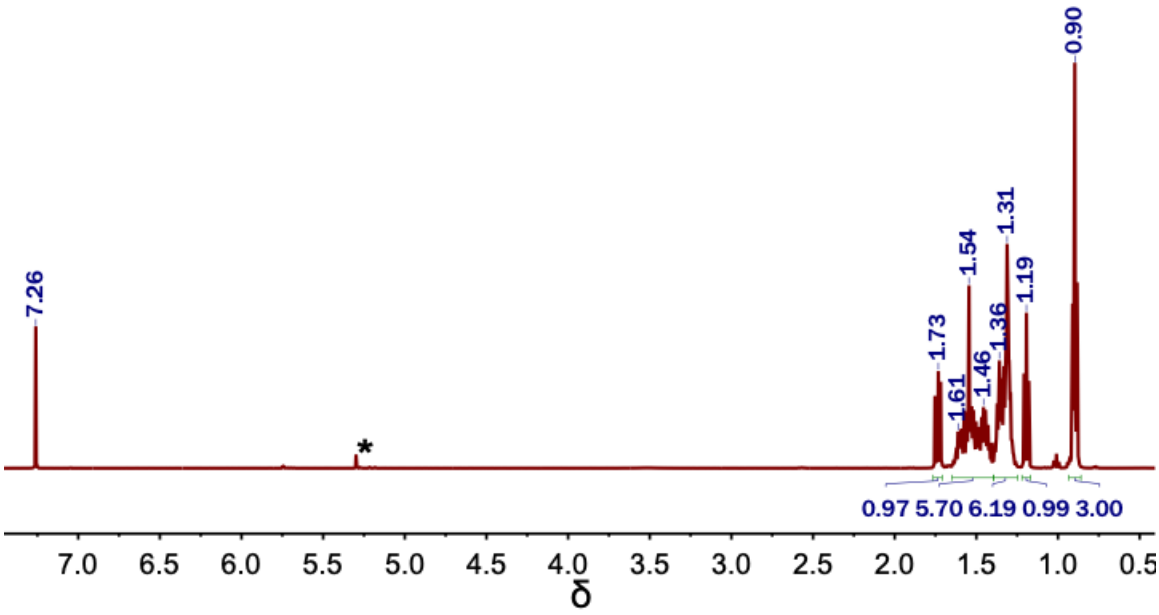

Figure 5.13: ^{1}H NMR spectrum of 1,1-dibromo-2-hexylcyclopropane in $CDCl_3$. Residual solvent (DCM: δ = 5.30) denoted with *.

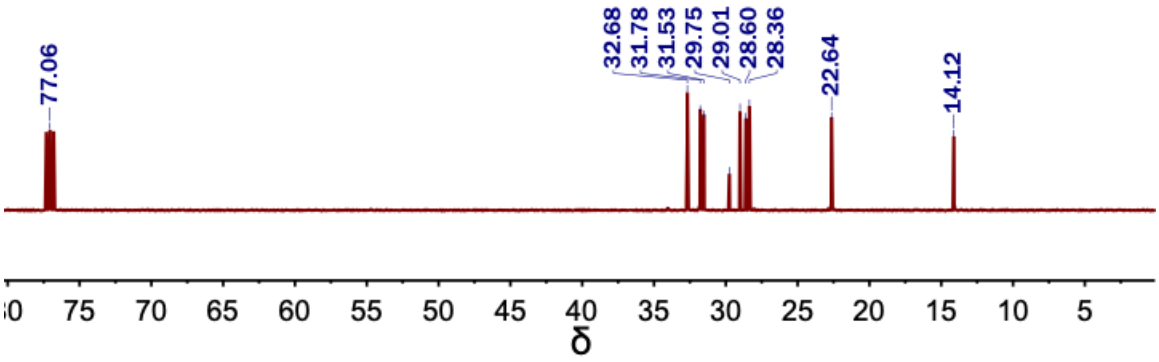

Figure 5.14: ^{13}C NMR spectrum of 1,1-dibromo-2-hexylcyclopropane in $CDCl_3$.

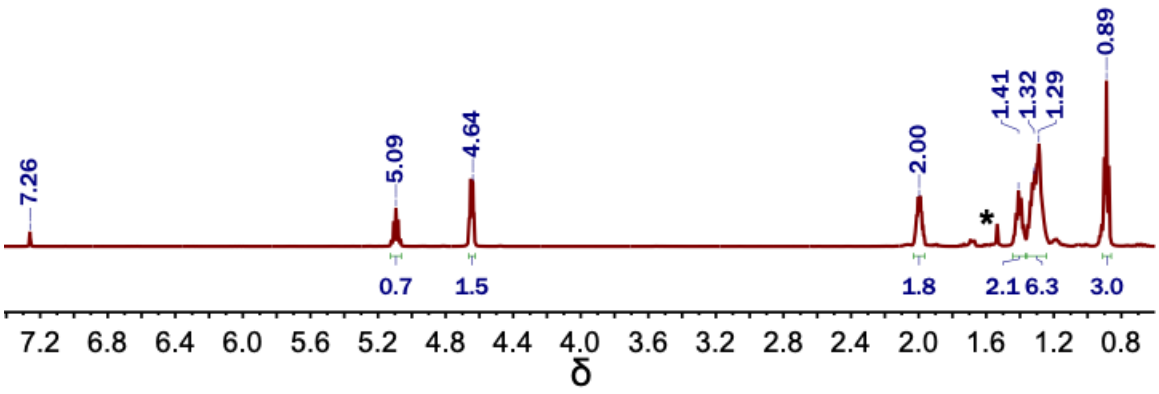

Figure 5.15: ^{1}H NMR spectrum of **5.7** in $CDCl_3$. Residual solvent (H_2O: δ = 1.56) denoted by *.

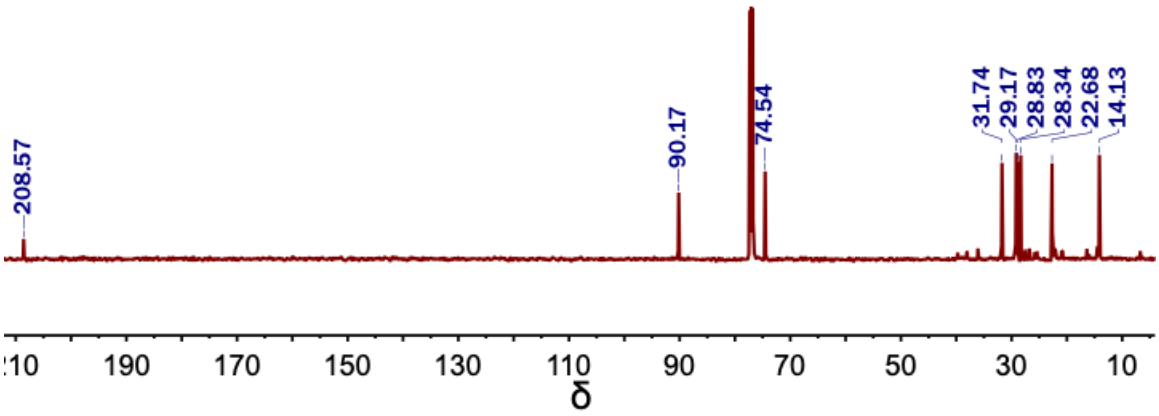

Figure 5.16: ^{13}C NMR spectrum of **5.7** in $CDCl_3$.

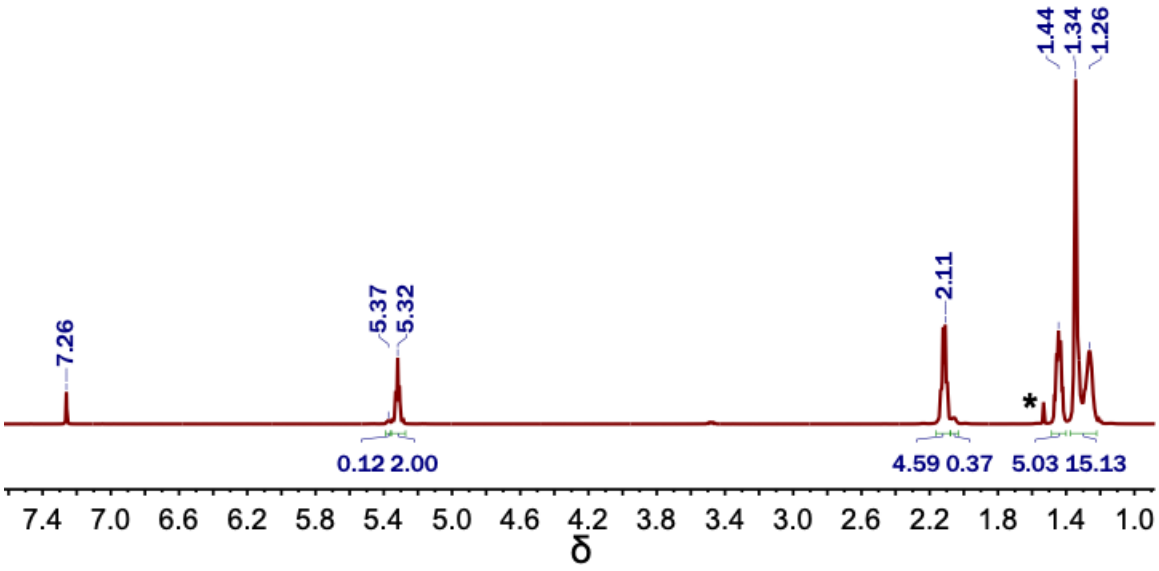

Figure 5.17: ^{1}H NMR spectrum of *cis*-cyclododecene in $CDCl_3$. Residual solvent (H_2O: δ = 1.56) denoted by *. *Cis*:*trans* ratio determined by relative integration of *cis* (δ = 5.32) and *trans* (δ = 5.37) resonances.

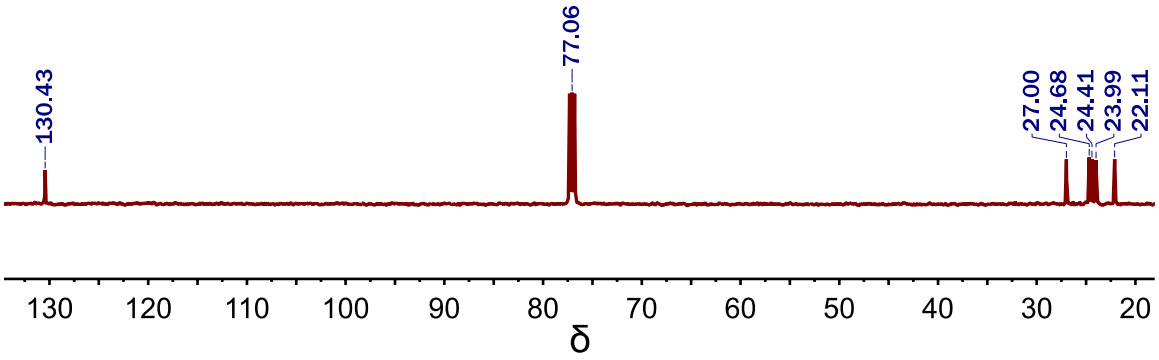

Figure 5.18: ^{13}C NMR spectrum of *cis*-cyclododecene in $CDCl_3$.

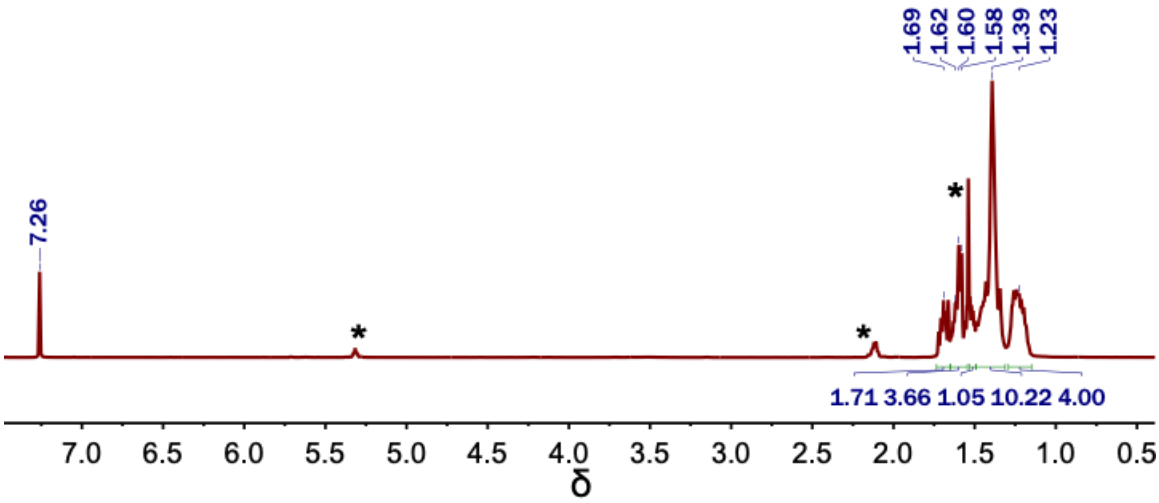

Figure 5.19: ^{1}H NMR spectrum of 13,13-dibromobicyclo[10.1.10]decane in $CDCl_3$. Residual solvent (H_2O: δ = 1.56) and *cis*-cyclododecene (δ = 5.32, 2.10) denoted by *.

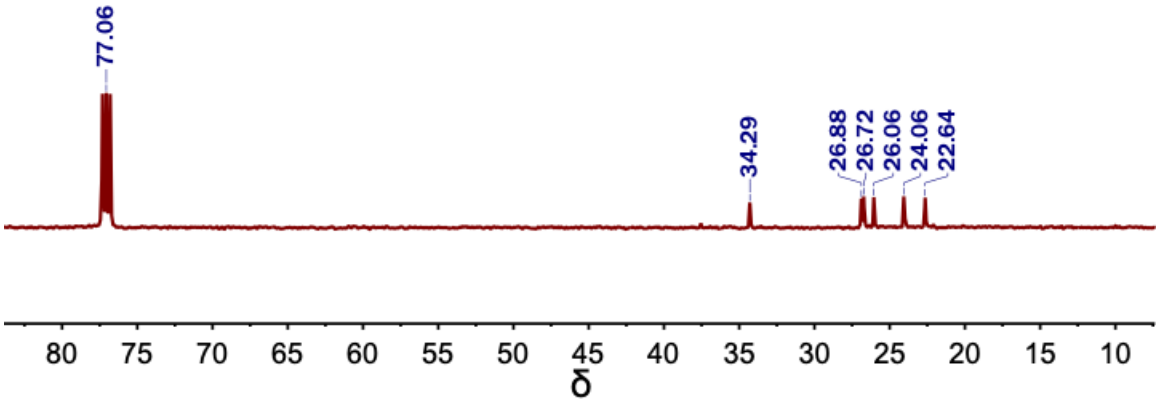

Figure 5.20: ^{1}H NMR spectrum of 13,13-dibromobicyclo[10.1.10]decane in $CDCl_3$.

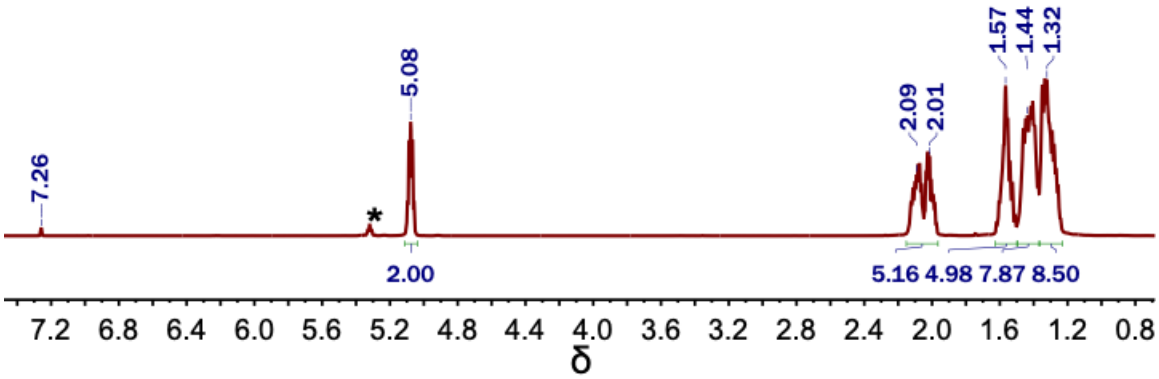

Figure 5.21: ^{1}H NMR spectrum of **5.8** in $CDCl_3$. Residual *cis*-cyclododecene (δ = 5.32) denoted by *.

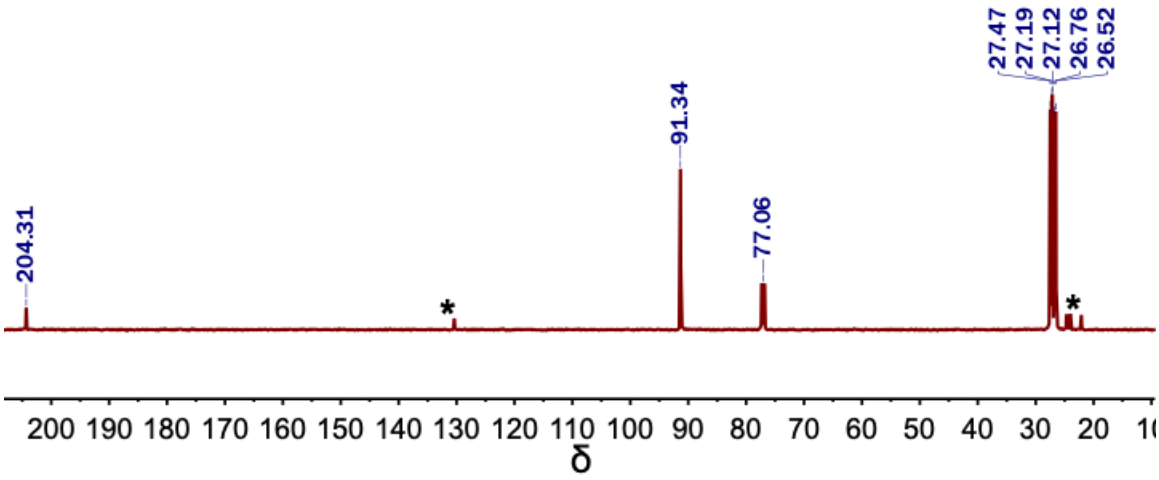

Figure 5.22: ^{1}H NMR spectrum of 5.8 in $CDCl_3$. Residual *cis*-cyclododecene (δ = 130.43, 24.65, 24.38, 23.95, 22.08) denoted by *.

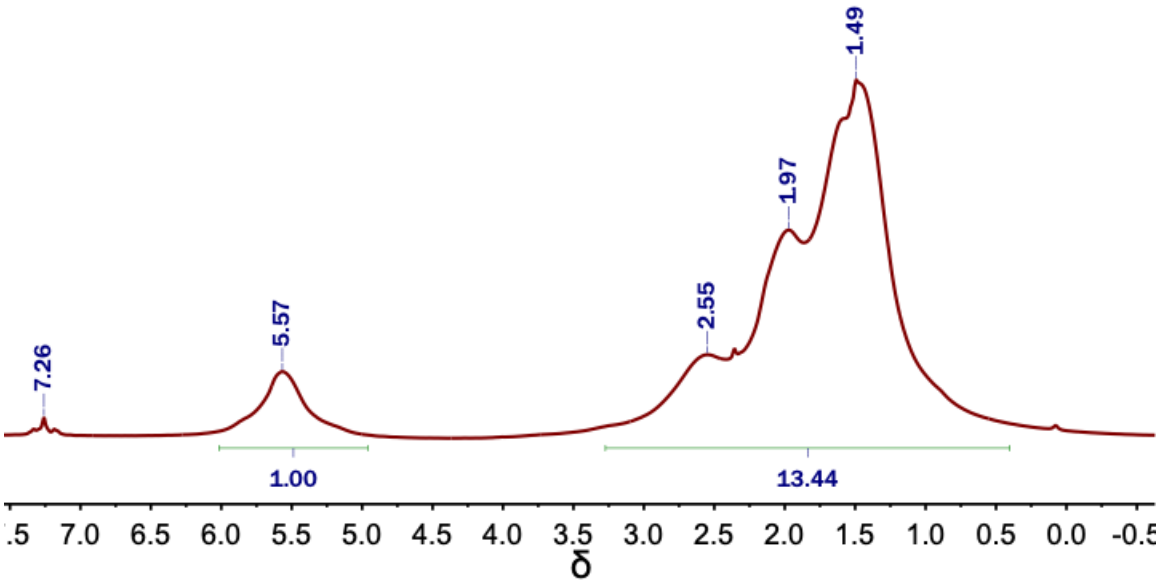

Figure 5.23: ^{1}H NMR spectrum of **5.2** in $CDCl_3$.

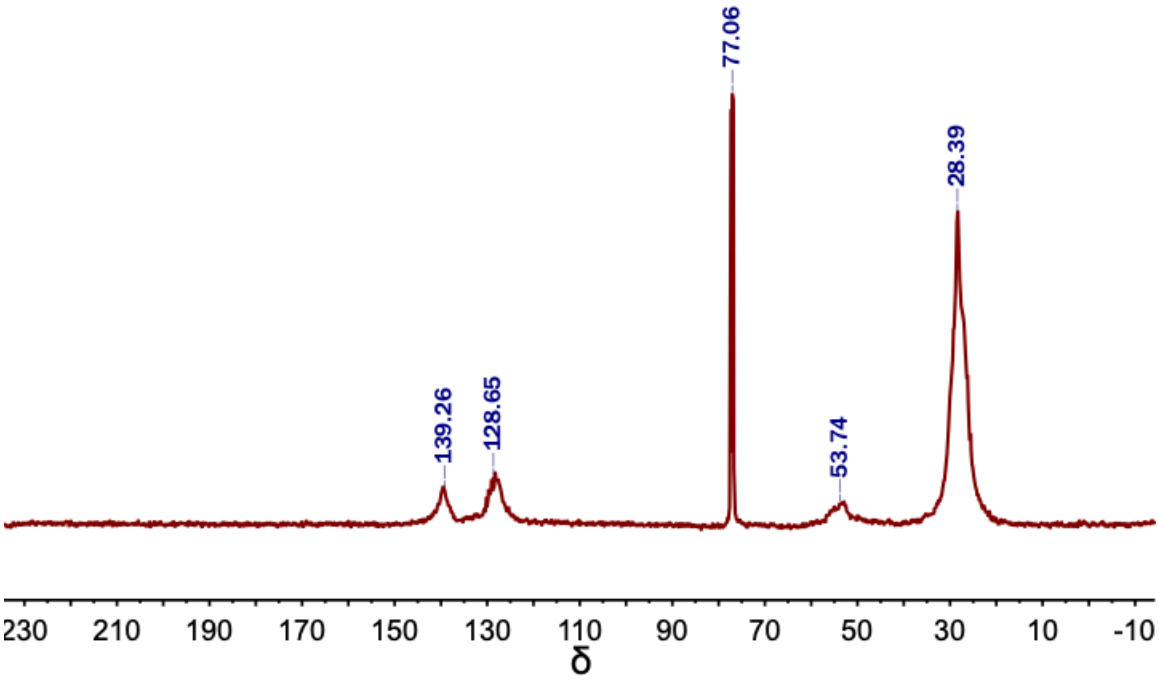

Figure 5.24: ^{13}C NMR spectrum of **5.2** in $CDCl_3$.

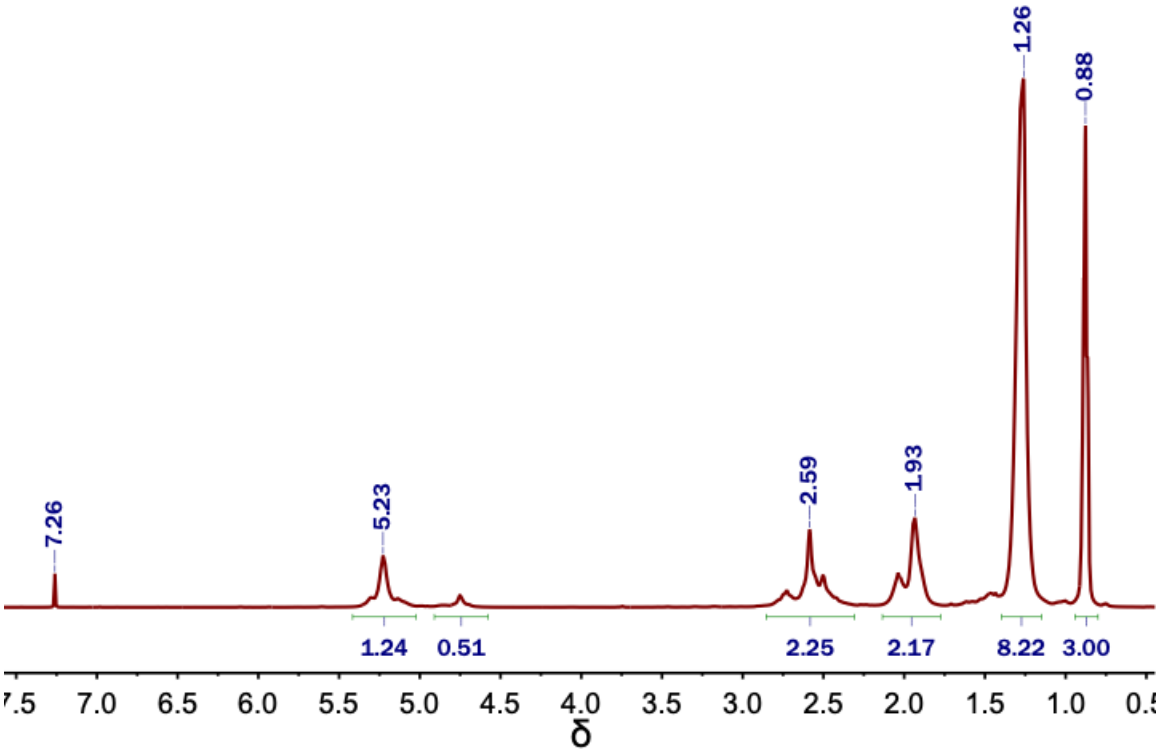

Figure 5.25: ^{1}H NMR spectrum of poly(1,2-nonadiene) in $CDCl_3$.

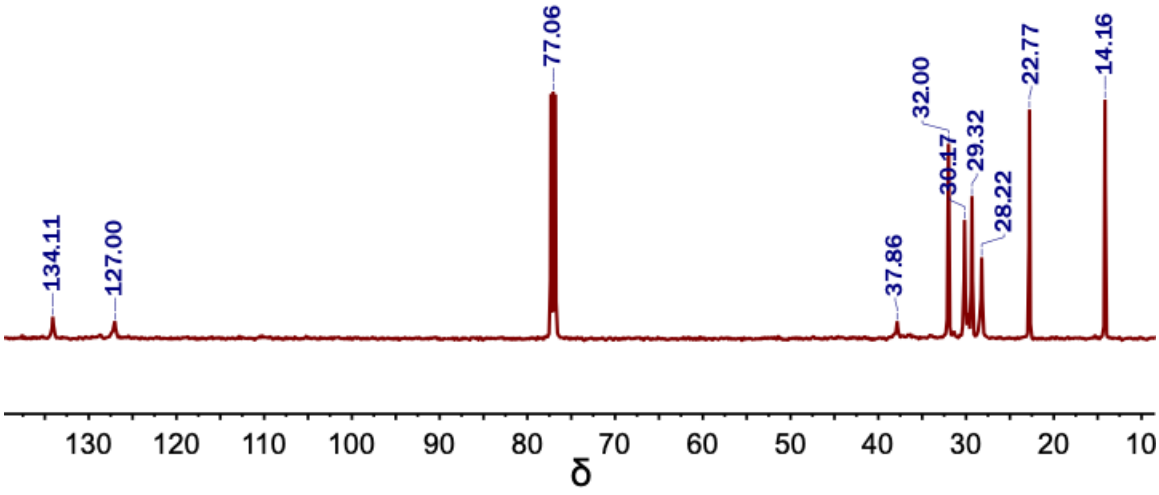

Figure 5.26: ^{13}C NMR spectrum of poly(1,2-nonadiene) in $CDCl_3$.

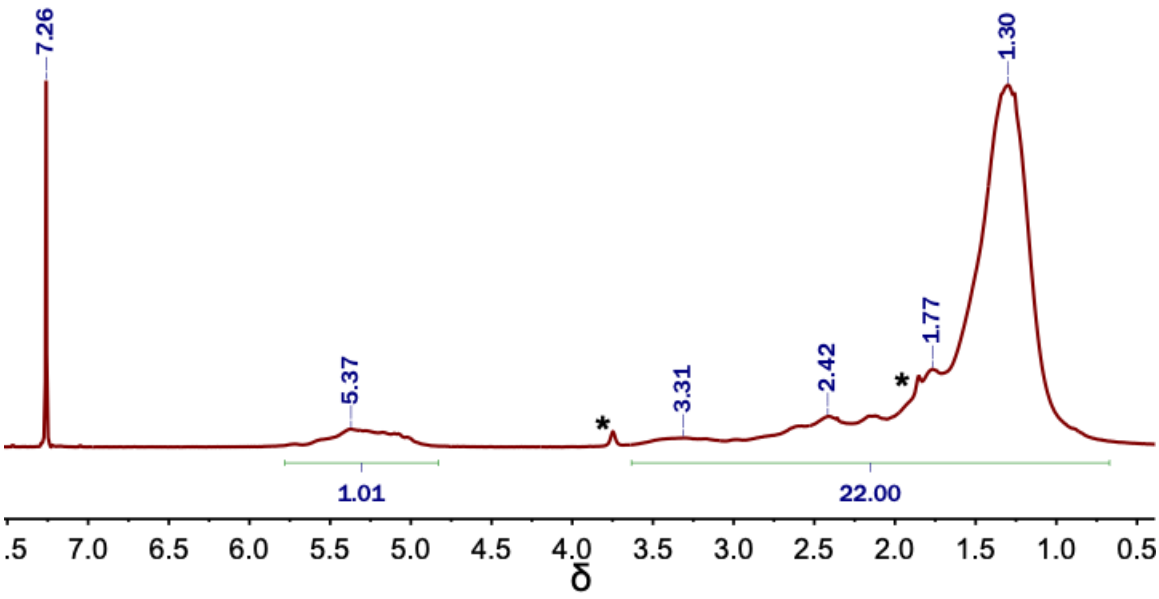

Figure 5.27: ^{1}H NMR spectrum of poly(1,2-cyclotridecadiene) in $CDCl_3$. Residual Solvent (THF: δ = 3.74, 1.85) denoted by *.

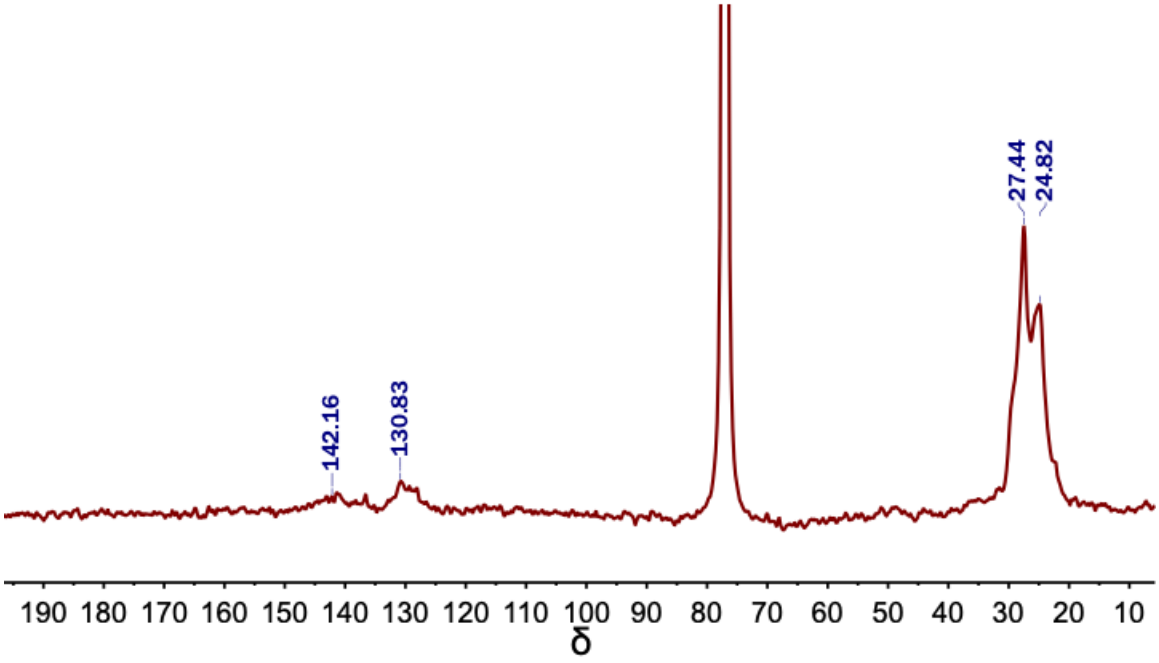

Figure 5.28: ^{13}C NMR spectrum of poly(1,2-cyclotridecadiene) in $CDCl_3$.

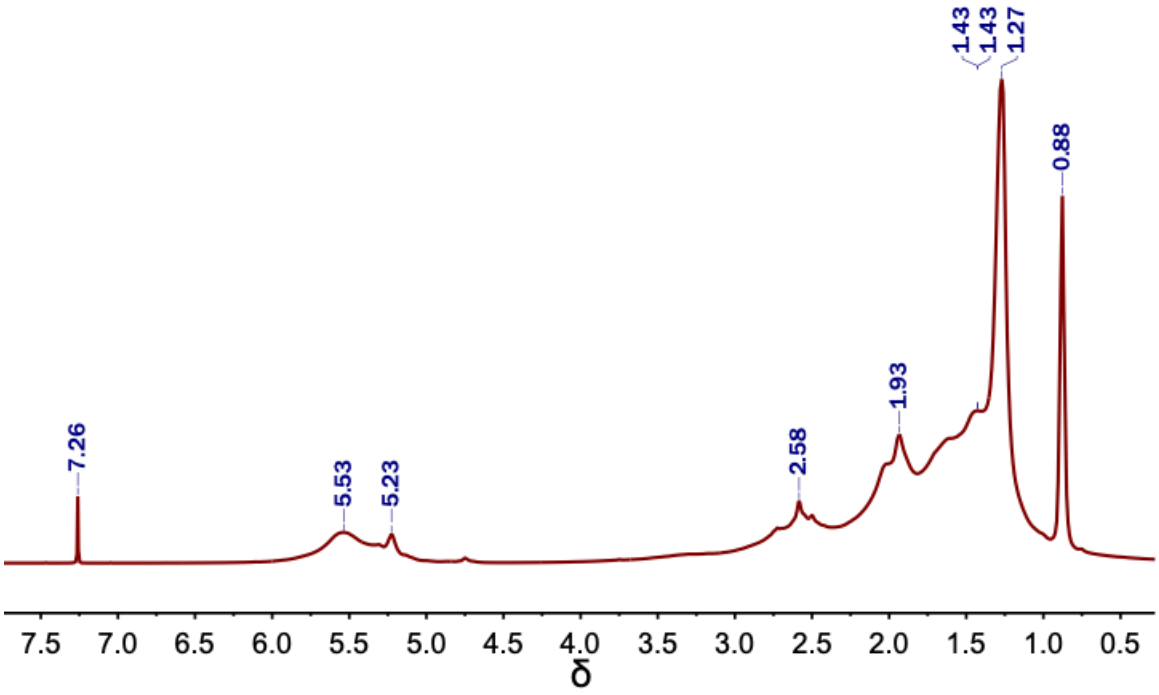

Figure 5.29: ^{1}H NMR spectrum of 70:30 (**5.1**:**5.7**) statistical copolymer in $CDCl_3$.

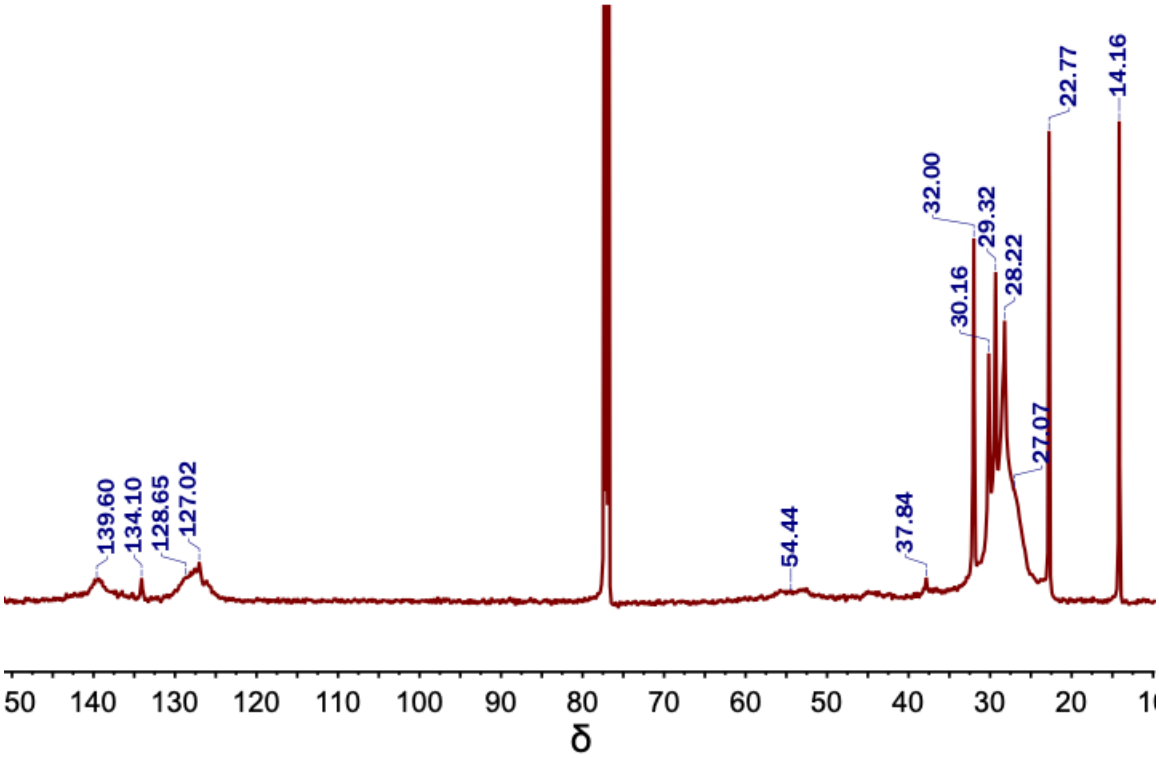

Figure 5.30: ^{13}C NMR spectrum of 70:30 (**5.1**:**5.7**) statistical copolymer in $CDCl_3$.

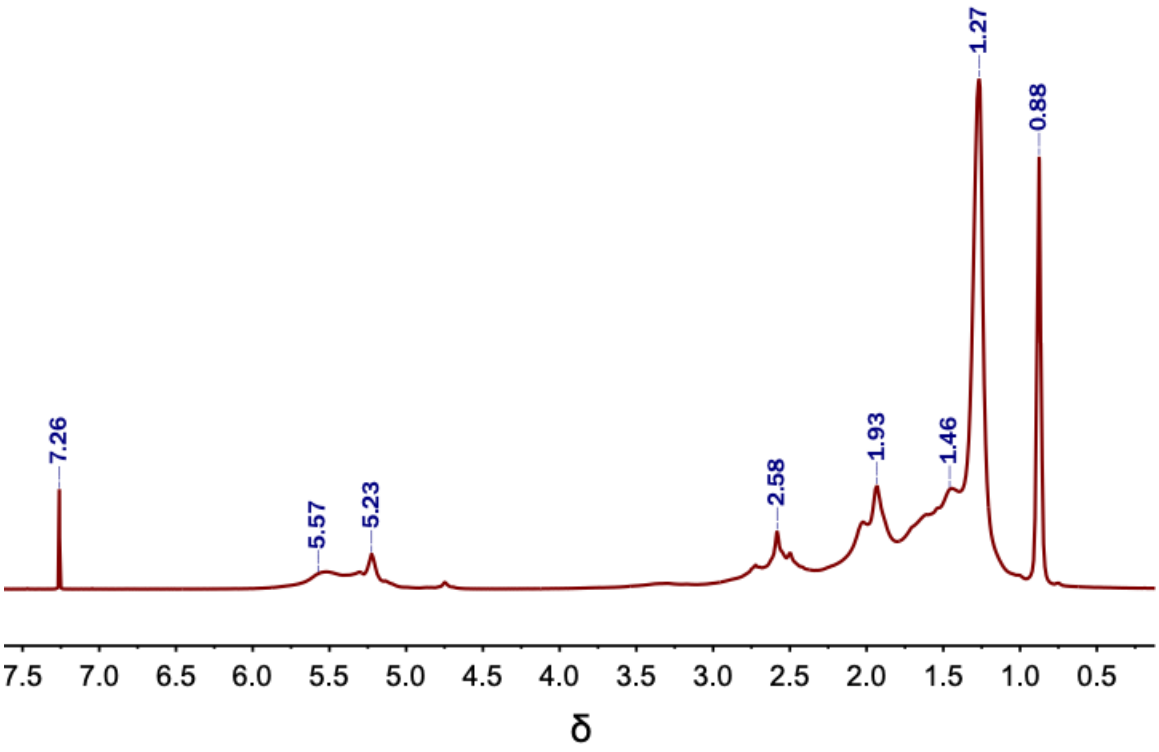

Figure 5.31: ^{1}H NMR spectrum of 50:50 (**5.1**:**5.7**) statistical copolymer in $CDCl_3$.

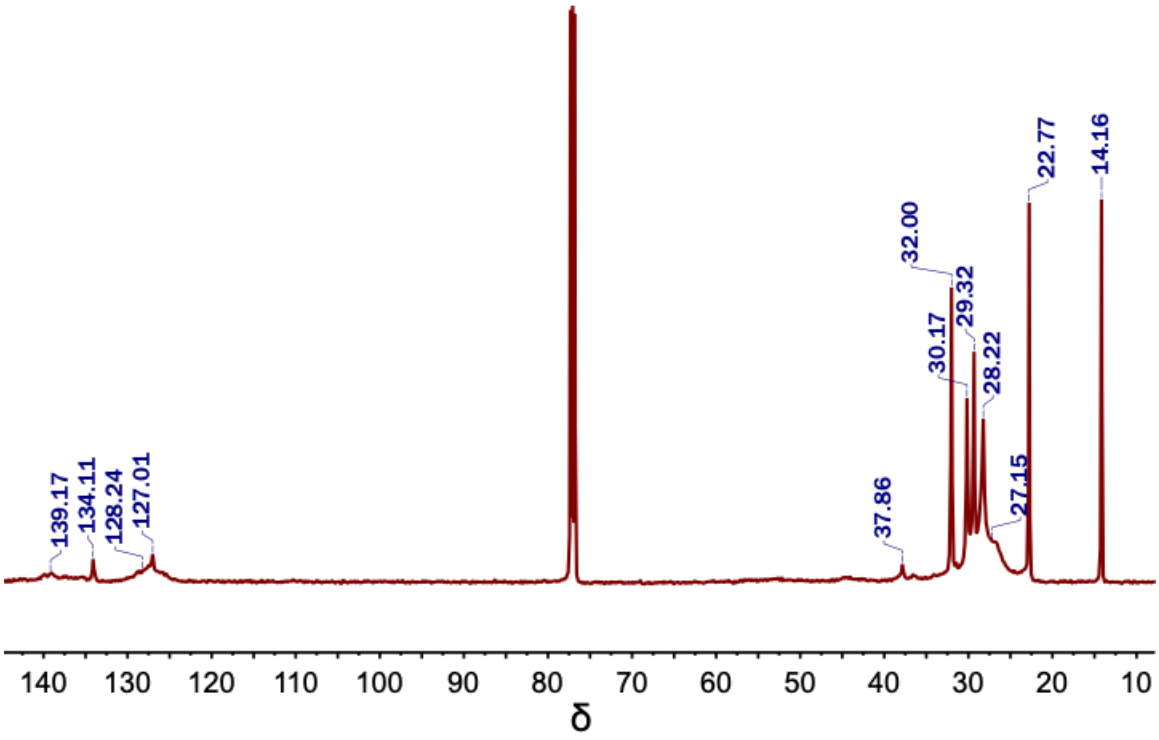

Figure 5.32: ^{13}C NMR spectrum of 50:50 (**5.1**:**5.7**) statistical copolymer in $CDCl_3$.

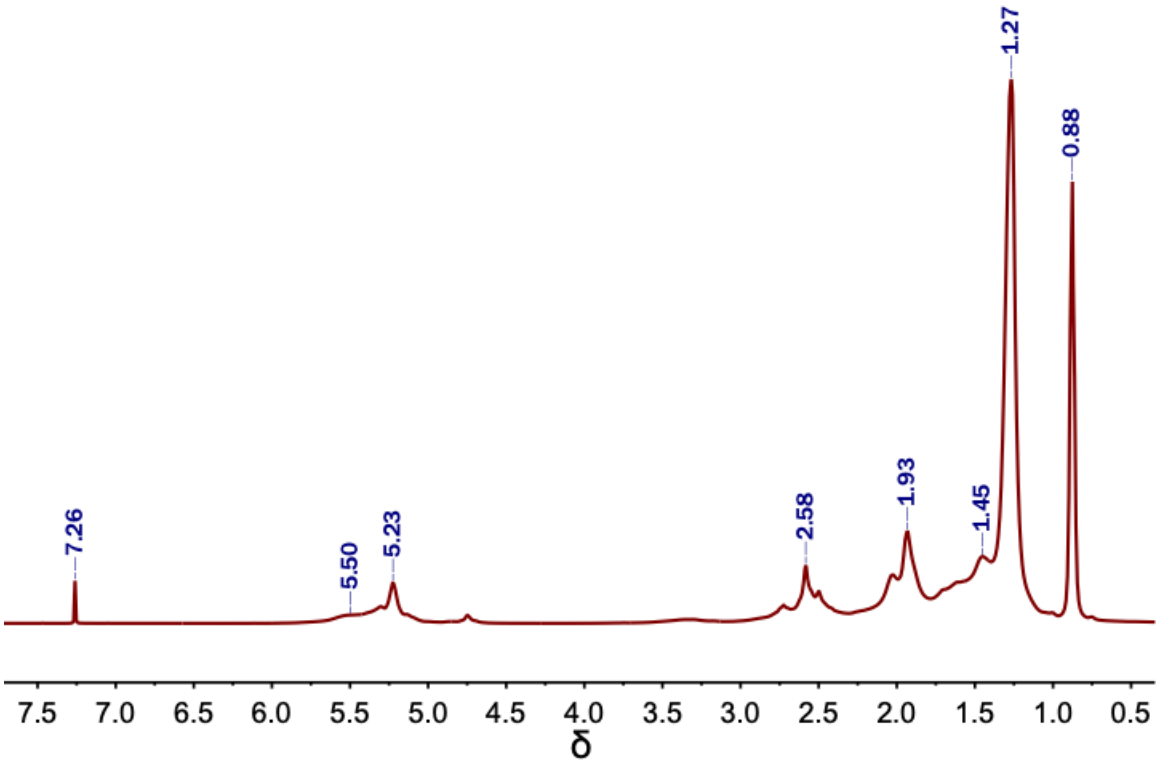

Figure 5.33: ^{1}H NMR spectrum of 30:70 (**5.1**:**5.7**) statistical copolymer in $CDCl_3$.

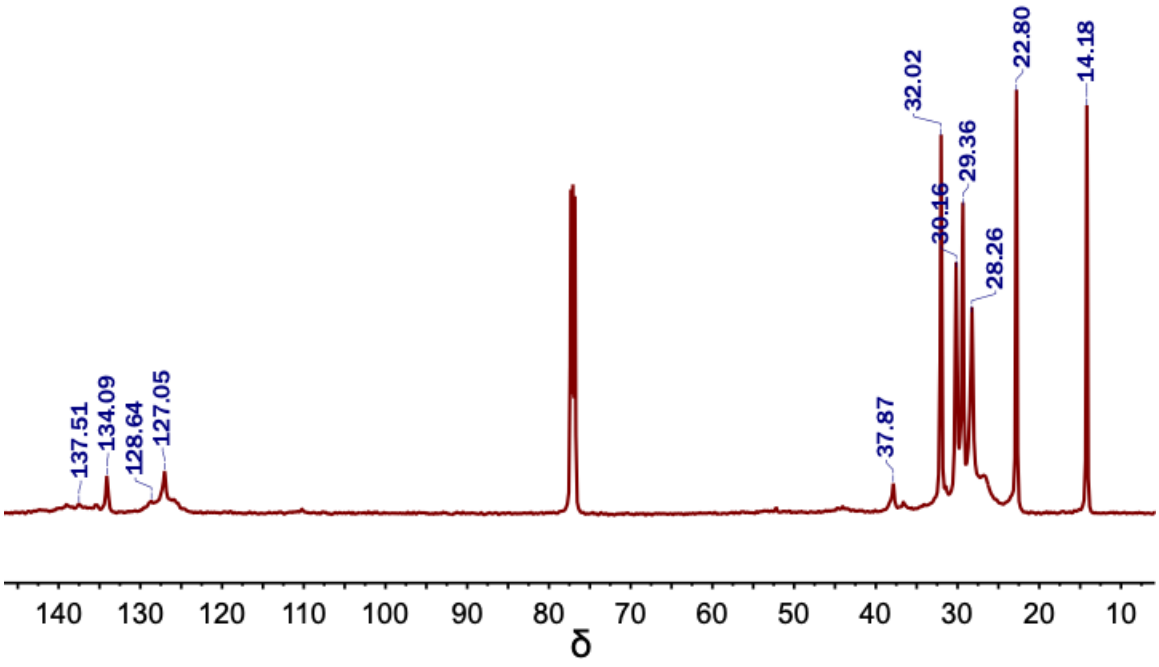

Figure 5.34: ^{13}C NMR spectrum of 30:70 (**5.1**:**5.7**) statistical copolymer in $CDCl_3$.

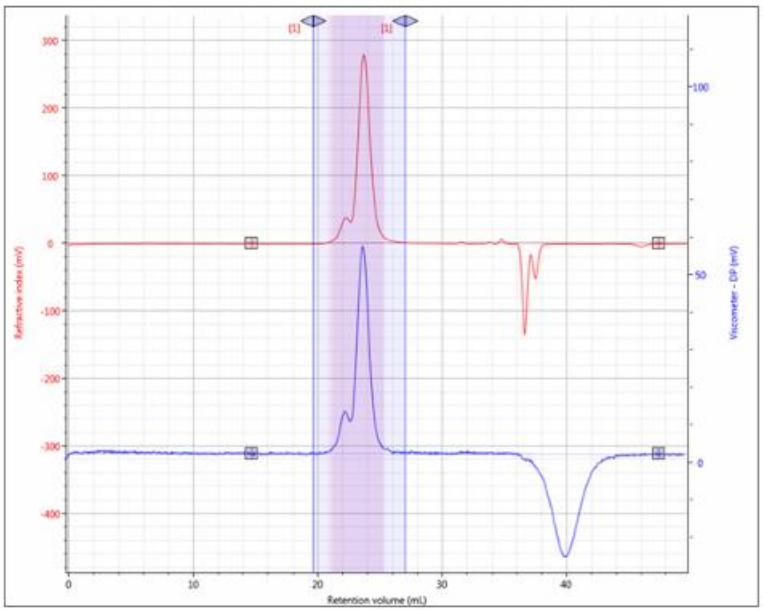

RV (mL)	23.73
Mn (g/mol)	73,840
Mw (g/mol)	85,440
Mz (g/mol)	107,100
Mw/Mn	1.157
IVw (dL/g)	0.2392
Rh(η)w (nm)	6.768
Rgw (nm)	N/C
M-H a	0.6672
M-H log K (dL/g)	-3.892
RI peak (mV·mL)	366.7
RALS peak (mV·mL)	66.25
LALS peak (mV·mL)	50.91
DP peak (mV·mL)	75.9
MALS peak (mV·mL)	N/C
Calc. dn/dc	0.1105
Recovery (%)	N/C

Figure 5.35: GPC trace of the polymerization of **5.1** with **5.3** in $CHCl_3$ (1 h).

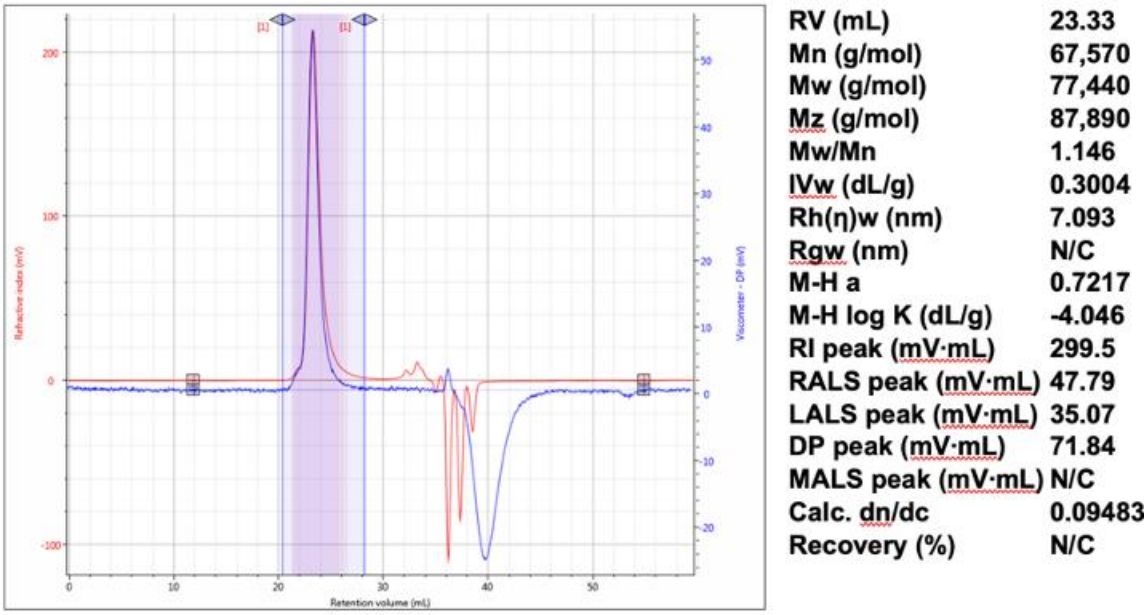

Figure 5.36: GPC trace of the polymerization of **5.7** with **5.3** (2 h).

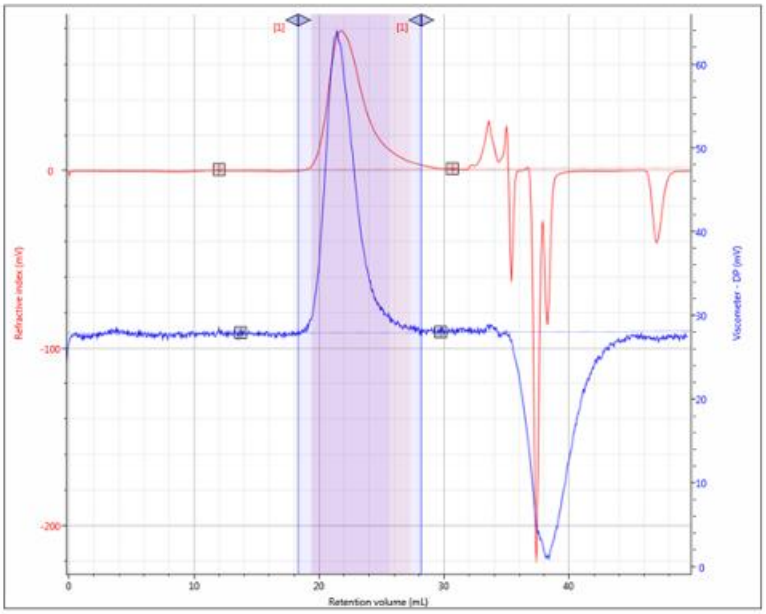

RV (mL)	21.79
Mn (g/mol)	128,200
Mw (g/mol)	211,000
Mz (g/mol)	369,200
Mw/Mn	1.646
IVw (dL/g)	0.4547
Rh(η)w (nm)	11.01
Rgw (nm)	6.66
M-H a	0.5896
M-H log K (dL/g)	-3.452
RI peak (mV·mL)	263.3
RALS peak (mV·mL)	118.3
LALS peak (mV·mL)	93.04
DP peak (mV·mL)	99.63
MALS peak (mV·mL)	N/C
Calc. dn/dc	0.1126
Recovery (%)	N/C

Figure 5.37: GPC trace of the polymerization of **5.1** with **5.4** (1 h).

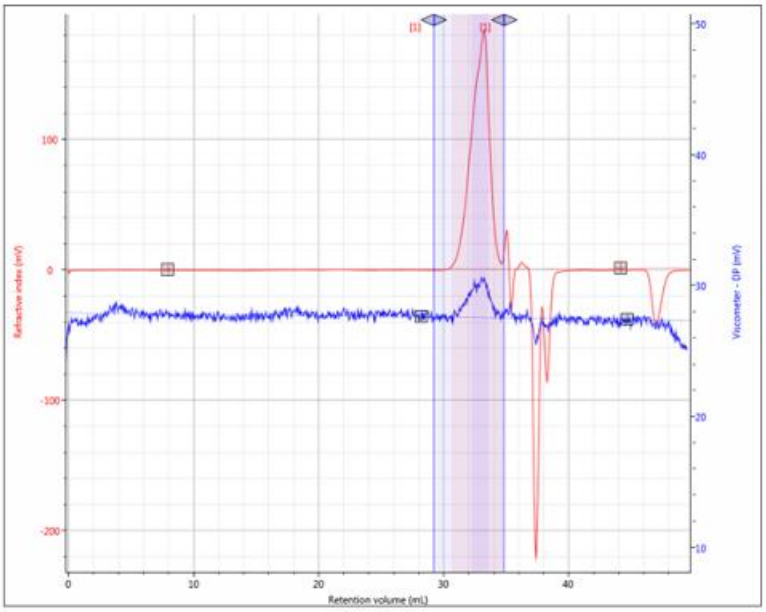

RV (mL)	33.25
Mn (g/mol)	33,650
Mw (g/mol)	45,040
Mz (g/mol)	187,600
Mw/Mn	1.338
IVw (dL/g)	0.02087
Rh(η)w (nm)	2.189
Rgw (nm)	N/C
M-H a	0.6906
M-H log K (dL/g)	-4.805
RI peak (mV·mL)	305.8
RALS peak (mV·mL)	29.97
LALS peak (mV·mL)	23.29
DP peak (mV·mL)	5.596
MALS peak (mV·mL)	N/C
Calc. dn/dc	0.109
Recovery (%)	N/C

Figure 5.38: GPC trace of the polymerization of **5.1** with activated **5.5** (24 h).

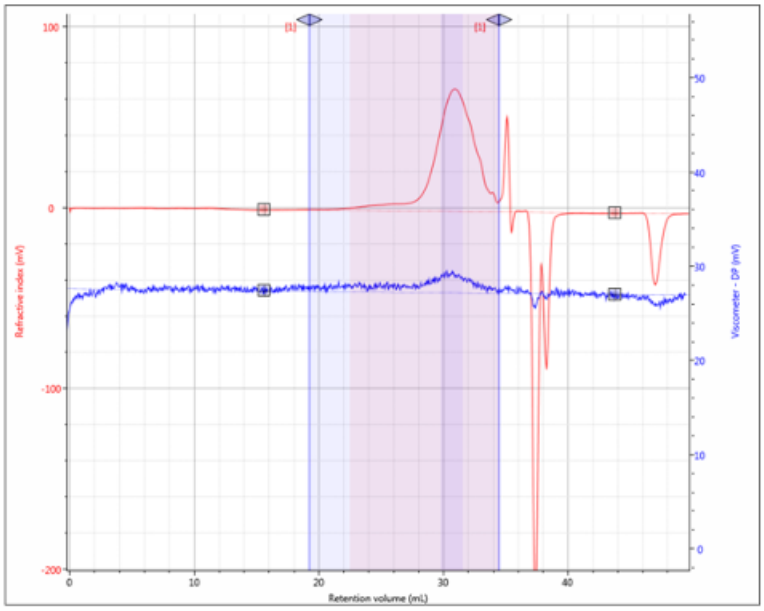

RV (mL)	30.94
Mn (g/mol)	6,691
Mw (g/mol)	12,040
Mz (g/mol)	29,520
Mw/Mn	1.799
IVw (dL/g)	0.09599
Rh(η)w (nm)	2.394
Rgw (nm)	N/C
M-H a	0.6738
M-H log K (dL/g)	-4.055
RI peak (mV·mL)	253.9
RALS peak (mV·mL)	5.593
LALS peak (mV·mL)	5.207
DP peak (mV·mL)	10.23
MALS peak (mV·mL)	N/C
Calc. dn/dc	0.1086
Recovery (%)	N/C

Figure 5.39: GPC trace of the polymerization of **5.1** with activated **5.6** (1 h).

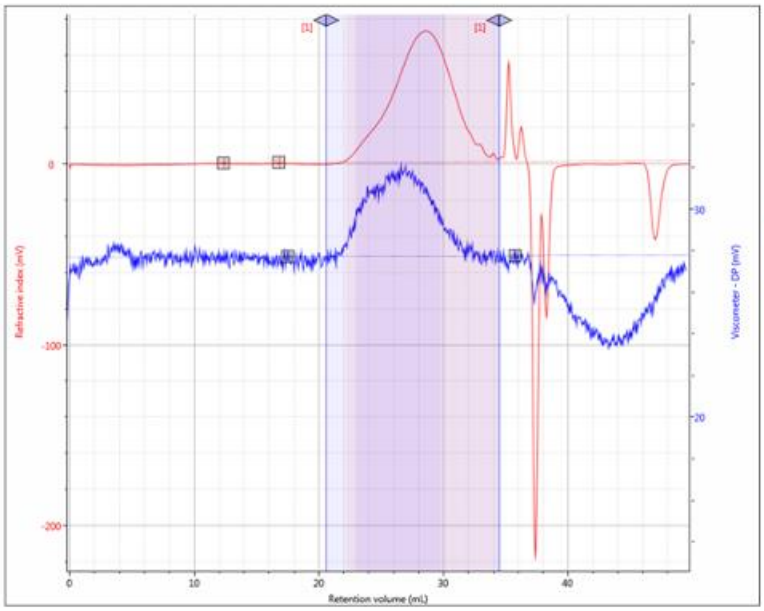

RV (mL)	28.63
Mn (g/mol)	8,071
Mw (g/mol)	22,040
Mz (g/mol)	50,520
Mw/Mn	2.731
IVw (dL/g)	0.08297
Rh(η)w (nm)	2.819
Rgw (nm)	N/C
M-H a	0.7349
M-H log K (dL/g)	-4.241
RI peak (mV·mL)	406.7
RALS peak (mV·mL)	23.41
LALS peak (mV·mL)	18.95
DP peak (mV·mL)	25.15
MALS peak (mV·mL)	N/C
Calc. dn/dc	0.1242
Recovery (%)	N/C

Figure 5.40: GPC trace of the polymerization of **5.1** with activated **5.3** (24 h).

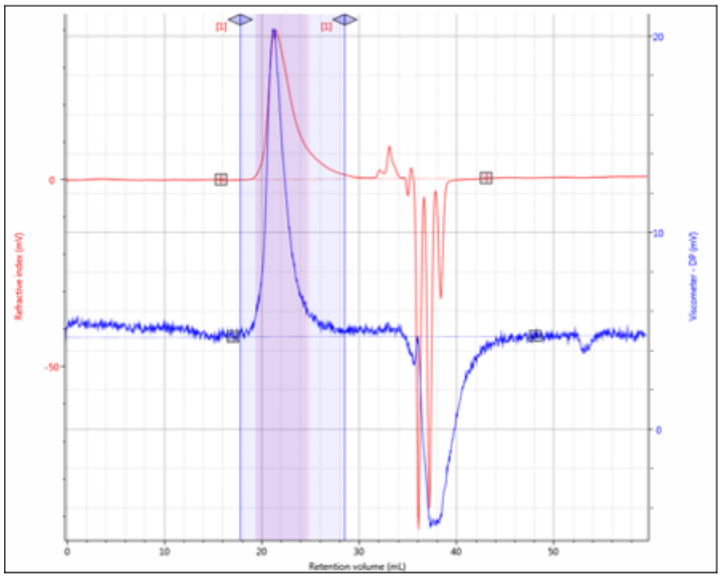

RV (mL)	21.43
Mn (g/mol)	99,270
Mw (g/mol)	174,100
Mz (g/mol)	257,500
Mw/Mn	1.754
IVw (dL/g)	0.4834
Rh(η)w (nm)	10.6
Rgw (nm)	8.074
M-H a	0.4886
M-H log K (dL/g)	-2.861
RI peak (mV·mL)	122.1
RALS peak (mV·mL)	52.59
LALS peak (mV·mL)	39.58
DP peak (mV·mL)	38.47
MALS peak (mV·mL)	N/C
Calc. dn/dc	0.1163
Recovery (%)	N/C

Figure 5.41: Raw GPC data for 70:30 (**5.1**:**5.7**) statistical copolymer

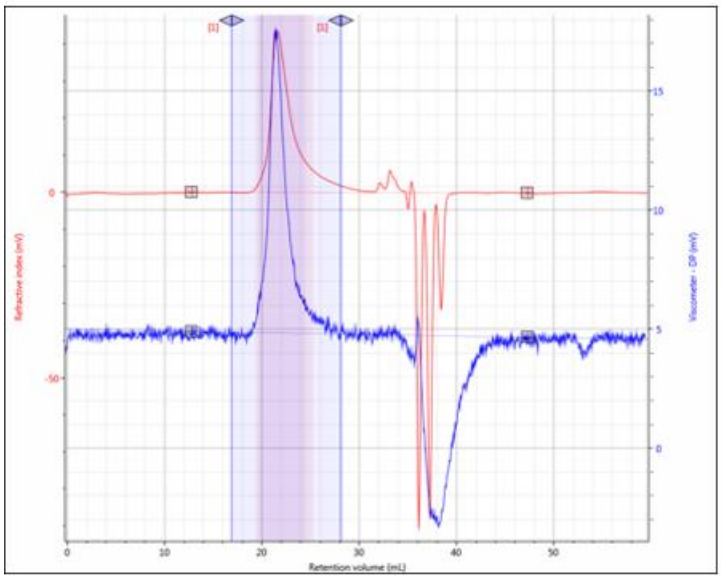

RV (mL) 21.63
Mn (g/mol) 98,360
Mw (g/mol) 181,800
Mz (g/mol) 297,500
Mw/Mn 1.849
IVw (dL/g) 0.4433
Rh(η)w (nm) 10.39
Rgw (nm) 9.095
M-H a 0.4434
M-H log K (dL/g) -2.667
RI peak (mV·mL) 116.9
RALS peak (mV·mL) 62.29
LALS peak (mV·mL) 47.05
DP peak (mV·mL) 27.8
MALS peak (mV·mL) N/C
Calc. dn/dc 0.137
Recovery (%) N/C

Figure 5.42: Raw GPC data for 50:50 (**5.1**:**5.7**) statistical copolymer.

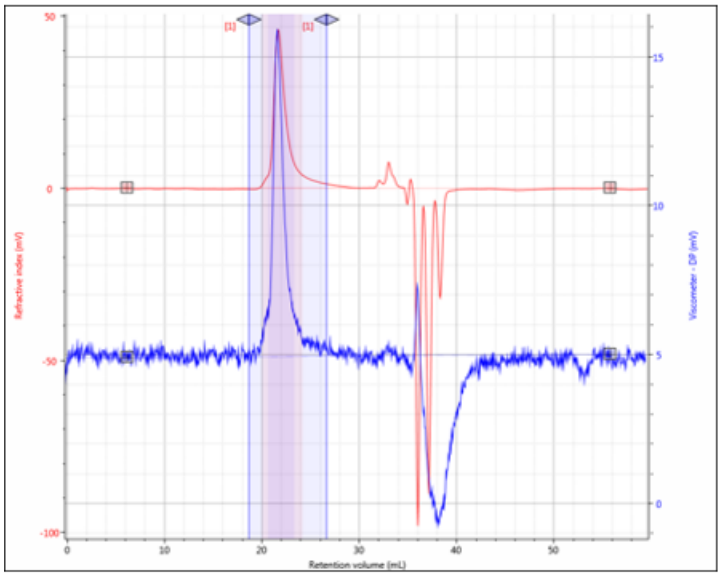

RV (mL) 21.71
Mn (g/mol) 129,100
Mw (g/mol) 178,400
Mz (g/mol) 237,100
Mw/Mn 1.382
IVw (dL/g) 0.4881
Rh(η)w (nm) 10.84
Rgw (nm) N/C
M-H a 0.9802
M-H log K (dL/g) -5.498
RI peak (mV·mL) 73
RALS peak (mV·mL) 45.56
LALS peak (mV·mL) 33.84
DP peak (mV·mL) 16.76
MALS peak (mV·mL) N/C
Calc. dn/dc 0.1613
Recovery (%) N/C

Figure 5.43: Raw GPC data for 30:70 (**5.1**:**5.7**) statistical copolymer.

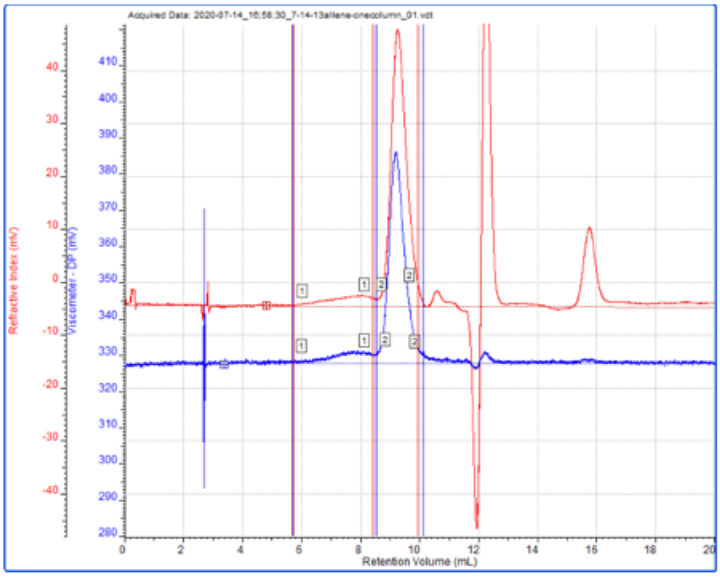

RV (mL) 9.217
Mn (Daltons) 47,289
Mw (Daltons) 94,522
Mz (Daltons) 1.141e6
Mw/Mn 1.999
IVw (dL/g) 0.0510
Rh(η)w (nm) 3.711
Rgw (nm) N/C
M-H a 0.260
M-H log K (dL/g) -2.508
RI peak (mV·mL) 32.12
RALS peak (mV·mL) 4.68
LALS peak (mV·mL) 1.76
DP peak (mV·mL) 36.81
MALS peak (mV·mL) N/C
Calc. dn/dc 0.0194
Recovery (%) N/C

Figure 5.44: High temperature GPC trace of poly(1,2-cyclotridecadiene).

CHAPTER VI: EXPLORING THE INFLUENCE OF RIGID CARBOCYCLES ON TERPENOID COPOLYMER PROPERTIES

A version of this chapter was originally published by Nicholas J. Galan, Alan D. Fried, Chase E. Cromer, Abigail Fish, Dominic R. Coughlin, and Johnathan N. Brantley:

Galan, N. J., Fried, A.D., Cromer, C. E., Fish, A., Coughlin, D. R., Brantley, J. N. *, Exploring the Influence of Rigid Carbocycles on Terpenoid Copolymer Properties. *J. Polym. Sci.* **2023**, 1-7.

In this article, I aided in designing and synthesizing polymers studied. I also performed most of the polymer characterization, kinetics, and glass transition temperature studies. Dr. Alan Fried also synthesized monomers, polymers, and performed tensile testing in this study. Chase Cromer helped with monomer synthesis and kinetics studies. Dr. Johnathan Brantley organized this project and facilitated the writing of the manuscript.

6.1 Abstract

Synthesizing soft polymers with uncommon architectural elements is critical for enhancing our understanding of fundamental structure-property relationships in macromolecules. Terpenoid materials are interesting candidates for addressing this grand challenge, as their constituent monomers can exhibit a diverse array of structural and functional groups. Moreover, these biologically-derived materials can potentially expand the sphere of knowledge surrounding trends in related petrochemically-derived polymers. For example, vinyl-addition copolymers of norbornene and acyclic olefins can exhibit predictable properties (e.g., linear changes in T_g as a function of composition). Due to synthetic limitations, however, it is not well understood if other rigid carbocycles engender similar

behavior in a range of copolymers. As numerous terpene scaffolds display rigid motifs (such as pinane systems), terpenoid polymers are uniquely positioned to address this deficiency. Here, we report the synthesis and characterization of terpenoid copolymers (both statistical and block) with systematically tailored compositions of pinene-based comonomers. We found that the pinane core (which is a constitutional isomer of norbornene) appears to promote ideal behavior with regard to bulk thermal properties of statistical copolymers, which mirrors the behavior of norbornene-based systems. We also found that block copolymers exhibited thermomechanical properties that were highly tunable (and apparently correlated to carbocycle composition).

6.2 Introduction

The rational design of polymers with bespoke properties and architectures is an enduring challenge in the polymer community. Indeed, efforts to predict bulk material properties from compositional information are often bedeviled by the subtleties of structure-property relationships (especially given that ideal behavior is relatively uncommon).[218] However, polymer architectures comprised of both rigid carbocycles and acyclic motifs seem to be an exception to this problem. These so-called cyclic olefin copolymers (COCs, Scheme 6.1) have emerged as popular engineering plastics due to their desirable properties (e.g., high T_g, optical clarity, good processibility, etc.).[63,66,210,219,220] Importantly, their bulk physical properties (e.g., T_g and Young's modulus) apparently correlate with cyclic monomer content in a linear/additive manner, consistent with the Fox relation.[65–67] However, a more complete understanding of how carbocycles influence

Scheme 6.1: Selected Examples of Polymers Containing Rigid Carbocycles

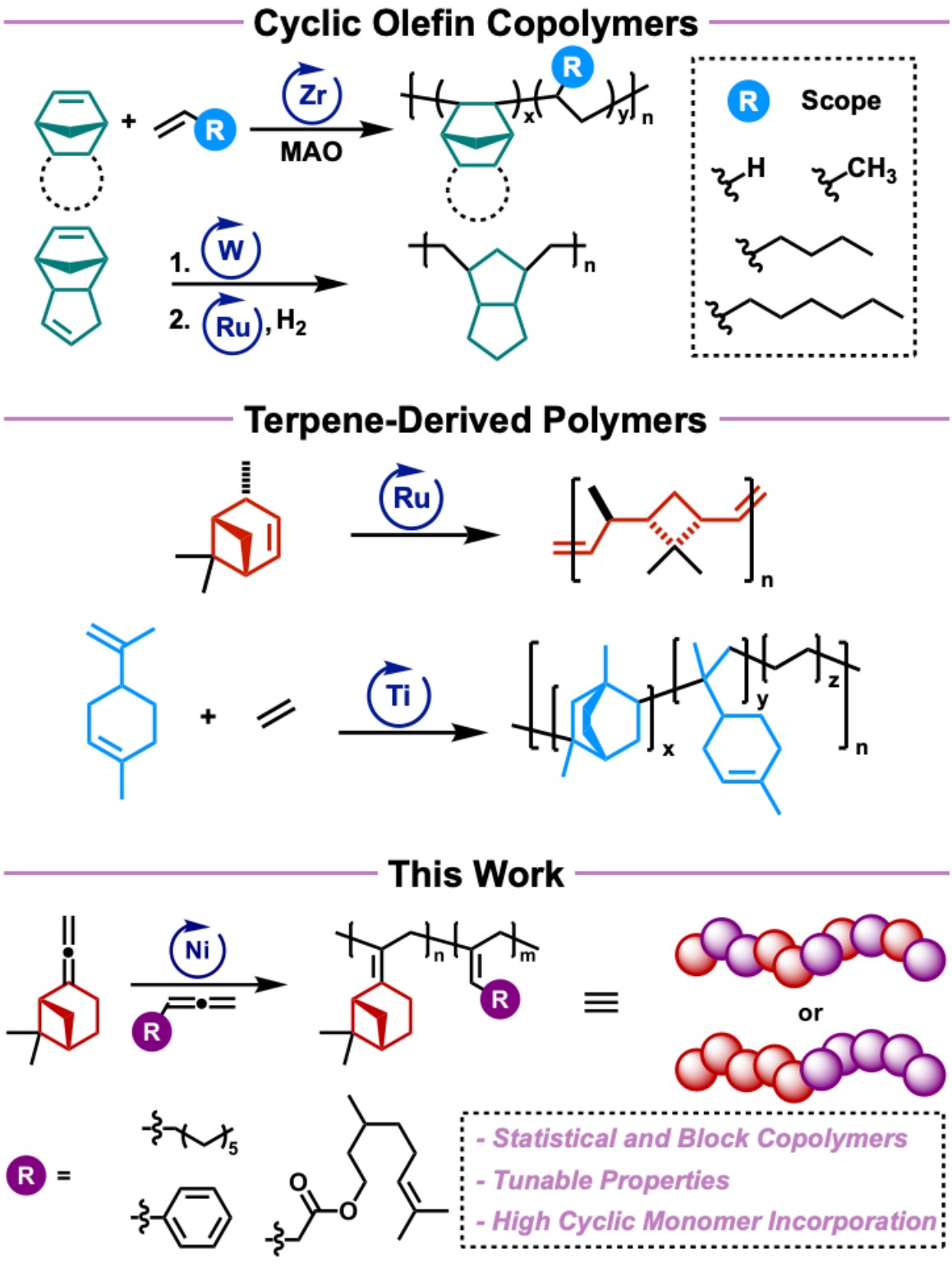

copolymer properties remains somewhat elusive. This is largely due to the fact that synthetic requirements severely limit the scope of cyclic motifs that can be reliably incorporated within polymers. For example, off-cycle reactions in vinyl-addition polymerizations (such as facile β-hydride elimination) often preclude the use of monomers other than norbornene.[71] Ring-opening metathesis polymerization (ROMP) intrinsically requires highly strained monomers,[70] and radical/cationic polymerizations often suffer from undesired chain-terminations or rearrangements.[68,69] As such, exploring new pathways to access materials comprised of rigid carbocyclic repeating units is vital for further elucidating how these structural elements influence bulk polymer properties

Terpenoids are attractive building blocks for addressing this challenge, given their wide availability and dazzling array of functionalized ring motifs.[221] Indeed, recent reports have showcased a range of COC-like materials that incorporate terpenoids (Scheme 1). For example, Nomura detailed the Ti-catalyzed copolymerization of limonene with ethylene (albeit with relatively low terpene incorporation).[85] Kennemur and coworkers reported the selective ROMP of δ–pinene in the presence of low quantities of α–pinene.[86] Furthermore, Howdle and colleagues recently disclosed the syntheses of terpenoid triblock copolymers from reversible-addition fragmentation chain-transfer (RAFT) polymerizations of functionalized pinene and tetrahydrogeraniol building blocks.[87,88] Despite these promising precedents, there have been relatively few studies that expand the scope of analogous terpenoid polymers. Given the abundance of complex multicyclic architectures inherent to the terpene family (e.g., pinene, camphene, sabinene, carnene, etc.), we surmised that

terpene-derived polymers would be ideal candidates for enhancing our understanding of how multicyclic systems impact copolymer properties.

Our group recently reported that pinane motifs can be readily incorporated into polymers through the living vinyl-addition polymerization of β-pinadiene (**6.1**).[44] As pinane is a constitutional isomer of norbornane, copolymers of **6.1** could potentially reveal how subtle changes to carbocycle constitution impact bulk material properties. Furthermore, the (π-allyl) Ni catalyst used in the polymerization of allenes circumvents many of the challenges associated with the synthesis of traditional COCs (e.g., it is compatible with carbocyclic[43,75,222] and acyclic allenes decorated with an array of functional groups[45,46,199,201]). Thus, our terpenoid materials could potentially expand structure-property studies to include congeners of polar cyclic olefin copolymers (which are materials that are difficult to access).[223]

6.3 Results and Discussion

6.3.1 Copolymer Preparation (6.1 and 6.2) and T_g Investigation

In direct analogy to conventional COCs, we initially explored copolymers comprised of both high and low T_g components. As homopolymers of **6.1** were found to afford high T_g (> 150 ºC) materials,[44] we targeted comonomers that would yield softer copolymer segments. For example, 1,2-nondadine (**6.2**) undergoes living vinyl-addition polymerization to afford a low T_g (-70 °C) material.[43,222] As such, **2** was selected as the comonomer for our preliminary studies. To facilitate our analyses, we first polymerized **6.1**[224] and **6.2** under previously reported conditions[43] to yield homopolymers **6.3** (Table

6.1, entry 1) and **6.4** (Table 6.1, entry 2), respectively. We then targeted a statistical copolymer, **[6.1-co-6.2]$_C$** (where the subscript denotes the experimentally determined percent of repeating units derived from **6.1**), from an equimolar mixture of **6.1** and **6.2**. In a nitrogen filled glovebox, **6.1** (171 mg) and **6.2** (143 mg) were added to a vial containing toluene (PhMe; 6 mL). In a separate vessel, allyl trifluoroacetate (4.7 μL) was added to a PhMe solution of Ni(cod)$_2$ (10 mg; 0.03 M) to generate the active (π-allyl) Ni catalyst. An aliquot of this catalyst solution was then added via syringe to the vial containing **6.1** and **6.2**. The polymerization was stirred at 23 °C, and quantitative consumption of **6.1** and **6.2** was observed after 6 h (as determined by ^{1}H NMR spectroscopy). The reaction was quenched by exposure to air, concentrated to a minimal volume, and subsequently added to stirring MeOH to precipitate any polymeric material. Filtration afforded **[6.1-co-6.2]$_{56}$** as an off-white solid (68%). The isolated polymer was analyzed by ^{1}H NMR spectroscopy, which was consistent with incorporation of repeating units from both **6.1** and **6.2**. The relative incorporation of both monomers could be determined via integration of one of the methyl resonances from **6.1** (δ = 0.74 ppm) relative to the new vinyl (δ = 5.08 ppm) or methyl (δ = 0.87ppm) proton resonances from incorporation of **6.2**. To our delight, the measured composition of **[6.1-co-6.2]$_{56}$** was in close agreement with the targeted **6.1**:**6.2** ratios (*c.f.* 56:44 versus 50:50, respectively; Table 6.1). Furthermore, analysis of **[6.1-co-6.2]$_{56}$** by size-exclusion chromatography (SEC) revealed a number average molecular weight (M_n) in good agreement with the theoretical value (*c.f.* 44 kDa versus 50 kDa, respectively). Analogous protocols were used to synthesize the remaining **[6.1-co-6.2]$_C$** materials and determine their relative compositions (Table 6.1).[225] With the target polymers

Table 6.1: Statistical Copolymerizations of **6.1** and **6.2**

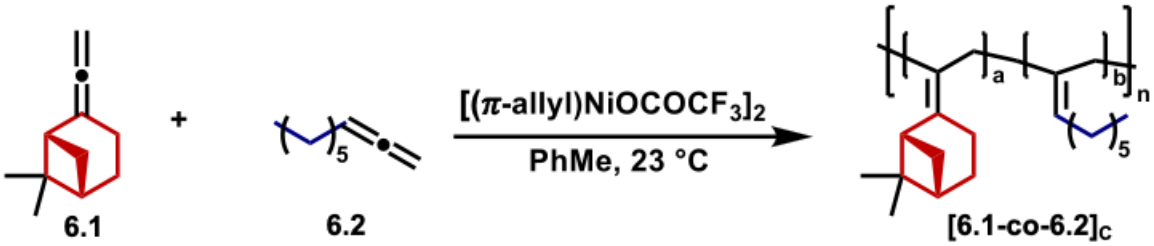

Entry	**6.1**[a] (%)	**6.1**$_{exp}$[b] (%)	M_n (Da)[c]	Đ[d]	Yield (%)	T_g (°C)
1	100	100	44,800	1.33	87.4	187.0
2	0	0	58,900	1.36	67.8	-69.5
3	25	30	49,980	1.30	45.6	-7.5
4	50	56	44,340	1.17	68.2	83.6
5	75	77	102,600	1.38	85.9	172.5

[a]Determined from monomer feed ratios. [b]Determined using ^{1}H NMR spectroscopy. [c]Measured by SEC (triple detection) and rounded. [d]Calculated using M_w/M_n.

in hand, we turned our attention to evaluating some of their intrinsic thermomechanical properties. Previous examples of COCs have shown linear changes in T_g as a function of cyclic repeating unit content (albeit with modest cycloolefin content); thus, we hypothesized that our COC congeners would exhibit analogous behavior.[210] Samples of **6.3**, **6.4**, and **[6.1-co-6.2]$_C$** were analyzed via differential scanning calorimetry (DSC)[226] with a heating rate of 10 °C per minute (Table 6.1). T_g values for each polymer were then plotted against the experimentally determined percent incorporation of **6.1** in each case. Consistent with our hypothesis, we observed a near linear correlation (R^2 = 0.96; Figure 6.65) between the measured T_g and **6.1** content across all compositions (Figure 6.1). To better understand the inherent relationships between copolymer T_g, comonomer identity, and intermolecular interactions, we analyzed our experimentally determined T_g values using established mathematical models. For example, the experimental T_g values were compared to the predicted values obtained from the Fox equation[227] (Equation 2; Table 6.4):

$$\frac{1}{T_g} = \frac{w_1}{T_{g1}} + \frac{w_2}{T_{g2}} \qquad (2)$$

Where T_g represents the predicted glass transition of the copolymer, T_{g1} and T_{g2} represent the measured T_g values of the corresponding homopolymers, and w_1 and w_2 represent the relative weight fractions of each monomer type in the copolymer. Our experimental values were found to deviate (± ~18%) from the values predicted using the Fox equation (Figure 6.1). This suggested to us that fitting the data using the linear form of the Gordon-Taylor equation (Equation 3; Table 6.5) might better elucidate subtle deviations from ideal behavior:

$$T_g - T_{gA} = C\left(T_{gB} - T_g\right)w_b/w_a \qquad (3)$$

Where T_g represents the predicted glass transition temperature of the copolymer, T_{gA} and T_{gB} represent the measured T_g of the homopolymers, and w_a and w_b represent the relative weight fractions of each monomer within the copolymer. The C value is considered to be an adjustable fitting parameter, and it is influenced by mixing interactions between the distinct repeating units in the copolymer.[228,229] We determined the C value for our statistical copolymers to be only slightly higher than unity (C = 1.08; Figure 6.1), but this provided a fit that more closely mirrored our experimental data than the Fox equation. This slight positive deviation from "ideal" (C = 1) Gordon-Taylor behavior is suggestive of a slight repulsive mixing of the two comonomer units (which we attribute to minor steric interference arising from the pinane motif).[228] Regardless, these results highlight that COC-like T_g trends can be recapitulated using bicyclic structures other than norbornene.

6.3.2 Copolymer Preparation (6.1 and 6.6) and T_g Investigation

Inspired by these results, we were curious if similar trends could be observed with other copolymer systems (especially those containing motifs that are difficult to access with current synthetic logic). For example, styrene is a comonomer that can be challenging to incorporate within COCs. To our knowledge, this has only been accomplished using highly reactive Sc based complexes with ethylene as a third comonomer.[230] As such, we decided to explore phenylallene (**6.6**) as a styrene surrogate in our materials. We first polymerized **6.1**and **6.6** under the previously reported conditions to yield homopolymers **6.3** (Table 6.2, entry 1) and **6.7** (Table 6.2, entry 2), respectively. We then prepared a series

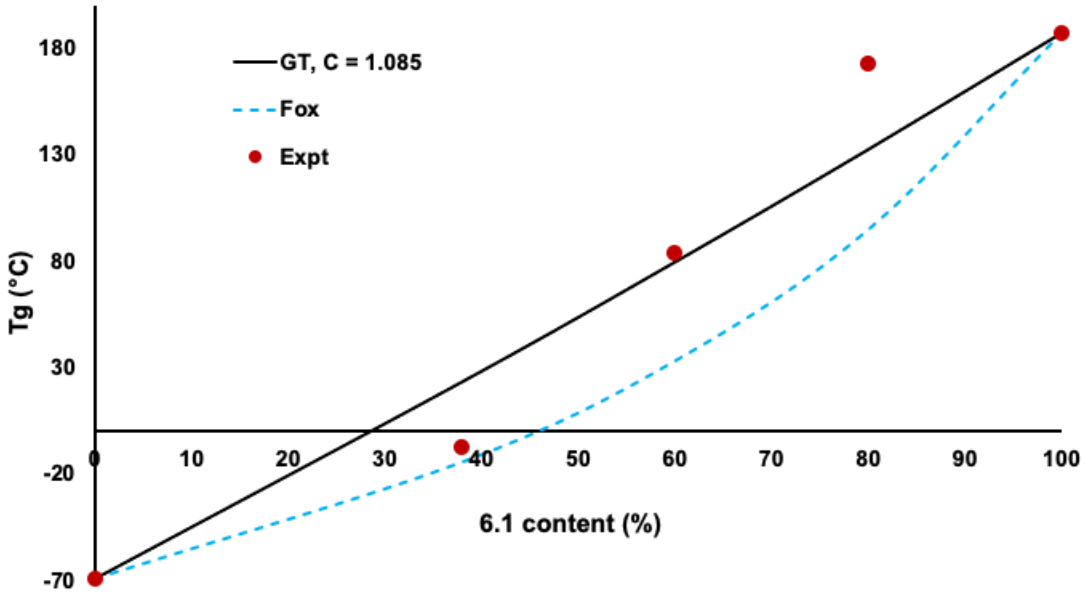

Figure 6.1: T_g correlations as a function of bicyclic content in COC-like copolymers. For comparison, the experimental (Red Circles) and theoretical T_g values predicted by the Fox (Blue Curve) and Gordon-Taylor (Black Curve) equations for **[6.1-co-6.2]**$_C$ are shown.

Table 6.2: Statistical Copolymerizations of **6.1** and **6.6**

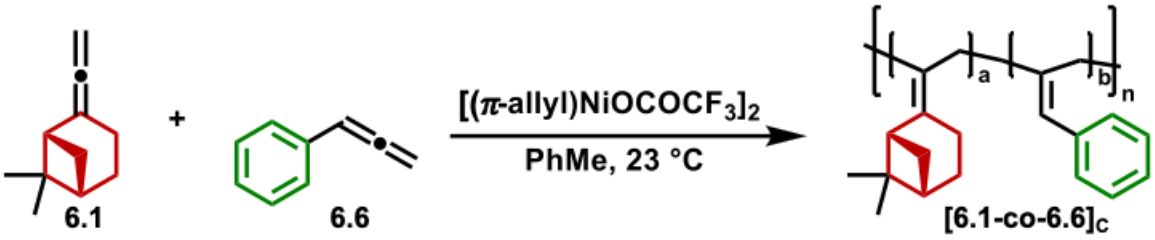

Entry	**6.1**$_{theo}$[a] (%)	**6.1**$_{calc}$[b] (%)	M_n^{expt} (Da)[c]	Đ[d]	Yield (%)	T_g (°C)
1	100	100	44,800	1.33	87.4	187.0
2	0	0	37,400	1.20	67.7	99.1[e]
3	25	20	58,300	1.16	83.2	109.0
4	50	44.2	70,600	1.22	94.3	123.6
5	75	69.5	46,100	1.40	92.9	149.8

[a]Determined from monomer feed ratios. [b]Determined by ^{1}H NMR spectroscopy. [c]Measured by SEC (triple detection) and rounded. [d]Calculated using M_w/M_n. [e]Determined using $\tan(\delta)_{max}$ from powder DMA.

of statistical copolymers of **6.1** and **6.6** using a similar protocol to that described for **[6.1-co-6.2]$_C$**. Briefly, solutions of **6.1** and **6.6** were prepared in PhMe, and a freshly prepared (π-allyl) Ni catalyst solution was added via syringe. Quantitative consumption of both **6.1** and **6.6** was confirmed by ^{1}H NMR spectroscopy after reacting for 24 h at room temperature. The reaction mixtures were subsequently quenched and added to MeOH to precipitate any polymeric material. Filtration afforded **[6.1-co-6.6]$_C$** as an off-white solid in good yield (81–99%).[231] Varying ratios of **6.1** (25%, 50%, and 75%) were targeted, and the actual copolymer compositions were determined by integrating the methyl proton resonances from **6.1** (δ = 0.74 ppm) relative to the new vinyl resonance from polymerization of **6.6** (δ =6.23 ppm). For all materials, their measured compositions and M_n values were commensurate with the initial monomer feed ratios (Table 6.2). Powder samples of these polymers were subjected to the same DSC analyses as described for the **[6.1-co-6.2]$_C$** materials. When relative composition was plotted against measured T_g, we were pleased to again observe a near linear correlation (R^2 = 0.94; Figure 6.66). Interestingly, while these copolymers were found to exhibit T_g values in very good agreement with those predicted (Table 6.6) from the Fox equation (± ~5%), they exhibited a greater deviation (Table 6.7) from "ideal" Gordon-Taylor behavior (C = 0.44; Figure 6.2). This suggested a higher degree of repulsive mixing between the **[6.1-co-6.6]$_C$** co-units compared to the purely aliphatic system in **[6.1-co-6.2]$_C$**. We attribute this to potential arene interactions between the styrenyl motifs that, in concert with steric interference from the bulky pinane core, can perturb chain-packing through backbone rigidification. This should lead to less free volume, and, thus, the negative deviation from the predicted T_g

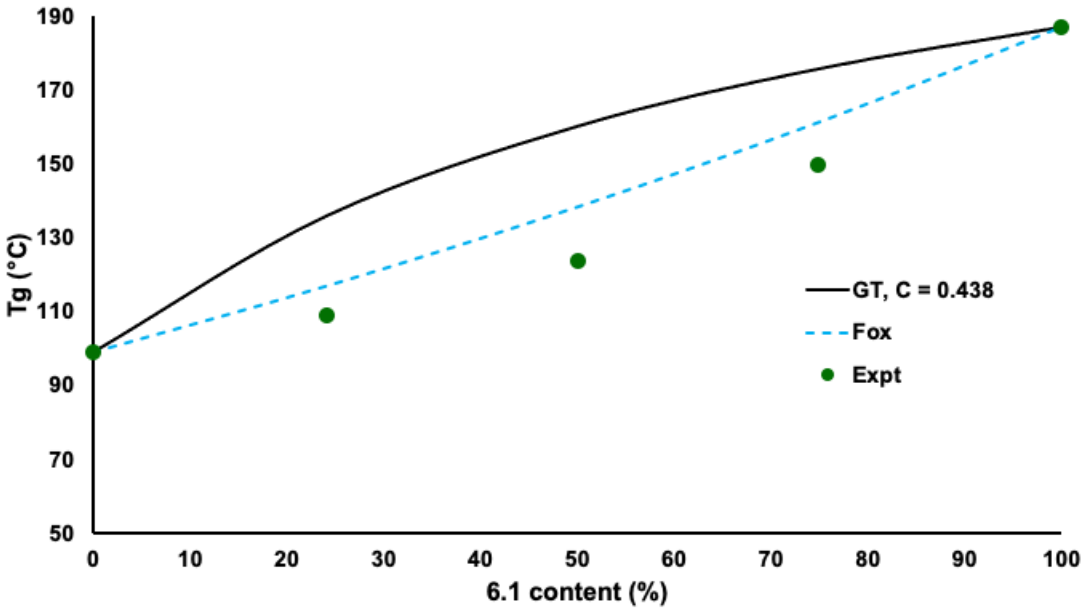

Figure 6.2: T_g correlations in materials comprised of mono- and bicyclic repeating units. For comparison, the experimental (Green Circles) and theoretical T_g values predicted by the Fox (Blue Curve) and Gordon-Taylor (Black Curve) equations for **[6.1-co-6.6]**$_C$ are shown.

values is expected.[229] The closer agreement with the Fox equation also suggests that noncovalent interactions (such as the putative arene interactions in this system) can act additively with steric exclusion. As such, this could represent an underexplored design space for new polymers with predictable physical properties.

6.3.3 Effects of a Polar Comonomer

As polar COCs are particularly challenging to synthesize, we also explored polar comonomers in our model platform. The citronellol-based allene, **6.9**, was selected as the comonomer of choice, given that this terpenoid would enable us to analyze trends in entirely biomass-derived materials. We first prepared a homopolymer of **6.9** (using an analogous protocol to the synthesis of **6.3** and **6.4**) to elucidate the T_g of this material. Briefly, an aliquot of the (π-allyl) Ni catalyst stock solution (0.026M) was added to a toluene solution of **6.9** and stirred for 4 h at 23 °C. The polymerization was quenched via sparging with air and concentrated to a minimal volume. Addition of this solution to MeOH between -40 ºC and -80 °C precipitated the homopolymer, **6.10**, as a tacky, pale-yellow material (82% yield). The resulting polymer was analyzed using SEC (M_n = 25 kDa) and DSC (which revealed a relatively low T_g = -49 °C; Figure 6.3). As we consistently observed highly linear correlations between T_g and pinane content in our models, we wondered if a simple linear fit using only two data points (i.e., the two homopolymer T_g values) would reasonably predict the T_g for a copolymer of arbitrary composition. To explore this concept, we prepared a single statistical copolymer from **6.1** and **6.9** using the protocol described above. The polymer, **[6.1-co-6.9]$_{65}$**, was isolated as a beige powder following precipitation from MeOH (86% yield),[232] and the relative composition of the material was in close

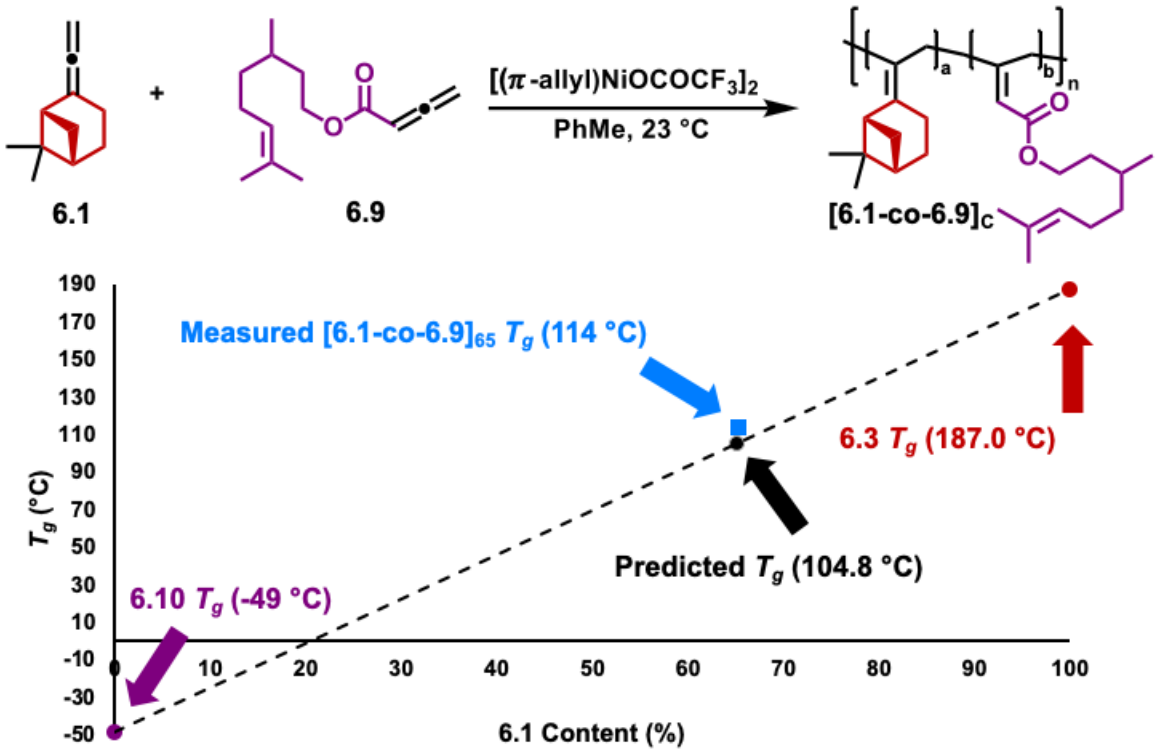

Figure 6.3: Predicting T_g in Polar COC-like Copolymers. (Top) Scheme depicting synthesis of **[6.1-co-6.9]$_{65}$**. (Bottom) A simple linear fit (Black Line) using homopolymer T_g values (Purple and Red Arrows) closely predicts (Black Arrow) the measured T_g of an arbitrary composition (Blue Arrow).

agreement with the **6.1**:**6.9** feed ratios (*c.f.* 65:35 versus 60:40, respectively).[233] We next created a linear fit between T_g and pinane composition using only the T_g values (Figure 6.20, Figure 6.23) from the endpoints of our copolymer sequence (i.e., **6.3** and **6.10**). Based on the calculated trendline, **[6.1-co-6.9]$_{65}$** was predicted to exhibit a T_g of 104.8 °C. To our delight, powder DMA analysis of **[6.1-co-6.9]$_{65}$** revealed a T_g of 114 °C, in close agreement with the predicted value (Figure 6.3). Although further studies are needed, this result suggests that frustrating chain packing through the incorporation of rigid carbocycles could have a stronger influence over bulk thermal properties than polarity mismatch/repeating unit mixing.

6.3.3 Block Copolymer (6.1 and 6.2) Synthesis and Tensile Testing

The living nature of the Ni catalyst used in our studies[43,234,235] also presented a unique opportunity to investigate innate trends in block copolymer analogues of COCs (which can be difficult to prepare using other strategies).[236] Initially, we explored a block copolymer from equimolar amounts of **6.1** and **6.2**. Briefly, a PhMe solution of **6.1** (111 mg; 0.10 M) was prepared in a glovebox. An aliquot of the (π-allyl) Ni catalyst stock solution (0.1 mL; prepared as described above) was added, and the polymerization was conducted at room temperature. Aliquots were periodically removed to monitor the reaction, and complete consumption of **6.1** was observed after 4 h. SEC analysis of the sample (M_n^{expt} = 30 kDa) closely matched the target value (M_n^{theo} = 36 kDa). A solution of **6.2** in PhMe (217 mg, 3.5 M) was subsequently added to the polymerization mixture and allowed to react for 16 h. The mixture was quenched via exposure to air, and the block copolymer, **[6.1-block-6.2]$_{34}$**, was isolated as a white solid following precipitation from

Table 6.3: Block Copolymerizations of **6.1** and **6.2**

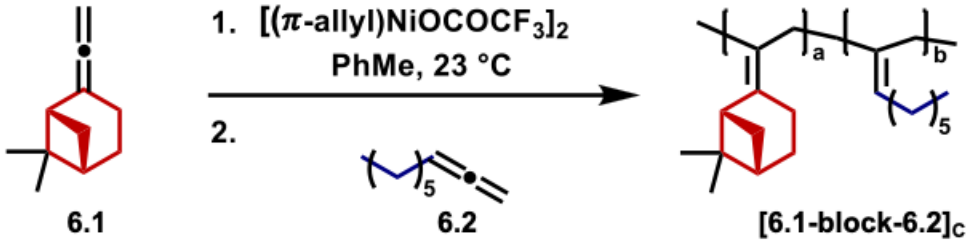

Entry	**6.1**$_{theo}$ (%)[a]	**6.1**$_{calc}$ (%)[b]	M_n^{expt} (Da)[c]	Đ[d]	Yield (%)	E (MPa)[e]	SAB (%)[e]
1	20	23.7	147,100	1.40	62.9	0.9	132.5
2	25	28.7	146,300	1.25	59.8	20.6	30.1
3	25	32.3	95,900	1.28	67.6	34.0	5.0
4	30	34.1	119,600	1.33	83.5	57.3	9.0

[a]Determined from monomer feed ratios. [b]Determined by ^{1}H NMR spectroscopy. [c]Measured by SEC (triple detection) and rounded. [d]Calculated using M_w/M_n. [e]Average of three experiments.

MeOH (84 % yield; Table 6.3). Successful chain extension was supported by SEC analysis, which revealed the M_n of the copolymer closely matched that of the expected value (*c.f.* M_n^{expt} = 119 kDa versus M_n^{theo} = 120 kDa; Table 6.3). Furthermore, ^{1}H NMR spectroscopy revealed the relative composition of the copolymer was ~34:66 (**6.1**:**6.2**), which was in good agreement with the targeted value. A series of **[6.1-block-6.2]$_C$** copolymers with varying composition were synthesized by altering the feed ratios of **6.1** and **6.2** (Table 6.3).

We hypothesized that discrete blocks of pinane units would frustrate chain packing to a larger degree than statistical incorporation (a result of enhanced rigidification due to increased steric interactions). This, in turn, could manifest through significant changes in bulk mechanical properties. To explore this concept, we further investigated our block copolymers under uniaxial strain. We were only able to prepare freestanding films from blocks with a modest **6.1** content (~20–35%), as films with higher relative incorporation of **6.1** (> 35%) were found to be extremely brittle (i.e., they cracked immediately upon isolation). Conversely, films with larger relative incorporation of **6.2** (> 80%) were too tacky for analysis with our instrument. We accordingly prepared a series of **[6.1-block-6.2]$_C$** materials exhibiting pinane contents ranging from 24% to 34%. Solid films were cast from a 10 wt% solution in $CHCl_3$ and dried for 16 h under vacuum at 40 °C prior to analysis (see experimental for additional details). The **[6.1-block-6.2]$_C$** films were then subjected to strain ramp experiments (0.1 strain%/min). As expected, the results from uniaxial tensile tests revealed the average Young's modulus (E) increased dramatically with increasing **6.1** content (Table 6.3, Figure 6.4). Concomitantly, the toughness of these materials decreased from 14.1(± 5.4) J·m^{-3} in **[6.1-block-6.2]$_{24}$** to 4.25 (± 0.26) J·m^{-3} with respect to **[6.1-block-**

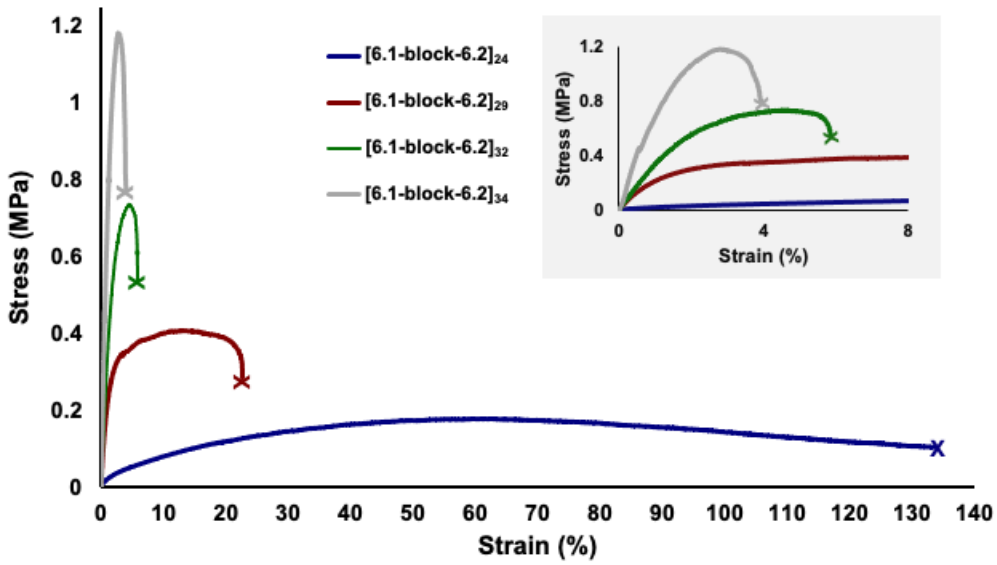

Figure 6.4: Representative stress-strain curves for **[6.1-block-6.2]$_C$.** Inset shows magnified view of the low strain region.

6.2]$_{34}$ (Figures 6.31-6.34). These results not only reflect properties observed in COCs,[237] but they also demonstrate that subtle changes to carbocycle incorporation can modulate bulk mechanical properties over orders of magnitude. While we are hesitant to invoke broad generalizations from these data (given the relatively small compositional window we were able to explore), we do note that an apparent exponential correlation exists between pinane content and E (Figure 6.67). Although phenomenological at this stage, we are currently pursuing additional studies with other block copolymers to ascertain the origins and generality of this putative correlation.

6.4 Conclusions

In conclusion, we have shown that rigid bicycles beyond norbornene can be leveraged to access copolymers with tunable (and even predictable) properties. Our findings demonstrate that trends observed in traditional COCs can be recapitulated by other bicyclic architectures, including those that are derived from biomass and/or include polymer comonomers. Additionally, we have demonstrated that block architectures exhibit highly tunable mechanical properties (even within a narrow range of relative carbocycle contents). Our work further advances efforts toward using biomass-derived materials as surrogates that can recapitulate the behavior of petrochemically-derived polymers. Moreover, the rich diversity of structures available in terpenoid systems is anticipated to provide exciting opportunities for enhancing fundamental knowledge of structure-property relationships.

6.5 Acknowledgements

We thank Prof. Mark Dadmun, Prof. Alexei Sokolov, Prof. Michael Kilbey, and Prof. Gila Stein for helpful discussions. This paper is dedicated to the memory of A.D.F. This work was supported by the National Science Foundation

6.6 Experimental

6.6.1 General Materials and Methods

Unless otherwise noted, solvents were dried on an MBraun solvent purification system with 3Å molecular sieves and degassed with three freeze pump thaw cycles. All other reagents were obtained from commercial sources and used without further purification. Oxygen and water sensitive manipulations were performed in a nitrogen filled MBraun glovebox or using standard Schlenk techniques. All polymerizations were performed in a N_2 filled glovebox. ^{1}H and ^{13}C NMR data were collected on a Varian 600 MHz NMR, Varian 500 MHz NMR, or Varian 300 MHz NMR spectrometer. Chemical shifts (δ) are reported in ppm using the residual solvent as reference. Thermogravimetric analysis (TGA) was performed on a TA Instruments TGA Q500 and Dynamic Mechanical Analysis (DMA) data was collected on a TA Instruments DMA Q800 with a powder clamp. Differential Scanning Calorimetry (DSC) was performed on a TA Instruments Q-2000 DSC. Size-Exclusion Chromatography (SEC) data was collected on an Omnisec Resolve and Omnisec Reveal System using triple detection with detectors in series: UV, light scattering, viscometer, and refractive index and three Viscotek styrene divinylbenzene copolymer columns (in series T3000, T4000, and T5000) at a flow rate of 1 mL/min and

thermostatted to 30 °C using tetrahydrofuran (THF) as the eluent. Molecular weight and dispersity data were determined using triple detection. The monomers β-Pinadiene (**6.1**) and 1,2-Nonadiene (**6.2**) were synthesized according to previously reported procedures.[44,43]

6.6.2 Procedure for gem-dibromocyclopropanation of Styrene (6.6a)

A 500 mL round bottom flask was charged with a Teflon stir bar, styrene (10 g; 96 mmol), dichloromethane (DCM; 100 mL), bromoform ($CHBr_3$; 18.5 mL; 192 mmol), and cetyltrimethylammonium bromide ($CTMA^+ Br^-$; 3.5 g; 9.6 mmol). The mixture was cooled to 0 °C in an ice bath, and KOH (50% w/w in water) was added dropwise (32.4 g; 576 mmol). The resulting mixture was left to stir for 25 h while warming to room temperature. The reaction mixture was then neutralized with 2M HCl, diluted with water, and filtered through a plug of Celite. The organic phase was separated, and the aqueous phase was extracted with DCM (2 x 50 mL). The combined organic layers were washed with brine (2 x 100 mL), dried over Na_2SO_4, filtered, and solvent removed under vacuum. The crude pale-yellow oil was taken up in hexanes and filtered through a SiO_2 plug. Subsequent solvent removal under vacuum afforded **6.6a** as a colorless oil (6.69 g; 25% yield). Representative ^1H NMR spectral data is shown in Figure 6.35.

6.6.2 Procedure for preparation of 1-phenylallene (6.6)

A 250 mL flame dried Schlenk flask was charged with a Teflon stir bar, **6.6a** (6.59 g; 23.9 mmol), and diethyl ether (Et_2O; 40 mL) before cooling the solution to -78°C (10 min isotherm). Methyllithium (1.6 M in Et_2O; 17.9 mL; 28.6 mmol) was then added dropwise

Scheme 6.2: Synthesis of **6.6a**

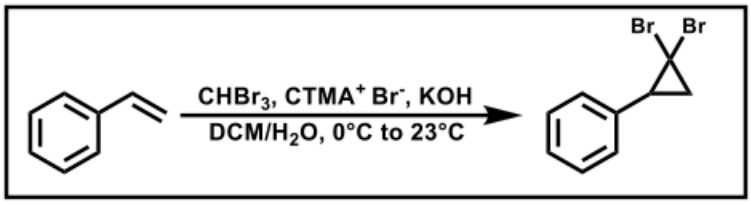

Scheme 6.3: Synthesis of **6.6**

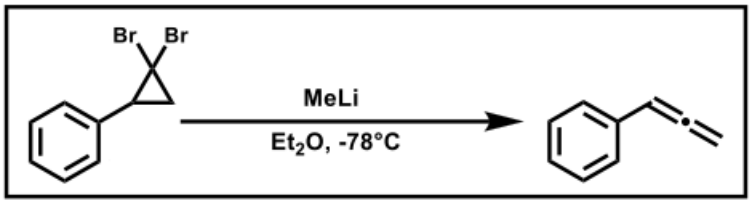

via gas-tight syringe, and the reaction was stirred at -78°C for 45 min. The reaction mixture was then warmed to 0 °C and quenched with water (30 mL). The mixture was warmed to room temperature, and the organic layer was separated. The aqueous layer was extracted with Et_2O (2 x 30 mL). The combined organic layers were washed with brine (2 x 40 mL), dried over Na_2SO_4, filtered, and dried under vacuum. Vacuum distillation (15 Torr) at 75 °C provided **6.6** as a colorless oil (1.27 g; 45.8% yield). Representative ^{1}H NMR data is shown in Figure 6.36. Spectral data were consistent with literature reports.[238]

6.6.3 Procedure for Esterification of β-Citronellol (6.9a)

Using a modified procedure,[239] a 250 mL flame-dried round bottom flask was charged with a Teflon stir bar, β-citronellol (7.11 g; 45.5 mmol), pyridine (4.03 mL; 50.1 mmol) and capped with a septum. The solution was stirred for 10 min at -78 °C. In a separate flask, bromoacetyl chloride (4.17 mL; 50.1 mmol) was taken up in dichloromethane (DCM; 90 mL) and transferred via cannula to the round bottom flask containing β-citronellol and pyridine. The solution was stirred at -78 °C for 10 min before warming to 23 °C. Water (50 mL) was added to the solution, and the organic layer was extracted using DCM (2 x 30 mL). The solution was concentrated to dryness under reduced pressure. The crude product was purified using flash-column chromatography (5:95 Ethyl Acetate:Hexanes) to yield **6.9a** as a pale-yellow oil (4.8 g; 38% yield). Representative ^{1}H NMR data is shown in Figure 6.37. Spectral data were consistent with literature reports.[240]

Scheme 6.4: Synthesis of **6.9a**

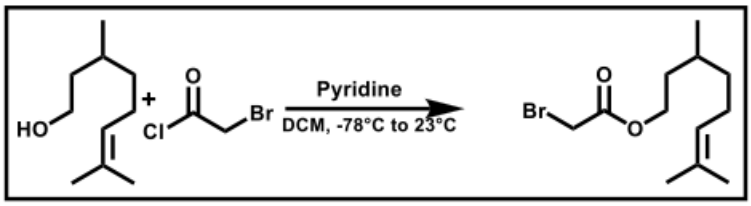

6.6.3 Procedure for Preparation of Wittig Salt (6.9b)

To a 250 mL flame-dried round bottom flask containing **6.9a** (7.56g, 27.27mmol) was added toluene (PhMe; 75 mL) and triphenylphosphine (7.51g; 28.6 mmol). The solution was stirred at room temperature for 42 h. After this, the solution was concentrated to dryness, triturated with hexanes, vacuum filtered, washed with hexanes, and dried on a vacuum line. The dried intermediate was taken up in a tetrahydrofuran/dimethyl sulfoxide solution (100 mL/8 mL). NaH (60% in oil suspension; 2.7g; 67.5 mmol) added, and the solution was stirred at room temperature for 5 h. The solution was concentrated and transferred to a separatory funnel containing DCM and water. The aqueous layer was extracted with DCM (2 x 20 mL). The combined organic layers were washed with brine (1 x 20 mL), dried over Na_2SO_4, and concentrated to dryness to yield **6.9b** (11.2g; 89.8%). Representative ^1H data are shown in Figure 6.38.

6.6.4 Procedure for Preparation of 6.9

To a 100 mL flame-dried round bottom flask containing **6.9b** (4.5g; 9.8 mmol) was added DCM (20 mL), triethylamine (1.5 mL; 10.8 mmol), and acetyl chloride (0.77 mL; 10.8 mmol) dropwise via gas-tight syringe. The solution was stirred at room temperature under N_2 for 1 h. The reaction was then quenched with methanol (0.9 mL). Hexanes (10 mL) were added to precipitate triphenylphosphine oxide, which was removed via vacuum filtration. The crude product was dissolved in minimal DCM and purified using flash-column chromatography (3:97 Ethyl Acetate:Hexanes). Drying over P_2O_5 afforded **6.9** as a colorless oil (1.05 g; 48% yield). Spectral data were consistent with literature reports.[239] Representative ^1H NMR data is shown in Figure 6.39.

Scheme 6.5: Synthesis of **6.9b**

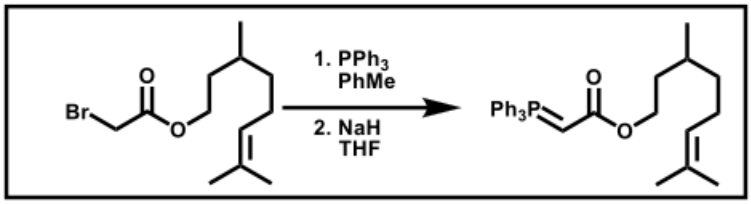

Scheme 6.6: Synthesis of **6.9**

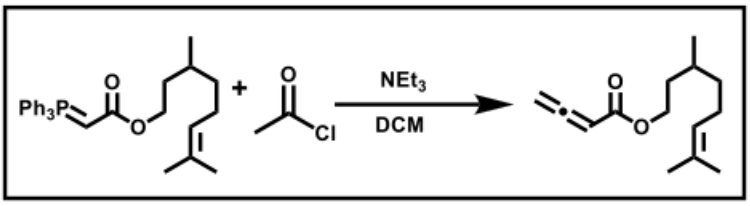

6.6.5 In-Situ Generation of Vinyl Addition Catalyst [(π-allyl)NiOCOCF$_3$]$_2$

In an N_2 filled glovebox, bis(1,5-cyclooctadiene)nickel(0) (10 mg, 0.036 mmol) was dissolved in toluene (1.34 mL) and stirred for 1 minute. To this solution was added allyltrifluoroacetate (4.75 μL, 0.036 mmol), and the subsequent orange solution was stirred for 1 minute to generate [(π-allyl)NiOCOCF$_3$]$_2$ *in situ*. This freshly prepared stock solution of [(π-allyl)NiOCOCF$_3$]$_2$ ([Ni] = 0.026 M) was subsequently used in polymerization studies. This stock solution is referred to as [(π-allyl)NiOCOCF$_3$]$_2$ in all polymerization procedures.

6.6.6 Polymerization of 6.1 using [(π-allyl)NiOCOCF$_3$]$_2$

In an N_2 filled glovebox, a 20 mL vial was charged with a Teflon stir bar, **6.1** (300 mg; 2.02 mmol), and toluene (PhMe; 8 mL). An aliquot of a freshly prepared [(π-allyl)NiOCOCF$_3$]$_2$ solution (0.23 mL; 0.006 mmol Ni) was added to this solution, and the polymerization reaction was stirred at room temperature for 1 h. The reaction vessel was removed from the glovebox, and the polymerization was quenched via sparging with air. The resultant solution was concentrated to a minimal volume under vacuum and added to excess MeOH to precipitate any polymeric material. The precipitated solids were collected via filtration and dried under vacuum to afford **6.3** (273.3 mg; 91% yield). A representative ^{1}H NMR spectrum is shown in Figure 6.40. Spectral data were consistent with literature reports.[44] Representative SEC data shown in Figure 6.5.

6.6.7 Polymerization of 6.2 using [(π-allyl)NiOCOCF$_3$]$_2$

In a N_2 filled glovebox, a 7 mL vial was charged with a Teflon stir bar, **6.2** (370 mg; 3.0 mmol) and toluene (PhMe; 6 mL). To this solution was added an aliquot of [(π-

Scheme 6.7: Generation of [(π-allyl)NiOCOCF$_3$]$_2$

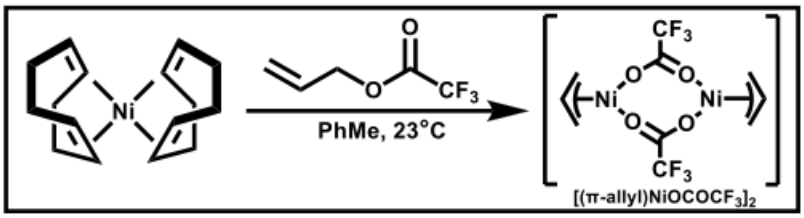

Scheme 6.8: Polymerization of **6.1**

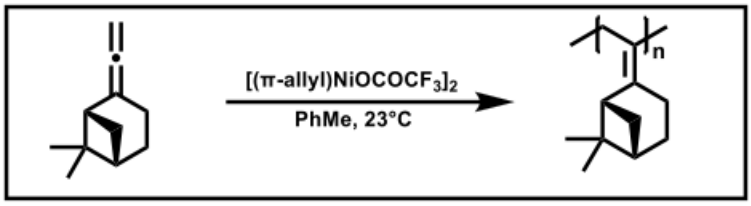

Scheme 6.9: Polymerization of **6.2**

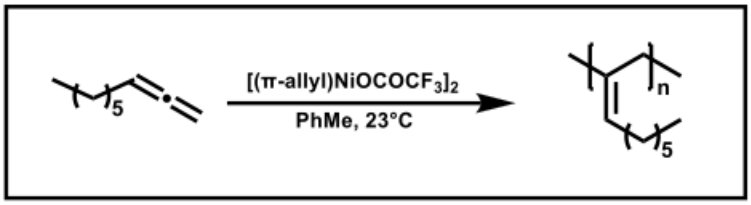

allyl)NiOCOCF$_3$]$_2$ (0.28 mL; 0.007 mmol Ni), and the polymerization was stirred at room temperature for 5 h. The reaction vessel was removed from the glovebox, and the polymerization was quenched via sparging with air. The resultant solution was concentrated to a minimal volume under vacuum and added to excess MeOH at -78 °C to precipitate any polymeric material. The precipitated solids were collected via filtration and dried under vacuum to afford **6.4** (252.1 mg; 68.1% yield). Representative ^{1}H NMR data is shown in Figure 6.41. Spectral data were consistent with literature reports.[43] Representative SEC data for the isolated polymer is shown in Figure 6.6.

6.6.8 Polymerization of 6.6 using [(π-allyl)NiOCOCF$_3$]$_2$

In a N_2 filled glovebox, a 20 mL vial was charged with a Teflon stir bar, **6.6** (230 mg; 1.98 mmol) and toluene (PhMe; 11 mL). To the solution was added an aliquot of [(π-allyl)NiOCOCF$_3$]$_2$ (0.2 mL; 0.005 mmol Ni), and the polymerization was stirred at room temperature for 17 h. The reaction vessel was removed from the glovebox, and the polymerization was quenched via sparging with air. The resultant solution was concentrated to a minimal volume under vacuum and added to excess MeOH to precipitate any polymeric material. The precipitated solids were collected via filtration and dried under vacuum to afford **6.7** (192.9 mg; 84% yield). Representative ^{1}H NMR data is shown in Figure 6.42. Spectral data were consistent with literature reports.[6] Representative SEC data for the isolated polymer is shown in Figure 6.7.

6.6.9 Polymerization of 6.9 using [(π-allyl)NiOCOCF$_3$]$_2$

In a N_2 filled glovebox, a 7 mL vial was charged with a Teflon stir bar, **6.9** (340 mg; 1.53 mmol) and toluene (PhMe; 3 mL). To the solution was added [(π-allyl)NiOCOCF$_3$]$_2$ (0.25

Scheme 6.10: Polymerization of **6.6**

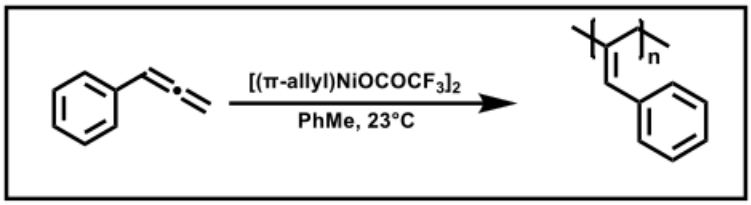

Scheme 6.11: Polymerization of **6.9**

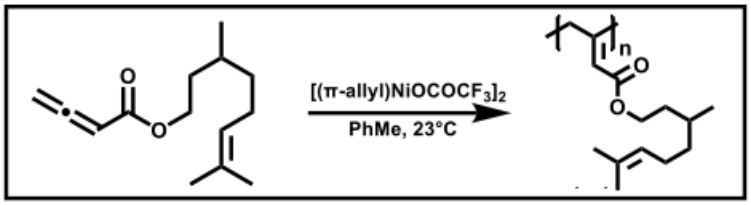

mL, 0.0065 mmol Ni), and the polymerization was stirred at room temperature for 5 h. The reaction vessel was removed from the glovebox, and the polymerization was quenched via sparging with air. The resultant solution was concentrated to a minimal volume under vacuum and added to excess MeOH at -78 °C to precipitate any polymeric material. The precipitated solids were collected via filtration and dried under vacuum to afford **6.10** (295 mg; 87% yield). **^{1}H NMR (500 MHz; $CDCl_3$):** δ = 0.9 (d, 3H), 1.17 (m, 1H), 1.32 (m, 1H), 1.42 (m, 1H), 1.54 (m, 1H), 1.58 (s, 3H), 1.66 (s, 3H), 1.94 (m, 2H), 3.54 (s, 2H), 4.05 (d, 2H), 5.07 (t, 1H), 5.86 (s, 1H). **^{13}C NMR (75 MHz; $CDCl_3$):** δ = 17.8, 19.58, 25.54, 29.79, 35.68, 37.28, 40.39, 62.63, 109.97, 119.70, 124.78, 131.30, 154.50, 165.98 Representative ^{1}H and ^{13}C NMR spectra are shown in Figure 6.43 and 6.44. Representative SEC data for the isolated polymer is shown in Figure 6.8.

6.6.10 Statistical Copolymerization of 6.1 and 6.2 using [(π-allyl)NiOCOCF$_3$]$_2$

In a N_2 filled glovebox, a 20 mL vial was charged with a Teflon stir bar, **6.1 (**171 mg; 1.15 mmol), **6.2** (143 mg; 1.15mmol) and toluene (PhMe, 8 mL). To the solution, an aliquot of a freshly prepared [(π-allyl)NiOCOCF$_3$]$_2$ solution (0.24 mL; 0.0062 mmol Ni) was added and the polymerization was stirred at room temperature for 6 h. The reaction vessel was removed from the glovebox, and the polymerization was quenched via sparging with air. The resultant solution was concentrated to a minimal volume under vacuum and added to excess MeOH to precipitate any polymeric material. The precipitated solids were collected via filtration and dried under vacuum to afford **[6.1-*co*-6.2]$_{56}$** (284.4 mg; 90.6% yield). The composition was determined using the relative integrations of the methyl protons arising from incorporation of each monomer (**δ** = 0.87 for **6.2** and **δ**= 0.73 for **6.1,** respectively).

Scheme 6.12: Statistical Copolymerization of 6.1 and 6.2

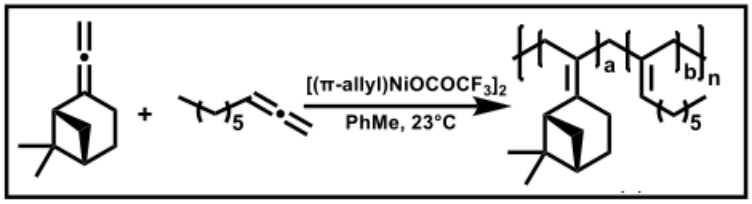

A similar method was used for all copolymers. Varying monomer feed ratios of **6.1** and **6.2** yielded statistical copolymers with varying compositions (see Table 6.1 in the main text). Molecular weight data is given in Table 6.1 in the main text. **^{1}H NMR (500 MHz; $CDCl_3$):** δ = 0.74 (s, 4H), 0.88 (s, 3H), 1.26 (s, 14H), 1.54 (s, 1H), 1.84 (d, 6H), 2.24 (s, 5H), 2.64 (s, 3H), 2.98 (s, 1H) 5.1 (m, 1H)**. ^{13}C NMR (125 MHz; $CDCl_3$):** δ = 14.28, 21.30, 22.88, 24.52, 26.59, 28.28, 29.42, 30.29, 32.12, 40.75, 46.60, 127.13, 134.25, 135.09, 138.31. Representative ^{1}H and ^{13}C NMR spectra for each composition are shown in Figures 6.45 – 6.50. Representative SEC data for the isolated polymers are shown in Figures 6.9 – 6.11.

6.6.11 Statistical Copolymerization of 6.1 and 6.6 using [(π-allyl)NiOCOCF$_3$]$_2$

In a N_2 filled glovebox, a 7 mL vial was charged with a Teflon stir bar, **6.1 (**170mg, 1.15mmol), **6.6** (134mg, 1.15mmol) and toluene (PhMe, 6 mL). To the solution, an aliquot of a freshly prepared [(π-allyl)NiOCOCF$_3$]$_2$ solution (0.23 mL, 0.006mmol) was added and the polymerization was stirred at room temperature for 27h. The reaction vessel was removed from the glovebox, and the polymerization was quenched via sparging with air. The resultant solution was concentrated to a minimal volume under vacuum and added to excess MeOH to precipitate any polymeric material. The precipitated solids were collected via filtration and dried under vacuum to afford **[6.1-co-6.6]$_{44}$** (280.7mg, 92% yield). Varying monomer feed ratios of **6.1** and **6.6** yielded statistical copolymers with varying compositions (see Table 6.2). Molecular weight data is given in Table 6.2 in the main chapter. Representative SEC data for the isolated polymers are shown in Figure 6.12 – 6.14. **^{1}H NMR (500 MHz; $CDCl_3$):** δ = 0.66 (s, 1H), 1.09 (s, 2H), 1.77 (s, 2H), 2.23 (s,

Scheme 6.13: Statistical Copolymerization of **6.1** and **6.6**

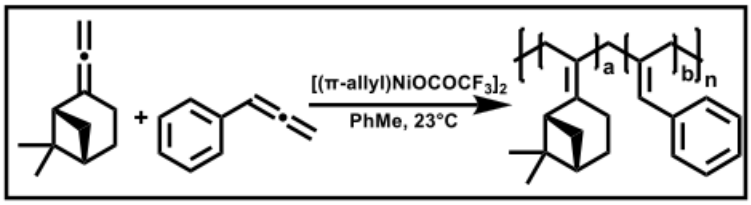

1H), 2.80 (m, 4H), 6.33 (s, 1H), 7.18 (m, 5H). **^{13}C NMR (125 MHz; $CDCl_3$):** δ = 21.61, 22.76, 24.34, 26.58, 27.92, 40.68, 46.20, 125.62, 126.05, 128.07, 129.05, 139.16**.** Representative ^{1}H and ^{13}C NMR spectra of each composition are shown in Figures 6.51–6.56.

6.6.12 Statistical Copolymerization of 6.1 and 6.9 using [(π-allyl)NiOCOCF$_3$]$_2$

In a N_2 filled glovebox, a 7 mL vial was charged with a Teflon stir bar, **6.1 (**171mg, 1.15mmol), **6.9** (165mg, 0.75mmol) and toluene (PhMe, 6 mL). To the solution, an aliquot of a freshly prepared [(π-allyl)NiOCOCF$_3$]$_2$ solution (0.25 mL, 0.0065mmol) was added and the polymerization was stirred at room temperature for 6h. The reaction vessel was removed from the glovebox, and the polymerization was quenched via sparging with air. The resultant solution was concentrated to a minimal volume under vacuum and added to excess MeOH to precipitate any polymeric material. The precipitated solids were collected via filtration and dried under vacuum to afford **[6.1-co-6.9]$_{65}$** (289.9mg, 86.3% yield). Representative SEC data for the isolated polymer is shown in Figure 6.15. **^{1}H NMR (500 MHz; $CDCl_3$):** δ = 0.74 (s, 4H), 0.89 (s, 3H), 1.21 (s, 6H), 1.33 (t, 4H), 1.59 (s, 3H), 1.67 (s, 3H), 1.94 (m, 6H), 2.27 (s, 5H), 2.66 (d, 4H), 4.07 (s, 2H), 5.08 (s, 1H), 5.85 (d, 1H)**.** **^{13}C NMR (125 MHz; $CDCl_3$):** δ = 17.81, 19.60, 21.65, 22.70, 24.67, 26.68, 29.83, 35.71, 36.45, 40.70, 46.42, 62.46, 124.83, 128.62, 131.31, 136.72, 165.89**.** Representative ^{1}H and ^{13}C NMR spectra are shown in Figures 6.57 and 6.58, respectively.

6.6.13 Block Copolymerization of 6.1 and 6.2 using [(π-allyl)NiOCOCF$_3$]$_2$

In a N_2 filled glovebox, a 7 mL vial was charged with a Teflon stir bar, **6.1** (93mg, 0.625mmol) and toluene (PhMe, 8 mL). To the solution, an aliquot of a freshly prepared

Scheme 6.14: Statistical Copolymerization of **6.1** and **6.9**

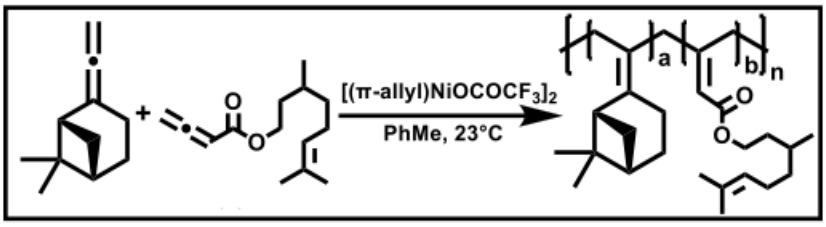

Scheme 6.15: Block Copolymerization of **6.1** and **6.2**

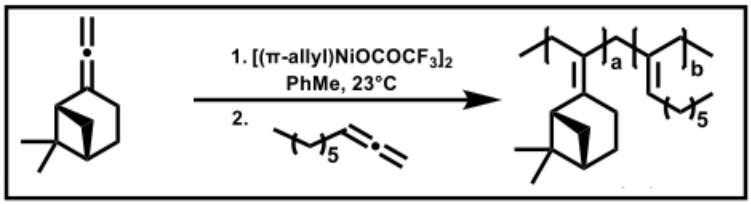

[(π-allyl)NiOCOCF$_3$]$_2$ solution (0.1 mL, 0.0026mmol) was added and the polymerization was stirred at room temperature for 3h. After which an aliquot (0.2 mL) was removed, quenched via exposure to air and diluted with $CDCl_3$ (0.5 mL). Complete consumption of **6.1** was confirmed via ^{1}H NMR spectroscopy and subsequent SEC analysis revealed the number average molecular weight (M_n) of the polymer was ~ 29 kDa (**[6.1-block-6.2]$_{29}$**; Table 6.3). In a separate vial, **6.2** (230mg, 1.875mmol) was taken up in toluene (0.5 mL) and added to the polymerization reaction and stirred for 15h. The bulk polymerization was removed from the glovebox and quenched via sparging with air. The solution was concentrated to a minimal volume and precipitated in stirring methanol. The precipitated solids were filtered and dried under vacuum to yield the product block copolymer (218.3mg, 68% yield) as an off-white solid or a tacky solid depending on composition. Varying ratios of **6.1** and **6.2** yielded block copolymers with the target compositions. (With varying M_n values; see Figures 6.16 – 6.19 for representative SEC data). **^{1}H NMR (500 MHz; $CDCl_3$):** δ = 0.75 (s, 2H), 0.87 (t, 3H), 1.27 (s, 10H), 1.55 (s, 1H), 1.93 (t, 3H), 2.32 (s, 2H), 2.58 (t, 1H), 2.94 (s, 1H), 5.22 (d, 1H). **^{13}C NMR (125 MHz; $CDCl_3$):** δ = 14.26, 21.69, 22.87, 24.72, 26.75, 28.31, 29.42, 30.26, 32.10, 34.20, 37.94, 40.72, 46.38, 127.12, 128.73, 134.20, 136.42**.** Representative ^{1}H and ^{13}C NMR spectra of each composition are shown in Figures 6.59–6.64.

6.6.14 General Procedures for Polymer Thermal Analysis

Dynamic Mechanical Analysis data of samples was acquired using a dynamic mechanical analyzer equipped with a powder clamp. Samples were heated at a rate of 2°C/min at 1 Hz (Figures 6.22, and 6.30).

Differential Scanning Calorimetry samples loaded in hermetic aluminum DSC pans and transferred into a glovebox under a Nitrogen atmosphere and subsequently sealed. Samples were heated at a rate of 10°C/min (Figures 6.20 – 6.21, 6.23 – 6.29)

6.6.15 Toughness Calculation for Stress/Strain Data (Figure 6.4)

Toughness values were calculated by integrating the area under each Stress/Strain curve in Figure 6.4 in the Main Text using Origin Pro 2022_SR1. Figures 6.31 – 6.34 are representative depictions of the integration parameters shown as the shaded area.

6.6.16 Procedure for Polymerization Kinetics

In an N2 filled glovebox, a 3 mL vial was charged with **6.1** (28.1 mg; 0.189 mmol), d_8-toluene (0.65 mL) and mesitylene (1 μL; 0.0072 mmol) as an internal standard. The solution was transferred to a septa-capped NMR tube and an initial (T0) ^{1}H NMR spectrum was collected. A separate 3 mL vial was charged with bis(1,5-cyclooctadiene)nickel(0) (7.71 mg; 0.028 mmol), a Teflon stir bar, d_8-toluene (1 mL), and allyltrifluoroacetate (3.65 μL; 0.028 mmol). Stirring at 23 °C for 20 minutes generated [(π-allyl)NiOCOCF$_3$]$_2$ *in situ* ([Ni] = 0.028 M). An aliquot (0.1 mL; 0.0028 mmol Ni) was drawn up by an air-tight syringe and the needle tip inserted into septa capped vial. The solution of [(π-allyl)NiOCOCF$_3$]$_2$ was quickly injected into the NMR tube (followed by mixing via inversion). ^{1}H NMR spectra were collected every three minutes over the course of 63 minutes. Monomer consumption was determined via integration of the allene vinyl protons (δ = 4.72 – 4.82) versus the internal standard (δ = 6.77 – 6.83 for mesitylene) (Figure 6.68).

Similar studies were conducted for **[6.1-co-6.6]** (Figure 6.69) and **[6.1-co-6.9]** (Figure 6.70) where the only difference is amount of d_8-toluene added to the monomer solution (0.629mL and 0.62mL respectively). Monomers were added in an equimolar ratio. Kinetics studies for 1,2-nonadiene reported previously.[43]

APPENDIX

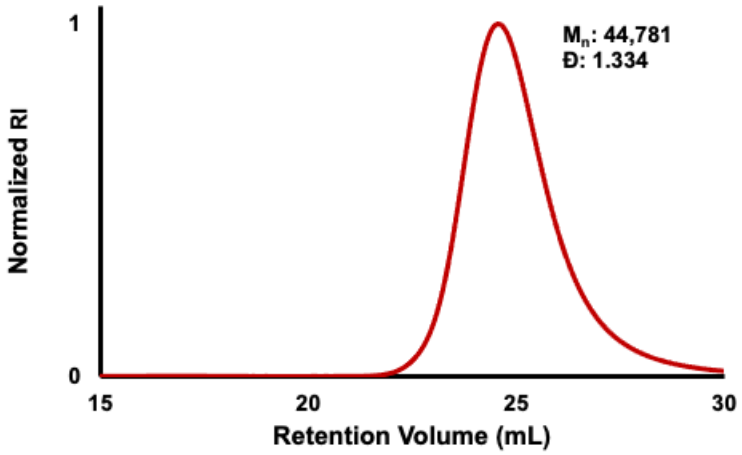

Figure 6.5: Representative SEC Trace of **6.3**

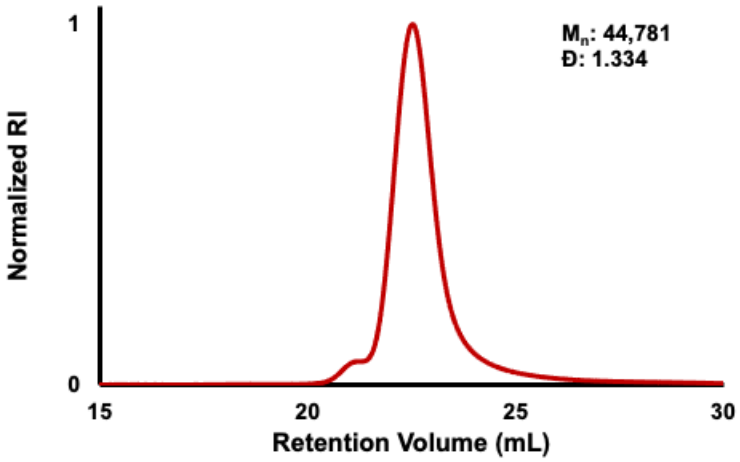

Figure 6.6: Representative SEC Trace of **6.4**

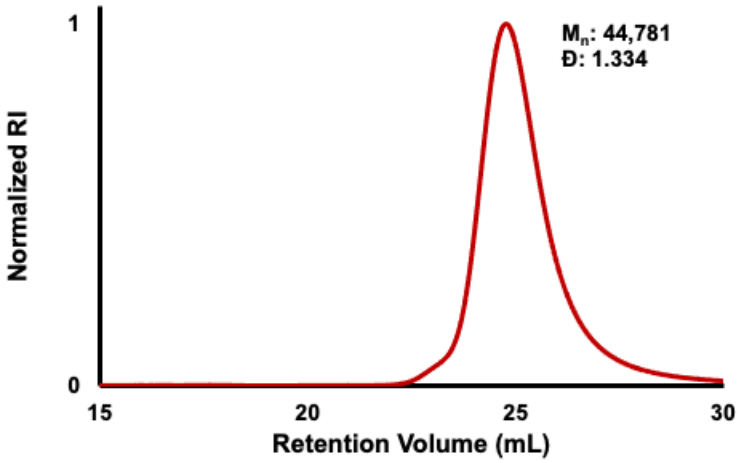

Figure 6.7: Representative SEC Trace of **6.7**

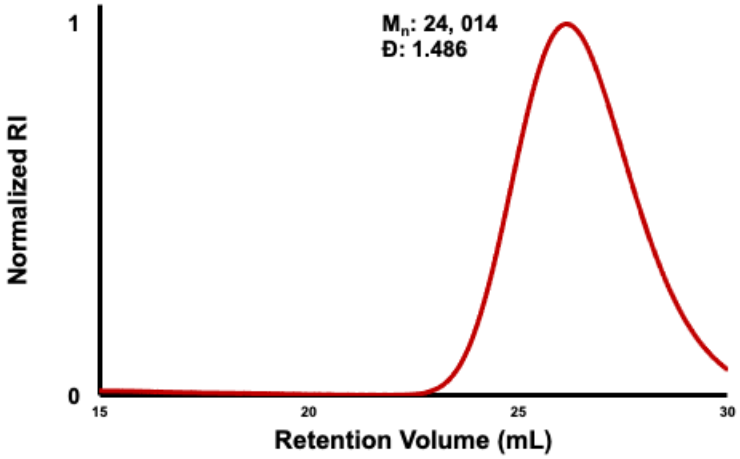

Figure 6.8: Representative SEC Trace of **6.10**

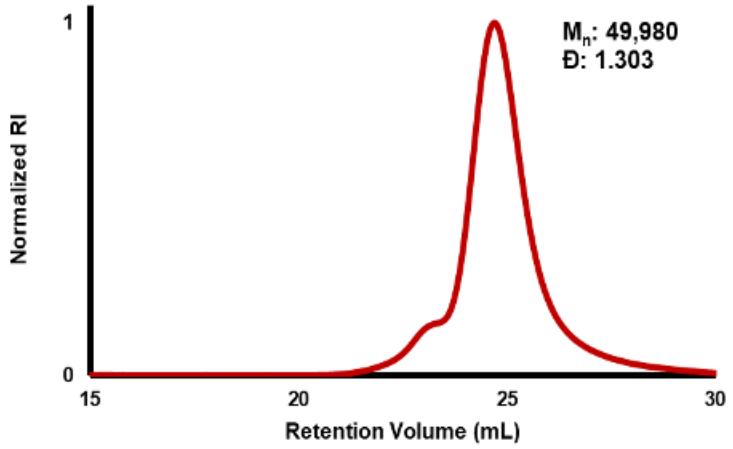

Figure 6.9: Representative SEC Trace of **[6.1-co-6.2]$_{30}$**

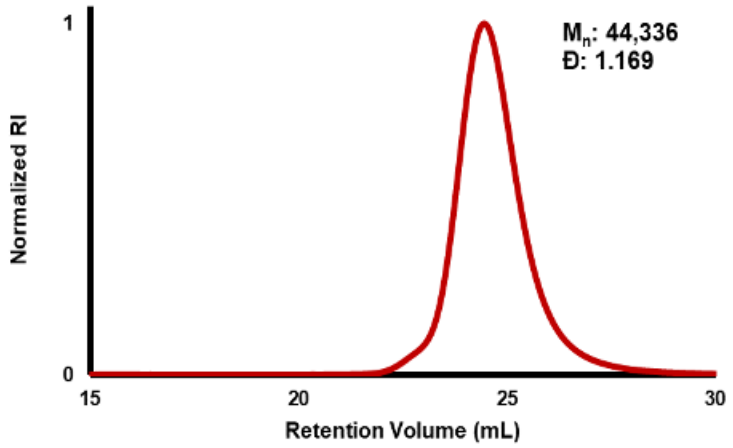

Figure 6.10: Representative SEC Trace of **[6.1-co-6.2]$_{56}$**

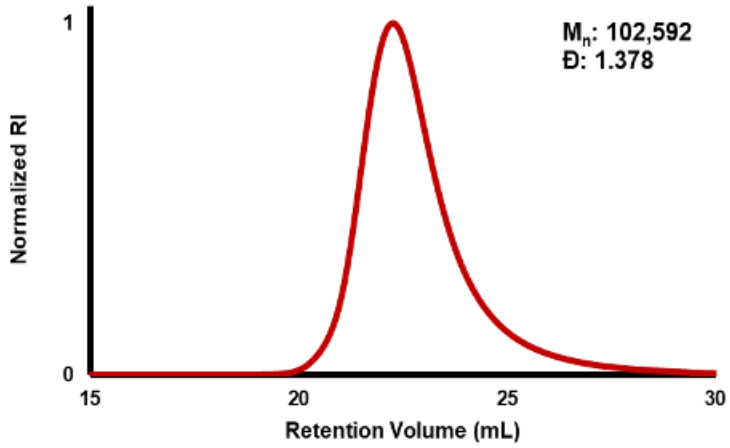

Figure 6.11: Representative SEC Trace of **[6.1-co-6.2]**$_{77}$

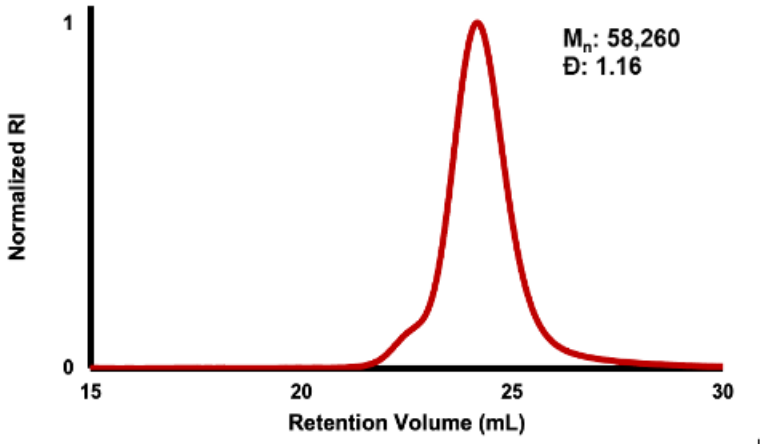

Figure 6.12: Representative SEC Trace of **[6.1-co-6.6]**$_{20}$

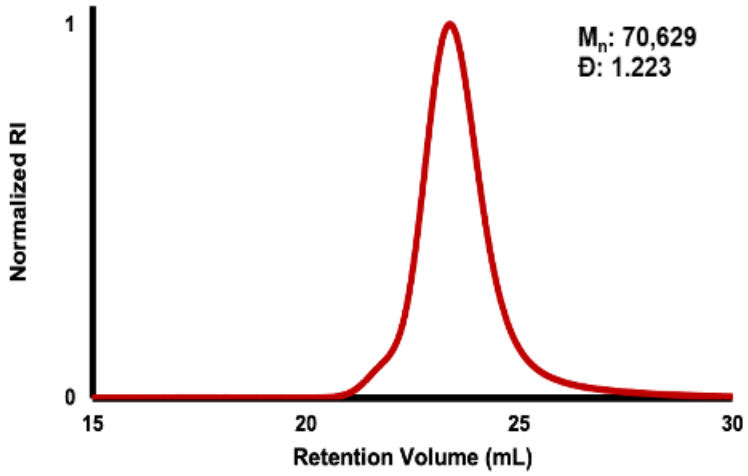

Figure 6.13: Representative SEC Trace of **[6.1-co-6.6]$_{44}$**

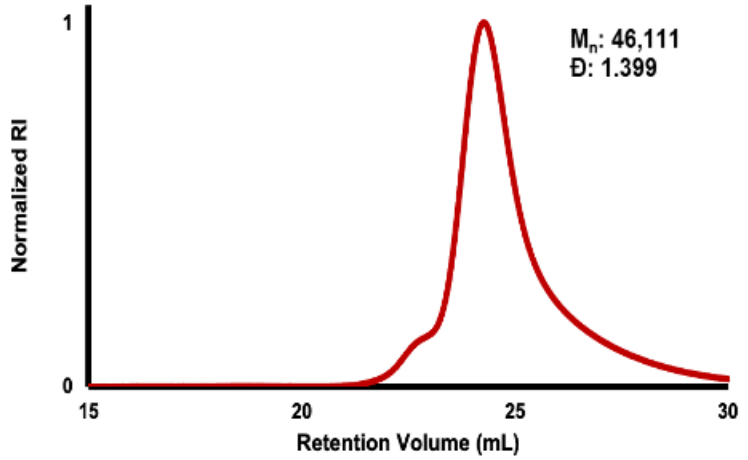

Figure 6.14: Representative SEC Trace of **[6.1-co-6.6]$_{70}$**

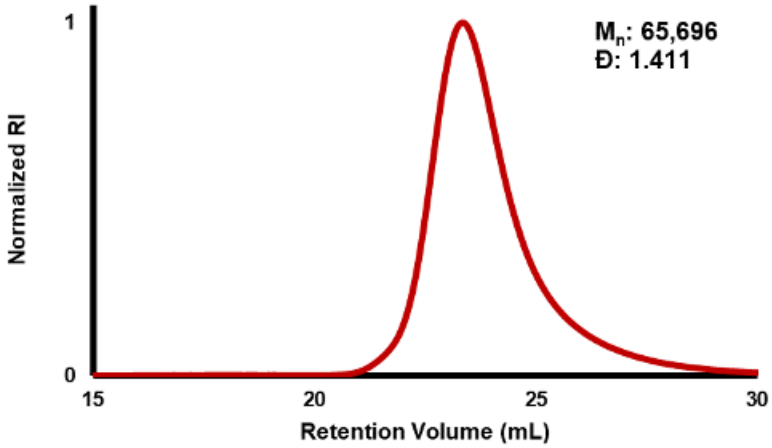

Figure 6.15: Representative SEC Trace of **[6.1-co-6.9]$_{65}$**

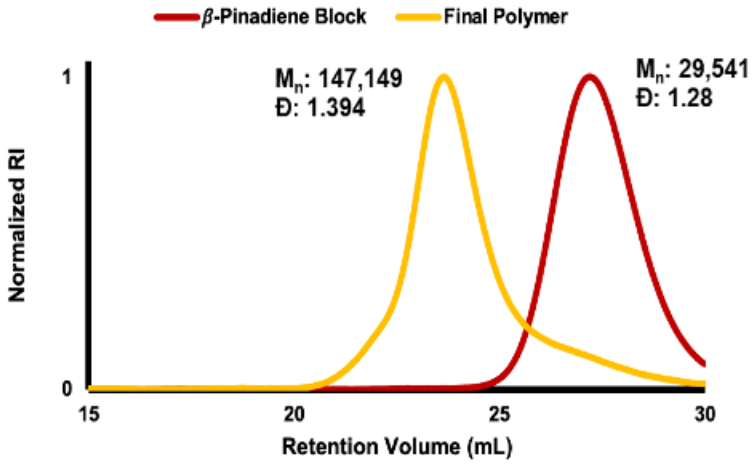

Figure 6.16: Representative SEC Trace of **[6.1-block-6.2]$_{24}$**

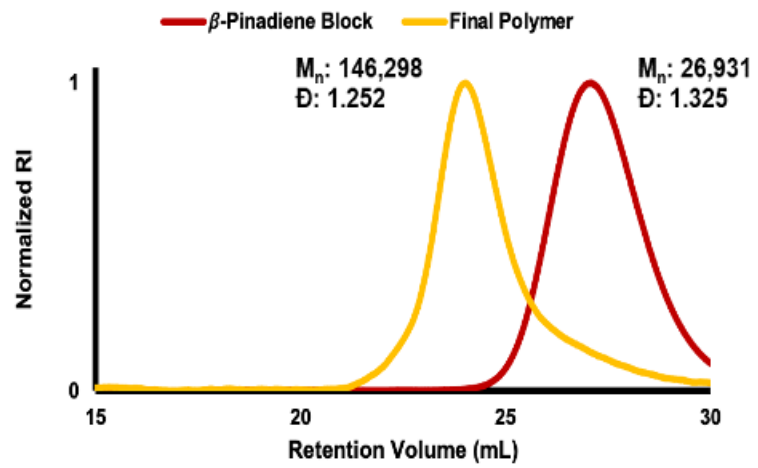

Figure 6.17: Representative SEC Trace of **[6.1-block-6.2]**$_{29}$

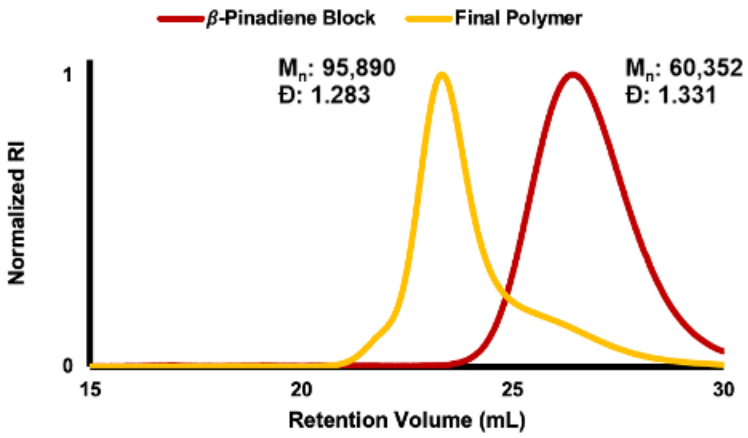

Figure 6.18: Representative SEC Trace of **[6.1-block-6.2]**$_{32}$

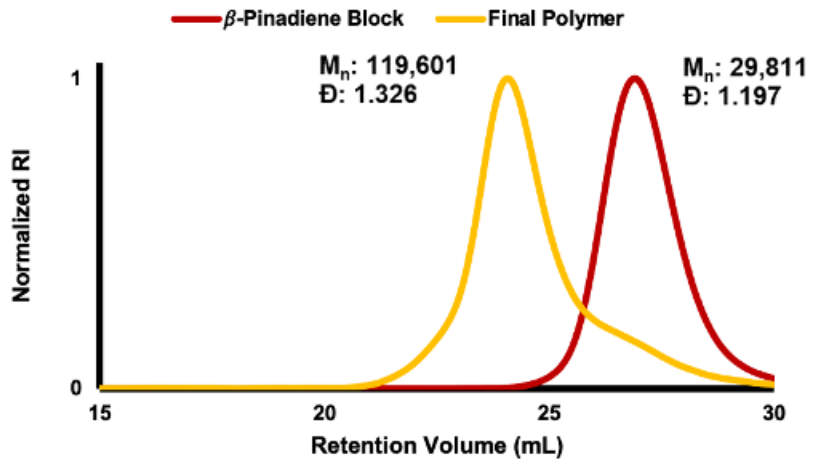

Figure 6.19: Representative SEC Trace of **[6.1-block-6.2]$_{34}$**

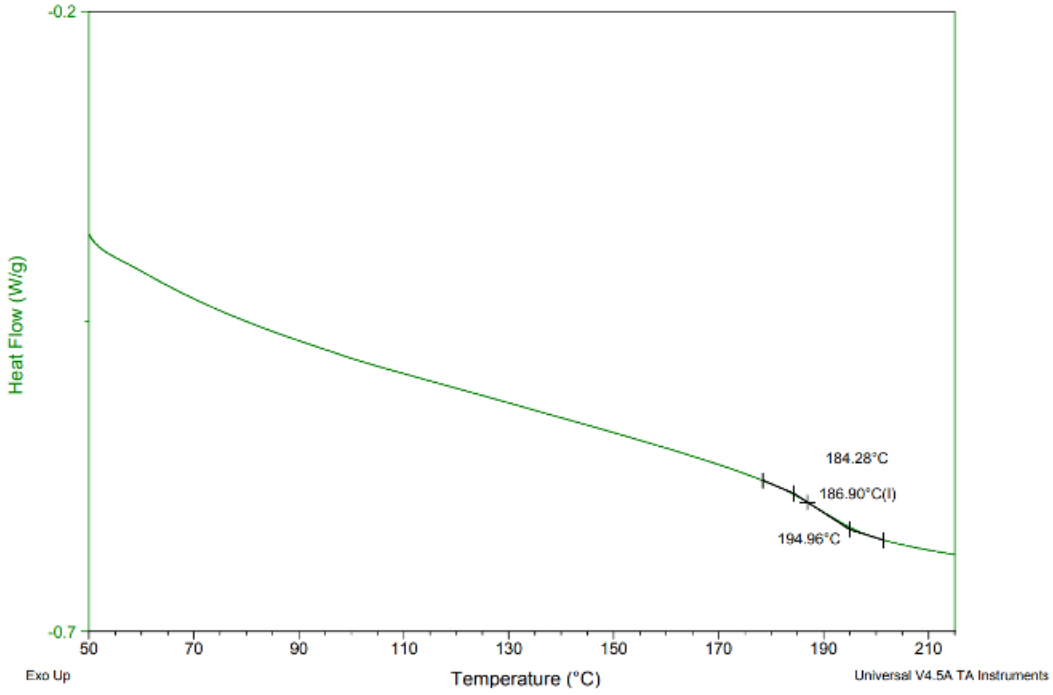

Figure 6.20: Representative DSC Data for **6.3**

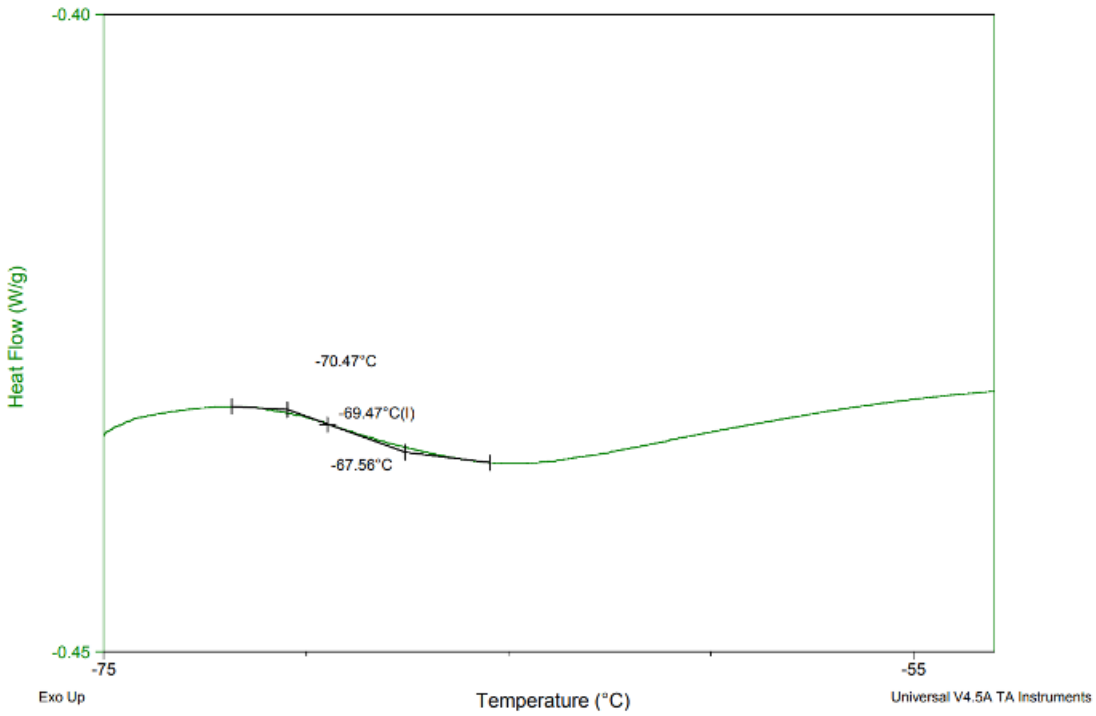

Figure 6.21: Representative DSC Data for **6.4**

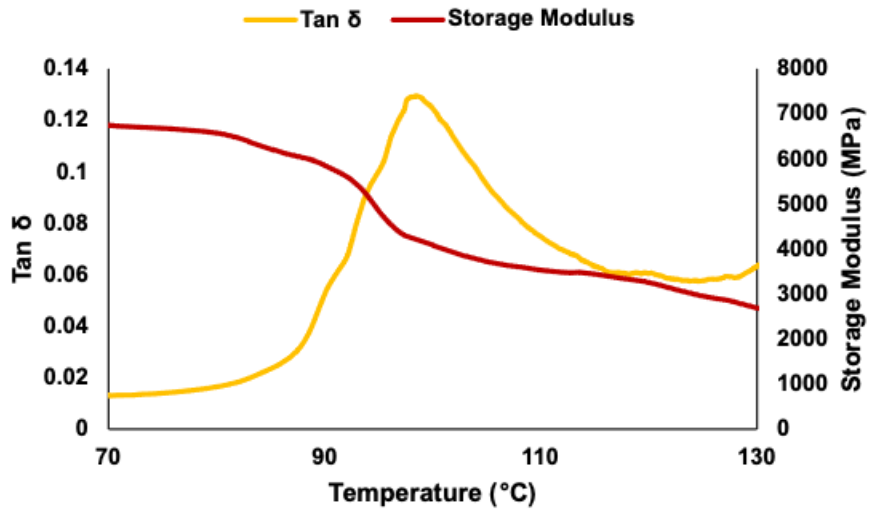

Figure 6.22: Representative Powder DMA Data for **6.7**

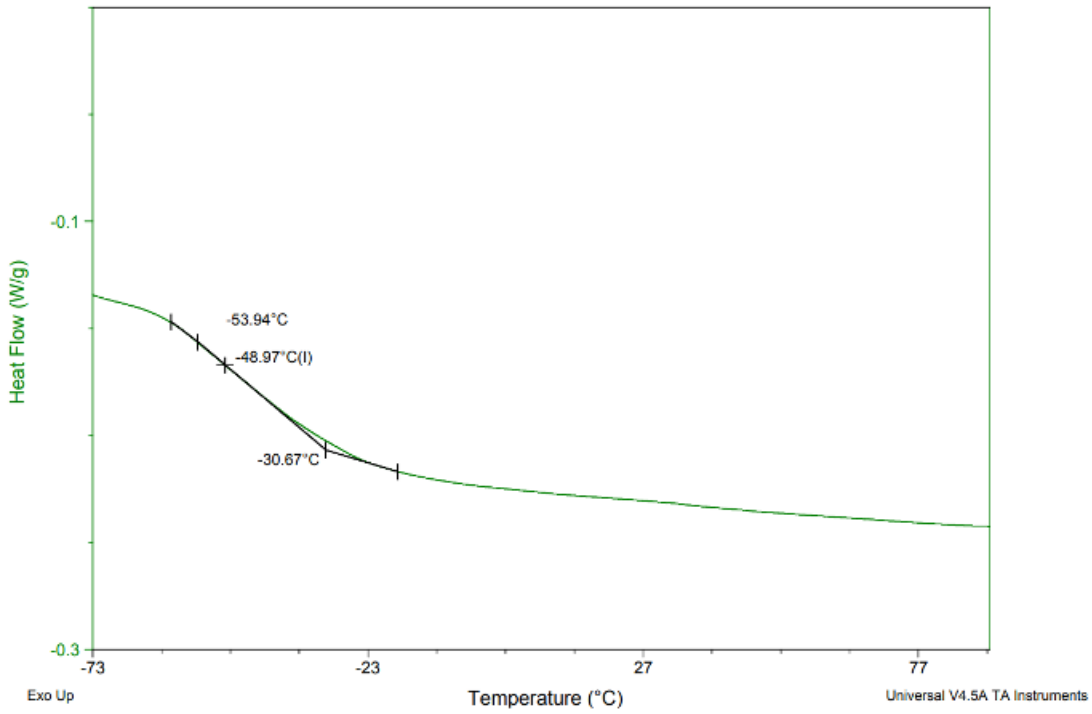

Figure 6.23: Representative DSC Data for **6.10**

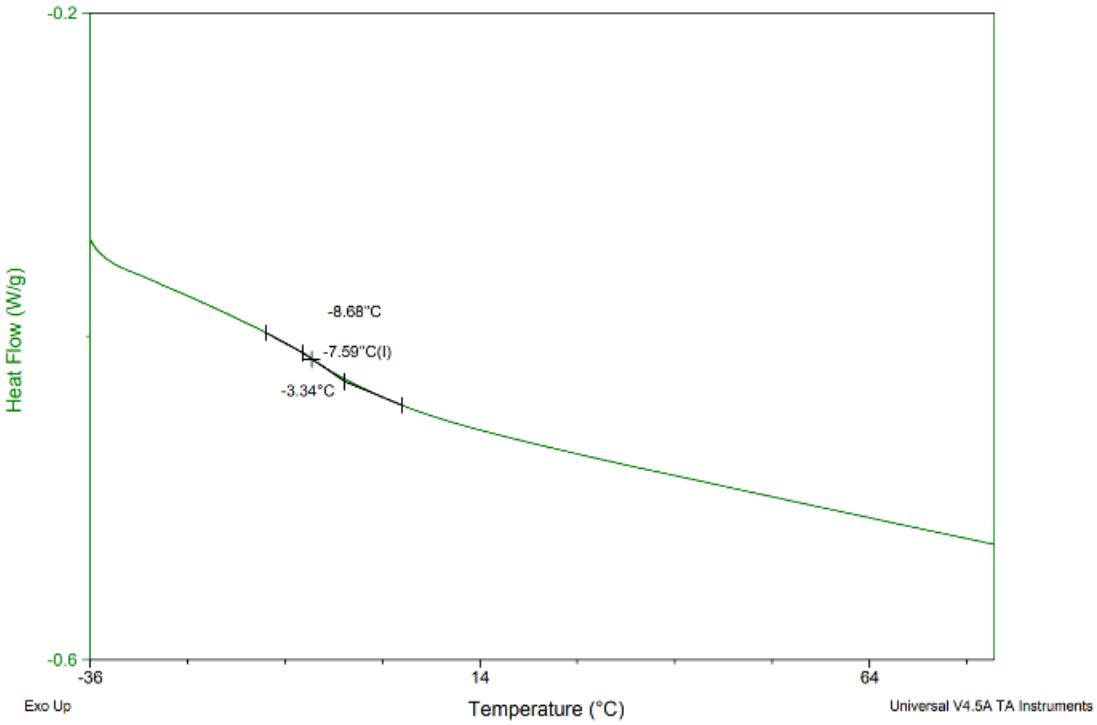

Figure 6.24: Representative DSC Data for **[6.1-co-6.2]$_{30}$**

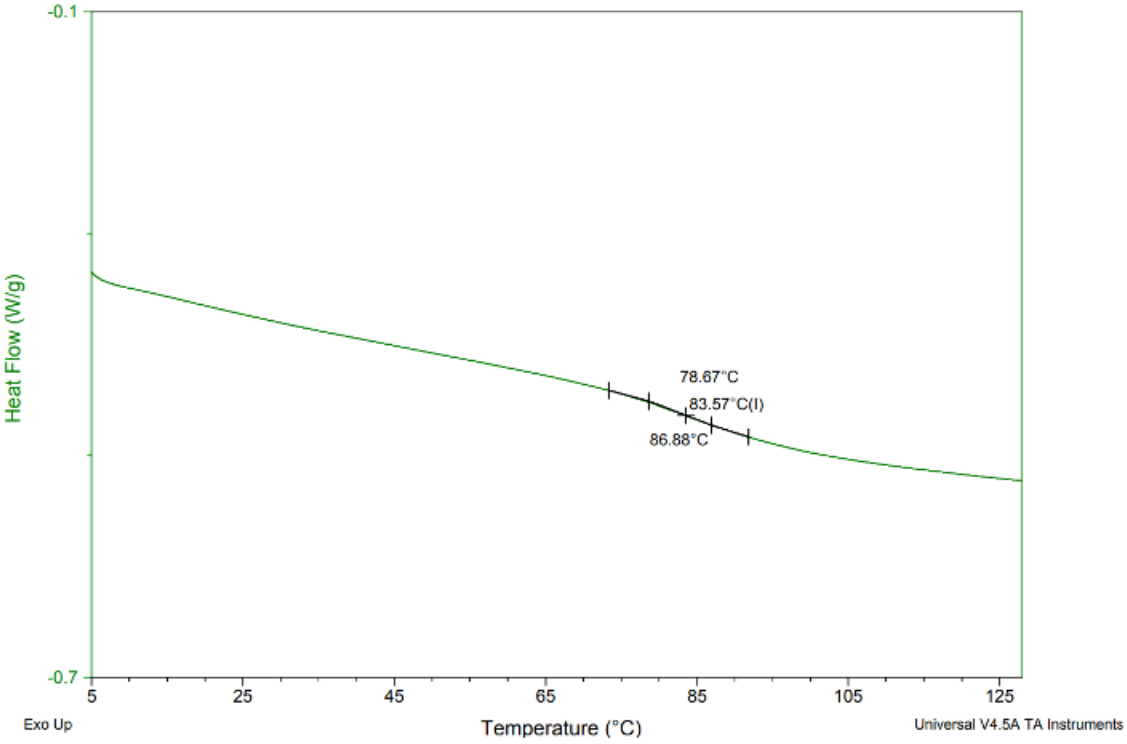

Figure 6.25: Representative DSC Data for **[6.1-co-6.2]$_{56}$**

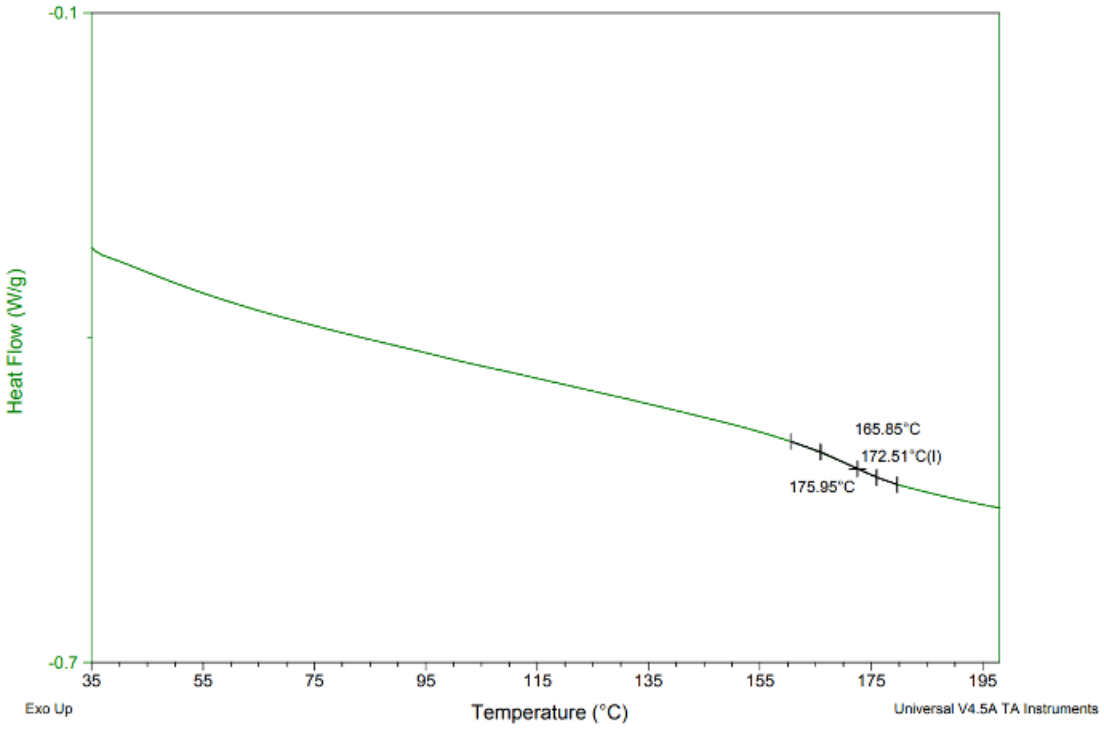

Figure 6.26: Representative DSC Data for **[6.1-co-6.2]**$_{77}$

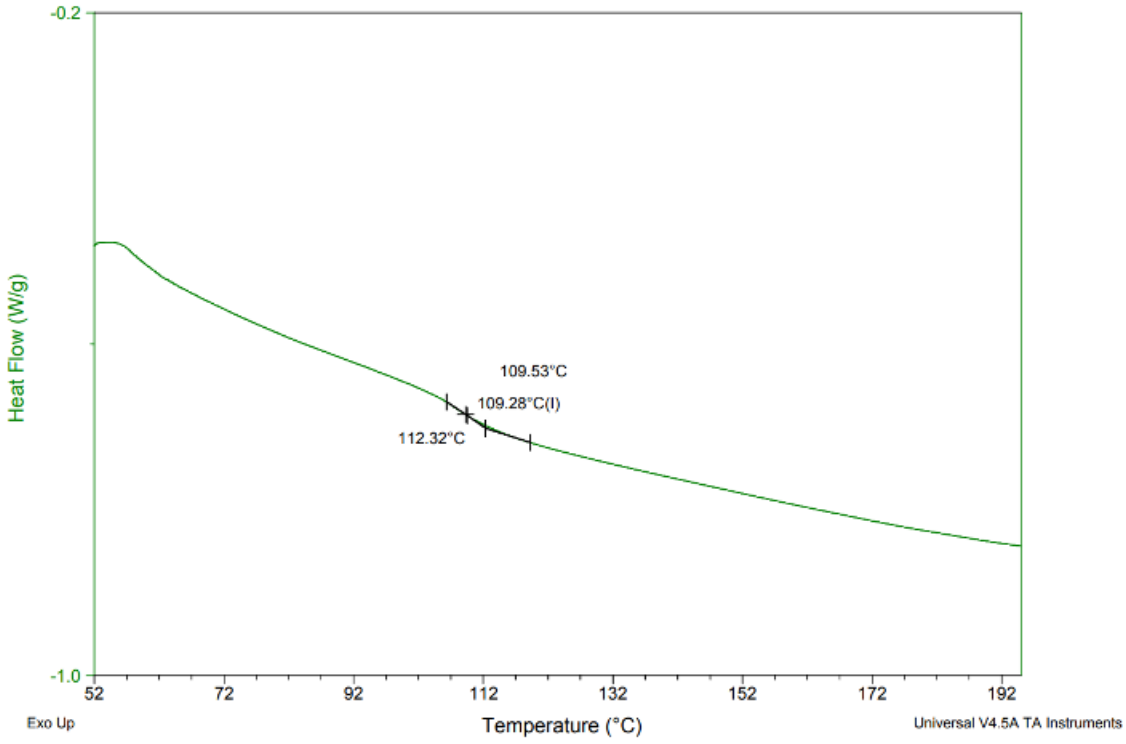

Figure 6.27: Representative DSC Data for **[6.1-co-6.6]$_{20}$**

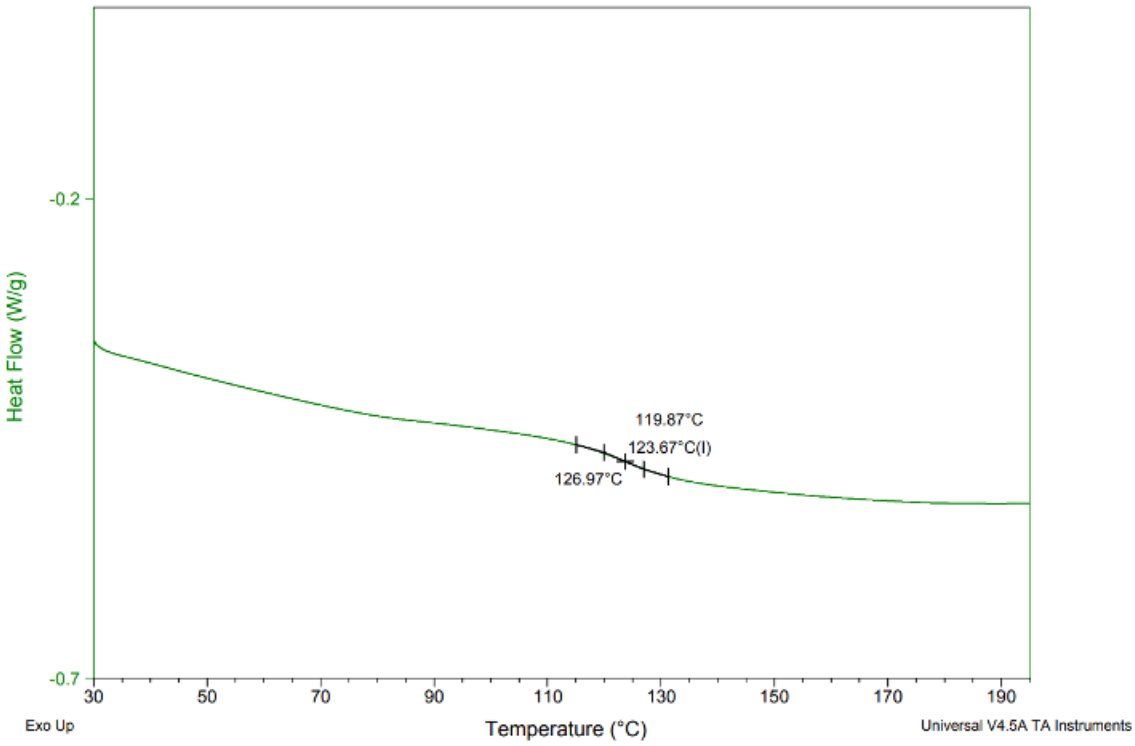

Figure 6.28: Representative DSC Data for [6.1-co-6.6]$_{44}$

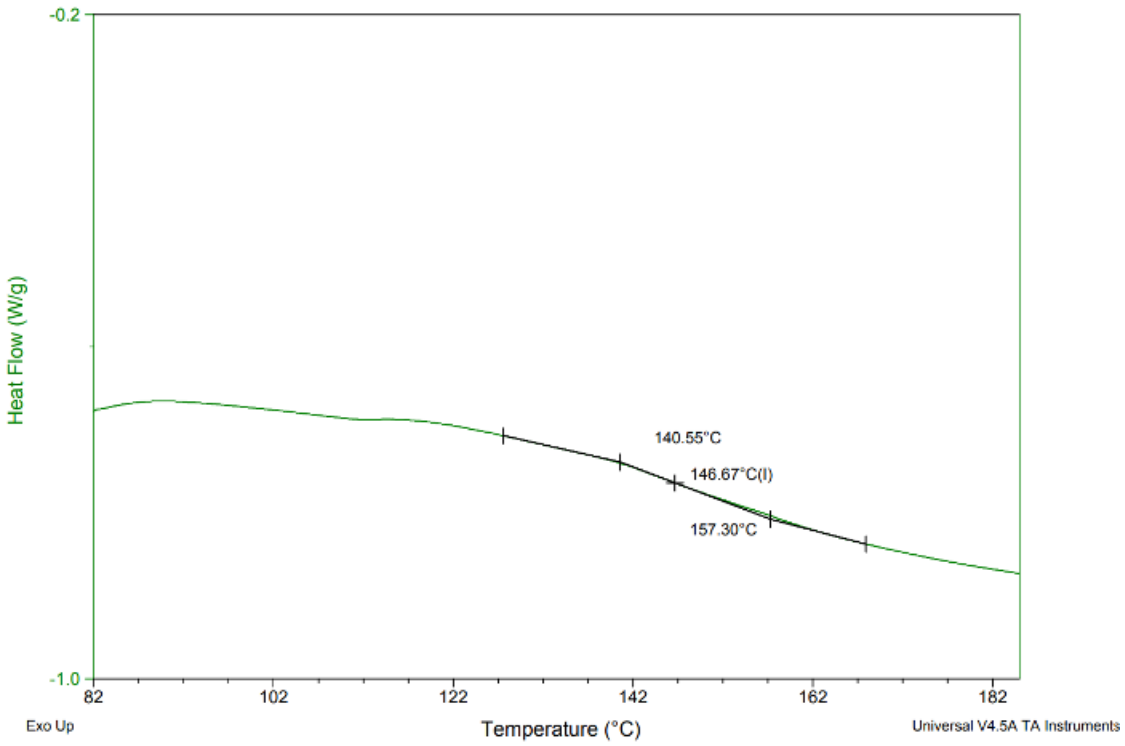

Figure 6.29: Representative DSC Data for **[6.1-co-6.6]$_{70}$**

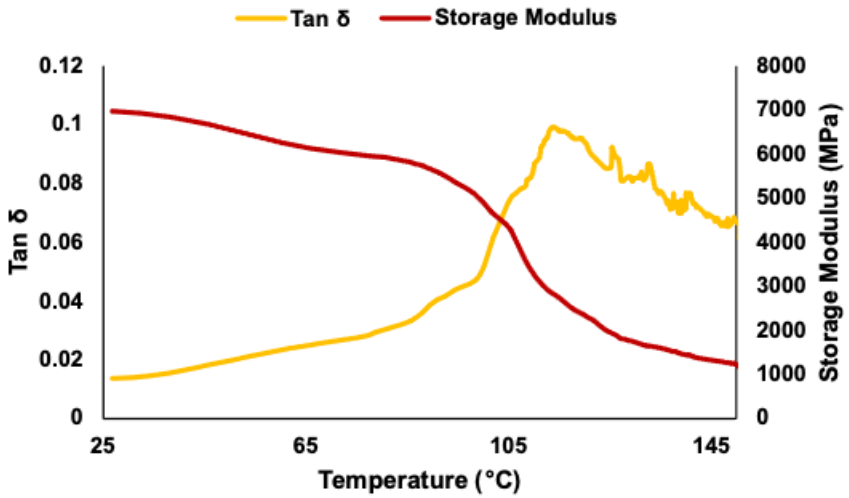

Figure 6.30: Representative Powder DMA Data for **[6.1-co-6.9]$_{65}$**

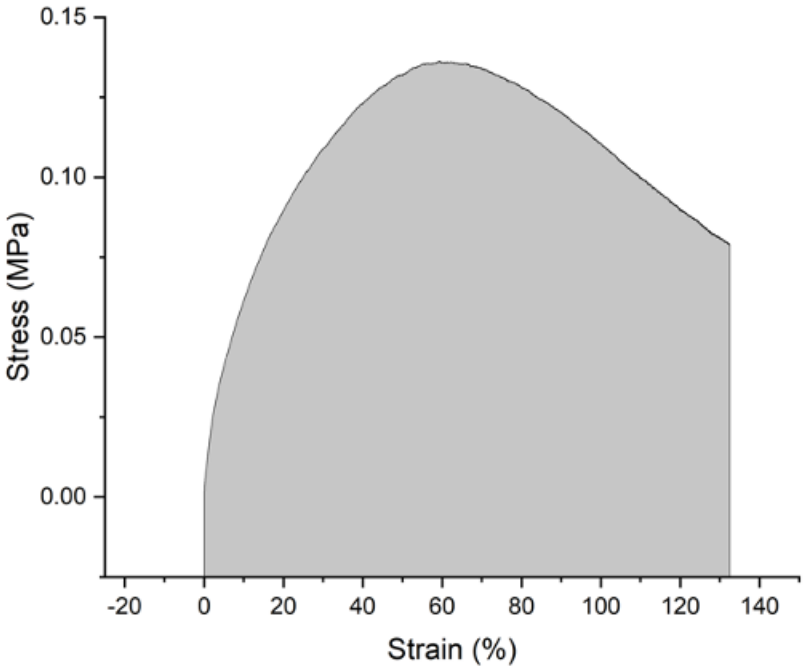

Figure 6.31: Integration for Toughness of **[6.1-block-6.2]$_{24}$** ($\bar{x}$ = 14.01497 ± 5.40606 J/m^3)

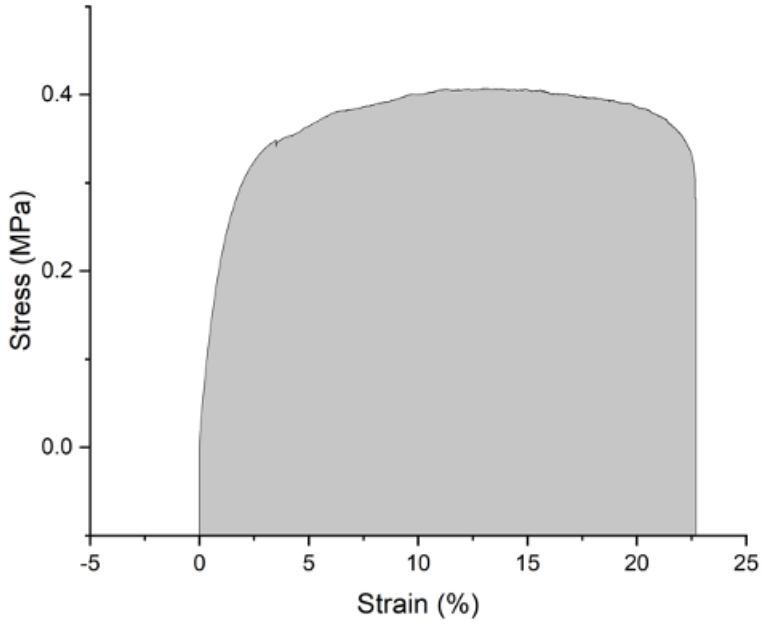

Figure 6.32: Integration for Toughness of **[6.1-block-6.2]$_{29}$** ($\bar{x}$ = 11.74878 ± 3.03905 J/m^3)

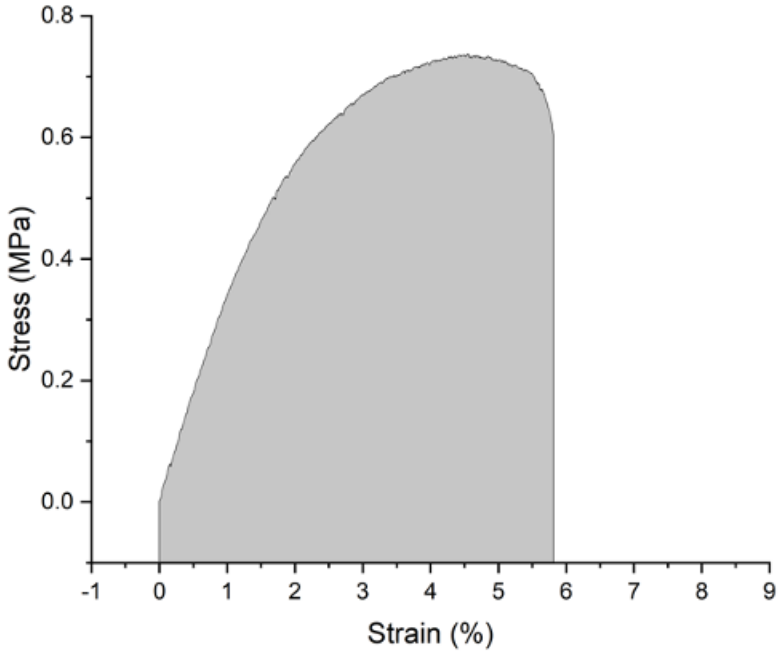

Figure 6.33: Integration for Toughness of **[6.1-block-6.2]$_{32}$** ($\bar{x}$ = 1.71634 ± 1.35818 J/m^3)

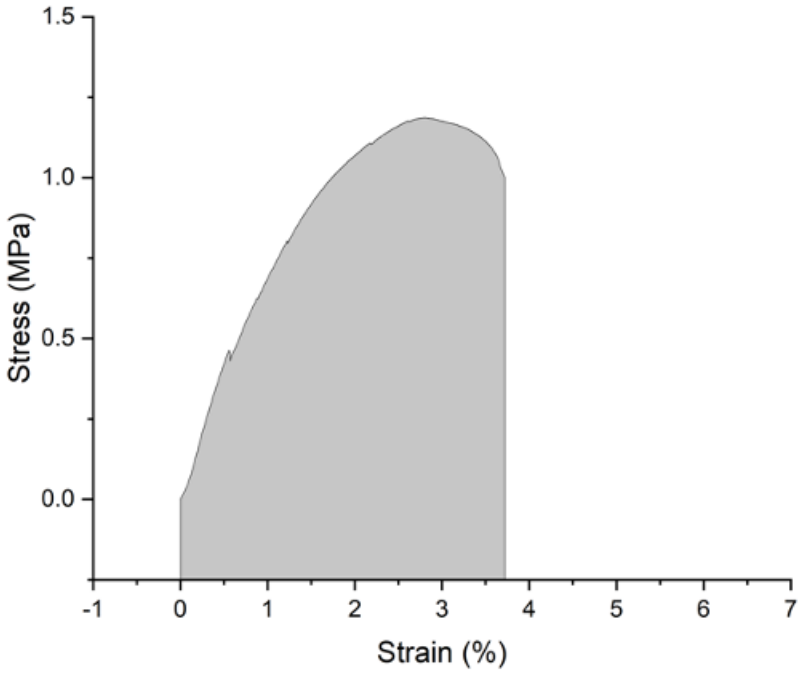

Figure 6.34: Integration for Toughness of **[6.1-block-6.2]$_{34}$** ($\bar{x}$ = 4.25155 ± 0.26631 J/m^3)

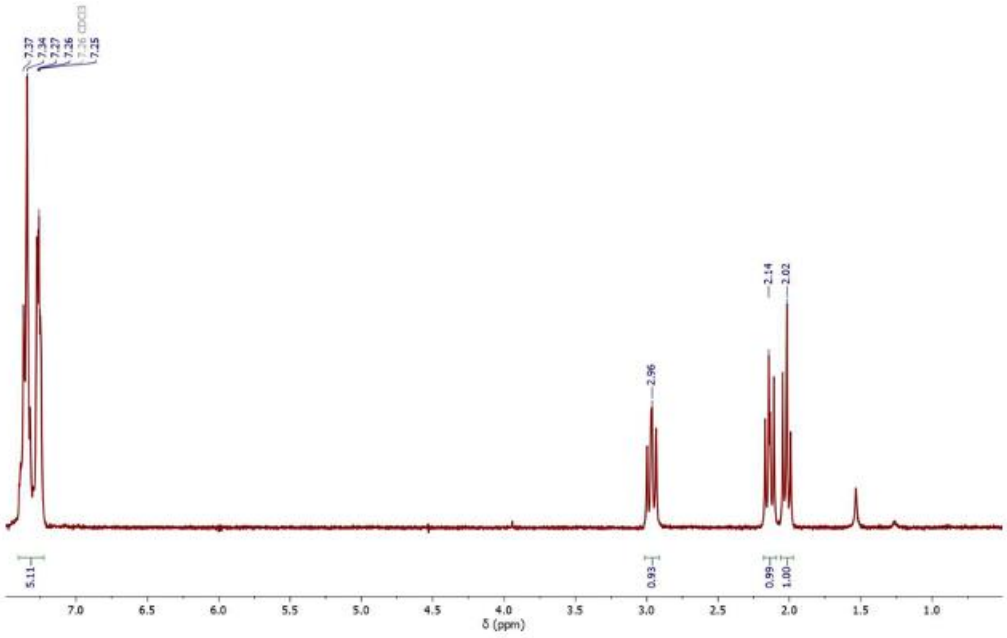

Figure 6.35: Representative ^{1}H NMR Spectrum of **6.6a** in $CDCl_3$.

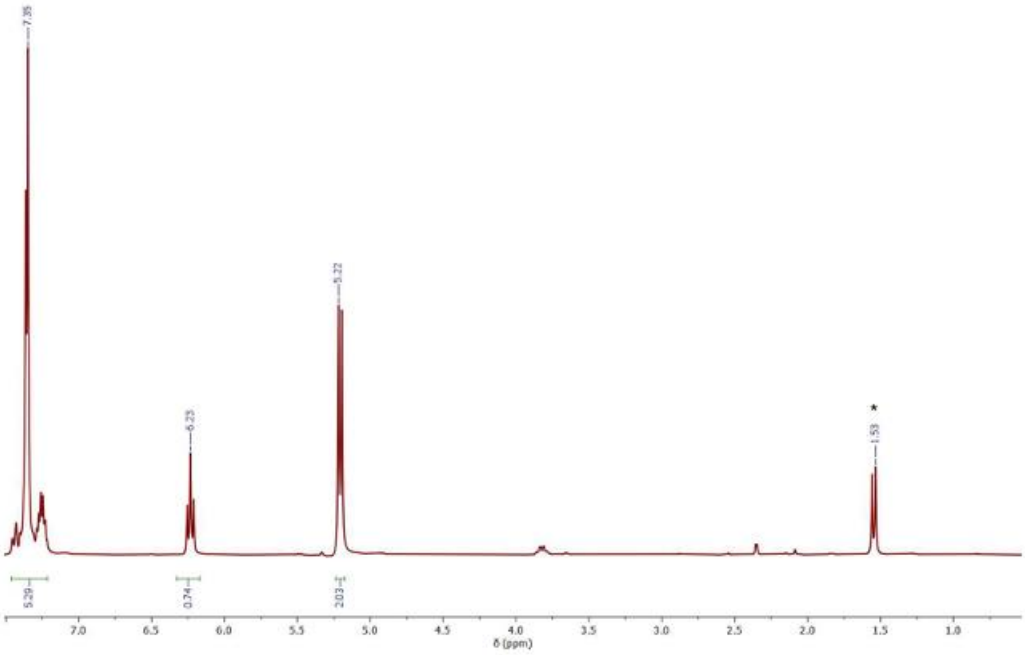

Figure 6.36: Representative ^{1}H NMR Spectrum of **6.6** in $CDCl_3$. Residual solvent: Water: $\delta = 1.53$, denoted by (*).

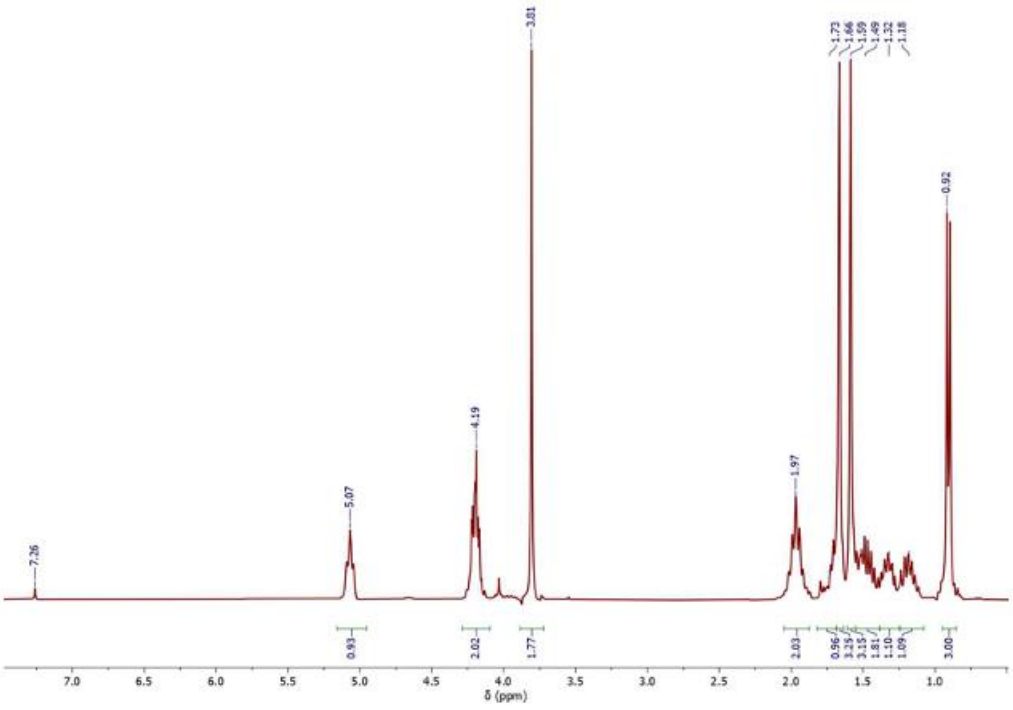

Figure 6.37: Representative ^{1}H NMR Spectrum of **6.9a** in $CDCl_3$

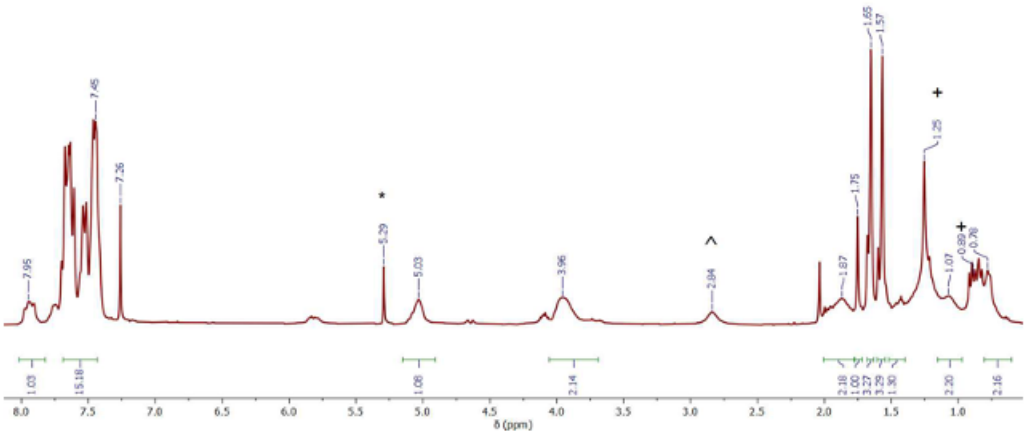

Figure 6.38: Representative ^{1}H NMR Spectrum of **6.9b** in $CDCl_3$. Residual solvents: DCM: δ = 5.29, denoted by (*); DMSO: δ = 2.84, denoted by (^); Hexanes: δ = 1.25, 0.89 denoted by (+)

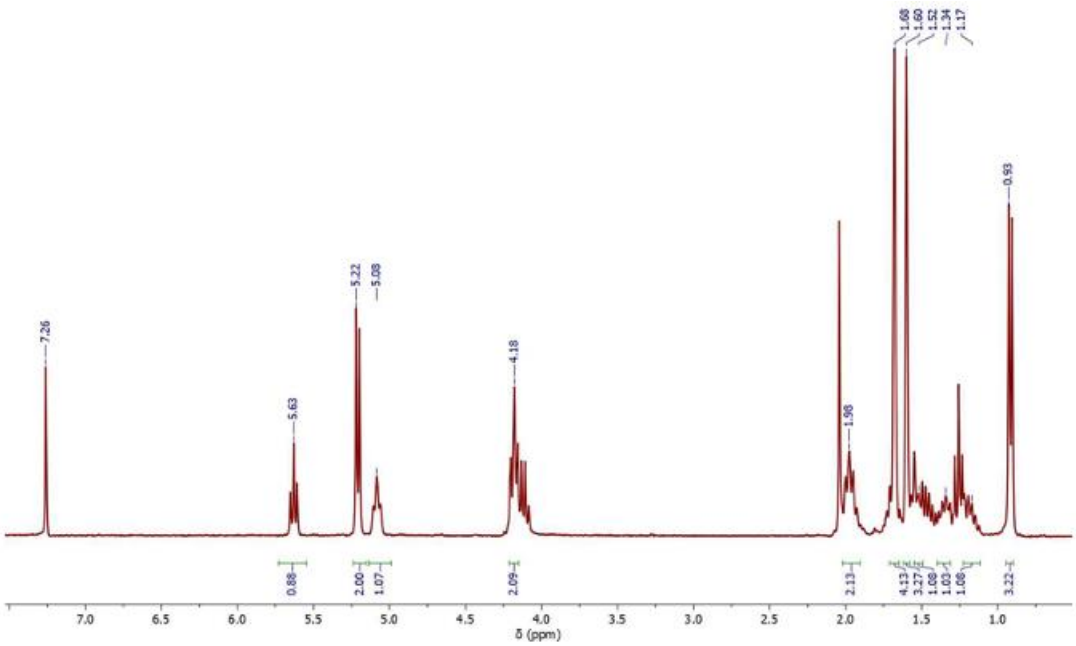

Figure 6.39: Representative ^{1}H NMR Spectrum of **6.9** in $CDCl_3$.

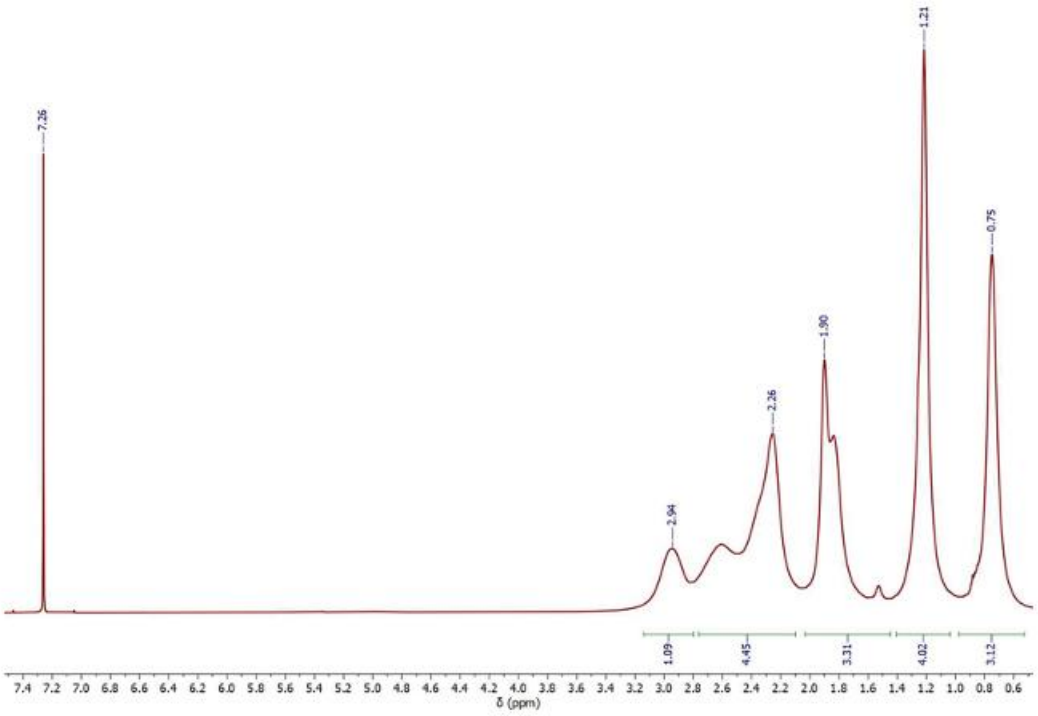

Figure 6.40: Representative ^{1}H NMR Spectrum of **6.3** in $CDCl_3$

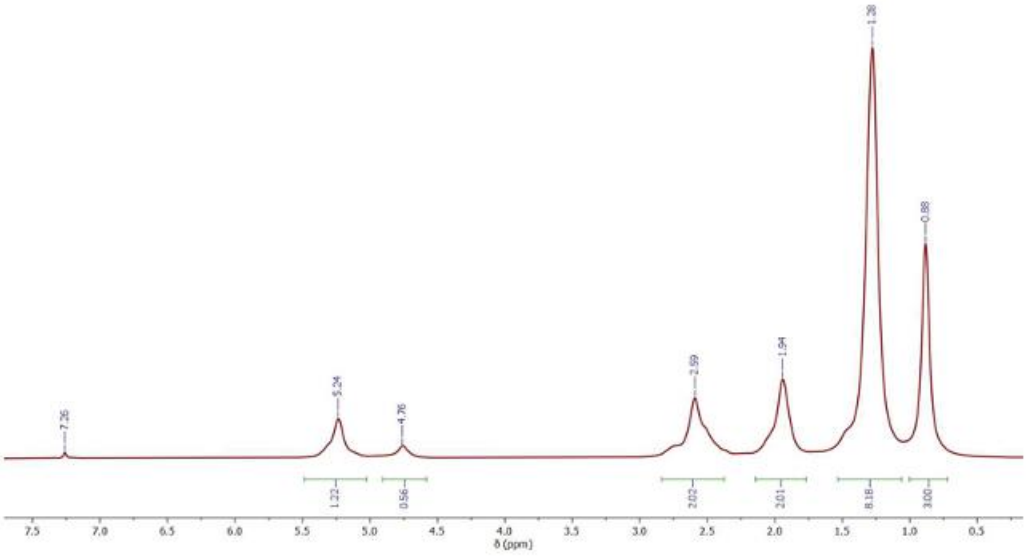

Figure 6.41: Representative ^{1}H NMR Spectrum of **6.4** in $CDCl_3$.

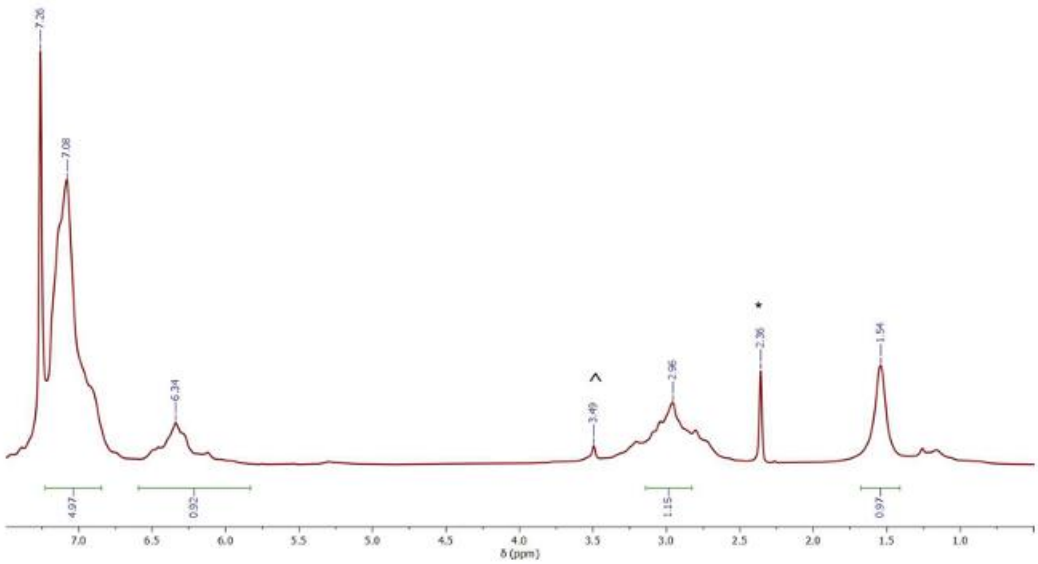

Figure 6.42: Representative ^{1}H NMR Spectrum of **6.7** in $CDCl_3$. Residual Solvents: Toluene: $\delta = 2.36$ denoted by (*); Methanol: $\delta = 3.49$ denoted by (^).

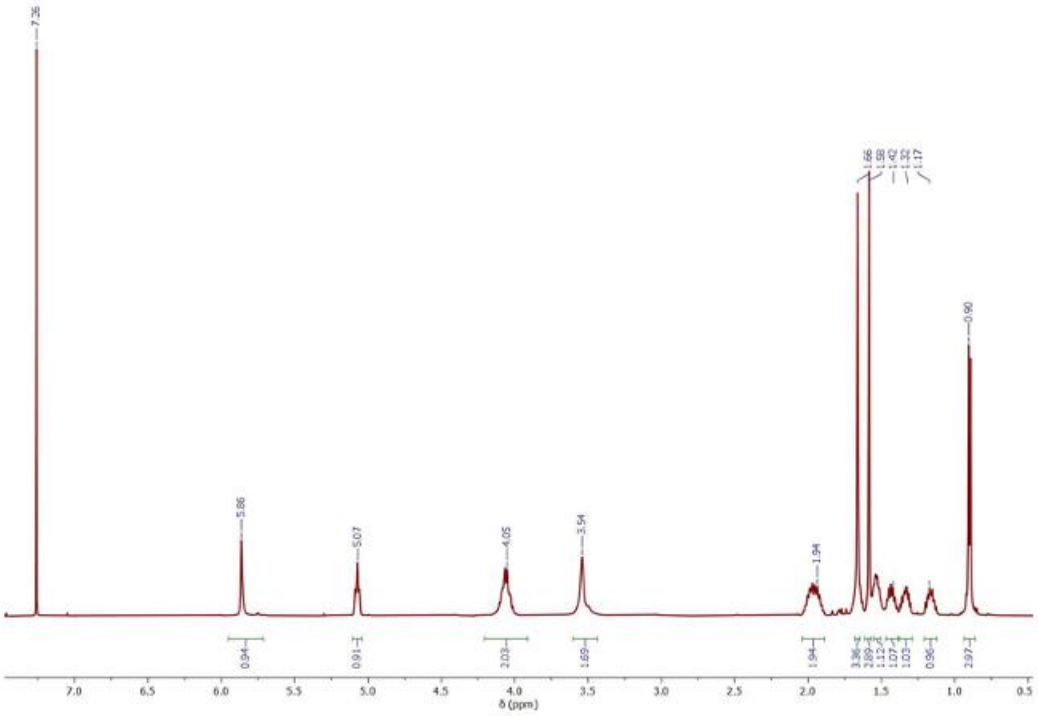

Figure 6.43: Representative ^{1}H NMR Spectrum of **6.10** in $CDCl_3$.

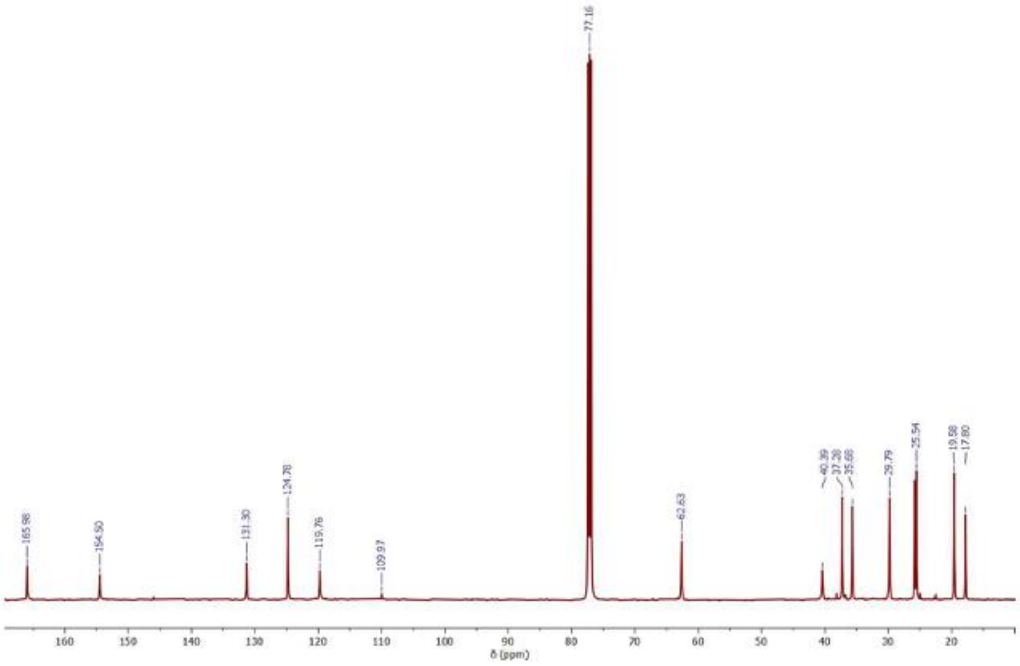

Figure 6.44: Representative ^{13}C NMR Spectrum of **6.10** in $CDCl_3$.

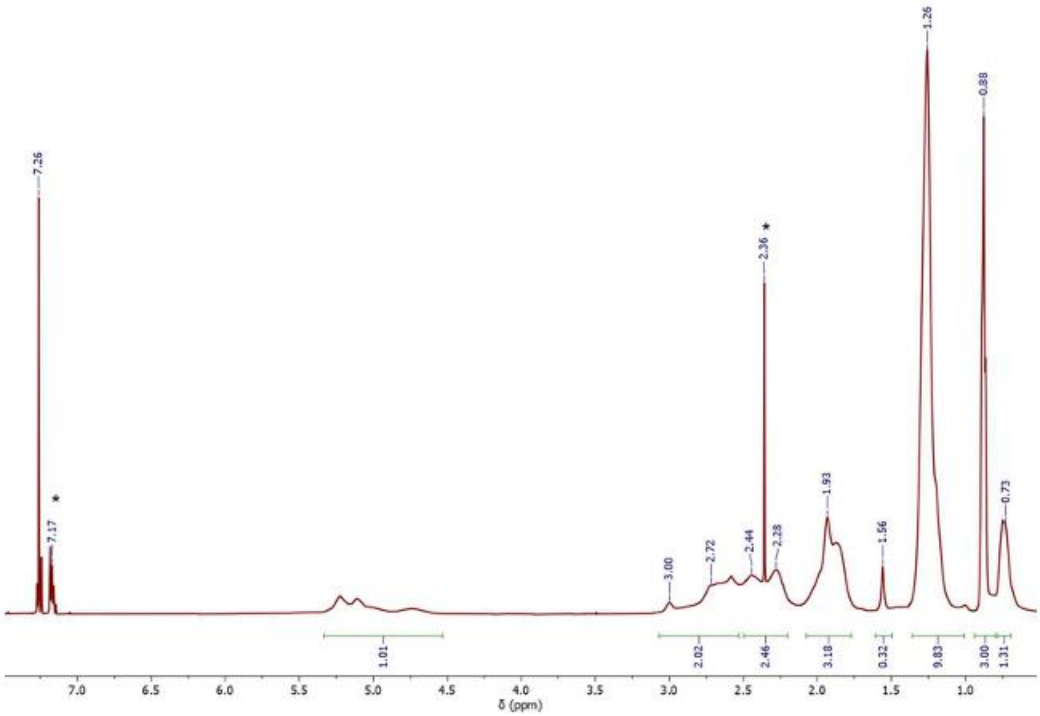

Figure 6.45: Representative ^{1}H NMR Spectrum of **[6.1-co-6.2]$_{30}$** in $CDCl_3$ Residual Solvents: Toluene: δ = 2.36, 7.17 denoted by (*)

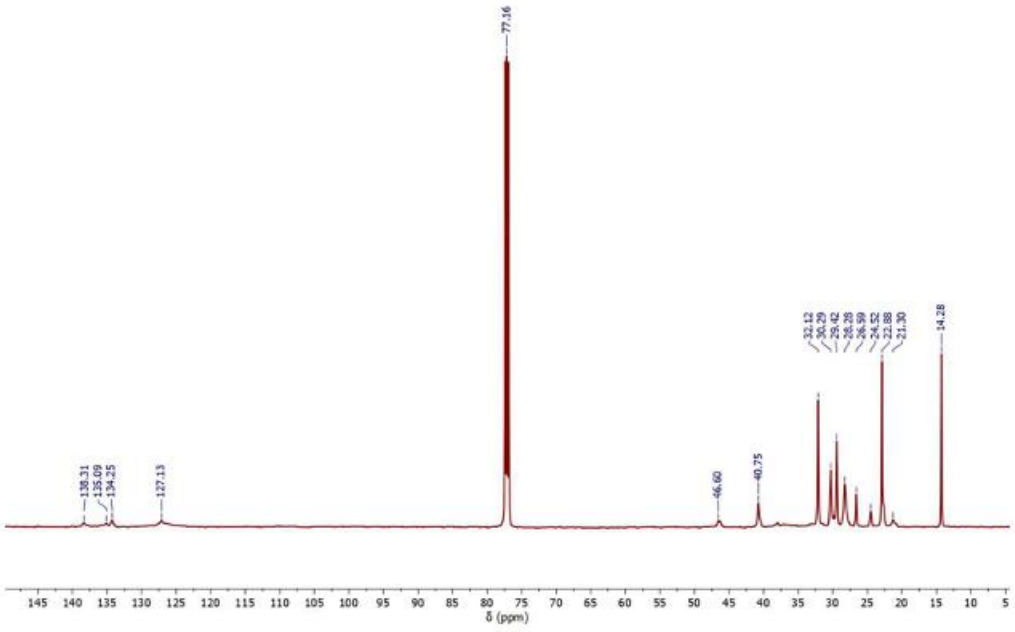

Figure 6.46: Representative ^{13}C NMR Spectrum of **[6.1-co-6.2]$_{30}$** in $CDCl_3$.

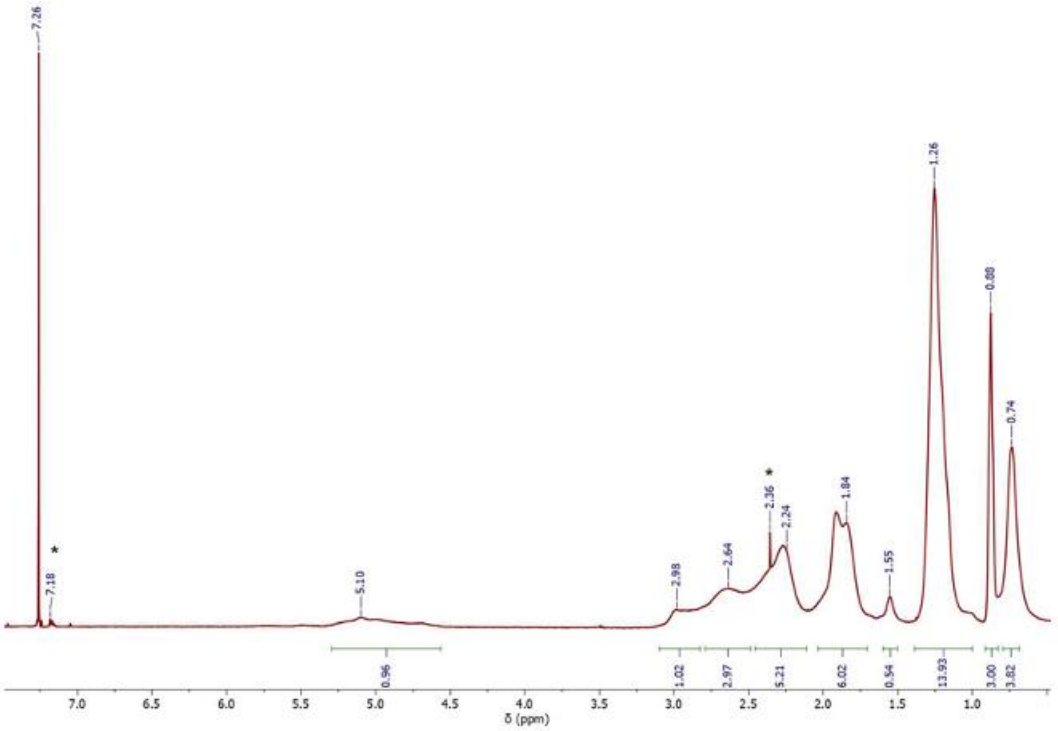

Figure 6.47: Representative ^{1}H NMR Spectrum of **[6.1-co-6.2]$_{56}$** in $CDCl_3$ Residual Solvents: Toluene: $\delta = 2.36, 7.18$ denoted by (*).

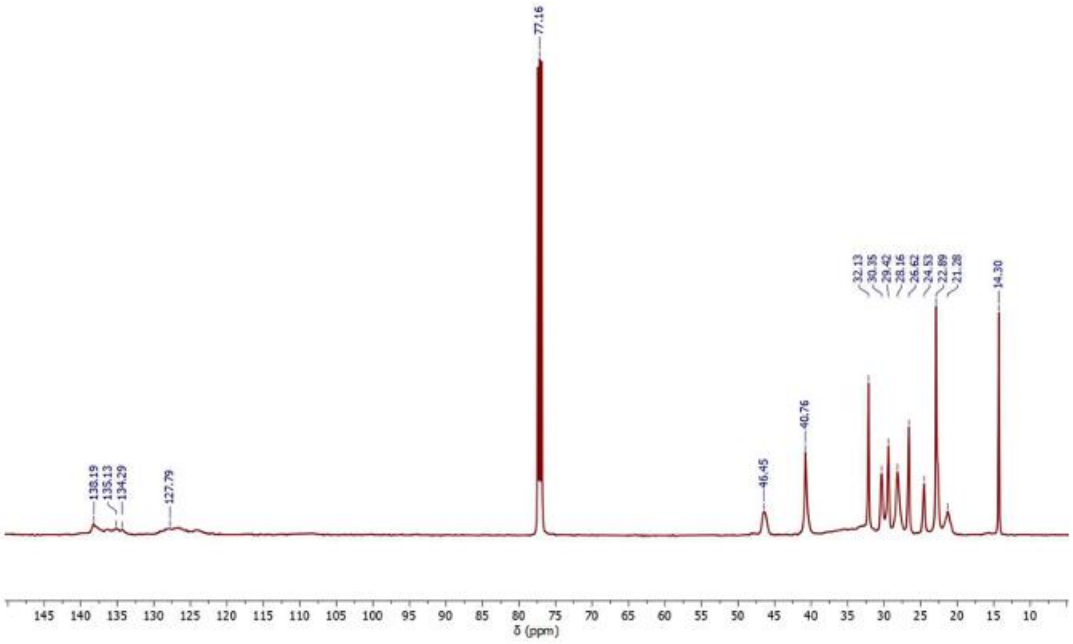

Figure 6.48: Representative ^{13}C NMR Spectrum of **[6.1-co-6.2]$_{56}$** in $CDCl_3$

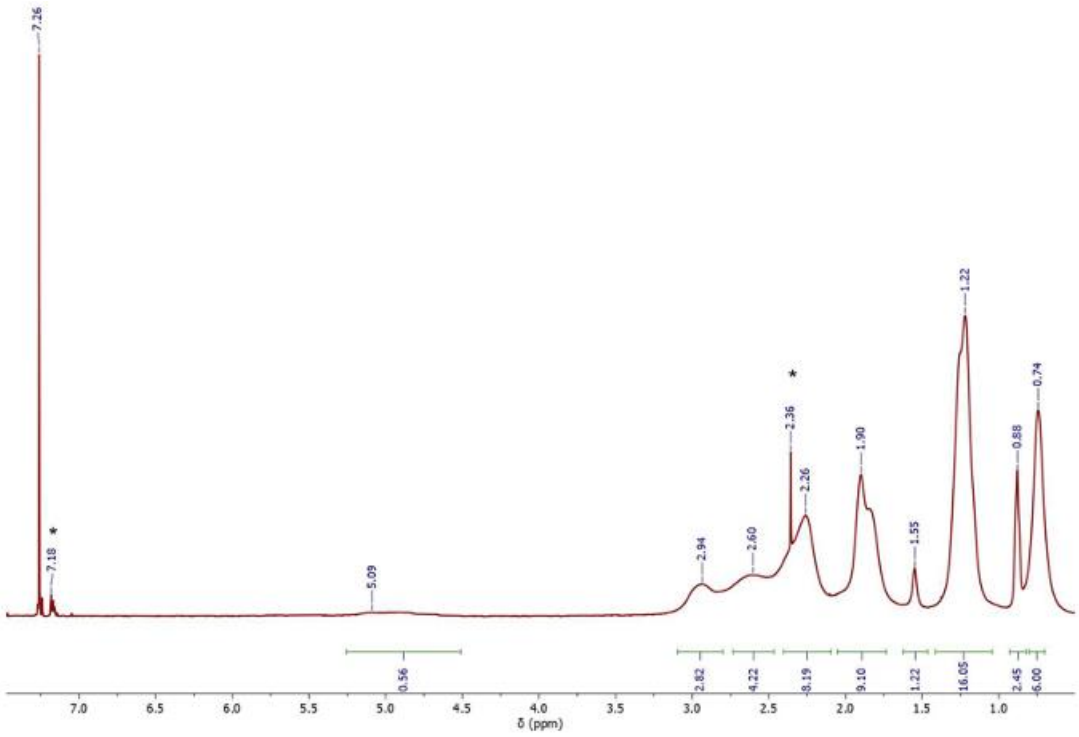

Figure 6. 49: Representative ^{1}H NMR Spectrum of **[6.1-co-6.2]**$_{77}$ in $CDCl_3$ Residual Solvents: Toluene: δ = 2.36, 7.18 denoted by (*)

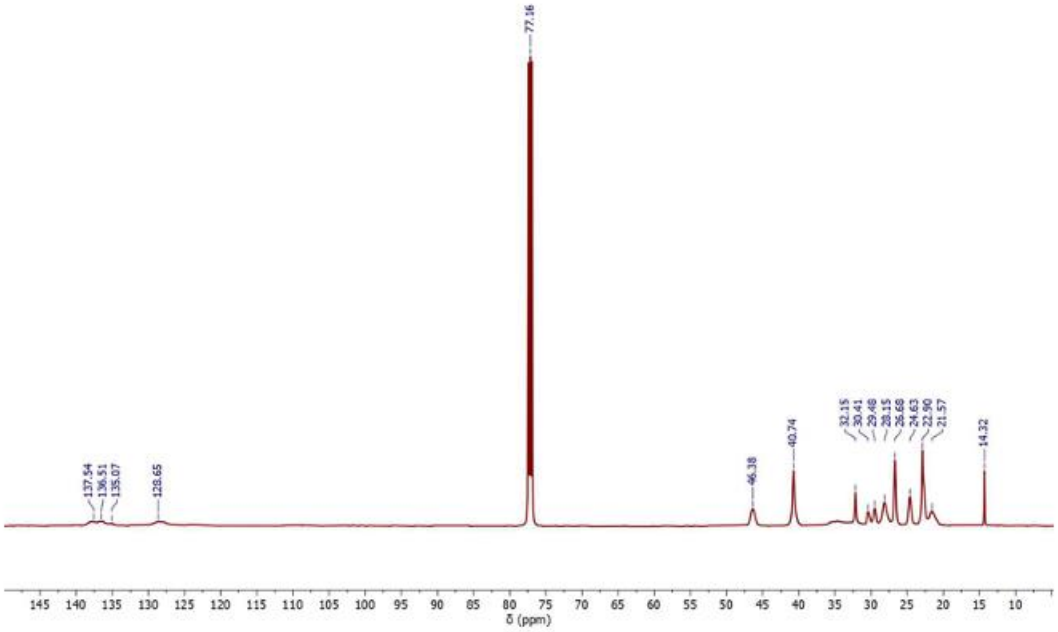

Figure 6.50: Representative ^{13}C NMR Spectrum of **[6.1-co-6.2]$_{77}$** in $CDCl_3$

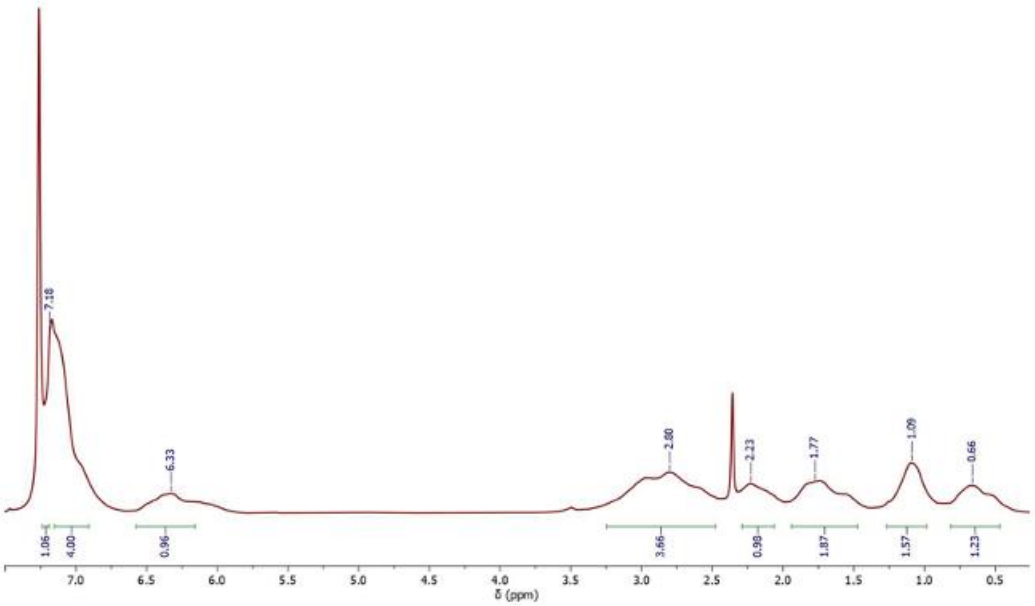

Figure 6.51: Representative ^{1}H NMR Spectrum of **[6.1-co-6.6]$_{20}$** in $CDCl_3$

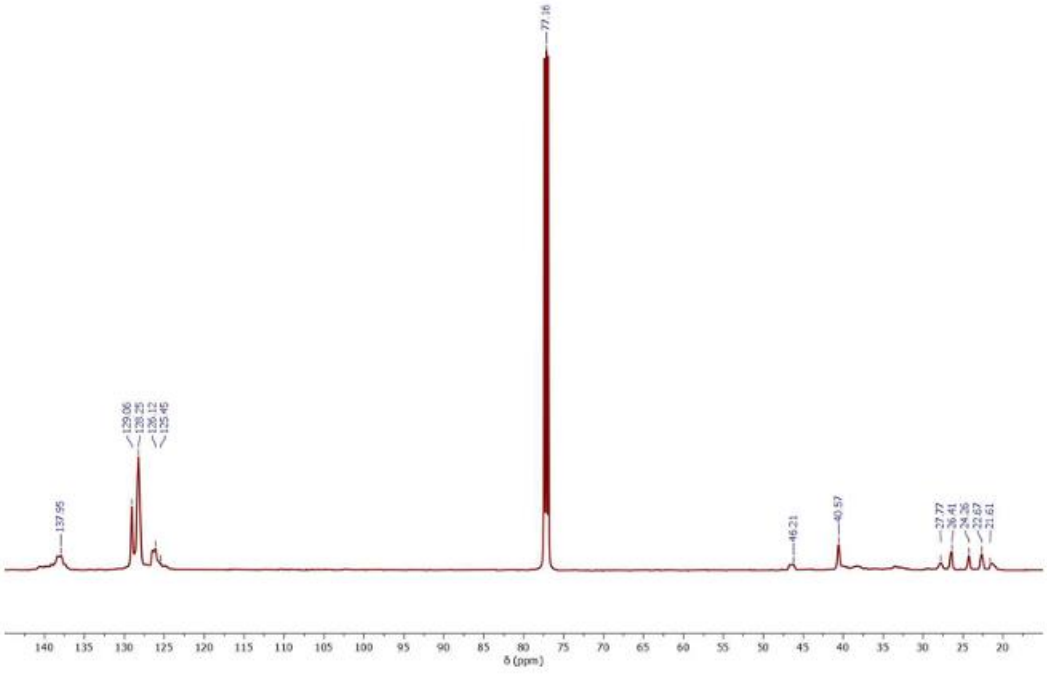

Figure 6.52: Representative ^{13}C NMR Spectrum of **[6.1-co-6.6]$_{20}$** in $CDCl_3$

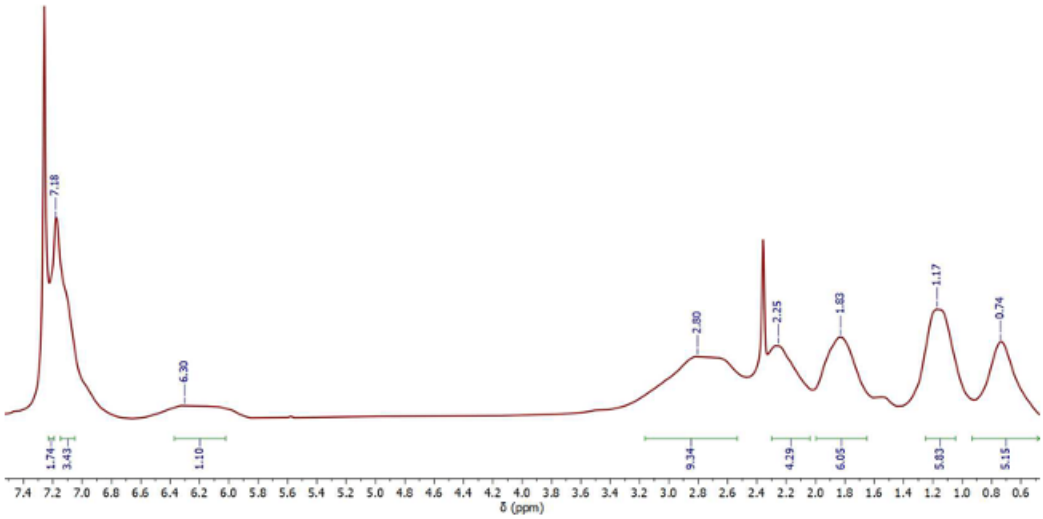

Figure 6.53: Representative ^{1}H NMR Spectrum of **[6.1-co-6.6]$_{44}$** in $CDCl_3$

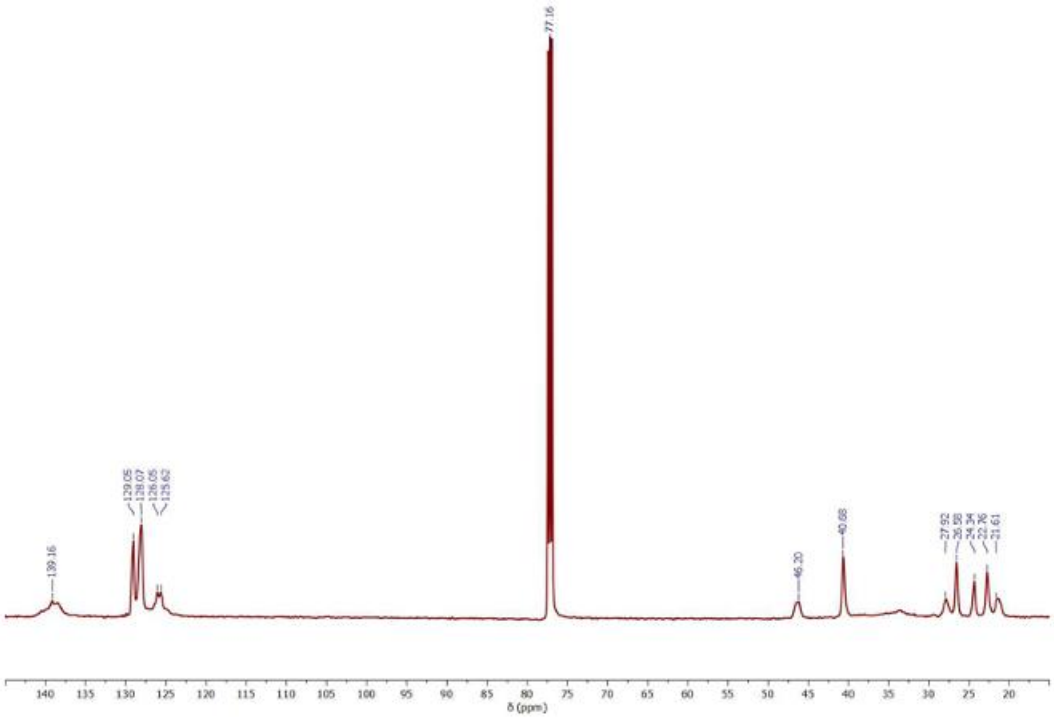

Figure 6.54: Representative ^{13}C NMR Spectrum of **[6.1-co-6.6]$_{44}$** in $CDCl_3$

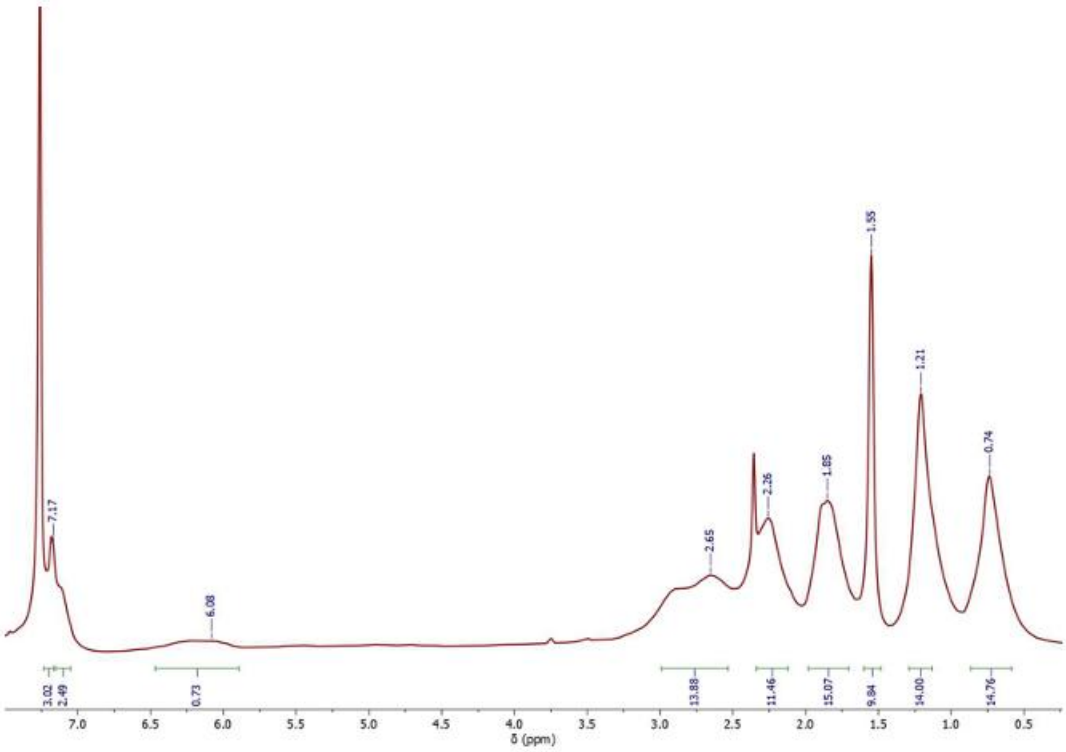

Figure 6.55: Representative ^{1}H NMR Spectrum of **[6.1-co-6.6]$_{70}$** in $CDCl_3$

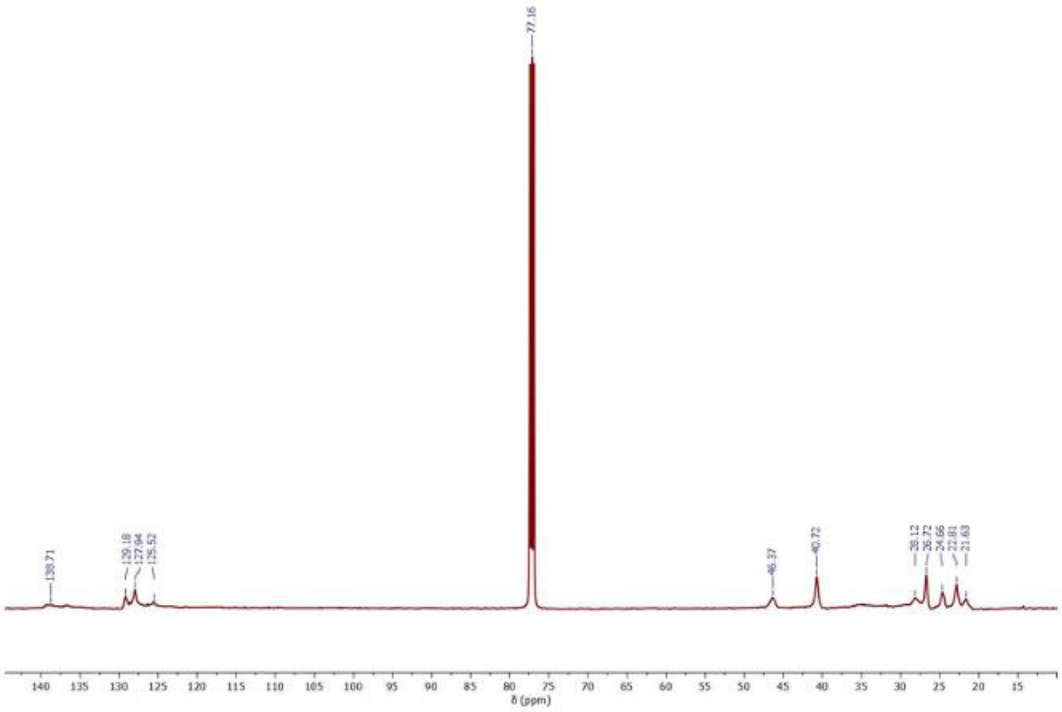

Figure 6.56: Representative ^{13}C NMR Spectrum of **[6.1-co-6.6]$_{70}$** in $CDCl_3$

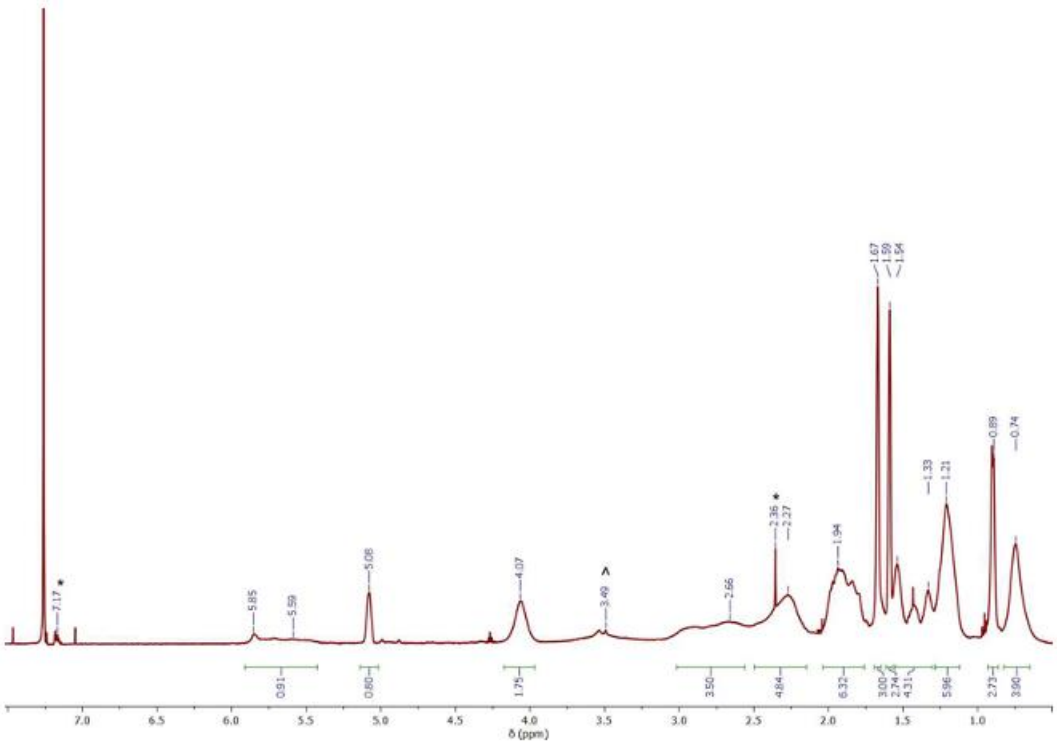

Figure 6.57: Representative ^{1}H NMR Spectrum of **[6.1-co-6.9]$_{65}$** in $CDCl_3$ Residual Solvents: Toluene: $\delta = 2.36, 7.17$ denoted by (*), Methanol $\delta = 3.49$, denoted by (^)

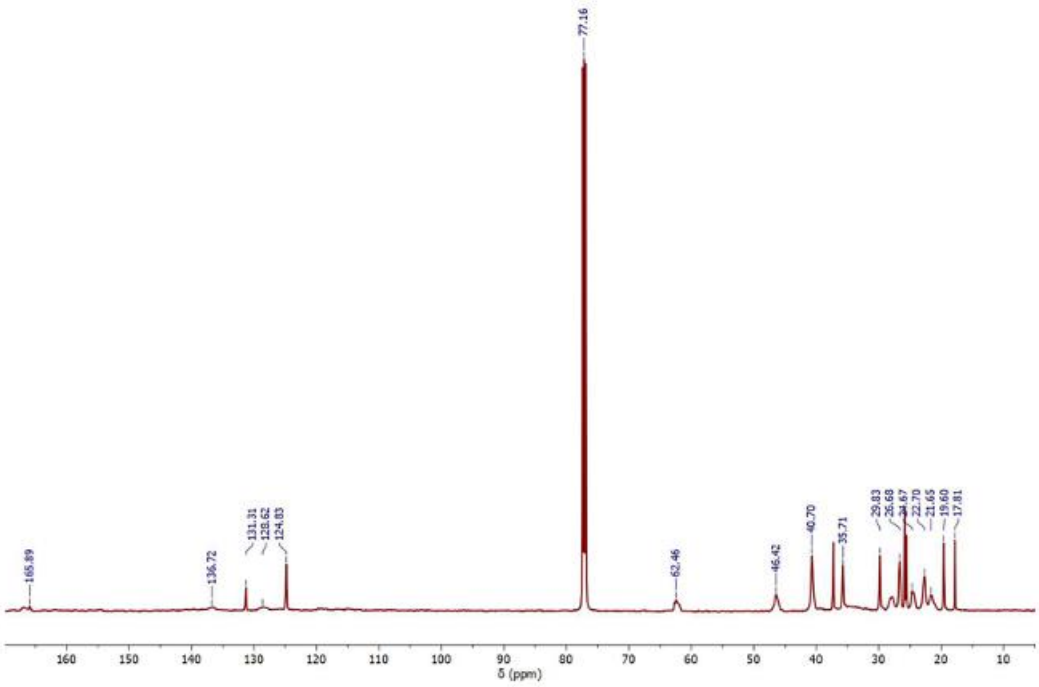

Figure 6.58: Representative ^{13}C NMR Spectrum of **[6.1-co-6.9]$_{65}$** in $CDCl_3$

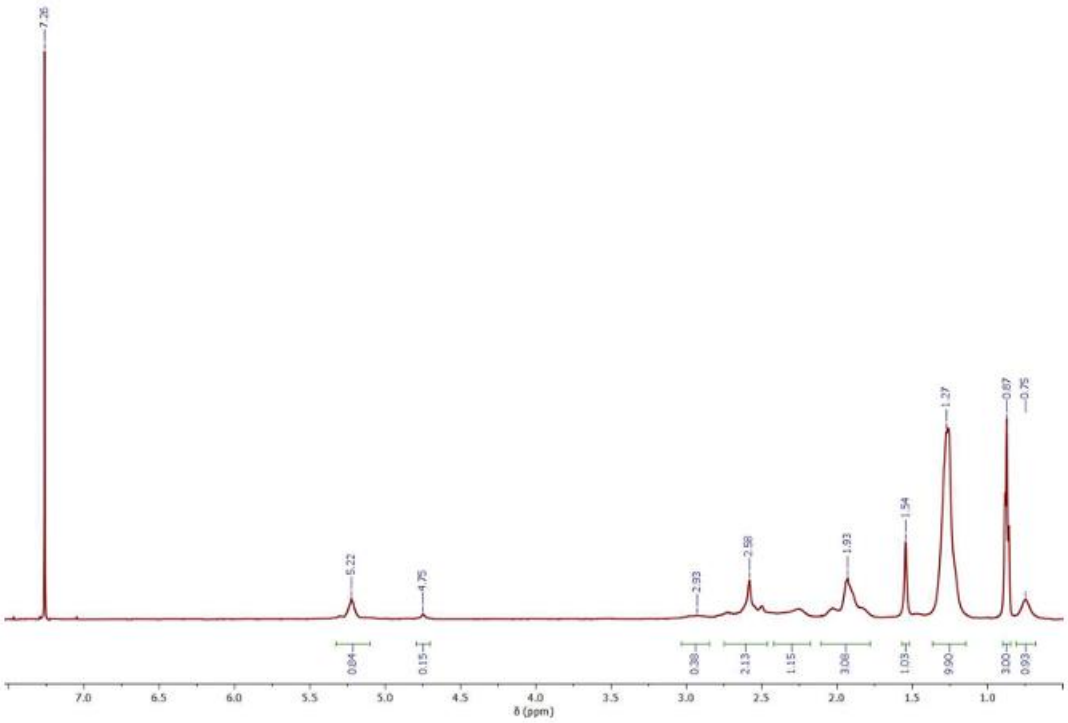

Figure 6.59: Representative ^{1}H Spectrum of **[6.1-block-6.2]$_{25}$** in $CDCl_3$

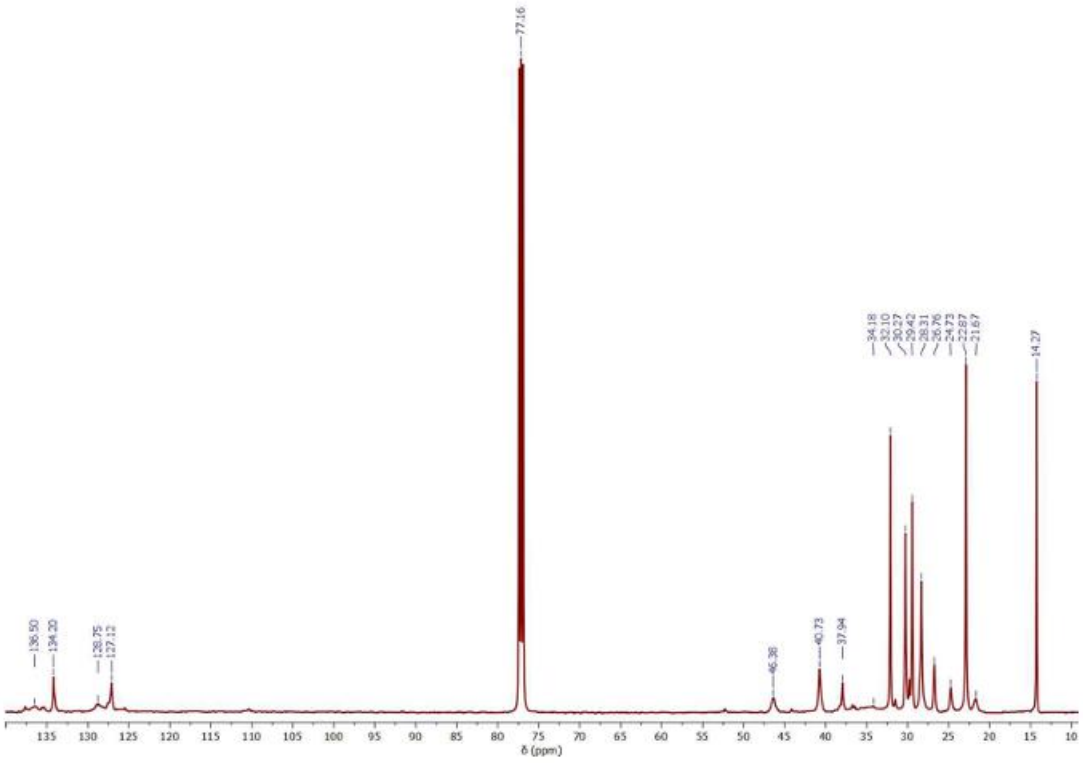

Figure 6.60: Representative ^{13}C NMR Spectrum of **[6.1-block-6.2]$_{25}$** in $CDCl_3$

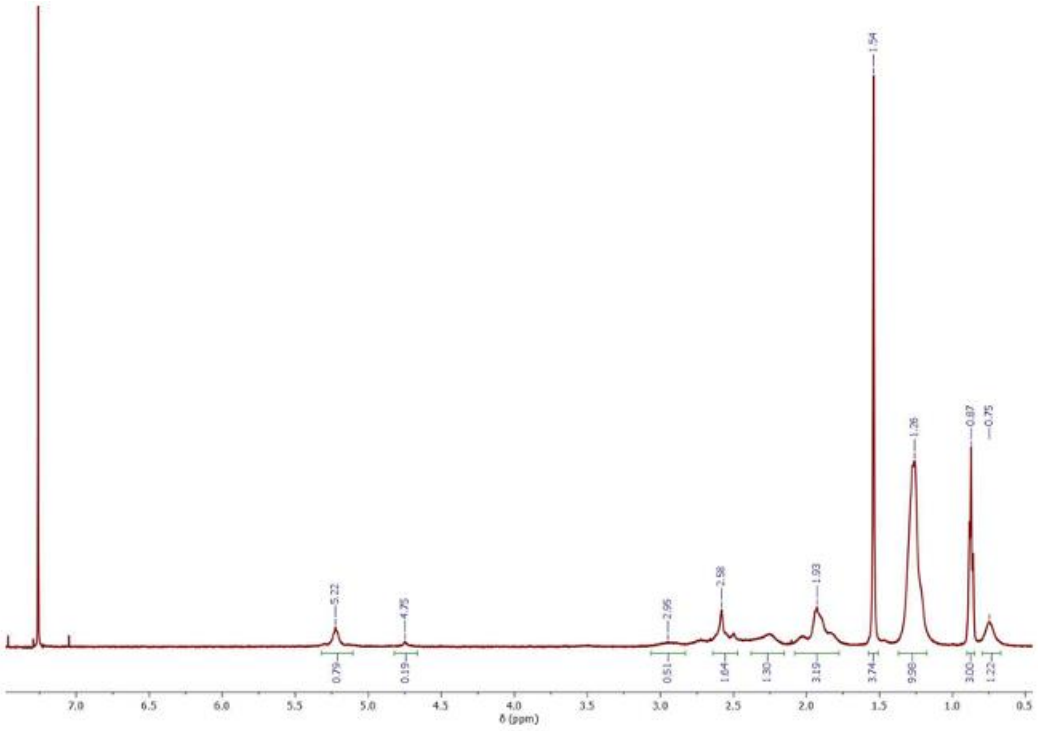

Figure 6.61: Representative ^{1}H NMR Spectrum of **[6.1-block-6.2]$_{30}$** in $CDCl_3$.

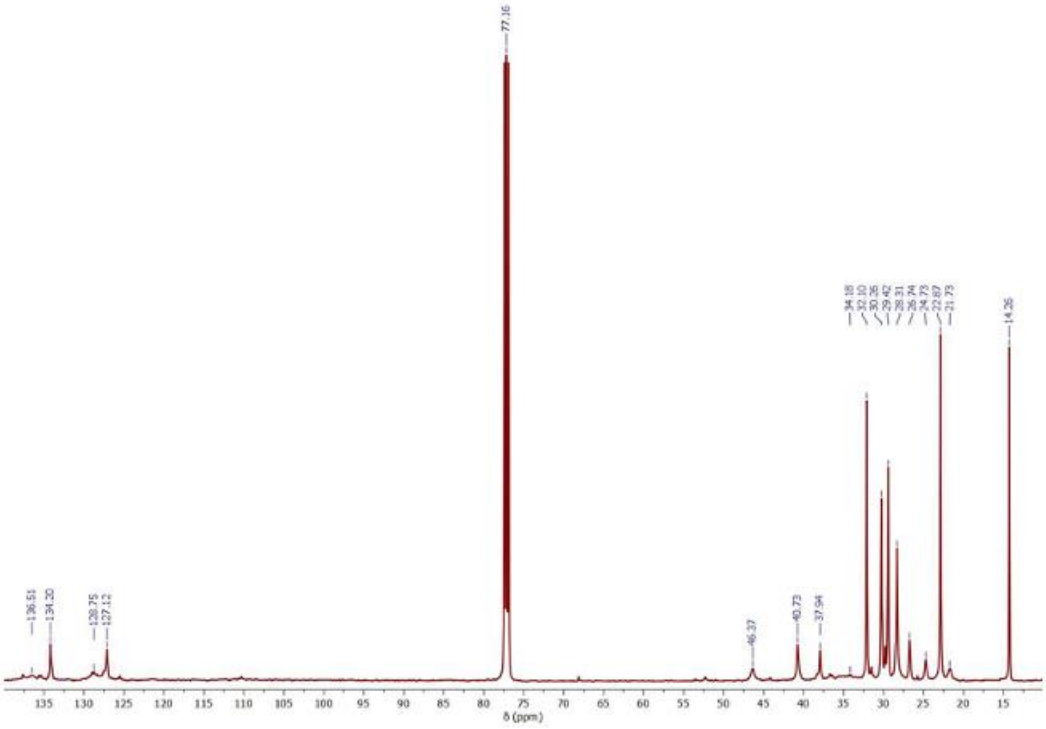

Figure 6.62: Representative ^{13}C NMR Spectrum of **[6.1-block-6.2]$_{30}$** in $CDCl_3$.

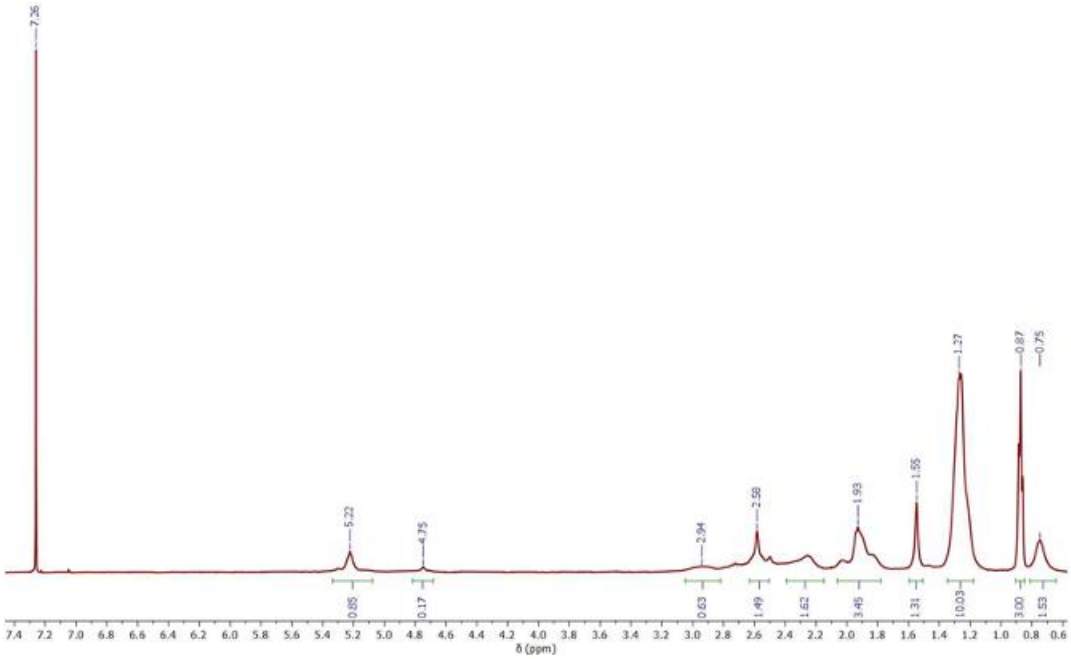

Figure 6.63: Representative ^{1}H NMR Spectrum of **[6.1-block-6.2]$_{35}$** in $CDCl_3$

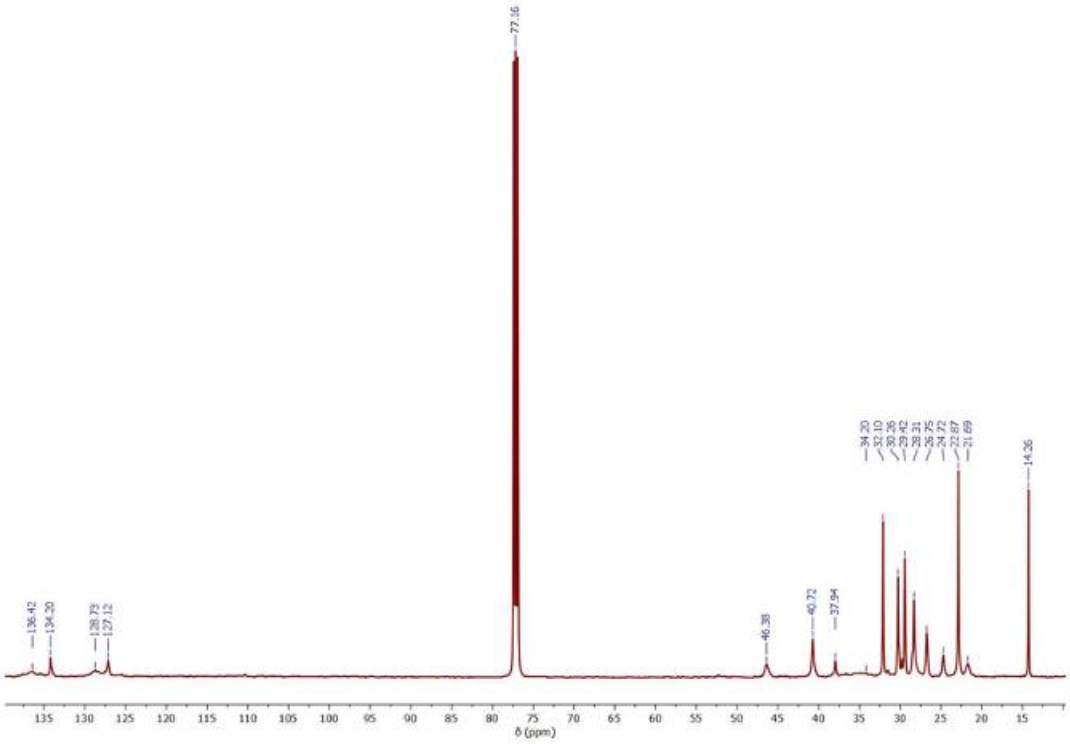

Figure 6.64: Representative ^{13}C NMR Spectrum of **[6.1-block-6.2]$_{35}$** in $CDCl_3$

Table 6.4: Fox Analysis of **[6.1-co-6.2]$_c$** Series Polymers

Polymer	Weight Fraction 1	Weight Fraction 2	T_g^{exp}	T_g^{theo}
4	0	1	-69.5	
[6.1-co-6.2]$_{30}$	0.38	0.62	-7.5	-14.6
[6.1-co-6.2]$_{56}$	0.6	0.4	83.6	32.8
[6.1-co-6.2]$_{77}$	0.8	0.4	172.5	94.6
3	1	0	187	

Table 6.5: Gordon Taylor Analysis of **[6.1-co-6.2]$_c$** Series Polymers

Polymer	Weight Fraction 1	Weight Fraction 2	T_g^{exp}	T_g^{theo}
4	0	1	-69.5	
[6.1-co-6.2]$_{30}$	0.38	0.62	-7.5	23.1
[6.1-co-6.2]$_{56}$	0.6	0.4	83.6	79.3
[6.1-co-6.2]$_{77}$	0.8	0.4	172.5	132.3
3	1	0	187	

Table 6.6: Fox Analysis of **[6.1-co-6.6]$_c$** Series Polymers

Polymer	Weight Fraction 1	Weight Fraction 2	T_g^{exp}	T_g^{theo}
7	0	1	99	
[6.1-co-6.6]$_{20}$	0.242	0.758	109	117.1
[6.1-co-6.6]$_{44}$	0.501	0.499	123.6	138.4
[6.1-co-6.6]$_{70}$	0.749	0.251	149.8	161.2
3	1	0	187	

Table 6.7: Gordon Taylor Analysis of **[6.1-co-6.6]$_c$** Series Polymers

Polymer	Weight Fraction 1	Weight Fraction 2	T_g^{exp}	T_g^{theo}
7	0	1	99	
[6.1-co-6.6]$_{20}$	0.242	0.758	109	136.1
[6.1-co-6.6]$_{44}$	0.501	0.499	123.6	160.2
[6.1-co-6.6]$_{70}$	0.749	0.251	149.8	175.7
3	1	0	187	

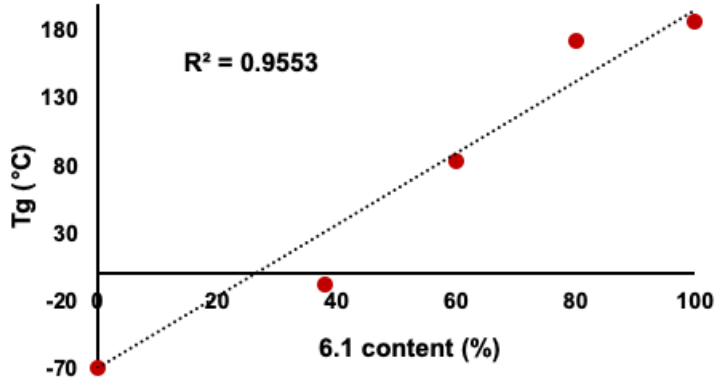

Figure 6.65: T_g vs β-Pinadiene Content for **[6.1-co-6.2]$_c$** Series Polymers

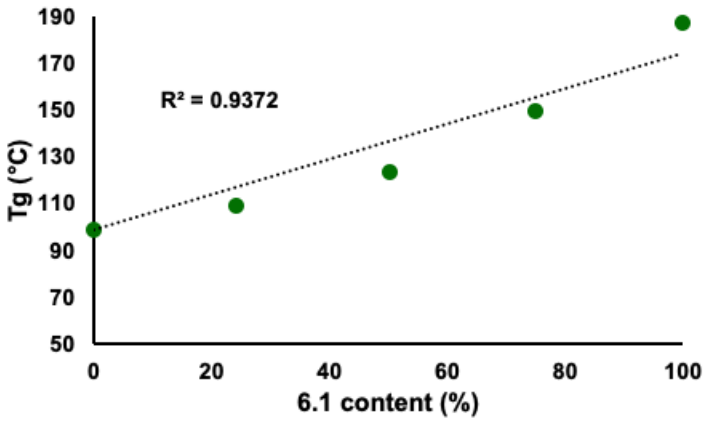

Figure 6.66: T_g vs β-Pinadiene Content for **[6.1-co-6.6]$_c$** Series Polymers

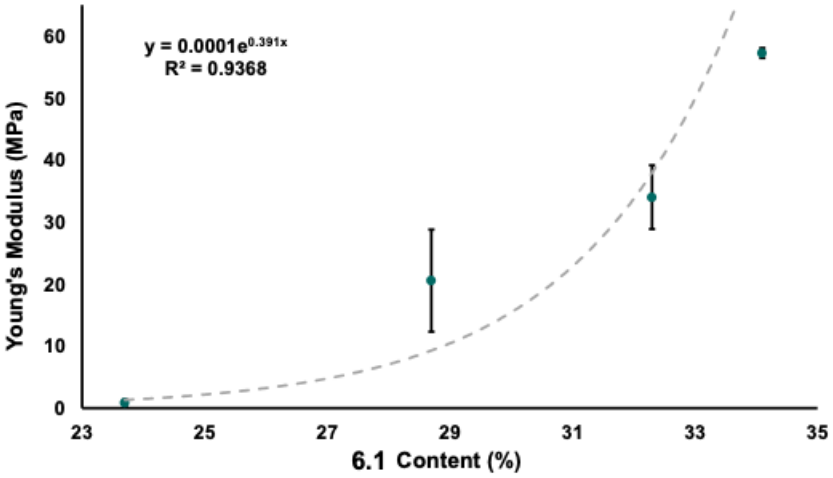

Figure 6.67: Young's Modulus vs β-Pinadiene Content for **[6.1-block-6.2]$_c$** Series Polymers

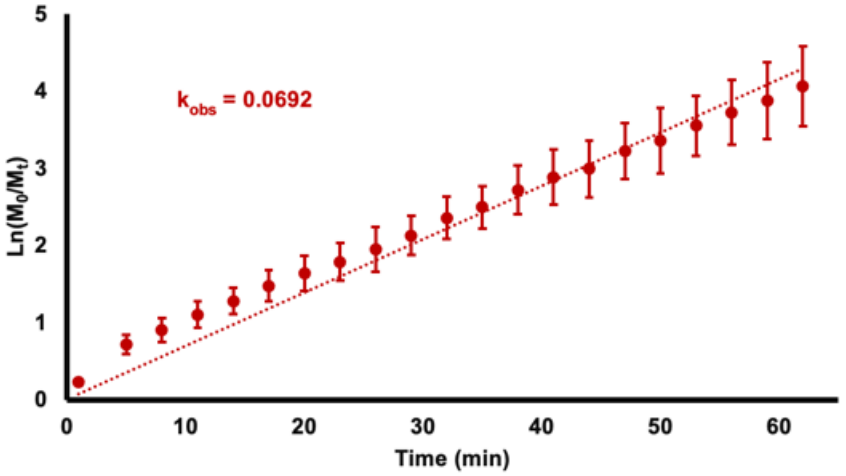

Figure 6.68: Polymerization Kinetics of **6.1**

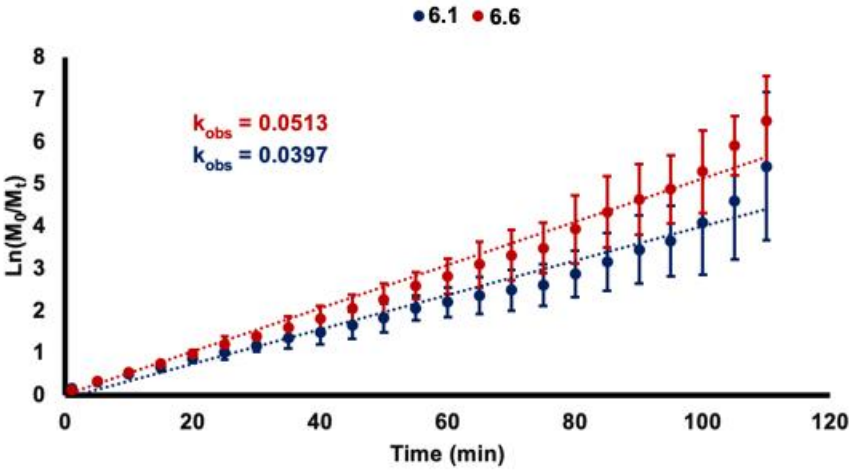

Figure 6.69: Polymerization Kinetics of **[6.1-co-6.6]**

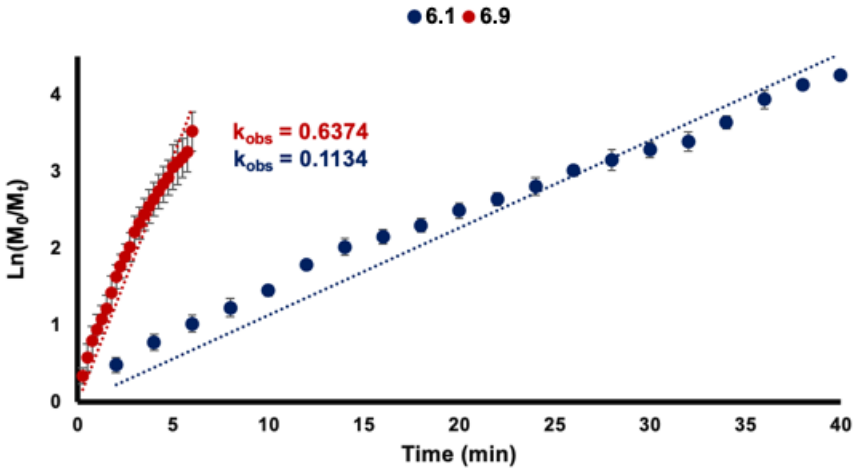

Figure 6.70: Polymerization Kinetics of **[6.1-co-6.9]**

CHAPTER VII: CONCLUSIONS AND OUTLOOK

7.1 Conclusions

Editing the structure of macromolecular substrates will not only alter bulk physical properties (such as T_g, optical transparency, Young's modulus, adhesion, among others) but can also modify chemical reactivity. Such strategies allow for the preparation of materials with bespoke properties and reactivities. Similarly, methods that facilitate the synthesis of structurally complex readily polymerizable monomers, which has been longstanding synthetic challenge, allow for further investigations of their innate structure property relationships. The first chapter of this dissertation provides the motivation for editing of both polymer and monomer substrates, accompanied by numerous examples in the literature which have demonstrated the utility of such editing methodologies.

Employing underexplored editing strategies that incorporate reactive moieties (i.e., allenes) or generate high energy species (e.g., radical ions) could allow for the preparation of 2nd generation daughter polymers or provide a pathway for degradation (via β-scission). Previous strategies to afford polyallenamers suffered from limitations such as poor molecular weight control, poor substrate scope, and incompatibility toward advanced architectures (i.e., block copolymers). Moreover, generating high-energy species along polymer backbones has been largely limited to synthetic electrochemistry, with only one class of photoredox transformations being reported for macromolecules (i.e., decarboxylation).

Polymers composed of rigid carbocyclic moieties and acyclic units demonstrate a linear relationship with respect to cyclic unit content (i.e., Fox behavior). However, polymerizing monomers with cyclic moieties is challenging, and the available monomer

scope is limited. As such, developing monomer editing methods which expand the current scope of available candidates is desirable. Herein, I present my contributions to the world's understanding of polymer and monomer editing methodologies.

My first project (Chapter II) explores how the installation of allenes, in a post-synthetic fashion, alters bulk physical properties and enhances the chemical reactivity. We found that allenes could be incorporated throughout a *cis*-polynorbornene scaffold in near quantitative conversion. These materials exhibited unique photophysical properties and were amenable to further elaborations. However, poor control of the starting molecular weight, and the stochastic nature of the *gem*-dihalocyclopropantion step precluded the synthesis of advanced architectures. Despite these limitations, this study demonstrated the utility of polyallenamers. Chapter III focused on improving our previous methodology by polymerizing a monomer with a "masked" allene. This allowed us to access polyallenamers with controlled molecular weights, and prepare block-like copolymers via judicious co-monomer selection. Furthermore, reduction of the residual olefin allowed us to investigate how photocuring of the allene units would modulate mechanical properties. Moving beyond allenes, Chapter IV detailed how single-electron oxidations, via excited state organic photoredox catalysts, promote the degradation and functionalization of various polyalkenamers. We found that this SEPE strategy allowed to access materials with a 96% reduction in molar mass. Furthermore, this chemistry could be conducted using natural sunlight, and extending the duration of irradiation facilitated a 99.5% reduction in molar mass. The high energy species could also be trapped with various nucleophiles such as alcohols, carboxylic acids, azides, and thiols to afford functionalized motifs.

Chapter V highlighted how cyclic and acyclic allenes could be leveraged to prepare congeners of COC materials via a monomer editing strategy which converts olefins to allenes. We found that the polymerization of the monomers proceeded in a living manner, and that cyclic allenes polymerized much faster than the acyclic analogue. We also determined that increasing the cyclic content led to a dramatic increase in mechanical properties (i.e., Young's Modulus) consistent with prior COC findings. Lastly, Chapter VI expanded this monomer editing methodology to naturally sourced terpenoids. We observed that copolymers possessing a pinane core, which is structurally analogous to norbornene, exhibited trends consistent with previous COCs (i.e., a linear correlation regarding T_g). Furthermore, we could leverage this strategy to incorporate monomers that are particularly synthetically challenging using traditional routes such as a congener of styrene (1-phenylallene). Moreover, the predictability observed across multiple copolymer systems allowed us to determine the T_g of a copolymer comprised of a polar co-unit.

7.2 Future Outlook

The work presented in this dissertation details how a union between synthetic methodology and polymer chemistry can expand the scope of available polymer and monomer editing strategies. This was accomplished through the investigation of underexplored functionalities and reaction manifolds to afford polymers/monomers with bespoke reactivities and properties. While our early efforts regarding polyallenamers have already inspired others to pursue alternative methods to access these intriguing materials, we have envisioned myriad pathways that our work could be expounded upon.

Regarding polyallenamers, we have discussed potential studies regarding their fluorescent properties. Since we have shown that electron deficient arenes (i.e., nitrobenzene) can “turn off” the fluorescence, we were curious if this mechanism is selective in nature. As such, analyte selectivity could further situate polyallenamers as a potential class of stimuli responsive materials. Furthermore, the abundance of available transition metal catalyzed transformations positions polyallenamers as modular platform to access a diverse library of daughter polymers. Finally, we have posited that exploring other methods for polyallenamer synthesis, such eliminations and propargyl rearrangements of enantiopure starting materials might yield allenes with defined stereochemistries (i.e., helical polymers), which could serve as chiral membranes or have unique physical properties. As for photoediting of macromolecular scaffolds, our lab is currently investigating methods toward the photoredox mediated dechlorination and functionalization of polyvinylchloride. Furthermore, recent C-H activations of small molecule alkanes disclosed by the Nicewicz group suggest that this strategy could be leveraged toward the editing of polyolefins such as polyethylene and polypropylene.

Finally, our lab is currently developing a library of novel allene based terpenoid monomers with varying structural complexities that will be incorporated into various copolymer architectures. Since these COC congeners have been prepared with a catalyst that exhibits living behavior, we have anticipated that this would be amenable to the synthesis of polymers comprised of high T_g, low T_g, high T_g units (i.e., thermoplastic elastomers). Further studies are also being planned regarding the influence rigid

carbocycles have on mechanical properties, and if reduction of the residual olefins could further influence both properties and processability.

REFERENCES

(1) Mülhaupt, R. Hermann Staudinger and the Origin of Macromolecular Chemistry. *Angew. Chemie Int. Ed.* **2004**, *43* (9), 1054–1063.

(2) Andrews, E. H. Structure-Property Relationships in a Polymer. *Angew. Chemie Int. Ed. English* **1974**, *13* (2), 113–121.

(3) Gabriel, C.; Münstedt, H. Influence of Long-Chain Branches in Polyethylenes on Linear Viscoelastic Flow Properties in Shear. *Rheol. Acta* **2002**, *41* (3), 232–244.

(4) Shinohara, K.; Yanagisawa, M.; Makida, Y. Direct Observation of Long-Chain Branches in a Low-Density Polyethylene. *Sci. Rep.* **2019**, *9* (1), 9791.

(5) Quintanilla, J. Microstructure and Properties of Random Heterogeneous Materials: A Review of Theoretical Results. *Polym. Eng. Sci.* **1999**, *39* (3), 559–585.

(6) Günay, K. A.; Theato, P.; Klok, H. Standing on the Shoulders of Hermann Staudinger: Post-polymerization Modification from Past to Present. *J. Polym. Sci. Part A Polym. Chem.* **2013**, *51* (1), 1–28.

(7) Gauthier, M. A.; Gibson, M. I.; Klok, H.-A. Synthesis of Functional Polymers by Post-Polymerization Modification. *Angew. Chemie Int. Ed.* **2008**, *48* (1), 48–58.

(8) Justynska, J.; Schlaad, H. Modular Synthesis of Functional Block Copolymers. *Macromol. Rapid Commun.* **2004**, *25* (16), 1478–1481.

(9) Yang, S. K.; Weck, M. Modular Covalent Multifunctionalization of Copolymers. *Macromolecules* **2008**, *41* (2), 346–351.

(10) Sessions, L. B.; Cohen, B. R.; Grubbs, R. B. Alkyne-Functional Polymers through Sonogashira Coupling to Poly(4-Bromostyrene). *Macromolecules* **2007**, *40* (6), 1926–1933.

(11) Jacobs, B. P.; Brantley, J. N. Exploring Combinatorial Approaches to Polymer Diversification. *Macromolecules* **2020**, *53* (21), 9287–9293.

(12) Williamson, J. B.; Lewis, S. E.; Johnson, R. R.; Manning, I. M.; Leibfarth, F. A. C−H Functionalization of Commodity Polymers. *Angew. Chemie Int. Ed.* **2019**, *58* (26), 8654–8668.

(13) Blanksby, S. J.; Ellison, G. B. Bond Dissociation Energies of Organic Molecules. *Acc. Chem. Res.* **2003**, *36* (4), 255–263.

(14) Kondo, Y.; García-Cuadrado, D.; Hartwig, J. F.; Boaen, N. K.; Wagner, N. L.; Hillmyer, M. A. Rhodium-Catalyzed, Regiospecific Functionalization of Polyolefins in the Melt. *J. Am. Chem. Soc.* **2002**, *124* (7), 1164–1165.

(15) Ray, A.; Zhu, K.; Kissin, Y. V; Cherian, A. E.; Coates, G. W.; Goldman, A. S. Dehydrogenation of Aliphatic Polyolefins Catalyzed by Pincer-Ligated Iridium Complexes. *Chem. Commun.* **2005**, No. 27, 3388–3390.

(16) Lewis, S. E.; Wilhelmy, B. E.; Leibfarth, F. A. Upcycling Aromatic Polymers through C-H Fluoroalkylation. *Chem. Sci.* **2019**, *10* (25), 6270–6277.

(17) Williamson, J. B.; Czaplyski, W. L.; Alexanian, E. J.; Leibfarth, F. A. Regioselective C−H Xanthylation as a Platform for Polyolefin Functionalization. *Angew. Chemie Int. Ed.* **2018**, *57* (21), 6261–6265.

(18) Fazekas, T. J.; Alty, J. W.; Neidhart, E. K.; Miller, A. S.; Leibfarth, F. A.; Alexanian, E. J. Diversification of Aliphatic C–H Bonds in Small Molecules and

Polyolefins through Radical Chain Transfer. *Science (80-.).* **2022**, *375* (6580), 545–550.
(19) Aravindu, K.; Cloutet, E.; Brochon, C.; Hadziioannou, G.; Vignolle, J.; Robert, F.; Taton, D.; Landais, Y. Poly(Arylene Vinylene) Synthesis via a Precursor Step-Growth Polymerization Route Involving the Ramberg–Bäcklund Reaction as a Key Post-Chemical Modification Step. *Macromolecules* **2018**, *51* (15), 5852–5862.
(20) Srivastava, V. K.; Basak, G. C.; Maiti, M.; Jasra, R. V. Synthesis and Utilization of Epoxidized Polybutadiene Rubber as an Alternate Compatibilizer in Green-Tire Composites. *Int. J. Ind. Chem.* **2017**, *8* (4), 411–424.
(21) Bowser, B. H.; Ho, C.-H.; Craig, S. L. High Mechanophore Content, Stress-Relieving Copolymers Synthesized via RAFT Polymerization. *Macromolecules* **2019**, *52* (22), 9032–9038.
(22) Wu, D.; Lenhardt, J. M.; Black, A. L.; Akhremitchev, B. B.; Craig, S. L. Molecular Stress Relief through a Force-Induced Irreversible Extension in Polymer Contour Length. *J. Am. Chem. Soc.* **2010**, *132* (45), 15936–15938.
(23) Klukovich, H. M.; Kouznetsova, T. B.; Kean, Z. S.; Lenhardt, J. M.; Craig, S. L. A Backbone Lever-Arm Effect Enhances Polymer Mechanochemistry. *Nat. Chem.* **2012**, *5*, 110.
(24) Colclough, T. New Method of Modifying Natural Rubber. *Trans. Inst. Rubber. Ind.* **1962**, *38*, 11.
(25) Lenhardt, J. M.; Black, A. L.; Craig, S. L. Gem-Dichlorocyclopropanes as Abundant and Efficient Mechanophores in Polybutadiene Copolymers under Mechanical Stress. *J. Am. Chem. Soc.* **2009**, *131* (31), 10818–10819.
(26) Fried, A. D.; Wilson, B. J.; Galan, N. J.; Brantley, J. N. Electroediting of Soft Polymer Backbones. *J. Am. Chem. Soc.* **2022**, *144* (20), 8885–8891.
(27) Häußler, M.; Eck, M.; Rothauer, D.; Mecking, S. Closed-Loop Recycling of Polyethylene-like Materials. *Nature* **2021**, *590* (7846), 423–427.
(28) Zeng, X.; Soleilhavoup, M.; Bertrand, G. Gold-Catalyzed Intermolecular Markovnikov Hydroamination of Allenes with Secondary Amines. *Org. Lett.* **2009**, *11* (15), 3166–3169.
(29) Li, C.; Yang, Z.; Wang, L.; Guo, Y.; Huang, Z.; Ma, S. Cobalt-Catalyzed Regio- and Stereoselective Hydroboration of Allenes. *Angew. Chemie Int. Ed.* **2020**, *59* (15), 6278–6283.
(30) Osborne, J. D.; Randell-Sly, H. E.; Currie, G. S.; Cowley, A. R.; Willis, M. C. Catalytic Enantioselective Intermolecular Hydroacylation: Rhodium-Catalyzed Combination of β-S-Aldehydes and 1,3-Disubstituted Allenes. *J. Am. Chem. Soc.* **2008**, *130* (51), 17232–17233.
(31) Khrakovsky, D. A.; Tao, C.; Johnson, M. W.; Thornbury, R. T.; Shevick, S. L.; Toste, F. D. Enantioselective, Stereodivergent Hydroazidation and Hydroamination of Allenes Catalyzed by Acyclic Diaminocarbene (ADC) Gold(I) Complexes. *Angew. Chemie, Int. Ed.* **2016**, *55* (20), 6079–6083.
(32) Barber, J. S.; Yamano, M. M.; Ramirez, M.; Darzi, E. R.; Knapp, R. R.; Liu, F.; Houk, K. N.; Garg, N. K. Diels–Alder Cycloadditions of Strained Azacyclic

Allenes. *Nat. Chem.* **2018**, *10* (9), 953–960.
(33) Barber, J. S.; Styduhar, E. D.; Pham, H. V; McMahon, T. C.; Houk, K. N.; Garg, N. K. Nitrone Cycloadditions of 1,2-Cyclohexadiene. *J. Am. Chem. Soc.* **2016**, *138* (8), 2512–2515.
(34) Kramer, S.; Fu, G. C. Use of a New Spirophosphine To Achieve Catalytic Enantioselective [4 + 1] Annulations of Amines with Allenes To Generate Dihydropyrroles. *J. Am. Chem. Soc.* **2015**, *137* (11), 3803–3806.
(35) Skotnitzki, J.; Kremsmair, A.; Keefer, D.; Schüppel, F.; Le Cacher de Bonneville, B.; de Vivie-Riedle, R.; Knochel, P. Regio- and Diastereoselective Reactions of Chiral Secondary Alkylcopper Reagents with Propargylic Phosphates: Preparation of Chiral Allenes. *Chem. Sci.* **2020**, *11* (20), 5328–5332.
(36) Mitchell, S. M.; Niradha Sachinthani, K. A.; Pulukkody, R.; Pentzer, E. B. Polymerization of Cumulated Bonds: Isocyanates, Allenes, and Ketenes as Monomers. *ACS Macro Lett.* **2020**, *9* (7), 1046–1059.
(37) Yokozawa, T.; Ito, N.; Endo, T. Radical Polymerization Behavior of Phenylallene. Synthesis of Functional Polymer Containing Styryl Moiety on the Backbone. *Chem. Lett.* **1988**, *17* (12), 1955–1958.
(38) Bao, Y.; Shen, G.; Liu, X.; Li, Y. RAFT Polymerization of a Novel Allene-Derived Asymmetrical Divinyl Monomer: A Facile Strategy to Alkene-Functionalized Hyperbranched Vinyl Polymers with High Degrees of Branching. *J. Polym. Sci. Part A Polym. Chem.* **2013**, *51* (13), 2959–2969.
(39) Takahashi, T.; Yokozawa, T.; Endo, T. Cationic Polymerization Behavior of Alkoxyallenes. *Macromolecules* **1995**, *28* (4), 866–869.
(40) Peska, J.; Benes, M. J. Anionic Polymerization of Cyanoallene. *Collect. Czechoslov. Chem. Commun.* **1969**, *34* (3), 1115–1117.
(41) Kanbayashi, N.; Ikegami, J.; Kataoka, Y.; Okamura, T.; Onitsuka, K. Cyclocopolymerization Based on Alternating Insertions of Isocyanide and Allene Units into a Palladium-Carbon Bond. *Macromol. (Washington, DC, United States)* **2018**, *51* (15), 6092–6098.
(42) Takenaka, Y.; Osakada, K. Rh Complex Catalyzed Alternating Copolymerization of Alkylallene or Aryloxoallene with Carbon Monoxide: Influence of Monomer Structures on the Reaction Rate. *Macromol. Chem. Phys.* **2001**, *202* (18), 3571–3578.
(43) Galan, N. J.; Burroughs, J. M.; Maroon, C. R.; Long, B. K.; Brantley, J. N. Vinyl-Addition Polymerizations of Cycloallenes: Synthetic Access to Congeners of Cyclic-Olefin Polymers. *Polym. Chem.* **2020**, *11* (35), 5578–5581.
(44) Fried, A. D.; Brantley, J. N. Controlled Polymerization of β-Pinadiene: Accessing Unusual Polymer Architectures with Biomass-Derived Monomers. *ACS Macro Lett.* **2020**, *9* (4), 595–599.
(45) Taguchi, M.; Tomita, I.; Endo, T. Living Coordination Polymerization of Allene Derivatives Bearing Hydroxy Groups by π-Allylnickel Catalyst. *Angew. Chemie Int. Ed.* **2000**, *39* (20), 3667–3669.
(46) Takagi, K.; Tomita, I.; Endo, T. Allylnickel-Catalyzed Living CoordinationPolymerization of Allenes with Ester Functionality. *Polym. Bull.*

2003, *50* (5), 335–342.
(47) Taguchi, M.; Tomita, I.; Yoshida, Y.; Endo, T. Block Copolymerization of Allene Derivatives with 1,3-Butadiene by Living Coordination Polymerization with π-Allylnickel Catalyst. *J. Polym. Sci. Part A Polym. Chem.* **1999**, *37* (21), 3916–3921.
(48) Hiroki, K.; Kijima, M. Synthesis and Properties of Conjugated Copolymer Having Alternate Structure of Diphenylanthracene and Allene. *Chem. Lett.* **2005**, *34* (7), 942–943.
(49) Kijima, M.; Hiroki, K.; Shirakawa, H. The First Conjugated Allene Polymer. *Macromol. Rapid Commun.* **2002**, *23* (15), 901–904.
(50) Hiroki, K.; Kikuchi, Y.; Kijima, M. Synthesis and Properties of Novel Acid-Sensitive Conjugated Allene Polymers. *Synth. Met.* **2003**, *135–136*, 389–390.
(51) Rivera-Fuentes, P.; Alonso-Gómez, J. L.; Petrovic, A. G.; Santoro, F.; Harada, N.; Berova, N.; Diederich, F. Amplification of Chirality in Monodisperse, Enantiopure Alleno-Acetylenic Oligomers. *Angew. Chemie Int. Ed.* **2010**, *49* (12), 2247–2250.
(52) Tzirakis, M. D.; Alberti, M. N.; Weissman, H.; Rybtchinski, B.; Diederich, F. Enantiopure Laterally Functionalized Alleno-Acetylenic Macrocycles: Synthesis, Chiroptical Properties, and Self-Assembly in Aqueous Media. *Chem. - A Eur. J.* **2014**, *20* (49), 16070–16073.
(53) Hasegawa, M.; Endo, J.; Iwata, S.; Shimasaki, T.; Mazaki, Y. Chiroptical Properties of 1,3-Diphenylallene-Anchored Tetrathiafulvalene and Its Polymer Synthesis. *Beilstein J. Org. Chem.* **2015**, *11*, 972–979.
(54) Kurioka, T.; Shida, N.; Tomita, I.; Inagi, S. Post-Functionalization of Aromatic C–H Bonds at the Main Chains of π-Conjugated Polymers via Anodic Chlorination Facilitated by Lewis Acids. *Macromolecules* **2021**, *54* (3), 1539–1547.
(55) Peters, B. K.; Rodriguez, K. X.; Reisberg, S. H.; Beil, S. B.; Hickey, D. P.; Kawamata, Y.; Collins, M.; Starr, J.; Chen, L.; Udyavara, S.; Klunder, K.; Gorey, T. J.; Anderson, S. L.; Neurock, M.; Minteer, S. D.; Baran, P. S. Scalable and Safe Synthetic Organic Electroreduction Inspired by Li-Ion Battery Chemistry. *Science (80-.).* **2019**, *363* (6429), 838–845.
(56) Siddiqi, Z.; Sarlah, D. Electrochemical Dearomatization of Commodity Polymers. *J. Am. Chem. Soc.* **2021**, *143* (50), 21264–21269.
(57) Fagnani, D. E.; Kim, D.; Camarero, S. I.; Alfaro, J. F.; McNeil, A. J. Using Waste Poly(Vinyl Chloride) to Synthesize Chloroarenes by Plasticizer-Mediated Electro(de)Chlorination. *Nat. Chem.* **2023**, *15* (2), 222–229.
(58) Izumiya, R.; Atobe, M.; Shida, N. Electrochemically Triggered Hole-Catalytic Benzylic Substitution Reaction at a Polymer Chain Containing β-O-4 Linkage. *Bull. Chem. Soc. Jpn.* **2023**, *96* (4), 353–358.
(59) Bellotti, V.; Parkatzidis, K.; Wang, H. S.; De Alwis Watuthanthrige, N.; Orfano, M.; Monguzzi, A.; Truong, N. P.; Simonutti, R.; Anastasaki, A. Light-Accelerated Depolymerization Catalyzed by Eosin Y. *Polym. Chem.* **2023**, *14* (3), 253–258.
(60) Liu, M. O.; Lin, H.-F.; Yang, M.-C.; Lai, M.-J.; Chang, C.-C.; Feng, M.-C.; Shiao, P.-L.; Chen, I.-M. Thermal Oxidation and Molding Feasibility of Cycloolefin Copolymers (COCs) with High Glass Transition Temperature. *Polym. Degrad.*

Stab. **2006**, *91* (7), 1443–1447.
(61) Khanarian, G. Rubber Toughened and Optically Transparent Blends of Cyclic Olefin Copolymers. *Polym. Eng. Sci.* **2000**, *40* (12), 2590–2601.
(62) Cherdron, H.; Brekner, M.-J.; Osan, F. Cycloolefin-Copolymere: Eine Neue Klasse Transparenter Thermoplaste. *Die Angew. Makromol. Chemie* **1994**, *223* (1), 121–133.
(63) Yamazaki, M. Industrialization and Application Development of Cyclo-Olefin Polymer. *J. Mol. Catal. A Chem.* **2004**, *213* (1), 81–87.
(64) Pegoretti, A.; Fambri, L.; Lonardi, C.; Slouf, M.; Dorigato, A.; Pegoretti, A.; Fambri, L.; Lonardi, C.; Slouf, M.; Kolarik, J. Linear Low Density Polyethylene/Cycloolefin Copolymer Blends. *EXPRESS polymer letters.* Budapest University of Technology and Economics Dept of Polymer Engineering: Budapest : 2011, pp 23–37.
(65) Shin, J. Y.; Park, J. Y.; Liu, C.; He, J.; Kim, S. C. Chemical Structure and Physical Properties of Cyclic Olefin Copolymers (IUPAC Technical Report). **2005**, *77* (5), 801–814.
(66) Forsyth, J. F.; Scrivani, T.; Benavente, R.; Marestin, C.; Pereña, J. M. Thermal and Dynamic Mechanical Behavior of Ethylene/Norbornene Copolymers with Medium Norbornene Contents. *J. Appl. Polym. Sci.* **2001**, *82* (9), 2159–2165.
(67) Fox, T. G.; Flory, P. J. Second-Order Transition Temperatures and Related Properties of Polystyrene. I. Influence of Molecular Weight. *J. Appl. Phys.* **1950**, *21* (6), 581–591.
(68) Nishida, S.; Nishida, H.; Endo, T. Radical Copolymerization Behavior of a Highly Fluorinated Cyclic Olefin with Vinyl Ether. *J. Polym. Sci. Part A Polym. Chem.* **2002**, *40* (8), 1151–1156.
(69) Mizote, A.; Tanaka, T.; Higashimura, T.; Okamura, S. Cationic Polymerization of Cyclic Olefins. *J. Polym. Sci. Part A-1 Polym. Chem.* **1966**, *4* (4), 869–879.
(70) Bielawski, C. W.; Grubbs, R. H. Living Ring-Opening Metathesis Polymerization. *Prog. Polym. Sci.* **2007**, *32* (1), 1–29.
(71) Jerschow, A.; Ernst, E.; Hermann, W.; Mueller, N. Nuclear Magnetic Resonance Evidence for a New Microstructure in Ethene-Cyclopentene Copolymers. *Macromolecules* **1995**, *28* (21), 7095–7099.
(72) Li, X.; Nishiura, M.; Mori, K.; Mashiko, T.; Hou, Z. Cationic Scandium Aminobenzyl Complexes. Synthesis, Structure and Unprecedented Catalysis of Copolymerization of 1-Hexene and Dicyclopentadiene. *Chem. Commun.* **2007**, No. 40, 4137–4139.
(73) Lavoie, A. R.; Waymouth, R. M. Catalytic Syntheses of Alternating, Stereoregular Ethylene/Cycloolefin Copolymers. *Tetrahedron* **2004**.
(74) Endo, T.; Tomita, I. Novel Polymerization Methods for Allene Derivatives. *Prog. Polym. Sci.* **1997**, *22* (3), 565–600.
(75) Takagi, K.; Tomita, I.; Endo, T. Living Coordination Polymerization of Alkylallenes by π-Allylnickel Catalyst: Observation of an Extremely High Polymerizability of 1,2-Cyclononadiene. *Chem. Lett.* **1997**, No. 11, 1187–1188.
(76) Auras, R.; Harte, B.; Selke, S. An Overview of Polylactides as Packaging

Materials. *Macromol. Biosci.* **2004**, *4* (9), 835–864.
(77) Gilding, D. K.; Reed, A. M. Biodegradable Polymers for Use in Surgery—Polyglycolic/Poly(Actic Acid) Homo- and Copolymers: 1. *Polymer (Guildf).* **1979**, *20* (12), 1459–1464.
(78) Castro-Aguirre, E.; Iñiguez-Franco, F.; Samsudin, H.; Fang, X.; Auras, R. Poly(Lactic Acid)—Mass Production, Processing, Industrial Applications, and End of Life. *Adv. Drug Deliv. Rev.* **2016**, *107*, 333–366.
(79) Mülhaupt, R. Green Polymer Chemistry and Bio-Based Plastics: Dreams and Reality. *Macromol. Chem. Phys.* **2013**, *214* (2), 159–174.
(80) Carmody, M. O.; Carmody, W. H. Polymerization of Terpenes. *J. Am. Chem. Soc.* **1937**, *59* (7), 1312.
(81) Ruckel, E. R.; Arlt, H. G.; Wojcik, R. T. The Chemistry of Tackifying Terpene Resins BT - Adhesion Science and Technology; Lee, L.-H., Ed.; Springer US: Boston, MA, 1975; pp 395–412.
(82) Silvestre, A. J. D.; Gandini, A. Chapter 2 - Terpenes: Major Sources, Properties and Applications; Belgacem, M. N., Gandini Polymers and Composites from Renewable Resources, A. B. T.-M., Eds.; Elsevier: Amsterdam, 2008; pp 17–38.
(83) Gandini, A. The Irruption of Polymers from Renewable Resources on the Scene of Macromolecular Science and Technology. *Green Chem.* **2011**, *13* (5), 1061–1083.
(84) Ahmad, N.; Abnisa, F.; Daud, W. M. A. W. Potential Use of Natural Rubber to Produce Liquid Fuels Using Hydrous Pyrolysis – a Review. *RSC Adv.* **2016**, *6* (73), 68906–68921.
(85) Kawamura, K.; Nomura, K. Ethylene Copolymerization with Limonene and β-Pinene: New Bio-Based Polyolefins Prepared by Coordination Polymerization. *Macromolecules* **2021**, *54* (10), 4693–4703.
(86) Yarolimek, M. R.; Coia, B. M.; Bookbinder, H. R.; Kennemur, J. G. Investigating the Effect of α-Pinene on the ROMP of δ-Pinene. *Polym. Chem.* **2021**, *12* (35), 5048–5058.
(87) Atkinson, R. L.; Elsmore, M.; Smith, S.; Reynolds-Green, M.; Topham, P. D.; Toolan, D. T. W.; Derry, M. J.; Monaghan, O.; Taresco, V.; Irvine, D. J.; Stockman, R. A.; De Focatiis, D. S. A.; Howdle, S. M. Sustainable ABA Triblock Methacrylate Copolymers Incorporating Both High and Low Tg Terpene-Derived Monomers. *Eur. Polym. J.* **2022**, *179*, 111567.
(88) Atkinson, R. L.; Monaghan, O. R.; Elsmore, M. T.; Topham, P. D.; Toolan, D. T. W.; Derry, M. J.; Taresco, V.; Stockman, R. A.; De Focatiis, D. S. A.; Irvine, D. J.; Howdle, S. M. RAFT Polymerisation of Renewable Terpene (Meth)Acrylates and the Convergent Synthesis of Methacrylate–Acrylate–Methacrylate Triblock Copolymers. *Polym. Chem.* **2021**, *12* (21), 3177–3189.
(89) Satoh, K.; Nakahara, A.; Mukunoki, K.; Sugiyama, H.; Saito, H.; Kamigaito, M. Sustainable Cycloolefin Polymer from Pine Tree Oil for Optoelectronics Material: Living Cationic Polymerization of β-Pinene and Catalytic Hydrogenation of High-Molecular-Weight Hydrogenated Poly(β-Pinene). *Polym. Chem.* **2014**, *5* (9), 3222–3230.
(90) Kukhta, N. A.; Vasilenko, I. V; Kostjuk, S. V. Room Temperature Cationic

Polymerization of β-Pinene Using Modified AlCl3 Catalyst: Toward Sustainable Plastics from Renewable Biomass Resources. *Green Chem.* **2011**, *13* (9), 2362–2364.

(91) Kenny, S. T.; Nikodinovic Runic, J.; Kaminsky, W.; Woods, T.; Babu, R. P.; Keely, C. M.; Blau, W.; O'Connor, K. E. Up-Cycling of PET (Polyethylene Terephthalate) to the Biodegradable Plastic PHA (Polyhydroxyalkanoate). *Environ. Sci. Technol.* **2008**, *42* (20), 7696–7701.

(92) Ragaert, K.; Hubo, S.; Delva, L.; Veelaert, L.; Du Bois, E. Upcycling of Contaminated Post-Industrial Polypropylene Waste: A Design from Recycling Case Study. *Polym. Eng. Sci.* **2018**, *58* (4), 528–534.

(93) Williamson, J. B.; Na, C. G.; Johnson, R. R.; Daniel, W. F. M.; Alexanian, E. J.; Leibfarth, F. A. Chemo- and Regioselective Functionalization of Isotactic Polypropylene: A Mechanistic and Structure–Property Study. *J. Am. Chem. Soc.* **2019**, *141* (32), 12815–12823.

(94) Liu, Y.; Hou, W.; Sun, H.; Cui, C.; Zhang, L.; Jiang, Y.; Wu, Y.; Wang, Y.; Li, J.; Sumerlin, B. S.; Liu, Q.; Tan, W. Thiol-Ene Click Chemistry: A Biocompatible Way for Orthogonal Bioconjugation of Colloidal Nanoparticles. *Chem. Sci.* **2017**, *8* (9), 6182–6187.

(95) Wang, Y.; Zhang, S.; Wang, L.; Zhang, W.; Zhou, N.; Zhang, Z.; Zhu, X. The Suzuki Coupling Reaction as a Post-Polymerization Modification: A Promising Protocol for Construction of Cyclic-Brush and More Complex Polymers. *Polym. Chem.* **2015**, *6* (25), 4669–4677.

(96) Beach, M. W.; Hull, J. W.; King, B. A.; Beulich, I. I.; Stobby, B. G.; Kram, S. L.; Gorman, D. B. Development of a New Class of Brominated Polymeric Flame Retardants Based on Copolymers of Styrene and Polybutadiene. *Polym. Degrad. Stab.* **2017**, *135*, 99–110.

(97) Hyvl, J.; Autenrieth, B.; Schrock, R. R. Proof of Tacticity of Stereoregular ROMP Polymers through Post Polymerization Modification. *Macromolecules* **2015**, *48* (9), 3148–3152.

(98) Kondo, Y.; García-Cuadrado, D.; Hartwig, J. F.; Boaen, N. K.; Wagner, N. L.; Hillmyer, M. A. Rhodium-Catalyzed, Regiospecific Functionalization of Polyolefins in the Melt. *J. Am. Chem. Soc.* **2002**, *124* (7), 1164–1165.

(99) Sherry, B. D.; Toste, F. D. Gold(I)-Catalyzed Propargyl Claisen Rearrangement. *J. Am. Chem. Soc.* **2004**, *126* (49), 15978–15979.

(100) Teller, H.; Flügge, S.; Goddard, R.; Fürstner, A. Enantioselective Gold Catalysis: Opportunities Provided by Monodentate Phosphoramidite Ligands with an Acyclic TADDOL Backbone. *Angew. Chemie - Int. Ed.* **2010**, *49* (11), 1949–1953.

(101) Trost, B. M.; Xie, J. Palladium-Catalyzed Asymmetric Ring Expansion of Allenylcyclobutanols: An Asymmetric Wagner−Meerwein Shift. *J. Am. Chem. Soc.* **2006**, *128* (18), 6044–6045.

(102) Chatani, N.; Takeyasu, T.; Hanafusa, T. Addition of Trimethylsilyl Cyanide to Allenes with the Aid of a Palladium or Nickel Catalyst. *Tetrahedron Lett.* **1986**, *27* (16), 1841–1844.

(103) Trost, B. M.; Jäkel, C.; Plietker, B. Palladium-Catalyzed Asymmetric Addition of

Pronucleophiles to Allenes. *J. Am. Chem. Soc.* **2003**, *125* (15), 4438–4439.
(104) Takagi, K.; Tomita, I.; Endo, T. A Novel Living Coordination Polymerization of Phenylallene Derivatives by π-Allylnickel Catalyst. *Macromolecules* **1997**, *30* (24), 7386–7390.
(105) Rivera-Fuentes, P.; Diederich, F. Allenes in Molecular Materials. *Angew. Chemie, Int. Ed.* **2012**, *51* (12), 2818–2828.
(106) Kijima, M.; Kinoshita, I.; Shirakawa, H. Syntheses and Properties of Conjugated Polymers with Cumulenic Bond in the Main Chain. *Synth. Met.* **1999**, *101* (1), 145–148.
(107) Liu, Y.; Liu, X.; Hu, H.; Guo, J.; Xia, Y.; Lin, L.; Feng, X. Synergistic Kinetic Resolution and Asymmetric Propargyl Claisen Rearrangement for the Synthesis of Chiral Allenes. *Angew. Chemie, Int. Ed.* **2016**, *55* (12), 4054–4058.
(108) Myers, A. G.; Zheng, B. New and Stereospecific Synthesis of Allenes in a Single Step from Propargylic Alcohols. *J. Am. Chem. Soc.* **1996**, *118* (18), 4492–4493.
(109) Skattebøl;, L. Chemistry of Gem-Dihalocyclopropanes. V.1 Formation of Tricyclo[4.1.0.04,6]Heptane and Derivatives. *J. Org. Chem.* **1966**, *31* (9), 2789–2794.
(110) Moore, W. R.; Ward, H. R. The Formation of Allenes from Gem-Dihalocyclopropanes by Reaction with Alkyllithium Reagents1,2. *J. Org. Chem.* **1962**, *27* (12), 4179–4181.
(111) Keitz, B. K.; Fedorov, A.; Grubbs, R. H. Cis-Selective Ring-Opening Metathesis Polymerization with Ruthenium Catalysts. *J. Am. Chem. Soc.* **2012**, *134* (4), 2040–2043.
(112) Although Allene Degradation Was Observed When Materials Were Heated at 80 °C for 48 h under an O2 Atmosphere, Minimal Degradation Was Observed at Room Temperature under an O2 Atmosphere (Figure S21). *Although allene Degrad. was Obs. when Mater. were heated 80 °C 48 h under an O2 Atmos. minimal Degrad. was Obs. room Temp. under an O2 Atmos. (Figure S21).*
(113) Brattesani, A. J.; Maverick, E.; Muscio Jr., O. J.; Jacobs, T. L. Dimerization of Substituted 1,3-Diarylallenes. *J. Org. Chem.* **1992**, *57* (26), 7346–7349.
(114) Skatteboel, L.; Solomon, S. Thermally Induced Reactions of Some Novel Allenes. *J. Am. Chem. Soc.* **1965**, *87* (20), 4506–4513.
(115) Two 4c' GPC Samples Were Analyzed with One Being Sonicated for 45 Minutes. A Đ of 1.86 Was Observed for the Normal Sample, Whereas a Narrower Đ of 1.49 Was Observed for the Sonicated Sample (Figure S28) Which Suggested Breaking up of Aggregates.
(116) Swager, T. M. The Molecular Wire Approach to Sensory Signal Amplification. *Acc. Chem. Res.* **1998**, *31* (5), 201–207.
(117) Jang, H.-S.; Cho, H.-S.; Uhrig, D.; Nieh, M.-P. Insight into the Interactions between Pyrene and Polystyrene for Efficient Quenching Nitroaromatic Explosives. *J. Mater. Chem. C* **2017**, *5* (47), 12466–12473.
(118) Sun, X.; Wang, Y.; Lei, Y. Fluorescence Based Explosive Detection: From Mechanisms to Sensory Materials. *Chem. Soc. Rev.* **2015**, *44* (22), 8019–8061.
(119) Alcaide, B.; Almendros, P.; Aragoncillo, C. Exploiting [2+2] Cycloaddition

Chemistry: Achievements with Allenes. *Chem. Soc. Rev.* **2010**, *39* (2), 783–816.
(120) A Control Experiment with 2c Was Also Performed after Which We Observed No Gelation (Figure S31), However the Z Olefins Were Partly Isomerized (See SI).
(121) Hurtado-Rodrigo, C.; Hoehne, S.; Muñoz, M. P. A New Gold-Catalysed Azidation of Allenes. *Chem. Commun.* **2014**, *50* (12), 1494–1496.
(122) 1H NMR spectroscopy of 5 revealed new vinyl resonances consistent with protodeauration to afford 1, 3-butadienes, which has been previously reported. See: Brown, T. J., Robertson, B. D. Widenhoefer, R. A. S. and X. crystal structure of a cationic. Gold (I) ?-(1,3- Diene) Complex Generated via Isomerization of a Gold ?-Allene Complex. J. Organomet. Chem. 758, 25-28 (2014); Ting, C.-M., Hsu, Y.-L. & Liu, R.-S. Gold-Catalyzed Isomerization of Unactivated Allenes into 1,3-Butadienes under Ambient Con. ditions. Chem. Commun. 48, 6577-6579 (2012).
(123) Shuler, W. E.; Fletcher, W. H. The Infrared Spectrum of Allene-1,1-D2. *J. Mol. Spectrosc.* **1957**, *1* (1), 95–106.
(124) Bunescu, A.; Lee, S.; Li, Q.; Hartwig, J. F. Catalytic Hydroxylation of Polyethylenes. *ACS Cent. Sci.* **2017**, *3* (8), 895–903.
(125) Maximilian, B.; Fei, L.; O., M. T.; Lukas, O.; Stefan, M. Polyethylene Materials with In-Chain Ketones from Nonalternating Catalytic Copolymerization. *Science (80-.).* **2021**, *374* (6567), 604–607.
(126) Mascareñas, J. L.; Varela, I.; López, F. Allenes and Derivatives in Gold(I)- and Platinum(II)-Catalyzed Formal Cycloadditions. *Acc. Chem. Res.* **2019**, *52* (2), 465–479.
(127) Alcaide, B.; Almendros, P. Progress in Allene Chemistry. *Chem. Soc. Rev.* **2014**, *43* (9), 2886–2887.
(128) Galan, N. J.; Brantley, J. N. General Access to Allene-Containing Polymers Using the Skattebøl Rearrangement. *ACS Macro Lett.* **2020**, 1662–1666.
(129) Park, G.; Bielawski, C. W. Ring Opening Metathesis Polymerization of Cyclic Allenes. *Macromolecules* **2021**, *54* (13), 6135–6143.
(130) Neary, W. J.; Sun, Y.; Moore, J. S. Selective Ring-Opening Allene Metathesis: Polymerization or Ruthenium Vinylidene Formation. *ACS Macro Lett.* **2021**, *10* (5), 642–648.
(131) Pinazzi, C. P.; Cattiaux, J.; Pleurdeau, A.; Brosse, J.-C. Polymérisation Par Ouverture de Cycle, 2. Polymérisation Des Dihalo-9,9-Bicyclo[6.1.0]Nonène-4. *Die Makromol. Chemie* **1974**, *175* (6), 1795–1811.
(132) Ramirez, A. L. B.; Kean, Z. S.; Orlicki, J. A.; Champhekar, M.; Elsakr, S. M.; Krause, W. E.; Craig, S. L. Mechanochemical Strengthening of a Synthetic Polymer in Response to Typically Destructive Shear Forces. *Nat. Chem.* **2013**, *5* (9), 757–761.
(133) Last, L. A.; Fretz, E. R.; Coates, R. M. Synthesis of Polycyclic Homocyclopropylcarbinols by Reductive Cyclization of Bromocyclopropyl Epoxides. *J. Org. Chem.* **1982**, *47* (17), 3211–3219.
(134) Sathe, D.; Zhou, J.; Chen, H.; Su, H.-W.; Xie, W.; Hsu, T.-G.; Schrage, B. R.; Smith, T.; Ziegler, C. J.; Wang, J. Olefin Metathesis-Based Chemically Recyclable

Polymers Enabled by Fused-Ring Monomers. *Nat. Chem.* **2021**, *13* (8), 743–750.
(135) Tang, J.; Xie, T.; Yuan, Y.; Hua, J.; Zhuang, T.; Luo, Y.; Geng, J. Degradation of Polydienes Induced by Alkyllithium: Characterization and Reaction Mechanism. *Macromolecules* **2021**, *54* (3), 1147–1158.
(136) Leibler, L. Theory of Microphase Separation in Block Copolymers. *Macromolecules* **1980**, *13* (6), 1602–1617.
(137) 5 Equiv. of MeLi per Cyclopropane Resulted in Only ~0.53 Equiv. Relative to the Total Mmol of 5 Used.
(138) Hahn, S. F. An Improved Method for the Diimide Hydrogenation of Butadiene and Isoprene Containing Polymers. *J. Polym. Sci. Part A Polym. Chem.* **1992**, *30* (3), 397–408.
(139) Halton, B.; Harvey, J. Electrocyclic Ring-Opening Reactions of Gem-Dibromocyclopropanes in the Synthesis of Natural Products and Related Compounds. *Synlett* **2006**, *2006* (13), 1975–2000.
(140) Crabtree, R. H.; Fujita, K.; Takahashi, Y.; Yamaguchi, R. (1,5-Cyclooctadiene)(Tricyclohexylphosphine)(Pyridine)Iridium(I) Hexafluorophosphate. *Encyclopedia of Reagents for Organic Synthesis*. March 13, 2018, pp 1–7.
(141) Mahittikul, A.; Prasassarakich, P.; Rempel, G. L. Hydrogenation of Natural Rubber Latex in the Presence of [Ir(Cod)(PCy3)(Py)]PF6. *J. Mol. Catal. A Chem.* **2009**, *297* (2), 135–141.
(142) Lower Mn Polymers (<15 KDa) Could Be Reduced Using Either Pd/C or Adam's Catalyst (PtO2).
(143) H2 Pressure Exceeding 600 Psi and Longer Reactions Times (70 h) Led to a Reduction in Mn, Which We Attributed to Possible Hydrogenolysis.
(144) Hibbitts, D. D.; Flaherty, D. W.; Iglesia, E. Effects of Chain Length on the Mechanism and Rates of Metal-Catalyzed Hydrogenolysis of n-Alkanes. *J. Phys. Chem. C* **2016**, *120* (15), 8125–8138.
(145) Flaherty, D. W.; Uzun, A.; Iglesia, E. Catalytic Ring Opening of Cycloalkanes on Ir Clusters: Alkyl Substitution Effects on the Structure and Stability of C–C Bond Cleavage Transition States. *J. Phys. Chem. C* **2015**, *119* (5), 2597–2613.
(146) These Materials Also Exhibited Photoluminescent Properties Consistent with Previous Reports22,24 (Figure S24 - S25), Could Be Thermally Crosslinked above 100 C (Figure S21), and Demonstrated Good Oxidative Stability in Solution (Figure S22).
(147) A 9Mn Sample Dissolved in D8-THF and Irradiated with 254 Nm Light Led to Complete Gelation after 7 Days (Figure SX).
(148) Ellen, M. Beyond Plastic Waste. *Science (80-.).* **2017**, *358* (6365), 843.
(149) M., G. J.; L., R. M. The Future of Plastics Recycling. *Science (80-.).* **2017**, *358* (6365), 870–872.
(150) Chatti, S.; Kricheldorf, H. R. Copolyesters of E-Caprolactone, Isosorbide and Suberic Acid by Ring-Opening Copolymerization. *J. Macromol. Sci. Part A* **2006**, *43* (7), 967–975.
(151) Yu, L.; Zhou, Q.; Gao, Y.; Fu, Z.; Xiao, Y.; Li, Z.-C.; Wang, J. Synthesis of

Polyallenoates through Copper-Mediated Cross-Coupling of Dialkynes and Bis-α-Diazoesters. *Chem. Commun.* **2022**, *58* (24), 3909–3912.
(152) Robin, J. J. Overview of the Use of Ozone in the Synthesis of New Polymers and the Modification of Polymers BT - New Synthetic Methods; Springer Berlin Heidelberg: Berlin, Heidelberg, 2004; pp 35–80.
(153) Nor, H. M.; Ebdon, J. R. Ozonolysis of Natural Rubber in Chloroform SolutionPart 1. A Study by GPC and FTIR Spectroscopy. *Polymer (Guildf).* **2000**, *41* (7), 2359–2365.
(154) Anachkov, M. P.; Rakovski, S. K.; Stefanova, R. V. Ozonolysis of 1,4-Cis-Polyisoprene and 1,4-Trans-Polyisoprene in Solution. *Polym. Degrad. Stab.* **2000**, *67* (2), 355–363.
(155) Akbulatov, S.; Tian, Y.; Boulatov, R. Force–Reactivity Property of a Single Monomer Is Sufficient To Predict the Micromechanical Behavior of Its Polymer. *J. Am. Chem. Soc.* **2012**, *134* (18), 7620–7623.
(156) Schneider, W. A.; Müller, M. F. Crystallinity of Trans-Polyoctenamer: Characterization and Influence of Sample History. *J. Mol. Catal.* **1988**, *46* (1), 395–403.
(157) Ramirez, A. L. B.; Kean, Z. S.; Orlicki, J. A.; Champhekar, M.; Elsakr, S. M.; Krause, W. E.; Craig, S. L. Mechanochemical Strengthening of a Synthetic Polymer in Response to Typically Destructive Shear Forces. *Nat. Chem.* **2013**, *5*, 757.
(158) Jiang, X.; Zhang, J.; Ma, S. Iron Catalysis for Room-Temperature Aerobic Oxidation of Alcohols to Carboxylic Acids. *J. Am. Chem. Soc.* **2016**, *138* (27), 8344–8347.
(159) Shaw, M. H.; Twilton, J.; MacMillan, D. W. C. Photoredox Catalysis in Organic Chemistry. *J. Org. Chem.* **2016**, *81* (16), 6898–6926.
(160) Naumann, R.; Goez, M. First Micelle-Free Photoredox Catalytic Access to Hydrated Electrons for Syntheses and Remediations with a Visible LED or Even Sunlight. *Chem. – A Eur. J.* **2018**, *24* (66), 17557–17567.
(161) Romero, N. A.; Nicewicz, D. A. Organic Photoredox Catalysis. *Chem. Rev.* **2016**, *116* (17), 10075–10166.
(162) Crespi, S.; Fagnoni, M. Generation of Alkyl Radicals: From the Tyranny of Tin to the Photon Democracy. *Chem. Rev.* **2020**, *120* (17), 9790–9833.
(163) Margrey, K. A.; Nicewicz, D. A. A General Approach to Catalytic Alkene Anti-Markovnikov Hydrofunctionalization Reactions via Acridinium Photoredox Catalysis. *Acc. Chem. Res.* **2016**, *49* (9), 1997–2006.
(164) Pistritto, V. A.; Liu, S.; Nicewicz, D. A. Mechanistic Investigations into Amination of Unactivated Arenes via Cation Radical Accelerated Nucleophilic Aromatic Substitution. *J. Am. Chem. Soc.* **2022**, *144* (33), 15118–15131.
(165) Riener, M.; Nicewicz, D. A. Synthesis of Cyclobutane Lignans via an Organic Single Electron Oxidant–Electron Relay System. *Chem. Sci.* **2013**, *4* (6), 2625–2629.
(166) Ramirez, N. P.; Bosque, I.; Gonzalez-Gomez, J. C. Photocatalytic Dehydrogenative Lactonization of 2-Arylbenzoic Acids. *Org. Lett.* **2015**, *17* (18),

4550–4553.
(167) Holmberg-Douglas, N.; Nicewicz, D. A. Photoredox-Catalyzed C–H Functionalization Reactions. *Chem. Rev.* **2022**, *122* (2), 1925–2016.
(168) Roth, H. G.; Romero, N. A.; Nicewicz, D. A. Experimental and Calculated Electrochemical Potentials of Common Organic Molecules for Applications to Single-Electron Redox Chemistry. *Synlett* **2016**, *27* (5), 714–723.
(169) Frech, S.; Theato, P. Synthesizing Polyethylene from Polyacrylates: A Decarboxylation Approach. *ACS Macro Lett.* **2022**, *11* (2), 161–165.
(170) Adili, A.; Korpusik, A. B.; Seidel, D.; Sumerlin, B. S. Photocatalytic Direct Decarboxylation of Carboxylic Acids to Derivatize or Degrade Polymers. *Angew. Chemie Int. Ed.* **2022**, *61* (40), e202209085.
(171) Korpusik, A. B.; Adili, A.; Bhatt, K.; Anatot, J. E.; Seidel, D.; Sumerlin, B. S. Degradation of Polyacrylates by One-Pot Sequential Dehydrodecarboxylation and Ozonolysis. *J. Am. Chem. Soc.* **2023**, *145* (19), 10480–10485.
(172) Perkowski, A. J.; You, W.; Nicewicz, D. A. Visible Light Photoinitiated Metal-Free Living Cationic Polymerization of 4-Methoxystyrene. *J. Am. Chem. Soc.* **2015**, *137* (24), 7580–7583.
(173) Kottisch, V.; Michaudel, Q.; Fors, B. P. Cationic Polymerization of Vinyl Ethers Controlled by Visible Light. *J. Am. Chem. Soc.* **2016**, *138* (48), 15535–15538.
(174) Lu, P.; Kensy, V. K.; Tritt, R. L.; Seidenkranz, D. T.; Boydston, A. J. Metal-Free Ring-Opening Metathesis Polymerization: From Concept to Creation. *Acc. Chem. Res.* **2020**, *53* (10), 2325–2335.
(175) Yang, X.; Murphy, L. M.; Haque, F. M.; Grayson, S. M.; Boydston, A. J. A Highly Efficient Metal-Free Protocol for the Synthesis of Linear Polydicyclopentadiene. *Polym. Chem.* **2021**, *12* (19), 2860–2867.
(176) Young, J. B.; Bowman, J. I.; Eades, C. B.; Wong, A. J.; Sumerlin, B. S. Photoassisted Radical Depolymerization. *ACS Macro Lett.* **2022**, *11* (12), 1390–1395.
(177) Wilger, D. J.; Gesmundo, N. J.; Nicewicz, D. A. Catalytic Hydrotrifluoromethylation of Styrenes and Unactivated Aliphatic Alkenes via an Organic Photoredox System. *Chem. Sci.* **2013**, *4* (8), 3160–3165.
(178) Hamilton, D. S.; Nicewicz, D. A. Direct Catalytic Anti-Markovnikov Hydroetherification of Alkenols. *J. Am. Chem. Soc.* **2012**, *134* (45), 18577–18580.
(179) Wang, Y.; Haze, O.; Dinnocenzo, J. P.; Farid, S.; Farid, R. S.; Gould, I. R. Bonded Exciplexes. A New Concept in Photochemical Reactions. *J. Org. Chem.* **2007**, *72* (18), 6970–6981.
(180) Miranda, M. A.; Garcia, H. 2,4,6-Triphenylpyrylium Tetrafluoroborate as an Electron-Transfer Photosensitizer. *Chem. Rev.* **1994**, *94* (4), 1063–1089.
(181) The Temperature of the Reaction Did Not Exceed 35 C.
(182) Wang, C.-S.; Dixneuf, P. H.; Soulé, J.-F. Photoredox Catalysis for Building C–C Bonds from C(Sp2)–H Bonds. *Chem. Rev.* **2018**, *118* (16), 7532–7585.
(183) The Temperature of the Reaction Did Not Exceed 40 C.
(184) (ΔMn = -89 KDa, Note: Initial Mn = 118 KDa).
(185) Andronico, L. A.; Quintavalla, A.; Lombardo, M.; Mirasoli, M.; Guardigli, M.;

Trombini, C.; Roda, A. Synthesis of 1,2-Dioxetanes as Thermochemiluminescent Labels for Ultrasensitive Bioassays: Rational Prediction of Olefin Photooxygenation Outcome by Using a Chemometric Approach. *Chem. – A Eur. J.* **2016**, *22* (50), 18156–18168.
(186) Smith, L. M.; Aitken, H. M.; Coote, M. L. The Fate of the Peroxyl Radical in Autoxidation: How Does Polymer Degradation Really Occur? *Acc. Chem. Res.* **2018**, *51* (9), 2006–2013.
(187) De Keer, L.; Van Steenberge, P.; Reyniers, M.-F.; Gryn'ova, G.; Aitken, H. M.; Coote, M. L. New Mechanism for Autoxidation of Polyolefins: Kinetic Monte Carlo Modelling of the Role of Short-Chain Branches, Molecular Oxygen and Unsaturated Moieties. *Polym. Chem.* **2022**, *13* (22), 3304–3314.
(188) Gesmundo, N. J.; Nicewicz, D. A. Cyclization–Endoperoxidation Cascade Reactions of Dienes Mediated by a Pyrylium Photoredox Catalyst. *Beilstein J. Org. Chem.* **2014**, *10*, 1272–1281.
(189) ΔMn = -176 KDa.
(190) Malhotra, S. L. Ultrasonic Modification of Polymers. II. Degradation of Polystyrene, Substituted Polystyrene, and Poly(n-Vinyl Carbazole) in the Presence of Flexible Chain Polymers. *J. Macromol. Sci. Part A - Chem.* **1982**, *18* (7–8), 1055–1085.
(191) ΔMn = -250 KDa.
(192) Hydrofunctionalization with MeOH Was Also Operative on a Low Mn 1 (9.7 KDa), However the Etherified Product Was Limited to 30% Conv.
(193) Perkowski, A. J.; Nicewicz, D. A. Direct Catalytic Anti-Markovnikov Addition of Carboxylic Acids to Alkenes. *J. Am. Chem. Soc.* **2013**, *135* (28), 10334–10337.
(194) Onuska Megan E.; Rosario Collazo, José L.; Nicewicz, David. A., N. P. R. . S.-H. Anti-Markovnikov Hydroazidation of Activated Olefins via Organic Photoredox Catalysis. *Synlett* **2020**, *31* (01), 55–59.
(195) Note: We Observe Slight Etherification of the Included Trifluoroethanol, and Extended Reaction Times Leads to Slight Thioether Formation (See SI).
(196) Brekner, M.-J.; Deckers, H.; Osan, F. Cycloolefin Copolymers with Low Melt Viscosity and Optical Damping for Use as Optical Wave Guides., August 18, 1994.
(197) Lavoie, A. R.; Waymouth, R. M. Catalytic Syntheses of Alternating, Stereoregular Ethylene/Cycloolefin Copolymers. *Tetrahedron* **2004**, *60* (34), 7147–7155.
(198) Takagi, K.; Endo, T.; Tomita, I.; Endo, T. Single-Feed One-Step Block Copolymerization of n-Octyloxyallene with Phenylallene Using π-Allylnickel as Initiator. *Chem. Commun.* **1998**, No. 6, 681–682.
(199) Tomita, I.; Kondo, Y.; Takagi, K.; Endo, T. A Novel Living Coordination Polymerization of Methoxyallene by .Pi.-Allylnickel Catalyst. *Macromolecules* **1994**, *27* (15), 4413–4414.
(200) Taguchi, M.; Tomita, I.; Endo, T. Living Coordination Polymerization of Allene (1,2-Propadiene) by π-Allylnickel Catalyst and Selective Hydrosilylation Reaction of Polymers Having Polyallene Units. *Macromol. Chem. Phys.* **2000**, *201* (17), 2322–2327.

(201) Takagi, K.; Tomita, I.; Endo, T. Living Coordination Polymerization of N-Allenylamides by π-Allylnickel Catalysts. *Macromolecules* **1998**, *31* (20), 6741–6747.
(202) Pearson, A. J.; Mallik, S.; Pinkerton, A. A.; Adams, J. P.; Zheng, S. Stereocontrolled Functionalization of 1,5-Cyclooctadiene Using Organomolybdenum Chemistry. *J. Org. Chem.* **1992**, *57* (10), 2910–2917.
(203) Moore, W. R.; Bertelson, R. C. The Synthesis and Some Reactions of 1,2-Cyclononadiene and 1,2-Cyclodecadiene. *J. Org. Chem.* **1962**, *27* (12), 4182–4186.
(204) No Title. *high Mol. Weight impurity Appear. to increase as a Funct. conversion, this Mater. also Appear. to Chain extend.*
(205) Liu, C.; Yu, J.; Sun, X.; Zhang, J.; He, J. Thermal Degradation Studies of Cyclic Olefin Copolymers. *Polym. Degrad. Stab.* **2003**, *81* (2), 197–205.
(206) Daoust, K. J.; Hernandez, S. M.; Konrad, K. M.; Mackie, I. D.; Winstanley, J.; Johnson, R. P. Strain Estimates for Small-Ring Cyclic Allenes and Butatrienes. *J. Org. Chem.* **2006**, *71* (15), 5708–5714.
(207) Gmernicki, K. R.; Hong, E.; Maroon, C. R.; Mahurin, S. M.; Sokolov, A. P.; Saito, T.; Long, B. K. Accessing Siloxane Functionalized Polynorbornenes via Vinyl-Addition Polymerization for CO2 Separation Membranes. *ACS Macro Lett.* **2016**, *5* (7), 879–883.
(208) Yu, S. T.; Na, S. J.; Lim, T. S.; Lee, B. Y. Preparation of a Bulky Cycloolefin/Ethylene Copolymer and Its Tensile Properties. *Macromol. (Washington, DC, United States)* **2010**, *43* (2), 725–730.
(209) Kolarik, J.; Krulis, Z.; Slouf, M.; Fambri, L. High-Density Polyethylene/Cycloolefin Copolymer Blends. Part 1: Phase Structure, Dynamic Mechanical, Tensile, and Impact Properties. *Polym. Eng. Sci.* **2005**, *45* (6), 817–826.
(210) Zhao, W.; Nomura, K. Copolymerizations of Norbornene and Tetracyclododecene with α-Olefins by Half-Titanocene Catalysts: Efficient Synthesis of Highly Transparent, Thermal Resistance Polymers. *Macromolecules* **2016**, *49* (1), 59–70.
(211) Shea, K. J.; Kim, J. S. Influence of Strain on Chemical Reactivity. Relative Reactivity of Torsionally Distorted Double Bonds in MCPBA Epoxidations. *J. Am. Chem. Soc.* **1992**, *114* (8), 3044–3051.
(212) Campbell, K. A.; House, H. O.; Surber, B. W.; Trahanovsky, W. S. Enones with Strained Double Bonds. 10. Use of Flash Vacuum Pyrolysis to Obtain Bicyclo[3.3.1]Non-1-En-3-One. *J. Org. Chem.* **1987**, *52* (12), 2474–2481.
(213) Becker, J. Y.; Zinger, B. Electrochemical Oxidation of Alkyl-Substituted Allenes in Methanol. *Tetrahedron* **1982**, *38* (11), 1677–1682.
(214) Zhu, Y.-Y.; Yin, T.-T.; Li, X.-L.; Su, M.; Xue, Y.-X.; Yu, Z.-P.; Liu, N.; Yin, J.; Wu, Z.-Q. Synthesis and Chiroptical Properties of Helical Polyallenes Bearing Chiral Amide Pendants. *Macromolecules* **2014**, *47* (20), 7021–7029.
(215) Ohno, M.; Okamoto, M. Cis-CYCLODODECENE. *Org. Synth.* **1969**, *49* (30).
(216) Han, X.; Hu, J.; Chen, C.; Yuan, Y.; Shi, Z. Copper-Catalysed, Diboron-Mediated Cis-Dideuterated Semihydrogenation of Alkynes with Heavy Water. *Chem.*

Commun. **2019**, *55* (48), 6922–6925.
(217) Erden, I.; Cao, W.; Price, M.; Colton, M. A Three-Carbon (N+1+2) Ring Expansion Method for the Synthesis of Macrocyclic Enones. Application to Muscone Synthesis. *Tetrahedron* **2008**, *64* (23), 5497–5501.
(218) Gordon, M.; Taylor, J. S. Ideal Copolymers and the Second-Order Transitions of Synthetic Rubbers. i. Non-Crystalline Copolymers. *J. Appl. Chem.* **1952**, *2* (9), 493–500.
(219) Kember, M. R.; White, A. J. P.; Williams, C. K. Highly Active Di- and Trimetallic Cobalt Catalysts for the Copolymerization of CHO and CO2 at Atmospheric Pressure. *Macromolecules* **2010**, *43* (5), 2291–2298.
(220) Song, X.; Cao, L.; Tanaka, R.; Shiono, T.; Cai, Z. Optically Transparent Functional Polyolefin Elastomer with Excellent Mechanical and Thermal Properties. *ACS Macro Lett.* **2019**, *8* (3), 299–303.
(221) Pichersky, E.; Raguso, R. A. Why Do Plants Produce so Many Terpenoid Compounds? *New Phytol.* **2018**, *220* (3), 692–702.
(222) Endo, T.; Takagi, K.; Tomita, I. Design and Synthesis of Polymerizable Cumulated Double Bond System. -Living Coordination Polymerization of Alkylallenes by π-Allylnickel Catalyst-. *Tetrahedron* **1997**, *53* (45), 15187–15196.
(223) Zhou, G.; Cui, L.; Mu, H.; Jian, Z. Custom-Made Polar Monomers Utilized in Nickel and Palladium Promoted Olefin Copolymerization. *Polym. Chem.* **2021**, *12* (27), 3878–3892.
(224) The Consumption of 1 Was Monitored via 1H NMR, and the Kobs Was Determined to Be 0.069 (Figure S63), Close to Our Previously Reported Rate of 2, Where Kobs = 0.052(Ref).
(225) Materials with a Monomer Feed Ratio of 25% 1, Were Precipitated at -78 °C as the Resulting Materials Were Tacky Oils That Were Difficult to Isolate at Room Temperature.
(226) DSC Samples Were Sealed in a Glovebox to Ensure the Samples Were Heated under an Inert Atmosphere.
(227) Fox, T. G.; Loshaek, S. Influence of Molecular Weight and Degree of Crosslinking on the Specific Volume and Glass Temperature of Polymers. *J. Polym. Sci.* **1955**, *15* (80), 371–390.
(228) Penzel, E.; Rieger, J.; Schneider, H. A. The Glass Transition Temperature of Random Copolymers: 1. Experimental Data and the Gordon-Taylor Equation. *Polymer (Guildf).* **1997**, *38* (2), 325–337.
(229) Wang, X.; Jeong, Y. L.; Love, C.; Stretz, H. A.; Stein, G. E.; Long, B. K. Design, Synthesis, and Characterization of Vinyl-Addition Polynorbornenes with Tunable Thermal Properties. *Polym. Chem.* **2021**, *12* (40), 5831–5841.
(230) Li, X.; Hou, Z. Organometallic Catalysts for Copolymerization of Cyclic Olefins. *Coord. Chem. Rev.* **2008**, *252* (15), 1842–1869.
(231) The Rate of Consumption for Both 1 and 6 during the Copolymerization Was Monitored via 1H NMR (Figure S64) Where a Slower Rate Was Observed for 1, Kobs = 0.040. Slightly Slower than the Measured Rate of 6, Kobs = 0.051.
(232) This Copolymerization Could Be Be Scaled up to >1 Gram Scale, Where the

Isolated Yield Was 93%.
(233) Upon Monitoring the Consumption of 1 and 9 (Figure S65) during the Copolymerization, We Observed That 9 Is Consumed within Minutes, Kobs = 0.63. While 1 Is Consumed Much Slower, Kobs = 0.11, Albeit Twice as Fast Compared to the Homopolymerization.
(234) Tomita, I.; Taguchi, M.; Takagi, K.; Endo, T. Block Copolymerization of Allene Derivatives with Isocyanides by the Coordination Polymerization with π-Allylnickel Catalyst. *J. Polym. Sci. Part A Polym. Chem.* **1997**, *35* (3), 431–437.
(235) Taguchi, M.; Tomita, I.; Yoshida, Y.; Endo, T. Block Copolymerization of Allene Derivatives with 1,3-Butadiene by Living Coordination Polymerization with π-Allylnickel Catalyst. *J. Polym. Sci. Part A Polym. Chem.* **1999**, *37* (21), 3916–3921.
(236) Song, X.; Yu, L.; Shiono, T.; Hasan, T.; Cai, Z. Synthesis of Hydroxy-Functionalized Cyclic Olefin Copolymer and Its Block Copolymers with Semicrystalline Polyolefin Segments. *Macromol. Rapid Commun.* **2017**, *38* (7), 1600815.
(237) Zhang, M.; Cui, Z.; Catherine Brinson, L. Mechanical Properties of Hard–Soft Block Copolymers Calculated from Coarse-Grained Molecular Dynamics Models. *J. Polym. Sci. Part B Polym. Phys.* **2018**, *56* (23), 1552–1566.
(238) Woof, C. R.; Durand, D. J.; Webster, R. L. Polymerization of Allenes by Using an Iron(II) β-Diketiminate Pre-Catalyst to Generate High Mn Polymers. *Chem. – A Eur. J.* **2021**, *27* (48), 12335–12340.
(239) Lin, L.-Z.; Che, Y.-Y.; Bai, P.-B.; Feng, C. Sulfinate-Engaged Nucleophilic Addition Induced Allylic Alkylation of Allenoates. *Org. Lett.* **2019**, *21* (18), 7424–7429.
(240) Lima, R. N.; Delgado, J. A. C.; Bernardi, D. I.; Berlinck, R. G. S.; Kaplaneris, N.; Ackermann, L.; Paixão, M. W. Post-Synthetic Functionalization of Tryptophan Protected Peptide Sequences through Indole (C-2) Photocatalytic Alkylation. *Chem. Commun.* **2021**, *57* (47), 5758–5761.

VITA

Nicholas Jose Galan was raised in Knoxville, Tennessee. In the spring of 2013, he graduated from Powell High School. The following fall, Nicholas started his studies at the University of Tennessee, Knoxville, where he would graduate with a B.S. in Chemistry in the spring of 2017. Nicholas decided to stay at the University of Tennessee, Knoxville to pursue a PhD in organic chemistry. Under the tutelage of Professor Johnathan Brantley, Nicholas published several peer-reviewed manuscripts, presented said work at national and regional conferences, co-authored a mini-review book chapter and mentored several undergraduate students. In addition, Nicholas volunteered at Science Olympiad events for multiple years. In his free time, Nicholas enjoys listening to music, tinkering on cars, specialty coffee, watching sports, and playing video games.